Universidad del País Vasco / Euskal Herriko Unibertsitatea

Facultad de Medicina y Enfermería

Departamento de Neurociencias

Metabolic and functional consequences of phagocytosis in microglia

Tesis doctoral para optar al grado de Doctor, presentada por:

Mar Márquez Ropero

2024

Directores de Tesis:

Dra. Amanda Sierra

Dra. María Domercq García

Esta tesis doctoral ha sido realizada gracias al disfrute de una beca de Ayuda de contratación para la Formación de Personal Investigador de UPV/EHU durante el periodo 2019-2023

Este trabajo fue apoyado por subvenciones del Ministerio de Economía y Competitividad de España con fondos FEDER (BFU2015-66689, RYC-2013-12817) y del Ministerio de Ciencia, Innovación y Universidades (MICIU/AE/10.13039/501100011033), una beca de la Fundación BBVA para Investigadores y Creadores Culturales; una beca de ERDF A way of making Europe (PID2022-136698OB-I00) y dos subvenciones del Gobierno Vasco (PI_2016_1_0011; IT1473-22); y una subvención para Proyectos de Investigación de la Fundación Tatiana Pérez de Guzmán para AS.

Sólo existe una llave para acceder a la sabiduría, y es el deseo.

- Amelie Nothomb

***

El alma errante volverá a su nido
Lo que ayer se perdió será encontrado
El sol será sin mancha concebido
y saldrá nuevamente en tu costado

Y dirás frente al mar: ¿Cómo he podido
anegado sin brújula y perdido
llegar a puerto con las velas rotas?

Y una voz te dirá: ¿Que no lo sabes?
El mismo viento que rompió tus naves
es el que hace volar a las gaviotas

- Óscar Hahn

***

A los que estuvieron, a los que están, a los que vendrán.

Me he pasado la vida eligiendo mis caminos de una forma más intuitiva que lógica, y cuando he hecho listas de pros y contras, cuando he asignado un valor

a cada ítem, cuando he ponderado hasta el milímetro cada variable, y la puntuación me ha sido revelada, me he dado cuenta de que yo ya había tomado esa decisión de manera anticipada, como si mi cerebro hubiese hecho esos cálculos de manera inconsciente. Me he pasado la vida sin saber bien cuanto de mi toma de decisiones es algo premeditado y conveniente, o si por el contrario son mis deseos los que me llevan a donde les da la gana.

Una vez, una persona a la que quise mucho me regaló un colgante que decía algo así como que "*yo* era/*vivía a merced de las rachas de viento – haize boladen menpe bizi; izan*". Han pasado unos cuantos años desde entonces y creo que esa afirmación se sigue manteniendo. Así, impulsada por una racha de viento llegué a la neurociencia, y a este laboratorio. Así es como acabó una psicóloga en un laboratorio de neurociencias y biología celular. Llegué durante las prácticas del máster, sin saber que las personas que conocería por el camino serían determinantes para que decidiera quedarme.

A todas las personas de nuestro laboratorio: Ainhoa, Jorge, Amanda. A los que me ayudaron cuando llegué y no sabía ni que era una pipeta.

A Amanda por acogerme durante las prácticas del máster y ofrecerme un lugar donde quedarme a aprender, a crecer y a vivir tanto. Gracias por transmitirme el compromiso de hacer buena ciencia, y por todas las oportunidades de participar en todos los proyectos que fueran saliendo, ya fueran de índole académico o más informales.

A Ainhoa, por mostrarse siempre accesible y disponible para cualquier cosa que pudiera necesitar. Gracias por tu humor y por tu buen hacer.

A Jorge Valero, el mejor del mundo entero, una persona culpable de que yo acabara por aquí. Gracias por tu entusiasmo por la ciencia, eso fue lo que me enganchó al principio, tu forma de trabajar y tu eterna amabilidad me animó a quedarme en el laboratorio unos añitos. Seguro que sigues creando adeptos allá donde estás ahora.

A Vir por tenerme tanta paciencia, por intentar enseñarme con tanto mimo y tanta profesionalidad. Gracias por hacer parte de este camino conmigo. Con personas como tú los momentos fáciles se disfrutan más y los difíciles se llevan mejor.

A Iñaki. Gracias por tu amistad y por los momentos compartidos: las cenas en tu casa, los cafés de después de la hora de comer, las interminables horas en el HCS (a.k.a aparato infernal), pero sobre todo gracias por descubrirme tan buena música. Tenemos pendiente una excursión a la nieve.

Alice. Cuando llegaste al laboratorio eran tiempos extraños. La pandemia no nos dejaba hacer muchos planes, pero aún así intentamos hacer que ese tiempo raro fuera más soportable y compartimos muchos momentos en los que casi nunca faltó la comida. Me hace feliz verte feliz con tu nueva vida en Barcelona.

Noelia. Comenzamos esta andadura juntas durante el máster. Tu fuiste la primera que entró a hacer las prácticas al laboratorio y me animaste a que yo

también lo hiciera. Gracias por los cafés compartidos al inicio. Juntas acabamos esta etapa y no tengo ninguna duda de que te irá estupendamente y encontrarás tu camino.

Joel. Eres un rayo de luz para el laboratorio. Siempre me has sacado una sonrisa, sobre todo cuando más lo he necesitado. Gracias por el apoyo y por escucharme siempre. Conserva siempre esa energía tan pura que tienes.

Marta. Hemos compartido muchísimas cosas y no sabría ni por dónde empezar. Gracias por tu calma, por tu escucha, por tu actitud de buscar siempre la solución a los problemas. Gracias sobre todo por tus consejos. Nos quedó pendiente ir a algún congreso juntas, pero la vida da tantas vueltas que quizá algún día ocurra. Vas a ser una científica increíble.

A Marco por cortar mis cerebros.

Isa. Coincidimos poquitos meses, pero desde el principio me pareciste una super sensata y divertida. Gracias por escucharme y por reírte de mis chistes malos.

Ane. Verte terminar la tesis me ha inspirado mucho y me ha dado muchas fuerzas. Para mi eres una referente. Gracias por ayudarme con la burocracia, por enseñarme acro y por compartir tanto jueves de pintxo-pote. Brindo por que sigan siendo muchos más.

Ter. Cómo valoro en la vida tener personas como tú. Tienes un don para hacernos reír incluso en los momentos más difíciles. No dudo de que encontrarás tu camino y seguirás haciendo felices a los que te rodean. Que la vida te devuelva todo el amor que das.

Laura. El PhD committee nos unió y desde entonces ha habido un montón de cambios inesperados. Gracias por proponer siempre planes tan guays. Seguiremos haciendo muchos más mientras estés en Bilbo. Gracias por las charlas, por nuestras divagaciones acerca de la vida y por escucharme y validarme siempre.

Joan. Gracias por esos abrazos que sanan. Por ser un tío tan auténtico y por esas conversaciones tan necesarias las veces que la oficina se quedaba vacías. gracias por recordarme que *la tranquilidad es lo que más se busca.*

María Alfonso. Gracias por tu bondad, eres un ser de luz, siempre dispuesta a ayudar y a dar lo mejor de ti en cada cosa que haces. Gracias por las reflexiones compartidas. Créete todo lo que vales porque eres una tía increíble.

Mari. Hemos compartido estos largos años juntas con cada una de sus alegrías y penas. Gracias por echarme un cable siempre que lo he necesitado, y por las cenas en tu casa. Muchísimo ánimo en el último empujón. Créeme que el esfuerzo merece la pena.

Josune. Gracias por las noches en las que hemos perreado hasta el suelo y por

alegrarme las mañanas en la oficina. Aunque te corte el pelo no pierdes la fuerza. Gracias por tu energía.

Aida. Gracias por todos los favores que me has hecho. Por enseñarme a cortar en el criostato y por todas las veces que sin dudarlo un segundo me has ayudado. Por aquel viaje de esquí del que sorprendentemente volvimos todos de una pieza. Eres una persona super trabajadora, te auguro muchos éxitos.

Rodrigo. Siempre recordaré nuestras “infiltraciones” en los Steering Boards y nuestros intentos por hacer las cosas un poquito mejor. Gracias por acompañarme a planes culturales, aunque no siempre acertemos. Siempre puedes contar conmigo para ir a más obras de teatro raras y para que me reía de tus chistes malos. Personalmente a mí me encantan. Gracias siempre por tu buena disposición y por ser tan buen tío. Eres un sol.

Lorena. Gracias por tu cariño y por las veces que nos hemos puesto a hablar de música en el confocal. Eres una tía increíble. Nos vemos por el barrio.

Pablo. Gracias por interesarte siempre por cómo estaba. Por aquellas tardes haciendo acroyoga en Karmela y por aquellas noches cantando y tocando la guitarra.

Leire. Te admiro muchísimo. Que mujer más valiente y más fuerte. De ti he aprendido que merece la pena hacer las cosas solamente por estar en paz con una misma. Eso es lo más importante. Lo único que nos vamos a llevar. Por más salidas al monte y por más noches de farra por Bilbo.

Ohiane. Siempre que hablo contigo siento que tenemos una conexión especial. Gracias por las cervezas compartidas esas noches de jueves que se alargan. Ahora toca confiar en que vienen cosas buenas, que la vida tiene cosas bonitas para regalarnos.

Sorey. Gracias por la honestidad que te caracteriza. La ciencia necesita a personas como tú y me alegra mucho que sigas luchando por conseguir lo que deseas.

Adhara. Nunca olvidaré la gymkana de papeleo que supuso hacer la estancia en EEUU en pleno COVID y todo lo que me ayudaste en el proceso. Gracias por aquellos días tan increíbles en Nueva York. Fueron un sueño.

A los inmensos profesionales que hay en Achucarro y en el Departamento de Neurociencias. Gracias a los predocs de los distintos laboratorios que siempre han estado para echarme una mano. Gracias a por post-docs y PIs, que me han enseñado que la ciencia va muchas veces de priorizar la importancia de las relaciones humanas.

A mis padres. No existen palabras ni gestos para expresar toda la gratitud que siento. Gracias por ser siempre tan generosos y tan sensatos, por quererme tanto, aunque a veces se nos resistan las palabras. Gracias por confiar en mí, y en mis decisiones. Gracias por entender que a veces me tengo que equivocar.

Por apoyarme tanto siempre, por animarme a seguir. Por enseñarme que lo más importante en la vida es querer y que te quieran bien, saber estar en las dificultades e intentar vivir con más ligereza y alegría, porque para el tiempito que estamos aquí hay que intentar ser felices, aunque sea a ratitos.

A mi nueva, no tan nueva, cuadrilla.

A Devi por estar siempre orgullosa de mí, y recordarme que algún día sería doctora. Ese día ha llegado, parece ser. Mi sorgiña favorita, nos conocimos haciendo cosas de brujas en teatro hace 9 años y mira todas las cosas que hemos vivido después. Gracias por integrarme en tu cuadrilla y presentarme a gente tan maja con la que he compartido tanto. Gracias por las conversaciones y las birras de la calle Somera. Descansa un poquito y déjate ver un poco más.

Eskerrik asko Aishari. Zure laguntzarik gabe ezin izango nuen tesi honen itzulpena burutu.

A Ibon. Mi leoncito. Gracias por todos estos años de poteo, charlas y de amistad. I know que soy tu bardo favorito. Por muchos años más compartiéndolos contigo. Tenemos pendiente un viaje a Pirineos.

A Iñi. Por ser el mejor máster de D&D que se pudiera tener. Porque aunque sea verdad que no callas ni debajo del agua a mi siempre me parece muy interesante todo lo que tienes que contar. Por que dentro de unos años yo también pueda llamarte Doctor a ti.

A Iñi Martinez. Te quería agradecer las risas que me echo siempre contigo pero no puedo: *Tengo que hacer tesis*. Gracias por los memes. Envíame más.

A mis amiguitos de Deusto. Gracias Edu por animarme siempre y por invitarnos a planes tan guays como un San Juan en un huerto perdido. Gracias Mikel por las tardes de escalada y por tenerme en cuenta.

A los que me acompañaron en mi breve pero intensa estancia en Nueva York. Those three crazy months in NYC were amazing and marked a significant transformation for me, especially in terms of my self-confidence and the realization that my life was mine to explore and live as I pleased.

I'm very grateful to the Hambardzaumyan lab for welcoming me during that time. Thanks to Dolores for all the opportunities and for considering me to participate in one of your papers. Thank you Z, Montse, Gonzalo, Tanvi, Angelo... I felt warmly welcomed and supported whenever I needed it. Special mention to Z because, apart from performing my irradiation experiments, he always radiated calm and a special light.

Thank you, Josh, for being my native guide and showing me the non-touristic USA. Gracias Rodrigo por las conversaciones, reflexiones y excursiones; y Agus por ser de esas personas que parece que conoces desde hace mucho tiempo. Gracias Ana por tus consejos y por recordarme que todo llega, y que no hay que conformarse. Sherry, thanks for all the walks by the Hudson River and the dinners

we shared, even the one where we got a bit too tipsy! Your company meant a lot to me.

Gracias Gabriel por tu magnetismo y tu intensidad. Qué frío hacía en NYC cuando te conocí y que remanso cálido me pareciste. Te mereces todo lo bueno que te está pasando.

A mis amigas de siempre. Gracias por demostrarme que en este mundo de capitalismo feroz donde todo es de usar y tirar hay relaciones que duran y se mantienen.

Jurema. Eres de las personas que más me ha aguantado estos años. Me has visto en mis picos de máxima locura y milagrosamente no has dejado de hablarme. Gracias porque siempre que he compartido contigo mi malestar y mis preocupaciones me he sentido escuchada y has conseguido calmarme y darme una perspectiva más amable. Me cuesta decir te quiero. Pero espero que sepas que te quiero mucho. Tenemos pendiente celebrar el haber sobrevivido a todos estos años con un viajecito a Japón, así que habrá que ir ahorrando.

Zuriñe. Siempre he admirado tu capacidad para hacer amigos. Cuando te conocí quería ser como tú. Quitarme miedos e inseguridades. Eres muy importante para mi y hemos compartido ya media vida juntas, que se dice pronto. Aunque estemos en ciudades distintas sabes que siempre estoy ahí para ti. Por seguir viéndonos crecer y evolucionar en los años de amistad venideros. Te quiero.

Gracias Sara. *Lo siento, había que hacerlo.* Gracias por decirme cosas que a veces una no quiere oir. Por tu comprensión. Porque juntas nos hemos metido en pozos emponzoñados y hemos salido vivas de ellos. Te quiero mucho. Nos esperan cosas bonitas. Lo sé.

Uge. Te has convertido en algo parecido a una hermana para mí. Gracias por estar de manera incondicional. Es una suerte y un honor tener a personas con las que puedes ser tú misma en la más pura esencia. Personas a las que les puedes enseñar tus rotos y tus partes feas y que nos quieren a pesar de nuestros defectos o quizá precisamente por nuestros defectos. Te quiero un montonazo. Indonesia nos espera.

A Alice, porque tu me recuerdas que en estos momentos de hiperconexión también hay amistades profundas con las que no tienes que hablar cada semana, ni siquiera cada mes. Y ahí, en la distancia, están para lo que puedes necesitar, ya sea una conversación profunda o 3 días de festival autodestructivo.

A los Laika. Unai y Alain. Cuántas tardes de ensayo tenemos a las espaldas, cuántas risas e ilusión he compartido con vosotros. Por seguir manteniendo nuestra amistad y por seguir haciendo música juntos.

A mis “Fuengiroleñas”. Gracias Aida, Carmen, Sara y Pilar por haber crecido conmigo y haber vivido tantos veranos maravillosos. Aunque la vida nos lo ponga cada vez más difícil para reunirnos, gracias por las veces que me habéis visitado

en Bilbao y por los sudokus que intentamos hacer para cuadrar las vacaciones y poder juntarnos todas. Gracias por estar en la distancia.

A Urtzi, porque compartir pasiones nos hace sentir un poco menos solos e incomprendidos. Muchas gracias por darle vida a nuestro disco, por todos esos momentos compartidos en el estudio y fuera de él. Ojalá seguir colaborando pronto. Ojalá conservarte como amigo para siempre.

A Miguel por compartir tanta música, tanta poesía y tantas noches. Qué bonito es encontrarte a personas con las que conectar y caer en delirios. Gracias por los domingos de resaca cuando me mandas canciones tan bonitas. Los haces más llevaderos.

A Eder, por decirme allá por 2014, "si alguien puede hacer una tesis esa eres tú". Siempre confiaste en mí, en todo, cuando aún era demasiado joven para que yo lo hiciera. A veces pienso lo distinta que hubiera sido mi vida si no te hubiese conocido. Gracias por seguir estando.

A Borja por regalarme casi 8 años de risas. Por haber sido durante mucho tiempo uno de mis mayores pilares. Mi mejor amigo, mi compañero, mi confidente. A estas alturas solo queda recordar lo bueno, y lo bueno es muchas veces lo sencillo, lo cotidiano. Eso me lo enseñaste bien. Gracias por las conversaciones eternas sobre música, por los memes, por poner pesadilla en la cocina en bucle mientras estábamos encerrados en la cuarentena, por hacerte una crisálida en tu saco verde enfrente de la estación de Canfranc, y por muchísimas otras cosas más. La lista sería eterna. Te sigo deseando lo mejor, a pesar de los pesares. Cuando pienso en ti siempre recuerdo esta frase. “Si yo pudiera darte una cosa en la vida, me gustaría darte la capacidad de verte a ti mismo a través de mis ojos". Ojalá hubiera podido regalarte eso. Solamente eso. Hubiéramos sido más felices.

A aquellas personas cuyo nombre no merece estar en estos agradecimientos, pero si el aprendizaje que dejaron.

A aquellas personas que me hubiese gustado que se quedasen un ratito más.

A Jon, por estar siempre disponible para lo que toque. Me alegra haberte recuperado. Tu alegría y tu determinación me hacen mucha falta.

A mis nuevas compañeras de trabajo en el Área de Juventud del Ayuntamiento. Gracias Ane, Maria, Leire y Mailen por ser compañía en esta nueva etapa, en este *impasse* raro en el que están ocurriendo tantas cosas buenas. Gracias por escuchar mis quejas sobre las montañas de papeleo y por animarme siempre. Espero seguir teniéndoos cuando esta etapa acabe. Eskerrik asko Itziar zure hitzengatik, beti animatsen nauzu tesiari buruz hitz egiten dizudanean. GazteKLUBEKO erreginak gara. Gazteriatik joan eta gero Gorka Urbizuren kontzertu batean topatuko gara ziur.

Al núcleo duro de talentia -Roberta, Carlos, Aitzol, Mario, Sandra, Asier, Maite- os conocí mientras cursaba el máster de Neurociencias y desde entonces hemos

compartido viajes, cambios y mucho crecimiento juntos. Espero que esto se mantenga y poder celebrar también con vosotros.

Esto ha quedado larguísimo. Soy muy afortunada de tener tantos amigos.
Aunque suena a tópico esto no hubiese sido posible sin vosotros.

Finalmente, gracias a Nerea. Lo que he evolucionado y crecido gracias a ti estos últimos tres años me sigue sorprendiendo. Has conseguido hacer salir a la Mar que se escondía detrás de tantas obligaciones autoimpuestas, de tanta falsa creencia de que debía ser como los demás deseaban y no como realmente yo quería. Ahora soy más libre, porque finalmente entendí que mis errores no me quitan valor si no que me dan experiencia y me permiten ser más auténtica, más humana. Eres una profesional inmensa y un referente para mí. Gracias de nuevo, de todo corazón.

Gracias a mí, por ser una cumplidora.

“Last but not least, I wanna thank me
I wanna thank me for believing in me
I wanna thank me for doing all this hard work
I wanna thank me for having no days off
I wanna thank me for, for never quitting

I wanna thank me for always being a giver
And tryna give more than I receive
I wanna thank me for tryna do more right than wrong
I wanna thank me for just being me at all times"

- Snoop Dogg

"Me lo dedico a mí también por ser tan trabajadora, tan valiente y tan maja"
- Úrsula Corberó

TABLE OF CONTENTS

1. ABBREVIATIONS

1. ABBREVIATIONS

AD	Alzheimer's Disease
ALIX	Apoptosis-linked gene 2-interacting protein X
ALS	Amyotrophic lateral sclerosis
AP	Anteroposterior
APCs	Antigen-presenting cells
ApoE	Apolipoprotein E
APP	Amyloid precursor protein
ATP	Adenosine triphosphate
Aβ	Amyloid β
Bak	BCL2 Associated K Protein
BAMs	Border associated macrophages
Bax	BCL2 Associated X Protein
BBB	Blood bran barrier
BDNF	Brain-derived neurotrophic factor
Birc5	Baculoviral IAP repeat containing 5
BrdU	5-bromo-2-deoxyuridine
BSA	Bovine serum albumin
C	Control
C1q	Complement protein 1q
CA	Cornu Amonis
CaCL2	Calcium Chloride
CAMs	CNS associated macrophages
CD11b	Cluster of differentiation molecule 11B
CD68	Cluster of differentiation 68 / Macrosialin
Cd74	Histocompatibility class II invariant chain peptide Class
Cenpe	Centromere protein e
CK-p25	Calcium/ calmodulin-dependent protein kinase II
CNS	Central nervous system
cpMs	Choroid plexus macrophages
CSF	Colony stimulating factor
CSF1R	Colony stimulating factor 1 receptor
Cst3	Cystatin 3
CTSB	Cathepsins B

CTSD	Cathepsins D
CX3CL1	Fractalkine
D	Day
DAM	Disease-associated microglia
DAMPs	Damage-associated molecular patterns
DAP12	DNAX-activation protein of 12 kD
DAPI	4',6-diamidino-2-phenylindole
DAVID	Database for Annotation, Visualization and integrated discovery
DBS	Double-strand breaks
dc-SAMe	Decarboxylated S-adenosylmethionine
DEPC	Diethyl Pyrocarbonate
DG	Dentate gyrus
DMEM	Dulbecco's Modified Eagle Medium
DPBS	Dulbecco's Phosphate-Buffered Saline
E	Embryogenic day
ECM	Extracellular matrix
EDTA	Ethylenediaminetetraacetic Acid
EGF	Epidermal growth factor
EMPs	Erythromyeloid precursors
ER	Endoplasmic reticulum
FAO	Fatty-acid oxidation
FasL	Fas ligand
FBS	Fetal Bovine Serum
Fcrl2	Fc receptor like 2
Fcrls	Fc receptor-like S, scavenger receptor
GAS6	Arrest-specific protein 6
gCSCs	Glioma cancer stem cells
GDNF	Glial cell-derived neurotrophic factor
GFP	Green fluorescent protein
γH2AX	Phosphorylated histone H2AX
GM-CSF	Granulocyte-macrophage colony-stimulating factor
GO	Gene ontology
GPC	Glycerylphosphorylcholine
GPR34	G protein-coupled receptor 34
GPR34	G protein-coupled receptor 34

GSSG	Glutathione disulfide
Gy	Gray (unit of ionazing radiation)
H	Hours
H2-Aa	Histocompatibility 2 class II antigen A alpha
H2-Ab1	Histocompatibility 2 class II antigen A beta 1
HAM	Highly-activated microglia
HAMs	Human AD microglia
HBSS	Hank's balanced salt solution
HCl	Hydrochloride acid
HEPES	4-(2-hydroxyethyl)-1-piperazineethanesulfonic acid
Hexb	β-hexosaminidase subunit β
HFRT	Hypofractionated radiotherapy
HGF/SF	Hepatocyte growth factor or scatter factor
HMGB1	High mobility group box 1 protein
HSCs	Hematopoietic stem cells
IBA1	Ionized calcium-binding adapter molecule 1
IFIT	Interferon induced protein
IFIT3	Interferon induced protein 3
IFN	Interferon
IL-10	Interleukin 10
IL-1β	Interleukin 1β
IL-4	Interleukin 4
IL-6	Interleukin 6
iPLA2	Phospholipase A2 enzyme
iPSCs	Induced pluripotent stem cells
IRM	Interferon responsive microglia
Irf7	Interferon regulatory factor 7
Isg20	Interferon stimulated exonuclease gene 20
KCl	Potassium Chloride
kVs	Kilovolts
LAMPs	Lysosome-Associated Membrane Proteins
LDAMs	Lipid-droplet-accumulating microglia
Lgals3	Galectin 3
LIMPs	Lysosomal Integral Membrane Proteins
LM	Lysosomal (transcriptional signature)

Log	Logaritmic
LPC	Lysophosphatidylcholine
LPS	Lipopolysaccharide
LysoPS	Lysophosphatydilserine
MACS	Magnetic-Activated Cell Sorting
Mcm5	Maintenance complex component 5
M-CSF	Macrophage colony-stimulating factor
MerTK	Mer tyrosine kinase
MGnD	Microglial neurodegenerative phenotype
MgSO4	Magnesium Sulfate
MHC	Major histocompatibility complexes
MKi67	Marker of proliferation Ki-67
MMP	Metalloproteinase
mMs	Leptomeningeal macrophages
MRC1/CD206	Mannose Receptor C-Type 1
MS	Multiple sclerosis
Ms4a7	Membrane spanning 4-domains A7
NaCl	Sodium Chloride
NaH2PO4	Sodium Dihydrogen Phosphate
NaHCO3	Sodium Bicarbonate
NKs	Natural killer cells
NLR	(nod)-like receptors
NO	Nitric oxide
NSCs	Neural stem cells
Ntv-a	Nestin promoter-driven tv-a
Oas	2'-5'-Oligoadenylate synthetase
OCT	Optimal Cutting Temperature
Olfml3	Olfactomedin-like protein 3
OPCs	Oligodendrocyte progenitors cells
P2RY12	Purinergic receptor P2Y12
PAM	Proliferative-region associated microglia
PBS	Phosphate-Buffered Saline
PC	Phosphatidylcholine
PD	Parkinson disease
Pf4	Platelet factor 4

PFA	Paraformaldehyde
PFKFB3	6-phosphofructo-2-kinase/fructose-2,6-biphosphatase 3
Ph	Phagocytosis
Ph-index	Phagocytic index
ProS	Protein S
PRRs	Pattern recognition receptors
PS	Phosphatidylserine
pvMs	Perivascular macrophages
RCAS	Retroviral vectors derived fromavian sarcoma-leukosis virus
RGCs	Retinal ganglion cells
ROS	Reactive oxygen species
Rpm	Revolutions per minute
RT	Room temperature
S1P	Sphingosine-1-phosphate
scRNA-seq	Single-cell RNA sequiencing
SDF-1	Stroma-derived factor 1
Sec	Seconds
SEM	Standard error of the mean
SGZ	Subgranular zone
Siglech	Sialic acid binding Ig-like lectin H
Socs3	Suppressor of cytokine signalling 3
SPF	Specific pathogen-free
SPP1	Secreted phosphoprotein 1
Stab1	Stabilin 1
Stat2	Interferon alpha induced transcriptional activator
STI1	Stress-inducible phosphoprotein 1
SVZ	Subventricular zone
TAMs	Tumor-associated macrophages
TCA	Tricarboxylic acid cycle
TGF-β	Transforming growth factor B
TLR	Toll like receptors
TM	Trabecular meshwork
TMEM119	Transmembrane protein 119
TNC	Tenascin C
TNF	Tumor necrosis factor

Top2a	DNA topoisomerase II alpha
Tr1 cells	Type 1 Regulatory T cells
Trem2	Triggering receptor expressed on myeloid cells-2
tSNE	t-Distributed Stochastic Neighbor Embedding
UMAP	Uniform Manifold Approximation and Projection
UMI	Unique Molecular Identifier
vATPases	Vacuolar ATPases
VNR	Vitronectin receptor
WAM	White matter associated microglia
WT	Wild-type
Xkr8	Xk-related protein 8
µm	Micron
2-DG	2-Deoxy-D-glucose

2. RESUMEN/SUMMARY

2. RESUMEN/SUMMARY

2.1 RESUMEN

Esta tesis doctoral se centra en una de las principales funciones de la microglía, la fagocitosis de material biológico en el parénquima, específicamente en la fagocitosis de células apoptóticas. El proceso de fagocitosis de células apoptóticas (eferocitosis) por parte de la microglía se ha estudiado ampliamente tanto en fisiología, como en enfermedad y comprende varias fases hasta que la célula apoptótica se elimina completamente del tejido. En el nicho neurogénico del hipocampo, concretamente en la zona subgranular del giro dentando (DG), se genera un exceso de neuroprogenitores que entran en apoptosis y son posteriormente eliminadas mediante fagocitosis microglial. El sistema-modelo del nicho neurogénico hipocampal ha sido ampliamente estudiado en nuestro laboratorio revelando que la fagocitosis no es un proceso terminal, ya que repercute en su entorno, regulando la neurogénesis hipocampal a través de la alteración del secretoma de la microglía fagocítica. Estos resultados previos nos llevan a especular que la **fagocitosis desencadena cambios en diferentes niveles de microglía, potencialmente afectando su estado transcripcional, metabólico y, en consecuencia, su función fagocítica**.

Para demostrar esta hipótesis, nuestro **Objetivo 1** se basó en poner en marcha un modelo *in vivo* de "superfagocitosis" mediante irradiación craneal baja (LCI) (2Gy), que induce la apoptosis de las células recién nacidas del DG 6h tras la exposición. En este primer momento, la microglía se vuelve "superfagocítica", engloba varios cuerpos apoptóticos y los elimina a las 24 horas. Este modelo no provoca la rotura del ADN microglial, ni la infiltración de monocitos, lo que nos permite estudiar específicamente los acontecimientos posteriores a la fagocitosis en la microglía.

En nuestro **Objetivo 2** estudiamos los cambios en la morfología y el estado transcripcional de la microglía tras la LCI para identificar y caracterizar a la microglía postfagocítica. El análisis morfológico reveló que la microglía no presentaba cambios estructurales en respuesta a la fagocitosis. Sin embargo, mediante el análisis de single-cell RNA-seq se comprobó que la LCI sí causaba cambios transcripcionales en la microglía. Observamos cambios en el tamaño y la firma de los diferentes clústers detectados, detectando cambios transcripcionales a corto y largo plazo desencadenados por la fagocitosis. A corto plazo (24h), detectamos que la microglía post-fagocítica experimentó cambios transitorios en su transcriptoma caracterizados por la sobreexpresión de genes lisosomales y galectina 3 (Gal-3), mientras que a largo plazo (7d) aumentaba el número de microglía proliferativa. Esta proliferación fue la consecuencia de la muerte microglial post-fagocítica mostrada por la reducción del número de microglía en el DG 24h después de la LCI, lo que sugiere que la fagocitosis desencadena estrés microglial que antecede a la proliferación observada.

Para explorar el mecanismo subyacente de este estrés, en el **Objetivo 3**, utilizamos un modelo de fagocitosis *in vitro* y analizamos el metabolismo y la función celular. Observamos que la microglía post-fagocítica aumentaba la producción de estrés oxidativo y reducía el metabolismo mitocondrial sin un aumento compensatorio de la glucólisis. El deterioro mitocondrial estaba relacionado con una remodelación de la red mitocondrial, con menos mitocondrias y menos complejas. Además, detectamos alteraciones en los niveles de poliaminas, que están estrechamente relacionadas con la resolución del estrés oxidativo y la proliferación celular. Por último, comprobamos si la microglía post-fagocítica recuperaba su función *in vivo*, exponiendo a la microglía a un segundo desafío de células apoptóticas 7 días después de la primera exposición. Tras la segunda exposición, la microglía fue capaz de fagocitar y eliminar las células apoptóticas, lo que sugiere una recuperación funcional tras el estrés inducido por la fagocitosis.

En general, demostramos que la fagocitosis no es un proceso terminal que finaliza con la eliminación de los restos. Más bien, la fagocitosis induce estrés microglial, desencadenando una serie de adaptaciones transcripcionales, metabólicas y mitocondriales, que en última instancia conducen a la apoptosis y la proliferación, apoyando la funcionalidad a largo plazo de la microglía. El estudio de los cambios post-fagocíticos es crucial para comprender cómo la microglía lleva a cabo la fagocitosis cuando las células se ven desafiadas por estímulos apoptóticos consecutivos en cortos periodos de tiempo.

En nuestro **Objetivo 4**, hemos estudiado un contexto patológico en el que es necesaria la fagocitosis repetitiva, como es el caso de los son los cánceres cerebrales. El glioblastoma (GBM) es uno de los tumores cerebrales primarios más comunes en adultos y se tratan con radioterapia secuencial hipofraccionada (HFRT) para eliminar las células tumorales, por lo que constituyen un modelo óptimo para estudiar la fagocitosis secuencial. Sin embargo, para entender cómo funcionaba la fagocitosis secuencial, en primer lugar caracterizamos la fagocitosis tras un solo pulso de radioterapia (RT) es dos subtipos de GBM y observamos que tanto la microglía como los monocitos infiltrantes del tumor, llamados macrófagos asociados al tumor (TAMs) en el contexto de los canceres cerebrales, eran capaces de fagocitar las células tumorales apoptóticas generadas tras la RT. De este modo proponemos que el estudio de la fagocitosis de los TAMs de los GBM expuestos a RT secuencial pudiera ser una estrategia válida para estudiar la función de la microglía post-fagocítica, al mismo tiempo que pudiera servir para optimizar estrategias de tratamiento.

2.2 SUMMARY

This PhD thesis focuses on one of the main functions of microglia, the phagocytosis of harmful biological material within the parenchyma, specifically focusing on the phagocytosis of apoptotic cells. The process of phagocytosis (efferocytosis) of apoptotic cells by microglia has been widely studied both in

physiology and disease and comprises several phases until the apoptotic cell is completely cleared from the tissue. In the neurogenic niche of the hippocampus, specifically in the subgranular zone of the dentate gyrus, an excess of neuroprogenitors undergo apoptosis and are subsequently eliminated through microglial phagocytosis. The neurogenic niche model of the hippocampus has been extensively studied in our laboratory, revealing that phagocytosis is not a terminal process, as it impacts its environment, regulating hippocampal neurogenesis. Additionally, phagocytosis also impacts microglia as it secretes factors that modulate the mentioned neurogenesis, so we speculate that **phagocytosis triggers changes at different levels of microglia, potentially affecting their transcriptional, metabolic, and consequently, phagocytic function.**

To demonstrate our hypothesis, **Objective 1** was based on implementing an in vivo model of "superphagocytosis" using low-dose cranial irradiation (LCI) (2Gy), which induces apoptosis of newly born cells in the dentate gyrus (DG) 6 hours post-exposure. At this early stage, microglia become "superphagocytic," engulfing multiple apoptotic bodies and eliminating them within 24 hours. This model does not cause microglial DNA breakage or monocyte infiltration, allowing us to specifically study events following microglial phagocytosis.

In **Objective 2**, we studied post-phagocytic changes in microglial morphology and transcriptional state to ultimately identify and characterize post-phagocytic microglia. Morphological analysis revealed no structural changes in microglia in response to phagocytosis. However, single-cell RNA-seq analysis confirmed that LCI caused transcriptional changes in microglia. We observed changes in the size and signature of different detected clusters, detecting short- and long-term transcriptional changes triggered by phagocytosis. In the short term (24 hours), we detected that post-phagocytic microglia underwent transient changes in their transcriptome characterized by the overexpression of lysosomal genes and galectin 3 (Gal-3), while in the long term (7 days), the number of proliferative microglia increased. This proliferation was the consequence of post-phagocytic microglial death shown by the reduction in the number of microglia in the DG 24 hours after LCI, suggesting that phagocytosis triggers microglial stress preceding the observed proliferation.

To explore the underlying mechanism of this stress, in **Objective 3**, we used an in vitro phagocytosis model and analyzed metabolism and cellular function. We observed that post-phagocytic microglia increased oxidative stress production and reduced mitochondrial metabolism without compensatory increase in glycolysis. Mitochondrial impairment was related to a remodeling of the mitochondrial network, with fewer and less complex mitochondria. Additionally, we detected alterations in polyamine levels, which are closely related to oxidative stress resolution and cell proliferation. Finally, we checked whether post-phagocytic microglia regained their in vivo function by exposing microglia to a second challenge of apoptotic cells 7 days after the first exposure. After the

second exposure, microglia were able to phagocytize and eliminate apoptotic cells, suggesting functional recovery after phagocytosis-induced stress.

Overall, we demonstrated that phagocytosis is not a terminal process that ends with the clearance of debris. Rather, phagocytosis induces microglial stress, triggering a series of transcriptional, metabolic, and mitochondrial adaptations that ultimately lead to apoptosis and proliferation, supporting long-term microglial functionality. Studying post-phagocytic changes is crucial for understanding how microglia carry out phagocytosis when cells are challenged by consecutive apoptotic stimuli in short periods of time.

In **Objective 4**, we studied a pathological context where repetitive phagocytosis is necessary, such as in brain cancers. Glioblastomas (GBM) are the most common primary brain tumors in adults and are treated with hypofractionated sequential radiotherapy (HFRT) to eliminate tumor cells, making them an optimal model to study sequential phagocytosis. However, to understand how sequential phagocytosis worked, we first characterized phagocytosis after a single pulse of radiotherapy (RT) in two GBM subtypes and observed that both microglia and tumor-infiltrating monocytes, called tumor-associated macrophages (TAMs) in the context of brain cancers, were capable of phagocytizing apoptotic tumor cells generated after RT. Thus, we propose that studying TAM phagocytosis in GBM exposed to sequential RT could be a valid strategy to study the function of post-phagocytic microglia while also serving to optimize treatment strategies.

3. INTRODUCTION

3. INTRODUCTION

3.1 INTRODUCTION TO MICROGLIA

Neuroscience encompasses a wide variety of fields that study the brain at different levels of depth. Cognitive Neuroscience investigates information processing and generation (Milner, 1998), while Molecular Neuroscience studies the biochemical and molecular processes of the cells that comprise brain tissue (Revest et al., 1998). Cellular Neuroscience focuses on brain cells, which include neurons and glial cells. Neurons have been widely defined as the primary components of the nervous system for being responsible of generating and transmitting the nerve impulse (Fodstad, 2002). However, a growing interest in glial cells has acknowledged that they occupy more than half of the volume of neural tissue with a 1:1 ratio of glia to neurons in the entire human brain, and play key roles in ensuring the proper functioning of the brain (Fields et al., 2014; Von Bartheld et al., 2016).

The first description of neurons and glial cells occurred in the early 19th century (Fan et al., 2018), although, at that time, these two cells were considered as a single cell type. It was not until 1856 when the term “neuroglia” (“Nervenkitt”) was coined to refer to a type of “connective tissue” that maintained “nervous elements” together (Hirbec et al., 2020), finally giving these cells the name glia, based on the Greek word for “glue”. However, improvements in fixation and staining procedures (Deiters, 1865; Golgi, 1873), later optimized by Ramon y Cajal (Ramón y Cajal et al., 1894; Andres-Barquin, 2002), revealed that each neuron and glial cell was anatomically separated from the other cells, providing the first direct histological evidence of the structural individuality brain cells (Ramón y Cajal, 1888; Ramón y Cajal, 1913; Fan et al., 2018). Cajal also identified a “third element” of the central nervous system in distinction from the “first element” (neurons) and “second element” (astrocytes) (Tremblay et al., 2015; Sierra et al., 2016; Fan et al., 2018). “The third element” was composed by oligodendrocytes and microglia, as discovered by Pío del Río Hortega, one of the disciples of Cajal's school, some years after the first description by Cajal (De Rio-Hortega, 1919; Sierra et al., 2016). Likewise, del Río-Hortega`s first observations described the ability of microglia to respond to stimuli and further depicted the regional distribution and heterogeneity of microglial cells (del Río-Hortega, 1919; Sierra et al., 2016).

After del Río-Hortega’s initial findings, the microglial research field stagnated until the end of the 1960s, when the group of Georg Kreutzberg’s discovered the participation of microglia in the postlesional reorganization of the facial nucleus by removing synaptic terminals (Blinzinger et al., 1968). Since then, our understanding in microglia has grown exponentially due to advances in three specific areas: cell culture of primary microglia, imaging methods for live and fixed cells, and the identification of microglial specific genes and proteins. With the arrival of the XXI century, this field evolved at an exponential rate, leading to a holistic understanding of microglia (Sierra et al., 2019; Paolicelli et al., 2022). Nowadays, microglia are considered the resident macrophages of the central nervous system (CNS) parenchyma, in charge of the constant surveillance of

brain parenchyma and constituting the main cellular barrier of the brain innate immune system (Paolicelli et al., 2022).

This PhD Thesis focuses on one of the main functions of microglia, the phagocytosis of detrimental biological material within the parenchyma, specifically centering on phagocytosis of apoptotic cells. The process of apoptotic cell phagocytosis (efferocytosis) by microglia has been extensively studied in both physiology and disease (Napoli et al., 2009; Sierra et al., 2013) and it involves several phases until the apoptotic cell is completely cleared from the tissue (Diaz-Aparicio et al., 2016). Moreover, phagocytosis is not a terminal process as it impacts in their environment and leads to transcriptional changes in microglia, which could lead to functional outcomes that are going to be studied as a main objective of this PhD thesis (Diaz-Aparicio et al., 2020; Márquez-Ropero et al., 2020). In the next sections, we explain in more detail how microglia originate, invade the brain, colonize and develop. Then we describe how microglia acquire their characteristic functions, mainly focusing on phagocytosis of apoptotic cells. Lastly, we explain the relevance of studying the effects of phagocytosis in one particular pathological context, brain tumors.

3.2 MICROGLIAL ONTOGENY

3.2.1 Microglial lineage and origin

Microglial cells are unique among other central nervous system (CNS) cells due to their distinct origin. While the rest of the brain cells derive from the ectoderm, the external layer of the embryo (Fujita et al., 1975), microglia share their origin with other macrophages and arise from the embryonic mesoderm (Ross et al., 2020), specifically from the yolk sac, the membranous sac attached to the embryo, following two main differentiation pathways. On one hand, certain populations of tissue-resident macrophages and monocytes originate from hematopoietic stem cells (HSCs), which are born intra-embryonically and later migrate to the fetal liver, where they start generating definitive HSCs around embryonic day 10.5 in mice (Kumaravelu et al., 2002; Márquez-Ropero et al., 2020). Fetal liver hematopoiesis gives raise to distinct macrophage populations that express and require the transcription factor c-Myb for proper development, such as alveolar or cardiac macrophages, among others (Mucenski et al., 1991; Sumner et al., 2000).

On the other hand, other macrophages such as microglia and CNS associated macrophages (CAMs), also known as border associated macrophages (BAMs), show a different origin compared to macrophages originated from HSCs. Microglia are considered the resident macrophages of the parenchyma, whilst CAMs are found in CNS interfaces which include perivascular macrophages (pvMs), dural and subdural leptomeningeal macrophages (mMs), and choroid plexus macrophages (cpMs), located in the perivascular space, meninges, and choroid plexus, respectively (Prinz et al., 2021). Both cell types originate from erythromyeloid precursors (EMPs) that are present in the yolk-sac earlier than HSCs (around E7.5-8.5 in mice) and do not express or require the c-Myb for

development and maturation (Ginhoux et al., 2010; Hoeffel et al., 2012; Schulz et al., 2012) (**Figure I1**).

The cell fate of CAMs and microglia depends on Mannose Receptor C-Type 1 (MRC1 or CD206) protein expression, and CD206+ and CD206- cells are already distinguished in the yolk sac prior to brain invasion at E10.5. CD206+ cells are mainly seeded in the developing choroid plexus and meninges, representing CAMs, whereas CD206- cells are distributed throughout the parenchyma and cells were positive for P2Y12 protein, representing microglial cells (Goldmann et al., 2016; Utz et al., 2020; Prinz et al., 2021). Microglial progenitors colonize the brain in E10.5 mice (Ginhoux et al., 2010; Ginhoux et al., 2015) and the 4th and 24th gestational week in humans (Menassa et al., 2018). These progenitors enter the CNS through leptomeninges and lateral ventricles and populate the brain in parallel to the formation and remodeling of blood-vessels (Bonney et al., 2020). The parallel formation between formation of vessels and the entrance of immature microglia allows these cells to colonize the parenchyma (Checchin et al., 2006; Pont-Lezica et al., 2011). Once microglia have entered the brain, the complete colonization takes place perinatally and occurs at different speeds according to the development of each brain structure (Monier et al., 2007; Verney et al., 2010; Menassa et al., 2018). When microglia are established, in the physiological state of an adult brain, they self-renew at a very low rate without contribution of circulating monocytes (Ajami et al., 2007; Bruttger et al., 2015; Goldmann et al., 2016; Zhan et al., 2019; Utz et al., 2020; Prinz et al., 2021). In summary, microglia are long-lived cells derived from the yolk sac that reside CNS parenchyma and persist into adulthood with self-renewal without the contribution of circulating monocytes under normal conditions.

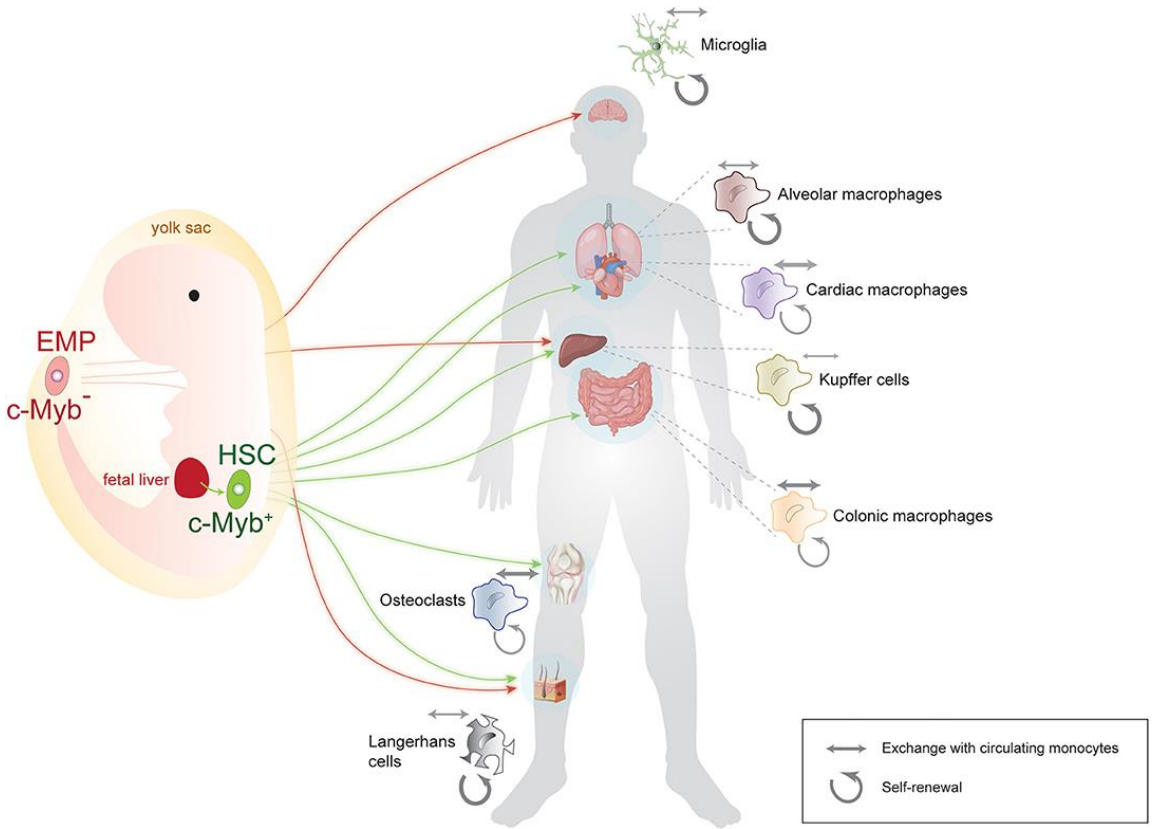

Figure 1. Summary of the origin, lineage, and population dynamics of main macrophage populations. *Microglia, originate exclusively from early, c-Myb-negative erythromyeloid precursors (EMPs) in the yolk sac. Colored arrows (green, red) indicate the main site of origin of macrophages and microglia. Weighted arrows next to each tissue-specific macrophage population indicate the relative contribution of self-renewal (circular arrows) vs. exchange with circulating monocytes (double-sided arrows) to that particular population. Microglia are mainly self-renewing, whereas other macrophages need bone-marrow derived monocytes for their generation. Some vector graphics were obtained from Vecteezy.com with permission. The image was published in (Marquez-Ropero et al., 2020)*

3.2.2 Microglial identity

Throughout the process of generation, colonization, and establishment of the microglial population in the brain, they acquire a transcriptional profile that confers them a unique identity. The current definition of microglial identity is based on the expression of genes highly enriched in microglia and commonly defined as "microglial markers". The consensus within the scientific community is that microglia can be identified by the expression of transcription factors like Pu.1, cytoplasmic markers like ionized calcium-binding adapter molecule 1 (IBA1), and cellular membrane markers such as the purinergic receptor P2YR12, the transmembrane protein 119 (TMEM119), and the colony stimulating factor 1 receptor (CSF1R) (Paolicelli et al., 2022).

Microglia are highly related to CAMs, and both populations are sometimes mixed up in studies in which shared proteins are used for their isolation and/or analysis (Mildenberger et al., 2022). For example, the cluster of differentiation molecule 11b (CD11b) protein, shared by both microglia and macrophages, is commonly used to select microglia and separate them from other cells during the sorting process (usually fluorescence-activated cell sorting or magnetic cell separation strategies (FACS or MACS)), which is the initial step is most single cell RNA-sequencing (scRNA-seq) studies. Thus, Cd11b sorted and sequenced cells include both microglia and CAMs, (Gerrits et al., 2020). However recent studies have defined specific markers for CAMs, which share a core transcriptional signature that comprises several common genes, such as MRC1, Platelet factor 4 (Pf4), Membrane-spanning 4-domains subfamily A member 7 (Ms4a7), among others. In addition each subtype is defined by its own genetic signature (Jordao et al., 2019; Mildenberger et al., 2022). All together, these data show that there are several subpopulations of CAMs defined according to their regional location and signature genes, which share some characteristics with parenchymal microglia and may be mixed up in sequencing studies. Both intrinsic transcription factors and external cues for the brain parenchyma guarantee a correct development of CAMs and microglia. In the next section, we will delve into the necessary transcription factors and environmental cues that lead to microglial maturation.

3.2.2.1 Transcription factors

The transcription factor **Pu.1** plays a crucial role in the regulation of hematopoiesis and determines the fate of hematopoietic progenitors, which

ultimately differentiate into different cell lineages (e.g. lymphoid, erythroid, and macrophage lineages) in a Pu.1 dose-dependent manner (Kastner et al., 2008; Mak et al., 2011). Moreover, Pu.1 regulates the expression of CD11b and early growth response 1 and 2 (Egr1/2), all of them critical for macrophage differentiation (Laslo et al., 2006). Ultimately, the absence of the transcription factor in Pu.1 in knock-out (KO) mice leads to the lack of macrophages, neutrophils, T and B cells, and microglia (McKercher et al., 1996; Mezey et al., 2000). Pu.1 interacts with another transcription factor, Interferon regulatory factor-8 (IRF8). **IRF8 i**s essential for the development of myeloid lineages, including monocytes/macrophages and dendritic cells (Xia et al., 2020). Unlike Pu.1, the lack of IRF8 expression does not completely prevent CNS colonization by microglia (Kierdorf et al., 2013). However, it leads to reduced expression of IBA1 in murine microglia, a hyperproliferative response to growth factors, functional deficits, and morphological and motility changes, highlighting the importance of this factor for a correct development of microglial function (Horiuchi et al., 2012; Masuda et al., 2014). Therefore, both transcription factors are crucial for microglial generation and promote its further maturation and function acquisition.

3.2.2.2 Environmental cues

Microglia also depend on environmental cues that guide the different phases of their development and determine their maturation. One major receptor is **CSF1R**, whose ligands CSF1 and IL-34 play a key role in the development of microglia. The signaling triggered by CSF1 is required for the development and differentiation of microglia by promoting their proliferation during embryonic development (Lee et al., 1993; Imai et al., 2002; Ginhoux et al., 2010; Smith et al., 2013). Likewise, IL-34 regulates proliferation, differentiation, and survival during development and promotes cytokine/chemokine expression, in addition to cellular adhesion and migration once microglia has established in the CNS (Lin et al., 2008; Elmore et al., 2014; Masteller et al., 2014; Zhao et al., 2018). Both ligands are crucial, since each of them is expressed differently depending on the brain region. While CSF1 drives microglial identity acquisition in the cerebellum without the influence of IL-34, leading to the expression of a unique molecular program that distinguished cerebellar microglia from forebrain microglia (Kana et al., 2019), in the hippocampus both ligands are required for microglial survival (Easley-Neal et al., 2019). When the signaling through CSF1R is abnormal, as in the case of IL-34 deficiency, microglial population is reduced ∼20% (Erblich et al., 2011; Nayak et al., 2014). Moreover, CSF1R−/− mice show a total loss of microglial cells, suggesting that the receptor is required for microglial development and survival (Erblich et al., 2011). Thus, signaling through CSF1R is not only determinant for microglia development, but may cause their complete absence when it is not expressed.

Another molecule that controls microglial maturation is the transforming growth factor beta (**TGF-β**) cytokine. Initially, studying the role of TGF- β in the development of microglia was not possible, because Tgfb1 KO mice develop a lethal auto-inflammatory syndrome shortly after birth (Kulkarni et al., 1993). The generation of a CNS-specific Tgfb1$^{-/-}$ under the IL2 promoter of T cells, permitted the study of the effects of TGF-β1 deficiency in the CNS on microglia, revealing

that lack of TGF-β1 decreases microglial numbers in 20-day-old mice, which was not recovered with age (IBA1+ cells). Moreover, TGF-β1 deficiency prevented the expression of the canonical microglial marker P2YR12 (Butovsky et al., 2014). Therefore, TGF- β is a necessary factor that acts in several steps of microglial maturation and ensures the acquisition of canonical microglial signature.

To summarize, microglial precursors develop through Pu.1 and Irf8-dependent pathways and depend on external environmental factors such as CSF1, IL-34 and TGF- β1 for its maturation and for the correct acquisition of their phenotype. Therefore, microglia need endogenous and exogenous information to completely develop and efficiently perform its functions.

In this section, we have provided a comprehensive overview of microglial identity, differentiating them from CAMs. We have discussed the internal factors and external signals that contribute to microglia's distinctive characteristics and functions, offering a general insight into microglial identification. Characterization of microglia is determinant for a further comprehension of microglial states, a dynamic concept that considers changes at different levels (transcriptomics, proteomics, ultrastructure, etc.) depending on the context or challenge that microglia need to face (Paolicelli et al., 2022).

3.2.3 Microglial states

For years microglia were considered a homogeneous population that uniformly responded to extrinsic factors (Butovsky et al., 2018), although early observations by Pío del Río Hortega showed that microglia exhibited different ways to respond and morphological differences when stimulated by diverse agents (Sierra et al., 2016). It was not until the mid-1970s when several studies detected morphological responses to distinct stimuli by microglia, giving rise to a dichotomous classification that divided microglia into "resting" and "activated". Following this trend, a nomenclature based on the *in vitro* response of macrophages to several stimuli, which triggered “M1” (pro-inflammatory) or “M2” (anti-inflammatory) activation types, began to be used in the 2000s to define microglial states. “M1” microglia were linked to an activated phenotype, presented an ameboid morphology, and released pro-inflammatory cytokines, whereas “M2” microglia represented a resting subtype, presented a ramified morphology and released anti-inflammatory factors (Gaikwad et al., 2013). However, this nomenclature soon became outdated when it was found that both macrophages and microglia responded in more varied and complex ways when stimulated by different types of threats. Likewise, with the advent of scRNA-seq technology, microglia ceased to be categorized dichotomously when it was shown that in the living brain microglia do not polarize to either of these categories, often co-expressing M1 and M2 markers (Ransohoff, 2016; Paolicelli et al., 2022).

Therefore, the dichotomous categorization of microglia does not consider the wide range of stimuli to which microglia are able to respond and the wide variety of functions these cells perform. In the past years, the development and rise of sequencing studies (bulk RNA-seq, scRNA-seq, etc) have contributed to the

assessment of the various microglial states, which will be further described below (**Figure I2**) (Paolicelli et al., 2022).

"Microglial states" refer to the diverse ways in which microglia adapt to varying contexts or respond to different situations. These adaptations involve notable alterations in transcriptional and metabolic activity, which serve as the biological manifestations of their contextual adaptations. Phagocytosis induces differentiated states, as evidenced by the fact that each stage of this process results in discernible transcriptional adaptations (Diaz-Aparicio et al., 2020).

The principal objective of this PhD thesis is to examine whether phagocytosis induces adaptations that underlie distinct states, through which microglia transition after engulfing apoptotic cells. Therefore, in this section, we will delineate the various states microglia can assume through the orchestration of transcriptional, metabolic and other changes in morphology and protein expression. Comprehending these microglial states is pivotal for evaluating potential modifications that may occur in response to phagocytosis. Next, we will delve into the description of which factors modulate microglial states and how microglia adapt to their context modulating their transcriptome and metabolism, both involved in triggering microglial heterogeneity.

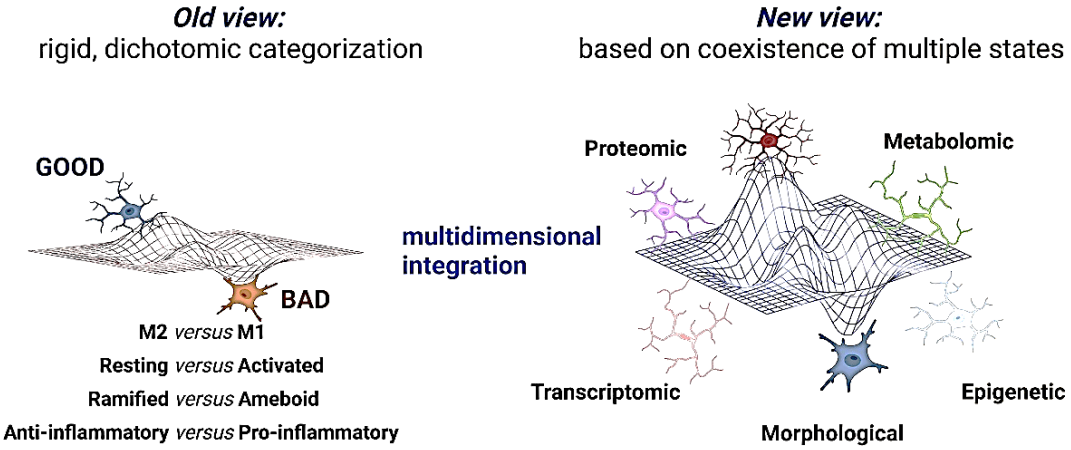

***Figure 2**. **Microglial nomenclatures: Past and future**. Microglia have been traditionally framed into dichotomic categories, but our current integration of epigenetic, transcriptomic, metabolomic, and proteomic data favors a multidimensional integration of coexisting states. The image was published in (Paolicelli et al., 2022).*

3.2.3.3 Context-dependent microglial heterogeneity

Factors that modify microglia leading to heterogeneous states include age, sex, circadian time, CNS signals, peripheral cues such as changes in microbiota and pathological conditions (Erny et al., 2015; Thion et al., 2018; Chen et al., 2021). **Age** influence microglia driving changes across the lifespan. Each stage (embryonic, perinatal, adult, and aging) is characterized by the expression of specific regulatory factors and genetic expression profiles. In the earliest stages of development, such as in early postnatal development, microglia become

extremely heterogeneous in their transcriptome, while in the adult CNS, microglial heterogeneity is reduced (Hammond et al., 2019). However, although transcriptional heterogeneity is reduced in adult microglia, there are still some differences mostly driven by regional location. Hippocampal and cerebellar microglia show transcriptional differences when compared to other areas (cortex and striatum), with increased expression of genes involved in immunity (Grabert et al., 2016). Likewise, microglia also respond to subtle cues, as evidenced with its phenotypic changes observed in the different layers of the sensorimotor cortex, where pyramidal neurons influence microglial density and molecular state of microglia (Stogsdill et al., 2022). **Sex** differences also impact microglial states, presumably due to sex chromosomes and gonadal hormones. Male and female microglia differ in their transcriptome, proteome and morphology, which are intrinsically maintained even after the transplantation to a brain from a different sex (Hanamsagar et al., 2017; Guneykaya et al., 2018; Villa et al., 2018). Interestingly the influence of sex differences in microglia could be key in pathologies that showed sexual dimorphism in different areas such as prevalence manifestation, and response to treatment (Lynch, 2022).

Beyond the environmental cues provided by the CNS, microglia also respond to **peripheral inputs**, including the capacity to sense changes in the microbiota from the gastrointestinal tract and the cytokines produced by peripheral macrophages after pathogen detection. On one hand, microbiota seems to control microglial maturation and function, through microbiota-derived short-chain fatty acids, which represent the mediators of the gut-brain axis (Erny et al., 2015; Thion et al., 2018; Erny et al., 2021). On the other hand, peripheral immune responses are also sensed by microglia. Acute systemic inflammation triggers the production of the inflammatory mediator Interleukin-1 beta (IL-1β), suggesting that microglia could mediate in the “sickness behavior” (e.g. lethargy, loss of appetite, sleepiness, etc.) during the course of an infection.

In summary, the presented data show the remarkable adaptability of microglia, as they respond to a multitude of cues. These adaptive responses underlie the observed heterogeneity across various parenchymal regions throughout the lifespan. Microglia accomplish these adaptations through alterations in their transcriptome and metabolism, which will be further elucidated in the subsequent discussion, commencing with an exploration of the transcriptional states.

3.2.3.1 Transcriptional states

In the preceding section, we described various contexts and environments that modulate microglial function, forming the foundation of their heterogeneity. A pivotal determinant of their functional versatility is their dynamic modulation of gene expression, giving rise to distinct transcriptional states. Beyond the classical and simplistic M1 and M2 states that categorized microglia as activated or resting, respectively, recent scRNA-seq studies have brought forth new knowledge to comprehend microglial diversity and introduced novel concepts to define microglial states. As delineated earlier, microglial states enclose the adaptations of microglia to diverse environments or stimuli, encompassing changes at multiple levels. Single-cell studies enable the categorization of microglia based on their transcriptome, specifically the expression of key genes, thus identifying

different states. In this section, we delve into major signatures outlined in scRNA-seq studies.

Homeostatic microglia

The definition of homeostatic microglia refers to cells in physiological conditions, which display diverse morphological and functional states depending on the signals from the CNS microenvironment (Paolicelli et al., 2022). Homeostatic mouse microglia specifically express P2yr12, Tmem119, sialic acid binding Ig-like lectin H (Siglech), G protein coupled receptor 34 (Gpr34), suppressor of cytokine signalling 3 (Socs3), β-hexosaminidase subunit β (Hexb), olfactomedin-like protein 3 (Olfml3), and Fc receptor-like S scavenger receptor (Fcrls) (Butovsky et al., 2018). Several of these microglial genes were also observed in human microglia, including P2RY12 and TMEM119 (Butovsky et al., 2014; Satoh et al., 2016; Zrzavy et al., 2017). Identification of this homeostatic microglial transcriptional signature improved the development of robust tools, including microglia-specific antibodies and transgenic mice to specifically target microglia, and the generation of microglia from induced pluripotent stem cells (iPSCs) (Muffat et al., 2016; Douvaras et al., 2017).

DAM microglia

Another signature found by the scRNA-seq analysis was disease-associated microglia (DAM). This signature was found for the first time in a genetic model of Alzheimer's disease (AD) characterized by the accumulation of amyloid β (Aβ), which is one the main hallmarks of the disease (Keren-Shaul et al., 2017). On one hand, this subpopulation featured reduced expression of homeostatic markers as Tmem119 and P2ry12, and other microglia expressed proteins, such as the purinergic receptor P2ry13, the chemokine (C-X3-C) receptor 1 (Cx3cr1), cystatin 3 (Cst3), and CSF1R. On the other hand, DAM microglia showed an increased expression of a wide variety of genes such as triggering receptor expressed on myeloid cells-2 (Trem2), apolipoprotein E (Apoe) and Dectin-1 (Clec7). The DAM signature was also identified in human microglia, which upregulated APOE and TREM2 (Olah et al., 2020). Importantly, both APOE and TREM” are risk genes for the development of human AD, suggesting that DAM may impact disease progression (Chen et al., 2021). Beyond AD, DAM microglia were also found in other diseases models such as a model the SOD1-G93A for amyotrophic lateral sclerosis (ALS) (Deczkowska et al., 2018) and multiple sclerosis (MS) (Krasemann et al., 2017). Together with DAM, similar signatures were found in other models of neurodegenerative disease, such as the microglial neurodegenerative phenotype (MGnD), human AD microglia (HAMs) microglia inflamed in multiple sclerosis (MS), lipid-droplet-accumulating microglia (LDAMs), white matter associated microglia (WAM), among others (Krasemann et al., 2017; Marschallinger et al., 2020; Srinivasan et al., 2020; Absinta et al., 2021; Safaiyan et al., 2021). Overall, these signatures describe microglial response to diseases, and most of them share signature genes, suggesting that DAM may represent a more universal core signature enriched in brains with a neurodegenerative pathology.

HAM microglia

Beyond the microglial signatures detected in neurodegenerative diseases, a model of aging without associated neurodegenerative pathologies revealed a signature defined as highly-activated microglia (HAM) (Jin et al., 2021). HAM microglia were only observed in 18-month-old mice, in which specific expression of several markers were observed, including lipoprotein lipase (Lpl), galectin-3 (Lgals3), cystatin-F (Cst7), and Cd74, was noted. HAM microglia triggered immuno-inflammatory responses in aged brains after sensing neuron-released macrophage migration inhibitory factor (Mif). Acting through the Cd74 receptor in HAM, Mif promoted the immunochemotactic activity of microglia. Thus, the HAM signature appears to be characteristic of microglia in aged brains without neurodegenerative pathologies.

MHC microglia

scRNA-seq studies have been carried out in other disease models such as the mouse neurodegeneration model based on overexpression of p25 human protein under the control of the calcium/ calmodulin-dependent protein kinase II (CK -p25) (Cruz et al., 2006), which seems to be accumulated in patients with AD and is closely linked to neuronal death. In CK-p25 mice another microglial subset was identified the MHC-II or MHC microglia (Mathys et al., 2017). This specific subset exhibited elevated gene expression levels of antigen presentation-related genes, including histocompatibility 2 class II antigen A alpha (H2-Aa), histocompatibility 2 class II antigen A beta 1 (H2-Ab1), and histocompatibility class II invariant chain peptide Class (Cd74, also expressed in the DAM signature). Significantly, the CAM signature displayed elevated expression levels of the MHC class II-related genes mentioned earlier. However, it also exhibited increased expression of additional genes, including Mrc1, platelet factor 4 (Pf4), membrane spanning 4-domains A7 (Ms4a7), stabilin 1 (Stab1), and Fc receptor like 2 (Fcrl2) (Prinz et al., 2021) -some of them describes previously in CAM population-, suggesting a potential relationship between these two cell populations. Moreover, MHC-II–related genes were increasingly upregulated during progression of neurodegeneration in the CK-p25 neurodegenerative model (Mathys et al., 2017) and in the amyloid precursor protein (APP) knock-in mouse model (APP^{NL-G-F}) for AD (Sala Frigerio et al., 2019), which suggests that exacerbation of pathology may amplify the MHC-II signature. Thus, neurodegenerative diseases seem to increase the presence of MHC microglia in the pathologic tissue.

IFN microglia

The interferon-related or IFN microglia cluster was also described for the first time in the CK-p25 model (Mathys et al., 2017) and further found in other disease models (e.g., Aβ accumulation (APP-PS1), tauopathy (P301S and P301L), amyotrophic lateral sclerosis, cuprizone-induced demyelination, ischemia, lipopolysaccharide exposure, viral infection, and glioma (Friedman et al., 2018). The IFN cluster included many well-known interferon-stimulated genes, such as members of the 2'-5'-Oligoadenylate synthetase (Oas1, Oas2, Oasl1, Oasl2), and interferon induced protein families (Ifit1, Ifit2, Ifit3), the interferon stimulated exonuclease gene 20 (Isg20), and the transcription factors interferon regulatory factor 7 (Irf7) and interferon alpha induced transcriptional activator (Stat2)

(Mostafavi et al., 2016). These genes were most highly induced in response to viral infection, but also overexpressed in mice treated with LPS and glioma models. Moreover, in a mouse model utilizing partial whisker deprivation, a known stressor that accelerates neural circuit remodeling in the somatosensory cortex, an IFN responsive microglial population was found (Dorman et al., 2022). Researchers further observed that microglia overexpressing IFN genes (e.g., Ifit3) were engulfing neurons, suggesting that IFN microglia participate in phagocytosis.

Proliferative microglia

In addition to the previously characterized homeostatic, DAM, MHC, and IFN microglial clusters/signatures, recent scRNA-seq studies conducted in the 5xFAD model for AD identified a fifth microglial cluster, the proliferative microglia. This population was notably enriched in cells in the growth (G)2/mitotic (M) phase and exhibited an upregulation of genes related to proliferation. It is characterized by the expression of genes such as DNA topoisomerase II alpha (Top2a), marker of proliferation Ki-67 (Mki67), centromere protein e (Cenpe), minichromosome maintenance complex component 5 (Mcm5), and baculoviral IAP repeat containing 5 (Birc5), (Chen et al., 2021). The identification of proliferative microglia corroborated previous reports of a cluster of microglia expressing the proliferation marker Ki67 around Aβ plaques in 5xFAD mice (Wang et al., 2016) and the increase of mitotic genes in neurodegenerative models (Friedman et al., 2018). Thus, microglia seemed to proliferate in response to neurodegeneration, confirming what had been previously observed in neurodegenerative conditions such as AD and Creutzfeldt Jakob disease (Gómez-Nicola et al., 2013).

PAM microglia

More recently, a microglial cluster associated with proliferative regions has been detected, named proliferative-region associated microglia (PAM) (Li et al., 2019). Their transcriptional signature is characterized by a dampened expression of homeostatic genes, such as Tmem119, P2ry12, and Siglech, and overexpression of secreted phosphoprotein 1 (Spp1), glycoprotein nonmetastatic melanoma protein B (Gpnmb), insulin-like growth factor 1 (Igf1), C-type lectin domain-containing 7A (Clec7a), lipoprotein lipase (Lpl), CD9 (Cd9), CD63 (Cd63), Galectin 3 (Lgals3), fatty acid-binding protein 5 (Fabp5), integrin subunit alpha X (Itgax), Apoe, and transmembrane immune signaling adaptor (Tyrobp). PAMs, or proliferative-region associated microglia, predominantly emerge in the developing corpus callosum and cerebellar white matter during the first postnatal week (Li et al., 2019). This specific timeframe coincides with their engagement in the phagocytosis of newly formed oligodendrocytes. Consequently, these observations lead to the conclusion that PAM are phagocytic cells.

In summary, scRNA-seq studies identify multiple microglial signatures depending on the developmental age of the animals and in the context of various diseases. Some of these populations appear to be closely related, as trajectory analysis addresses the relationships among certain microglial populations (Ellwanger et al., 2021), showing that homeostatic microglia differentiate through a continuum and ultimately branch into four separate trajectories: DAM, IFN-I, MHC, and

proliferative microglia. Thus, microglia appear to transition flexibly from one transcriptional signature to another, each possibly related to a unique state, depending on the demands of the environment.

However, scRNA-seq studies also have limitations. While gene expression signatures indicate biological pathways, the functional implications of these transcriptional signatures and whether they represent stable subpopulations remain unclear. Moreover, sample processing artifacts and interspecies differences hamper comparisons and data integration, avoiding the consensus between research groups (Gosselin et al., 2017; Wu et al., 2017; Geirsdottir et al., 2019; Marsh et al., 2022a). The lack of consensus can lead to different names for the same cluster, as well as to over-fragmentation of clusters. Thus, although scRNA-seq studies provide useful information to understand the diversity of microglial states, it is critical to start defining microglial states not only considering mRNA expression levels, but also exploring other layers of complexity (e.g., epigenetic, transcriptional, translational, and metabolic signatures), which will ultimately determine cellular phenome (i.e., motility, morphology, and ultrastructure) and function (Paolicelli et al., 2022). Next, we will address two distinct topics: first, the metabolic changes associated with microglial states, and second, the influence of various contextual factors such as species, sex, spatial considerations, and developmental timing on microglial diversity.

3.2.3.2 Metabolic states

Beyond their transcriptional states, microglia exhibit specific metabolic profiles intricately linked to the environmental cues they encounter. These metabolic profiles are tailored to meet the functional demands dictated by the prevailing context. Many immune cells, including T cells and macrophages possess remarkable metabolic flexibility, allowing them to adapt to changing inflammatory conditions and thereby support coordinated immune responses (Bernier et al., 2020b). Similarly, other non-immune cells such as tumor cells switch from mitochondrial oxidative phosphorylation to a more rapid energy production through glycolysis (Warburg effect), leading to increased proliferation, (Vaupel et al., 2021). Apart from cancer cells, rapidly proliferating mammalian cells, acutely regenerating tissues and mature human red blood cells also show a switch to a Warburg-type glucose metabolism (Ghashghaeinia et al., 2019; Sun et al., 2019). Similarly, the transition from oxidative metabolism to an enhanced glycolytic state serves as a mechanism responsible for the development of innate immunity in macrophages exposed to a bacterial and fungal wall compound, β-glucan. Mouse macrophages exposed to β-glucan undergo the Warburg metabolic shift through activation of the dectin-1-Akt-mTOR-HIF-1α pathway, leading to epigenetic changes that are responsible for long term enhanced functional responses to secondary infections enhanced way (Cheng et al., 2014). This innate memory differs from adaptive memory, which is defined as the production of highly specific immune responses through the action of T and B cells, which recognize and remember specific antigens, such as proteins or other molecules from pathogens, to provide long-term protection against those specific invaders. Thus, different immune cell types use their metabolism to change their function.

Microglia face a unique metabolic microenvironment, as the brain, an organ representing 2% of body weight, consumes ~20% of the body's glucose and oxygen (Mergenthaler et al., 2013). The blood-brain barrier (BBB) regulates the input of substrates to the brain parenchyma, with astrocytes being the main key players in glucose uptake and lactate shuttle that ultimately serves as a source of energy to neurons (Jurcovicova, 2014). But microglia also sense the metabolic environment though transporters and enzymes that allow them to metabolize glucose, amino acids, and fatty-acids (Bennett et al., 2016). Under baseline homeostatic conditions, microglia preferentially metabolize glucose. Microglia, however, display metabolic flexibility in vitro and display the ability to maintain oxidative metabolism when either glucose, glutamine, pyruvate, lactate, or ketone bodies were the only metabolite available in the medium (Nagy et al., 2018). When glucose is not available, such as during insulin-induced hypoglycemia, microglia rely on in glutamine and rapidly switch from glycolysis to glutaminolysis to maintain oxidative phosphorylation and their surveillance capacity (Bernier et al., 2020a). Thus, microglia are able to internalize and metabolize diverse substrates showing their capacity to adapt to metabolic fluctuations of the environment.

However, microglia are not just passive agents that adapt to the surrounding metabolic environment, but they undergo metabolic changes as a consequence of inflammatory stimuli. For example, in pro-inflammatory environments, microglia undergoes a metabolic switch that results in a decreased oxidative phosphorylation, linked to mitochondrial fission and an upregulated glycolysis (Orihuela et al., 2016; Nair et al., 2019). This glycolytic shift involves changes in the regulation of enzymes and transcription of metabolic genes participating in the signaling pathway of glycolysis. For example, both the glucose receptor GLUT1 and the enzyme 6-phosphofructo-2-kinase/fructose-2,6-biphosphatase 3 (PFKFB3) show an increased transcription in microglia when exposed to inflammatory stimulation and also in diseases in which inflammation is exacerbated, such as in AD (Holland et al., 2018; Wang et al., 2019; Piers et al., 2020). In contrast, exposing microglia to anti-inflammatory mediators induces metabolic changes characterized by a reduced glucose consumption and an increase in fatty-acid oxidation (FAO) (Gimeno-Bayón et al., 2014; Geric et al., 2019). Thus, microglia not only adapt metabolically to changes in their environment, but also need to reprogram their metabolism to perform some of their functions (**Figure I3**).

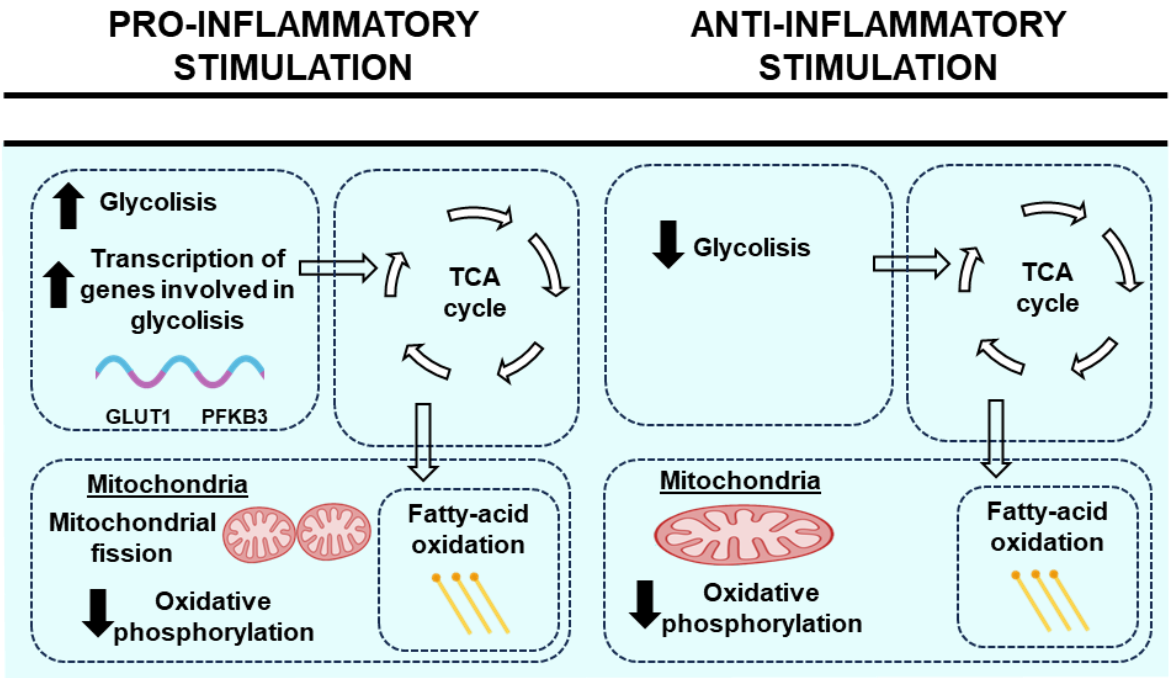

Figure 3. Metabolic adaptations of microglia to pro- and anti-inflammatory stimulation. *The stimulation of microglia with pro-inflammatory factors triggers a metabolic switch that potentiates glycolysis while reducing oxidative phosphorylation, while anti-inflammatory stimuli reduces glycolysis and increase fatty-acid oxidation. Created with BioRender.com. and adapted from (Márquez-Ropero et al., 2020).*

In summary, microglia exhibit remarkable adaptability in response to environmental challenges, which stems from alterations in gene expression and metabolism leading to distinct microglial states. While this section has outlined various factors influencing microglial states (e.g. developmental-time, age, sex, parenchymal region, etc.), the current knowledge of how phagocytosis affects the microglial state is still limited (will be reviewed in **section 1.5.2**). Our laboratory's research has already shown that *in* vitro microglia undergo transcriptional modifications after phagocytosis, with some genes implicated in cellular metabolism, suggesting that phagocytosis induces both transcriptional and metabolic adaptations in microglia (Diaz-Aparicio et al., 2020). Consequently, one of the main objectives of this PhD thesis is to unravel and describe in more detail the transcriptional and metabolic changes in microglia triggered by phagocytosis.

Thus, microglia remodel their transcriptomic profile and metabolism to acquired determined states and ultimately to perform specific functions that respond to acute or chronic stimulation. To delve into the plethora of functions that microglia perform in the CNS, in the next section we will describe microglial functions in more detail.

3.3 MICROGLIAL FUNCTIONS

As resident macrophages of the brain parenchyma, microglia play integral roles in various essential functions of the central nervous system (CNS). Among their classic immune functions are the inflammatory response and phagocytosis, which will be described first. Through mechanisms that participate in both inflammation and phagocytosis, such as the release of soluble factors and the clearance of debris, microglia perform brain-specific functions that encompass gliogenesis, vasculogenesis, neurogenesis, synaptic maintenance, and myelination (**Figure I4**). In the forthcoming sections, we will provide a general overview of the classical immune functions: inflammation and phagocytosis, followed by a detailed exploration of brain-specific functions fulfilled by microglia. Among these diverse functions, microglia are continuously scanning their surroundings in a process called surveillance, which will be described in first place.

3.3.1 Surveillance

In order to effectively respond to changes in their environment, microglia must "sense" their surrounding tissue and perceive its alterations. For this purpose, microglial processes continuously scan the brain tissue, and are ready to act when any type of disturbance occurs (Hanisch et al., 2007). Microglia are capable of sensing a wide range of environmental changes, including the presence of invading microbes, damaged or dead cells, alterations in the pH of the surrounding tissue, changes in the composition or integrity of the extracellular matrix, and the release of various substances such as inflammatory cytokines and chemokines (Hickman et al., 2013). Surveillance takes place through cellular processes that maintain non-overlapping regions of scanning (Nimmerjahn et al., 2005). Moreover, emerging evidence suggests that microglial processes can operate autonomously, as observed in phagocytic microglia, where one process engages in phagocytosis while another continues to surveil the surrounding territory with equal efficiency (Kamei et al., 2023). However, some pathological conditions, such as stroke (Beccari et al., 2023), epilepsy (Abiega et al., 2016), and Alzheimer's disease (Franco-Bocanegra et al., 2019), impair microglial motility, further affecting surveillance and downstream functions.

3.3.2 Immune response

The immune response is divided into the innate immune response and the adaptive immune response. The former is considered the first line of defense of the body against pathogens, and is characterized by a rapid and nonspecific response. Once pathogens reach the organism, the innate immune system acts as the earliest line of defense (Riera Romo et al., 2016; McComb et al., 2019). The cells that compose the innate immune system are natural killer cells (NKs), dendritic cells, and white blood cells, and tissue macrophages, including microglia and CAMs in the brain (Turvey et al., 2010; Prinz et al., 2021). After the detection of a harmful stimuli, these immune cells trigger two mechanisms to cope with the threat: inflammation and phagocytosis. In the innate immune system, trained immunity functions as a memory process, whereby a second exposure to an infection triggers a more heightened response by the system (Netea, 2013).

On the contrary, adaptative immunity specifically targets pathogens after their recognition, leading to a delayed and more efficient immune response. Moreover, it is characterized by having the ability to recognize pathogens to which it has been previously exposed, which is defined as immunological memory (Janeway Jr et al., 2001; Brandes et al., 2019). However, both forms of memory differ in that adaptive memory is specific, responding to particular pathogens to which the immune cells have been previously exposed, whereas innate immunity memory is unspecific and generalized.

Innate and adaptive immunity are connected through different mechanisms, such as the release of cytokines by the cells of the innate system, which lead to the activation of cells of the adaptive system, or through antigen presenting cells (APCs) that capture and process antigens of noxious agents for immune presentation through major histocompatibility complexes (MHC-I and MHC-II) (Kumar et al., 1994; Hoebe et al., 2004; Rossi et al., 2005). While it has been suggested that microglia may play a role in mediating the connection between the innate response and the adaptive response by potentially participating as antigen-presenting cells (APCs) (Aloisi, 2001; Gregerson et al., 2004; Sutter et al., 2022), there is a lack of clear evidence regarding their role in adaptive immunity.

Nevertheless, a distinctive feature of microglia is their engagement in the realm of innate immunity, particularly in the specialization of inflammatory response and phagocytosis—two classical functions inherent to innate immunity. First, we will discuss the molecular effectors of inflammation and in the next section, we will delve into phagocytosis, the main topic of this PhD thesis.

3.3.2.1 Inflammation

Inflammation is triggered by harmful stimuli, such as pathogens, toxics substances, irradiation, or damaged cells, and it is characterized by pain, heat, redness, swelling and loss of tissue function (Lucas et al., 2006; Isailovic et al., 2015). The main objective of inflammation is to clear the threat and further restore the tissue (Chen et al., 2018). Within the brain parenchyma, microglia are the major orchestrators of the inflammatory response by the release of inflammatory mediators such as cytokines, chemokines and the complement proteins (Nayak et al., 2014).

The cytokine family comprises small molecules, such as peptides, proteins and glycoproteins and act either on the producer cells, in an autocrine way, and in a paracrine way in neighboring cells (Borish et al., 2003). Cytokines are classified as pro- and anti-inflammatory according to their function. Pro-inflammatory cytokines trigger the inflammatory response, while anti-inflammatory ones resolve it. Next, we will further describe them in more detail.

Pro-inflammatory cytokines are a group of signaling molecules that are released to promote inflammation upon detection of noxious stimuli by microglia through pattern recognizing receptors, such as toll like receptors (TLR), nucleotide binding oligomerization domain (nod)-like receptors (NLR), and TREM, among others (Franchi et al., 2009; Hanamsagar et al., 2012; Owens et al., 2017). The

recognition leads to the production of cytokines that initiate the inflammatory response(Vezzani, 2005). The production of pro-inflammatory cytokines is necessary to cope with external threats, but an exacerbated release can lead to detrimental consequences as tissue injury (Raziyeva et al., 2021). In the particular case of the brain, several pathologies such as AD, Parkinson disease (PD), multiple sclerosis (MS), epilepsy, and stroke have shown abnormal increased levels of pro-inflammatory cytokines, which are usually linked to a worsening of the pathology (Schwartz et al., 2010; Fung et al., 2012). These cytokines trigger the production and release of other inflammatory mediators like reactive oxygen species (ROS) and nitric oxide (NO), that can be neurotoxic if their action is not limited (Bilbo et al., 2012; Lyman et al., 2014). The most common detrimental consequences of uncontrolled cytokine release are apoptosis of neurons and glial cells, increased BBB permeabilization accompanied by increased migration and infiltration of immune cells towards the brain parenchyma, which increases the damage (Ramesh et al., 2013; Salmina et al., 2021).

In contrast, anti-inflammatory cytokines participate in resolving inflammation. With the potential exception of interleukin (IL)-1 receptor antagonist (IL-1ra), all the anti-inflammatory cytokines have at least some pro-inflammatory properties as well (Opal et al., 2000). The well-known anti-inflammatory cytokines include interleukin 4 (IL-4), interleukin 10 (IL-10), and transforming growth factor B (TGF-β) (F. Su et al., 2016). In addition to these cytokines, there are specific cytokine inhibitors and soluble cytokine receptors that help to attenuate the pro-inflammatory cytokine function (Opal et al., 2000). In the particular case of microglia, the release and sensing of anti-inflammatory cytokines leads to protective response in pathological conditions, caused by decreased antigen presentation and reduced the release of proinflammatory cytokines, chemokines, and nitric oxide (NO) (Aloisi, 1999; Loane et al., 2010).

Beyond pro- and anti-inflammatory cytokines, another class of cytokines, the chemokines, promote the motility of several cells towards the injury site, where they will further initiate the inflammatory response (Hughes et al., 2018). Thus, chemokines lead to a cell migration process called chemotaxis, that is also executed in physiological conditions, as in the acquisition of neuronal identities (neural patterning) during development (Jin et al., 2008). Microglia express the macrophage chemokine CX3CR1, which together with its ligand CX3CL1 are essential for the neuron-microglia communication axis (Wolf et al., 2013). Some chemokines and their receptors have been proposed to be upregulated in pathological situations such as AD, MS, brain trauma or stroke (Mennicken et al., 1999; Ubogu et al., 2006; Savarin-Vuaillat et al., 2007), and seem to be influencing microglial migration towards the pathological sites (El Khoury et al., 2007).

Another key released component of the inflammatory response is the complement system, which plays a crucial role in host defense and inflammation. The complement consists of more than 30 proteins, receptors and modulators that rapidly response to threats (Morgan & Harris, 2015). Complement activation results in opsonization of pathogens and their removal by phagocytes, which is triggered by opsonins, extracellular proteins that bound harmful content to induce

phagocytosis (Sarma et al., 2011). Thus, the activation of the complement system is key to initiate phagocytosis and will be describe in more detail in the section below.

3.3.2.2 Phagocytosis

Phagocytosis is the cellular process by which a potentially harmful element is recognized, ingested and digested by a phagocyte, a cell with the ability to eat large particles (larger than 0.5 μm) (Mukherjee et al., 1997). In unicellular organisms, phagocytosis is their basic nutritional process, whereas in multicellular organisms different types of cells perform phagocytosis to maintain tissue homeostasis. Among them, specialized cells, the professional phagocytes, perform phagocytosis efficiently and rapidly respond to threats. Most phagocytes combine the inflammatory response and the phagocytic function to eliminate and clear pathogens and toxic substances. As the professional phagocytes of the CNS, microglia perform the phagocytosis of a wide variety of cargo that will be described below.

Microbes. The chance of invasion of the CNS by pathogens is low since the BBB acts a physical barrier difficult to penetrate for invaders (Pardridge, 2005). However, when organism such as viruses, bacteria, fungi or parasites enter the CNS microglia rapidly recognize them triggering the immune response (Dando et al., 2014). Beyond recognition of pathogens, microglia efficiently clear these organisms as demonstrated in microglial cultures engulfing bacteria after lipopolysaccharide (LPS) stimulation (Diesselberg et al., 2018; Cockram et al., 2019). Phagocytosis of bacteria as well as exposure to LPS triggered the inflammatory response in microglia and therefore LPS stimulation was implemented as a model to mimic human sepsis (Deitch, 1998). Like bacteria, fungi are also phagocytosed by microglia both *in vitro* and *in vivo* (Neglia et al., 2006; Lionakis et al., 2011). Hence, microglia effectively battle invading microbes in the CNS.

Amyloid β (Aβ). Aβ is a 36-43 amino acid peptide derived from the amyloid precursor protein (APP) (Hamley, 2012). The release, oligomerization, and deposition of Aβ in the brain is one of the main pathological features of AD (Hardy et al., 2014) (Ondrejcak et al., 2010). Once Aβ begins to accumulate in the parenchyma, it triggers a detrimental cascade of events that start from synapse loss and neurodegeneration, and finish with cognitive impairment and loss of memory. Several studies have stated that the progression of AD may be related to a deficient clearance of Aβ (Mawuenyega et al., 2010; Subramanian et al., 2020). However, the role of microglia in the phagocytosis of Aβ is still controversial. Although microglia phagocytose in Aβ *in vitro* cultures, the role of microglia in plaque clearance in vivo remains unclear (Majumdar et al., 2011; Hellwig et al., 2015; Feng et al., 2020). While some studies have shown that microglia have no effects on the disease, as microglia depletion do not affect Aβ plaque size (Grathwohl et al., 2009), other studies suggest that microglia exert beneficial effects reducing plaque size by the activity of phagocytosis related tyrosine kinases receptors Axl and Mertk (Huang et al., 2021). Likewise, another microglial receptor, TREM2, is also involved in the disease, as its deletion leads to plaque accumulation (Ulrich et al., 2017) (Yuan et al., 2016). Thus, microglia

are involved in the progression of AD, although the precise role they play in the development and maintenance of the disease remains a matter of controversy.

Synapses. Synapses represent the connections between neurons, which are dynamic and change as a consequence of neuronal activity, developmental events and neurodegeneration (Hong et al., 2016). When excessive synapses are formed, this excess is eliminated by synaptic pruning. This phenomenon has been observed in situations of excessive synapse formation during development (Katz et al., 1996; Hua et al., 2004), and certain studies have even indicated the presence of synaptic components within microglia. For instance, microglial processes have been observed containing both presynaptic (SNAP25) and postsynaptic (PSD95) proteins following synaptic contacts. However it has not yet been clarified how this process occurs, nor have the different stages and signaling pathways involved in it been detailed contacts (Paolicelli et al., 2011; Lim et al., 2021). It has been suggested that synaptic pruning is regulated by factors such as fractalkine (Paolicelli et al., 2011), the complement system, and the MERTK phagocytic pathways (Schafer et al., 2012; Chung et al., 2013). Therefore, while further research is necessary to fully comprehend the mechanisms governing synapse phagocytosis, these findings strongly suggest that microglia efficiently engulf synaptic material, thus contributing to the process of synaptic pruning.

Myelin. This process has been mainly studied in diseases that trigger the loss of myelin after an insult, as in MS, or ischemic stroke (Jia et al., 2022; Sen et al., 2022). In MS, inflammatory lesions cause oligodendrocyte damage and demyelination, and microglia actively participates in the removal of myelin debris, which promotes posterior remyelination (Trapp et al., 1998; Napoli et al., 2010; Dobson et al., 2019). Studies in animal models of MS, such as the cuprizone model that causes demyelinating lesions, have shown that microglia play a key role in remyelination since mice deficient in the microglial receptors CX3CR1 and TREM2 showed a reduced clearance of myelin debris concomitant with slower remyelination (Lampron et al., 2015; Cignarella et al., 2020). Axons and myelin are also damaged after ischemic stroke and microglia also contribute to myelin removal, further synthetizing activate liver X receptor (LXR) signaling, which further resolves inflammation and creates a favorable environment for oligodendrocyte differentiation and recovery (Liu et al., 2020).

Apototic cells. In this Thesis project, we will focus on the apoptotic cells and their phagocytosis. Apoptosis, or programmed cell death, takes place regularly in both normal physiological contexts (such as during development or maintaining balance) and in disease states (Henson et al., 2001). Regardless of whether apoptotic cells arise from physiological or disease-related events, it is essential for microglia to efficiently clear these cells. Microglial phagocytosis of apoptotic cells guarantees the timely and effective removal of these dying cells, promoting tissue homeostasis and preventing the release of potentially harmful cellular debris and pro-inflammatory signals that could otherwise lead to neuroinflammation and tissue damage (Neher et al., 2012; Sierra et al., 2013).

In the next section **(section 1.4**), after the detailed description of brain-specific functions, we will further detail the relevance of apoptotic cells phagocytosis,

further explaining the different phases of the process, experimental procedures for studying this function and the effects of phagocytosis in microglial cells.

3.3.3 Brain-specific functions of microglia

Through surveillance and mechanisms related to both inflammation and phagocytosis, such as soluble factor release and debris removal, microglia perform brain-specific functions which include neurogenesis, synaptic maintenance, gliogenesis, vasculogenesis, BBB permeability, and myelination.

In the developing brain, microglia regulate neurogenesis in the two main neurogenic niches in the mammalian brain: the subgranular zone (SGZ) of the dentate gyrus (DG) of the hippocampus and the subventricular zone (SVZ) (Saharan et al., 2013). In the murine SGZ, microglia phagocytose apoptotic neuroblasts in the early postnatal period to regulate their incorporation into hippocampal circuits and continue performing this function also in adulthood (Sierra et al., 2010). In the SVZ, microglia also phagocytose neuroprogenitors (NPCs) and regulate NPC population density (Cunningham et al., 2013; Fourgeaud et al., 2016). Pathological conditions causing the release of pro-inflammatory cytokines by microglia lead to a reduced formation of new neurons in the DG (Ekdahl et al., 2003; Monje et al., 2003). Likewise, direct modulation of microglial phenotype also abrogates neuroblast differentiation (Buttgereit et al., 2016), suggesting the relevance of a proper functioning of microglia for sustaining neurogenesis. Taken together, these findings emphasize the multi-faceted ways microglia can regulate neurogenesis.

Beyond neurogenesis, microglia are also central regulators of survival and activity of newborn neurons after embryonic development. Microglia perform different strategies to shape neuronal function. Through signaling via some membrane receptors, such as fractalkine and Cx3cr1, microglia contribute to the maturation and survival of photoreceptors in the retina (Jobling et al., 2018). Likewise, microglia release cytokines and growth factors that mediate neuronal survival and it has been further demonstrated that the disruption of TGF-β signaling leads to an impaired microglial maturation (Frade et al., 1998; Sedel et al., 2004; Ueno et al., 2013). In addition to secretory mechanisms, microglial processes can directly contact neurons through purinergic receptors, which regulates neuronal calcium load and further modulate neuronal connectivity (Cserép et al., 2020). Collectively, these findings indicate that microglia are not only vital for maintaining neuronal populations, but are also indispensable for the modulation of neural activity.

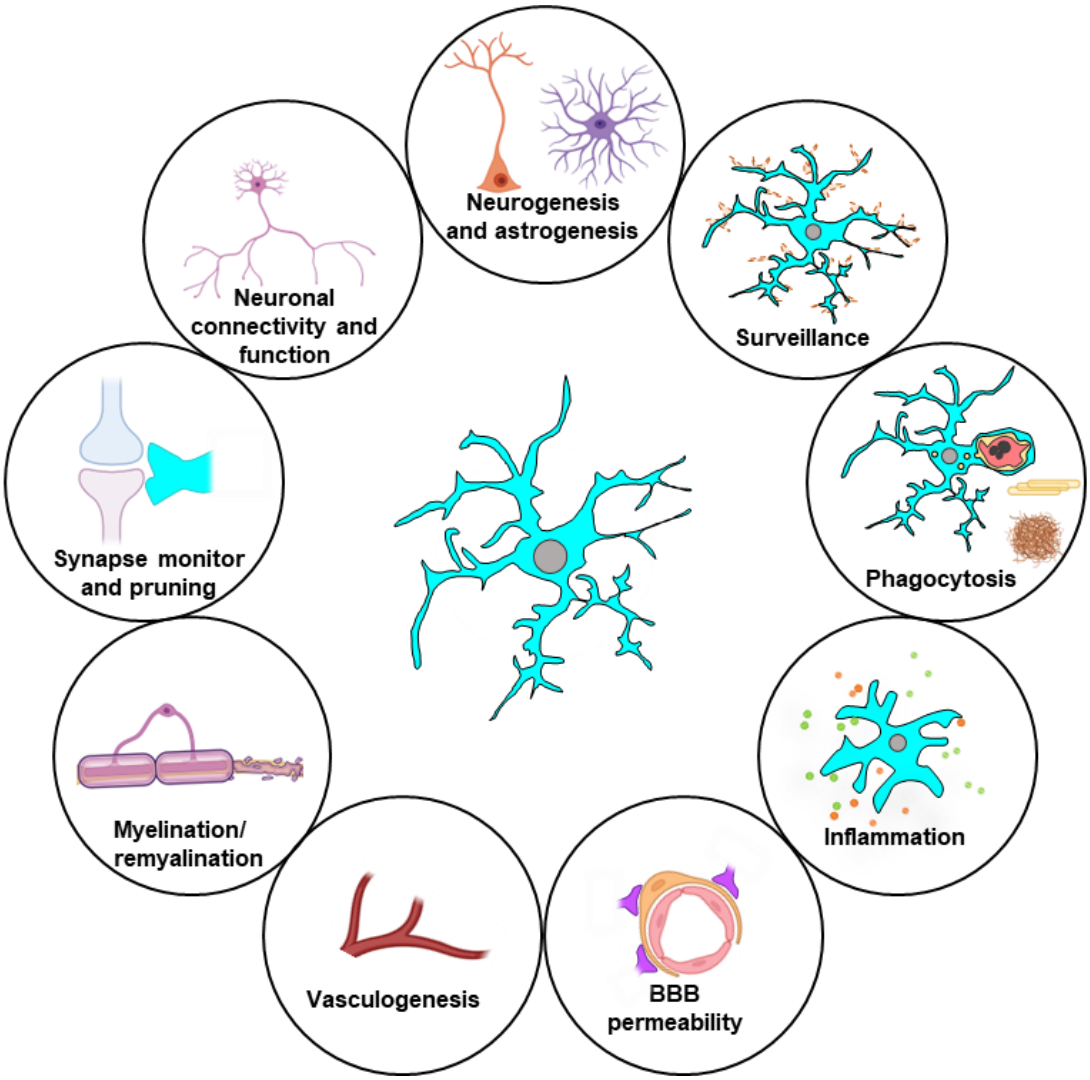

Figure 4. Microglial key functions. *Microglia perform several key functions in both brain physiology and pathology. In constant surveillance, microglia senses environmental changes and respond to them. As immune cells of the brain, microglia execute innate immune functions in response to pathological conditions. They release inflammatory factors and phagocytose cellular debris (e.g. apoptotic cells, protein aggregates, and myelin fragments). Moreover, microglia also perform various essential tasks under physiological conditions, which may be disrupted during pathological states. These tasks include the previously mentioned phagocytosis, which is also key during development and in the neurogenic niches and synaptic monitoring and pruning. Microglia are versatile, as they can interact with other types of brain cells, influencing their activities. This interaction extends to neurons and their network connections, neural stem cells (NSCs) and the process of neurogenesis, oligodendrocytes and the myelination/remyelination of axons, endothelial cells and the formation/reformation of blood vessels in the brain, as well as astrocytes and the permeability of the blood-brain barrier (BBB). Created with BioRender.com. and adapted from (Sierra et al., 2019).*

Another key role that microglia perform to ensure the correct functioning of neurons is synapse remodeling. Microglia participates in several functions that shape synapsis, as formation, maturation and refinement. In the formation of synapses, brain-derived neurotrophic factor (BDNF) acts as potent regulator of synaptic development and the removal of microglial BDNF resulted in reduced

synapsis (Parkhurst et al., 2013). Likewise, microglia also play a key-role during synapse maturation, as observed in microglia lacking the receptor CX3CR1, which causes a delayed microglial colonization and delayed synaptic maturation (Hoshiko et al., 2012). Proposed mechanisms that underlie synaptic modifications by microglia include stripping, a non-phagocytic mechanism based on the interposition of microglia between pre- and post-synaptic membranes, and trogocytosis, which is defined as a partial phagocytosis of the membrane, both of which affect synaptic excitability or stability (Eyo et al., 2023). Beyond synaptic modifications, microglia also participate in synapse clearance, which has been reviewed in the previous **section 1.3.2.2 (Phagocytosis of synapses)**. In short, microglia promote proper synapse function by acting at different stages of synapse maturation and performing their clearance when necessary.

Moreover, microglia promote the generation of vasculature and non-neuronal cells such as oligodendrocytes and astrocytes especially during development. Brain vasculature is formed in parallel to neurogenesis and matures with time (Checchin et al., 2006). Both disrupted microglial M-CSF signaling and microglial depletion reduce the complexity of the vasculature, highlighting the importance of microglia for proper blood vessel development (Checchin et al., 2006; Kubota et al., 2009). Microglia also participates in myelination through the release of growth factors that promote the survival and proliferation of oligodendrocytes (Pang et al., 2013). During remyelination, microglia phagocytose the degenerated myelin (Domingues et al., 2016), promoting the recruitment and differentiation of oligodendrocyte precursors (Domingues et al., 2016; Voet et al., 2019). However, the release of pro-inflammatory cytokines can also limit remyelination in pathologies such as MS, showing that chronic inflammation linked to the disease impairs the proper functioning of microglia (Guerrero et al., 2020). The generation of astrocytes is also mediated by microglia, which through several secreted factors such as interleukin 1 and 6 (IL-1 and IL-6), leukemia inhibitory factor (Lif) and nitric oxide (NO) stimulate astrogenesis (Nakanishi et al., 2007; Béchade et al., 2011). Thus, microglial secreted factors are a primary mechanism by which microglia regulate putative astrocyte development. Overall, microglia contribute to the generation and development of non-neuronal cells, which is crucial to maintain the proper functioning of cerebral parenchyma.

In conclusion, microglia perform a diverse array of functions tailored to the brain's environment, all of which are crucial for optimal parenchymal operation throughout an organism's lifespan. This PhD thesis will specifically center on one function of microglia: the phagocytosis of apoptotic cells.

3.4 PHAGOCYTOSIS OF APOPTOTIC CELLS

Apoptosis is a tightly regulated form of programmed cell death initiated by two main signaling pathways: the intrinsic (mitochondrial) pathway and the extrinsic (death receptor) pathway (Vitale et al., 2017; Galluzzi et al., 2018). Intrinsic apoptosis is triggered by various intracellular signals, such as DNA damage, oxidative stress, or the loss of survival signals. These signals activate pro-apoptotic proteins belonging to the Bcl-2 family, such as BCL2 Associated X Protein (Bax) and BCL2 Associated K Protein (Bak)(Roufayel, 2016). Activation

of Bax and Bak leads to mitochondrial outer membrane permeabilization, resulting in the release of cytochrome c and other apoptotic factors into the cytosol. This, in turn, activates caspase enzymes (D'Orsi et al., 2017), which are essential for the cleavage and degradation of proteins. The activation cascade of caspases represents the stage at which intrinsic and extrinsic apoptosis pathways intersect. The extrinsic pathway is initiated by the binding of death ligands from the extracellular environment, such as tumor necrosis factor (TNF) and Fas ligand (FasL), to their corresponding death receptors on the cell surface. This binding triggers the formation of death receptor signaling complexes ultimately causing activation of caspases (Nair et al., 2014). In the final stages of apoptosis, cells undergo nuclear fragmentation (karyorrhexis), chromatin condensation (pyknosis), cytoplasm reduction, and the formation of apoptotic bodies (Santavanond et al., 2021). Throughout this entire process, the cell maintains the integrity of its plasma membrane to prevent the leakage of its cytoplasmic contents, which is toxic to the surrounding tissue. Impaired phagocytosis would hinder this safeguard, leading primary apoptotic cells to progress into a secondary necrotic state if their plasma membrane is compromised, resulting in the overflow of their harmful intracellular contents (Dias et al., 2021).

In physiological conditions, apoptosis regulates cell numbers in response to excessive cell proliferation (Oppenheim, 1991; Paronetto et al., 2016). During embryonic and postnatal development, apoptosis plays a major role balancing the surplus of proliferative cells, while in adult organisms apoptosis is crucial for cellular turnover (Pellettieri et al., 2007; Voss et al., 2020). In pathological conditions, apoptosis occurs in response to pathogen exposure and is also observed in neurodegenerative diseases such as Alzheimer's disease, amyotrophic lateral sclerosis (ALS), Parkinson's disease, and Huntington's disease (Czabotar et al., 2023). In the CNS, regardless of the physiological or pathological cause for apoptosis, microglia are responsible for the removal of the dead corpses to ensure tissue homeostasis.

One of the contexts in which the microglial phagocytic process is extensively described is the engulfment of progenitor cells undergoing apoptosis. Specifically, microglia engage in the phagocytosis of apoptotic retinal ganglion cells (RGCs) shortly after birth in the retina (Anderson et al., 2019), and oligodendrocyte progenitors cells (OPCs) within the corpus callosum (Nemes-Baran et al., 2020). In the adult brain, apoptosis continues to take place in adult neurogenic niches such as the subventricular zone (SVZ) and the hippocampal DG. In the DG, most of newborn cells undergo apoptosis before their integration into the circuitry (Xavier et al., 2015). The efficient phagocytosis of apoptotic cells by microglia occurs through three distinct stages known as "find-me," "eat-me," and "digest-me", preventing the spillover of toxic intracellular compounds and ensuring tissue homeostasis(Magnus et al., 2002; Henson et al., 2006; Neumann et al., 2008). In the following section, we will detail the process of phagocytosis and the different signals involved throughout its three stages: “find-me”, “eat-me” and “digest-me” stages.

3.4.1 Stages of phagocytosis

Phagocytosis of apoptotic cells takes place sequentially in a process governed by different signals. First, apoptotic cells release “find-me” signals to attract microglia towards them, which will produce microglial mobilization to the cargo that need to be phagocytosed (Sierra et al., 2013; Yu et al., 2022). Subsequently, microglia will directly interact with the apoptotic cell through “eat-me” ligands and receptors, which are found respectively on apoptotic cells and microglia. This step enables the recognition and docking of the apoptotic cells and leads to the physical engulfment of the apoptotic cargo in which microglia form the phagocytic pouch allowing apoptotic cell internalization (Gardai et al., 2006; Sierra et al., 2010; Li, 2012; Sierra et al., 2013). Apoptotic cargo internalization results in the formation of the phagosome, which is delivered to the lysosome to finally form the phagolysosome and be degraded in the latest “digest-me” step (Kinchen et al., 2008a; Kinchen et al., 2008b; Hochreiter-Hufford et al., 2013) (**Figure I5**). Next, we will describe in detail the set of molecules and receptors involved in the whole process individually, classifying them according to the step in which they participate.

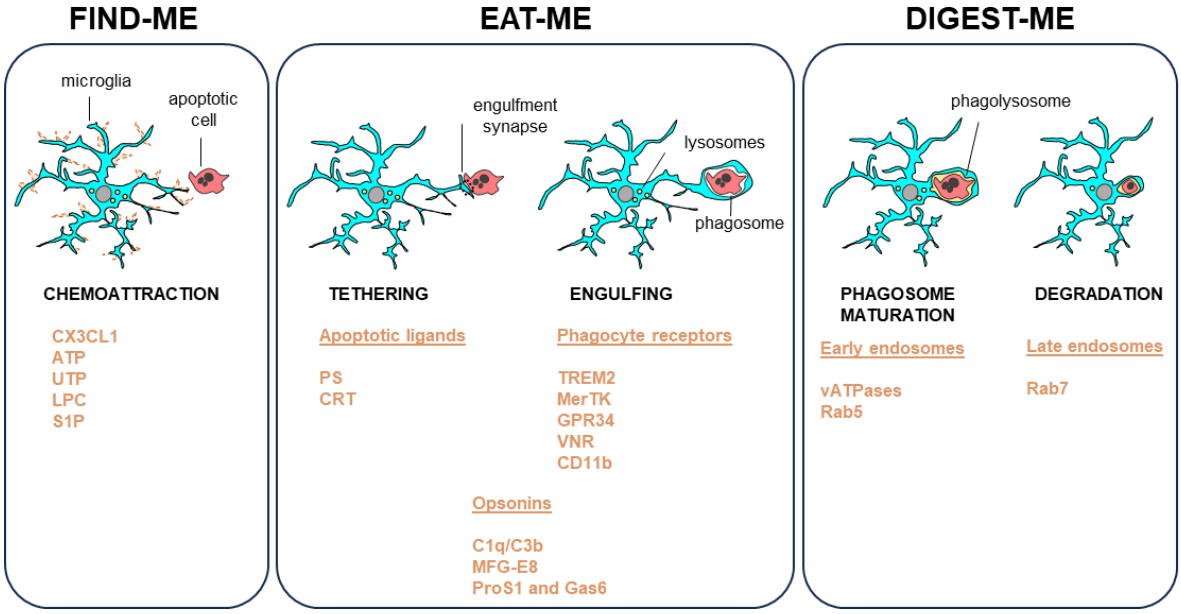

Figure 5. Microglial phagocytic process and its stages. *Phagocytosis of apoptotic cells by microglia is divided into three stages: “find-me”, “eat-me” and “digest-me” steps. First, apoptotic cells, during their death process, release molecules that participate in the chemoattraction process by stimulating the movement of microglia towards the damaged cell. Once, microglia reach the damage cell, apoptotic cell ligands bind microglial receptors allowing the tethering of the microglial process to the apoptotic cell. During this step, opsonins facilitate the recognition of the apoptotic bodies. After recognition and tethering, microglia engulf the apoptotic cell by forming the phagocytic pouch around the cell. Lastly, the engulfed cargo is delivered to the lysosomes where it is finally degraded. Modified from Sierra 2013.*

3.4.1.1 ‘Find-me’ stage

The molecules released by apoptotic cells termed as “find-me” signals include the chemokine fractalkine (CX3CL1), and extracellular nucleotides (ATP, UTP),

and the lipids lysophosphatidylcholine (LPC) and sphingosine-1-phosphate (S1P) (Truman et al., 2008; Arandjelovic et al., 2015)

Fractalkine (CX3CL1). CX3CL1 is a membrane bound protein, which needs to be proteolitically cleaved to be released from apoptotic cells. The resultant soluble molecule binds to the microglial-specific CX3C motif chemokine receptor 1 (CX3CR1) promoting phagocyte migration to the site of apoptotic cells (Jung et al., 2000; Truman et al., 2008; Mizutani et al., 2012; Eyo et al., 2016).

Nucleotides (ATP, UTP). ATP and ADP nucleotides are released from apoptotic cells through 1 channel after caspase 3 activation (Elliott et al., 2009; Chekeni et al., 2010). Once located in the extracellular space, these nucleotides and their hydrolyzed form forms ADP and UDP are recognized by the plethora of purinergic receptors expressed in microglia, which finally results in the attraction of the phagocytes towers the dying cell (Inoue, 2008; Domercq et al., 2013).

Lysophosphatidylcholine (LPC). During the apoptotic process phosphatidylcholine is cleavaged by phospholipase A2 enzyme (iPLA2) and converted into LPC, which ultimately binds to the G-coupled receptor G2A promoting the chemoattractic migration of the microglia (Lauber et al., 2003) (Peter et al., 2008; Xu et al., 2016).

Sphingosine-1-phosphate (S1P). S1P is produced from sphingosine by sphingosine kinase after caspase 3 activation. When released it binds to S1P receptors expressed on microglia, leading to a process of chemoattraction that remains poorly understood (Gude et al., 2008; O'Sullivan et al., 2018)

After microglia has approached to the apoptotic cell, the second stage of phagocytosis is initiated, so called “eat me” stage, in which physical contact between microglia a target cell occurs in order to perform recognition and tethering of the apoptotic cell (Sierra et al., 2013).

3.4.1.2 ‘Eat-me’ stage

The “eat me” phase involves a plethora of molecules released by the apoptotic cells (‘eat-me’ ligands), their corresponding microglial membrane receptors (‘eat-me’ receptors) and opsonins and bridge molecules, which bind to target apoptotic cells to facilitate their phagocytosis.

- Apoptotic ‘eat-me’ ligands

Phosphatidylserine (PS). PS is a phospholipid localized on the inner membrane leaflet of the plasma membrane, which is externalized to the cell surface upon apoptotic stimuli (Fadok et al., 1998). PS externalization process is irreversible due to the action of the Xk-related protein 8 (Xkr8), as well as by the inactivation of ATP11C ATPase by caspase-3-mediated cleavage (Suzuki et al., 2016) (Segawa et al., 2014).

Calreticulin (CRT). CRT is a protein associated to the endoplasmic reticulum (ER) involved in the quality control of newly generated proteins, and both ER stress

and apoptosis signaling cause its exposure on the cell surface (Kleizen et al., 2004; Obeid et al., 2007). CRT exposure takes place either alone or bound to PS and it is sensed by by microglial low-density lipoprotein receptor (LRP), promoting apoptotic cell engulfment (Gardai et al., 2003; Wijeyesakere et al., 2016).

- Phagocyte 'eat-me' receptors

TREM2. TREM2 is an immunoglobulin-like transmembrane receptor and it is expressed in dendritic cells (DCs), macrophages and microglia (Neumann et al., 2007). TREM2 is associated with an adapter protein named DNAX-activation protein of 12 kD (DAP12), and the disruption of either TREM2 or DAP12 results in impairment in the uptake of apoptotic cells by microglia (Paloneva et al., 2002) (Hsieh et al., 2009; Thrash et al., 2009). Furthermore, TREM2 is involved in the recognition of Aβ in AD and acts as a receptor of the apolipoprotein E (ApoE), which is linked to AD pathology (Atagi et al., 2015; Parhizkar et al., 2019; Joshi et al., 2021).

Mer tyrosine kinase (MerTK). MerTK is a the most extensively studied TAM (Tyro3, Axl, and Mer) receptor (Lemke, 2013). It is expressed in DCs, macrophages and microglia and interact with apoptotic cells through soluble proteins bound to PS, like arrest-specific protein 6 (GAS6), protein S (ProS) and mediate in apoptotic cell removal in vitro through Galectin-3 (Gal-3) (Wu et al., 2005; Caberoy et al., 2012; Lemke, 2013; Jiménez-García et al., 2022).

G protein-coupled receptor 34 (GPR34). GPR34 belongs to PY2 family of receptors (Lin et al., 2017). It is mainly expressed in microglia and macrophages, and other immune cell populations like B cells and lymphoid cells (Makide et al., 2013; Schoeneberg et al., 2018) (Wang et al., 2021a). The main ligand of GPR34 is lysophosphatydilserine (LysoPS), a deacetylated form of previously mentioned PS (Makide et al., 2013), which acts as an "eat-me" ligand. GPR34 deficiency in microglia lead to a reduced capacity in the engulfment of beads, apoptotic cells and myelin (Preissler et al., 2015), providing evidence of the important role of the receptor in phagocytosis,

Vitronectin receptor (VNR). VNR belongs to the integrin superfamily of macrophagial adhesion molecules. It binds to the opsonin MFG-E8 (milk fat globule EGF factor 8), to which we will refer when describing opsonins in more detail (Hanayama et al., 2002; Lauber et al., 2004). VNR participates in the binding process mediated in the phagocytosis of apoptotic cells, both *in vivo* and *in vitro,* triggering the cytoskeletal arrangement of microglia through the interaction with MerTK receptor (Wu et al., 2005; Brown et al., 2014; Arcuri et al., 2017).

Complement receptor 3 (CR3/CD11b). CR3 is a member of beta-2 integrins family and binds to different molecules of the complement cascade such as C1q or C3b (Linnartz et al., 2012; Vorup-Jensen et al., 2018). It plays an important role enabling cellular adhesion and phagocytosis of pathogen and apoptotic cells on microglia in vitro (Trouw et al., 2008). Moreover, CR3 also triggers an anti-inflammatory response in microglia helping to maintain immune tolerance (Fraser et al., 2010).

- Opsonins and bridge molecules

In order to facilitate phagocytosis, other soluble molecules such as opsonines and bridge molecules target the cells that must be engulfed. The most described classic opsonins are complement components C1q and C3b. In addition, in microglial phagocytosis the molecules that bind PS acting like bridge molecules include milk fat globule EGF factor 8 (MFG-E8), and the aforementioned MerTK ligands Gas6 and ProS.

Complement component C1q and C3b. C1q protein performs a variety of functions in the innate immune system such as cellular lysis, inflammatory response, virus neutralization and opsonization (Beurskens et al., 2015). During opsonization C1q binds to the apoptotic cell membrane and promotes the cleavage of C3, resulting in opsonin C3b (Martin et al., 2016). Opsonin deposition in the apoptotic cells surface ultimately leads to microglial phagocytosis (Diaz-Aparicio et al., 2019).

Milk fat globule EGF factor 8 (MFG-E8). Produced by DCs, macrophages and microglia, MFG-E8 binds to PS on apoptotic cells, leading to phagocytosis (Aziz et al., 2011; Spittau et al., 2015). MFG-E8 mediated phagocytosis has been directly assessed both *in vitro* and *in vivo* in macrophages (Hanayama et al., 2002; Akakura et al., 2004) and in microglia *in vitro* (Fuller et al., 2008).

Protein S (ProS1) and Gas6. ProS1 and Gas6 are homologous vitamin K-dependent proteins. Both, soluble molecules are TAM receptor ligands that bind to PS acting as bridging molecules to recognize and engulf apoptotic cells (Manfioletti et al., 1993; Lemke et al., 2008).

Once “eat-me” phase is completed, the apoptotic body is finally surrounded by the 3-dimensional phagocytic pouch and internalized within microglia. Next, microglia must deliver the cargo to the lysosomes for the digestion process (Yu et al., 2008), which will be further explained in the next section.

3.4.1.3 ‘Digest-me’ stage

The digestion process following phagocytosis consists of several steps ranging from maturation of the engulfed phagosome, its transport to fuse with lysosome and the subsequent total degradation of the phagocytosed cargo (Desjardins et al., 1994) (Harrison et al., 2003; Keller et al., 2017). In the maturation process the phagosome becomes acidified and gains hydrolytic function through interaction with endocytic organelles (Desjardins, 1995). First, early phagosome fuses with early endosomes acquiring vacuolar ATPases (vATPases) and membrane associated proteins, such as the Rab GTPase Rab5, resulting in a pH close to 6.5 (Duclos et al., 2000). After Rab5 recruitment, the phagosome acquires Rab7 expression on its membrane, its pH decreases to 5.5 and its ultimately considered as late phagosomes (Vieira et al., 2003). During maturation process phagosomes are transported for its fusion with the lysosome to form the phagolysosome (Keller et al., 2017). The phagolysosomal formation leads to the degradation of the cargo by using a pH of 4.5 and approximately 60 different hydrolytic enzymes (Ballabio,

2016). Overall, the degradation process triggers a signaling cascade, which has been proposed to further regulate phagocytosis by remodeling lysosomes to increase their degradation capacity (Hipolito et al., 2018).

In summary, phagocytosis consists of a cascade of events involving numerous molecules that are grouped in three major steps: “find-me”, “eat-me” and “digest-me”. Thesestages must operate correctly and in an integrated manner, as the impairment of any one of them will adversely affect the entire process, thereby impairing or hindering phagocytosis. The activation of this cellular machinery for efficient phagocytosis may have consequences for microglia, which presumably seeks to restore the system for subsequent phagocytic activities. One of the goals of this PhD thesis is to examine how phagocytosis affects microglial cells. In the next section, we will describe different strategies that have been used to identify phagocytic microglia and we will detail both *in vitro* and *in vivo* methods to assess phagocytosis.

3.4.2 Methods for the study of phagocytosis

The analysis of microglial phagocytosis has traditionally relied on indirect methods, including the assessment of microglial morphology or the expression of specific markers in contexts where phagocytosis is presumed to occur (Diaz-Aparicio et al., 2016). In this section, we will delineate morphological changes and proteins associated with phagocytosis. Additionally, we will conduct a comprehensive review of methods that replicate microglial phagocytosis, employing both *in vivo* and *in vitro* approaches (**Figure I6**).

3.4.2.1 Phagocytosis “markers”

Regarding indirect methods to identify phagocytosis, an ameboid morphology was long linked to microglial phagocytosis (Young et al., 2018) but, our laboratory demonstrated that ramified microglia is very efficient performing phagocytosis either in physiological conditions and showing a more hypertrophic morphology after LPS stimulation (Sierra et al., 2010; Sierra et al., 2013).

Among the proteins proposed for labeling phagocytic microglia, both membrane-associated proteins and cytoplasmic proteins associated with lysosomes have been suggested. The former category includes Axl, MerTK, TREM2, and CD11b, which have been proposed as markers for phagocytosis as membrane receptors involved in the early stages of the phagocytic process, primarily the "eat-me" stage. In this section, we will first refer to them. Regarding the cytoplasmic proteins, these include lysosomal enzymes, lysosomal-associated membrane proteins (LAMPs), and other proteins associated with the degradative metabolism of lipids. These proteins are mainly involved in the "digest-me" stage of phagocytosis and will be described after membrane proteins. Beyond these two categories, other proteins such as IBA1 have been associated with phagocytosis.

The protein IBA1, has been used as indicator of phagocytic microglia (Hendrickx et al., 2017; Nelson et al., 2017). However, this protein, expressed basally in microglia, is increased by numerous stimuli such as encephalitis (Mori et al.,

2000), ischemia (Ito et al., 1998), or exposure to brain tumors (Tran et al., 1998). Thus, IBA1, exhibits increased expression in response to various stimuli beyond phagocytosis and cannot be used as a marker of phagocytosis.

Axl and MerTK have also been proposed as phagocytosis markers (Jenkins et al., 2023). Both belong to TAM receptors, which mediate the engulfment of apoptotic cells (Scott et al., 2001; Burstyn-Cohen et al., 2012), but also participate in innate immune responses leading to an increase expression of both receptors in conditions showing high levels of inflammation, such as neurodegenerative diseases and ageing (Ransohoff et al., 2010; Zagórska et al., 2014; Fourgeaud et al., 2016). Hence, the increased expression of TAM receptors cannot be considered solely a consequence of phagocytosis.

The same holds true for TREM2, whose disrupted expression results in impaired uptake of apoptotic cells (Paloneva et al., 2002; Hsieh et al., 2009; Thrash et al., 2009), and it has also been implicated in the phagocytosis of synapses (Filipello et al., 2018). However, it is noteworthy that TREM2 often considered a marker of phagocytosis of Aβ in AD, has also been linked to the risk of developing AD and a higher progression of the disease (Frank et al., 2008; Lue et al., 2015; Wang et al., 2016).

Likewise, the surface protein CD11b, which is known for participating in the phagocytosis of opsonized particles (Fu et al., 2014), leads to an inhibited phagocytosis when the protein is blocked (Allendorf et al., 2020). Nevertheless, CD11b also experiences an increase in its expression as a consequence of pro-inflammatory (e.g., LPS) and oxidative stress (e.g., H_2O_2) insults (Roy et al., 2008).

Overall, these surface receptors, which have been used phagocytosis markers, play a crucial role during this process. However, they also participate in other processes, and their increased expression cannot be linked exclusively to phagocytosis.

Several lysosomal proteins (e.g. enzymes and LAMPs) have been proposed as potential markers for phagocytosis (Colombo et al., 2021), given the crucial role of lysosomal activity in the final "digest-me" stage of phagocytosis. Lysosomal proteins can be categorized into enzymes that participate in the acidification and degradation of substrates, such as acid hydrolases and cathepsins and their inhibitors cystatins. These proteins play a central role in the digestive activity of microglia, leading to an increase in lysosomal enzyme activity after phagocytosis (Axline et al., 1970)

Among these enzymes, cathepsins constitute a group of protease enzymes crucial for cellular processes, particularly the degradation of proteins within lysosomes (Repnik et al., 2012). Proper functioning of cathepsins appears to be crucial during the process of phagocytosis. Following phagocytosis, certain cathepsins, such as cathepsin B, are upregulated in response to a phagocytic challenge (Porter et al., 2013). Additionally, the deficiency of cathepsin K results in impaired digestion and accumulation of phagocytosed cargo (Everts et al., 2003). Cystatins act as inhibitors of cathepsins, which are cysteine proteases.

The primary function of cystatins is to bind to cathepsins and inhibit their enzymatic activity (Turk et al., 2012). The depletion of cystatin B impairs microglial phagocytosis in the hippocampus in a Cstb KO mouse model (Sierra-Torre et al., 2020), whereas in an AD mouse model the deletion of cystatin B show contrary effects by enhancing lysosomal activity (Yang et al., 2014). Thus, the role of cathepsins and cystatins during the degradative phase of phagocytosis appears to be significant.

Additionally, there are lysosomal membrane proteins that play vital roles in the structure, function, and stability of lysosomes. Examples include Lysosome-Associated Membrane Proteins (LAMPs) and Lysosomal Integral Membrane Proteins (LIMPs) (Saftig et al., 2010). Lysosomal membrane proteins are crucial during degradation, as their proper functioning is required for the fusion of lysosomes with phagosomes (Huynh et al., 2007). The LAMP family protein macrosialin (also known as lysosomal protein CD68) has also been considered to label phagocytic microglia in a model for PD (Silva et al., 1999). Moreover, in the model of neurodegeneration caused by a mutation in the Niemann-Pick type C (NPC1) gene, a scRNA-seq signature of microglia characterized by an increase in the expression of the CD68 gene and other genes encoding lysosomal proteins such as LAMP1, LAMP2, and the previously mentioned cathepsins D and B (CTSD and CTSB) is identified (Colombo et al., 2021). This microglial population also exhibits an enhanced phagocytic uptake of myelin. This same study also identifies that in the microglial signature associated with an increase in lysosomal function, there is an upregulation of genes related to myelin phagocytosis, such as LGALS3 and LPL, both also described in another signature detected in aged mice, described as highly-activated microglia (HAM) (Jin et al., 2021). Moreover, the product of LGALS3, galectin-3 (Gal-3), also participated in phagocytosis of neuron-like cells *in vitro* (Nomura et al., 2017), and its increased expression, together with LPL, have also been reported in microglia in PAM signature (Li et al., 2019). However, Gal-3 appears to be upregulated in the transcriptomic profile of microglia in various neurodegenerative environments and damaged brain sites. It is also involved in triggering the proinflammatory response through its interaction with Toll-like receptors (TLRs) (García-Revilla et al., 2022).

In conclusion, currently, no specific marker has been defined for phagocytosis. Instead, many of the proteins upregulated after phagocytosis are also upregulated as a result of other types of stimuli and contexts. The main problem relies in the interpretation that phagocytosis is a microglial state, instead of a process. Microglia are engaged in engulfment when they display phagocytic pouches, in degradation when the cargo is being digested, and later on, they develop post-phagocytosis adaptations. Therefore, discussing specific markers for phagocytosis is incorrect, because microglia will show different alterations in each one of these stages. In this PhD Thesis, we will identify transcriptional, metabolic and functional alterations associated to phagocytosis using *in vitro* and *in vivo* models.

3.4.2.2 Phagocytosis models

Phagocytosis has been traditionally studied using *in vitro* systems. *In vitro* modelling of phagocytosis allows the study of the signaling pathways involved in

the process and the dissection of the mechanisms involved. However, *in vivo* approaches of phagocytosis fully recapitulate the phagocytic process in living organism allowing a more integrated study of the process itself and of the functional outcome of phagocytosis. Next, we will detail the various techniques used to model both *in vitro* and *in vivo* phagocytosis.

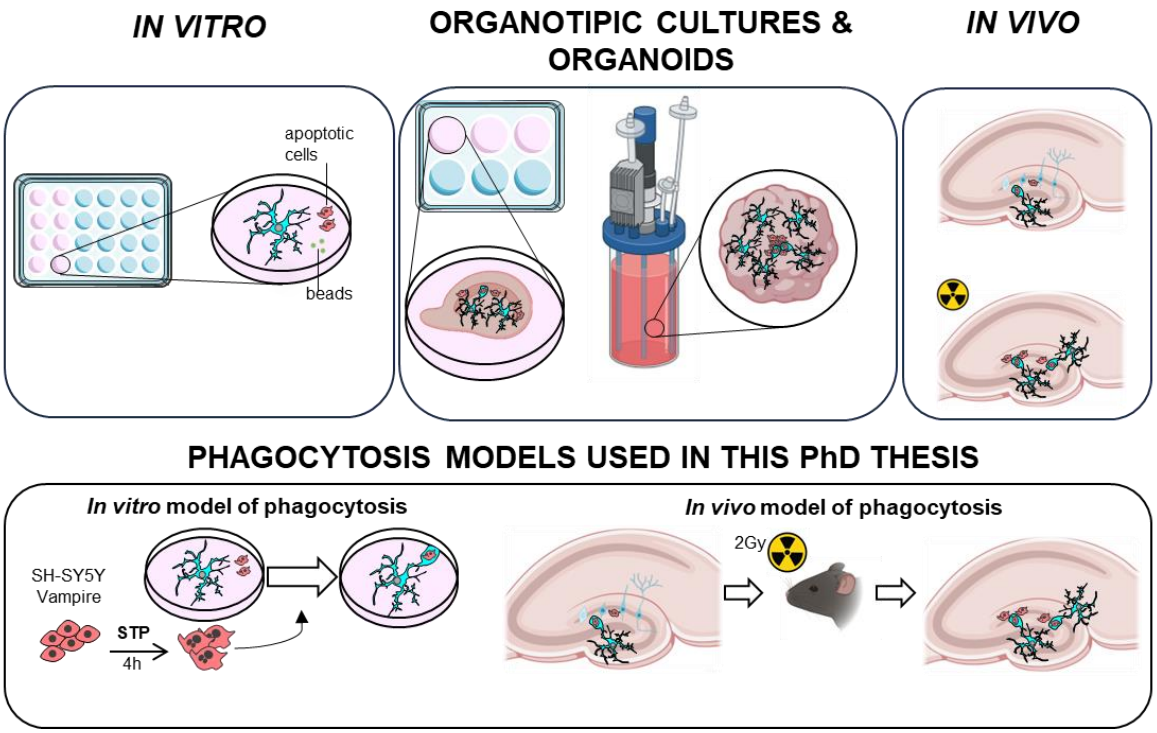

Figure 6. Methods for the study of microglial phagocytosis. *Different models are currently used to study phagocytosis. The choice of model depends on the study's objectives. In vitro models enable the investigation of phagocytosis in isolated microglial cells, with precise control over the quantity of apoptotic cells or beads introduced into the culture. The in vitro approach is invaluable for exploring the extracellular and intracellular mechanisms involved in phagocytosis. Models developed in organotypic cultures and organoids represent intermediate approaches between in vitro and in vivo systems, allowing the study of more complex interactions in a controlled environment. Finally, in vivo systems offer the opportunity to investigate microglia in physiological conditions, as the basal apoptosis in the dentate gyrus provides a baseline for analysis. For the development of this PhD thesis, both an in vitro and an in vivo model have been employed. The in vitro model involves the culture of primary mouse microglia "fed" with human apoptotic cells. In contrast, the in vivo "superphagocytosis" consist in using low-cranial irradiation (LCI) at 2Gy to induce apoptosis that already occurs basally and boost phagocytosis. This in vivo approach provides the opportunity to closely examine the microglial response under physiological conditions and its ability to enhance phagocytosis in a controlled experimental environment. Created with BioRender.com.*

In vitro methods to study phagocytosis

Back in 1986, Guilian and Baker, performed the first approach to study microglial phagocytosis, establishing the culture of adherent primary microglia and "feeding" the cells with potential phagocytic substrates (Giulian et al., 1986). This study laid the foundation in the field and microglial phagocytosis began to be studied using

primary cultures (Sierra et al., 2013). In addition to primary cultures, microglial cells lines, such as the microglial immortalized line BV2 (Blasi et al., 1990), have been and still are commonly used in phagocytosis assays (Bocchini et al., 1992). Furthermore, in the last years, the development of induced pluripotent stem cells (iPSCs) technology has allowed to generate human derived microglia, in which phagocytosis has been also studied (Healy et al., 2018; Dräger et al., 2022). In short, these three approaches are commonly used to study the phagocytic process. Each of them renders different advantages and disadvantages that will change depending on the type of the assay, for example, depending on the phagocytic substrate added to the culture. The characteristics of each model, as well as the importance of choosing the most convenient phagocytic substrate, will be detailed below. We will first discuss the pros and cons of using different microglia (immortalized cells lines, primary cultures and microglial cells derived from induced pluripotent stem cells), to further continue with the different substrates that are usually added to the cultures (beads and apoptotic cells).

Feeding culture models:

Feeding *in vitro* systems guarantee the controllability of the experiments and allow to directly assess the effect of the treatment in individualized microglial cells and can be performed using different sources of microglia. Microglial cell lines are easy to maintain and highly available because of their unrestricted proliferative capacity and to their easy storage (Timmerman et al., 2018). One of the most widely used murine cell lines mentioned above, the BV2, respond to LPS and present phagocytic capacity (Stansley et al., 2012). Primary cultures have also the advantage of genetic homogeneity and the acquisition of an specific pathogen-free (SPF) population due to the origin of the rodents used for their generation (Timmerman et al., 2018). Likewise, iPSCs also have advantages as they recapitulate human microglial features (Healy et al., 2018). However, *in vitro* systems also have limitations. BV2 cells do not completely replicate the microglial phenotype and significantly differ from the profile of adult mouse brain microglia. Consequently, these cells exhibit reduced motility in response to chemokines, diminished responsiveness to LPS, and downregulation of the TGF-β pathway (Butovsky et al., 2014; Das et al., 2016; He et al., 2018). Primary cultures of microglia lack the environmental signals required for their subsequent maturation, leading to an immature transcriptional profile (Butovsky et al., 2014). Moreover, in the brain microglia are constantly receiving certain signals, such as fractalkine, that inform about the homeostatic state of the environment. The lack of these stimuli leads to an increase in inflammatory profile of microglia that do not recapitulate the homeostatic state of brain microglia, which could lead to some artifacts (Wolf et al., 2013). Another primary culture handicap is the difference between rodent and human microglia, which has been tried to be solved through human derived primary microglia. However he limited availability of (healthy) human brain tissue hinder the possibility of using human primary microglia (Watkins et al., 2014; Timmerman et al., 2018). iPSC present a higher risk of mutagenesis and oncogene activation (Friedman et al., 2018), a limitation despite which they remain to be the most accurate model for mimicking human microglia (Hasselmann et al., 2020). Thus, *in vitro* approaches are valuable for studying cellular mechanisms in a controlled environment. However, cultured microglia differ from their in vivo counterparts, and their function may not fully replicate the complexity of the brain environment.

The choice of substrate is also critical in in vitro phagocytosis assays. Latex beads have been commonly used in a procedure that involves coating the beads with serum to promote the interaction with the phagocyte. It has been recently proposed that C1q, present in the culture serum, participates in the phagocytosis of apoptotic cells, which also highlights the relevance of using a non-inactivated serum when performing phagocytosis assays (Fraser et al., 2010; Diaz-Aparicio et al., 2019). Nevertheless, beads do not release chemokines, thus preventing microglial chemoattraction towards the substrate in the "find-me" phagocytic stage. Moreover, these particles can not be degraded, not allowing to study the final step of phagocytosis. Therefore, to mimic phagocytosis in physiological conditions, our lab has used an *in vitro* phagocytosis assay by "feeding" microglia with apoptotic neurons in the presence of C1q (non-activated serum). The method allows the release of "find-me" signals from apoptotic cells and their subsequent digestion once phagocytosed by microglia (Diaz-Aparicio et al., 2020).

Organotypic cultures and organoids:

In addition to cell cultures treated with apoptotic cells, other methods allow to study phagocytosis in 3D environments, such as organotypic cultures and brain organoids. In hippocampal organotypic slices apoptosis occurs naturally, all the neural cell types are present, and connectivity is preserved; therefore they can be used to both mimic physiological phagocytosis and to model several diseases such as epilepsy or stroke (Garbayo et al., 2011; Abiega et al., 2016; Gerace et al., 2021). However, organotypic slices show some disadvantages as the modification of the environment after adding culture medium, the loss of connection with other brain areas, and the ultimate fact that an organotypic slice does not encompass the full complexity and functionality of a complete brain (Humpel, 2015; Abiega et al., 2016). More recently, brain organoids have allowed to model the human brain maintaining cellular heterogeneity and making the whole structure to act in a tissue-like manner (Sabate-Soler et al., 2022). All these characteristics make organoids very complete systems for the study of neural development and neurological disorders (Lancaster et al., 2013; Lindborg et al., 2016). However, for years, microglia were absent in brain organoids. Because of the mesodermal origin of microglia, they do not differentiate within the neuroectodermal tissue of brain organoids, whereby iPSCs derived microglia need externally assembled in the culture (Fagerlund et al., 2021; Popova et al., 2021). Lately, these co-culture protocols have shown that microglia exhibited phagocytic capacity after the observation of caspase3 particles within microglial cells (Xu et al., 2021; Zhang et al., 2023). Thus, organoids open a new field of research in which the human brain can be modeled on a plate without the need for animal experiments; however, their novelty and scarce development still make *in vivo* models necessary.

In vivo methods to study phagocytosis

To analyze phagocytosis *in vivo*, the apoptotic cargo must be observed within microglia. The phagocytic pouch, a three-dimensional structure usually located in a microglia process, surrounds the apoptotic body and through this observation phagocytosis will be assessed. Currently, imaging techniques allow us the direct

visualization of the 3D pouch and the content inside. Our laboratory uses immunofluorescence and confocal imaging, which allows immunolabelling and posterior visualization of microglial, apoptotic cells and other phagocytic contents, such as myelin or axonal debris (Sierra et al., 2013). However, fixed tissue image analysis has the limitation of providing information at a given time-point. This problem can be solved using the live imaging technique of 2-photon microscopy in transgenic zebrafish with fluorescent reporters in target cells that ultimately develop to be used in transgenic mice, allowing the visualization of the complete phagocytic process (Sieger et al., 2012; Abiega et al., 2016; Kamei et al., 2023).

Our laboratory has used the neurogenic niche of the DG as an in vivo model to study phagocytosis in physiological conditions. During the process of neurogenesis that occurs in the hippocampal DG in a process known as neurogenic cascade, some newborn cells die. This basal apoptosis allows us to establish a baseline of microglial phagocytosis in physiological conditions (Sierra et al., 2010). Our group was a pioneer in the study of microglial phagocytosis in the DG, and by the analysis of microglia, apoptotic cell and phagocytosed apoptotic cell numbers determined useful to calculate parameters that indicate phagocytic efficiency (Sierra et al., 2010). In physiological conditions, most of the apoptotic cells (near to 90%) were engulfed by microglia, while the remaining apoptotic cells because their early apoptotic characteristic were not recognized by microglia yet (Sierra et al., 2010). The percentage of phagocytosed apoptotic cells engulfed by microglia is defined as the phagocytic index (Ph index) and represent microglial phagocytic ability. Moreover, phagocytosis occurs rapidly removing the apoptotic cell in a clearance time of 90 minutes approximately. Likewise, the number of phagocytic pouches (presumably indicating phagocytosed apoptotic cells) per phagocytic microglia indicates the phagocytic capacity of the cells. In basal conditions most of the phagocytic microglia display 1 phagocytic pouch containing an apoptotic body (Sierra et al., 2010). Therefore, in physiology microglia efficiently remove the apoptotic cells of the DG niche through apoptosis-coupled phagocytosis.

Nevertheless, the model has some limitations. Apoptosis occurs unpredictably and sporadically. Consequently, among all microglial cells present in the neurogenic niche, only a few cells will be engaged in phagocytosis. As a result, a mixed population comprising both non-phagocytic and phagocytic microglia coexists in the hippocampal neurogenic niche of young-adult and adult mice. To address this issue, in this PhD thesis we have developed an *in vivo* “superphagocytosis” model that consisted of using low-cranial irradiation (LCI) to induce apoptosis of neuroprogenitors in the DG and boost phagocytosis. This model produces a massive apoptosis which allows to synchronize DG microglia in a phagocytic state while engulfing the damaged cells and a post phagocytic state once they have been cleared. This significantly increases the number of phagocytic microglia in the DG, which allows to study the postphagocytic changes of that microglial population that has been exposed to the phagocytic challenge.

3.5 FUNCTIONAL CONSEQUENCES OF PHAGOCYTOSIS

As reviewed in the last section, microglial phagocytosis is very efficient in physiological conditions in the DG as they rapidly engulf and clear apoptotic cells. The proper removal of apoptotic debris by microglia has effects both on surrounding nerve tissue and on the microglial cells themselves. We will describe both in more detail below.

3.5.1 Functional outcome of phagocytosis for the CNS environment

The rapid and efficient removal of apoptotic debris by microglia avoids the spillover of apoptotic intracellular content, as primary apoptotic cell loss their membrane integrity and became into secondary apoptotic or necrotic cells (Kolb et al., 2017). The release of intracellular contents into the extracellular space is known to cause the inflammatory response, since some molecules such as DNA, RNA, nucleotides, or chromatin proteins such as HMGB1 (high mobility group box 1 protein) termed damage-associated molecular patterns (DAMPs) are recognized by pattern recognition receptors (PRRs) expressed by microglia , initiating a complex immune inflammatory response (Huber-Lang et al., 2018). On one hand, an inefficient phagocytosis results in a generalized inflammatory response and tissue damage, as observed in an *in vivo* mouse model of epilepsy widely studied in our laboratory, in which impaired phagocytosis is linked to a pro-inflammatory profile in microglia (Abiega et al., 2016; Morioka et al., 2019). On the other hand, *in vitro* microglia performing apoptotic cell phagocytosis showed dampened responses to inflammatory stimuli such as LPS (Magnus et al., 2002; De Simone et al., 2003). On the contrary, our laboratory has demonstrated that in vitro primary microglia exposed to LPS exhibit a cytokine expression profile highly similar to that of phagocytic microglia (Diaz-Aparicio et al., 2020). In summary, despite seemingly contradictory findings that may be related to procedural differences (e.g. post-phagocytic time, or LPS dosage), these data suggest that microglial phagocytosis exerts immunomodulatory effects (Szondy et al., 2017; Morioka et al., 2019).

3.5.2 Functional outcome of phagocytosis in microglia

In **section 1.2.3.3** we have reviewed how microglial function and especially inflammatory responses are regulated by changes in their metabolism and transcription. Thus, microglial phagocytosis could also trigger intracellular changes at the transcriptional and metabolic level.

In macrophages, phagocytosis elicit a repertoire of transcriptional and metabolism adaptation that led to the modulation of immune function, a process called innate immunity training (**section 1.2.3.3**). In fact, phagocytosis triggers mitochondrial fission (Wang et al., 2017; Morioka et al., 2018) and decreased mitochondrial membrane potential via mitochondrial uncoupling protein 2 (UCP2) (Park et al., 2011), which, together with increased glycolysis (Morioka et al., 2018), ensure the continued uptake of corpses. In addition, increased lactate release promotes the establishment of an anti-inflammatory environment (Morioka et al., 2018). However, phagocytosis-induced metabolic adaptations not only have an effect during phagocytosis, but also trigger long-lasting effects. There are several examples of how phagocytosis reprograms the function of macrophages. For instance, during Drosophila early development, naïve

macrophages are insensitive to tissue damage or infection. However, upon corpse uptake macrophages become capable of migrating into damaged regions, and phagocytose bacterial pathogens, through the activation of the Jun kinase-signaling pathway and increased the expression of the damage receptor Draper (Weavers et al., 2016). Thus, phagocytosis of apoptotic corpses in macrophages triggers metabolic adaptations that immediately modulate cell function and also drives a long-term that potentiate the phagocyte.

In contrast, little is known about the metabolic adaptations to phagocytosis in microglia. In culture, phagocytic microglia undergo transcriptional modulations showing time-dependent expression changes. While some genes are transiently regulated at 3 h after engulfment, most are regulated in the post-degradation phase at 24 h after engulfment (Diaz-Aparicio et al., 2020). Some of these genes were involved in cell metabolism suggesting that phagocytosis triggers metabolic adaptations also in microglia (Diaz-Aparicio et al., 2020). In this PhD thesis we will test the hypothesis that upon phagocytosis microglia remodel their metabolism and may impact their function.

3.6 PHAGOCYTOSIS IN BRAIN TUMORS

The study of microglial post-phagocytic changes is crucial to understand how microglia performs phagocytosis when cells are challenged by apoptotic stimuli consecutively in short periods of time. One pathological case in which repetitive phagocytosis is necessary are brain tumors, which are commonly treated using radiotherapy to kill tumor cells in brain cancer (Scaringi et al., 2018). The treatment is usually administered in sequential doses (Hingorani et al., 2012a), leading to several waves of apoptotic cells that microglia need to clear. In this section, we will discuss various types of brain tumors, with a subsequent emphasis on glioblastoma, the most prevalent and aggressive form of primary malignant brain tumors, and its associated treatment modalities. Additionally, we will delve into the role of microglia within the tumor microenvironment, finally focusing in microglial phagocytosis of tumor cells.

3.6.1 Categories of brain tumors

The most prevalent brain tumors are grouped into three categories: intracranial metastases from systemic cancers, meningiomas, and gliomas (McFaline-Figueroa et al., 2018). Metastatic brain tumors are considered secondary brain tumors because they do not originate in the brain and their prevalence is 10 times higher than primary tumors (Arvold et al., 2016). As most brain metastases are a consequence of an advanced systemic disease, the prognosis remains generally poor (Sperduto et al., 2012). Among primary brain tumors, meningiomas originate from meningothelial cells, are further developed in the cranial or dural surface and present a good prognosis, being mostly benign (Buerki et al., 2018). Conversely, gliomas originate from glial cells and include astrocytomas, oligodendrogliomas, ependymomas, glioblastomas and a variety of tumors with rare histology. Among gliomas, glioblastomas are the most frequent and aggressive primary malignant brain tumors, showing a limited treatment efficiency and low survival rates (Fu et al., 2014). So far, available treatments have failed

to increase survival rates and have only increased patients' lifespan by a few months (Silantyev et al., 2019). Thus, the optimization of treatments is key to improve the quality of life and lifespan of patients with glioblastoma.

Although the new classification of glioblastomas, which relies on molecular and histological features, aims to obtain more adequate diagnoses and therapies, the classical therapeutic approach includes a combination of neurosurgery, radiotherapy, and chemotherapy (McFaline-Figueroa et al., 2018). First, the tumor is resected. The resection has to guarantee the maximum removal of the cancerous tissue without affecting or little affecting the brain functions (Sanai et al., 2011). Then, the "Stupp protocol" is implemented, as this procedure represents the consensus standard for postoperative treatment. The protocol consists of 6 weeks of hypofractionated radiotherapy (HFRT), in which consists the total dose of radiation is divided into smaller doses and administered sequentially (60Gy divided into 2Gy fractions per day, allowing for rest periods of two days every five days) together with the adjuvant temozolamide, which is administered daily during radiotherapy and followed by six subsequent cycles (Stupp et al., 2005). Nevertheless, the latest research on HFRT that has explored different fractions and doses has failed to significantly increase survival time (Liu et al., 2021). Furthermore, HFRT optimization has often overlooked the crucial role of phagocytes in removing apoptotic tumor cells, as research on tumor cell phagocytosis by microglia remains relatively limited, as we will describe in the next section. Therefore, the post-radiation phagocytosis needs to be more explored in order to optimize the treatments.

3.6.2 Microglial and TAMs in the tumor microenvironment

In the tumor, microglia coexist with circulatig monocytes that infiltrate the tumor after BBB permeabilization, and both constitute a mixed population called tumor-associated macrophages (TAMs). TAMs comprise around the 30-40% of tumor mass and have a bidirectional relationship with cancer cells and tumor microenvironment (Badie et al., 2000; Watters et al., 2005; Buonfiglioli et al., 2021a). As a consequence of this relationship, TAMs have been proposed to contribute to tumor worsening by both promoting tumor progression and by exerting immunosuppressive functions (Buonfiglioli et al., 2021a) (**Figure I7**).

TAM-glioma cell crosstalk is mediated by both chemoattractant molecules released by glioma cells that contribute to TAM recruitment, and by TAMs released factors that promote tumor progression (Buonfiglioli et al., 2021a). Among the factors released by tumor cells are the following chemoattractant proteins that favor the recruitment of TAMs to tumor sites: the cytokines CCL2 and CCL7, interleukin 33 (IL-33), and growth factors such as granulocyte-macrophage colony stimulating factor (GM-CSF), hepatocyte growth factor or scatter factor (HGF/SF), stroma-derived factor 1 (SDF-1), and glial cell-derived neurotrophic factor (GDNF) (Wang et al., 2012; Ku et al., 2013; Sielska et al., 2013; Chen et al., 2017a; Chen et al., 2017b; De Boeck et al., 2020). Likewise, tumor cells release other agents, such as CSF1 and secreted phosphoprotein 1 (SPP1), which not only attract TAMs but also induce a switch to a more immunosuppressive phenotype on TAMs (Sielska et al., 2013; Wei et al., 2019). Lastly, proteins secreted by the tumor also favor the progression of the tumor

itself, this is the case of the Versican that bind toll-like receptors (TLR) directly favoring tumor growth, and the cell adhesion molecule Tenascin C (TNC), which positively regulate tumor proliferation via TAMs (Hu et al., 2015; Xia et al., 2015). Overall, glioblastoma cells orchestrate a complex process of production and release of molecules that in turn favor their growth and expansion through the action of TAMs.

After being reprogramed by tumor cells derived factor, TAMs contribute to tumor progression through released factors released. The production of the cytokines, TGF-β and interleukins 1β and 6 (IL-1β and IL-6) is increased in TAMs, and each of them contribute to tumor progression in different ways. The secretion of TGF-β leads to the disruption of the extracellular matrix (ECM) and thus increase the invasion of glioblastoma cells (Wick et al., 2001). Moreover, IL-1β overexpression promotes the proliferation and tumor cells; and IL-6 is involved in tumor progression by contributing to the formation of blood vessels by tumor cells (Feng et al., 2015; Zhang et al., 2017). Likewise, both the release of stress-inducible phosphoprotein 1 (STI_1) and epidermal growth factor (EGF) and the production of metalloproteinases (MMP_{14}, MMP_2 and MMP_9) through TLR activation promote tumor growth and invasion (Markovic et al., 2009; Coniglio et al., 2012; Vinnakota et al., 2013; da Fonseca et al., 2014; Hu et al., 2014). Thus, TAMs directly contribute to tumor growth representing an interesting therapeutic target that could slow down tumor progression.

Moreover, TAMs also dampen the immune response influencing other cells, as T cells, and decreasing their own immune functions as phagocytosis. T-cells perform the anti-tumor response by the recognition and destruction of tumor cells (Sakaguchi et al., 2007; Qian et al., 2018). When it comes to tumor cell recognition, T cells need to recognize antigens from target cells and TAMs, which are antigen-presenting cells (APCs), facilitate the identification of cancerous cells. However, glioma-derived factors decreased antigen presentation through the impairment of MHC class II expression of TAMs, which dampened T cell activity leading to tumor progression (Qian et al., 2018). Thus, TAMs also contribute to tumor progression by influencing surrounding immune cells.

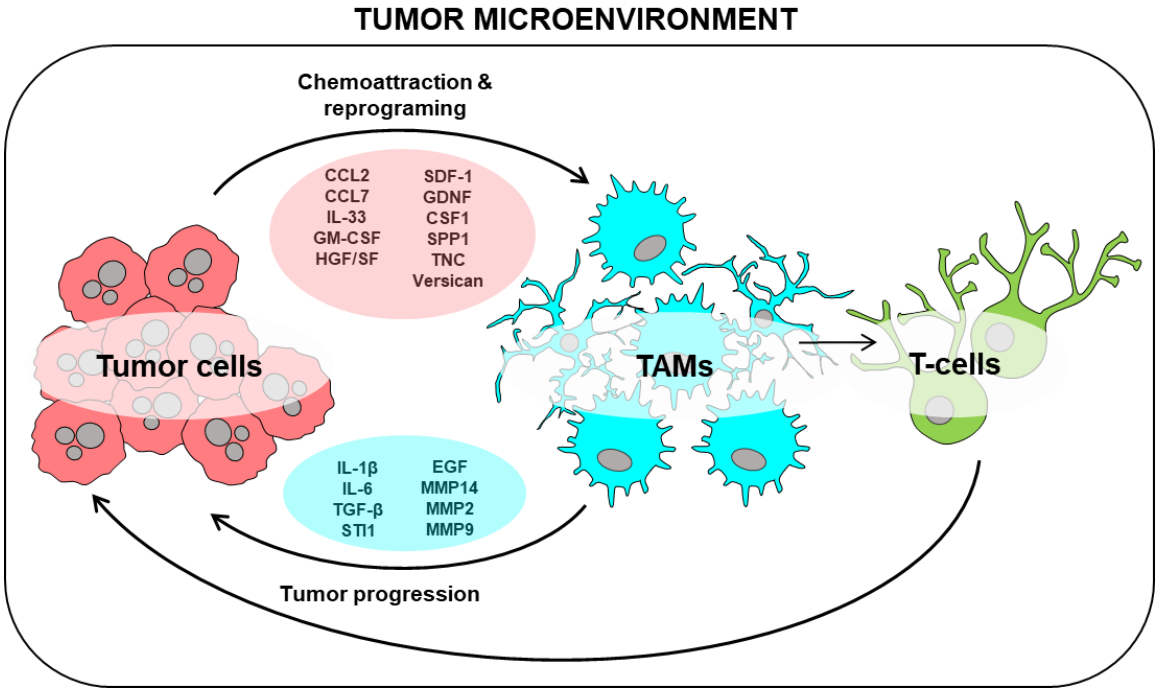

Figure 7. TAMs-tumor cells crosstalk in the tumor microenvironment. *Factors released in the tumor microenvironment in the TAMs-tumor cells crosstalk promote tumor growth and decrease the immune response. Glioma cells release chemoattractant molecules that recruit and reprogram TAMs. In turn, TAMs release that promote tumor progression and dampen the response of the adaptative immune system (T-cells). Created with BioRender.com. and adapted from (Buonfiglioli et al., 2021a).*

3.6.3 Tumor cell phagocytosis

The ability of TAMs to perform phagocytosis in the tumor microenvironment is still contradictory. On the one hand, tumor cells are not phagocytosed by TAMs, since like healthy cells they exhibit "don't eat-me" signals that prevent phagocytosis (Cockram et al., 2021; Kelley et al., 2021). Moreover, in the tumor microenvironment "don't eat-me" signals increase, that is the case of the augmented expression of the anti-phagocytic ("don't eat me") surface protein CD47, which binds to its homologous receptor SIRPa on TAMs cell to inhibit phagocytosis (Willingham et al., 2012; Li et al., 2021). In this regard, treatment with anti-CD47 antibodies induced phagocytosis tumor phagocytosis by TAMs in a glioblastoma xenograft model and reduced tumor expansion (Hutter et al., 2019). On the other hand, at least in vitro, TAMs showed a reduced phagocytic capacity of microbeads when exposed to glioma cancer stem cells (gCSCs) (Wu et al., 2010). However, when apoptosis is induced in the tumor by cytotoxic agents or UV light, astrocytes, glioma cells and TAMs are able to perform phagocytosis in the tumor microenvironment (Chang et al., 2000; Kulprathipanja et al., 2004). Moreover, the number of apoptotic cells engulfed by TAMs was four-fold higher than those engulfed by astrocytes and glioma cells, indicating that TAMs were the most efficient phagocytes in brain tumors (Chang et al., 2000). The effect of radiotherapy on both apoptosis and phagocytosis has been less explored. Therefore, given that radiotherapy is the most common strategy for treating glioblastoma, one of the primary objectives of this PhD Thesis is to evaluate the phagocytosis of apoptotic tumor cells by TAMs. Understanding how

radiation impacts apoptosis and the subsequent phagocytosis of tumor cells by TAMs will open a new path for studying HFRT, which is the most widely used therapy to combat glioblastoma

4. HYPOTHESIS AND OBJECTIVES

4. HYPOTHESIS AND OBJECTIVES

Microglial phagocytosis of apoptotic cells has been extensively studied in both physiology and disease and it involves several phases until the apoptotic cell is completely cleared from the tissue (Napoli et al., 2009; Diaz-Aparicio et al., 2016). Moreover, phagocytosis is not a terminal process, as it impacts in both the environment and in the microglia cells themselves. The consequences of phagocytosis avoids the spillover of apoptotic intracellular content and suppressed the inflammatory response (Kolb et al., 2017; Huber-Lang et al., 2018). Likewise, phagocytosis regulates the neurogenic cascade by the production of neuromodulatory factors (Diaz-Aparicio et al., 2020), elucidating that microglia undergo functional changes following phagocytosis. In this study we hypothesize that phagocytosis will trigger changes at different levels of microglia, potentially affecting their transcriptional, metabolic status and consequently their downstream phagocytic function.

Aim 1. To develop and validate a "superphagocytosis" *in vivo* model. For the development of the model , we will adapt a model based in the administration of cranial irradiation (8Gy), which induced neuroprogenitor apoptosis and microglial phagocytosis in the DG (Beccari et al., 2023), to a low-cranial irradiation model (LCI) (2Gy) to reduce the number of generated apoptotic cells and minimize side effects. Afterwards we will use immunofluorescence and confocal imaging to assess the efficacy of the model to synchronize microglia in a phagocytic state, and to assess DNA damage and monocyte extravasation.

Aim 2. To study phagocytosis-induced changes on microglial morphology and their transcriptional state. To find markers of post-phagocytic microglia, we will explore different parameters that could undergo changes after phagocytosis such as changes in morphology, and gene expression. Microglial morphology will be examined using immunofluorescence and confocal imaging, while the postphagocytic transcriptional state of microglia will be assessed using single-cell RNA sequencing (scRNA-Seq) and immunofluorescence and RNAScope.

Aim 3. To unravel the mechanisms by which microglia is stressed after phagocytosis we will explore different functions and intracellular components in post-phagocytic microglia, such as oxidative stress, mitochondria, and cellular metabolism, all of them associated with cellular stress and death. Oxidative stress, mitochondria, and cellular metabolism will be explored using an *in vitro* model of phagocytosis, followed by fluorescence expression analysis, confocal and electron microscopy analysis, and Seahorse and mass spectrometry metabolomic analysis, respectively.

Aim 4. To address microglial phagocytic function after post-phagocytic stress. Microglial function will be assessed using the *in vivo* “superphagocytosis” model followed by immunofluorescence and confocal imaging.

Aim 5. To assess microglial phagocytosis in radiotherapy exposed glioblastoma tumors, as a preliminary approach to study phagocytosis in the context of hypofractionated radiotherapy (HFRT). we will used two different animal models that recapitulate the proneural and mesenchymal subtype of glioblastoma in mice (Lenting et al., 2017), which will be exposed to one pulse of radiotherapy (RT). Phagocytosis will be assessed using immunohistochemistry, immunofluorescence and imaging techniques.

5. EXPERIMENTAL PROCEDURES

5. EXPERIMENTAL PROCEDURES

5.1 ANIMALS

All experiments were performed in mice expressing the enhanced green fluorescent protein, under the control of the mouse colony stimulating factor 1 receptor (fms-EGFP) (MacGreen, B6. Cg-Tg (Csf1r-EGFP)1Hume/J; Jackson Laboratory stock #018549) mice. In the fms-EGFP mice microglia constitutively express the green fluorescent protein (GFP) under the expression of c-fms gene (Sasmono et al., 2003; Sierra et al., 2007). Single cell RNA-Seq experiments, were performed in WT mice. Experiments in tumor-bearing mice were performed WT mice crossed with mice expressing a transgene expressing the avian cell surface receptor for subgroup A avian leukosis viruses directed by a promoter derived from the human nestin gene (Ntv-a mice) (Ntv-a, STOCK Tg(NES-TVA)J12Ech/J; Jackson Laboratory stock #003529)(Holland et al., 1998). These mice were generated via 10 generations of back crosses (Hambardzumyan et al., 2009). All animals were housed in a climate controlled, pathogen-free facility with *ad libitum* food and water under a 12-hour light/dark cycle. All mice used were in a C57BL/6 background.

All procedures conducted in Spain followed the European Directive 2010/63/EU and NIH guidelines, and were approved by the Ethics Committees of the University of the Basque Country EHU/UPV (Leioa, Spain; CEBA/205/2011, CEBA/206/2011, CEIAB/82/2011, CEIAB/105/2012). All procedures conducted in USA were approved by the Institutional Animal Care and Use Committee (IACUC) of the Icahn School of Medicine at Mount Sinai (Protocol #2019-00619).

5.2 CELL CULTURES

5.2.1. Red fluorescent SH-SY5Y cell line (Vampire SH-SY5Y)

SH-SY5Y (American Type Culture Collection), a human neuroblastoma cell line derived from the bone marrow of 4-year-old female, was used for phagocytic assay experiments. Vampire-SH-SY5Y cells were developed through stable transfection of SH-SY5Y cell line with tFP602 (InnoProt, P20303), and expresses red fluorescent protein as a free cytoplasmatic protein. SH-SY5Y cells were grown as an adherent culture in non-coated culture flasks covered with 10-15ml of Dulbecco's Modified Eagle Medium (DMEM, PAN-Biotech), supplemented with 10% Fetal Bovine Serum (FBS) (PAN-Biotech),1% antibiotic/antimycotic (Gibco) and 0.5 % geneticin (Fisher). When confluency was reached, cells were trypsinized and replated at 1:4.

5.2.2 BV2 cell line

BV2 cells (Interlab Cell Line Collection San Martino-Instituto Scientifico Tumori-Instituto Nazionale per la Ricerca sul Cancro), a line derived from raf/myc-immortalized murine neonatal microglia, was used to perform phagocytosis *in vitro* assays for the analysis of the mitochondrial network. BV2 cells were grown as an adherent culture in non-coated culture flasks covered with 10ml DMEM (PAN-Biotech), supplemented with 10% FBS (PAN-Biotech) and 1% antibiotic/antimycotic (Gibco). When confluency was reached, cells were trypsinized and replated at 1:4. For experiments, BV2 cells were counted and plated in a density of 80,000 cell/well on poly-l-lysine-coated glass coverslips in 24-well plates (BioLite, Thermofisher). For transfection experiments BV2 cells were allowed to rest and settle for at least 24h before transfection of mitoGFP7 plasmid.

5.2.3 Primary Microglia Cultures

Primary microglia cultures were performed as previously described (Abiega et al., 2016; Beccari et al., 2018). Postnatal day 0-1 (P0-P1) fms-EGFP mice pup brains were extracted and the meninges were peeled off in Hank's balanced salt solution (HBSS, Gibco) under a binocular magnifier. The olfactory bulb and cerebellum were discarded and the rest of the brain was then mechanically homogenized by careful pipetting and enzymatically digested in an enzymatic solution (116mM NaCl, 5.4mM KCl, 26mM $NaHCO_3$, 1mM NaH_2PO_4, 1.5mM $CaCL_2$, 1mM MgSO4, 0.5mM EDTA, 25mM glucose, 1mM L-cysteine) with papain (20U/ml, Sigma), and deoxyribonuclease (DNAse; 150U/µl, Invitrogen) for 15min at 37°C. The resulting cell suspension was then filtered through a 40µm nylon cell strainer (Fisher) and transferred to a 50 ml Falcon tube quenched by 5 ml of 20% FBS (PAN-Biotech) in HBSS. Afterwards, the cell suspension was centrifuged at 200 g for 5 min, the pellet was resuspended in 1ml DMEM (PAN-Biotech) complemented with 10% FBS (PAN-Biotech),1% Antibiotic/Antimycotic (Gibco), and 5ng/ml granulocyte-macrophage colony stimulating factor (GM-CSF, Sigma), and seeded in poly-L-lysine-coated (15µl/ml, Sigma) culture flasks with a density of two brains per flask. Medium was changed the day after and then every 3–4 days. After confluence (at 37°C, 5% CO2 for approximately 11-14 days), microglia cells were harvested by shaking at 140 rpm, 37°C, 4h.

5.2.4 DF-1 cell line

DF-1 cell line (American Type Culture Collection, CRL-3586), is a spontaneously immortalized fibroblast cell line derived from chicken. DF-1 cells were transfected with viruses and consecutively employed in brain injections to induce brain tumors. DF-1 cells were grown as an adherent culture in non-coated culture T25 flasks covered with 6ml of DMEM (ATCC), supplemented with 10% FBS (ATCC), 1% penicylin/streptomycin (, Gibco) and 1% GlutaMax (Gibco). Cells were grown at 39°C according to ATCC instructions, used in early passages, and tested for mycoplasma. Cells were split every other day using trypsin and replated at 1:8. The day of the transfection with mitoGFP7 plasmid, cells were 30-50% confluent.

5.3 CELLULAR TRANSFECTIONS

5.3.1 BV2 cell line transfection with mitoGFP7

GFP-Mito-7 plasmid DNA (Addgene, 57148) was transfected into BV2 cells using lipofectamine 2000 Mito-7 corresponds to the mitochondrial targeting sequence from subunit VII of cytochrome C oxidase (Kitay et al., 2013). BV2 cells were cultured in poly-lysine-treated coverslips in a 24-multiwell plate at a density of 50.000 cells per well. To facilitate cellular internalization of the plasmid, plasmid DNA and Lipofectamine 2000 (Thermofisher) were diluted in OPTI-MEM with no serum (Gibco) at a 2:1 ratio. Following a 20-minute incubation at RT, the mixture was added to the cells and they were further incubated with the transfection mix for 18 hours at 37°C.Transfection media was then changed to DMEM 10% FBS, 1% antimycotic-antibiotic.

5.3.2 DF-1 cell line transfection with glioblastoma inducing viruses

Transfections with retroviral vectors derived from avian sarcoma-leukosis virus (RCAS): RCAS-hPDGFB-HA and RCAS-shRNA-p53-RFP for Proneural GBM induction, and with RCAS-shRNA-Nf1, RCAS-hPDGFA-myc, RCAS-shRNA-p53-RFP, RCAS-shRNA-Pten-RFP Mesenchymal GBM induction were performed using a Fugene 6 transfection kit (Roche #11814443001) according to the manufacturer's protocol. The Fugene 6 reagent (60µl/ml) was mixed with DMEM (without antibiotics or serum) (ATTC), followed by a 5min incubation at RT. Subsequently, DNA was added to the transfection mix at a 3:1 ratio and incubated for 20 minutes at RT before being added to the flask containing the cells. The entire transfection setup was then incubated at 39°C with 5% CO2. A cell passage was performed the following day.

5.4 IN VITRO PHAGOCYTOSIS ASSAY

5.4.1 Primary microglia

Primary microglia were allowed to rest and settle for at least 24h before phagocytosis experiments. To adapt the glucose concentration of the proliferation media (poner aquí la concentración) to a more physiological concentration (Mot et al., 2016) in Seahorse metabolic measurements, in the analysis of metabolites, and in ROS measurement assays, primary microglia were maintained at low glucose concentration (2.5mM) for 3 days prior and during the phagocytosis assay. SH-SY5Y cells were treated with staurosporine (Sigma) 3 µM for 4h at 37°C to induce apoptosis. The floating dead cell fraction was collected from the supernatant and apoptotic cells were visualized and quantified by trypan blue in a Neubauer chamber. Because cell membrane integrity is still maintained in early induced apoptotic cells, trypan blue unlabeled cells were considered apoptotic. Primary microglia were fed for 5h with apoptotic Vampire SH-SY5Y cells (with

subsequent cell washout), by adding them at a 1:3 proportion for Seahorse, metabolomics, and ROS measurement experiments. For TEM experiments microglia was fed for 1h with apoptotic SH-SY5Y by adding the cells in a 1:1 proportion to ensure most microglia will become phagocytic. All the analyses were performed 24h after adding the apoptotic cells.

5.5 SEAHORSE EXTRACELLULAR FLUX ANALYSIS

Primary microglia were plated at a density of 100,000 cells/well in a Seahorse XFe96 cell culture microplate (Agilent) in a cell suspension of 80 µl/well to avoid cells attaching to the well's walls. The four corner wells were not seeded and were used as background. 24h after plating, the media was changed and cells were maintained in low glucose DMEM (2.5mM) for 3 days. Apoptosis of Vampire SH-SY5Y was induced as described above (see section **5.4**)) and cells were added in a 1:3 proportion. 5h after later, the cell media was changed to remove non-phagocytosed apoptotic cells. Phagocytosis assay was also performed in low glucose concentration the analysis was performed in each experimental condition (naïve/phagocytic).

5.5.1 Oxidative phosphorylation analysis

The analysis of the mitochondrial function was done using the Seahorse XF Cell Mito Stress Kit (Agilent), which targets several components of the mitochondrial ETC. The kit is composed of three drugs, which were sequentially injected. First, oligomycin (1 µM) inhibited ATPase synthase (ETC complex V), causing a decrease in the oxygen consumption rate (OCR) of cells (pmol/min), which indicates mitochondrial respiration coupled to ATP production. Second, FCCP (1 µM) was injected and, as a consequence, oxygen was maximally consumed by complex IV of the ETC (mitochondrial membrane potential enhancement), producing an increase in the OCR that indicated the maximal mitochondrial respiration. Third, a mix of rotenone (complex I inhibitor, 0.5 µM) and antimycin A (complex III inhibitor, 0.5 µM) was injected and mitochondrial respiration was completely inhibited, permitting to estimate the non-mitochondrial respiration. Drugs were pipetted in an XFe96 Sensor Cartridge (Agilent)pretreated with XF Calibrant solution (200 µl/well) overnight at 37°C in a non-CO2 incubator. XF Seahorse Medium (1mM pyruvate (Merck), 2mM glutamine (Sigma), 2.5 mM glucose (Sigma) and HEPES buffer 5 mM) were added in each well, including those at the corners (background correction or blank wells). The media was heated at 37°C and then the pH was adjusted to 7.4 with NaOH 1N. Cells were maintained with the supplemented medium for 1h before assay in a non-CO2 incubator (180 µl/ well).

5.5.2 Glycolysis analysis

The analysis of the glycolytic function was performed using the Seahorse XF Glycolysis Rate Assay Kit (Agilent). Two drugs were sequentially injected in order to obtain an accurate measurement of the glycolytic proton efflux rate (glycoPER; pmol/min) in cells through the estimation of the oxygen consumption rate (OCR) and the extracellular acidification rate (ECAR). First, a mix of rotenone and antimycin A (0.5 µM) was injected to block mitochondrial oxygen consumption. Thereby, PER from mitochondrial respiration (produced by the extrusion of protons via the Krebs cycle) could be calculated and removed from the total PER, obtaining the glycoPER. Second, 2-DG (2-Deoxy-D-glucose) 50 mM was injected. This glucose analogue inhibits glycolysis through the competitive binding of glucose hexokinase, the first enzyme in the glycolytic pathway. The consequence was a stop of glycolytic acidification, measuring the non-glycolytic acidification. Drugs were pipetted in a XFe96 Sensor Cartridge pretreated with XF Calibrant solution (200 µl/well) O/N at 37°C in a non-CO2 incubator. DMEM 10% FBS, 1% Antimycotic/antibiotic was replaced by XF Seahorse Medium (1mM pyruvate (Merck), 2mM glutamine (Sigma), 2.5 mM glucose (Sigma), and HEPES buffer 5 mM for each well including background wells. The media was heated at 37°C and then the pH was adjusted to 7.4 with NaOH 1N. Cells were maintained with the supplemented medium for 1h before assay in a non-CO2 incubator (180 µl/ well).

5.6 ANALYSIS OF TCA AND METHIONINE CYCLE METABOLITES

Primary microglia were plated in a density of 1 million cell/well in 6-well plates (BioLite, Thermofisher). 3 wells were seeded for each experimental condition (naïve/phagocytic) and for each metabolic pathway (TCA (tricarboxylic acid cycle)/ Methionine cycle). 24h after plating, media was changed and cells were maintained in low glucose concentration (2.5mM) for 3 days. Phagocytosis assay was performed as described above (see section **5.3**), Vampire SH-SY5Y cells were added in a 1:3 proportion and media was changed 5h after. Phagocytosis assay was performed in low glucose concentration and the experiment was performed 24h after adding the apoptotic cells. 24h after adding apoptotic cells all the wells were washed 3-times with ice-cold PBS 1X, the plate was sealed with Parafilm (Bemis, Parafilm) and then frozen at -80°C. Analysis of metabolites was performed by Diana Cabrera and Juan Manuel Falcón in CIC-bioGUNE.

5.6.1 Analysis of TCA cycle

For extraction of metabolites of the TCA cycle 500 µL ice-cold methanol/water (50/50 %v/v) was added to the wells of the culture plates (6-wells-plate). The plates were left on dry ice for 15 minutes. Subsequently 400 µL of the homogenate plus 400 µL of chloroform was transferred to a new aliquot and shaken at 1400 rpm for 60 minutes at 4 °C. Next, the aliquots were centrifuged for 30 minutes at 13000 rpm at 4 °C. The organic phase was separated from the aqueous phase. From the aqueous phase 250µL was transferred to a fresh

aliquot and placed at -80 °C for 20 minutes. 150 µL of supernatants were evaporated with a speedvac in approximately 1.5h. The resulting pellets were each resuspended in 150 µL water/acetonitrile (MeCN)(40/60v/v/%).

Samples were measured with a UPLC system (Acquity, Waters Inc., Manchester, UK) coupled to a Time-of-Flight mass spectrometer (ToF MS, SYNAPT G2, Waters Inc.). A 2.1 x 100 mm, 1.7 µm BEH amide column (Waters Inc.), thermostated at 40 °C, was used to separate the analytes before entering the MS. Mobile phase solvent A (aqueous phase) consisted of 99.5% water and 0.5% FA while solvent B (organic phase) consisted of 4.5% water, 95% MeCN and 0.5% FA. In order to obtain a good separation of the analytes the following gradient was used: from 10% A to 99.9% A in 2.6 minutes in curved gradient (#9, as defined by Waters), constant at 99.9% A for 1.6 minutes, back to 10% A in 0.3 minutes.

The flow rate was 0.250 mL/min and the injection volume was 4 µL. After every 8 injections sample was injected. The MS was operated in negative electrospray ionization in full scan mode. The cone voltage was 25 V and capillary voltage was 250 V. Source temperature was set to 120 °C and capillary temperature to 450 °C. The flow of the cone and desolvation gas (both nitrogen) were set to 5 L/h and 600 L/h, respectively. A 2 ng/mL leucine-enkephalin solution in water/acetonitrile/formic acid (49.9/50/0.1 %v/v/v) was infused at 10 µL/min and used for a lock mass which was measured each 36 seconds for 0.5 seconds.

Spectral peaks were automatically corrected for deviations in the lock mass. Extracted ion traces for relevant analytes were obtained in a 20 mDa window in their expected m/z-channels. These traces were subsequently smoothed and peak areas integrated with TargetLynx software. Signals of labelled analytes were corrected for naturally occurring isotopes. These calculated raw signals were adjusted for by median fold-change (MFC) adjustment. This is a robust adjustment factor for global variations in signal due to difference in tissue amounts, signal drift or evaporation. The MFC is based on the total amount of detected mass spectrometric features (unique retention time/mass pairs). The calculations and performance of the MFC adjustment factors are described in the following publications (Dieterle et al., 2006; Veselkov et al., 2011).

5.6.2 Analysis of metabolites from the methionine cycle

For extraction of metabolites of the Methionine cycle 500 µL ice cold methanol containing 200 mM acetic acid was added to the wells of the culture plates (6-wells-plate). The plates were left on dry ice for 15 minutes. Subsequently the extraction liquid was transferred from the wells to Eppendorf tubes and centrifuged at 3750 rpm at 4 °C during 30 minutes. 250 µL of the chilled supernatants were evaporated with a speedvac in approximately 1.5 h. The resulting pellets were resuspended in 150 µL water/acetonitrile (40/60 v/v/).

Samples were measured with an ultra-performance liquid chromatographic system (Acquity, Waters Inc., Manchester, UK) coupled to a Time-of-Flight mass spectrometer (SYNAPT G2, Waters Inc.). A 2.1 x 100 mm, 1.7 µm BEH amide column (Waters Inc.), thermostated at 40 °C, was used to separate the analytes before entering the MS. Mobile phase solvent A (aqueous phase) consisted of 99.5% water, 0.5% formic acid (FA) and 20 mM ammonium formate while solvent B (organic phase) consisted of 29.5% water, 70% ACN, 0.5% FA and 1 mM ammonium formate. In order to obtain a good separation of the analytes the following gradient was used: from 5% A to 50% A in 2.4 minutes in curved gradient (#8, as defined by Waters), from 50% A to 99.9% A in 0.2 minutes constant at 99.9% A for 1.2 minutes, back to 5% A in 0.2 minutes. The flow rate was 0.250 mL/min and the injection volume was 4 µL. All samples were injected randomly. After every 8 injections QC sample (pooled samples) was injected. The MS was operated in positive electrospray ionization mode in full scan (50 Da to 1200 Da). The cone voltage was 25 V and capillary voltage was 250 V. Source temperature was set to 120 °C and capillary temperature to 450 °C. The flow of the cone and desolvation gas (both nitrogen) were set to 5 L/h and 600 L/h, respectively. A 2 ng/mL leucine-enkephalin solution in water/acetonitrile/formic acid (49.9/50/0.1 %v/v/v) was infused at 10 µL/min and used for a lock mass which was measured each 36 seconds for 0.5 seconds. Spectral peaks were automatically corrected for deviations in the lock mass.

5.7 ROS MEASUREMENT ASSAY

Primary microglia were plated at a density of 40,000 cell/well on poly-L-lysine-coated 96-well plates (Thermofisher) and the cells were allowed to rest and settle for at least 24h before phagocytosis experiments. Phagocytosis assay was performed as previously described (see section **5.3**) and microglia was fed with apoptotic Vampire SH-SY5Y cells for 24h and 6h in a 1:3 proportion. Apoptotic cells were washed 5h after the exposure. 1h before the measurement the media was replaced and cells were incubated with CellROX (5 µM, Invitrogen) and the nuclear dye NucBlue (8µl/well, Invitrogen) added to phenol-free DMEM 10% FBS, 1% antimycotic-antibiotic, 2.5mM glucose, 1mM pyruvate in the incubator of the CellInsight CX7 Pro high-content screening system (ThermoFisher) at 37°C and 5% CO2. After incubation at least 3 images/well were taken at 644/665 nm were taken using a 40x (0.6 NA) Olympus objective for a maximum time of 2 hours. Images were analyzed using ImageJ software (https://fiji.sc/) and the mean intensity ROS fluorescence was measured in each image and normalized by the total count of microglial nuclei.

5.8 TRANSMISSION ELECTRON MICROSCOPY (TEM)

Three million primary microglial cells were cultured in poly-L-lysine coated 60mm diameter plates (Nunc, Thermofisher) and the cells were allowed to rest and settle

for at least 24h before phagocytosis experiments. Afterwards, phagocytosis assay was performed by adding apoptotic Vampire SH-SY5Y in a 1:1 proportion and washing them 1h after. 24h after adding the apoptotic cells, the plates were rinsed in PBS and pre-fixed as an adherent cell monolayer using 0.5% glutaraldehyde solution in Sörensen buffer (SB) 0.1M pH=7.4 (10 mins, RT). After scraping the pre-fixed cells, primary microglia were centrifuged (800g, 5 mins, RT) to form a pellet and fixed in 2% glutaraldehyde solution in SB (overnight, 4°C). Primary microglia were then rinsed with 4% sucrose in SB and post-fixed with 1% osmium tetroxide in SB (1h, 4ºC, darkness). After rinsing, primary microglia were dehydrated in a growing concentration series of acetone. After dehydration, primary microglia samples were embedded in epoxi resin EPON Polarbed 812 (Electron Microscopy Sciences). Semi-thin sections (1µm thick) were stained with toluidine blue to identify the regions of interest. Ultra-thin sections were cut using a LEICA EM UC7 ultramicrotome and contrasted with uranyl-acetate and lead citrate. The ultrastructural analysis was done with a Transmission Electron Microscope JeoJEM 1400 Plus at 100 kVs equipped with a SCMOS digital camera.

5.9 GLIOBLASTOMA (GBM) INDUCTION

Injections of what were performed using a stereotactic fixation device (Stoelting, Wood Dale, IL). Mice used for these experiments were adults ranging from 6 to 12 weeks old as previously utilized (Alcantara Llaguno et al., 2009; Hambardzumyan et al., 2009). Mice were anaesthetized with intraperitoneal (ip) injections of ketamine (0.1 mg/g) and xylazine (0.01 mg/g). For brain injections, one microliter of 4×10^4 transfected DF-1 cells in suspension was delivered using a 30-gauge needle attached to Hamilton syringe. A 1:1 mixture of cells and culture medium was used for co-injections. Locations were determined according to the coordinates in the mouse brain atlas (Franklin et al., 2019). Coordinates for SVZ injections were: AP-0mm from bregma, Lat-0.5 mm (right of midline), and depth-1.5 mm from the dural surface. Right frontal striatum coordinates were: AP-1.7 mm from bregma, Lat-0.5 mm (left or right), and depth-2 mm from the dural surface. Mice were monitored carefully and sacrificed when they displayed endpoint symptoms.

5.10 IRRADIATION

For the in vivo LCI model, fms-EGFP 2-month-old-mice were anaesthetized with 2.5% avertine (10 µl/gr) and exposed to X irradiation using a model YXLON SMART 200 tube (Yxlon International, Hamburg, Germany) at RT. Only the head of the animals was exposed to irradiation, while the rest of the body was covered with a lead blanket. The radiation was delivered as a single dose of 2 Gy at a dose rate of 0.92 Gy/min during a total time of 2 min 17 sec. The source-half-depth distance was initially calculated to obtain a constant dose rate of 0.92 Gy/min. After exposure mice were sacrificed at 6h, 24h, 3d, 7d and 30d by transcardial perfusion with 30ml of PBS followed by 30ml of 4% PFA. In the

double irradiation experiments, animals were sequentially exposed to a 2Gy X-ray cranial irradiation twice, 7 days apart, and were posteriorly sacrificed at 6h and 24h. Brain tissue was posteriorly processed for immunofluorescence and/or *in situ* hybridization.

For the irradiation of GBM, tumor bearing mice were monitored and irradiated when they started to display endpoint symptoms (approximately 2 months after the injection). Mice were anaesthetized with ketamine (0.1 mg/g) and xylazine (0.01 mg/g), and exposed to X irradiation using an X-RAD 320 from Precision X-Ray. Only the head of the animals was exposed to irradiation, while the rest of the body was shielded with a lead cover in a homemade apparatus. The radiation was delivered as a single dose of 10 Gy at a dose rate of 1.2 Gy/min during a total time of 8 min 33. After exposure, mice were sacrificed at 6h and 24h, by transcardial perfusion with 30ml of PBS followed by 30ml of 4% PFA. The tissue was posteriorly processed for immunofluorescence.

5.11 IMMUNOFLUORESCENCE AND IMMUNOHISTOCHEMISTRY

5.11.1 Primary microglial cultures and BV2

Primary microglial cultures were fixed for 10 min in 4% PFA and then transferred to PBS. Fluorescent immunostaining was carried out following standard procedures (Abiega et al., 2016; Beccari et al., 2018). Coverslips with primary microglial cultures were blocked in 0.1% Triton X-100, 0.5% BSA in PBS for 30 min at RT. The cells were then incubated with primary antibodies (**Table 1**) in blocking solution (0.1% Triton X 100, 0.5% BSA in PBS) overnight at RT, rinsed in PBS and incubated in the secondary antibodies containing DAPI (5 mg/ml) in the permeabilization solution for 1h at RT. After washing with PBS, primary cultures were mounted on glass slides with Dako Fluorescent Mounting Medium (Agilent).

5.11.2 Brain tissue sections

Mice were transcardially perfused with 30ml of PBS followed by 30ml of 4% PFA. The brains postfixed with the same fixative for 4h at RT, then washed in PBS and kept at 4°C. Six series of 50µm-thick sagital sections of mouse brains were cut using a Leica VT 1200S vibrating blade microtome (Leica Microsystems GmbH, Wetzlar, Germany). Fluorescent immunostaining was carried out following standard procedures (Sierra et al., 2010; Beccari et al., 2018). Free-floating vibratome sections were blocked in permeabilization solution (0.3% Triton-X100, 0.5% BSA in PBS; all from Sigma) for 2 hr at RT, and then incubated overnight with the primary antibodies (**Table 1**) diluted in the permeabilization solution at 4°C. For BrdU (bromodeoxyuridine), activated caspase 3 and Iba1(guinea pig) labelling an antigen retrieval procedure was performed by incubating in 2M HCl for 20min at 37°C and then washing with 0.1M sodium tetraborate for 15min at

RT (3 washes of 5min each) prior to the blockade of the sections. After overnight incubation with primary antibodies, brain sections were thoroughly washed with 0.3% triton in PBS. Next, the sections were incubated with fluorochrome-conjugated secondary antibodies and DAPI (5mg/ml; Sigma) diluted in the permeabilization solution for 2h at RT. After washing with PBS, the sections were mounted on glass slides with DakoCytomation Fluorescent Mounting Medium (Agilent).

For immunohistochemistry of activated-caspase 3 in GBM, mice were transcardially perfused with 30ml of PBS followed by 30ml of 4% PFA. 24h post-fixation, brains were embedded in 30% sucrose-DEPC treated until brain sink and frozen at -80ºC in O.C.T. Compound (Cell Path). 20µm sections were cut onto Superfrost Plus slides using a LEICA CM1950 Cryostat (Leica) and kept at -20ºC until use. The tissue was air-dried and antigen retrieval was performed by immersing the slides in a jar containing antigen retrieval buffer pH 6 (Vector labs) diluted in Milli-Q H_2O. The jar was inserted into a container with boiling water and the samples were maintained at 93ºC for 15-25min. Samples were put back to RT in an histology box and blocked in permeabilization solution (0.3% Triton X-100 (Sigma) and 5% normal goat serum in PBS) for 1h at RT followed by 3% H_2O_2 incubation for 30min. Slides are incubated in caspase 3 primary antibody (prepared in PBS) at 4ºC overnight. After overnight incubation with primary antibodies, slides were washed with 0.3% triton in PBS. Next, the sections were incubated with biotinylated goat anti-rabbit secondary antibody (prepared in PBS) for 1h at RT. Secondary antibody was washed with 0.3% triton in PBS. Biotin labeling was developed by incubating the samples with ABC solution (Avidin Biotin Complex Elite Kit; Vector labs) following manufactures instructions, followed by incubation with 3,3′-Diaminobenzidine tetrahydrochloride (DAB) (Sigma) diluted in Milli-Q H2O (the final solution must include 1.5% buffer stock solution, 1.5% H_2O_2 and 2% DAB solution). Samples were washed with 0.3% triton in PBS. Nuclei staining was developed by 1min incubation in hematoxylin solution (Sigma). After washing with PBS, the sections were mounted on glass slides with 100% glycerol (Sigma).

5.12 RNASCOPE IN SITU HYBRIDIZATION

To detect mRNA, RNAscope was performed on 4% PFA-DEPC treated fixed mice brains from control and mice exposed to LCI 24h and 7d. 24h post-fixation, brains were embedded in 30% sucrose-DEPC treated until brain sink and frozen at -80ºC in O.C.T. Compound (Cell Path). 20µm sections were cut onto Superfrost Plus slides using a LEICA CM1950 Cryostat (Leica) and dried at -20ºC for 2h and kept at -80ºC. RNAscope was carried out according to manufacturer's instructions with the following catalogue probes: Mm-Ifit3 (ACDBio, 508251) and Mm-Ms4a7 (ACDBio, 314601). The probe APOE (ACDBio, 313271) was used as a positive internal control. For the development of the fluorescent signal the fluorophore OPAL 570 dye (Akoya) was used. RNAscope was followed by immunofluorescence with anti-P2Y12.

Primary antibodies				
Brain tissue sections				
Primary	Host	Dilution	Source	Catalogue #
Activated caspase 3	Rabbit	1:1,000 (IFF) 1:250 (IHC)	Cell Signalling	9664
BrdU	Rat	1:500	Bio-Rad	MCA2060GA
CD68	Rat	1:600	BioRad	MCA1957
cFos	Rabbit	1:1,000	Santa Cruz	sc-7202
GFP	Chicken	1:1,000	Aves Lab	GFP-1020
γH2AX	Mouse	1:1,000	Millipore	05-636-25UG
Iba1	Rabbit	1:1,000	Abcam	019-19741
Iba1	Guinea pig	1:500	Synaptic systems	234 308
Ifitm3	Rabbit	1:250	Protein Tech	11714-1-AP
Ki67	Rabbit	1:750	Abcam	ab16667
P2Y12	Rabbit	1:1,000	AnaSpec	AS-55043A
Pu.1	Rabbit	1:400	Cell Signaling	#2258
Cell cultures				
Primary	Host	Dilution	Source	Catalogue #

DsRed	Rabbit	1:1000	Santa Cruz	Sc-33353
CD11b	Rabbit	1:500	Bio-Rad	MCA711G
GFP	Chicken	1:1000	Aves Lab	GFP-1020
Secondary	Host	Dilution	Source	Catalogue #
AlexaFluor 488 donkey anti-chicken	donkey	1:500	Fisher	17777517
AlexaFluor RRX donkey anti-rabbit	donkey	1:500	Jackson Immunology Research	711-295-152
AlexaFluor 647 donkey anti-rabbit	donkey	1:500	Jackson Immunology Research	711-605-152
AlexaFluor RRX donkey anti-rat	donkey	1:500	Jackson Immunology Research	712-005-153
AlexaFluor 488 goat anti-chicken	goat	1:500	Fisher	10286672
AlexaFluor RRX goat anti-rat	goat	1:500	Jackson Immunology Research	112-545-003
AlexaFluor 647 goat anti-rabbit	goat	1:500	Jackson Immunology Research	111-605-144
AlexaFluor 647 donkey anti-mouse	donkey	1:500	Fisher	A31571
Biotinylated Goat Anti-Rabbit IgG	goat	1:500	Abcam	ab64256

Table 1. List of antibodies used in this PhD thesis.

5.13 CONFOCAL IMAGING

All fluorescence immunostaining images were collected using a SP8 laser scanning microscope (Leica) or a Stellaris confocal microscope (Leica) using a 40X oil-immersion objective and a z-step of 0.7 µm for phagocytosis analysis, and a 63X objective and a z-step of 0.3 µM for mitochondrial morphology analysis. All images were saved in a Tiff format and used for further analysis in ImageJ. For the analysis of cells in cultures, 4 random images per coverslip were

acquired. For mouse tissue sections, at least 3 15-20 µm-thick z-stacks located at random positions containing the DG and CA were collected per hippocampal section, and a minimum of 6 sections per series were analyzed. Quantitative analysis of apoptosis and phagocytosis, was performed using unbiased stereology methods as previously described (Sierra et al., 2010).

5.14 IMAGE ANALYSIS AND QUANTIFICATION

5.14.1 Mitochondrial morphology

Mitochondrial confocal images taken in naïve or phagocytic microglia were analyzed adapting a preexisting protocol (Valente et al., 2017) during my Master Thesis (Márquez, 2018) with the aid of image analysis software ImageJ and Huygens. Mitochondrial images were deconvoluted with Huygens professional program (Scientific Volume Imaging) by using the Classic Maximum Likelihood Estimation algorithm (CMLE). Deconvolution parameters were established as 40 maximum iterations, signal to noise ratio 20, 0.05 of quality threshold, and optimized iteration mode. The analysis carried out with ImageJ started with background removal by using FIJI "substract background" tool. Additionally, cell-specific background was eliminated by substracting the cell nucleus intensity. Images were then converted to binary (black and white) by thresholding, where a foreground pixel is assigned the maximum value (255) and background pixels are assigned the minimum value (0). The "skeletonize" tool of FIJI allowed us to define the mitochondrial features of the original image ("skeleton") and it was analyzed using the plugin Analyze Skeleton 2D/3D (Arganda-Carreras et al., 2010). This plugin classified the spatial distribution of each skeleton pixel to measure the length of each branch and the number of them. Two types of mitochondrial structures were distinguished: individual mitochondria (unbranched) and mitochondria networks (branched). Individual mitochondria were defined as those objects in the image that did not contain junction pixels and were comprised of 1 or 0 branches (defined as a single point). Mitochondrial networks were defined as those objects which contained at least 1 junction pixel and were comprised of more than 1 branch. Based on this categorization, several parameters were determined in our images: the number of mitochondria and their length per cell; the number of branches per cell; and the number of junctions between branches per cell. The analysis with Huygens worked with deconvoluted images. First, out of focus and noisy stacks were removed with "crop" option. Then the image is opened with "object analyzer" tool and the values from the maximum intensity of the original image and the maximum intensity of the nucleus are selected to establish a threshold. Then "watershed segmentation" option was selected and a sigma value of 0.2 of was chosen. Objects smaller than 0.06µm^3 were removed by applying a 38-voxel equivalent size filter as they were not considered mitochondria. Finally, the following data from the mitochondrial objects resulting from the processing was extracted: nº of mitochondrial objects,

total and mean volume of objects, total and mean length of objects, and mean lateral width, axial width, roughness, sphericity and surface of objects.

5.14.2 TEM analysis

Image analysis was performed using ImageJ software . Mitochondria were identified manually, and their perimeter was selected to generate regions of interest (ROIs) in each image. The area of the cellular cytoplasm (μm²) was also identified and selected manually to generate a ROI in each image. Subsequently, the number following information about the mitochondrial ROIs was extracted: area, density, perimeter, circularity, ferret diameter, roughness, and solidity. Finally, the quantitative data coming from ROIs of the images belonging to the same cell were grouped and the number of per μm² was calculated dividing the number of mitochondria present in the cell by its cytoplasm area (μm²). The percentage of cytoplasm area occupied by mitochondria per each cell was calculated by summing up the areas of individual vesicles and relating it to the cellular cytoplasmic area, which was considered 100%.

5.14.3 Phagocytosis analysis

In brain tissue sections, the number of apoptotic cells, phagocytosed apoptotic cells and the density of microglial cells were quantified using ImageJ image analysis software. The quantification was estimated per volume by using the DG contained in the z-stack (by multiplying the thickness of the stack by the area of the DG at the center of the stack). The estimation per hippocampus was only performed in brain tissue sections. For that purpose, the estimation per volume was multiplied by the volume of the septal hippocampus (spanning from -1mm to -2.5 in the AP axes, from Bregma), which was calculated by taking pictures of the last 6-7 brain slices cut with the vibratome, where the septal hippocampus is contained, with an epifluorescent microscope (Zeiss Axiovert) at 20X. To calculate the phagocytosis parameters, the following formulas were used (Beccari et al., 2018).

Ph Index: Proportion of apoptotic cells engulfed by microglia. Phagocytosed apoptotic cells (apo^{Ph}); total apoptotic cells (apo^{tot}).

$$\text{Ph index}=\frac{\text{apo}^{\text{Ph}}}{\text{apo}^{\text{tot}}} \text{ X } 100$$

Ph capacity: proportion of microglia with one or more phagocytic pouches, each containing one apoptotic cell (Sierra et al., 2010). Microglia (mg); microglia with one or more phagocytic pouches (Phn).

$$\text{Ph capacity}=\frac{\text{mgPh1+ mgPh2+ mgPh3 } \ldots nmgPhn}{\text{mg}}$$

Ph/A coupling: Phagocytosis/Apoptosis coupling: net phagocytosis (number of microglia multiplied by their phagocytic capacity) divided by the number of apoptotic cells (Abiega et al., 2016).

$$\text{Ph/A coupling}=\frac{\text{Ph } capacity\ x\ microglia}{\text{apo}^{tot}}$$

5.14.4 γH2AX analysis

For the analysis of DNA damage, γH2AX nuclear staining was analyzed within nuclear DAPI and Pu.1 staining. 2-3 images from 6-7 brain slices were analyzed using a homemade ImageJ Macro. The Macro extracted the values for the total volume of nuclei (DAPI staining), the total volume of microglia nuclei (Pu staining) and the total volume of double-strand breaks (DBS) (γH2AX staining). Finally, the values of the % volume occupied by γH2AX in both DAPI and Pu.1 were extracted as indicators of overall nuclear damage and microglia damage, respectively. The number of γH2AX+ cells, which represented those cells that had their entire nucleus occupied by γH2AX staining, were manually quantified and finally the number of γH2AX/mm3 cells was extracted.

5.14.5 Monocyte infiltration analysis

To quantify monocyte infiltration, we analyzed 2-3 images from 6-7 brain slices. Manual counting was carried out for both microglia cells (GFP+/P2Y12+) and monocytes (GFP+/P2Y12-). Subsequently, the percentage of GFP+ cells identified as microglia and monocytes was determined.

5.14.6 In situ validation of scRNA-seq analysis

For the analysis of MS4A7 and IFIT3 probes using RNAScope, 2-3 images from 6-7 brain slices were analyzed, with an average of 38 total cells analyzed per experimental condition. The labeling of MS4A7 and IFIT3 probes was visually inspected and microglial cells were classified as $MS4A7^{+}$ or $MS4A7^{-}$ and $IFIT3^{+}$ or $IFIT3^{-}$. Subsequently, total microglia were manually counted and the % MS4A7+ and IFIT3+ microglia were extracted. In all RNAscope procedure reactions, both positive (ApoE) and negative (DapB) controls were included.

The assessment of CD68 and Gal-3 expression using immunofluorescence was conducted using at least 3 images from 6-7 brain slices. For CD68 labeling, cells were considered $CD68^{+}$ microglia if they exhibited >5% of their cytoplasm labeled with CD68, as measured by a homemade volumen colocalization macro. Once $CD68^{+}$ microglia were identified, the percentage of $CD68^{+}$ microglia relative to the total number of microglia was determined. For Gal-3 labeling, microglia expressing Gal-3 were classified as Gal-3^{+} microglia, and the percentage among

all microglia was calculated. Additionally, Gal-3$^+$ microglia were classified based on low (intensity values 0-85), medium (intensity values 85-170), and high (intensity values 170-255) expression levels to assess changes in protein expression levels.

Both Ki67$^+$ microglia and BrdU$^+$ microglia analysis was performed using unbiased stereological methods as previously described in (Beccari et al., 2018). In brief, microglial cells labeled with Ki67 or BrdU were quantified from 2-3 images of 6-7 and the volume estimate was multiplied by the volume of the septal hippocampus (ranging from -1mm to -2.5 in the AP, Bregma axes), which was calculated by imaging the last 6-7 brain slices cut with the vibratome, where the septal hippocampus is contained, with an epifluorescent microscope (Zeiss Axiovert) at 20X.

5.15 SINGLE CELL RNA- SEQUENCING

WT 2-month-old-mice were anaesthetized with 2.5% avertine (10 µl/gr) and exposed to 2Gy X-ray cranial irradiation. After exposure mice were sacrificed at 24h and 7d by a terminal dose of avertine (20 µl/gr) and posteriorly perfused with PBS 1X. The hippocampi were extracted with a scalpel and 6 hippocampi per group (3 animals) were pooled in a 2ml tube with a mixture of DNase (50ug/ml) and papain (2mg/ml) dissolved in DPBS (Dulbecco's Phosphate-Buffered Saline ,HyClone). Then, EDTA (10µl/tube) was added and tubes were placed on the Stuart S83 Rotator for shaking at 11 rpm at 37°C for 30 minutes. The rest of the procedure was performed cold (4°C). Subsequently, the samples were homogenized with a Pasteur pipette. The resulting cell suspension was filtered through a 70µm cell strainer (BD Bioscience) and transferred to a 15 ml tube filled with 1 ml DPBS. After. 1 mL DPBS was added and centrifuged at 300 g for 10 min. After centrifugation, the supernatant was discarded and 1 ml of Percoll 25% (Cytiva) was added for myelin removal. After resuspension, cells were transferred to a 1.5 ml tube for centrifugation at 1000 g (full acceleration, full brake) at RT for 10 min. The myelin was removed, discarding the supernatant and the cells were resuspended and incubated for 15 min at 4ºC in 90µl of cytometry buffer and 10µl of anti-CD11b microbead solution (Miltenyi Biotec). 1 ml of cytometry buffer was added and centrifuged at 300 g for 10 min. The supernatant was removed and cells were resuspended in 500µl cytometry buffer in a 15ml Falcon tube for magnetic separation of CD11b$^+$ cells using AutoMACS (posseld and rise options) (Miltenyi Biotec). CD11b$^+$ cells were resuspended at a concentration of 1,200 cells/µl for further preparation.

Cells were encapsulated using the Chromium Next GEM Chip microfluidic chamber (10X Genomics) and the corresponding libraries were subsequently generated with Chromium Controller and Single Cell Gene Expression 3´ according to the Chromium Next GEM Single Cell reagent kits user guides. 3´ Reagent Kits v3.1. The quality and quantity of the libraries were checked with a

high sensitivity DNA kit (Agilent Technologies) on a BioAnalyzer 2100 (Agilent Technologies). Sample processing for encapsulation and analysis was conducted in CIMA (University of Navarra) by Leyre Ayerra and Amaia Vilas with the collaboration and support of Marysol Aymerich.

5.15.1 Bioinformatic analysis of scRNA-seq

10x-barcoded sequencing libraries were generated using 10x Single Cell 3' v3 kits (10x Genomics, inc.) and sequenced to about 300M/sample (control 24h (Ctrl24h): 316.580.458; control 27d (Ctrl7d): 297.113.513; irradiated 24h (irr24h): 305.341.402; irradiated 7d (irr7d): 338.536.344). Raw FASTQ from gene expression libraries were aligned on the mm10-2020-A mouse genome and processed using CellRanger Count (10X Genomics Cell Ranger v5.0.1) with default parameters. We retrieved 15745 cells in Ctrl24h, 16704 in Ctrl7d, 14295 in Irr24h, and 18601 in Irr7d. Sequencing depth was between 17.787 and 21.360 read pairs per cell, with sequencing saturation between 44.4% and 52.2%. Multiplet artifacts were removed using Scrublet v0.2.3 python package (Wolock et al., 2019) (python v3.7.10 (Van Rossum et al., 2009) (with default parameters. Upon doublet removal, we retrieved 15397 cells in Ctrl24h, 15949 in Ctrl7d, 13813 in Irr24h, and 18069 in Irr7d. All subsequent single cell transcriptomics analyses were performed using R Statistical Software (v4.0.5) and the Seurat V4 (v4.1.1) package (R Core Team, 2013; Hao et al., 2021).

For quality control, genes expressed in fewer than 3 cells were removed. All cells with unique feature counts (detected genes) over 4500 or less than 1300 were excluded. Finally, cells with more than 5% mitochondrial counts were filtered out. The remaining cells, 45,249 high quality cells (10,955 cells in control 24h, 11,801 in control 7d, 9,281 in LCI 24h, and 13,212 in LCI 7d), were then used for downstream analyses. For each sample, UMI (Unique Molecular Identifier) count data were normalized using a regularized negative binomial regression with SCTransform (sctransform 0.3.3). SCTransform was executed with the additional flags vst.flavor="v2" to invoke the v2 regularization and method="glmGamPoi" to fit a Gamma-Poisson Generalized Linear Model which improves the speed of the learning procedure. Furthermore, we regressed out mitochondrial content in a second non-regularized linear regression. Next, to ensure that the sctransform residuals for the top variable genes across all samples are computed, we used the functions SelectIntegrationFeatures with nfeatures=3000 (getting the top 3,000 highly variable genes (HVGs) across all the samples) and PrepSCTIntegration (recomputing the residuals for missing values across the previous 3,000 HVGs using the stored model parameters). Then the four Seurat objects were merged into a single object that contains all the 45,249 high quality cells with all the needed values calculated in the SCT assay, the default assay for the downstream analysis. Principal Component Analysis was performed on top 3,000 HVGs to reduce dimensionality of the dataset. Non-linear dimensional

embedding was performed using Uniform Manifold Approximation and Projection (UMAP) on the 30 most significant dimensions of the PCA. PrepSCTFindMarkers was performed on the merged object prior differential expression testing on the SCT assay. Shared Nearest-Neighbor (SNN) graph was constructed using FindNeighbors function on the 30 most significant principal components (PCs), and cell clusters were identified using FindClusters. Differentially expressed genes between clusters were obtained by Seurat-implemented Wilcoxon rank sum tests with default parameters. Module enrichment score (AddModuleScore with default parameters) was performed using gene signature from Marsh (Marsh et al., 2022a) to identify microglia cells. Populations showing low scores for microglia markers, macrophages and non-myeloid cells, were filtered out. Microglia cells were then scored for micro/myeloid shared activation score gene list from Marsh et al., (Marsh et al., 2022a) using AddModuleScore function with default parameters. This analysis led to the identification of a cluster of activated microglia cells that was present in all the samples, probably due to enzymatic digestion-based isolation of microglia (see above). Microglia a reactive profile resulting from the dissociation procedure were removed and UMAP was recomputed using previous 30 most significant PCs on the remaining 32,591 high quality cells (8,453 cells in Ctrl24h, 8,961 in Ctrl7d, 6,282 in Irr24h, and 8,895 in Irr7d). PrepSCTFindMarkers function was used prior to differential testing on the SCT assay, using FindAllMarkers to identify enriched genes detected in at least 25% of the cells in a given subpopulation or in the rest of microglia, with all other parameters at default values. Differentially expressed genes in response to LCI for each microglia cluster were obtained by Seurat-implemented Wilcoxon rank sum tests (FindMarkers function with logfc.threshold = 0.1). The analysis was performed by Ángel Márquez and José Pascual López Atalaya.

5.15.2 Functional enrichment analysis

The Database for Annotation, Visualization and Integrated Discovery (DAVID) (https://david.ncifcrf.gov/) v6.8 provides a comprehensive set of functional annotation tools to understand biological meaning behind large list of genes. DAVID was used to generate a gene-GO term enrichment analysis that identified enriched biological themes and to highlight the most relevant GO terms associated with the array gene list. The generated gene lists were inserted in DAVID website and of rsq> 0.9 was used for this gene profile analysis. The analysis of each expression pattern was performed separately and only terms with an adjusted p-value (Benjamini-Hochberg) > 0.05 were considered significant.

5.16 STATISTICAL ANALYSIS

SigmaPlot (San Jose, CA, USA) and GraphPad Prism (San Diego, CA, USA) were used to perform the statistical analysis. Data was tested for normality and

homocedasticity. When the data did not comply with these assumptions, a logarithmic transformation (Log10, Log10+1, of Ln) or a square root was performed, and the data was analyzed using parametric tests. Two-sample experiments were analyzed by Students' t-test and more than two sample experiments with one-way or two-way ANOVA. In case that homoscedasticity or normality were not achieved with a logarithmic transformation, data were analyzed using a Kruskal-Wallis ranks test, followed Dunn method as a posthoc test. Two sample non-parametric data was analyzed using Mann Whittney U test. Only $p < 0.05$ is reported to be significant.

The equipment and processing software used are summarized and below (**Table 2**).

Resources	
Equipment	Source
Leica Stellaris 5 (DM6 B CS)	Leica
Leica TCS STED CW SP8	Leica
Carl Zeiss ApoTome2	Zeiss
Automated digital slide scanner Pannoramic MIDI II	3DHistech
ThermoFisher CellInsight CX7	Thermo Fisher
Seahorse XFe96 – Extracellular Flux Analyzer	Agilent
Software	Source
Image J (Fiji)	https://imagej.nih.gov/ij/
Huygens	https://svi.nl/Huygens-Software
SigmaPlot	https://sigmaplot.co.uk/index.php
GraphPad Prism	https://www.graphpad.com

Table 2. Summary of equipment used in this PhD thesis.

6. RESULTS

6. RESULTS

6.1: Validation of the *in vivo* model of "superphagocytosis"

Phagocytosis of apoptotic cells by microglia is crucial to ensure proper elimination of toxic debris from the brain parenchyma. This process occurs quickly and efficiently and avoids tissue damage produced by the spillover of cytotoxic content that result from cell death. However, phagocytosis is not a terminal process and leads to multiple transcriptional changes in microglia that affect surrounding cells (Diaz-Aparicio et al., 2020). To further examine the implications of phagocytosis-induced changes in microglia we used a previously developed *in vitro* model of phagocytosis (Diaz-Aparicio et al., 2020), and here we developed an *in vivo* "superphagocytosis" model that consisted of using low-cranial irradiation (LCI) to induce apoptosis and boost phagocytosis. Irradiation prominently affects proliferating cells (Jiao et al., 2022), such as radial neural stem cells (rNSCs) and their daughter cells, the newborn granule cells (NGCs), which are located in neurogenic niches such as the subgranular zone (SGZ) of the hippocampal DG (Ehninger et al., 2008). In the past, we showed that irradiation (8Gy) induces neuroprogenitor apoptosis and microglial phagocytosis in the DG (Beccari et al., 2023). In this PhD Thesis we reduced the dose to 2Gy, which is 15-25 times lower than the dose used in antitumor treatments in mice (Gan et al., 2016), to reduce damage to non-proliferative cells and minimize side effects.

This *in vivo* model of "superphagocytosis" allowed us to analyze transcriptional and functional changes in phagocytic microglia *in vivo* microglia, which complemented the data obtained from the *in vitro* model. In this section, we introduced the *in vivo* "superphagocytosis" model and showed that microglia are synchronized in a phagocytic stage, specifically in the DG. We also determined whether LCI induced microglial DNA breaks and monocyte extravasation.

6.1.1. Microglia becomes "superphagocytic" in the DG after LCI.

We studied the effects of irradiation in apoptosis and microglial phagocytosis and observed an increase in apoptotic cells expressing activated caspase 3, which is cleaved during apoptotic process and label apoptotic cells, specifically located in the SGZ of the DG 6h after the exposure (**Figure 8**). Next, we compared control (non-irradiated) mice with mice euthanized at different time points after LCI (6h, 24h, 3d, 7d and 30d) (**Figure 9A**) and performed immunofluorescence and confocal imaging to observe microglia, expressing the green reporter EGFP under the Csf1r (colony stimulating factor 1 receptor) promoter (fms-EGFP mice); and apoptotic cells, with abnormal nuclear morphology (pyknosis, karyorrhexis) using the DNA stain, 4'-6-diamidino-2-phenylindole (DAPI). To facilitate the identification of apoptotic cells and microglia, activated caspase 3 and the nuclear microglial marker Pu.1 were also used, respectively (**Figure 9B, C**).

LCI induced increased apoptosis at 6h in the SGZ of the DG, determined by an increase in both pyknotic/karryorhectic cells and cells expressing activated

caspase-3 (**Figure 8**, **Figure 9B, D**). The majority of these cells were engulfed by microglial processes, which formed 3D phagocytic pouches around them (**Figure 9C**), as shown by the Ph index (% of apoptotic cells engulfed by microglia). In control mice, microglia phagocytosis was very efficient (Ph index 93.6 ± 2.7%), but it was slightly reduced by 6h after LCI (75.7 ± 2.5%), (**Figure 9E, F**), likely because of the large number of apoptotic cells. At 6h microglia counteracted the augmented apoptosis increasing their total phagocytic capacity (mean phagocytic pouches per microglia). Whereas in control conditions only 9.1 ± 1.5% of microglia was phagocytic, by 6h 83.1 ± 14.9% of microglia had become phagocytic, and each cell contained 1-6 phagocytic pouches (**Figure 9C,G,H**). This active, synchronized phagocytosis led to effective clearance and by 24h the apoptotic cells induced by LCI had disappeared from the DG (**Figure 9B-D**). These numbers also provide a rough estimate of the clearance time of 46.4 ± 8.5 min per cell, calculated as the ratio of apoptotic cells between 6h and 24h, multiplied by the time interval (18h) and the number of phagocytic pouches per microglia at 6h (Ph capacity) (**Figure 9I**). At later time points (3d-30d), apoptosis and phagocytosis returned to basal levels (**Figure 9D-H**), confirming that the LCI caused massive generation of apoptotic cells and their subsequent phagocytosis.

All combined, these data suggest that LCI induced apoptosis and synchronized microglia in a phagocytic stage by 6h. These cells rapidly and efficiently removed apoptotic debris from the hippocampal parenchyma, becoming post-phagocytic after 24h. Therefore, this “superphagocytosis” model allowed us to analyze how phagocytosis impacts microglia. Next, we determined whether apoptosis and phagocytosis were restricted to the DG and the post-phagocytosis changes induced in microglia.

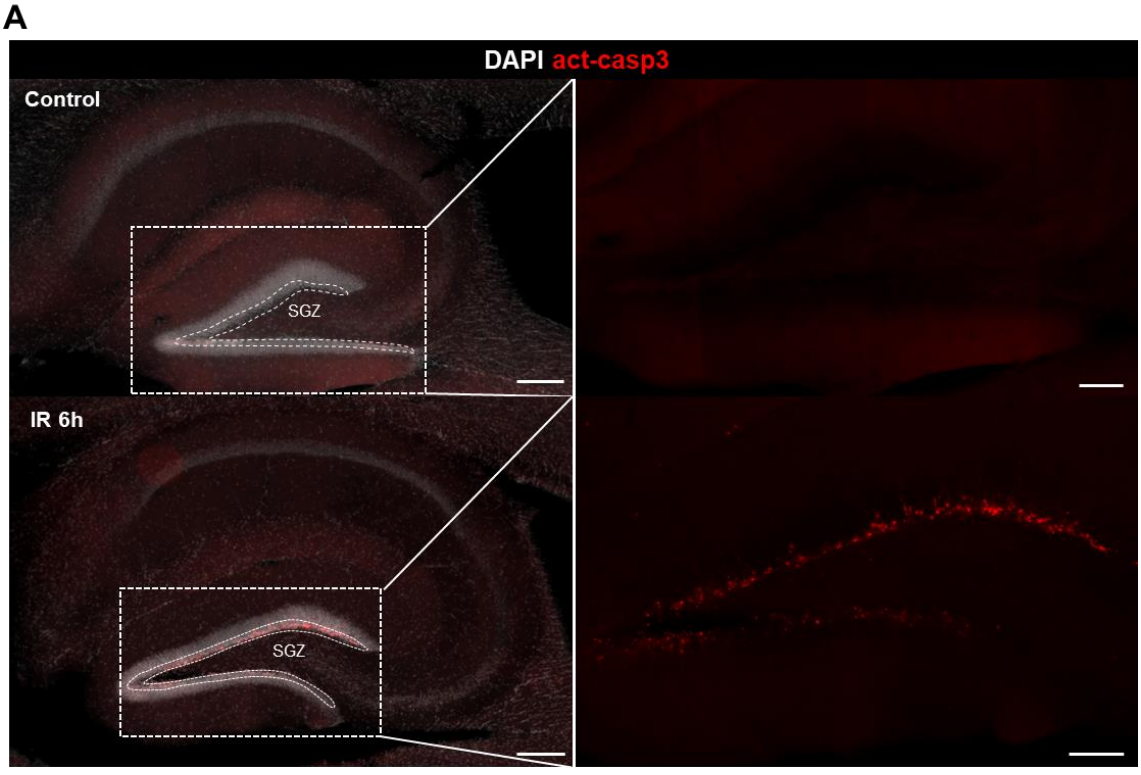

Figure 8. Induction of apoptosis in the neurogenic niche of the hippocampus after LCI. ***(A)*** *Representative image of the hippocampus in control condition and 6h after LCI showing DAPI (white) and activated caspase 3 (act-casp3, red). The right panel shows*

a higher magnification of apoptotic cells in the SGZ (indicates using a dotted line) of the hippocampus. Scale bars= 200μm, [insert, 100μm], z=1μm.

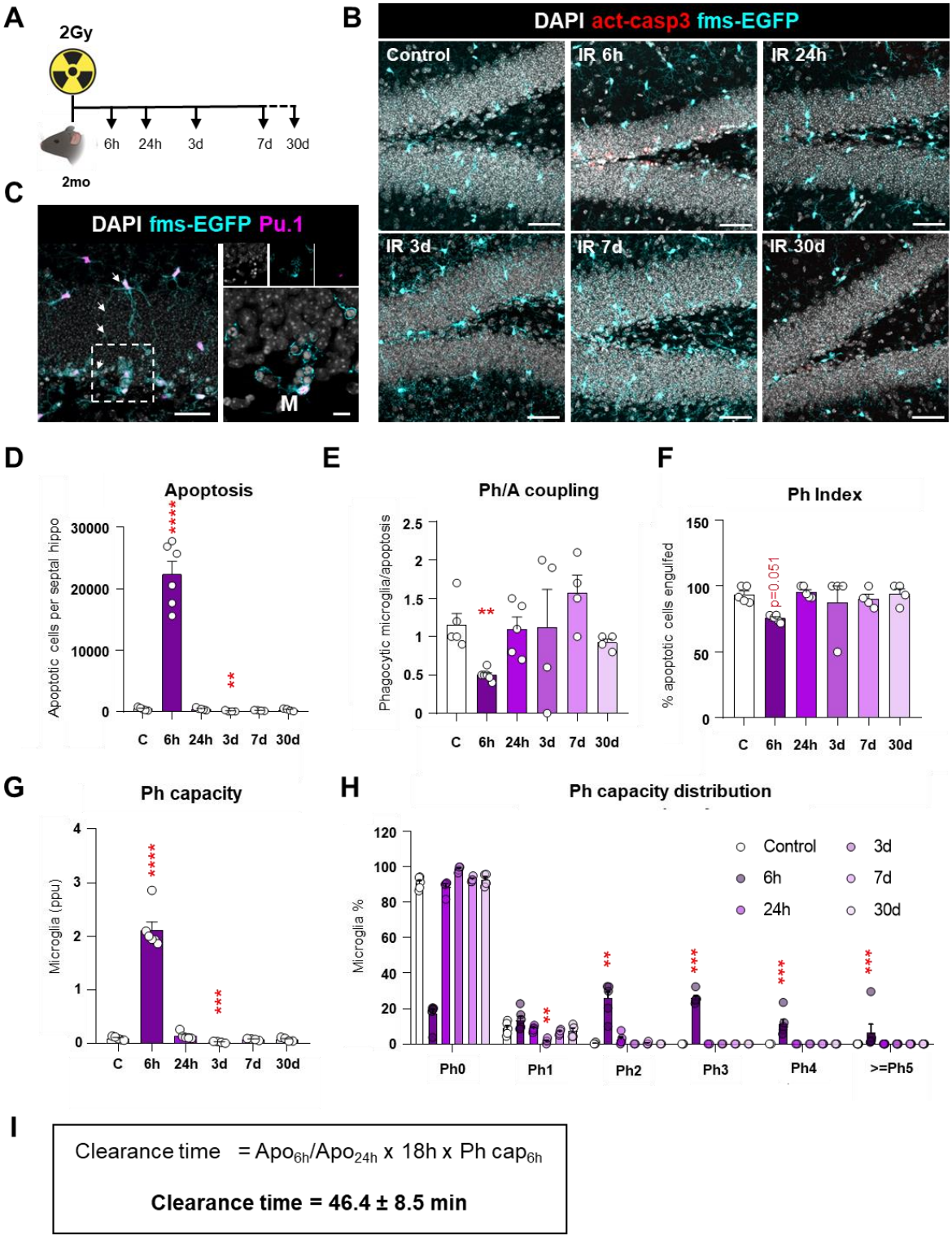

Figure 9. In vivo model of "superphagocytosis" driven by Low Cranial Irradiation (LCI). ***(A)*** *Experimental design of "superphagocytosis" by LCI.* ***(B)*** *Representative confocal images of the different experimental conditions (Control, 6h, 24h, 3d, 7d, 30d) showing DAPI (white), activated caspase 3 (red) y GFP (cyan) staining.* ***(C)***

Representative images of "superphagocytic" microglia 6h after LCI showing DAPI (white), Pu.1 (magenta) y GFP (cyan) staining. ***(D)*** *Number of apoptotic cells in the DG per septal hippocampus.* ***(E)*** *Ph/A coupling in fold change (net phagocytosis with respect to total levels of phagocytosis).* ***(F)*** *Ph index (% of apoptotic cells phagocytosed by microglia)* ***(G)*** *Weightened Ph capacity (number of phagocytic pouches filled with apoptotic nuclei per microglia) in parts per unit (ppu).* ***(H)*** *Ph capacity (% of microglia containing phagocytic pouches) at several time-points after LCI (Control, 6h, 24h, 3d, 7d, 30d)* ***(I)*** *Clearance time showing the mean time in which microglia removes an apoptotic cell. Bars show mean ± SEM of n=4-6 mice. Data was analyzed by one-way ANOVA followed by Holm-Sidak post hoc tests when appropriate. Some data [D, E, G, H] was Log transformed to comply with homoscedasticity. When homoscedasticity was not accomplished Kruskal-Wallis test was performed [F, H]. Asterisks represent significance between control and LCI (6h, 24h, 3d, 7d, 30d). ** represents p<0.01, *** represents p<0.001. Scale bars= 50μm [B], 20μm [C], 10μm (inserts in [C]); z=21μm, z=17.5μm, z=25.2μm, z=13.3μm, z=16.1μm, z=14.7μm [B], z=13.3μm [C], z=4.2μm (inserts in [C]). Created with BioRender.com.*

6.1.2. Phagocytic microglia is specifically located in the DG.

As previously observed, LCI-induced apoptosis concentrated in the neurogenic niche located in the SGZ of the DG. To further examine whether LCI caused apoptosis in non-neurogenic hippocampal regions, we next focused on the CA (Cornu Ammonis) at 6h after LCI and used immunofluorescence and confocal imaging to observe microglia expressing GFP, and apoptotic cells using DAPI (**Figure 10A**).

We found that after LCI there was a small induction of apoptosis in CA (**Figure 10B**), but it was nonetheless not comparable with that of the DG, which was 26.3 ± 2.3 times larger than in CA after LCI (**Figure 9D & Figure 10B**). In CA, phagocytosis did not occur in control mice and by 6h after LCI the Ph index was 2.7 ± 0.6 times smaller than in the DG. (**Figure 9D & Figure 10C**). Importantly, the percentage of phagocytic microglia was 28.9 ± 10.3 times smaller in CA, representing only 4.0 ± 1.5% of microglia (**Figure 9H & Figure 10D**). All together, these data showed that LCI caused less apoptosis in CA than in the DG, and that CA microglia were less efficient phagocytosing apoptotic debris than their DG counterparts, suggesting that in this non-neurogenic region cells were less susceptible to die and microglia were less trained to phagocytose. Thus, we confirmed that phagocytic microglia were largely located in the hippocampal DG. Therefore, in the following sections we compared microglia in the DG and the CA to discriminate the changes induced by irradiation (occurring in both DG and CA) from those induced by phagocytosis (specific of the DG).

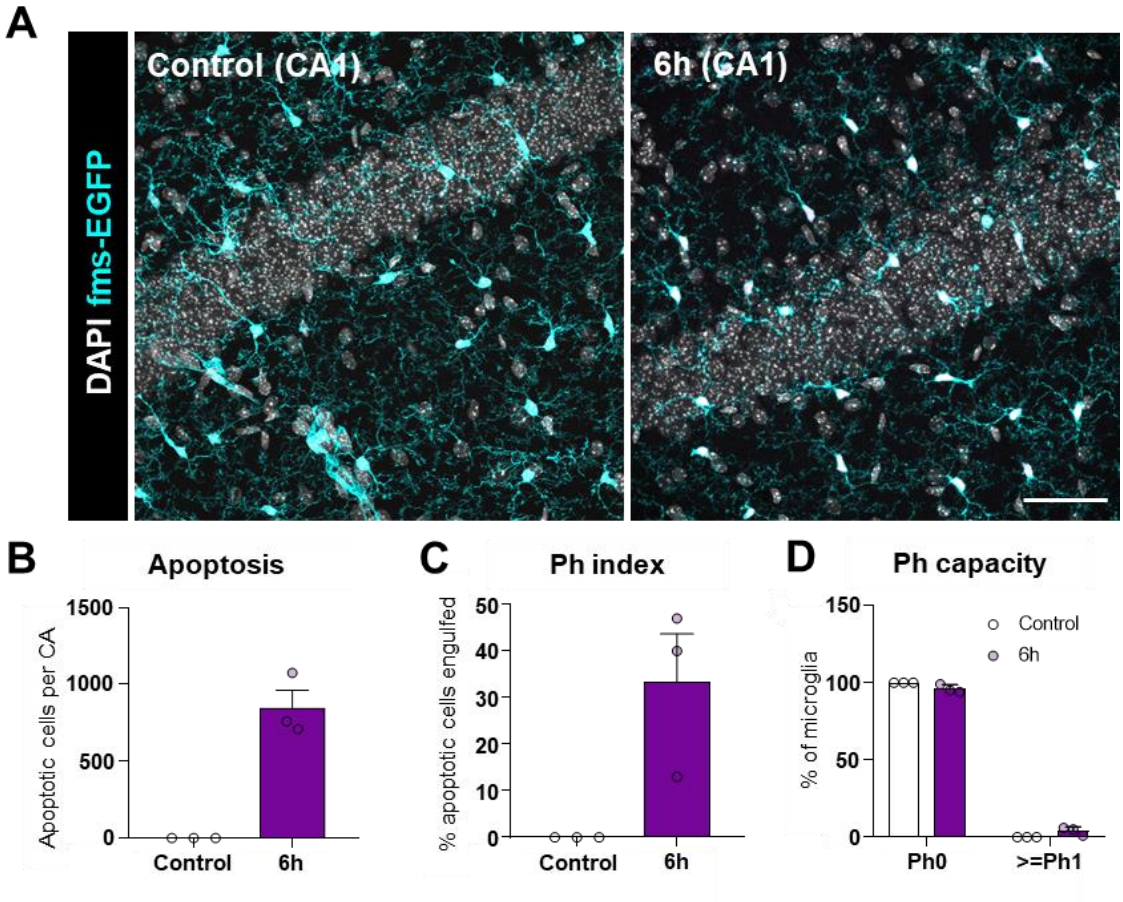

Figure 10. Analysis of phagocytosis in CA region in control at 6h after LCI. ***(A)*** *Representative confocal images of CA at different experimental conditions (Control and 6h) showing DAPI (white) and GFP (cyan) staining.* ***(B)*** *Number of apoptotic cells in the CA per septal hippocampus.* ***(C)*** *Ph index (% of apoptotic cells phagocytosed by microglia).* ***(D)*** *Ph capacity (% of microglia containing phagocytic pouches) at Control and 6h after LCI. When homoscedasticity was not accomplished [B, C, D] Mann Whitney test was performed. Bars show mean ± SEM of n=3 mice. Scale bars= 50μm [A], z=14μm, z=21μm.*

6.1.3 LCI does not cause DSBs in microglia.

Next, we assessed whether LCI damaged microglia by inducing DNA double-strand breaks (DBS). We analyzed the expression of phosphorylated histone H2AX, also known as gamma-H2AX, to identify DSBs caused by irradiation (Kavanagh et al., 2013). For this purpose, we performed immunofluorescence and confocal imaging to observe γH2AX in all nuclei (labeled with DAPI) or within microglial nuclei (labeled with Pu.1). We found two patterns of expression: γH2AX$^+$ nuclei, which represented severely damaged cells; and nuclei with γH2AX puncta, which represented less damaged cells (Scarpato et al., 2013). Both the number of γH2AX$^+$ nuclei and the volume of nuclei with γH2AX puncta increased at 6h, decreasing at later time-points (**Figure 11A,C**). Importantly, none of the γH2AX$^+$ nuclei belonged to microglia (identified with Pu.1) and we only found a small volume of γH2AX puncta in microglial nuclei, which was 7.2 ± 1 times smaller than the rest of the nuclei in the DG (**Figure 11B,E**). This data suggests that LCI caused robust DNA damage on DG nuclei, but a much residual

damage on microglial DNA, likely because microglia are quiescent and do not proliferate in physiological conditions (Reu et al., 2017). Thus, we confirmed that LCI is a good model to study changes induced by phagocytosis with minimal effects of irradiation on microglia.

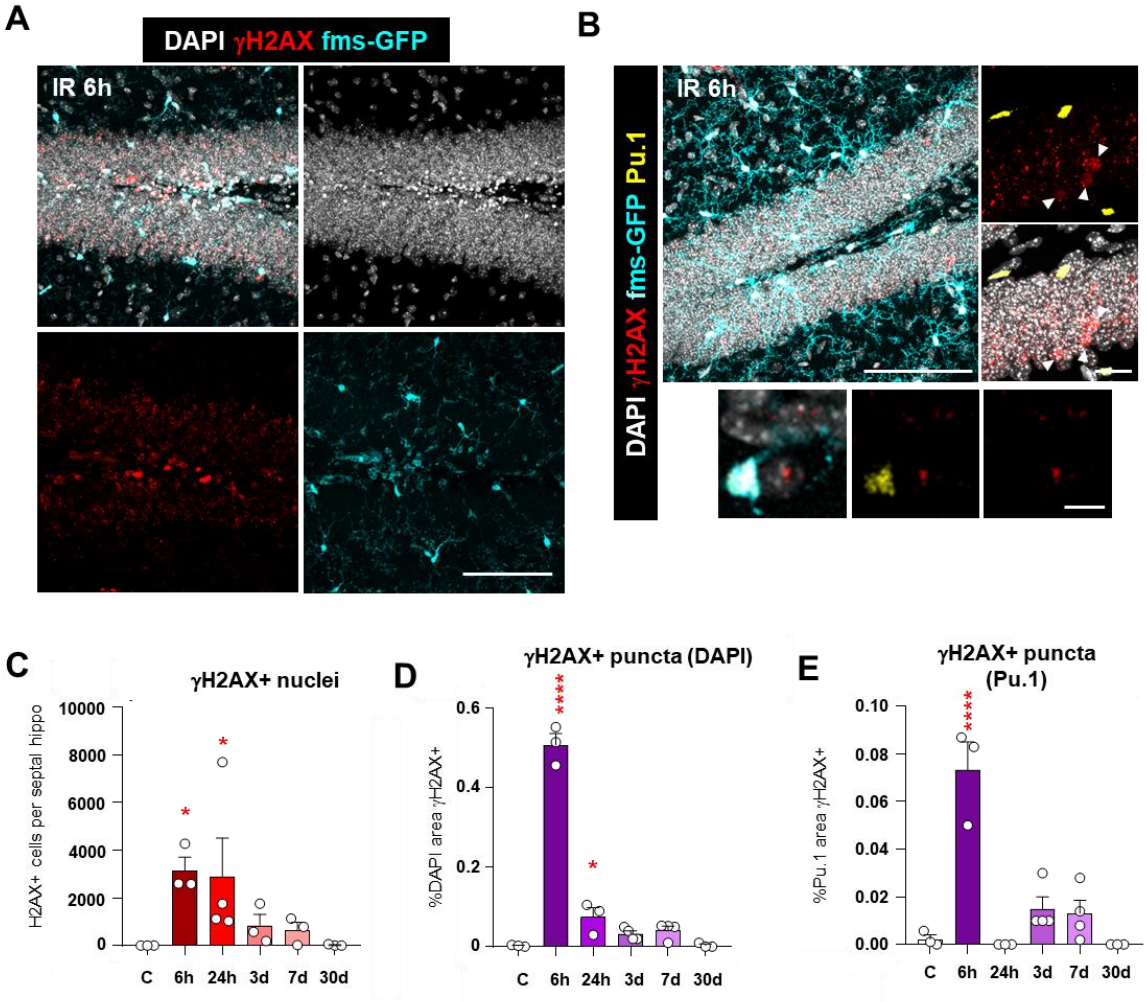

Figure 11. Analysis of DNA damage by assessing DSB ***(A)*** *Representative confocal images of γH2AX puncta at 6h after LCI showing DAPI (white), γH2AX (red) and GFP (cyan) staining.* ***(B)*** *Representative images of nuclei γH2AX+ cells (red) indicated with white arrowheads and non-microglial DAPI (white) and microglial nuclei containing DAPI and Pu.1 (white and yellow). Microglia is shown with GFP (cyan) staining.* ***(C)*** *Number of γH2AX+ cells in the DG per septal hippocampus.* ***(D)*** *Percentage of nuclear volume (DAPI) occupied by the puncta of γH2AX.* ***(E)*** *Percentage of microglial nuclear volume (Pu.1) occupied by the puncta of γH2AX. Bars show mean ± SEM of n=3-4 mice. Data was analyzed by one-way ANOVA followed by Holm-Sidak post hoc tests when appropriate. When homoscedasticity was not accomplished Kruskal-Wallis test was performed [C]. Asterisks represent significance between control and LCI (6h, 24h, 3d, 7d, 30d). * represents p<0.05, *** represents p<0.001. Scale bars= 100μm [A], 100μm [B], 20μm, 10μm (inserts in [C]); z=16.8μm [A], z=26.6μm, z=0.7μm [B].*

6.1.4 LCI does not cause monocyte infiltration.

To further assess the extent of LCI-induced damage, we assessed monocyte infiltration, because ionizing radiation is known to compromise the integrity of the blood-brain barrier (BBB) (Trnovec et al., 1990). Since in our fms-EGFP mice both microglia and macrophages express GFP, we discriminated between these two populations performing immunofluorescence for GFP and for the microglial-specific marker P2Y12 (Paolicelli et al., 2022). We observed that irradiation did not increase the percentage of monocytes (GFP+/P2Y12-) at any time-point after LCI (**Figure 12A-B**), suggesting that there was not monocyte infiltration after LCI.

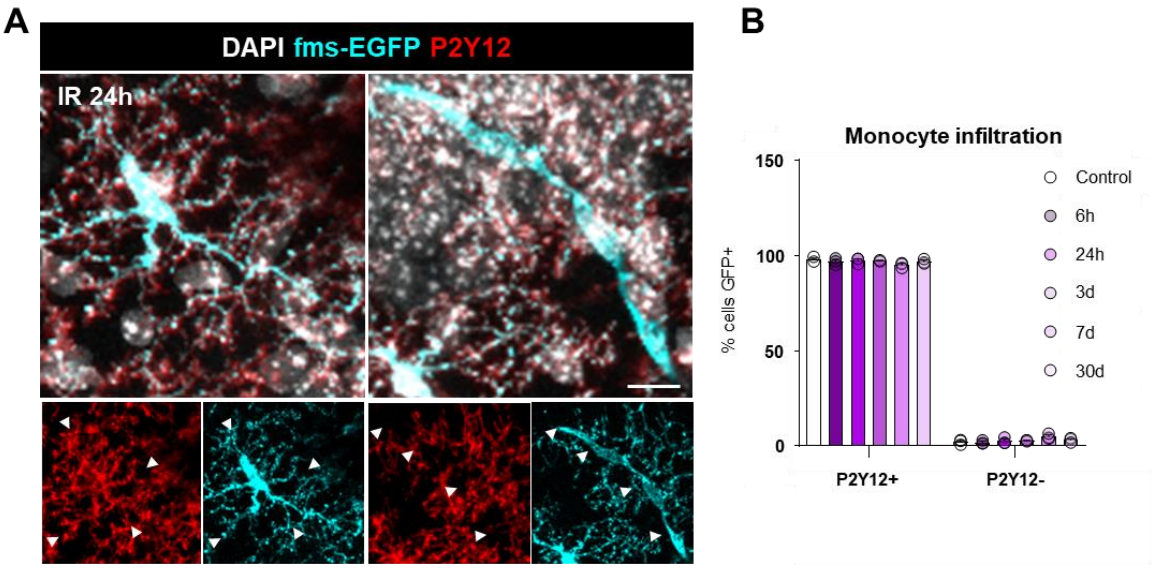

Figure 12. Analysis of monocytic infiltration after LCI. ***(A)*** *Representative confocal images microglia and monocyte at 24h after LCI. Microglia is labelled with both P2Y12(red) and GFP (cyan), while monocytes only express GFP (cyan). DAPI (white) staining shows nuclei. Cells are indicated with white arrowheads.* ***(B)*** *Percentage of GFP+ cells that are microglia (GFP+/P2Y12+) and that are monocytes (GFP+/P2Y12-). Bars show mean±SEM of n=3 mice. Scale bar 10μm; z= 17,5μm.*

In summary, the *in vivo* model of "superphagocytosis" is a valid model to study post-phagocytic changes in microglia because it synchronized DG microglia in a phagocytic stage, causing minimal microglial DNA damage, and without detectable monocyte infiltration.

Thus, LCI allowed us to obtain a microglia population enriched in phagocytic cells specifically located in the DG of the hippocampus. In the following sections, we described several strategies to find possible markers to identify post-phagocytic microglia. To this end, we analyzed morphological and transcriptional changes of microglia following phagocytosis and examine whether any of them are useful as identifiers of phagocytic microglia.

6.2: Identification and characterization of post-phagocytic microglia.

In the first section of Results, we validated the “superphagocytosis” model that synchronized DG microglia in a phagocytic stage, allowing us to study the effects of phagocytosis on these cells. In this section, we explored different parameters that could undergo changes after phagocytosis to find markers of post-phagocytic cells, such as changes in morphology, and gene or protein expression.

6.2.1 Microglial morphology does not identify post-phagocytic cells.

Microglial morphology has commonly been used as an indicator of their function (Young et al., 2018). However, the connection between function and morphology has been widely discussed, concluding that they are not always related (Paolicelli et al., 2022). For example, an “ameboid” morphology has been associated with phagocytic microglia, but it is clear now that in physiology ramified microglia execute phagocytosis through their terminal branches (Sierra et al., 2010), and only in some diseases (e.g., epilepsy and stroke) they perform phagocytosis by apposition, engulfing only apoptotic cells that are close to their cellular bodies (Abiega et al., 2016; Beccari et al., 2023). To study microglial morphology in our *in vivo* model of “superphagocytosis”, we performed a Sholl analysis of microglia to quantify process length and number of processes in microglia in the time course after LCI (**Figure 13A**).

We found no differences in the distribution of the processes length, measured from the cell center, nor on the maximum process length (**Figure 13B-C**) along the time course (6h, 24h, 3d, 7d, 30d). Likewise, we found no differences in the frequency distribution of number of processes nor in the total number of processes (**Figure 13D-E**). To analyze the effect of phagocytosis more specifically, we compared “superphagocytic” vs non-phagocytic cells at 6h after LCI. We observed that “superphagocytic” cells had fewer processes and a decreasing trend in the maximum distance of processes (**Figure 13F-I**). Thus, when microglia were engaged in phagocytosis, they showed pouches and displayed a less ramified morphology, raising the interesting possibility that phagocytic microglia has reduced surveillance of the tissue surrounding the apoptotic cell. However, post-phagocytic microglia did not display robust morphological alterations that could validate morphology as a reliable marker of post-phagocytosis. In short, our data demonstrates that morphology is not a proper indicator to identify post-phagocytic microglia.

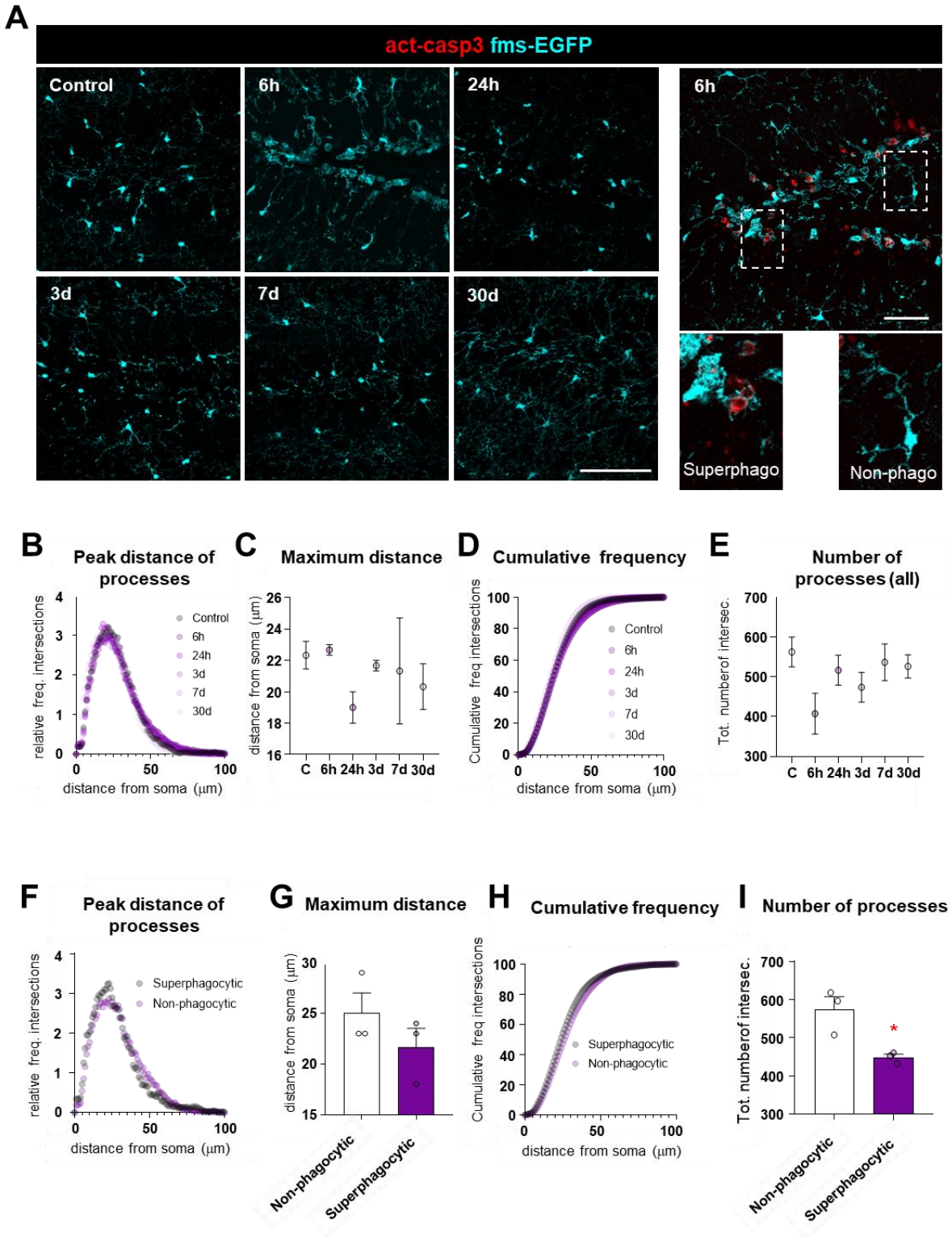

Figure 13. Morphology analysis of microglia after phagocytosis. ***(A)*** *Representative confocal images of microglial morphology at different experimental conditions (Control, 6h, 24h, 3d, 7d, 30d) and a representative detail (dotted white square) of "superphagocytic" and non-phagocytic microglia at 6h showing activated caspase 3 (red) y GFP (cyan) staining. Sholl analysis of microglial morphology after LCI comparing Control, 6h, 24h, 3d, 7d and 30d showing:****(B)*** *relative frequency of intersections correlated to distance from soma,* ***(C)*** *maximum distance of the most distal process,* ***(D)*** *cumulative frequency of intersections correlated to distance from soma,* ***(E)*** *total number of intersections meaning total number of processes. Sholl analysis of microglial*

morphology after LCI 6h comparing Non-phagocytic and Super-phagocytic microglia showing: ***(F)*** *relative frequency of intersections correlated to distance from soma,* ***(G)*** *maximum distance of the most distal process,* ***(H)*** *cumulative frequency of intersections correlated to distance from soma,* ***(I)*** *total number of intersections meaning total number of processes. Colored dots show mean values of n=3 mice. Colored dots [C,E] with error bars show mean ± SEM of independent experiments. Data was analyzed by one-way ANOVA followed by Holm-Sidak post hoc tests when appropriate [C, E] and by Student's t-test [G,I]. Asterisks represent significance between non-phagocytic and super-phagocytic. * represents p<0.05. Scale bars= 100μm [A], 50μm [A, 6h detail]. z=21μm, z=15.4μm, z=18,9; z=8.4μm, z=14μm, z=12.6μm[A], z=11.9μm [A, 6h detail].*

6.2.2 Single-cell RNAseq of hippocampal microglia as a tool for identification of "superphagocytic" population in the DG.

Since morphology was not useful to identify post-phagocytic microglia, we next assessed whether transcriptional changes could identify phagocytic microglia from the LCI model using single-cell RNA sequencing (scRNA-Seq) and validated these changes *in situ* using immunofluorescence and RNA Scope. We expected to find that some transcriptional changes were due to irradiation (in spite of the low microglial nuclei damage), and some transcriptional changes due to post-phagocytosis adaptations. Irradiation would lead to broader changes in all microglial regardless of their location, whereas phagocytosis would lead to changes specifically located in the DG.

Our lab had previously identified transcriptional changes induced by phagocytosis in microglia *in vitro*, revealing thousands of genes that were either up- or down-regulated at 3h and 24h in cultured microglia that had engulfed apoptotic cells (Diaz-Aparicio et al., 2020). Based on this data, we assessed post-phagocytic changes in the *in vivo* "superphagocytosis" model at short term (24h) and long term (7d), comparing both groups with their respective non-irradiated controls (control 24h and control 7d). (**Figure 14A-B**). We first removed circulating monocytes by perfusing the mice with saline, and then purified CD11b+ cells, which include both microglia and CNS associated macrophages (CAMs) (Masuda et al., 2022), and encapsulated the cells using a 10X Genomics microfluidic chamber, which allowed us the generation of libraries and the subsequent bioinformatic analysis (**Figure 14A**).

The sequencing data was filtered and analyzed in collaboration with Jose Pascual López Atalaya and Ángel Márquez Galera (Neuroscience Institute – CSIC/UMH). Our analysis pipeline consisted on a quality control filtering low quality cells. Then we plotted the data for visualization and chose those clusters that did not over-segment the point cloud. Next, we removed small clusters (< 200 cells), and defined the remaining clusters based on their gene expression and previous literature. Finally, we analyzed cluster-specific changes (cluster size and genes) and validate them *in situ* (**Figure 14B**).

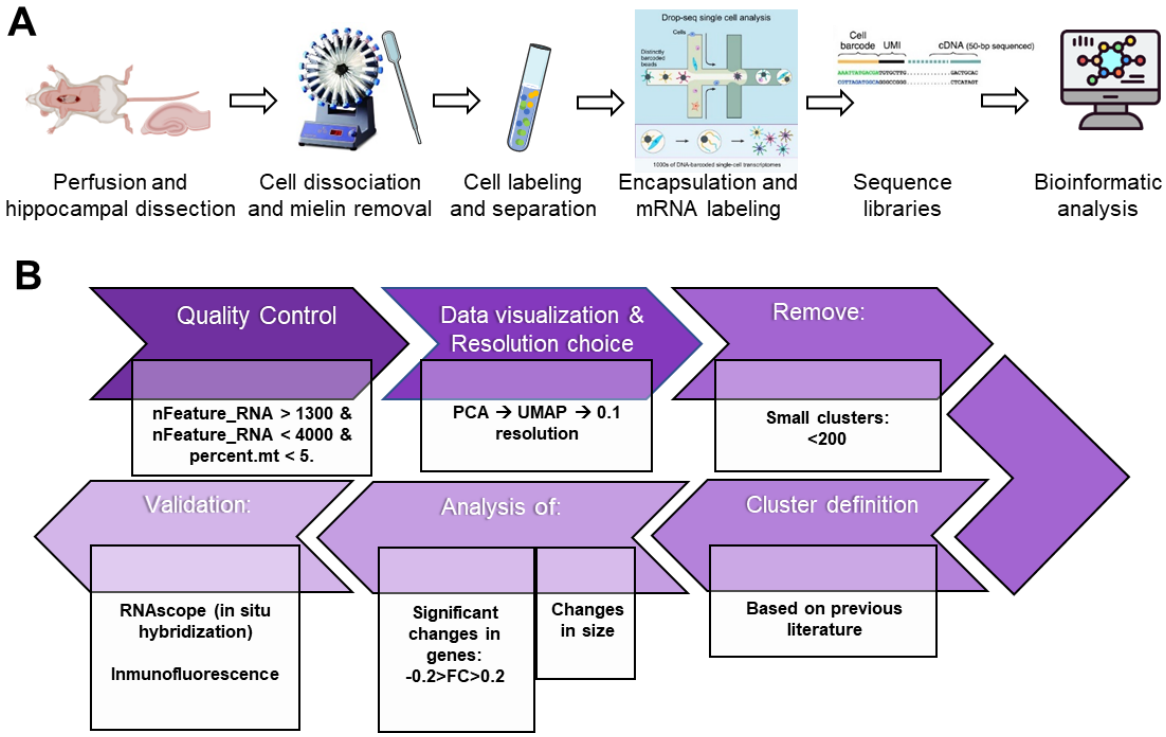

Figure 14. Graphical abstract of Single-cell RNAseq (sample processing and data filtering). ***(A)*** *Summary of sample processing.* ***(B)*** *Time-line of data filtering, analysis and validation.*

6.2.3 Quality control of scRNA-Seq data.

We first performed a quality control of the transcriptional data from the different experimental conditions that consisted on removing three types of events: 1, putative multiplets, i.e., cells that have not been correctly individualized (cells with >4,000 genes); 2, low-quality cells (with <1,300 genes); and 3, damaged cells (with >5% of mitochondrial genes). Filtering resulted in the removal of 18,484 cells, resulting in a final number of 46,861 cells. (**Figure 15**).

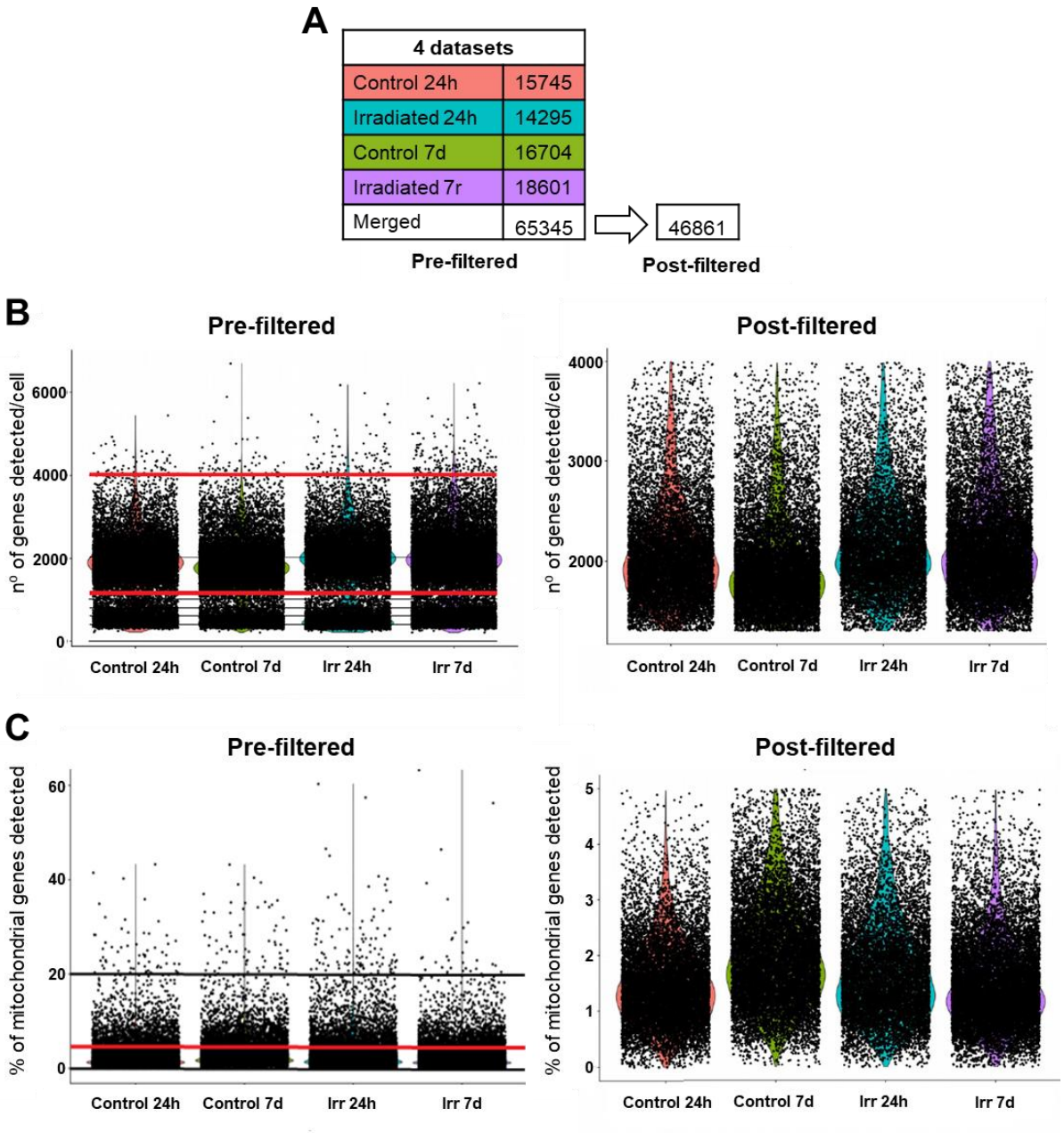

Figure 15. Quality Control of Single-cell RNAseq data. ***(A)*** *Summary table of total number of sequenced cells by condition and the final cell number after filtering* ***(B)*** *Violin-plot of the number of genes detected per cell before filtering (left) and after filtering (right). Red lines indicate the thresholds set for filtering.* ***(C)*** *Violin-plot of the % of mitochondrial genes detected per cell before filtering (left) and after filtering (right). Red lines indicate the thresholds set for filtering.*

6.2.4 Dimensionality reduction, resolution choice, and removal of small-sized clusters.

Once doublets, low-quality, and damaged cells were removed, we analyzed the cell clusters in the dataset by performing dimensionality reduction. Dimensionality reduction consists of transforming the original high-dimensional matrix, which contains information from the transcriptome of each cell, into a lower-dimensional subspace enriched with useful signals (Nguyen, 2022). First, we performed

principal component analysis (PCA) to linearly transform the data into a new coordinate system and then Uniform Manifold Approximation and Projection (UMAP) (**Figure 16A-B**). UMAP, a gold-standard for single-cell RNAseq data visualization, plots cells according their transcriptional similarities, in order to find relationships among them (clustering) (Sivarajah, 2020). We also performed unsupervised clustering analysis using shared nearest neighbor (SNN) modularity optimization-based clustering algorithm, which were visualized in the UMAP graph. We identified cell clusters for further analysis using the resolution parameter, which divides the cells into clusters according to the transcriptional differences that exist between them. Applying a high resolution leads to more sensitivity in detecting these differences, while lower values represent lower sensitivity. We tested 3 different resolution values (minimum distance = 0.8, 0.5 and 0.1) and opted for the minimal resolution (0.1), as it best represented the cloud shape represented in the UMAP, although we may miss subtle changes in microglial clusters (**Figure 16C**). With this resolution, we identified 8 clusters (0-7), of which clusters 5, 6 and 7 were eliminated because of low cell number (<200). The selected resolution of 0.1 did not result in oversegmentation, preserving small clusters such as the 3rd and 4th subpopulations, which remained the same size. This suggests that the chosen resolution effectively maintained well-defined populations. The remaining clusters (0, 1, 2, 3 and 4) were analyzed downstream (**Figure 16D-E**).

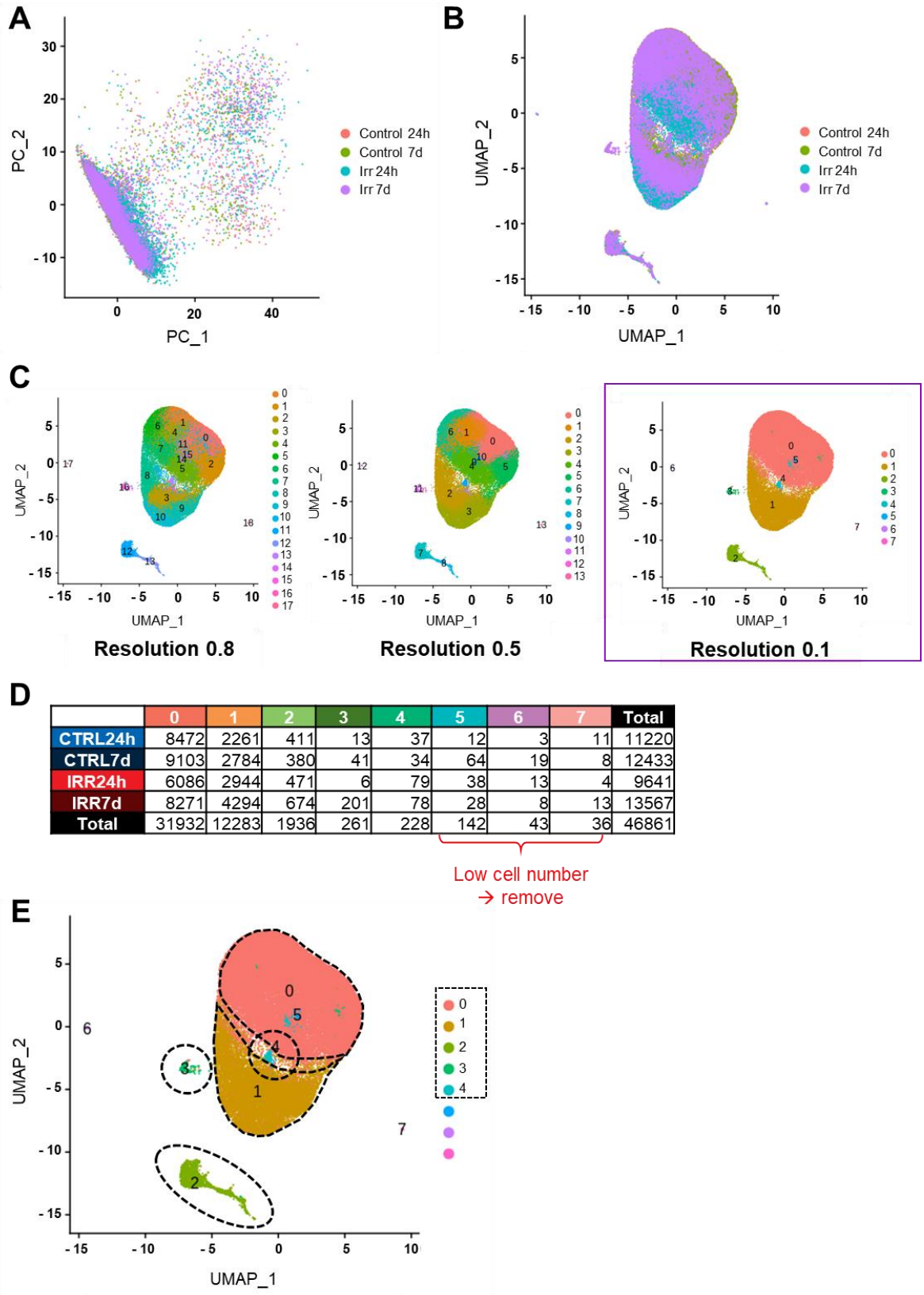

	0	1	2	3	4	5	6	7	Total
CTRL24h	8472	2261	411	13	37	12	3	11	11220
CTRL7d	9103	2784	380	41	34	64	19	8	12433
IRR24h	6086	2944	471	6	79	38	13	4	9641
IRR7d	8271	4294	674	201	78	28	8	13	13567
Total	31932	12283	1936	261	228	142	43	36	46861

Low cell number
→ remove

Figure 16. Dimensionality reduction, resolution choice and removal of small-sized clusters. ***(A)*** *PCA analysis.* ***(B)*** *UMAP visualization of merged data from different treatments.* ***(C)*** *UMAP graphs showing their cluster outputs with different resolution parameters (0.8, 0.5 and 0.1).* ***(D)*** *Summary table of detected cells per cluster and treatment. Annotations in red shows removed cluster due to low cells number.* ***(E)*** *UMAP of selected clusters surrounded by dotted-lines in black.*

6.2.5 Cluster annotation

To identify the finally selected clusters we examined their signature genes (Top 20 expressed genes) and defined them based on previous literature (**Figure 17A-B**). Recent scRNA-Seq studies define 5 main clusters of microglia: homeostatic, disease-associated (DAM), major histocompatibility complex (MHCII), interferon responsive (IFN), and proliferative (Chen et al., 2021). In addition, there are several other specialized macrophage populations as CAMs, which may also be present in our preparation (Masuda et al., 2022). Furthermore, microglia respond to ex vivo tissue processing resulting in an artifactual transcriptional signature (Marsh et al., 2022b), which must be removed from the analysis. By matching the signature genes obtained in our analysis with the signature genes from these studies we defined our clusters, identified the CAM cluster, and determined which cells had been activated by the processing.

We identified cluster 0 as "homeostatic" because four genes (P2RY12, SIGLECH, HEXB, TMEM119) matched with the homeostatic gene signature. We identified cluster 1 as "*ex vivo* activated" (exAM) because seven genes (EGR1, ZFP36, NFKBIZ, CCL4, FOS, JUNB, ATF3) matched with the processing-reactive signature (Marsh et al., 2022b). We identified cluster 2 as "MHC" because four genes (CD74, H2-EB1, H2-AA, H2AB1) matched with the genes described for the MCHII signature. However, three other signature genes of cluster 2 have been identified in other signatures: APOE (DAM signature), and PF4 and MS4A7 (CAM signature). Therefore, as most of the signature genes corresponded to the MHC population this cluster was finally named as such. We identified cluster 3 as "proliferative" because four genes (TOP2A, H2AFZ, MKI67, CENPE) matched with the proliferative signature. We identified cluster 4 as "IRM" (interferon responsive microglia) because five genes (IFITM3, ISG15, IRF, USP18, OASL2) matched with the IRM signature. (**Figure 17B**).

Therefore, based on previous studies, we define our clusters as homeostatic (0), reactive (1), MHCII (2), proliferative (3), and IRM (4) (**Figure 17C**). Next, we analyzed changes of the homeostatic, MHCII, proliferative and IFN clusters in size and gene expression to identify which of those clusters was related to phagocytosis. The reactive cluster, an artifact caused by sample processing, was not further analyzed.

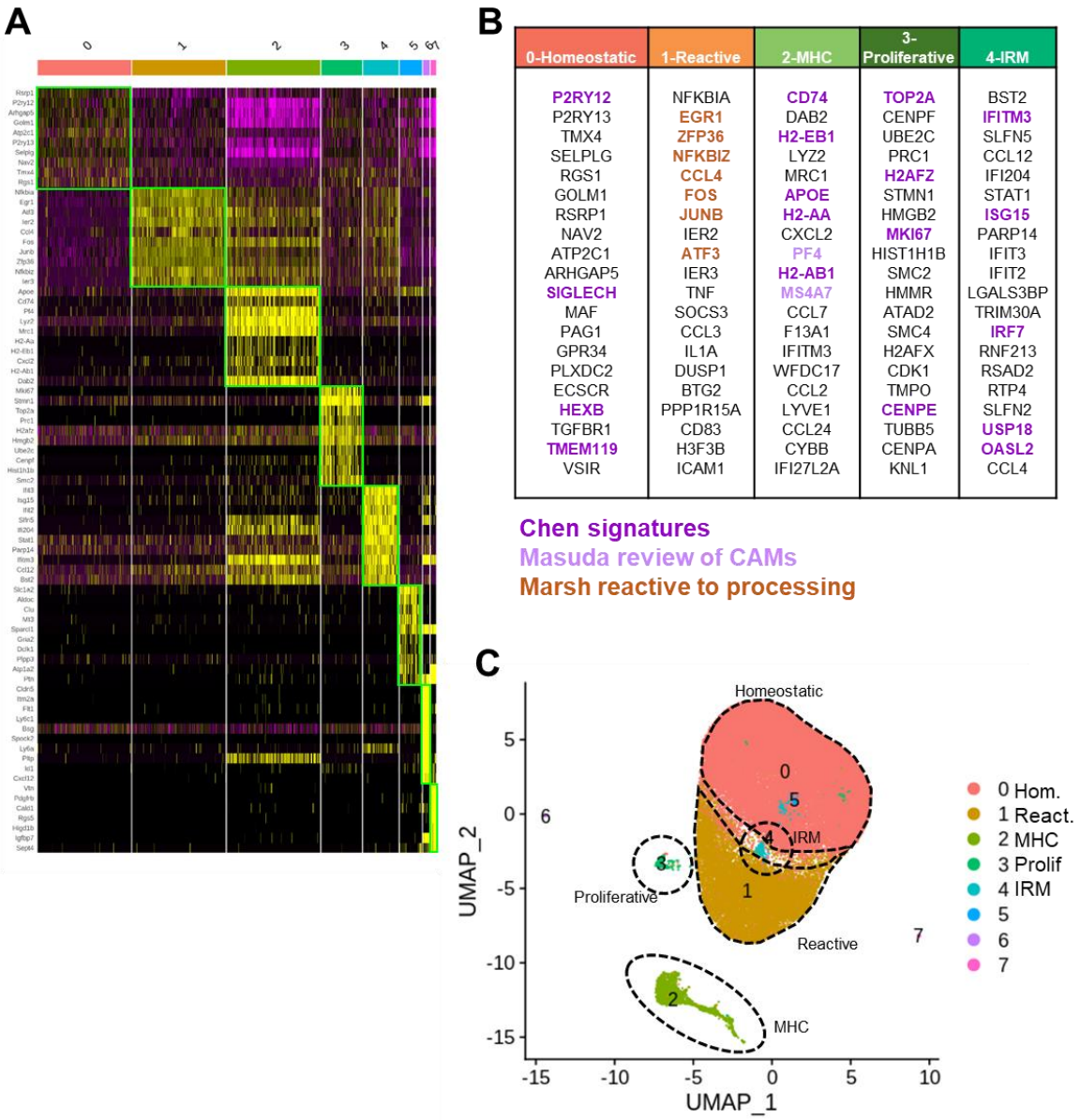

Figure 17. Cluster identification based in previous scRNA-seq studies. ***(A)*** *Heat-map of 10 most expressed genes per cluster.* ***(B)*** *Summary table with the top 20 signature genes of each cluster. In dark purple, genes described for different microglial sub-populations defined by the Colonna´s lab (Chen et al., 2021).* *In light purple, genes described for CAMs by the Prinz´s lab (Masuda et al., 2022).* *In orange, genes described for processing-reactive microglia by the Steven´s lab (Marsh et al., 2022b)* ***(C)*** *UMAP of selected clusters surrounded by dotted-lines in black and labeled with their respective names.*

6.2.6 LCI induced changes in size and transcriptional signature

Once we identified the different microglia clusters, we analyzed how each cluster changed between treatments (controls 24h and 7d, irradiated 24h and 7d) by assessing their location (transcriptional profile) and size (population size) in the UMAP. The homeostatic cluster shifted downwards towards the reactive cluster 24h after irradiation, returning to its basal state by 7d, suggesting that LCI triggers transcription of reactive microglia genes in the homeostatic population. Another

evident change occurred in the proliferative cluster, which notably increased its size 7d after irradiation (**Figure 18**). Next, we assessed gene expression changes in all clusters.

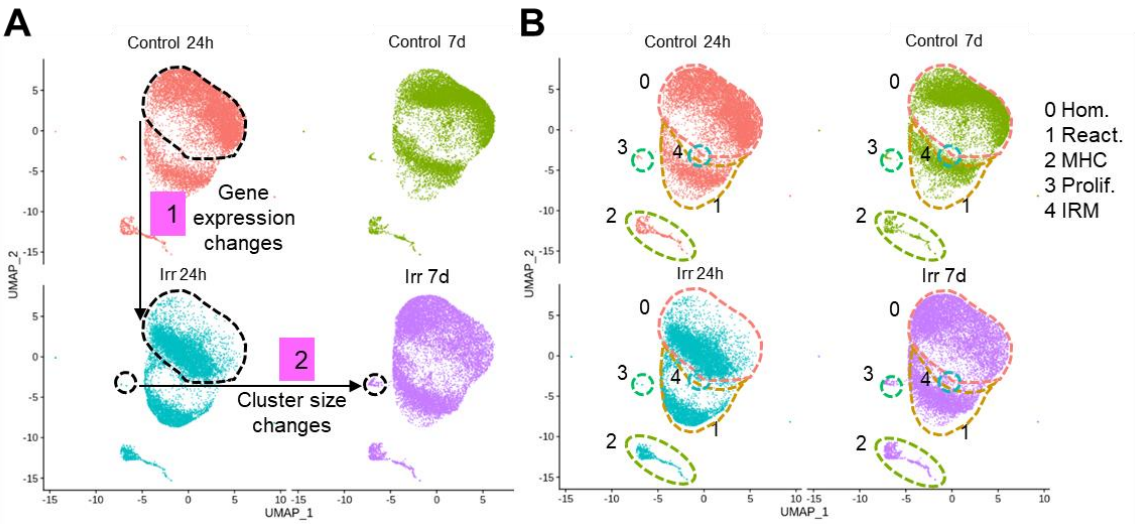

Figure 18. General analysis of changes in cluster size and transcriptome. ***(A)*** *UMAP of the different treatments with annotations (purple) describing the in cluster size and change in the cluster transcriptome.* ***(B)*** *UMAP of the different treatments with dotted lines indicating the original distribution (24h control) of each cluster (0=homeostatic, 1=reactive, 2=MHC, 3=proliferative, 4=IRM).*

6.2.7 Transcriptional changes in genes shared between clusters

In order to discriminate between transcriptional changes induced by irradiation from those induced by phagocytosis, we first examined the global gene expression 24h and 7d after LCI in all clusters combined, and in the next section we focused on the specific changes in each cluster. We found two types of genes whose expression was altered after LCI: genes expressed in different clusters (shared genes), possibly representing global changes induced by irradiation; and genes that were cluster-specific, some of which may be related to phagocytosis. Then, we analyzed their functional implications with the functional annotation tool DAVID. DAVID allows to annotate our genes of interest and identify enriched functional groups based on Gene Ontology (GO) that usually covers three domains: molecular function, biological process, and cellular components (Huang et al., 2007).

LCI caused strong transcriptional changes at 24h affecting 140 shared genes and 114 cluster-specific genes **(Figure 19A)**. DAVID analysis revealed that shared genes were related to specific GOs, such as the biological processes of protein kinase B signaling (GO:0043491) and inflammatory response (GO:0006954) (**Figure 19C**). Protein kinase B signaling is involved in cellular survival pathways, by inhibiting apoptotic processes (Chen et al., 2001). The brain inflammatory response is commonly executed by microglia in the presence of neurodegeneration or damage (Muzio et al., 2021a), suggesting that hippocampal microglia reacted to LCI triggering a response of self-protection and performing immune functions that may reestablish surrounding damaged tissue.

At 7 days, LCI induced the expression in 32 shared genes and 61 cluster-specific genes (**Figure 19B**), showing a decrease of affected genes suggesting that the effects of irradiation were fading off. The DAVID analysis revealed that shared genes were related to specific GOs, such as the upregulated cellular component of cyclin dependent protein kinase holoenzyme complex (GO:0000307), involved in the regulation of cell cycle and the downregulated cellular components of mitochondria (GO:0005739), mitochondrial inner membrane (GO:0005743), and cellular respiration (GO:0045333) (**Figure 19D-E**), suggesting that microglia continue to recover in the long term. Thus, in spite of the minimal DNA damage found (**Figure 11**) LCI was not innocuous for microglia, which implemented mechanisms to survive right after irradiation, and recover over time.

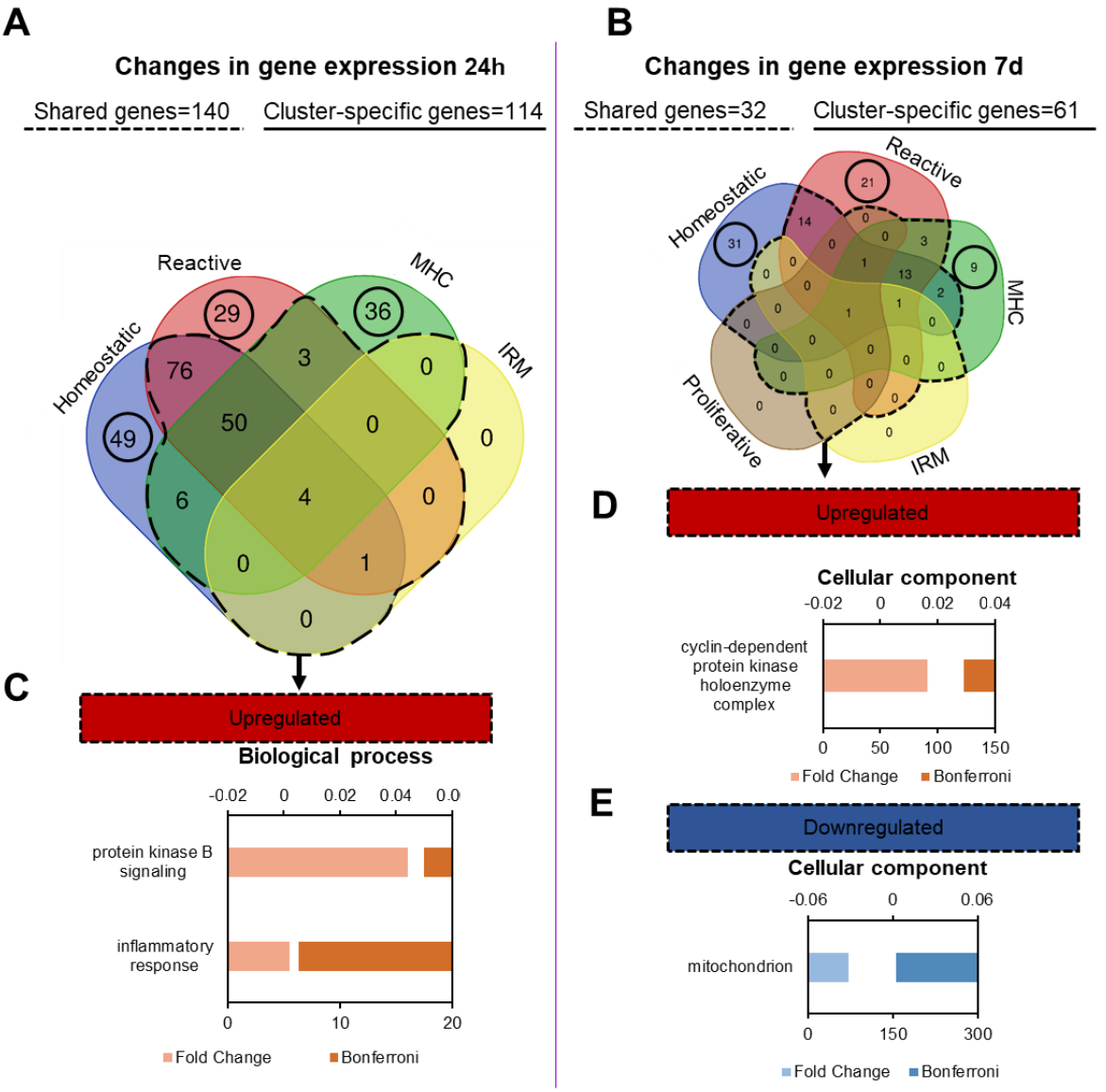

Figure 19. Transcriptional changes in cluster shared-genes. ***(A, B)*** *Venn diagram showing expression changes in shared and cluster-specific genes at 24h (**A**) and 7d (**B**) after LCI. Black circles indicate cluster-specific genes, while the dotted lines indicate shared-genes that were further analyzed based on Gene Ontology (GO).* ***(C)*** *Analysis of the up-regulated biological processes using DAVID at 24h.* ***(D)*** *Analysis of both up-regulated, and* ***(E)*** *down-regulated cellular components using DAVID at 7d. Left axis represents the fold enrichment of each biological function and right axis represents the*

adjusted p-value of each GO term. Only statistically significant changes are shown. Only GO term domains with statistically significant changes are shown (GO domains: biological process and cellular component).

6.2.8 Transcriptional changes in homeostatic microglial cluster

In addition to the transcriptional changes in shared genes caused by LCI, we found cluster-specific transcriptional changes, some of which could represent phagocytic microglia.

First, we explored these changes in the homeostatic cluster although it was unlikely to harbor the phagocytic population because it was the largest population in control mice and it was slightly reduced after LCI (**Figure 20A,C**). In contrast, we expect that the phagocytic microglia, a minority among all cells in the hippocampus, would be increased after LCI. This cluster represents 80% of the sequenced cells and it is reduced in size after exposure to LC1. These data mismatch our previous results where we observed that in the DG gyrus phagocytic microglia increased from 9.1 ± 1.5% in control conditions to 83.1 ± 14.9% at 6h LCI post-exposure (**Figure 9**).

In the homeostatic cluster, LCI caused transcriptional changes in 49 cluster-specific genes at 24h and 31 cluster-specific genes at 7d (**Figure 20D**). Of these 80 cluster-specific genes, 8 of them changed their expression at both time-points. Genes regulated at 24h were related to several GOs, such as the upregulated molecular function of C3HC4-type RING finger domain binding (GO:0055131), and the downregulated cellular component of the cytosolic ribosome (GO:0022626) (**Figure 20E-F**). C3HC4-type RING finger domain plays a key role in ubiquitination (Guo et al., 2022), the biochemical process by which most proteins are degraded; and a downregulated function of the ribosome may imply a decrease in protein synthesis, suggesting that proteins within the cell undergo a recycling process, perhaps as a consequence of their action to counteract the damage that can result from both irradiation and phagocytosis.

Genes regulated at 7d were related to upregulated GOs involved in the following biological processes: cellular response to calcium ion (GO:0071277), transcription from RNA polymerase II promoter (GO:0006367), and response to cAMP (GO:0051591) (**Figure 20H**). Overall, these genes participate in transcription of DNA into precursors of messenger RNA (mRNA), suggesting that the homeostatic cluster becomes active again at the transcriptional level in the long term (7d after irradiation). Moreover, the cells seem to respond to signals such as calcium and cyclic adenosine monophosphate (cAMP), indicating that homeostatic microglia recover their sensing activity in the long-term. On the other hand, the downregulated GOs at 7d include the biological process of aerobic respiration (GO:0009060) (**Figure 20I**), suggesting a decreased mitochondrial activity, and a reduced energy production by the cells. Therefore, it is possible that the aforementioned recovery has not been fully completed and that the cells still have metabolic deficits that need to resolve. Regarding those genes regulated at both time-points, they were related to the upregulated GO of the molecular function double-stranded DNA binding (GO:0003690). This molecular function brings together other more specific functions, such as transcription,

packaging or cleaving of DNA, suggesting that microglia undergo changes at the nuclear level. Thus, LCI downregulates transcription in homeostatic cells that try to recover at the long-term, However, this recovery is partial, since microglial metabolism may continue downregulated in the long term.

Therefore, the homeostatic cluster was discarded as a candidate to represent the phagocytic population, and the rest of the clusters were further examined.

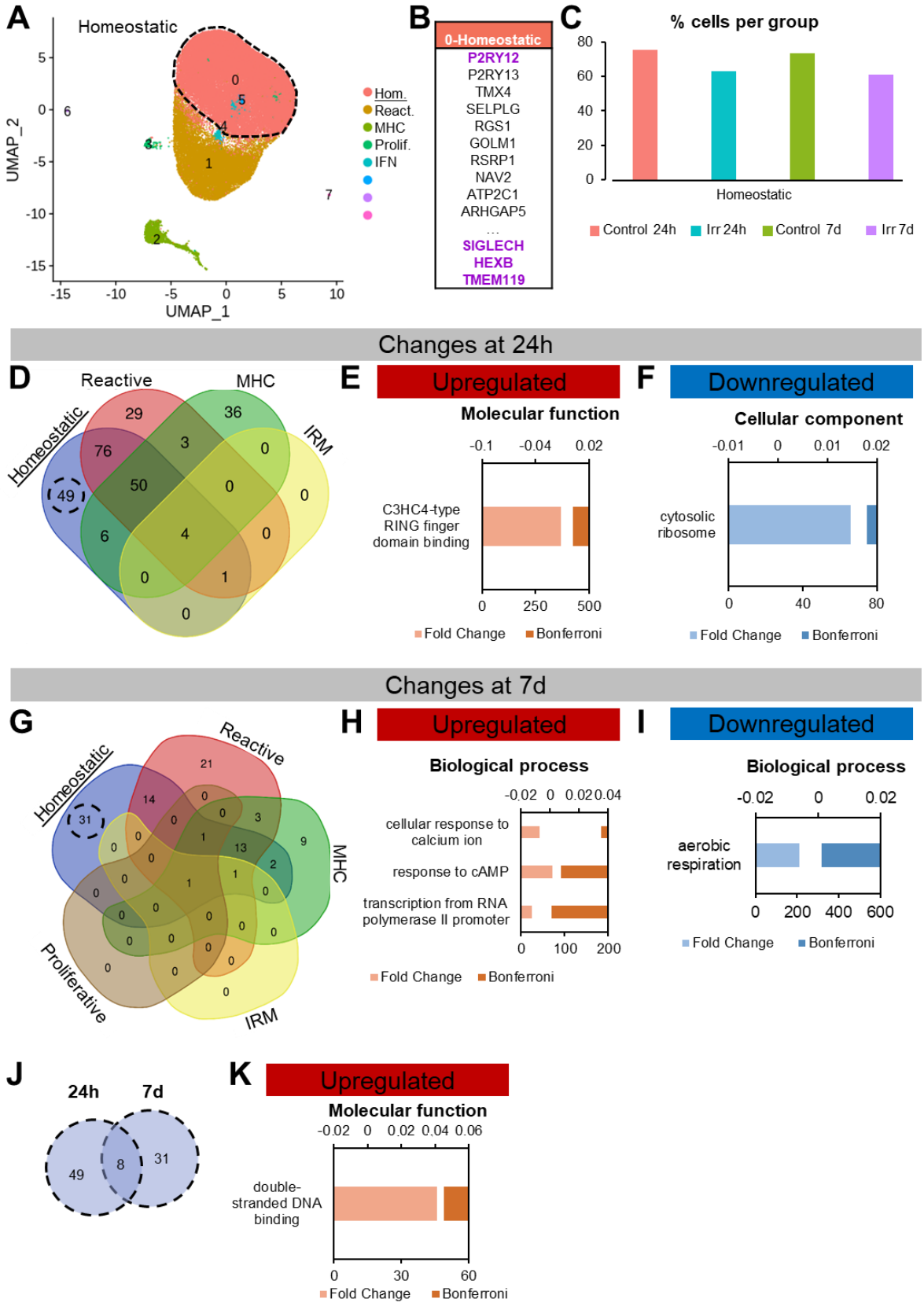

Figure 20. Transcriptional changes in the homeostatic cluster. ***(A)*** *UMAP showing the homeostatic cluster surrounded by a dotted-line.* ***(B)*** *List of signature genes characteristic of the homeostatic cluster.* ***(C)*** *% of cells belonging to homeostatic cluster*

in each experimental condition. ***(D, G, J)*** *Venn diagram showing expression changes in shared and cluster-specific genes at 24h (D) and 7d (G) after LCI, including cluster-specific genes that are shared among both time-points(J)****.*** *Analysis of both up-regulated* ***(E)*** *and down-regulated (****F****) GOs at 24h using DAVID software. Analysis of both up-regulated* ***(H)*** *and down-regulated (****I****) GOs at 7d using DAVID software. Analysis of up-regulated GO of time-shared genes (****J****). Left axis represents the fold enrichment and right axis represents the adjusted p-value of each GO term. Only statistically significant changes are shown.*

6.2.9 Transcriptional changes in MHC cluster

The MHC cluster was a potential candidate for harboring the phagocytic population, as it increased in size in response to LCI in the short and long term (**Figure 21C**). However, this cluster may also represent CAMs, as some genes of the cluster (MSA47 and PF4) have been identified in the CAM signature (**Figure 21B**). To further analyze the cluster specific transcriptional changes that the treatment cause in the MHC population, we examined cluster specific transcriptional changes at short and long-term.

In the MHC cluster, LCI caused transcriptional changes in 36 cluster-specific genes at 24h and 9 cluster-specific genes at 7d, sharing 1 specific gene among the two timepoints (**Figure 21D**). Analysis of these genes with DAVID did not reveal that they were significantly involved in any GO, likely because they were few genes involved. Therefore, the function of each gene was examined and those involved in similar processes were grouped together.

Genes regulated at 24h and 7 d were classified according to their function in the following categories: metabolism, motility phagocytosis/degradation, inflammation, antigen presentation, oxidative/cellular stress, DNA damage-recovery, regulation of apoptosis/growth, metabolism of mRNA, membrane receptor, and unknown functions (**Figure 21F**). Interestingly, the gene Lgals1 shared among both time-points showed an up-regulated pattern and was implicated in cell-cell and cell-matrix interactions, acted as a negative growth factor and exerted pro-survival effects (Ruvolo et al., 2020).

Overall, these results suggest that MHC population undergoes short-term changes at the intracellular level following LCI. Interestingly some of these changes were related to increased oxidative stress and to the downregulation of genes involved in the main function of the MHC cluster, the antigen presentation. In the long-term MHC population seem to recover from oxidative stress, but still show some alterations in phagocytosis, inflammation, mRNA metabolism, regulation of apoptosis and cellular metabolism. To identify the MHC population in our tissue, we validated these findings by RNAscope *in situ* hybridization in the following section.

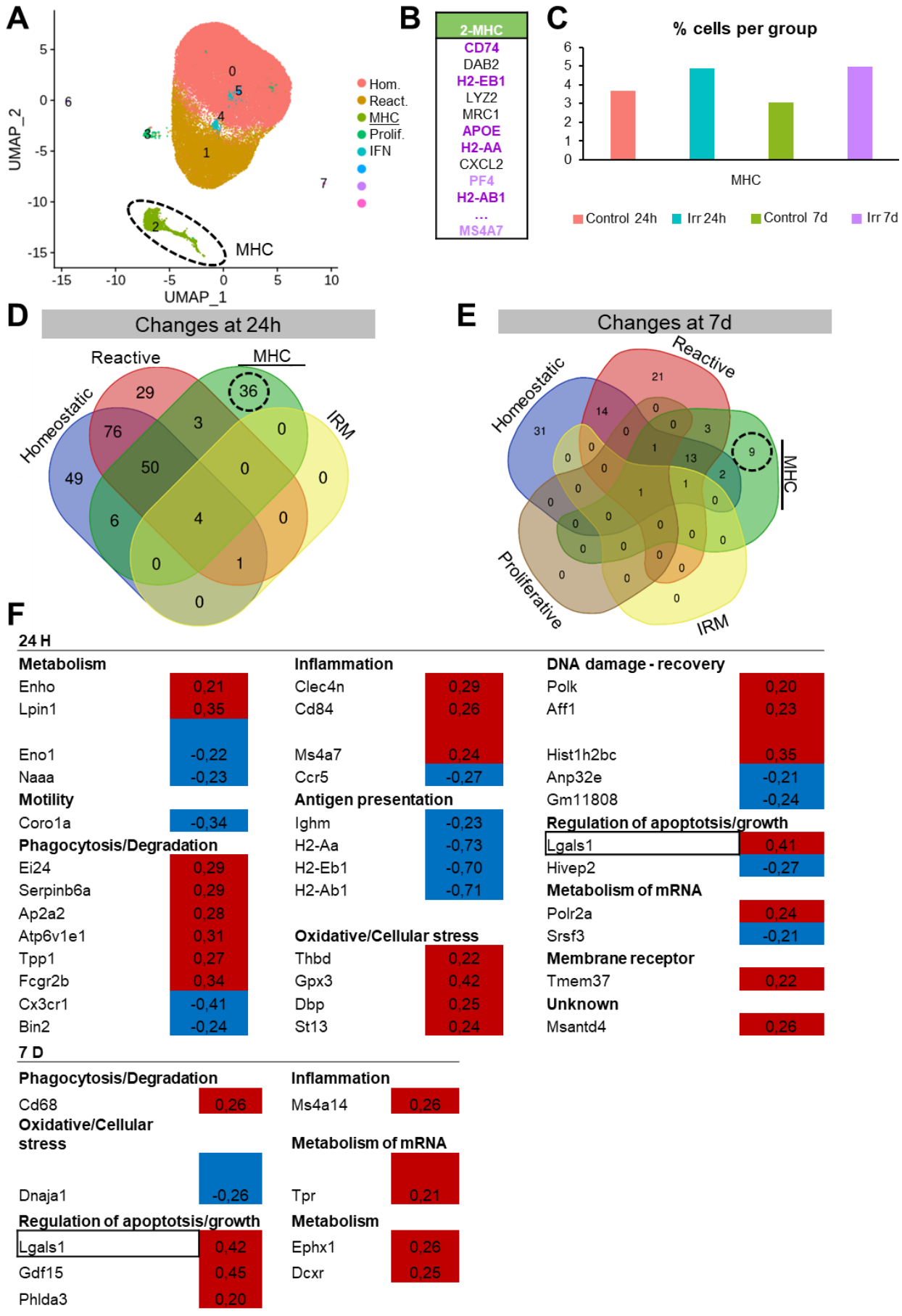

Figure 21. Transcriptional changes in the homeostatic cluster. ***(A)*** *UMAP showing*

MHC population surrounded by a dotted-line. ***(B)*** *List of signature genes characteristic of the MHC cluster. In dark purple, genes described for different microglial sub-populations in Chen et al. 2021 (Chen et al., 2021)****.*** *In light purple, genes described for CAMs in Masuda et al. 2022 (Masuda et al., 2022)****. (C)*** *% of cells belonging to MHC cluster in each experimental condition.* ***(D,E)*** *Venn diagram of shared and cluster-specific genes at 24h (D) and 7d (E) after LCI. Specific changes of MHC cluster surrounded by a dotted-line. (****F****) Summary table of cluster-specific gene changes grouped by their functional classification. FC means the fold-change. Numbers within red boxes represent up-regulated genes, whereas numbers in blue boxes represent gown-regulated genes. Black bordered boxes label the repeated gene at both time points.*

6.2.10 Expression of MHC genes *in situ* after LCI.

The MHC cluster was a potential candidate for harboring the phagocytic population, as it increased in size in response to LC) at 24h and 7d. However, this cluster may also represent CAMs, as some genes in the cluster (MSA47 and PF4) have been identified in the CAM signature (Prinz et al., 2021) (**Figure 21B-C**). To examine whether this cluster represented phagocytic microglia, we selected one of the genes of this signature, MS4A7, a member of the membrane-spanning 4A gene family associated commonly associated with mature cellular function in the monocytic lineage (Mattiola et al., 2021).

MS4A7 was expressed in 81% of the cells of the MHC cluster, as showed in pct.1 (percentage of cells where the gene is detected in the cluster for condition), while only 1% of cells from other clusters expressed it, as showed in pct.2 (percentage of cells where the gene is detected on average in the other clusters for condition) (**Figure 22A**), showing a pct1/pc2 ratio of 57.57, which suggested that MS4A7 was a strong candidate for identifying the MHC population. In addition, this gene increased its expression by 0.24 (FC, fold-change) at 24h after LCI in the MHC cluster (**Figure 22A-B**). We analyzed MS4A7 expression *in situ* using RNAScope. As there was limited MS4A7 labeling in the analyzed regions, the expression of the APOE probe was used as an internal control (**Figure 22D,E**). In adult microglia APOE expression is low (Lee et al., 2023) , and our images shows no colocalization between P2Y12 and APOE labeling (**Figure 22F**), demonstrating that the hybridization process was functioning correctly.

Cells positive for MS4A7 had a low expression of P2Y12, an amoeboid morphology, and represented a very low percentage of the $P2Y12^{+}$ microglial population in DG, and no cells from this population were observed in CA (**Figure 22D**). Although the higher expression of MS4A7 in DG than in CA coincides with the expected pattern of expression in phagocytic microglia, their low expression of P2Y12 and their ameboid morphology suggests that the MHC cluster represents CAMs and does not characterize the phagocytic microglia population.

A

Gene	avg_logFC	pct.1	pct.2	ratio	changes expresion within the cluster after tratment 24h? (FC)	changes expresion within the cluster after tratment 7d? (FC)
Ms4a7	2,39	0,81	0,01	57,57	0,24	no

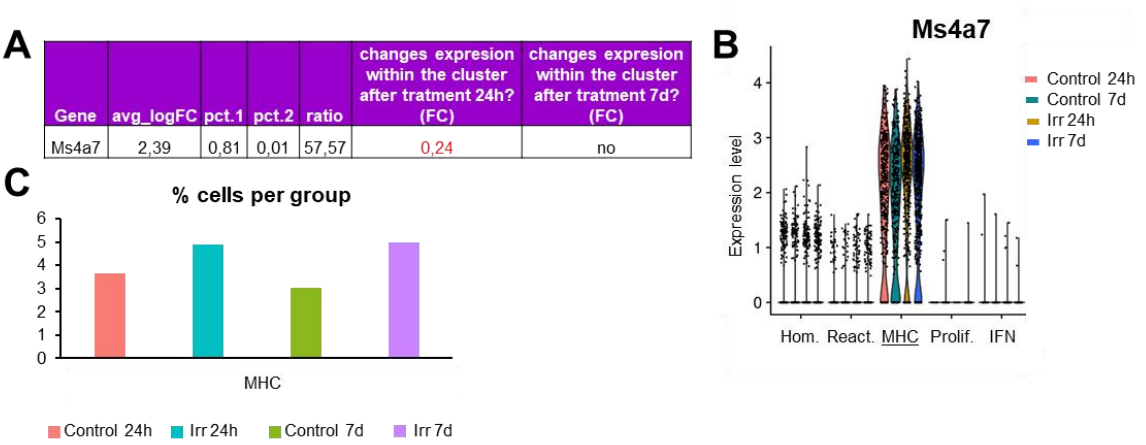

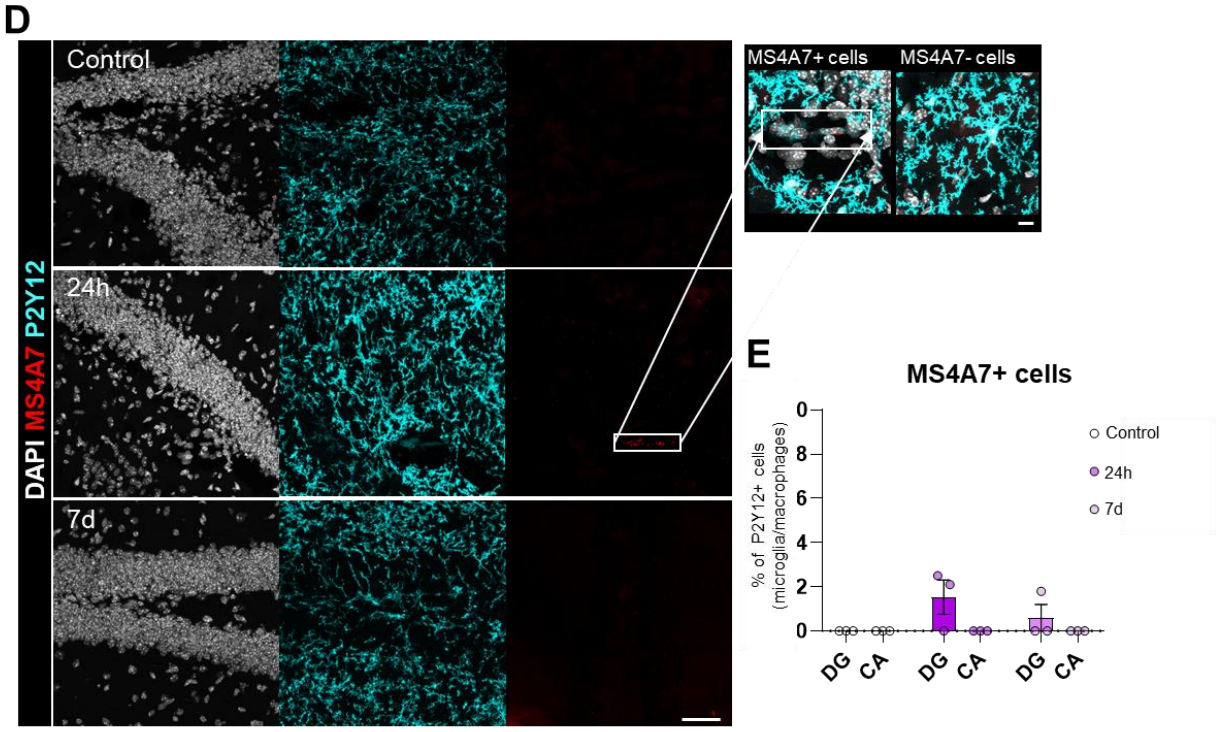

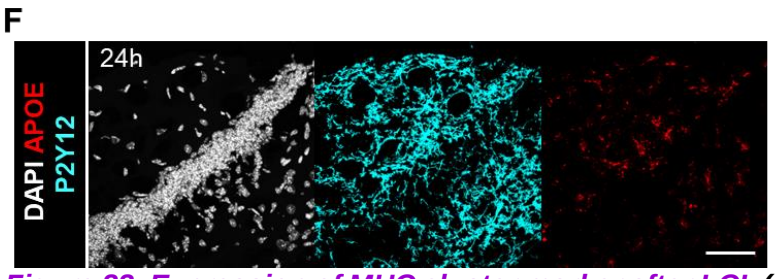

Figure 22. Expression of MHC cluster marker after LCI. ***(A)*** *Summary table of MS4A7 gene expression in the MHC cluster. The following parameters are shown are the average FC, pct1, pct2, the pct1/pct2 ratio and expression changes after LCI (24h and 7d).* ***(B)*** *Violin-plots showing MS4A7 in different clusters among different conditions.* ***(C)*** *% of cells belonging to MHC cluster in each experimental condition.* ***(D)*** *Representative images of the DG showing DAPI (white), MS4A7 (red) and P2Y12 (cyan) staining in different experimental conditions (Control, 24h and 7d). Within the white rectangle MS4A7+ cells are indicated.* ***(E)*** *Analysis of cells expressing high content in MS4A7 mRNA showing the percentage of cells in DG and CA regions in different experimental conditions (Control, 24h and 7d).* ***(F)*** *Representative images of the DG showing the labeling of the positive control APOE (red), also showing DAPI (white) and P2Y12 (cyan).*

Bars show mean ± SEM of n=3 mice. Data was analyzed by one-way ANOVA [D] followed by Holm-Sidak post hoc tests when appropriate. Scale bars=50μm, 10μm (inserts in [D]). z=16.45, z=17.5, z=8.75 [D]; z=15.4 [F].

6.2.11 Transcriptional changes in IRM cluster and expression of IRM genes *in situ* after LCI.

The IRM cluster was also a potential candidate for harboring the phagocytic population, as it was a small cluster that increased in size in response to treatment (LCI) at 24h and 7d, but showed no change in gene expression (i.e., had no cluster-specific transcriptional changes) (**Figure 23A,C).** This microglial signature has been observed in cells responsible for phagocytosis of what during cortical development (Escoubas et al., 2021). Thus, to validate and identify the IRM cluster *in situ*, we performed RNAscope of the signature gene IFIT3.

IFIT3 was expressed in 80% of the cells of the IRM cluster (pct.1), while only 4% of cells from other clusters expressed it (pct.2), showing a pct.1/pct.2 ratio of 44.61, which suggests that IFIT3 was a strong candidate for identifying the IRM population (**Figure 23D-E**). Microglial cells were classified as IFIT3+ or IFIT3- based on their content of IFIT3 mRNA. Cells with evident IFIT3 content were categorized as $IFIT3^{+}$, and they were further analyzed within the microglial population. Although in basal conditions the $IFIT3^{+}$ microglia population was more numerous in DG than in CA (25.1±1.0 vs. 0.7±0.7), the percentage of $IFIT3^{+}$ cells did not change after treatment in either region (**Figure 23F-G**), suggesting that this cluster does not represent the post-phagocytic microglia either. Furthermore, to confirm these results, we analyzed the expression of IFITM3, another signature gene of this cluster, by immunofluorescence. The analysis revealed that IFITM3 was primarily expressed in blood vessels (**Figure 23H**), without colocalization with microglial cells. Thus, the IRM cluster does not represent the post-phagocytic microglia population.

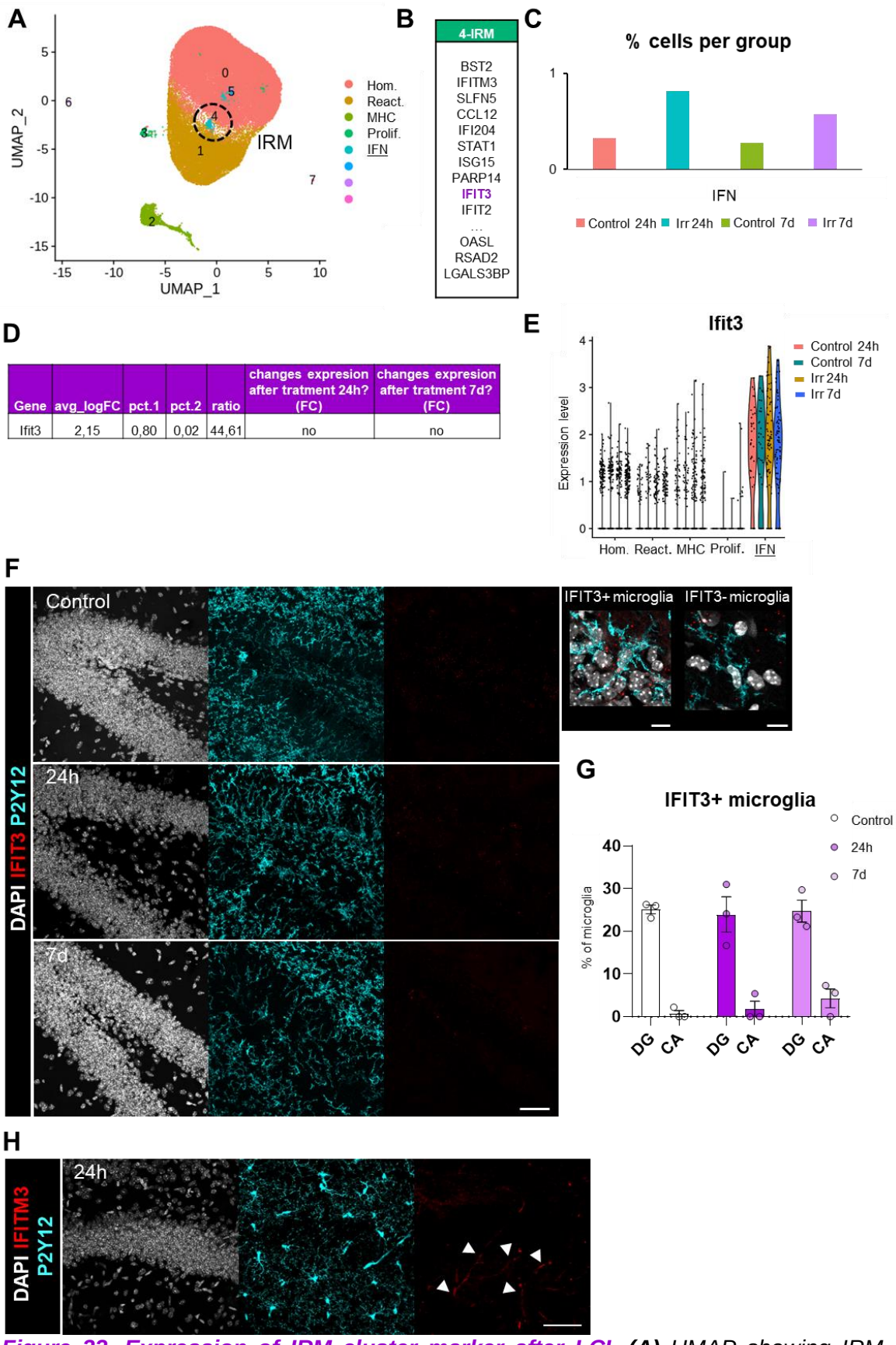

Gene	avg_logFC	pct.1	pct.2	ratio	changes expresion after tratment 24h? (FC)	changes expresion after tratment 7d? (FC)
Ifit3	2,15	0,80	0,02	44,61	no	no

Figure 23. Expression of IRM cluster marker after LCI. ***(A)*** *UMAP showing IRM population surrounded by a dotted-line.* ***(B)*** *List of signature genes characteristic of the IRM cluster.* ***(C)*** *% of cells belonging to IRM cluster in each experimental condition.* ***(D)*** *Summary table of IFIT3 gene expression in the IRM cluster. The following parameters*

are shown are the average FC, pct1, pct2, the pct1/pct2 ratio and expression changes after LCI (24h and 7d). ***(E)*** *Violin-plots showing IFIT3 in different clusters among different conditions.* ***(F)*** *Representative images of the DG showing DAPI (white), IFIT3 (red) and P2Y12 (cyan) staining in different experimental conditions (Control, 24h and 7d).* ***(G)*** *Analysis of the percentage of IFIT3+ in DG and CA regions in different experimental conditions (Control, 24h and 7d).* ***(H)*** *Representative images of the DG showing DAPI (white), IFITM3 (red) and P2Y12 (cyan) staining. Bars show mean ± SEM of n=3 mice. Data was analyzed by one-way ANOVA [D] followed by Holm-Sidak post hoc tests when appropriate. Scale bar=50μm, 10μm (inserts in [F]). z=12.25, z=11.2, z=10.15 [F]; z=27.3 [G] z=40 [H].*

6.2.12 Phagocytic microglia is characterized by high CD68 and galectin 3 expression.

As the post-phagocytic population was not found within any of the clusters identified by scRNA-Seq, we performed a literature search for proteins associated with phagocytosis, such as CD68 and galectin 3 (Gal3) (Rotshenker, 2009; Rotterman et al., 2020). CD68 is predominantly located in the endosomal and lysosomal compartments of cells, actively participating in the degradation of extracellular materials (Bobryshev et al., 2013). Additionally, CD68 has been associated with phagocytosis processes, and its expression is also upregulated in phagocytic contexts, such as ischemia or proliferative regions in development (Silva et al., 1999; Li et al., 2019). Gal3, a member of the galectin family, it is well known for its pleiotropic nature and its involvement in triggering immune responses (Sciacchitano et al., 2018). The LGALS3 gene, which codes for Gal3, is upregulated in microglia when they phagocytose myelin and oligodendrocytes (Nomura et al., 2017; Li et al., 2019). The expression of both proteins was analyzed by immunofluorescence in control and after LCI (24h and 7d) (**Figure 24A,C**).

The percentage of CD68+ microglia increased in DG both at 24h and 7d after LCI while there were no changes in CA (**Figure 24A-B**). Likewise, the percentage of Gal3+ microglia increased in DG both at 24h and 7d after LCI. This increase occurred only in the DG, while there were no changes in CA (**Figure 24C-D,E**). $Gal3^+$ microglia from the DG was specifically located in the subgranular zone (SGZ) of the DG, the region where phagocytosis mainly occurs (Sierra et al., 2010) (**Figure 24G**). In contrast to the DG, where $Gal3^+$ microglia were localized specifically in the SGZ, CA $Gal3^+$ microglia were distributed throughout the different layers, suggesting that DG microglia responded to changes occurring specifically in the SGZ **(Figure 24H,F)**. Likewise, DG $Gal3^+$ microglia showed higher levels of Gal3, as most of the cells showed a medium-high intensity, whereas most of CA Gal3+ microglia displayed low intensity, revealing differences between DG and CA microglia. (**Figure 24E-F**). Thus, we concluded that there was a population of overexpressing both CD68 and Gal3 specifically located in the SGZ, that increased its size after phagocytosis, suggesting that post-phagocytic microglia is characterized by the expression of both markers.

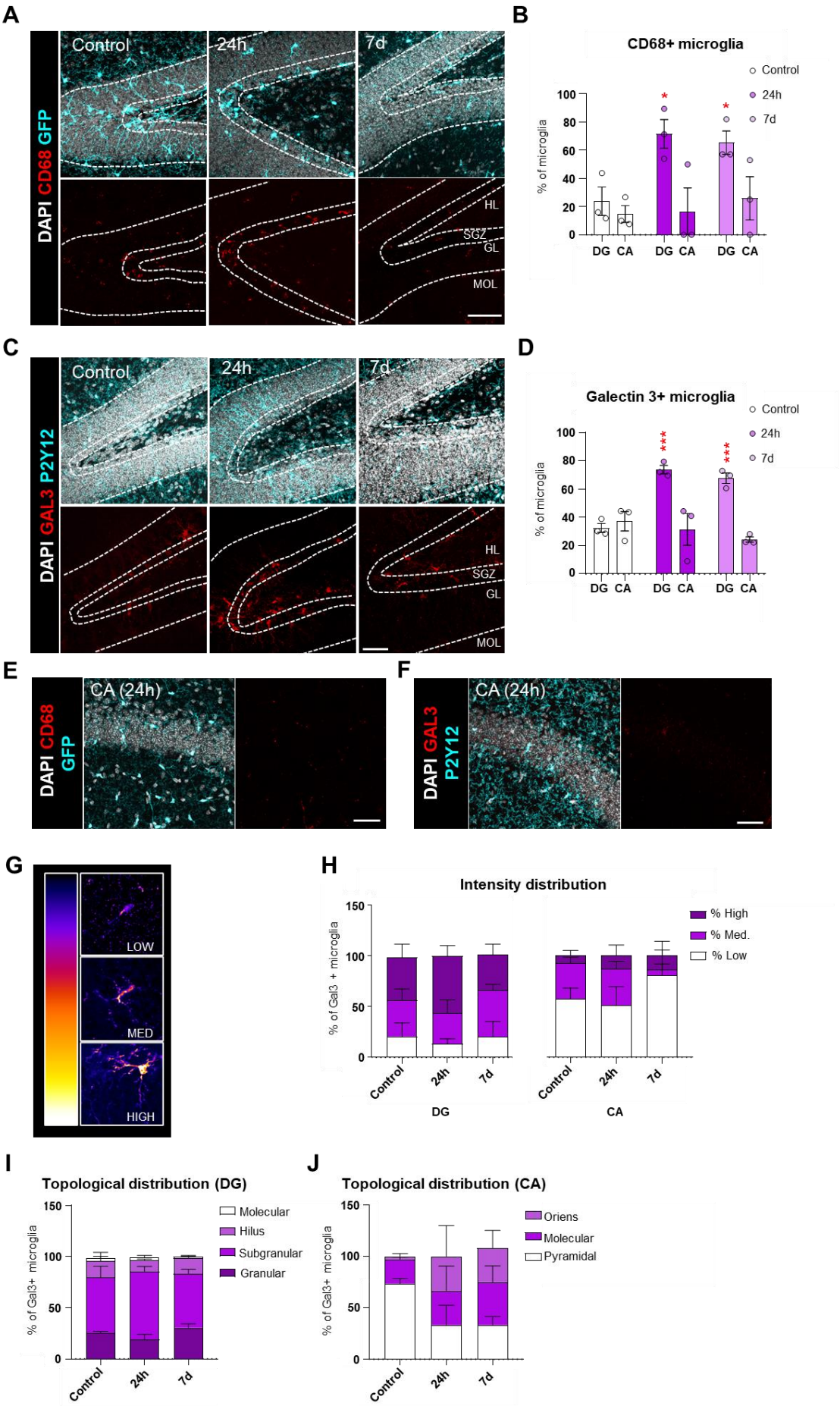
A
Control
24h
7d
DAPI CD68 GFP
HL
SGZ
GL
MOL
B
CD68+ microglia
Control
24h
7d
% of microglia
DG CA DG CA DG CA
C
DAPI GAL3 P2Y12
D
Galectin 3+ microglia
E
CA (24h)
DAPI CD68 GFP
F
DAPI GAL3 P2Y12
G
LOW
MED
HIGH
H
Intensity distribution
% of Gal3 + microglia
% High
% Med.
% Low
DG
CA
I
Topological distribution (DG)
% of Gal3+ microglia
Molecular
Hilus
Subgranular
Granular
J
Topological distribution (CA)
Oriens
Molecular
Pyramidal

Figure 24. Expression of phagocytosis related proteins after LCI. ***(A)*** *Representative confocal images of microglia expressing CD68 in the DG at different experimental conditions (Control, 24h, 7d), showing DAPI (white), CD68 (red), and GFP (cyan) staining. Different cellular layers (hilus, HL; subgranular zone, SGZ; granular layer, GL; molecular, MOL) are labelled with white dotted lines.* ***(B)*** *Analysis of the percentage of CD68+ microglia in DG and CA regions in different experimental conditions (Control, 24h and 7d).* ***(C)*** *Representative confocal images of microglia expressing galectin3 in the DG at different experimental conditions (Control, 24h, 7d), showing DAPI (white), galectin3 (red), and P2Y12 (cyan) staining. Different cellular layers (hilus, HL; subgranular zone, SGZ; granular layer, GL; molecular, MOL) are labelled with white dotted lines.* ***(D)*** *Analysis of the percentage of Gal3+ microglia in DG and CA regions in different experimental conditions (Control, 24h and 7d). (**E**) Representative confocal image of microglia expressing CD68 in the CA 24h after LCI showing DAPI (white), CD68 (red), and GFP (cyan) staining. (**F**) Representative confocal image of microglia expressing GAL3 in the CA 24h after LCI showing DAPI (white), GAL3 (red), and GFP (cyan) staining. (**G**) Graphical representation of the classification criteria to define cells according to gal3 intensity using a LUT (lookup table) from Image J. (**H**) Percentage of Gal3+ microglia in the DG and CA classified according to the expressed fluorescence intensity. (**I**) Percentage of Gal3+ microglia in the DG clustered according their topological distribution (granular, subgranular, hilus, molecular). (**J**) Percentage of Gal3+ microglia in the CA clustered according their topological distribution (oriens, molecular, pyramidal). Bars show mean ± SEM of n=3-4 mice. Data was analyzed by one-way ANOVA [B,D,F,G,H] followed by Holm-Sidak post hoc tests when appropriate. Asterisks represent significance between control and LCI (24h, and 7d). * represents p<0.05 and *** represents p<0.001. Scale bars=50μm. z=20.3, z=8.4, z=23.1[A]; z=12.6, z=28.7; z=18.98 [C]; z=17.5 [E]; z=17.5 [F].*

6.2.13 Reclustering of the pre-existing scRNA-seq data identified a CD68/GAL-3 high microglial cluster.

We examined the expression of *Cd68* and *Lgals3*, the gene encoding Gal-3, in our initial embedding and identified distinct co-expression patterns of these genes in specific territories of the UMAP graph (**Figure 25**). However, our initial unsupervised clustering approach (shared nearest neighbor (SNN) modularity optimization-based clustering algorithm with resolution parameter set to 0.1) did not reveal a defined population for these cells, which were assigned to the homeostatic microglia category. We reasoned that our initial approach did not achieve a good balance between underclustering and overclustering. Therefore, to gain a deeper understanding of compositional heterogeneity in microglia, we conducted a new analysis using the same mapped read data (refer to the table below for a summary of the relevant parameters for both analyses (**Table 3**)).

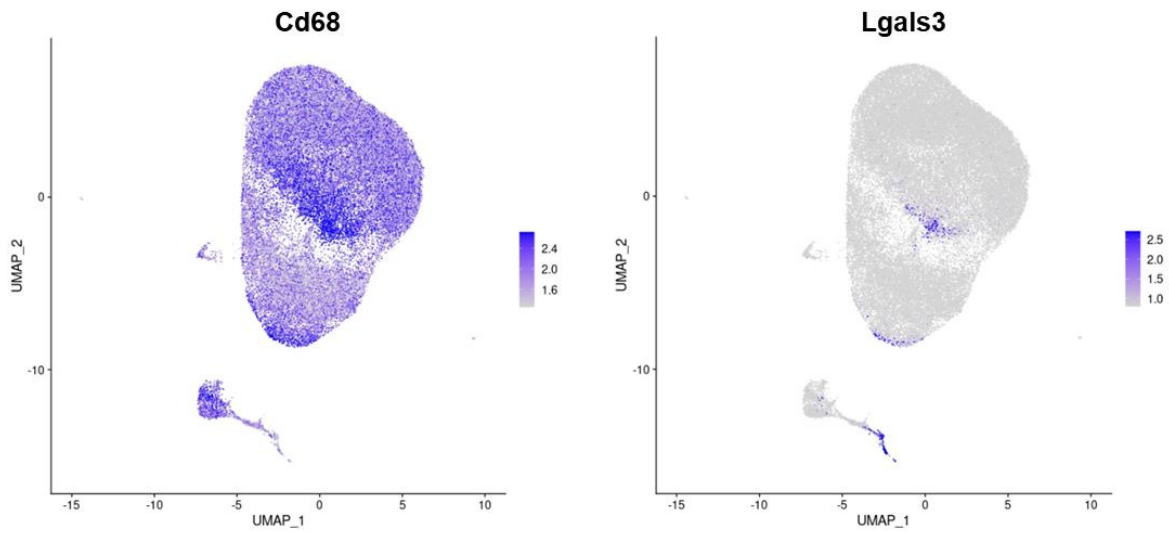

Figure 25. Cd68 and Lgals3 show co-expression patterns in specific territories of the UMAP graph.

Briefly, we performed computational identification of doublets using Scrublet tool (Wolock et al., 2019). Next, we filtered out cells based on read content and the relative proportion of mitochondrial genes using the same parameters as in our initial analysis, except for the upper threshold of per-cell read content, which was set to 4,500 reads. We then performed generalized linear model (GLM)-based data normalization and variance stabilization using SCT v2 (Choudhary et al., 2022). This is a relevant difference with our initial analysis where data were normalized using standard log-normalization (UMI counts are first scaled by the total sequencing depth ("size factors") followed by pseudocount addition and log-transformation) (Satija et al., 2015; Hafemeister et al., 2019). Next, we performed a supervised clustering approach, using several resolution parameters in the SNN algorithm (0.1, 0.5, 0.8) and clusters were visualized in a UMAP embedding generated using 30 most significant dimensions (PCs) from principal component analysis (PCA) (compared to 12 PCs used in the initial approach) (**Figure 26A**). Finally, we filtered out non-myeloid cells, MHC CAMs, and *ex vivo* "activated" microglia ("reactive") and reembeded the subset of microglia (32,591 cells) in low-dimensional space using the 30 most significant dimensions of the initial Seurat object (**Figure 27A**).

	1st analysis	2nd analysis
Doublet detection	No	Yes (Scrublet)
QC filtering	<1000; >4000; mt<5%	<1000; >4500; mt<5%
Normalization	Log norm	SCT v2
UMAP	12 PCs	30 PCs
Clustering	SNN, res=0.1 (unsupervised)	SNN, res=0.1;0.5;0.8 (supervised)

Table 3. Summary of the main steps performed in scRNAseq data analysis pipelines.

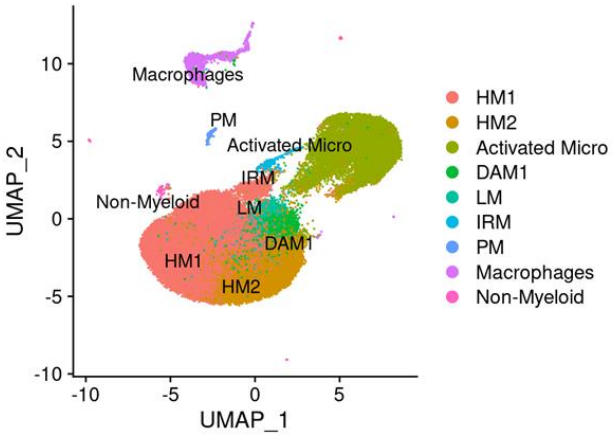

Figure 26. UMAP illustrating the outcomes of a supervised clustering. *This analysis relies on information derived from the 30 most significant dimensions (Principal Components, PCs) obtained through Principal Component Analysis (PCA).*

This approach revealed that microglia are largely homogeneous, in line with previous studies (Keren-Shaul et al., 2017; Hammond et al., 2019; Marsh et al., 2022a) (**Figure 27A**). In addition to two major populations of homeostatic microglia (HM1, 19050 cells; HM2, 9,818 cells), we also identified four smaller populations of microglia, which we annotated on the basis of the cluster-specific marker genes (Chen et al., 2021): disease-associated microglia 1 (DAM1; 1,944 cells; *APOE*, *B2M*), lysosomal microglia (LM; 1,319 cells; *APOE*, *CTSB*, *CST7*, *LPL*, *AXL*, *ITGAX*), interferon-responsive (IRM; 278 cells; *IFITM3*, *IRF7*), and proliferative (PM; 180 cells; e.g. *TOP2A*, *MKI67*) (**Figure 27A-C**). Notably, LCI was associated with a significant decrease in the proportion of cells in the HM2 cluster and a concomitant increase in proportion of cells in the LM and IRM clusters at 24h (**Figure 27B**). Thus, LCI seem to trigger short-term effects in the transcriptome of microglia and slightly affected homeostatic functioning of cells as previously reported in **6.2.8 section.**

LM population showed significant decrease in bona fide markers of homeostatic microglia such as P2ry12 and Tmem119 (**Figure 28A)**. Seven days after LCI treatment, the proportions of microglia populations were similar to control

condition, except for a marked increase in proliferative cells (**Figure 28B**). Interestingly, LM population showed increased levels of genes related with lysosomal activity, including *CTSB*, CTSZ, *CD68*, *ATP6V0*, and *CD63* (**Figure 28D**). Moreover, this cluster exhibited specific expression of *Lgals3* (**Figure 28D-E**), and increased levels of *Cd68* (**Figure 28B-C**), thereby confirming that the DAM2 harbors the post-phagocytic microglial population.

We speculate that the rise in CD68 could result from an increase in lysosomes for the degradation of phagocytic cargo (Chistiakov et al., 2017), whereas the increase in Gal3 may be linked to its participation in the recovery of damaged lysosomes (Rotshenker, 2022). The LM cluster bare some similarities with PAM, which have been associated with phagocytosis as both of them share core signature genes such as CD9, CD63 and LGALS3 (Li et al., 2019). The data presented herein demonstrates that early post-phagocytosis events appear to manifest a transient transcriptional signature shared among different phagocytic contexts (LCI and phagocytosis of PAMs in the *corpus callosum*) and conceivably associated with the degradative activities of the cell. Thus, phagocytic microglia adopt a transient transcriptional state linked to the requisite functions for proper degradation of the phagocytic cargo.

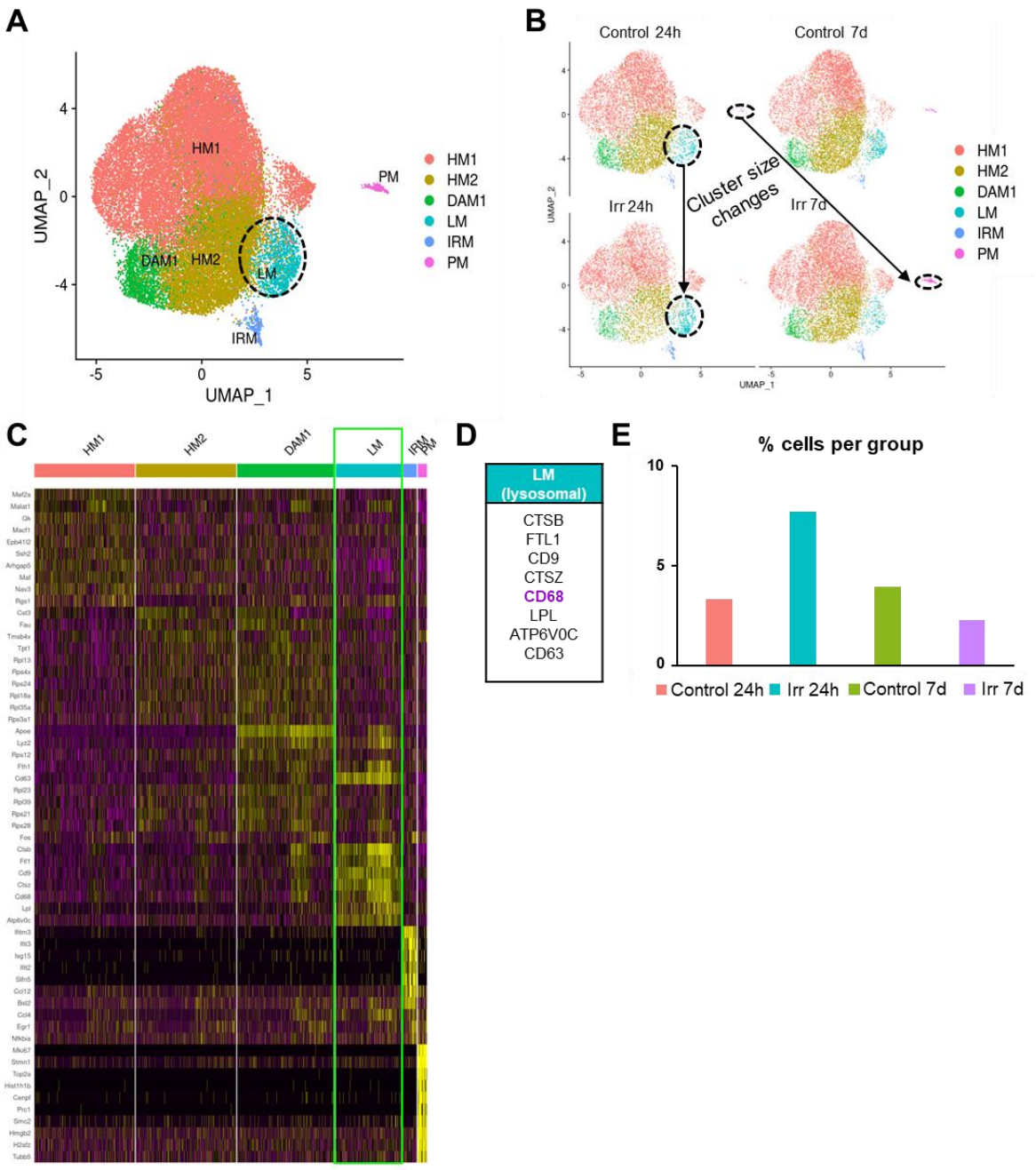

Figure 27. Lysosomal cluster detection by the re-analysis of pre-existing sc-RNA-seq data. ***(A)*** *UMAP of selected clusters, where LM cluster is surrounded by dotted-lines in black.* ***(B)*** *UMAP of the different treatments with annotations showing LM increase 24h after LCI. (**C**)Heat-map of most expressed genes per cluster. LM cluster is surrounded in light green.* ***(C)*** *Summary table with the top 10 signature genes of LM cluster. In dark purple, CD68 (highly expressed in post-phagocytic cells) is shown.* ***(D)*** *% of cells belonging to LM cluster in each experimental condition.*

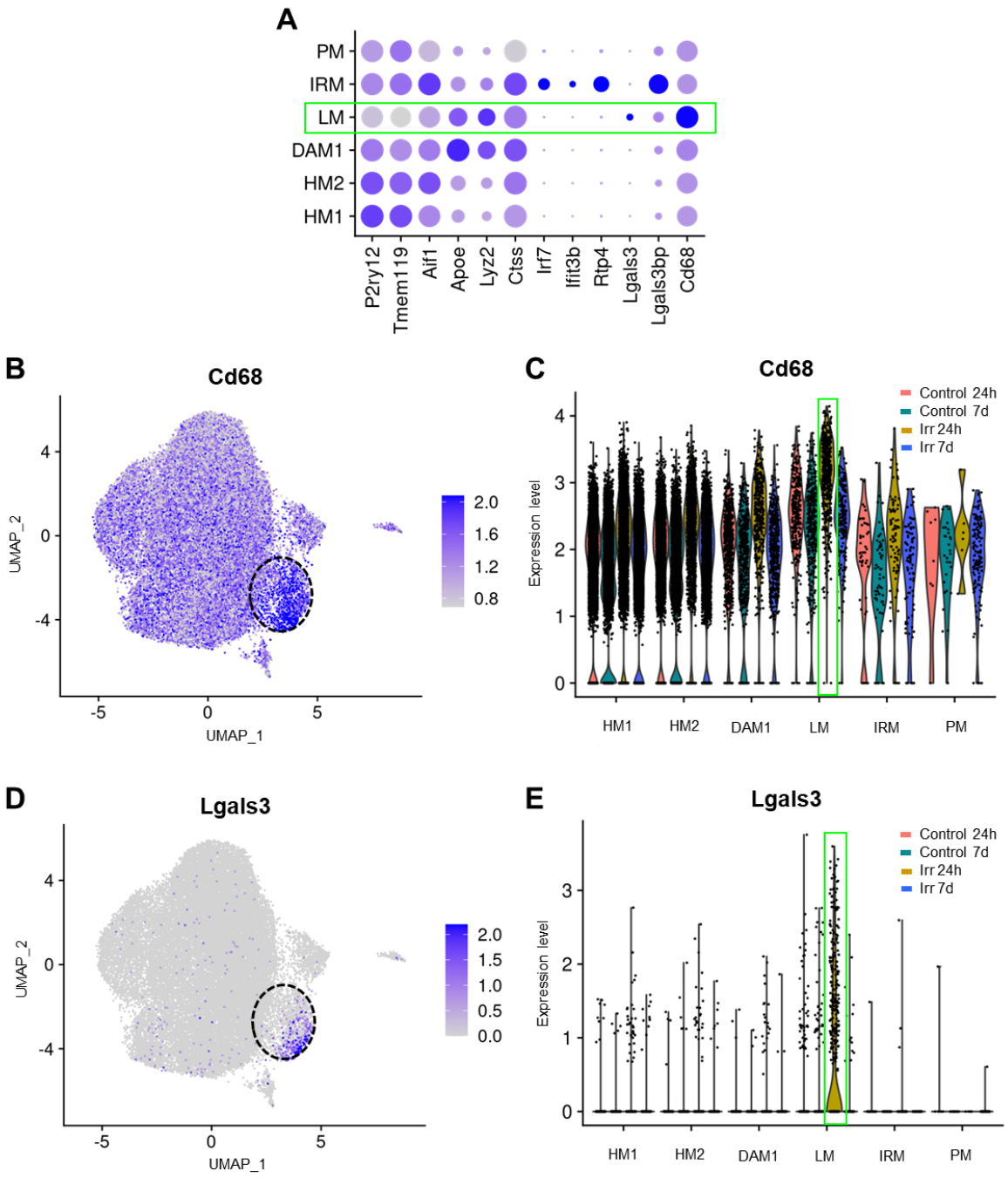

Figure 28. Characterization of the LM cluster. ***(A)*** *Dot-plot showing the main expression changes among the different clusters. LM clusters is showed surrounded by a light green rectangle.* ***(B)*** *UMAP showing CD68 expression indicated by FC. LM cluster is surrounded by dotted-lines in black.* ***(C)*** *Violin-plots showing CD68 in different clusters among different conditions. Increased expression in LM cluster at 24h after LCI is indicated by a light green rectangle.* ***(D)*** *UMAP showing LGALS3 expression indicated by FC. LM cluster is surrounded by dotted-lines in black.* ***(E)*** *Violin-plots showing LGALS3 in different clusters among different conditions. Increased expression in LM cluster at 24h after LCI is indicated by a light green rectangle.*

6.2.14 Microglia proliferates after phagocytosis

Once the changes induced by phagocytosis in the short term (24h) were defined, transcriptional changes in the long term (7d) were analyzed. Both the first and second scRNA-seq analyses and clustering revealed a proliferative cluster that increased in size after LCI, specifically at 7d. (**Figure 29C**).

To validate and identify the proliferative population in the hippocampal DG, we performed immunofluorescence and confocal imaging of microglia and Ki67, a proliferation-associated nuclear protein encoded by MKi67, a signature gene of the proliferative cluster in control (non-irradiated) and along the LCI time course (6h, 24h, 3d, 7d and 30d) (**Figure 30A**).

We observed a decreased number of total Ki67 cells in the DG right after LCI exposure (6h and 24h), which was recovered later on (**Figure 30B**). This reduction and posterior recovery suggested that LCI impaired the proliferation of neuroprogenitors that was reestablished with time. DG microglia was not proliferative in control mice, however, 7 days after LCI they started to proliferate, a trend that continued increasing at later time-points (30d) (**Figure 30A,C**). Moreover, microglial proliferation was specific from the DG, since almost no proliferative microglial cells were found CA, suggesting that phagocytosis triggered microglial proliferation (**Figure 30D**). Thus, we confirmed that phagocytosis induced microglial proliferation of microglia at 7d and validated that changes in proliferative population observed by sc-RNASeq were a consequence of phagocytosis. Therefore, phagocytosis initiated a protracted proliferative program in microglia.

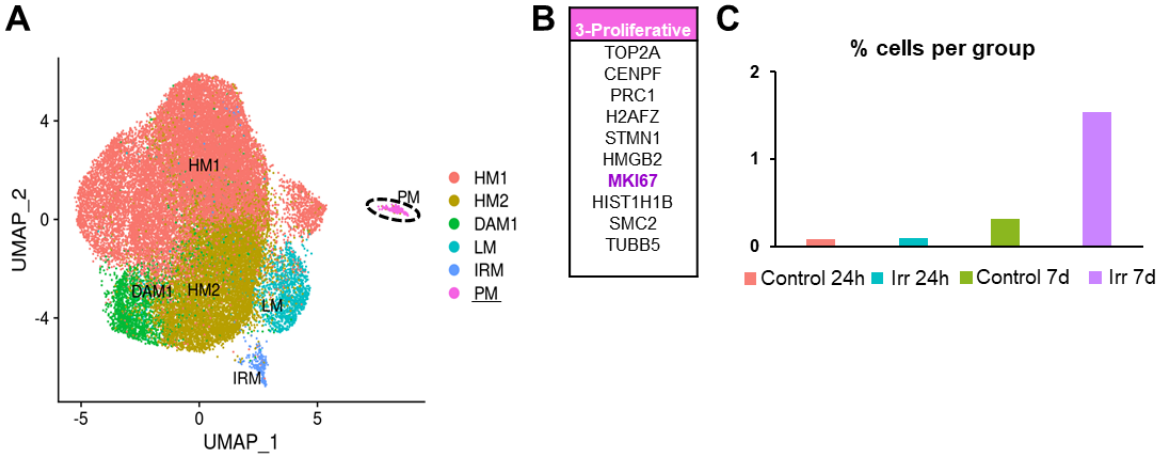

Figure 29. Characterization and analysis of proliferative cluster. ***(A)*** *UMAP showing the proliferative population surrounded by a dotted-line.* ***(B)*** *List of signature genes characteristic of the proliferative cluster.* ***(C)*** *% of cells belonging to proliferative cluster in each experimental condition.*

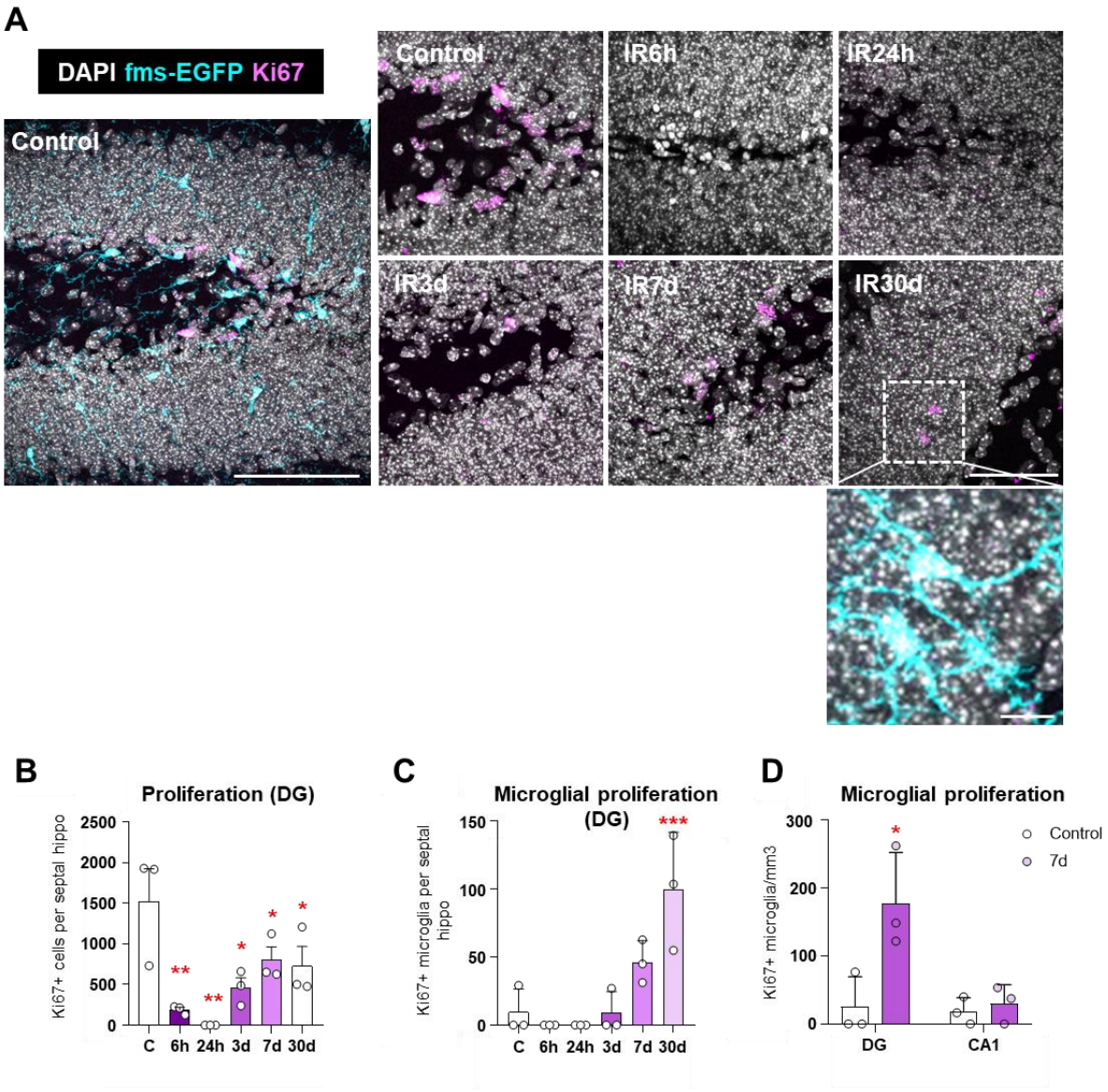

Figure 30. Analysis of proliferation after LCI. ***(A)*** *Representative confocal images of the different experimental conditions (control, and 6h, 24h, 3d, 7d, and 30d after LCI) showing DAPI (white), Ki67 (magenta), and GFP (cyan) staining. Detail of proliferative microglia is indicated within the white dotted square.* ***(B)*** *Number of Ki67$^+$ cells in the DG per septal hippocampus.* ***(C)*** *Number of microglia Ki67$^+$ in the DG per septal hippocampus.* ***(D)*** *Number of microglia Ki67$^+$ per mm3 in DG and CA regions. Bars show mean ± SEM of n=3 mice. Data was a was analyzed by one-way ANOVA [B,C] followed by Holm-Sidak post hoc tests when appropriate, and by Student's t-test [D]. Asterisks represent significance between control and LCI (6h, 24h, and 7d) [B,C] and between control and LCI 7d [D]. * represents p<0.05, ** represents p<0.01, *** represents p<0.001. Scale bars= 100μm and 50μm respectively [A], 10μm (inserts in [A]); z=8.4μm, z=11.2μm, z=16.1μm, z=14.7μm, z=16.1μm, z=16.1μm [A].*

6.2.15 The proliferative program caused after phagocytosis is abortive

Next, we assessed whether this proliferative program altered the number of microglia. We found that the microglial population dropped at 24h but recovered basal levels later on (**Figure 31A**), suggesting that some of the cells may die soon after phagocytosis. To directly track the new born microglia, 7 days after

LCI we injected bromodeoxyuridine (BrdU), a synthetic analog of the nucleoside thymidine that is incorporated into DNA during S-phase of the cell and labels proliferative cells (Duque et al., 2015). To analyze the lifespan of proliferative microglia, mice were euthanized at 24h and 48h post-injection (hpi), and we performed immunofluorescence and confocal imaging of microglia (fms-EGFP) and BrdU (**Figure 31A-B**). We observed that, unlike the total BrdU$^+$ population, which remained at similar numbers at both time points (24hpi and 48hpi), the BrdU$^+$ microglia population declined at 48h dpi (**Figure 31C-E**). Overall, these data demonstrates that phagocytosis-induced microglial proliferation was abortive, suggesting that only a few newly generated cells were maintained in the long term.

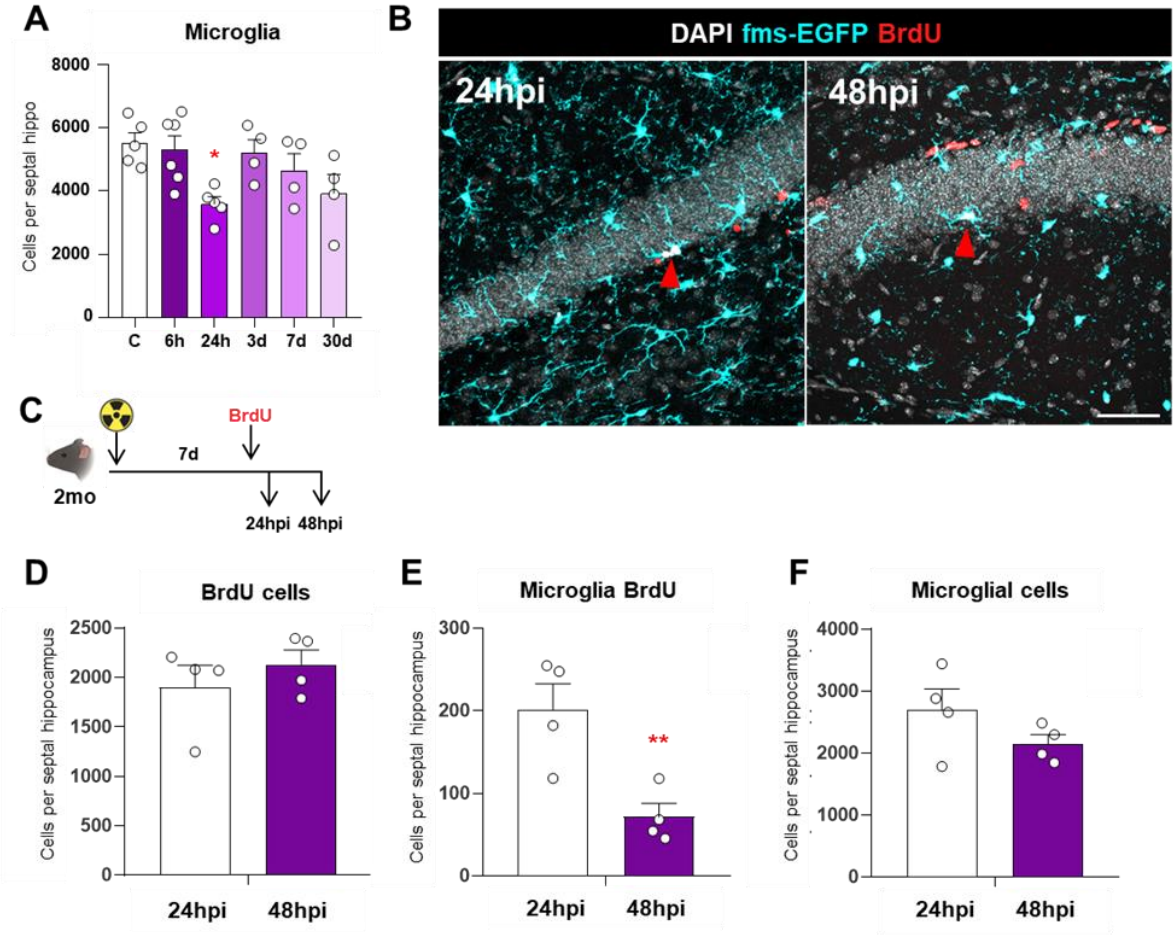

Figure 31. Analysis of functional proliferation after phagocytosis. ***(A)*** *Number of microglia in the DG per septal hippocampus at several time-points after LCI (Control, 6h, 24h, 3d, 7d, 30d).* ***(B)*** *Representative confocal images of the different experimental conditions (24hpi, 48hpi) showing DAPI (white), BrdU (red) y GFP (cyan) staining.* ***(C)*** *Experimental design of BrdU assay after LCI "superpagocytosis" model.* ***(D)*** *Number of BrdU+ cells in the DG per septal hippocampus.* ***(E)*** *Number of BrdU+ microglia in the DG per septal hippocampus.* ***(F)*** *Number of microglia in the DG per septal hippocampus at 24hpi and 48hpi. Bars show mean ± SEM of n=4 mice. Data was analyzed by Student's t-test. Asterisks represent significance between 24hpi and 48hpi. ** represents p<0.01. Scale bar= 50μm; z=13.3μm, z=27.3μm.*

6.2.16 Microglia proliferation compensates cell death caused after phagocytosis

As we observed a reduction of microglia 24h after LCI (**Figure 31A**), we next assessed early microglial death more directly and observed apoptotic microglia engaged in phagocytosis as early as 6h (pyknotic/karryorhectic Pu.1 nuclei) (**Figure 32A**). Nevertheless, the numbers were too small to quantify, possibly because they were immediately phagocytosed by nearby microglia. To independently analyze if microglial death was a consequence of phagocytosis, we performed an *in vitro* phagocytosis assay, feeding naïve microglia with apoptotic SH-SY5Y cells (Diaz-Aparicio et al., 2020) (**Figure 321B-C**). After phagocytosis microglia increased the expression of genes involved in both apoptosis (GO apoptosis: 0006915) and proliferation (GO proliferation: 0008283) (**Figure 32D**), and underwent apoptosis as early as 1h after the exposure to apoptotic cells (2.3% ± 1.2), a trend that continued to increase over time reaching a peak by 24h (12.6% ± 0.9) (**Figure 32E).** Thus, phagocytosis seemed to induce early (6-24h) apoptosis of microglia both *in vivo* an *in vitro*, followed by protracted (3-30d), abortive cell proliferation.

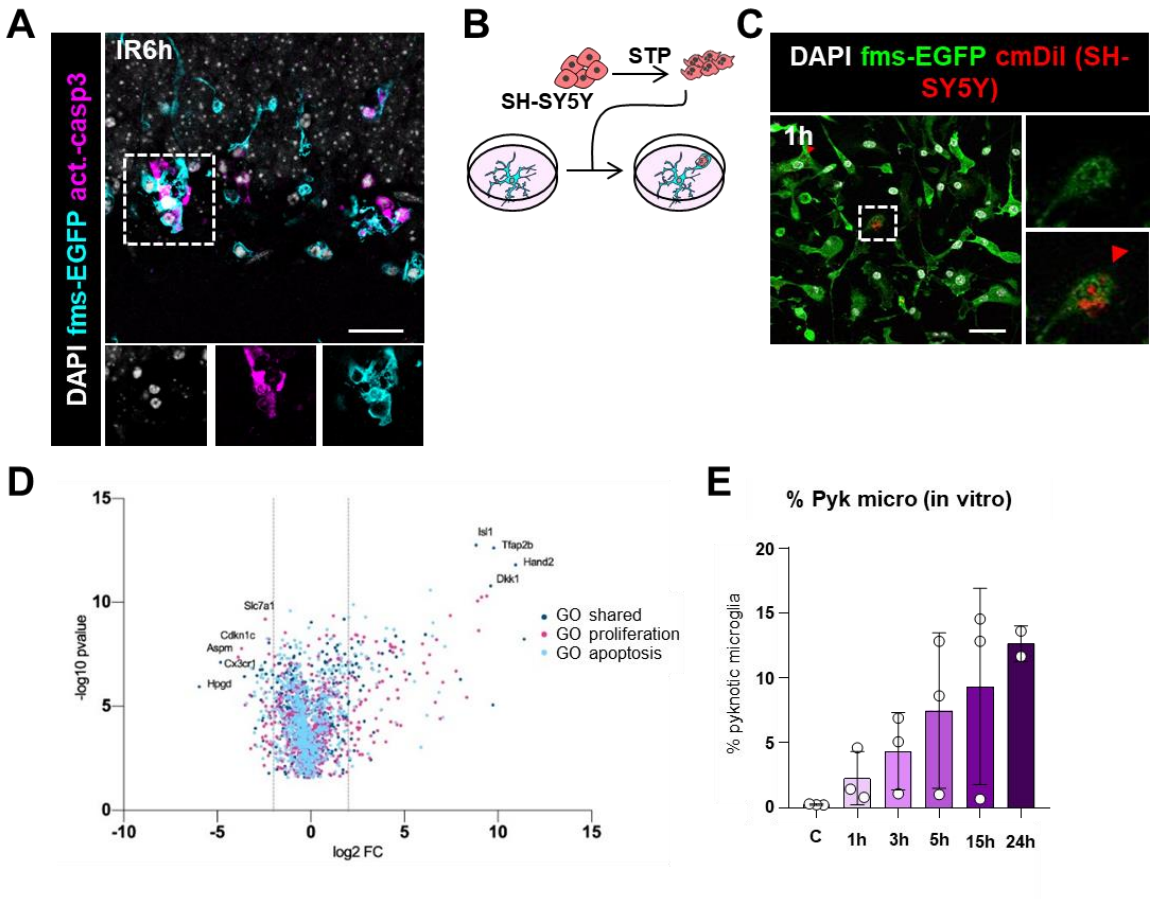

Figure 32. Analysis microglial death after phagocytosis. ***(A)*** *Representative confocal image of apoptotic microglia showing DAPI (white), activated caspase 3 (magenta) and GFP (cyan) staining. The detail is showed within a dotted square.* ***(B)*** *Experimental design of in vitro phagocytosis assay.* ***(C)*** *Representative confocal images of in vitro phagocytosis at 1h showing DAPI (white), Vampire SH-SY5Y (red) and GFP (cyan) staining. Detail of SH-SY5Y content within microglia.* ***(D)*** *Volcano plot showing most expressed genes in the microarray.* ***(E)*** *Percentage of pyknotic microglia after*

*phagocytosis. Bars show mean±SEM of 3-6 independent experiments. Data was analyzed by one-way ANOVA followed by Holm-Sidak post hoc tests when appropriate. Asterisks represent significance between control and LCI (6h, 24h, and 7d). * represents p<0.05. Scale bars= 30μm [B], 20μm [E]; z=6.3μm [B], z=0.7μm [E].*

In summary, the exploration of different parameters that label/identify the post-phagocytic microglia resulted in the identification of two different post-phagocytic populations: An early post-phagocytic population (24h) that specifically expressed Gal3 and overexpressed CD68; and a late post-phagocytic population (7d) that proliferated in response to the death induced by phagocytosis.

To further determine which was the mechanism causing microglial death, in the next aim we explore oxidative stress, mitochondrial alterations, and metabolic changes as possible causes of microglial death. Subsequently, we analyze whether the aforementioned renewed population recovers its phagocytic capacity in the long term.

6.3: Unraveling the mechanism by which microglia is affected by phagocytosis.

In the second section of Results, we aimed to find markers for post-phagocytic microglia and identified a $Gal3^{+}/CD68^{high}$ microglial population at the short-term and a population of proliferative microglia that compensates death caused after phagocytosis. This section focused on exploring the mechanisms underlying cell death in post-phagocytic microglia, with a specific emphasis on post-phagocytic oxidative stress, mitochondria, and cellular metabolism. These factors were chosen due to their intrinsic interrelationships and their known associations with cell death.

6.3.1 Phagocytosis increases oxidative stress in microglia

First we analyzed radical oxygen species (ROS) production, which is generated during various cellular processes such as proliferation, differentiation, metabolic adaptation, regulation immunity (Glasauer et al., 2013) and phagocytosis (Dupre-Crochet et al., 2013). In phagocytosis, ROS is generated in the phagosome and contribute to cargo degradation (Minakami et al., 2006). However, excess levels of ROS cause damage to proteins, nucleic acids, lipids, membranes and organelles, which can lead to activation of cell death processes such as apoptosis (Redza-Dutordoir et al., 2016). Thus, to analyze whether oxidative stress was induced in response to phagocytosis leading to a further damage of the cells, we used the *in vitro* model of phagocytosis and measured ROS with the fluorogenic probe CellROX. 6h after phagocytosis ROS levels were 2.1 ± 0.3 times higher than in naïve microglia, while at 24h a downward trend was observed that suggested that ROS levels were returning to basal levels in naïve microglia. This data suggested that ROS production could be involved in the generation of oxidative stress leading to cellular dysfunction and posterior death (**Figure 33**). Nevertheless, this result needs to be confirmed by analyzing whether antioxidants could revert this effect and avoid microglial death after phagocytosis.

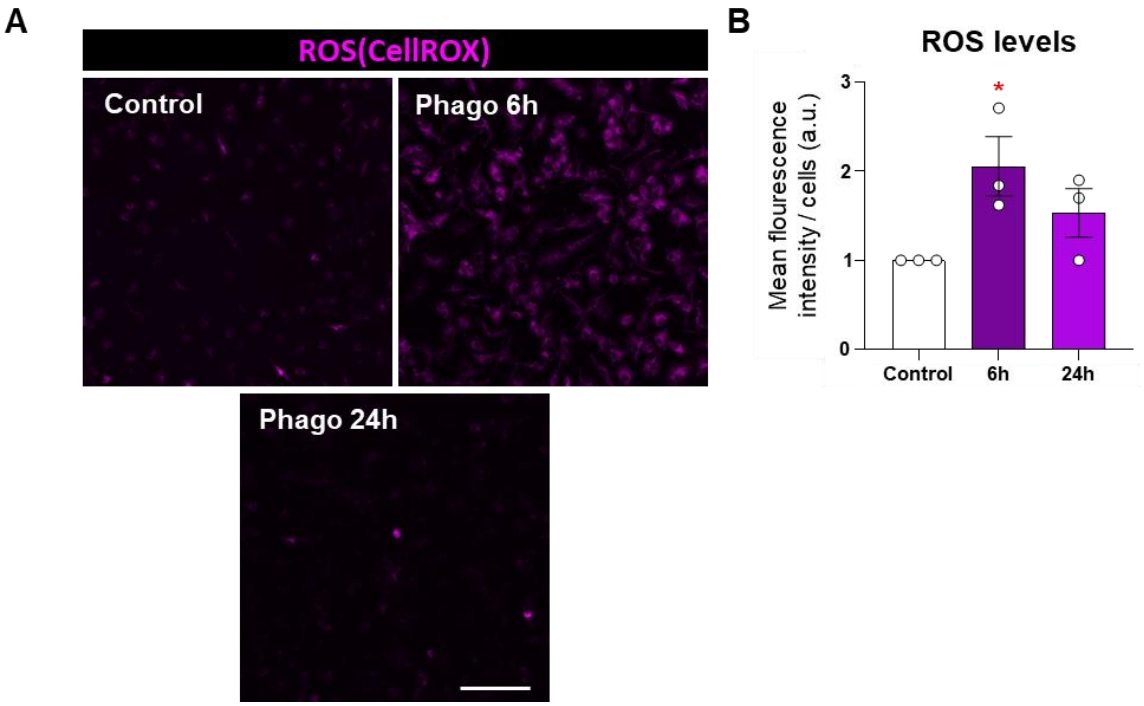

Figure 33. ROS analysis after phagocytosis. **(A)** Representative images of primary microglia expressing ROS at different conditions (Control, 6h and 24h). **(B)** ROS levels indicated in arbitrary units (a.u.). Bars show mean±SEM of n=3 independent experiments. Data was analyzed by one-way ANOVA followed by Holm-Sidak post hoc tests when appropriate. Asterisks represent significance between control and phagocytic (6h,24h) microglia. * indicates p <0.05. Scale bar= 50μm.

6.3.2 Phagocytosis remodels mitochondria decreasing the mitochondrial number and simplifying the networks.

Approximately 90% of ROS are produced by the mitochondria (Tirichen et al., 2021). Furthermore, this ROS production often leads to mitochondrial damage and mitochondria undergo changes such as remodeling (Muliyil et al., 2014) and mitophagy (Schofield et al., 2021). To further examine alterations in mitochondria of post-phagocytic microglia at 24h, we analyzed the mitochondrial network, morphology, and ultrastructure using our *in vitro* phagocytosis model with both the microglial cell line BV2 and primary microglia. The mitochondrial network and morphology were examined in BV-2 cells transfected with the plasmid GFP-Mito-7 (Garcia-Moreno et al., 2014), which labels the mitochondria targeting the subunit VII of cytochrome C oxidase (Olenych et al., 2007). Mitochondria were visualized using confocal microscopy to analyze the mitochondrial network (using Fiji) and mitochondrial morphology in 3D (using Huygens) (**Figure 33A**). Both types of analysis were equivalent and detected a comparable number of mitochondrial objects per cell (**Figure 34B**), showing a high correlation between methods (R^2=0.89). The mitochondrial network analysis represented the mitochondrial objects in a simplified way, generating a central line or skeleton showing the basic shape of the network, which allowed us to examine its complexity. Thus, we observed that phagocytosis reduced the number of both individual and network-forming mitochondria. We also found a trend of

decreasing length, branches, and junctions, suggesting a reduction in network complexity (**Figure 34C**). The mitochondrial morphology analysis also revealed that after phagocytosis the total number of mitochondrial objects and their total length decreased. However, there was no change in the average dimensions (volume and length) of mitochondrial objects (**Figure 34D**). These data showed that phagocytosis caused a reduction in the mitochondria of the microglia-like cell line BV2.

To validate these changes, we performed the same phagocytosis assay in primary microglia and analyzed the mitochondria by transmission electron microscopy (TEM) (**Figure 35A**). We observed that after phagocytosis there were fewer mitochondrial objects that occupied less cytoplasmic area (**Figure 35B-C**). After phagocytosis mitochondrial objects were smaller, supporting the decreased complexity of the mitochondrial network observed earlier (**Figure 35D**). All together, these data suggest that phagocytosis reduced mitochondrial numbers and simpler networks. This mitochondrial reduction may be a consequence of ROS production, as increased ROS levels disrupts mitochondrial dynamics and causes mitophagy (Chuang et al., 2020). Also, since mitochondria have a central role in cellular metabolism, their reduction may also imply a decrease in catabolic metabolism and consecutive microglial death.

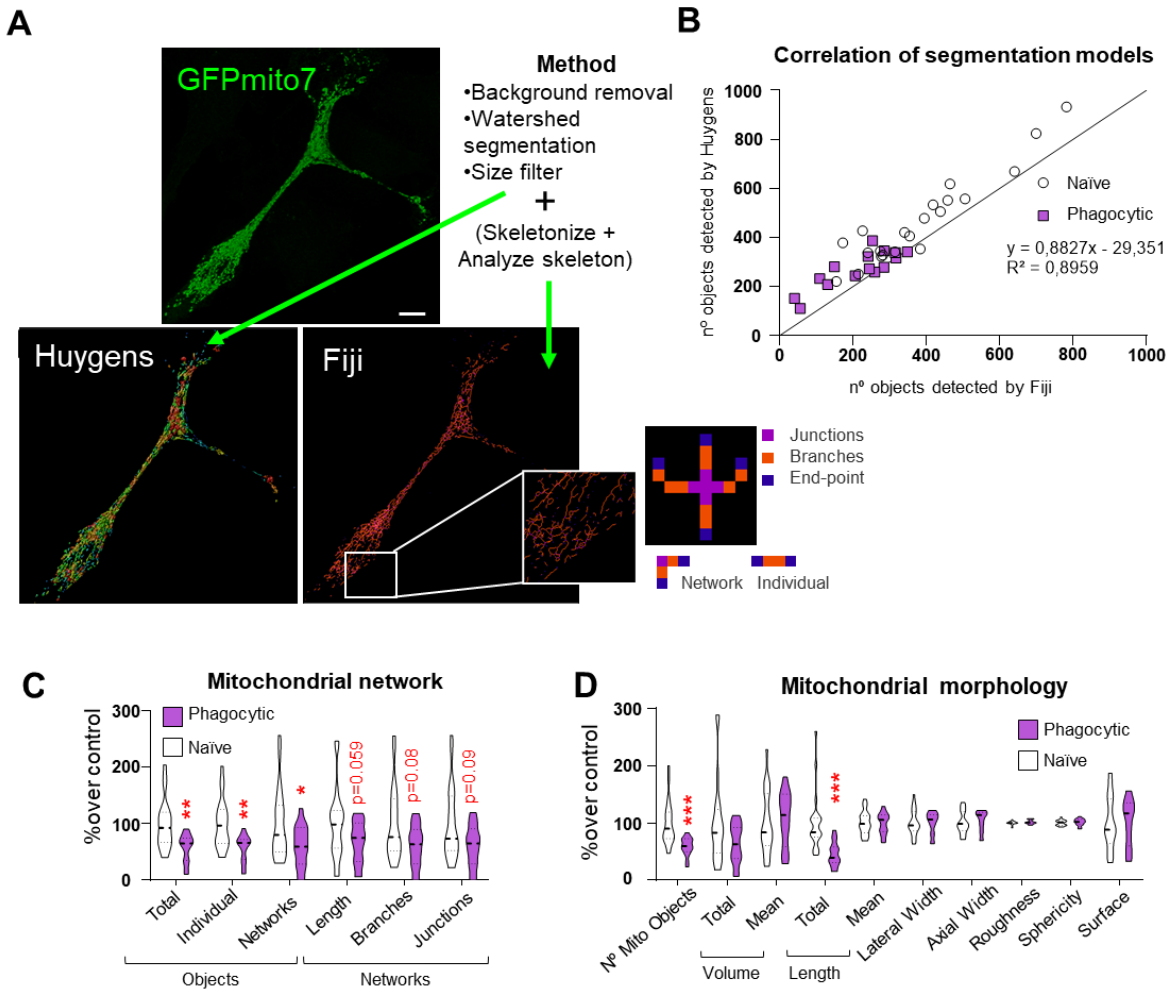

Figure 34. Confocal microscopy analysis of mitochondria in BV2 cells after phagocytosis. ***(A)*** *Graphical summary of the analysis methods. The images show mitochondria labelled in with GFPmito7 (green) and the analysis of mitochondrial morphology by Huygens and Fiji image analysis softwares respectively.* ***(B)*** *Correlation of the analysis of mitochondrial objects using Fiji and Huygens.* ***(C)*** *Analysis of mitochondrial network showing the percentage of different mitochondrial parameters normalized to control.* ***(D)*** *Analysis of mitochondrial morphology showing the percentage of different mitochondrial parameters normalized to control. White dots and coloured squares show the correlation of the values detected (number of mitochondrial objects per cell) with each method of analysis. Violin plots show the data distribution including extreme values; lower and upper hinges correspond to the third quartile respectively. Data shows an of n=3 independent experiments. Data was analyzed by Student's t-test. Some data [C,D] was Log transformed to comply with homoscedasticity. When neither normality nor homoscedasticity were accomplished Mann-Whitney test performed [C,D]. * indicates p <0.05, ** indicates p <0.01, *** indicates p <0.001. Scale bar= 10mm; z=7.64mm.*

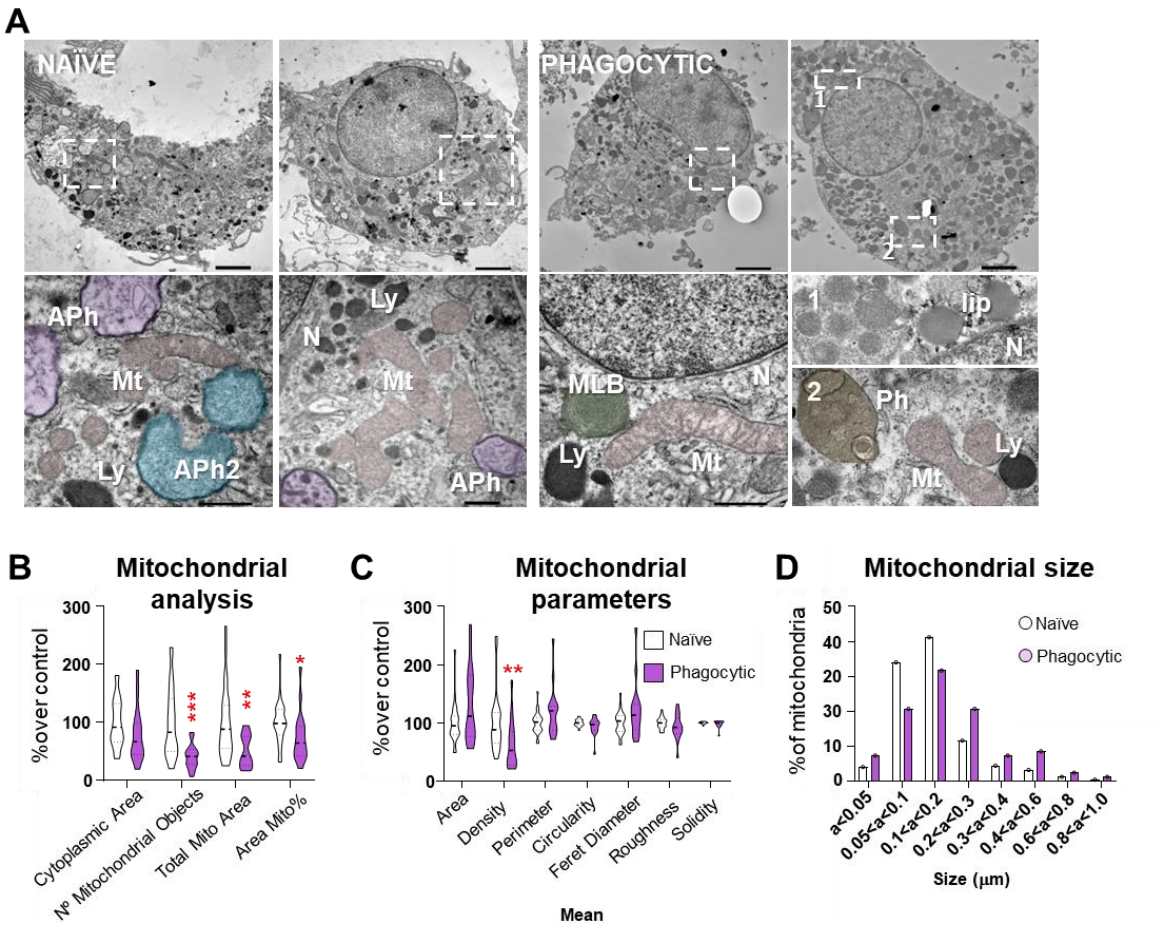

Figure 35. TEM analysis of mitochondria in primary microglia after phagocytosis. ***(A)*** *Representative TEM images of nave and phagocytic microglia. Images show mitochondria (pink,Mt) and other organelles, such as lysosomes (dark,Ly). In control cells, abundant primary and secondary autophagosmes (purple and blue, respectively; APh) were found, whereas in phagocytic cells several degradative organelles such as multilamelated bodies (green,MLB) were found. Lipidic content (lip) and phagosomes (Ph) were also found in phagocytic cells.* ***(B)*** *EM analysis of mitochondrial object number and area in microglial cytoplasm showing the percentage of the different measurements normalized to control.* ***(C)*** *EM*

analysis of mitochondrial parameters showing the percentage of the measurements normalized to control. ***(D)*** *Classification of mitochondrial objects according their size (% of mitochondria). Violin plots show the data distribution including extreme values; lower and upper hinges correspond to the third quartile respectively. Data was analyzed by Student's t-test. Some data [B,C] was Log transformed to comply with homoscedasticity and/or normality. * indicates p <0.05, ** indicates p <0.01, *** indicates p <0.001. Scale bar, 2µm for whole cells images and 0.5µm for details [A].*

6.3.3 Phagocytosis downregulates catabolic metabolism.

Mitochondria are essential for the generation of most of the energy needed by cells. Through a process called cellular respiration, which involves a series of metabolic pathways, these organelles, convert glucose and other fuels into ATP, the universal energy currency of cells (Judge et al., 2020). Since phagocytosis remodeled the mitochondrial network by reducing the number of mitochondria, we explored whether catabolic metabolism was affected after phagocytosis by analyzing the different pathways involved (glycolysis, tricarboxylic acid cycle (TCA) and mitochondrial respiration (**Figure 36A**). Using the *in vitro* phagocytosis model, we analyzed post-phagocytic metabolic changes at 24h by performing metabolomics and measuring extracellular acidification (ECAR) and oxygen consumption rate (OCR) using the Seahorse technology (Zhang et al., 2019) and metabolites using mass spectrometry.

Metabolomics analysis revealed no changes in post-phagocytic microglia in the production of major metabolites involved in glycolysis (glucose) and in the TCA cycle (succinate, fumarate and malate) (**Figure 364B-E**). To further analyze the glycolytic pathway using Seahorse, we examined the contribution of glycolysis to ECAR by measuring the proton extrusion rate (PER) generated by this process (**Figure 36F**). PER analysis showed that in naïve microglia glycolysis contributed to 71.4 ± 13.8% of acidification, while mitochondrial respiration contributed to the remaining 28.6 ± 13.8%, whereas in phagocytic microglia the contribution of glycolysis to acidification increased to 92.43 ± 1.2% (**Figure 36G**). Thus, glycolysis of phagocytic cells seemed to be increased. However, the analysis of compensatory glycolysis, which was examined by measuring the glycolytic PER after blockade of mitochondrial respiration with Rotenone and Antimycin A (Rot/AA), showed that unlike naïve microglia, phagocytic microglia were not able to increase glycolysis after inhibition of oxidative phosphorylation (**Figure 36H**). Therefore, phagocytosis impaired the glycolytic metabolism by reducing the spare capacity of microglia to cope with energetic demands when mitochondrial respiration is pharmacologically impaired.

Next, we analyzed mitochondrial metabolism by measuring the OCR in the presence of ATP synthase inhibitors and observed that phagocytosis led to an increased proton leak, a measurement of mitochondrial malfunctioning, while decreasing ATP production (**Figure 36I-J**). Next, the measurement of OCR before and after the uncoupling agent FCCP (carbonyl cyanide 4-(trifluoromethoxy)phenylhydrazone) which disrupts the proton gradient across the mitochondrial inner membrane, showed the maximal capacity of mitochondria. After phagocytosis both the maximal respiration and the spare capacity showed a decreased trend. Furthermore, when the spare capacity of phagocytic microglia was normalized to that of naïve microglia, we observed a decreased ability of the

cells to increase OCR in response to an increased demand for energy (**Figure 36J-K**). Moreover, increased OCR and ECAR after both glycolytic and mitochondrial inhibition (**Figure 36H-J**) revealed that other metabolic pathways could be upregulated after phagocytosis. Altogether, phagocytosis leads to a downregulated catabolic metabolism with an impaired mitochondrial respiration and compensatory glycolysis, while other compensatory metabolic pathways seem to be increased. This downregulated catabolic metabolism could be a cause of mitochondrial damage triggered by ROS and cause cell death.

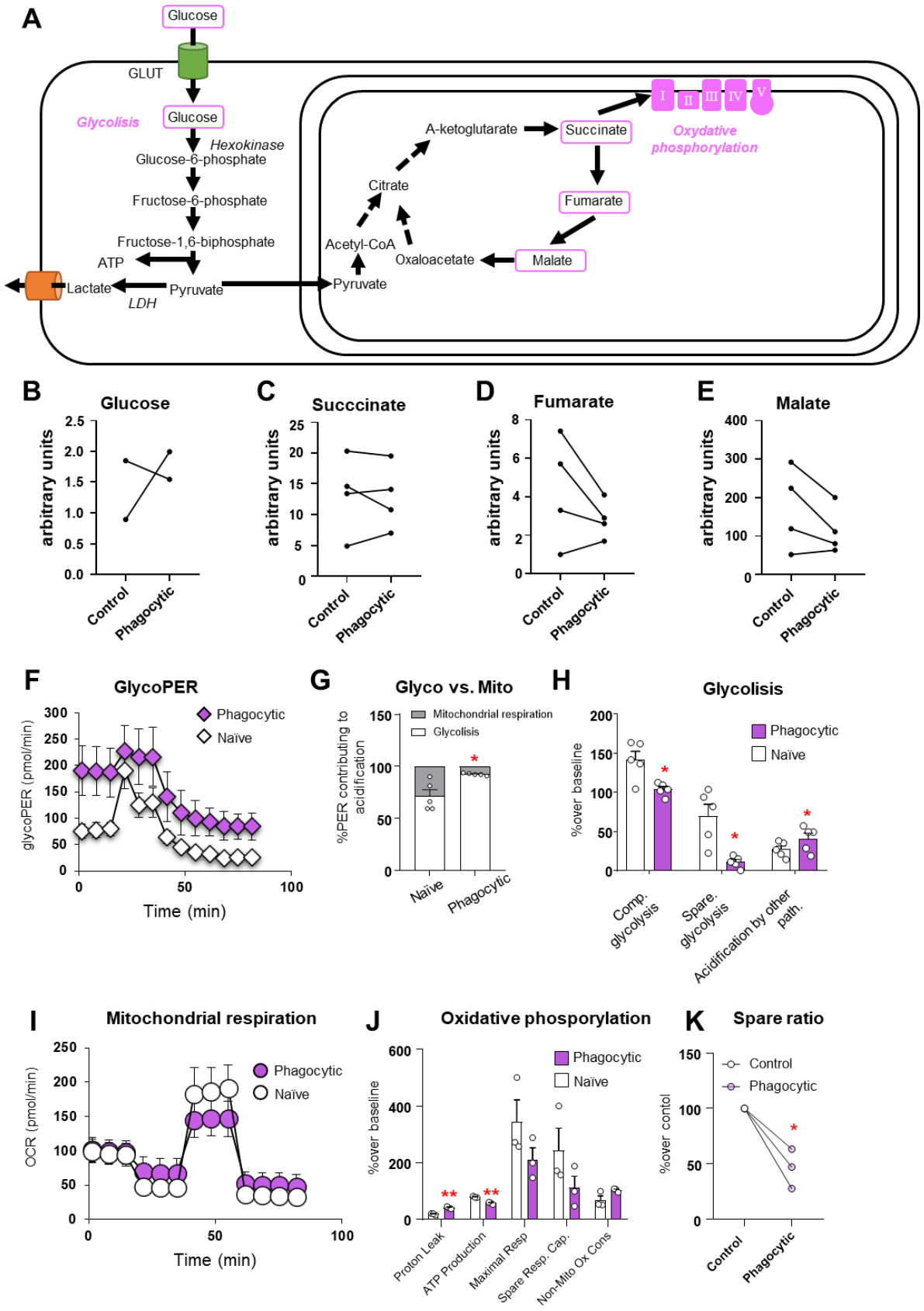

Figure 36. Analysis of catabolic metabolism after phagocytosis. ***(A)*** *Graphical summary of the metabolic pathways explored. The metabolites analyzed by mass spectrometry are labeled in magenta.* ***(B)*** *Glucose levels measured in arbitrary units*

(a.u.). ***(C)*** *Succinate levels measured in arbitrary units (a.u.).* ***(D)*** *Fumarate levels measured in arbitrary units (a.u.).* ***(E)*** *Malate levels measured in arbitrary units (a.u.).* ***(F)*** *Proton Extrusion Rate (PER) in pmol/min caused by glycolysis of naïve and phagocytic microglia (the data of a representative experiment was chosen).* ***(G)*** *Percentage of PER originated by both glycolysis and oxidative phosphorylation.* ***(H)*** *Analysis of glycolysis by measuring changes in PER over baseline.* ***(I)*** *Oxygen Consumption Rate (OCR) in pmol/min of naïve and phagocytic microglia microglia (data from a representative experiment is shown).* ***(J)*** *Analysis of oxidative phosphorylation by measuring changes in OCR over baseline.* ***(K)*** *Spare capacity of mitochondrial respiration normalized to control. Dots represent individual measurements and lines connect independent experiments (B-E). Icons (diamonds and circles) from F and I represent the mean of the different conditions of a representative experiment, while error bars show the SD. Bars show mean±SEM of n=3/5 independent experiments in G, H and J. Data was analyzed by Student's t-test. Some data ([G,J]) was Log transformed to comply with homoscedasticity. When homoscedasticity was not accomplished Welch's t-test was performed ([K]). Asterisks represent significance between control and phagocytic microglia. * indicates p <0.05. ** indicates p <0.01.*

6.3.4 Metabolomic analysis after phagocytosis reveals an increased production of metabolites involved in resolution of oxidative stress and cell proliferation

To further analyze which other metabolic pathways were upregulated after phagocytosis, we used mass spectrometry to identify other major metabolites from the folate cycle (serine), the methionine cycle (methionine, choline, betaine, GPC, SAMe and dc-SAMe) and interconnected pathways (threonine, glutamate and glutamine), which are involved in several key function as the syntheses of the antioxidant glutathione (GSH, GSSG) and polyamine synthesis (spermidine and spermine) (**Figure 37**). All these pathways could be altered after phagocytosis. On one hand, the methionine cycle participates in methylation reactions, which are crucial for the regulation of gene expression (Zhang, 2018). Our transcriptomic results have shown changes in gene expression after phagocytosis, suggesting that the methionine cycle may be altered in post-phagocytic microglia. Additionally, glutathione and polyamines play a key role in situations of oxidative stress (Diaz-Vivancos et al., 2015; Lenis et al., 2017), which is increased after phagocytosis, so their synthesis could also be altered in post-phagocytic microglia.

Post-phagocytic microglia produced a significant increase in the oxidized form of glutathione (GSH), glutathione disulfide (GSSG) (**Figure 37D**), which is generated when glutathione acts as an antioxidant (Owen et al., 2010a), suggesting that glutathione had been involved in resolving oxidative stress. Additionally, phagocytosis also induced changes in polyamine synthesis, decreasing the amount decarboxylated S-adenosylmethionine (dc-SAMe), and increasing spermidine levels while decreasing spermine, and finally leading to an increased Spd/Spm ratio (**Figure 37B-C**). These polyamines are involved in the recovery from oxidative stress, e.g., increased of spermidine mitigates oxidative stress by reducing ROS levels (Kumar et al., 2022b), cell proliferation, and differentiation (Pegg, 2016). Decreased dc-SAMe, which is a precursor of the increased spermidine, and increased Spd/Spm ratio suggested a potentiation of spermidine production, which seem to be used immediately after its synthesis as it is not posteriorly transformed into spermine. Additionally, phagocytosis also

increased levels of the metabolite glycerylphosphorylcholine (GPC) (**Figure 37C**), a precursor of phosphatidylcholine (PC), which is a major component of cellular membranes in the body. The metabolite serine, which is involved in protein synthesis showed an increased tendency also after phagocytosis. All together, the metabolomic data suggested that after phagocytosis microglia synthetized molecules that participate in oxidative stress resolution; in cell recovery, by the generation of proteins and lipidic membranes that may have been degraded during the phagocytotic process; and in cell proliferation.

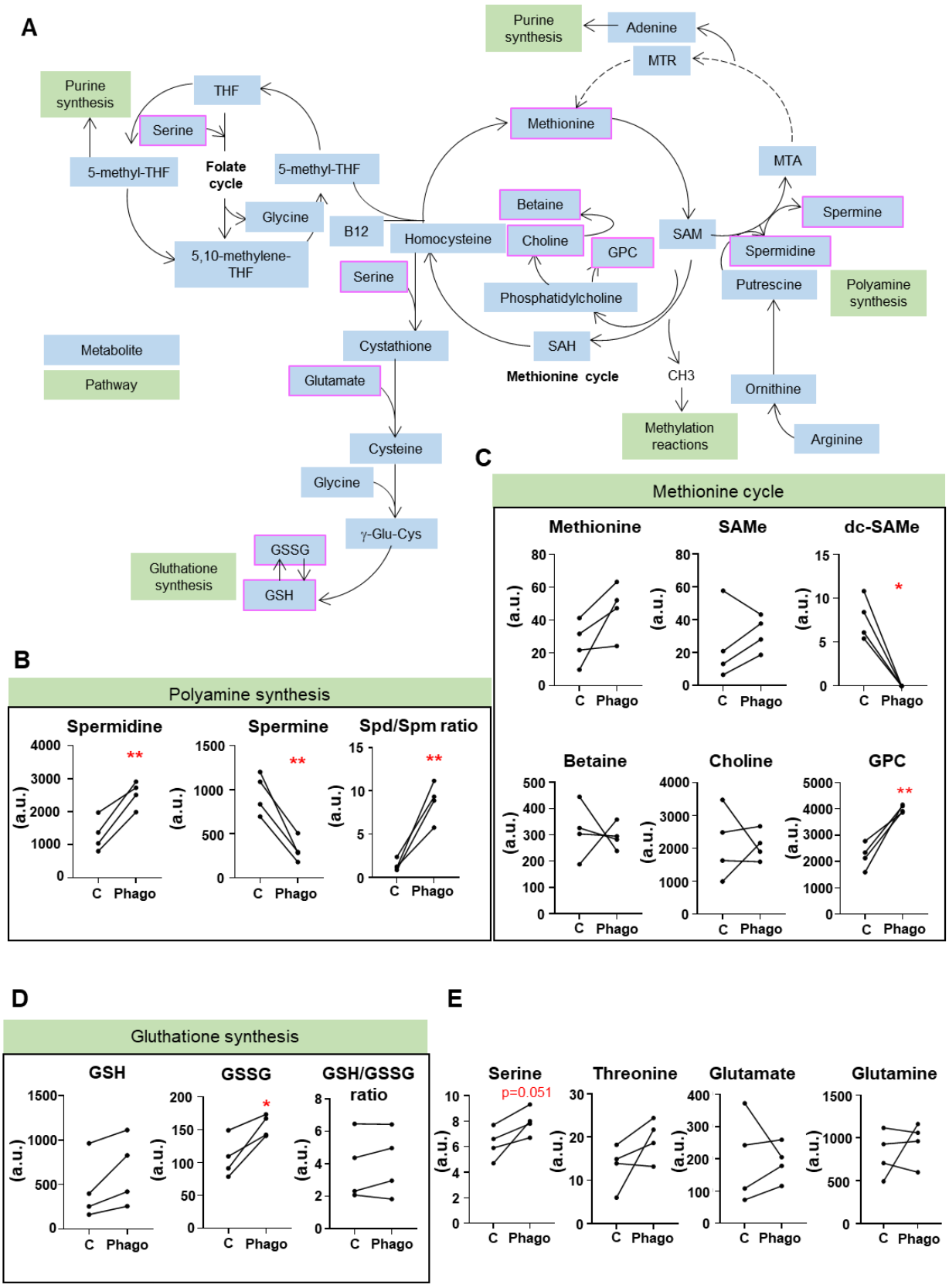

Figure 37. Analysis of metabolites of methionine cycle, polyamine synthesis and glutathione synthesis. ***(A)*** *Graphical summary of analyzed metabolites(purple) by mass spectrometry and the metabolic pathway in which they are involved.* ***(B)*** *Measurements of polyamine synthesis metabolites (spermidine, spermine, Spd/Spm*

ratio) in arbitrary units(a.u.). ***(C)*** *Measurements of methionine cycle metabolites (methionine, SAMe, dc-SAMe, betaine, choline, GPC) in arbitrary units(a.u.).* ***(D)*** *Measurements of glutathione synthesis metabolites (GSH, GSSG, GSH/GSSG) in arbitrary units (a.u.).* ***(E)*** *Measurements of other metabolites involved in methionine cycle (Serine, Threonine, Glutamate, Glutamine) in arbitrary units (a.u.). Dots represent individual measurements and lines connect independent experiments (n=4). Data was analyzed by Student's t-test. Some data [B,C] was Log transformed to comply with homoscedasticity. When neither normality nor homocedasticity were accomplished Mann-Whitney test performed [C]. * indicates p <0.05, ** indicates p <0.01.*

6.3.5 Phagocytosis efficiency is recovered in the long term.

We next asked whether after the observed cellular stress that microglia undergo after phagocytosis and the posterior compensatory proliferation, the cells were able to recover their function. To analyze whether these changes helped preserving phagocytic efficiency of microglia, we challenged microglia sequentially *in vivo*, by administering LCI twice with a time interval of 7 days. Thus, we exposed microglia to 2 pulses of apoptotic cells that need to be phagocytosed and studied the efficiency of post-phagocytic microglia after the second exposure to analyze their phagocytic (6h) and clearance efficiency (24h) (**Figure 38A**).

The second LCI pulse induced apoptosis, although this death was 7.8 ± 0.78 times smaller than that generated in the first pulse (**Figure 38B-C**), since the pool of proliferating neuroprogenitors had been reduced during the first LCI exposure (**Figure 38B**). Nonetheless, microglia were equally efficient in clearing apoptotic corpses in the first and the second pulse, as all apoptotic cells disappeared by 24h (**Figure 38B-C**). Likewise, the phagocytic index and the number of microglia were unaffected by the sequential irradiation. The maintenance of the total microglia count following this second challenge may be imply that phagocytosis-induced microglial cell death is proportional to the number of apoptotic cells that are cleared. That is, as microglia phagocytose fewer apoptotic cells in the second irradiation challenge, they are less stressed and therefore a reduction in their number is not observed. (**Figure 38D-E**). Despite the limitations of this model, which generates a minor phagocytic challenge after the second irradiation, post-phagocytic microglia seemed to preserve their phagocytic capacity and were able to remove apoptotic debris efficiently. Thus, the mitochondrial and metabolic adaptations that microglia undergo after phagocytosis seem to preserve their function in the long-term.

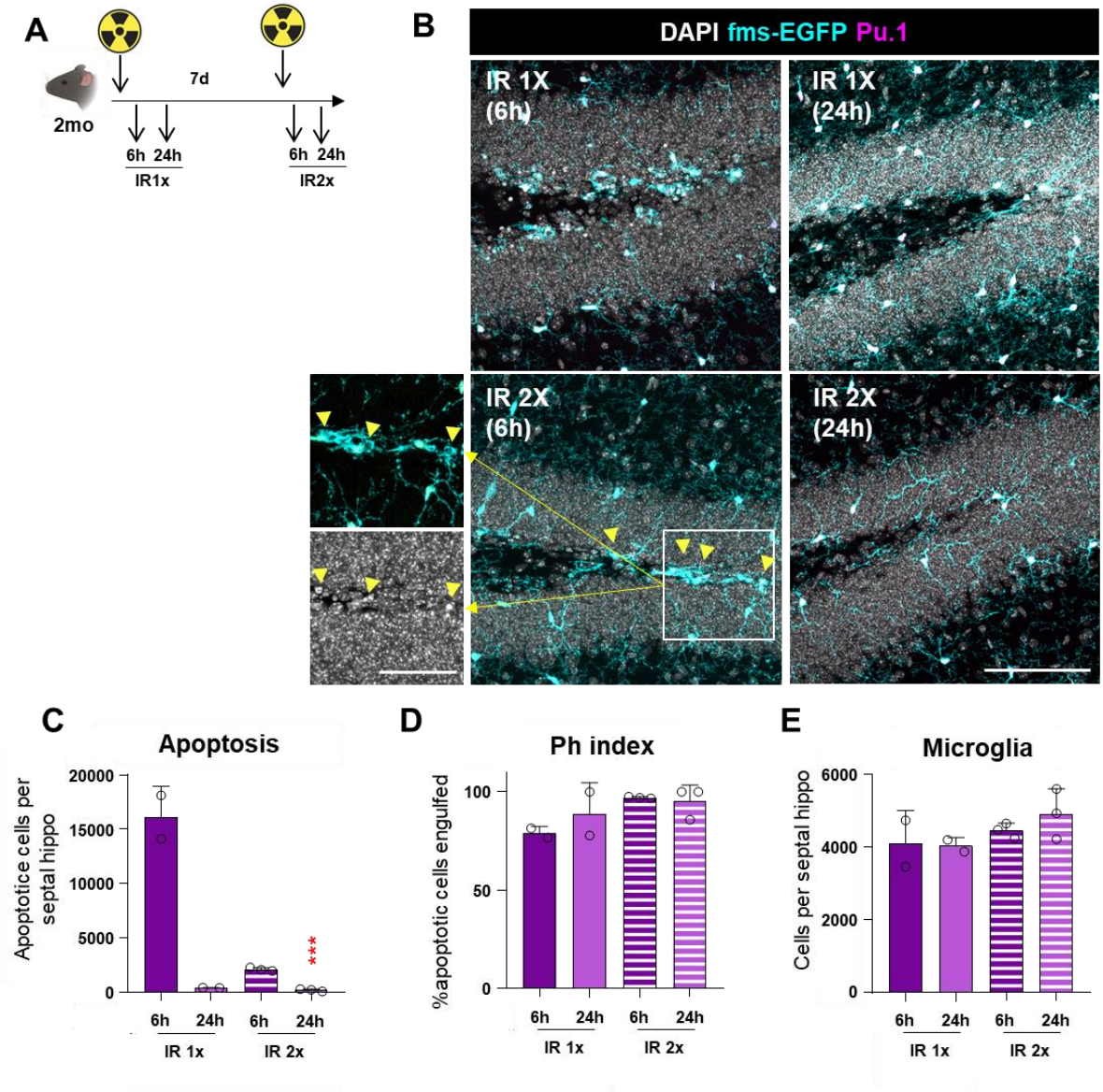

Figure 38. Functional analysis of microglial phagocytosis exposed to a second apoptotic challenge. ***(A)*** *Experimental design of Double Phagocytosis exposing mice to LCI twice.* ***(B)*** *Representative confocal images of the different experimental conditions (IR 1x 6h and 24h, and IR 2x 6h and 24h) showing DAPI (white) Pu.1 (magenta) and GFP (cyan) staining. Detail of phagocytic microglia indicated within a White square. Phagocytic pouches indicated with yellow arrowheads.* ***(C)*** *Number of apoptotic cells in the DG per septal hippocampus.* ***(D)*** *Ph index (% of apoptotic cells phagocytosed by microglia).* ***(E)*** *Number of microglia in the DG per septal hippocampus. mean ± SEM of n=3 mice (n=2 for positive controls). Data was analyzed by Student's t-test when comparing time-dependent differences (6h vs 24h). *** indicates p <0.001. Scale bar= 100μm [B], 50μm (inserts in [B]); z=16.1μm, z=17.5μm, z=18.2μm, z=13.3μm [B].*

In short, in this 3rd section of results, the analysis of mechanism by which microglia are affected after phagocytosis revealed that the cells increased ROS production, reduced mitochondria and catabolic metabolism, while increasing the synthesis of polyamines related to proliferation which, ultimately results in the recovery of phagocytic function.

Understanding how phagocytosis affects microglia and their further recovery is crucial to comprehend how microglia performs phagocytosis when cells are challenged by apoptotic stimuli consecutively in short periods of time. One pathological condition in which sequential apoptotic challenges occur is the radiation therapy (RT) used to kill tumor cells in brain cancer (Scaringi et al., 2018). RT is usually administered in sequential doses (Hingorani et al., 2012), which lead to several waves of apoptotic tumor cells that microglia would need to clear. However, there is little research on how microglia function in the removal of the generated debris. In the following section, we analyze microglial phagocytosis in glioblastoma, a very aggressive type of brain cancer, after exposure to radiation.

6.4: Assessing phagocytic capacity of microglia in brain tumors (Glioblastoma).

In the previous sections we have described how phagocytosis impacts microglia leading to transcriptional and metabolic changes, and inducing cellular stress that further translates into cell death and compensatory proliferation. To test the impact of these findings in a disease context, we focused on cerebral cancers. Tumor associated macrophages (TAMs), which include resident microglia and tumor infiltrating monocytes (Chen et al., 2017b), are usually exposed to several consecutive waves of apoptotic cells, as the most used type of RT is hypofractionated radiotherapy (HFRT), in which the total dose of radiation is divided into smaller doses and administered sequentially (Hingorani et al., 2012b). Thus, TAM phagocytosis could be impaired when HFRT pulses are too close in time, preventing the recovery of phagocytosis efficiency that we have observed 7 days after the first phagocytic challenge. Before addressing the effect of HFRT, we assessed TAM phagocytosis after a single dose of irradiation, as some research claims that the factors released in the tumor microenvironment leads to phenotypic changes in microglial impairing phagocytosis (Buonfiglioli et al., 2021b).

For this purpose, I visited the laboratory of Dr. Hambarzumyan's laboratory (Icanh School Medicine at Mount Sinai, New York), an expert in animal models that replicate human glioblastoma (GBM), using the RCAS-TVA system (Lenting et al., 2017), which uses avian leukosis virus (ALV)-based vectors to selectively infect cells containing the TVA receptor. First, the RCAS plasmid with the desired mutations is transfected into DF-1 cells, which are then injected into genetic engineered animals expressing TVA in target cells. Finally, the integrated mutations will convert target cells into cancer cells, developing the tumor. During my internship I specifically worked with two different animal models that replicated two subtypes of glioblastoma (proneural and mesenchymal). Once animals developed the tumor, we assessed the effects of radiotherapy after one pulse of RT (10Gy).

6.4.1 RT causes apoptosis of tumor cells and partial clearance in Proneural (PDGFβ1) gliobastoma subtype.

We studied the effects of irradiation in apoptosis and microglial phagocytosis in different brain regions (healthy tissue, tumor border, tumor core) of mice bearing the Proneural (PDGFβ1) subtype, comparing control (non-irradiated) mice with mice euthanized at different time points after RT (6h and 24h). The dose administered was 10Gy, 5 times higher than that used in the "superphagocytosis" model, since previous studies showed that this dose was able to kill tumor cells and to induce cell cycle arrest, prolonging survival of mice (Becher et al., 2010). We then performed immunofluorescence and confocal imaging to observe microglia, labeled with P2Y12; monocytes, labeled with IBA1, tumor cells expressing RFP; and apoptotic cells with DAPI. For a first general overview of apoptosis caused by RT, we performed immunohistochemistry of activated caspase-3.

We first analyzed the cellular composition of the different regions (heathy tissue, tumor border and tumor core) by assessing the volume occupied by RFP (tumor cells), P2Y12 (microglia) and IBA1 (microglia/macrophages) to determine the identity of the phagocytes outside and within the tumor (**Figure 39A**). In healthy tissue there was little volume occupied by tumor cells (RFP+), supporting that few cells infiltrated healthy tissue. Moreover $P2Y12^{+}$ and $IBA1^{+}$ cells occupied a similar % of tissue volume, suggesting that outside the tumor most of the phagocytes were microglia (**Figure 39B).** In the tumor border, the volume occupied by tumor cells (RFP+) increased compared to the healthy tissue, showing an augmented presence of cancer cells, while, $IBA1^{+}$ cells occupied 5 ± 2 times more than $P2Y12^{+}$ cells regardless of the treatment applied (Control, RT 6h and RT 24h) (mean ± SEM across all animals, regardless the experimental condition) (**Figure 39C)**. Within the tumor core, the volume occupied by RFP continued to increase compared to what and IBA1+ cells occupied 8.4 ± 3.8 times more than P2Y12+ cells regardless of the treatment applied (Control, RT 6h and RT 24h) (mean ± SEM across all animals, regardless the experimental condition) (**Figure 39D)**, showing that P2Y12 expression is almost lost within the tumor. Thus, we conclude that as the presence of cancer cells increased, P2Y12 expression was reduced until its disappearance, suggesting that either microglia do not infiltrate the tumor or that the tumor reprograms microglia altering their phenotype as previously suggested (Buonfiglioli et al., 2021b).

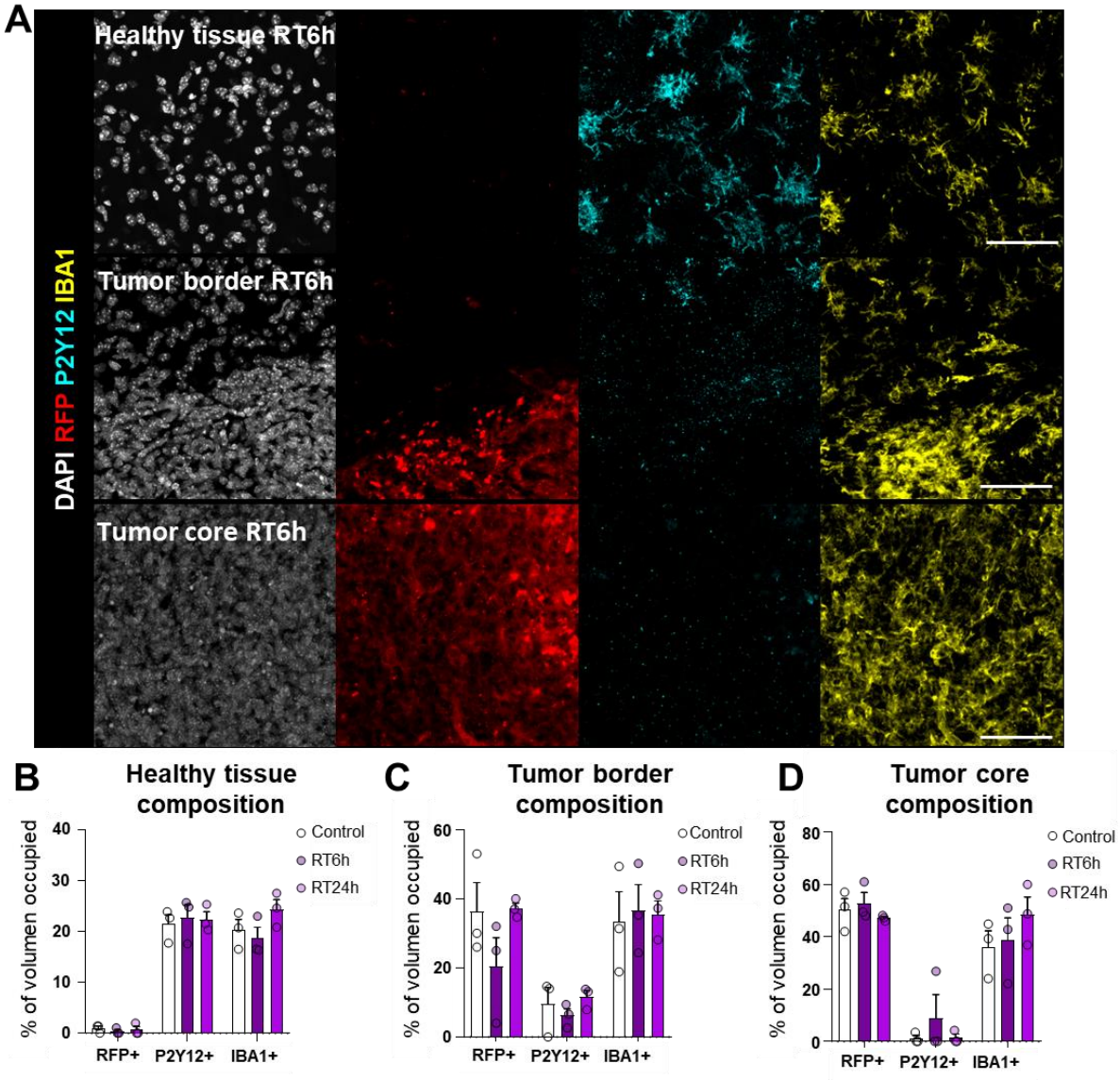

Figure 39. Cell populations among brain regions in Proneural Glioblastoma (PDGFβ1) after RT. ***(A)*** *Representative confocal images of the different brain regions (healthy tissue, tumor edge and inside tumor) healthy 6h after irradiation showing DAPI (white), P2Y12 (cyan), IBA1 (yellow) and RFP (red) staining.* ***(B)*** *% of volume occupied by different cell populations: tumoral (RFP+), microglia (P2Y12+) and microglia/macrophages (IBA+) in healthy tissue.* ***(C)*** *% of volume occupied by different cell populations: tumoral (RFP+), microglia (P2Y12+) and microglia/macrophages (IBA+) in tumor border.* ***(D)*** *% of volume occupied by different cell populations: tumoral (RFP+), microglia (P2Y12+) and microglia/macrophages (IBA+) in tumor core. Bars show mean ± SEM of n=3 mice. Data was analyzed by one-way ANOVA followed by Holm-Sidak post hoc tests when appropriate [B-D]. Scale bars = 50μm; z=20.3μm, z=15.4μm, z=19.6μm.*

We next analyzed the effect of RT and observed an increase in both activated caspase 3 expressing cells and cells with pyknotic/karyorrhectic nuclei (**Figure 40A-F),** suggesting an augmented apoptosis after irradiation. At the tumor border, apoptosis occurred mainly at 24h, while in the tumor core the generation of

apoptotic cells that mainly occurred at 6h (**Figure 40E).** RT also induced apoptosis in healthy tissue, mainly at 6h, however this death was 9.9 ± 2.1 and 68.7 ± 14.6 times lower compared to apoptosis occurring at the border and in the tumor core, respectively (**Figure 40D**). Overall, these data showed that apoptosis was more abundant as tumor cell density increased. However, to directly assess tumor cell apoptosis, we differentiated between tumor (RFP+) and non-tumor (RFP-) cells. In healthy tissue, RT caused the death of non-tumor cells (RFP-), while at the border and the tumor core the % of RFP+ apoptotic cells increased to 60.9 ± 8.6% and 73.4 ± 6.5% (mean ± SEM of apoptotic cells at 6h and 24h) respectively (**Figure 41A-D**). Thus, RT killed both tumor and healthy cells, suggesting that the dose used (10Gy) could be optimized to reduce the damage caused to non-tumor cells. Likewise, we assessed the proliferative capacity of tumor cells after RT by counting mitotic figures using DAPI and observed that RT abolished cell proliferation at 6h, which was recovered by 24h (**Figure 41E-H**), suggesting that, as expected, RT killed mostly proliferative tumor cells. Thus, RT was a useful strategy to induce apoptosis in PDGFβ1 tumors, but also killed non tumor cells.

The reduction of apoptotic cells observed in the tumor core between 6h and 24h (**Figure 40E**) suggested their partial clearance. Thus, to examine more directly the efficiency of microglial phagocytosis, we analyzed the Ph index (% of apoptotic cells phagocytosed) and observed that at 6h and 24h around 50% of the apoptotic cells were engulfed regardless of the region (**Figure 42A-D**). Therefore, phagocytes within the tumor were capable of engulfing apoptotic cells. However, the Ph index in the tumor was lower than the Ph Index in the DG, which under control conditions was 93.6 ± 2.3%, while at 6h after LCI it was 75.7 ± 1%, both showing higher values when compared to phagocytosis within the tumor. Moreover, the reduction of apoptotic cells observed in the tumor core at 24h was not observed in the tumor border. On the contrary the number of apoptotic cells increased at 24h in the tumor border, suggesting a continued/delayed apoptosis and/or a decreased efficiency of TAMs. Altogether, tumor-associated phagocytes seemed less efficient than microglia in a physiological context as they show a lower Ph capacity and a decreased clearance capacity of apoptotic cells.

In summary, the results obtained after analyzing the effects of irradiation in apoptosis and phagocytosis of the Proneural GBM reveal that 10 Gy RT caused apoptosis of tumor cells by depleting tumor cell proliferation. However, it also caused apoptosis of non-tumor cells, and thus a lower dose could prevent apoptosis of healthy cells. Moreover, tumor phagocytes, TAMs that have lost the characteristic expression of the microglial marker P2Y12, were able to engulf and clear tumor cells, although they showed less efficiency than microglia under physiological conditions.

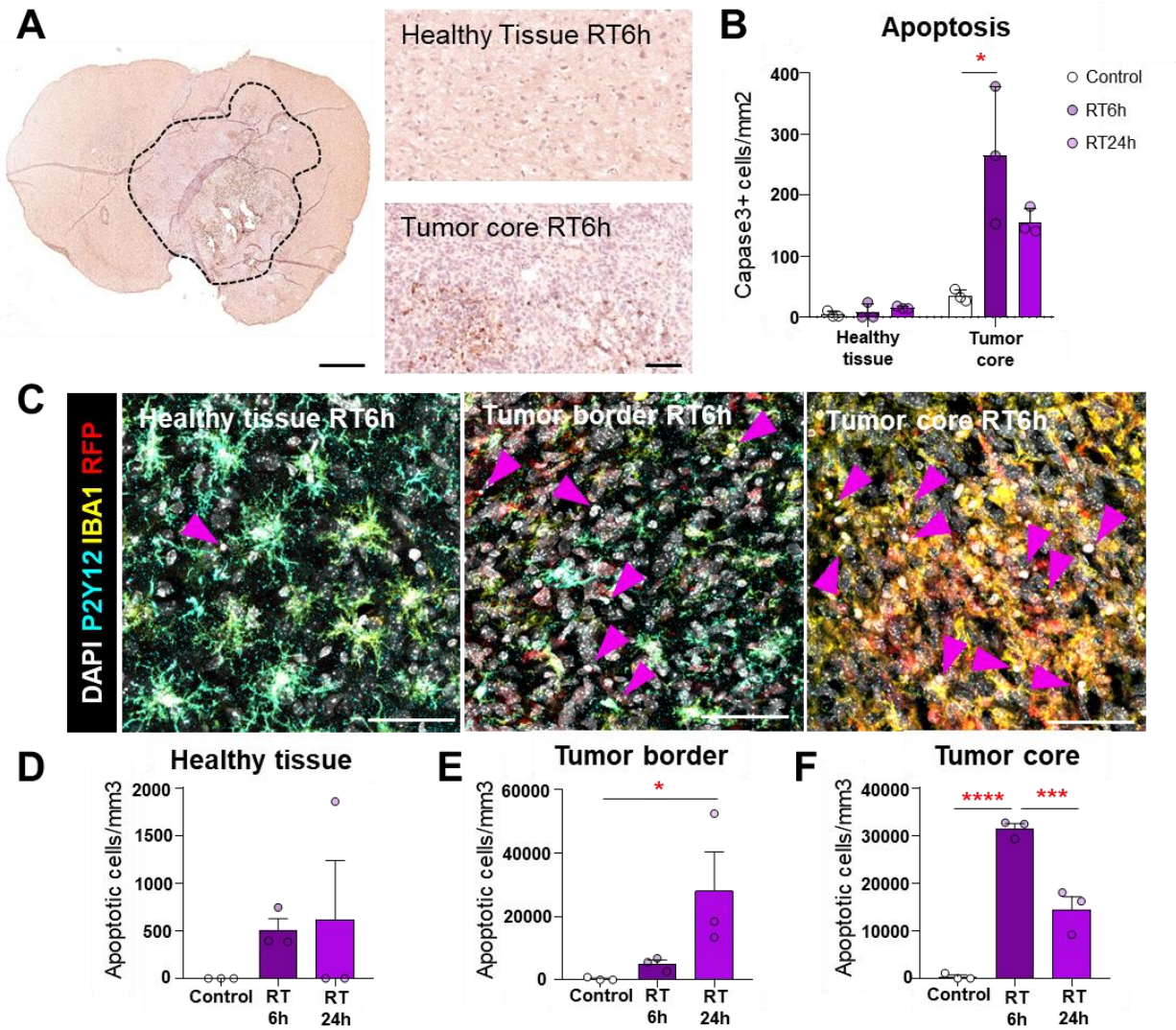

Figure 40. Analysis of apoptosis in PDGFβ1 after irradiation. ***(A)*** *Representative scanner image of brain slice bearing a PDGFβ1 subtype glioblastoma immunostained for activated caspase 3.* ***(B)*** *Number of apoptotic cells per mm2 in healthy tissue vs. Tumor core after exposure to radiation (control, 6h and 24h).* ***(C)*** *Representative confocal images of different brain regions (Healthy tissue, tumor edge and inside tumor) 6h after the exposure to 10Gy irradiation showing DAPI (white), P2Y12 (cyan), IBA1 (yellow) and RFP (red) staining. Pink arrowheads show apoptotic cells.* ***(D)*** *Number of apoptotic cells per mm3 in healthy tissue after exposure to radiation (Control, 6h, 24h).* ***(E)*** *Number of apoptotic cells per mm3 in tumor border after exposure to radiation (Control, 6h, 24h).* ***(F)*** *Number of apoptotic cells per mm3 in tumor core after exposure to radiation (Control, 6h, 24h). Bars show mean ± SEM of n=3 mice. Data was analyzed by one-way ANOVA followed by Holm-Sidak post hoc tests when appropriate [D,E]. When homoscedasticity was not accomplished Kruskal-Wallis test was performed [F, H]. * indicates p <0.05, *** indicates p <0.001, **** indicates p <0.0001. Scale bars = 1mm [A], 100μm (inserts in [A]), 50μm [C]; z=23.8μm, z=16.8μm, z=6.3μm[C].*

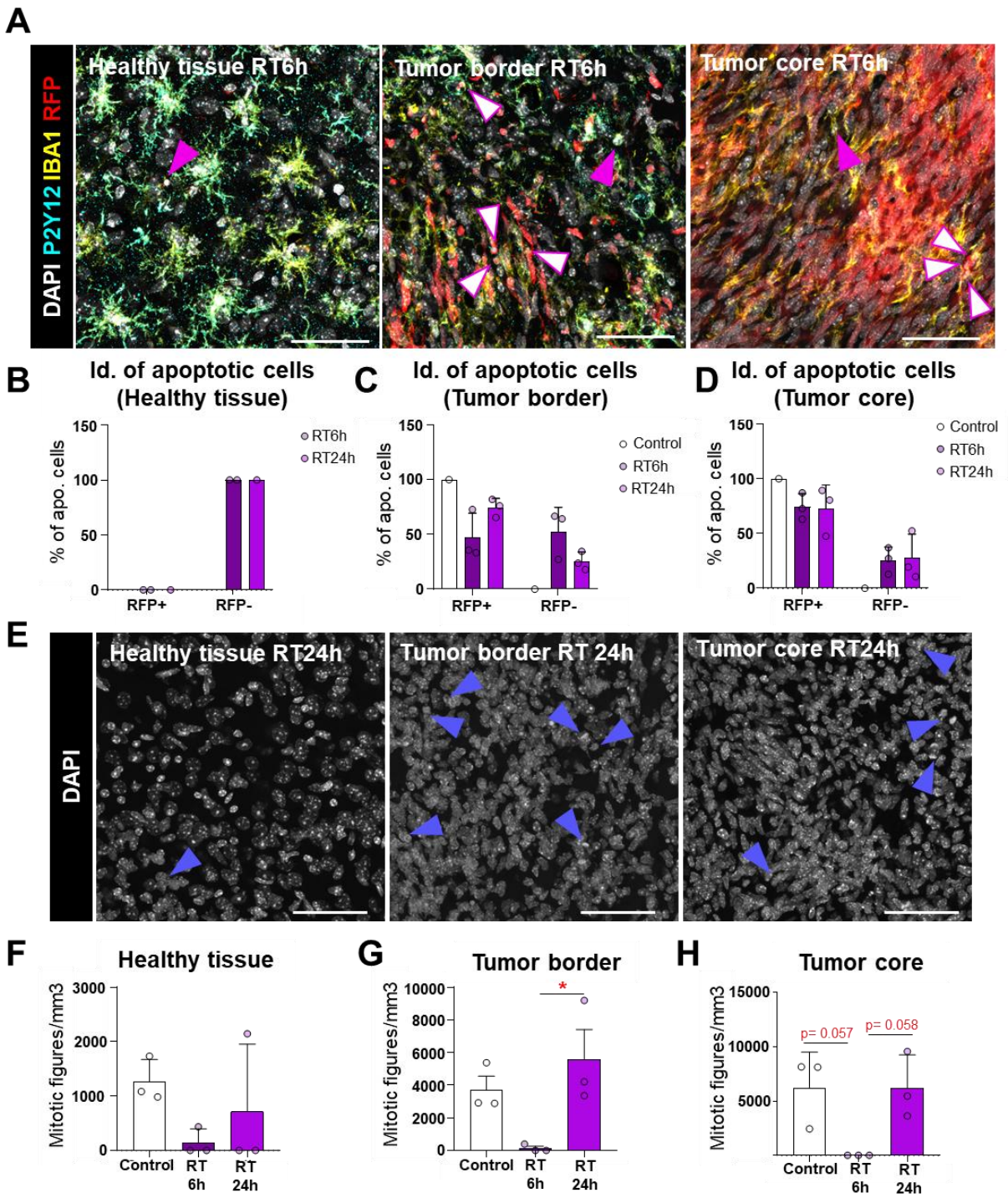

Figure 41. Identity of apoptotic cells and analysis of proliferation in PDGFB1 after RT. ***(A)*** *Representative confocal images of different regions (healthy tissue, tumor border and tumor core) 6h after irradiation showing DAPI (white), P2Y12 (cyan), IBA1 (yellow) and RFP (red) staining. Pink arrowheads show RFP- apoptotic cells and arrowheads filled in white show RFP+ apoptotic cells.* ***(B)*** *Percentage of apoptotic cells that are tumoral (RFP+) and non-tumoral (RFP-) in healthy tissue after irradiation (6h and 24h).* ***(C)*** *Percentage of apoptotic cells that are tumoral (RFP+) and non-tumoral (RFP-) in tumor border after irradiation (control, 6h and 24h).* ***(D)*** *Percentage of apoptotic cells that are tumoral (RFP+) and non-tumoral (RFP-) in tumor edge after irradiation (6h and 24h).* ***(E)*** *Representative confocal images of different brain regions (Healthy tissue, tumor edge and inside tumor) in control condition showing DAPI (white). Blue arrowheads show*

mitotic figures. ***(F)*** *Number of mitotic figures per mm3 in healthy tissue after exposure to radiation (Control, 6h, 24h).* ***(G)*** *Number of mitotic figures per mm3 in tumor border after exposure to radiation (Control, 6h, 24h).* ***(H)*** *Number of mitotic figures per mm3 inside the tumor after exposure to radiation (Control, 6h, 24h). Bars show mean ± SEM of n=3 mice. Data was analyzed by one-way ANOVA followed by Holm-Sidak post hoc tests when appropriate [F,G,H] and by t-test comparing the values of at least n=3 mice per condition (6h vs 24h) [C,D]. * indicates p <0.05. Scale bars = 50μm [A,E]; z=23.8μm, z=15.4μm, z=7.7μm[A], z=18.2μm, z=14.7μm, z=17.5μm [E].*

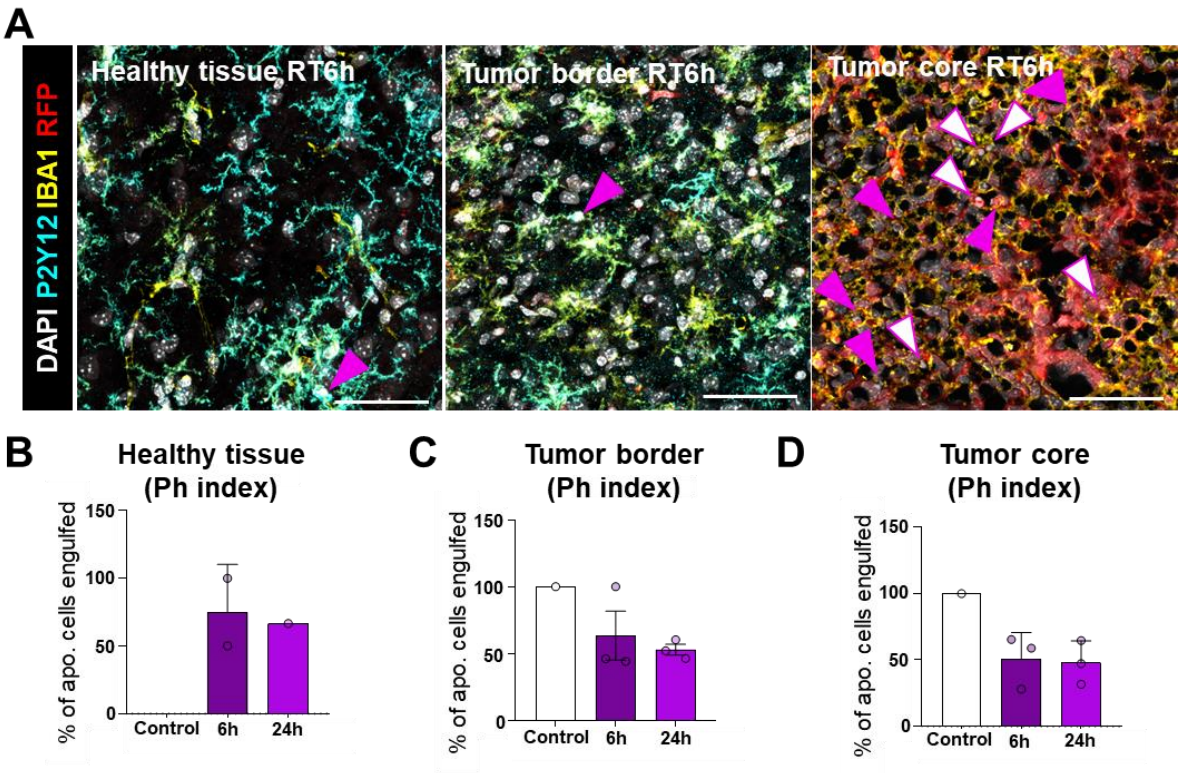

Figure 42. Analysis of phagocytosis in PDGFβ1 after RT. ***(A)*** *Representative confocal images of different regions (healthy tissue, tumor border and tumor core) 6h after irradiation showing DAPI (white), P2Y12 (cyan), IBA1 (yellow) and RFP (red) staining. Pink arrowheads show engulfed apoptotic cells and arrowheads filled in white show non-phagocytosed apoptotic cells.* ***(B)*** *Ph index (% of apoptotic cells phagocytosed) in healthy tissue.* ***(C)*** *Ph index (% of apoptotic cells phagocytosed) in the tumor border.* ***(D)*** *Ph index (% of apoptotic cells phagocytosed) in tumor core. Bars show mean ± SEM of n=3 mice. Data was analyzed by t-test comparing the values of at least n=3 mice per condition (6h vs 24h). Scale bars = 50μm [A]; z=8.4μm, z=22.4μm, z=2.8μm [A].*

6.4.2 RT causes apoptosis of tumor in Mesenchymal (NF1) gliobastoma subtype.

For the characterization of the Mesenchymal (NF1) subtype, we replicated the experimental procedure and analyses carried out in the PDGFβ1 subtype.

When we analyzed the composition of the different regions (healthy tissue, tumor border, tumor core), we observed that in healthy tissue there was very little volume occupied by tumor cells (RFP+) (**Figure 43A-B**). Moreover P2Y12+ and

IBA1+ cells occupied a similar volume (**Figure 43A-B**), suggesting that outside the tumor most of the phagocytes were microglia. In the tumor border, the volume occupied by tumor cells (RFP+) increased compared to the healthy tissue, showing an augmented presence of cancer cells, while P2Y12 expression was reduced 1.9 ± 0.3 times when compared with the healthy tissue (**Figure 43A,C**). In the tumor core, the volume occupied by RFP increased when compared to the tumor border (among all the experimental conditions) and P2Y12 expression was even more reduced in the core than in the border (among all the experimental conditions), which was showed by a decrease of 2.7 ± 0.5 times when compared with the healthy tissue (**Figure 43A,D**). However, in spite of P2Y12 reduction and in contrast to PDGB1, P2Y12 expression was maintained in the tumor core. Therefore, the identification of P2Y12+ cells within these regions indicates the presence of microglial cells within the tumor.

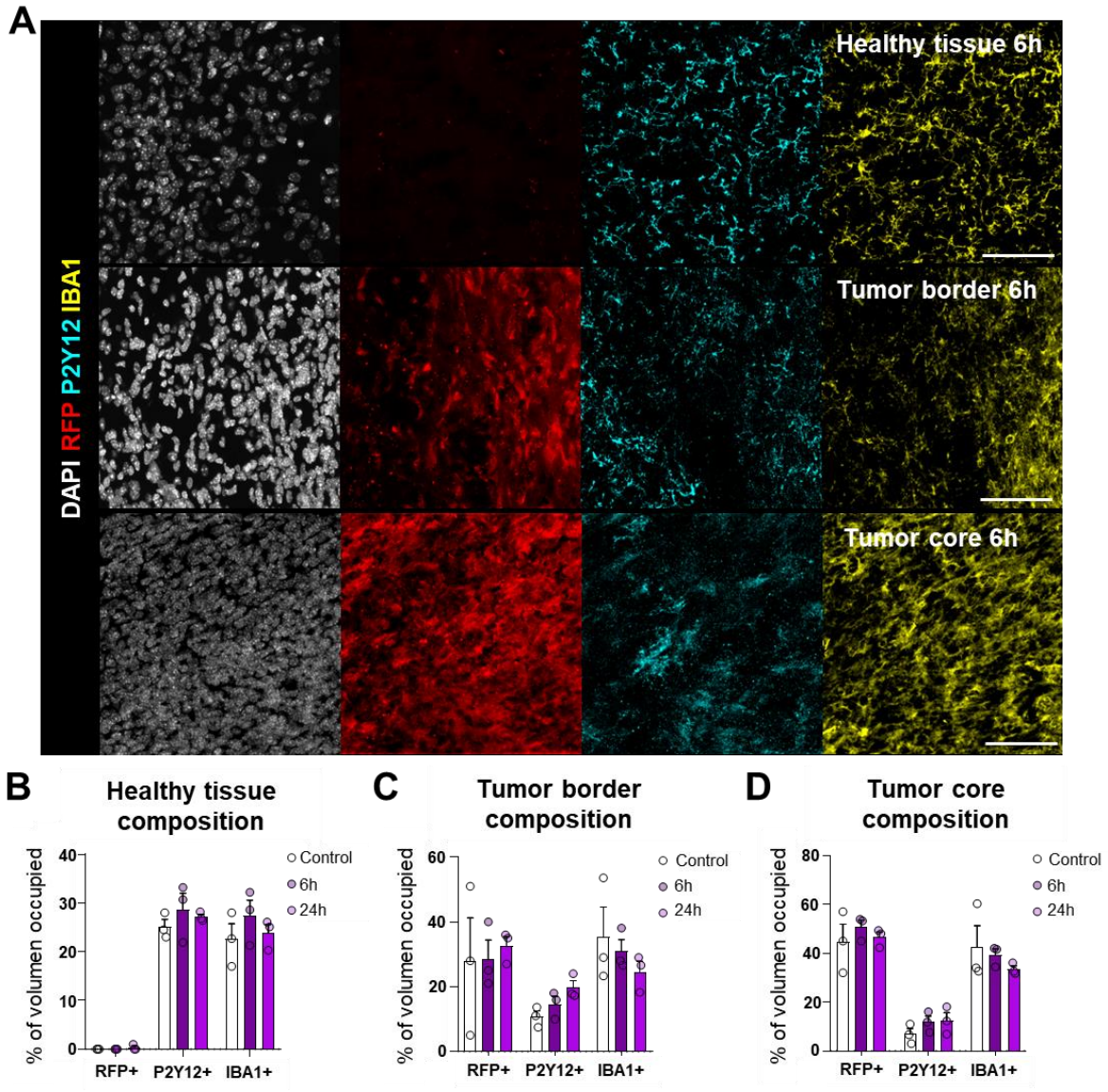

Figure 43. Cell populations among brain regions in Mesenchymal Glioblastoma (NF1) after RT. ***(A)*** *Representative confocal images of the different brain regions (healthy tissue, tumor edge and inside tumor) healthy 6h after irradiation showing DAPI*

(white), P2Y12 (cyan), IBA1 (yellow) and RFP (red) staining. ***(B)*** *% of volume occupied by different cell populations: tumoral (RFP+), microglia (P2Y12+) and microglia/macrophages (IBA+) in healthy tissue.* ***(C)*** *% of volume occupied by different cell populations: tumoral (RFP+), microglia (P2Y12+) and microglia/macrophages (IBA+) in tumor border.* ***(D)*** *% of volume occupied by different cell populations: tumoral (RFP+), microglia (P2Y12+) and microglia/macrophages (IBA+) in tumor core. Bars show mean ± SEM of n=3 mice. Data was analyzed by one-way ANOVA followed by Holm-Sidak post hoc tests when appropriate [B-D] Scale bars = 50μm; z=20.3μm, z=18.2μm, z=15.4μm.*

We then analyzed the effects of RT and observed that it induced apoptosis by increasing the number of cells expressing activated caspase 3 at 6h in the healthy tissue and leading to an increased trend of apoptotic cells within the tumor (**Figure 44A-B**). Likewise, the analysis of pyknosis/karyorrhexis showed an increased trend of apoptotic cells both in tumor border and in the tumor core 6h and 24h after irradiation (**Figure 44C-F**), which contrary to what was observed in the PDGFβ1 subtype, did not decrease with time. Moreover, when comparing the NF1 subtype with the PDGFβ1 subtype we observed that RT generated 6 ± 17 times more cells in the tumor core in the PDGFβ1 subtype than in the NF1 subtype at 6h. However, RT generated a similar number of apoptotic cells within the tumor core at 24h: 14,490 ± 2,695 and 19,912 ± 9,601 pyknotic nuclei respectively (**Figure 44F, Figure 40F)**. Therefore, RT efficiently induced apoptosis of tumor cells, and slightly affected healthy tissue by killing non-tumor cells. To direct asses more reliably the apoptosis of tumor cells, we discriminated between tumor (RFP+) and non-tumor (RFP-) apoptotic cells after RT. In healthy tissue, RT caused the death of non-tumor cells (RFP-), while in tumor border and core most of the apoptotic cells were RFP+ at 24h (96.6 ± 5.7% and 73.6 ± 3.6% respectively) (**Figure 45A,B,D**). Thus, RT killed both tumor and healthy cells, suggesting that the dose used (10Gy) could be optimized to reduce the damage caused to non-tumor cells. Likewise, we assessed the proliferative capacity of tumor cells after RT by mitotic figure counting and observed that RT abolished cell proliferation at 6h, which was recovered by 24h (**Figure 45E-I**), suggesting that RT kills mostly proliferative tumor cells. So far, we have found that RT causes apoptosis of tumor cells while abolishing proliferation, suggesting that RT mostly kills tumor cells both in PDGFβ1 and NF1 tumors.

Finally, to examine more directly the efficiency of microglial phagocytosis in removing these apoptotic cells, we analyzed the Ph index (% of apoptotic cells phagocytosed) and observed that at 6h and 24h around the 50% of the apoptotic cells were engulfed regardless of the region (**Figure 46**). Therefore, we conclude that phagocytes within the tumor were capable of engulf apoptotic cells, whereas the observed decrease in clearance be a consequence of continued/delayed apoptosis and/or of an impairment in the degradation mechanism of the phagocytes. Therefore, we conclude that RT causes apoptosis of tumor cells in the NF1 tumor and although the clearance detected in the PDGFβ1 subtype at 24h was not observed.

In summary, the analysis of both glioblastoma subtypes in response to RT revealed intrinsic differences in each subtype, such as the expression of the microglia-specific marker P2Y12 that was totally lost in the Proneural subtype, while it was partially maintained in the Mesenchymal subtype. RT had similar

effects on apoptosis in both subtypes, inducing apoptosis of tumor cells, and to a lower extent, the apoptosis of non-tumor cells, suggesting that this dose could be optimized to reduce the number of non-tumor cells affected. Also, in both subtypes RT reduced tumor cell proliferation, which could inhibit tumor progression if RT is applied sequentially. However, the generation of apoptotic within the tumor was higher in the Proneural subtype, as the Mesenchymal subtype is more resistant to RT (Wang et al., 2021b). Likewise, in the Proneural subtype the clearance of apoptotic cells was observed in the tumor core, contrary to what was observed in the Mesenchymal subtype. However, when phagocytosis was analyzed, the phagocytic index was similar in both subtypes. Therefore, the lack of clearance observed in the Mesenchymal subtype may be caused by the inability of the phagocytes to degrade the cargo, or to a continued/postponed apoptosis. Altogether, these data show that RT was capable of causing tumor cell apoptosis and subsequent phagocytosis by TAMs in both GBM models.

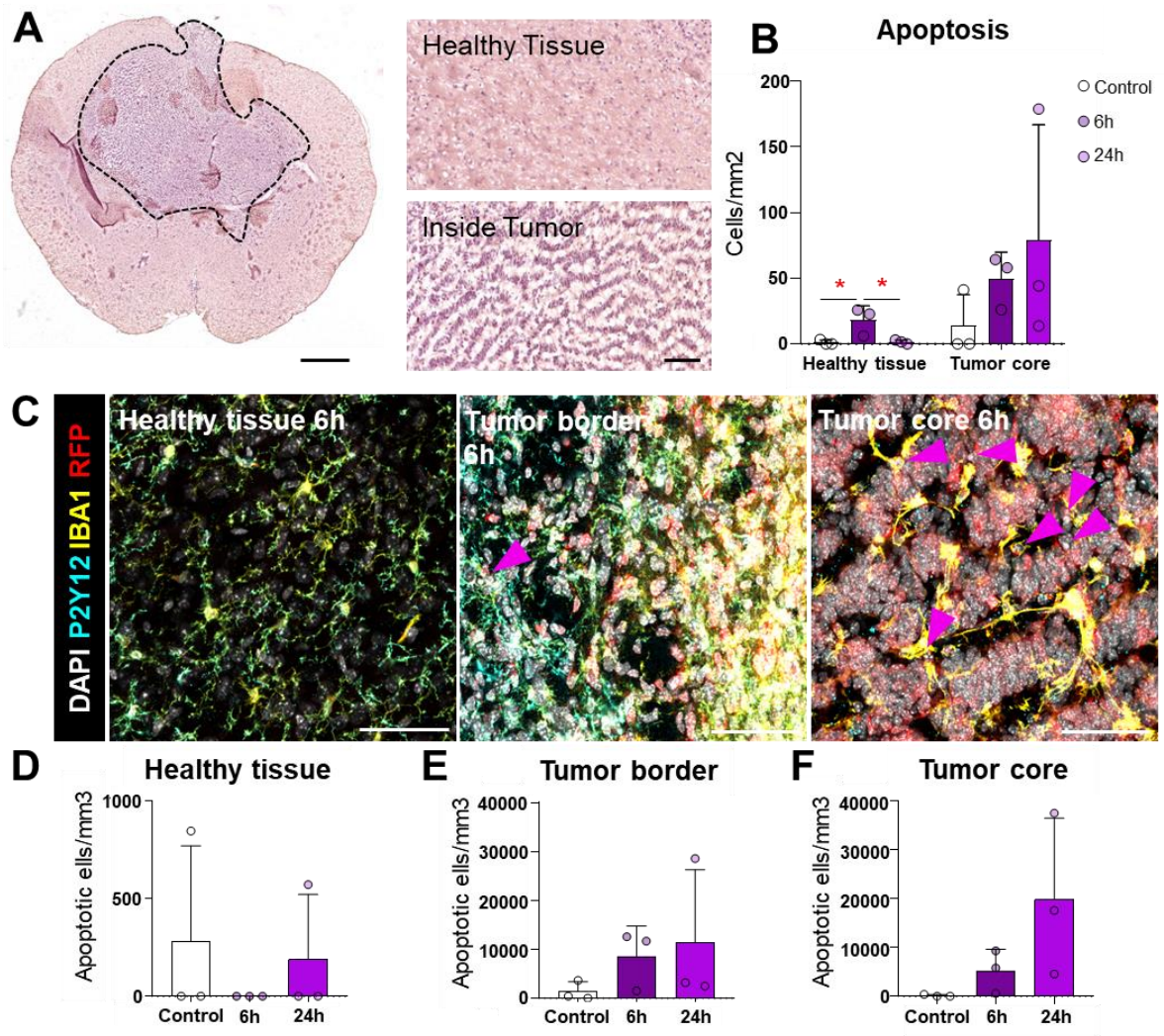

Figure 44. Analysis of apoptosis in NF1 after RT. ***(A)*** *Representative scanner image of brain slice bearing a NF1 subtype glioblastoma immunostained for activated caspase 3.* ***(B)*** *Number of apoptotic cells per mm2 in healthy tissue vs. Inside the tumor after exposure to radiation (control, 6h and 24h).* ***(C)*** *Representative confocal images of*

different brain regions (Healthy tissue, tumor edge and inside tumor) 6h after the exposure to 10Gy irradiation showing DAPI (white), P2Y12 (cyan), IBA1 (yellow) and RFP (red) staining. Blue arrowheads show apoptotic cells. ***(D)*** *Density of apoptotic cells (apoptotic cells per mm3) in healthy tissue after exposure to radiation (Control, 6h, 24h).* ***(E)*** *Density of apoptotic cells (apoptotic cells per mm3) in tumor border after exposure to radiation (Control, 6h, 24h).* ***(F)*** *Density of apoptotic cells (apoptotic cells per mm3) in tumor core after exposure to radiation (Control, 6h, 24h). Bars show mean ± SEM of n=3 mice. Data was analyzed by one-way ANOVA followed by Holm-Sidak post hoc tests when appropriate. * indicates p <0.05. Scale bars = 1mm [A], 100μm (inserts in [A]), 50μm [C]; z=20.3μm, z=18.2μm, z=17.5μm[C].*

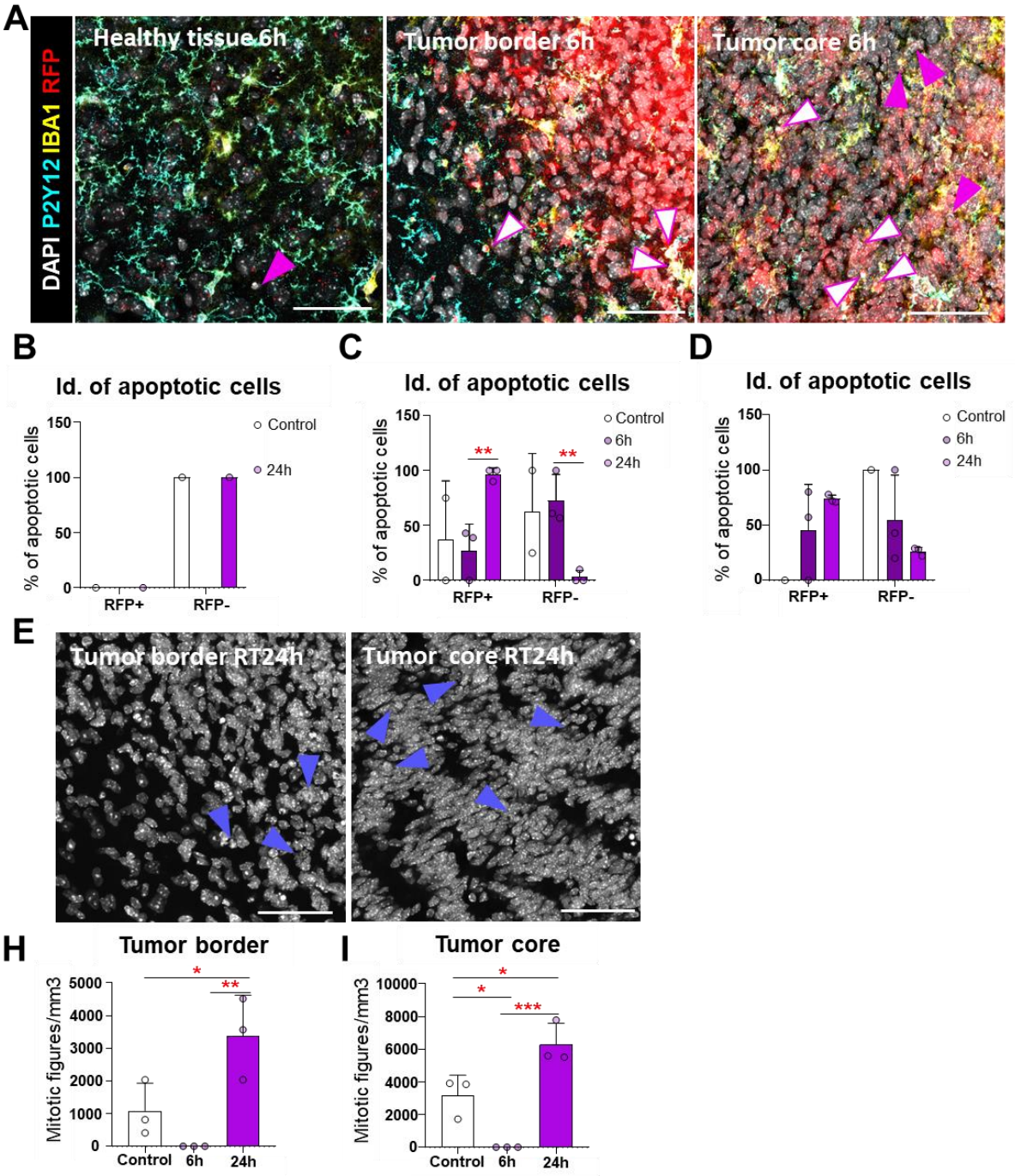

Figure 45. Identity of apoptotic cells and analysis of proliferation in NF1 after RT. ***(A)*** *Representative confocal images of different regions (healthy tissue, tumor border and tumor core) 6h after irradiation showing DAPI (white), P2Y12 (cyan), IBA1 (yellow) and RFP (red) staining. Pink arrowheads show RFP- apoptotic cells and arrowheads filled in white show RFP+ apoptotic cells.* ***(B)*** *Percentage of apoptotic cells that are tumoral (RFP+) and non-tumoral (RFP-) in healthy tissue after irradiation (6h and 24h).* ***(C)*** *Percentage of apoptotic cells that are tumoral (RFP+) and non-tumoral (RFP-) in tumor border after irradiation (control, 6h and 24h).* ***(D)*** *Percentage of apoptotic cells that are tumoral (RFP+) and non-tumoral (RFP-) in tumor edge after irradiation (6h and 24h).* ***(E)*** *Representative confocal images of different brain regions (Healthy tissue, tumor edge and inside tumor) in control condition showing DAPI (white). Blue arrowheads show mitotic figures.* ***(F)*** *Density of mitotic figures (mitotic cells per mm3) in healthy tissue after exposure to radiation (Control, 6h, 24h).* ***(G)*** *Density of mitotic figures (mitotic cells per mm3) in tumor border after exposure to radiation (Control, 6h, 24h).* ***(H)*** *Density of mitotic figures (mitotic cells per mm3) in tumor core after exposure to radiation (Control, 6h, 24h). Bars show mean ± SEM of n=3 mice. Data was analyzed by one-way ANOVA followed by Holm-Sidak post hoc tests when appropriate [F,G,H] and by t-test comparing the values of at least n=3 mice per condition (6h vs 24h) [C,D]. * indicates p <0.05. ** indicates p <0.01. *** indicates p <0.001. Scale bars = 50μm [A,E]; z=2.8μm, z=7μm, z=17.5μm[A], z=14μm, z=4.9μm E].*

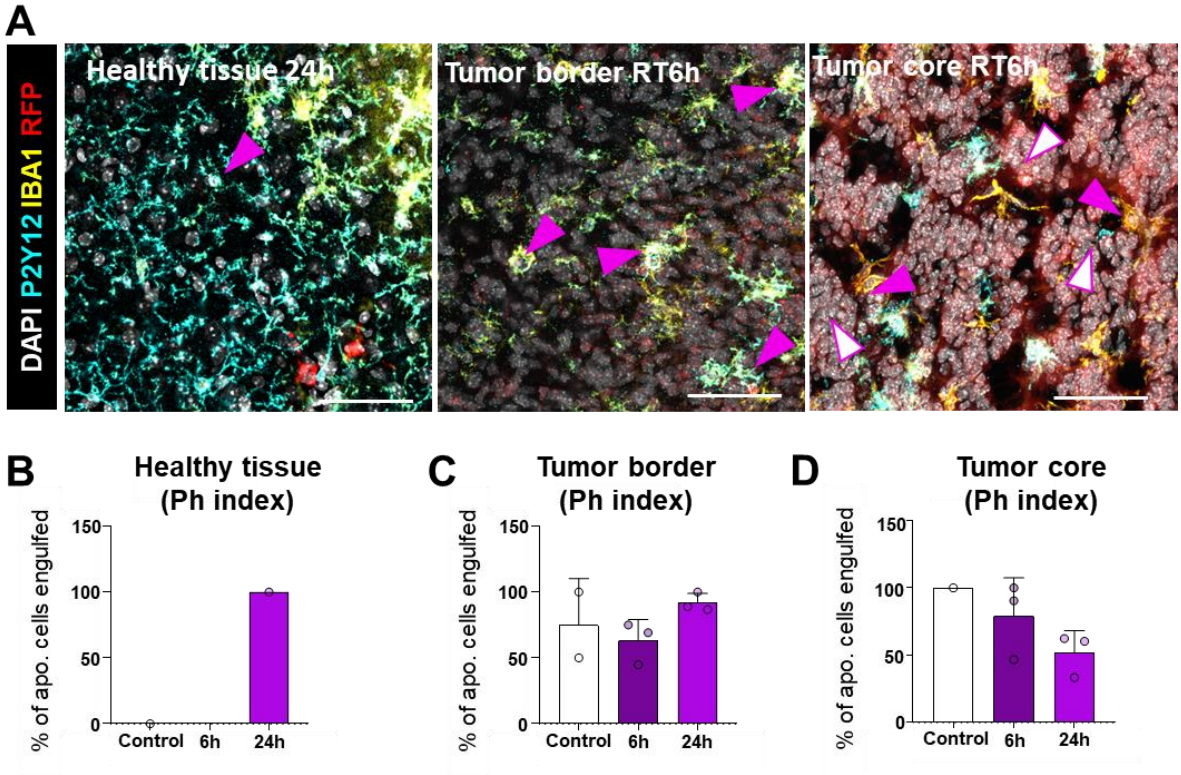

Figure 46. Analysis of phagocytosis in NF1 after RT. ***(A)*** *Representative confocal images of different regions (healthy tissue, tumor border and tumor core) 6h after irradiation showing DAPI (white), P2Y12 (cyan), IBA1 (yellow) and RFP (red) staining. Pink arrowheads show engulfed apoptotic cells and arrowheads filled in white show non-phagocytosed apoptotic cells.* ***(B)*** *Ph index (% of apoptotic cells phagocytosed) in healthy tissue.* ***(C)*** *Ph index (% of apoptotic cells phagocytosed) in the tumor border.* ***(D)*** *Ph index (% of apoptotic cells phagocytosed) in tumor core. Bars show mean ± SEM of*

n=3 mice. Data was analyzed by t-test comparing the values of at least n=3 mice per condition (6h vs 24h). Scale bars = 50μm[A]; z=15.4μm, z=7μm, z=10.5μm[A].

7. DISCUSION

7. DISCUSION

Phagocytosis of apoptotic cells by microglia is a crucial function that guarantees tissue homeostasis and has an impact on the surrounding environment, while also influencing microglial cells. To clearly understand how microglia are affected by the process of phagocytosis, we first developed an in vivo "superphagocytosis" model using LCI that synchronized DG microglia to a phagocytic state. This allowed us to study subsequent post-phagocytic changes while causing minimal radiation-driven effects in microglia in particular and the parenchyma in general. The model was used to identify post-phagocytosis changes that occurred specifically in DG microglia, revealing minimal changes on microglial morphology at 6h, and altered transcriptomic profiles at 24h and 7d. On one hand, short-term transcriptional changes (24h) led to the expression of novel signature characterized by galectin 3 and the overexpression of lysosomal genes, such as CD68 (LM signature), possibly implicated in the process of cargo degradation or in the subsequent recovery of lysosomes in microglia. On the other hand, long term-changes (7d) showed the increase of a microglial cluster related to proliferation, which was further confirmed using BrdU pulse-and-chase experiments. However, phagocytosis-induced proliferation was abortive, and not all newly generated cells survived, leading to the stabilization of the microglial density. To understand the link between microglial phagocytosis, proliferation and cell death, we used an *in vivo* approach that revealed a post-phagocytotic increase in ROS production, a reduced mitochondrial complexity and catabolic metabolism, and increased the synthesis of polyamines related to recovery and proliferation. Finally, we tested whether these changes altered microglial phagocytosis efficiency in a double irradiation model *in vivo*. Altogether, our data supports that phagocytosis induces microglial stress, triggering a series of transcriptional, metabolic, and mitochondrial adaptations, which ultimately lead to apoptosis and proliferation, supporting the long-term functionality of microglia (**Figure 47**).

Understanding how phagocytosis affects microglia and their further recovery is crucial to comprehend the performance of microglia upon consecutive apoptotic challenges. Brain tumors are an example of consecutive apoptosis of tumor cells driven by sequential doses of radiotherapy (HFRT), which may prevent microglia from recovery, as microglia must engage in phagocytosis each time radiation is administered (daily or every other day). Understanding how microglia responds to HFRT will be useful to optimize brain cancer therapies. As a first step, we have explored microglial phagocytosis in glioblastoma exposed to a single dose of RT, to set up a baseline of how efficient they are phagocytosing apoptotic tumor cells. The analysis of phagocytosis in the tumor context revealed that microglia and macrophages were able to engulf and clear apoptotic tumor cells, although they were less efficient than phagocytosing apoptotic newborn cells. In the upcoming sections, we will examine the strengths and weaknesses of the "superphagocytosis" model, the signature of post-phagocytic microglia, and the functional consequences of phagocytosis. Finally, we will conclude with a discussion on the implications of microglial post-phagocytosis for glioblastoma treatment.

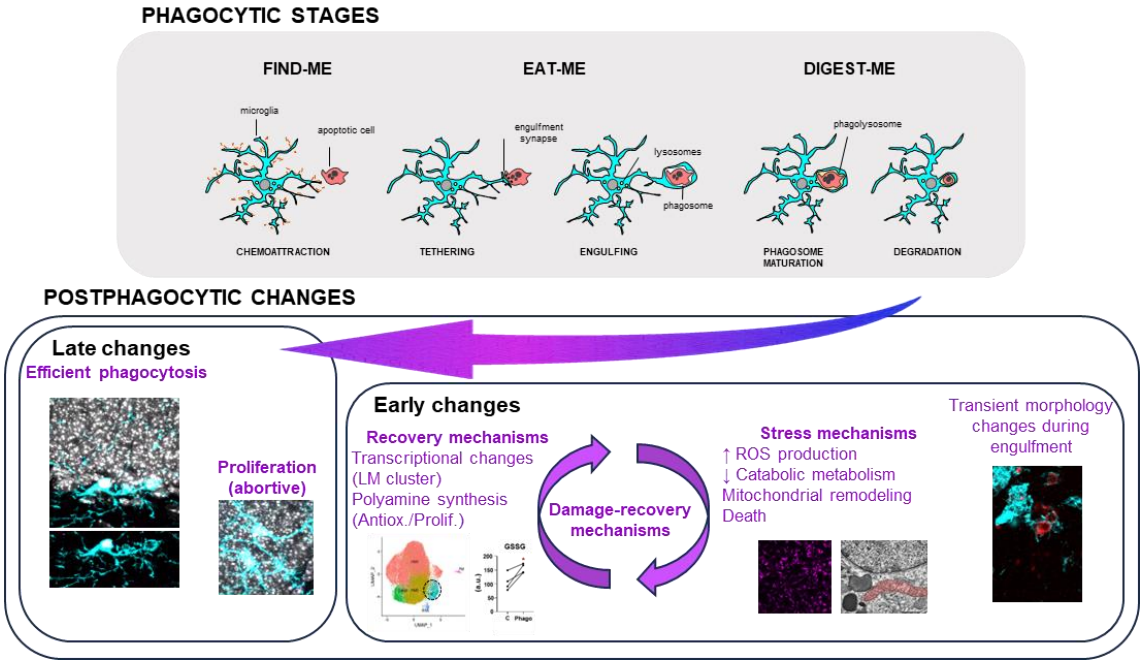

Figure 47. Graphical abstract summarizing microglial post-phagocytosis adaptation. *Microglia experience early post-phagocytosis changes characterized by damage and recovery mechanisms, which indicated stress processes initiated by phagocytosis (oxidative stress, downregulated catabolism, simplification of mitochondria) and the activation of recovery mechanisms (transcription of lysosomal related genes, and synthesis of metabolites involved in resolving oxidative stress and proliferation). Ultimately, microglia proliferate in response to phagocytosis and phagocytic function is sustained in the long-term.*

7.1 THE "SUPERPHAGOCYTOSIS" IN VIVO MODEL IS A VALID STRATEGY TO ASSESS PHAGOCYTOSIS INDUCED CHANGES IN MICROGLIA

7.1.1 The "Superphagocytosis" model synchronizes DG microglia in phagocytosis, while avoiding major damage caused by high doses of radiation

In order to study phagocytosis-induced microglial changes, we have developed a "superphagocytosis" model based on our previous understanding of basal apoptosis and phagocytosis within the mouse dentate gyrus (DG) neurogenic niche (Sierra et al., 2010). Assessing phagocytosis in physiological conditions has limitations. In the hippocampus, newborn cell apoptosis and subsequent phagocytosis depend on the level of neurogenesis, which is age-dependent (Sierra et al., 2010), resulting in low apoptosis levels during adulthood. In young adult animals at one month of age, phagocytic microglia constituted approximately 35% of total DG microglia (Sierra et al., 2010), decreasing to 15% at two months of age (data presented in this PhD Thesis). Consequently, a mixed population of non-phagocytic and phagocytic microglia coexists in the hippocampal neurogenic niche of young-adult and adult mice. To investigate the effects of phagocytosis, a more robust model was required to synchronize the majority of DG microglia into a phagocytic state for subsequent comparison with non-phagocytic microglia populations,

For this purpose, we needed to adapt the preexisting model to enhance phagocytosis and synchronize DG microglia. One potential alternative considered was the utilization of younger animals (<1 month). However, microglia in such younger animals may not accurately recapitulate adult microglia, as microglial transcriptional maturation typically occurs around postnatal day 30 (P30) (Hammond et al., 2019). This approach could affect the interpretation of our results with information related to the developmental process of microglia rather than solely reflecting the consequences of phagocytosis.

Another alternative involved the use of models to increase newborn cell apoptosis, and we selected irradiation, which predominantly affects proliferating cells (Jiao et al., 2022), including radial neural stem cells (rNSCs) and their progeny, the newborn granule cells (Ehninger et al., 2008). In the initial attempt to induce apoptosis through cranial irradiation, an acute dose of 8 Gy was administered to 3-month-old mice (Beccari et al., 2023). This dosage is equivalent to the clinical dose of 18 Gy used in the treatment of pediatric medulloblastoma. Clinically relevant doses of irradiation have well-established effects, causing both acute and late responses, which include DNA damage leading to proliferative cell apoptosis (Hendry et al., 1997; Stone et al., 2003), neuroinflammatory responses triggered by microglia (Mizumatsu et al., 2003; Lumniczky et al., 2017) (Kalm et al., 2009; Chen et al., 2016; Lumniczky et al., 2017), and other abnormalities such as demyelination, gliosis, and blood-brain barrier permeabilization (Trnovec et al., 1990; Sundgren et al., 2009), which ultimately lead to functional impairments including endocrinopathies and cognitive impairment (Sklar et al., 1995; Duffner, 2004).

Consequently, to optimize our model, two crucial parameters for apoptosis induction were adjusted to mitigate damage and circumvent adverse effects. These parameters included the irradiation dose and the age of the animals. In our model, the irradiation dose was reduced to a subclinical level of 2Gy, a magnitude 15-25 times lower than the dosage employed in antitumor treatments in mice (Gan et al., 2016). This LCI model aimed to minimize harm to non-proliferative cells and reduce potential side effects. Through the utilization of 2-month-old mice, we successfully induced apoptosis in approximately 20,000 cells per hippocampus—a quantity 3.33 times greater than that elicited by an 8Gy dose in 3-month-old mice (Beccari et al., 2023). Nevertheless, low-dose irradiation was not innocuous, causing subtle effects in both the parenchyma in general and, specifically, microglial cells. Next, we will discuss, low-dose irradiation effects in more detail.

7.1.2 LCI causes minimal damage in the brain and in microglia themselves

LCI induced apoptosis specifically in the SGZ of the hippocampus, where neural progenitors reside, leading to a persistent reduction in proliferative cell numbers 30 days post-LCI. This particular effect is likely associated with the fact that irradiation adversely affects proliferative cells due to the heightened vulnerability of their DNA during replication (Santivasi et al., 2014). Consequently, the DNA undergoes stress, potentially resulting in DNA breakage, such as DSBs. This

phenomenon has been assessed in our results as a consequence of LCI in neuroprogenitors of the DG. The impact of low-dose irradiation, ranging from 0.1-2Gy (Safwat, 2000), has been investigated in various contexts, with a primary focus on understanding the consequences of radiotherapeutic diagnostics. On one hand, the exposure to low-dose irradiation in children increases the risk of brain tumors (Pearce et al., 2012; Mathews et al., 2013), and early-life exposure in mice leads to cognitive impairment in adulthood (Buratovic et al., 2016; Eriksson et al., 2016), highlighting the vulnerability of the developing brain. The pronounced effects observed may be attributed to the immature nature of the brain. On the other hand, low-dose radiation in the adult brain induces transcriptional changes associated with cellular metabolism, oxidative stress, protein synthesis, mitochondria, and negative regulation of neurogenesis (Lowe et al., 2009). Even very low doses (0.1 Gy) induce alterations in genes related to protective and reparative functions, impacting stress response, cell cycle control, DNA repair, and neural signaling activity (Yin et al., 2003). Low doses also directly affect neurogenesis and microvasculature in the hippocampus but, unlike high doses, they do not result in cognitive impairments (Casciati et al., 2016). Therefore, low-dose irradiation is not innocuous to the brain parenchyma, and predominantly affects neurogenic regions. In conclusion, these effects must be carefully considered as an essential factor when contemplating the utilization of a model with low irradiation to replicate our *in vivo* “superphagocytosis” model.

Regarding the effect of radiation on brain immune cells, low-dose irradiation does not have a significant impact on either macrophage or microglial populations. In the case of macrophages, they enter the parenchyma after the disruption of the BBB; however, low-dose irradiation does not induce monocyte infiltration as higher doses are necessary to affect the BBB (Sundgren et al., 2009). Thus, using lower doses result in minimal monocyte and BBB disturbances in the brain. Concerning microglia, low-dose irradiation does not alter their numbers and causes minimal DNA damage. This lack of effect is attributable to the quiescent nature of adult microglia, as they do not proliferate under physiological conditions (Réu et al., 2017). However, we did observe changes in gene transcription induced by irradiation, which included changes at early (24h) and later (7d) stages. Early alterations affected 140 genes, shared across different clusters (cluster-shared genes), indicating the widespread effect of irradiation on microglia. These genes were associated with protein kinase B signaling and the inflammatory response. Protein kinase B is implicated in cellular survival pathways by inhibiting apoptotic processes (Thakkar et al., 2001), while the inflammatory response is typically orchestrated by microglia in the presence of neurodegeneration or damage (Muzio et al., 2021b) indicating that hippocampal microglia responded to LCI by initiating a self-protective response and performing immune functions to potentially restore surrounding damaged tissue. Late changes (7d) induced the expression of only 32 cluster-shared genes, suggesting a waning effect of irradiation. These genes were related to the upregulation of the cellular component of the cyclin-dependent protein kinase holoenzyme complex, involved in cell cycle regulation, and the downregulated cellular components of mitochondria: mitochondrial inner membrane and cellular respiration.

Altogether, these data indicates that microglia recover from irradiation, even though some alterations persist at later time points. This protective response

differ from observation in other studies, in which low-dose ranging between 0.1-0.5 Gy activate protective mechanisms, attenuating the inflammatory response while suppressing ROS-mediated damage (Yin et al., 2003). This could be due to the fact that our dose is four times higher than the dose used in these studies. Thus, despite the minimal DNA damage observed, LCI proved not to be innocuous for microglia. Instead, microglia underwent transcriptional changes that suggested microglia to be slightly affected. In summary, LCI not only has general effects on the parenchyma but also directly impacts microglia with changes detected by transcriptomic alterations.

Overall, using LCI as a model to explore post-phagocytic changes has shown practical benefits. It efficiently induces microglial phagocytosis in the DG, a phenomenon specific to this region, enabling comparisons with non-phagocytic microglia from different regions. Nonetheless, it comes with the caveat that LCI is not entirely harmless and subtly impacts microglia by triggering transcriptomic changes that suggest protective mechanisms.

7.2 MICROGLIAL PHAGOCYTOSIS IS NOT A STATE BUT A MULTI-STAGE PROCESS.

The second objective of this study focused on exploring different parameters that characterize and identify post-phagocytic microglia, including morphological changes assessed by immunofluorescence and transcriptional changes by single-cell RNA sequencing (scRNA-seq). Next we will discuss the limitation of using morphology as a parameter to identify post-phagocytic microglia, whereas specific transcriptional changes could be useful to useful to address post-phagocytosis at least at early stages.

7.2.1 Early post-phagocytic microglia underwent transitory changes, which suggest post-phagocytosis as a dynamic process.

Our results revealed that during engulfment, “superphagocytic” cells displayed morphological features characterized by pouches and a less branched morphology. This observation suggested that "superphagocytic" microglia might extend their processes towards neighboring areas of apoptotic cells, potentially responding to "find-me" signals and reducing overall morphological complexity. However, these results contradict the statement that for years has equated ameboid microglia to phagocytic microglia (Paolicelli et al., 2022), and support previous laboratory findings that demonstrate ramified microglia engaging in phagocytosis through their terminal branches (Sierra et al., 2010), and only in specific pathological conditions such as epilepsy and stroke, microglia perform phagocytosis by apposition, engulfing only apoptotic cells in close proximity to their cellular bodies (Abiega et al., 2016; Beccari et al., 2023). Likewise, it was recently demonstrated that during phagocytosis, microglial processes operate autonomously, as observed when one process engages in phagocytosis while another continues to surveil the surrounding territory with equal efficiency (Kamei

et al., 2023). Overall, in physiology phagocytosis seem to occur through the branches of ramified microglia, as our data has repeatedly confirmed.

However, post-phagocytic microglia rapidly recovered their morphology, and by 24 hours after LCI, they exhibited a branching cell morphology similar to that of their control counterparts. The morphological analysis was conducted using the Sholl analysis, which may have limitations in detecting subtle morphological differences (Binley et al., 2014). Nevertheless, at a gross level, significant morphological changes were not observed. In summary, morphology proved inadequate for discerning post-phagocytic cells. Therefore, to identify these cells, we conducted an analysis of transcriptional changes in genes associated with post-phagocytic microglia.

The results of the reanalysis of scRNA-seq revealed a new cluster with a signature characterized by the expression of genes mostly associated with lysosomes, leading to its designation as LM cluster. Interestingly, the LM cluster increased in size shortly after phagocytosis and exhibited overexpression of both CD68 and LGALS3 genes. Subsequent validation via in situ analysis of the DG confirmed that the LM cluster corresponded to the early post-phagocytic microglial population (24h). The LM cluster exhibits similarities with the proteomic profile identified in microglia engaged in myelin phagocytosis (Colombo et al., 2021), sharing lysosomal genes such as CD68 and CTSB and other genes such as LGALS3 and LPL. The LM cluster also shares genes like CD63, CD9, and LGALS3 with the proliferative-region associated microglia (PAM), also involved in the phagocytosis of oligodendrocytes in the developing mice brain (Li et al., 2019). These coincidences indicate that microglia that have participated in the phagocytosis of different cells and cellular materials, shares a common transcriptional program.

The signature genes of early post-phagocytic microglia play diverse roles. Gal-3, encoded by LGALS3, is a member of the galectin family well known for its pleiotropic nature. Gal-3 plays a central role in the repair and removal of damaged structures, as demonstrated in the study of the repair and elimination of damaged lysosomes, where Gal-3 recruits the protein Apoptosis-linked gene 2-interacting protein X (ALIX), leading to the repair and restoration of lysosomal function (Jia et al., 2020). Likewise, Gal-3 also plays a key role in other recovery mechanisms, such as cellular proliferation. (Lalancette-Hébert et al., 2012), as will be discussed below. In addition, in microglia, Gal-3 appears upregulated in the transcriptomic profile of microglia in distinct neurodegenerative conditions (García-Revilla et al., 2022), and it is involved in triggering the inflammatory response in several pathological contexts (Rahimian et al., 2021). Therefore, beyond its participation in lysosomal repair and proliferation, the upregulation of Gal-3 in post-phagocytic microglia could also be implicated in regulating inflammatory processes. Overall, Gal-3 seems to participate in the recovery of microglia after phagocytosis, a hypothesis that could be tested testing the effects of irradiation and superphagocytosis in LGALS3 KO mice.

The LM signature also expressed lysosomal genes are directly involved in building the lysosomal structure and participating in its specialized degradation process. For example, CD68 is predominantly located in the endosomal and lysosomal compartments, actively engaging in the degradation of extracellular materials (Yu et al., 2015). In addition to the previously mentioned increased transcription of CD68 in microglia involved in phagocytosis of myelin and developing oligodendrocytes (Li et al., 2019; Colombo et al., 2021), the overexpression of CD68 protein has been linked to myelin phagocytosis by microglia (Hendrickx et al., 2013), in microglia around infarcted areas in cerebral stroke (Ito et al., 2001; Perego et al., 2011), and in phagocytic BV-2 cells (Wong et al., 2005). The elevated CD68 levels may stem from an increased lysosomal biogenesis to facilitate the degradation of phagocytic cargo. However, CD68 is also upregulated in microglia mediating inflammation after LPS and IFN-γ stimulation (Chistiakov et al., 2017), so its increase cannot be considered specific to post-phagocytosis.

Other genes of the LM signature are CTSB and CTSZ, which encode for cathepsins B and Z, respectively, located in the endosomal and lysosomal compartment (Xie et al., 2023). Although our results demonstrate the upregulation of both genes in post-phagocytic microglia, the role of cathepsins in phagocytosis has been poorly explored. Cathepsin B has been observed to be upregulated in cells following phagocytic challenges outside the nervous system, as in the specific case of highly phagocytic cells in the trabecular meshwork (TM) located near the eye (Porter et al., 2013), and it is also involved in lysosomal biogenesis (Qi et al., 2016). Therefore, its upregulation could be implicated in the recovery of lysosomes that have been depleted during the degradation of phagocytic cargo. On the other hand Cathepsin Z´s link to phagocytosis is even more unknown, but it plays a key role in protein degradation (Bhutani et al., 2012), suggesting that it could be vital in ensuring proper degradation of the phagocytic cargo. Therefore, the overexpressed lysosomal proteins in early post-phagocytic microglia in the LM signature seem to be involved in both cargo degradation and subsequent recovery of lysosomal structures.

Other non-lysosomal genes in the phagocytic population, such as CD63 and CD9 (both coding for tetraspanins), and LPL may be implicated in various post-phagocytic functions. Tetraspanins have been demonstrated to play a crucial role in phagocytosis performed by neutrophils (Ciuntu, 2017). Additionally, CD9 is proposed to be involved in signal transduction coupled with cell motility and proliferation (Kaji et al., 2001). The role of LPL has been extensively described in models of neurodegeneration such as AD and ALS (Nadjar, 2018). Although LPL upregulation has not been directly described in the context of phagocytosis of cells, it has been related with lipid uptake. The observed increase in LPL expression in these contexts, coupled with its implication in lipid metabolism, suggests that elevated lipid metabolism is essential to support a correct functioning of the cell. Furthermore, LPL loss has been linked to a pro-inflammatory microglial phenotype. Therefore, we speculate that the

overexpression of LPL could potentially act as a brake to prevent an exacerbated pro-inflammatory response (Bruce et al., 2018).

Overall, the early post-phagocytic transcriptional changes appear to be closely related to the process of phagocytic cargo degradation and subsequent lysosomal recovery. However, some of these genes and proteins also participate in other cellular functions and are overexpressed in contexts beyond the phagocytosis of neurons. Additionally, the increased expression of these genes is transient, labeling microglia only during the early post-phagocytosis stage. For these reasons, the signature LM signature and its associated genes and proteins cannot be interpreted as unequivocal markers of post-phagocytic microglia.

7.2.2 Late post-phagocytic changes are related to microglial proliferation following previous death.

In our examination of long-term post-phagocytic transcriptional changes, a significant observation from the sc-RNASeq analysis was the notable increase in the proliferative cluster at 7 days after irradiation compared to the control. To further investigate whether this population was a consequence of phagocytosis, we assessed the expression of the proliferation marker Ki67 (Klöppel et al., 2018) and analyzed the survival of proliferative microglia with BrdU within tissue samples. Our observations revealed an elevation in post-phagocytic microglia expressing Ki67 at 7 days post-LCI, specifically within the DG, which indicated an increase of proliferative microglia triggered by phagocytosis. Thus, we verified that phagocytosis induced microglial proliferation at 7 days and validated that the changes in the proliferative population identified through sc-RNASeq were indeed a consequence of phagocytosis. However, the proliferation proved to be abortive, resulting in the death of many newly generated cells within a few hours after their proliferative phase. Consequently, the increase in proliferative microglia did not culminate in a corresponding augmentation of the total microglial population. The concept of abortive proliferation has been described in T cells during the activation of the adaptive immune response. Antigen-presenting B cells triggered the response of rare T cells, leading to their proliferation and subsequent disappearance once their function was fulfilled (Townsend et al., 1998). Additionally, further research conducted on Type 1 Regulatory T cells (Tr1 cells) cells revealed a correlation between higher proliferative rates and increased rates of cell death. The low survival of proliferative cells was attributed to an Akt/Survivin pathway unique to this T cell type, not observed in other cell types (Meiffren et al., 2006). Thus, we speculate that the diminished survival of proliferative microglia may be a consequence of the internal cellular machinery that drives cells to proliferate in response to environmental demands temporarily and then triggers their death to prevent cellular overpopulation.

It is important to note, however, that markers of proliferation are not exclusive to phagocytosis, as microglia may proliferate in response to various stimuli such as neurodegeneration (Gómez-Nicola et al., 2013; Wang et al., 2016). Therefore, while we can affirm that phagocytic microglia proliferate in the long term after

phagocytosis, it is crucial to recognize that proliferative microglia are not always a direct consequence of phagocytosis.

Microglial proliferation may have occurred as a consequence of previous death reported in our study both *in vivo* and *in vitro*. Such death of microglia was reported by the observation of pyknotic microglia 6h after LCI and corroborated by the increased of pyknotic microglia observed in an *in* vitro model consisted in feeding microglia with apoptotic cells. The in vitro model further showed that apoptosis and proliferation genes increased in cultured phagocytic microglia by 24h (Diaz-Aparicio et al., 2020). These results indicate that phagocytosis is stressful in microglia, and that some of these cells undergo early cell death after phagocytosis. Phagogocytosis seems to initiate an abortive proliferation program at later time points, which may aim at the renewal of the damaged microglial population while maintaining its density.

Our results suggest that microglia proliferate and die as a consequence phagocytosis. In the next section, we will discuss the underlying causes and mechanism of microglial death. The compensatory proliferation will be further discussed in the following section **7.3.**

7.3 PHAGOCYTOSIS IS STRESFULL FOR MICROGLIA, WHICH SET IN MOTION A RECOVERY PROGRAM.

7.3.1 Phagocytosis leads to oxidative stress and metabolic deficits that underlie microglial death.

Our results revealed that the mechanisms underlying cellular death after phagocytosis include increased ROS production, reduced mitochondria, and catabolic metabolism. In this section, we will discuss how these changes are directly related to cellular stress and death.

Phagocytosis-induced cell death could be mediated by oxidative stress. Post-phagocytic microglia increased cytoplasmic ROS and the synthesis of the metabolite GSSG, which is generated when glutathione acts as an antioxidant (Owen et al., 2010b), and the polyamine spermidine, which could be used to recover from oxidative stress (Kumar et al., 2022a). Exacerbated levels of oxidative stress cause cellular death, as it induces damage to cellular components such as proteins, lipids, and DNA, disrupting vital cellular functions and triggering apoptotic pathways (Redza-Dutordoir et al., 2016). When the production of ROS, typically generated during cellular processes such as proliferation, differentiation, metabolic adaptation, and immune regulation (Glasauer et al., 2013), surpasses the cellular antioxidant capacity, oxidative stress is generated, leading to cellular damage (Adwas et al., 2019). These data suggest that phagocytosis leads to oxidative stress and a series of compensatory adaptations in microglia that involve the production of antioxidants such as GSSG and spermidine when oxidative stress levels exceed compensatory mechanism

cells may die, indicating that ROS production could underlie cellular death of microglia.

Microglial cell death could also result from the remodeling of the mitochondria. Our study has shown that phagocytosis simplified the mitochondrial network, reduction in both the number of mitochondria and the complexity of the mitochondrial network. This effect was consistently observed in both the in vitro model of phagocytosis using the BV2 microglia cell line and primary microglia. These results differ from the mitochondrial fragmentation observed after phagocytosis of apoptotic cells in macrophages, which was characterized by an increase of mitochondrial objects (Wang et al., 2017). The mitochondrial number could be reduced through mitophagy, a hypothesis that was not tested here. Mitophagy contributes to a decrease in mitochondria as a response to stress (De Gaetano et al., 2021). During mitophagy, preserved mitochondria undergo fusion, which results in an elongation of the mitochondrial network. This serves as a protective mechanism to shield the remaining organelles from the autophagic process (Gomes et al., 2011), and ensures the sustained functioning of the cellular bioenergetics, which would prevent cell collapse and subsequent cell death (Sheridan et al., 2008; Kubli et al., 2012; Liesa et al., 2013). Thus, the mitochondrial simplification observed in our study could be a consequence of a stress-recovery mechanism that attempts to ensure the survival of the cell. In summary, the simplification of the mitochondrial network could be a consequence of mitophagy, which is proposed as a potential trigger for cell death.

Finally, phagocytosis-induced cell death could result from impaired mitochondrial respiration and overall metabolic impairment. The decrease in mitochondrial respiration and the subsequent energy impairment generated within the cell have been associated with cellular death. Interestingly, lysosomal damage was also associated with downregulated oxidative phosphorylation (Bussi et al., 2022), suggesting that the lysosomal damage occurring during the degradation of phagocytic cargo could be affecting both the mitochondria and its functionality. The compromise of the cell's bioenergetic reserve can lead to cell death if the cell fails to acquire the necessary energy for its functions (Kubli et al., 2012). Therefore, this downregulation of catabolic metabolism may also play a role in microglial apoptosis induced by phagocytosis.

In summary, the various explored cellular processes and pathways are intricately interconnected. Thus, phagocytosis, which elevates ROS levels, induces a simplification of the mitochondrial network and results in metabolic deficits impact microglia at multiple levels, causing oxidative stress and impairing the cell's energy capacity for functional processes, and initiating apoptosis However, compensatory mechanisms appear to counteract this stress, such as the generation of antioxidants after phagocytosis or the formation of more compact mitochondrial networks, potentially serving as a defense against mitophagy and enhancing energy efficiency. After microglial death caused by phagocytosis-induced stress, microglia appear to proliferate to recover from such damage. In the present section, we will discuss the various mechanisms that may trigger

microglia proliferation, linking it specifically to the context of phagocytosis and to the previously mentioned metabolic stressors.

7.3.2 Phagocytosis triggers the synthesis of proteins and metabolites involved in cell proliferation

Phagocytosis triggers microglial proliferation, as evidenced by the increase in proliferative cells through both single-cell transcriptomics and BrdU labeling in a period ranging from 7 to 30 days after phagocytosis. Microglia proliferate during development and in contexts of neurodegeneration, responding to both neuronal death and axonal injury (Dissing-Olesen et al., 2007; Zusso et al., 2012; Gómez-Nicola et al., 2013), suggesting that microglia proliferate as a consequence of internal and external damage.

Our findings indicate that phagocytosis initiates mechanisms potentially linked to cellular growth and proliferation. The generation ROS and the synthesis of molecules, including Gal-3, polyamines, glycerylphosphorylcholine, and serine, have been implicated in the regeneration of cellular structures, fostering cellular growth, and ultimately facilitating cell proliferation (Yang et al., 1996; Inuzuka et al., 2005; Valko et al., 2006; Ridgway, 2013; Wei et al., 2022)

Microglial proliferation after phagocytosis could be a compensatory mechanism to recover after cell death. As previously mentioned, phagocytosis triggered ROS increase and beyond its implication in causing oxidative stress, ROS is also involved in cell growth regulatory processes through signaling pathways, such as activating protein-1 (AP-1) and nuclear factor-kappaB, playing essential roles in the control of cell proliferation and differentiation (Valko et al., 2006). Thus, ROS production may not only underlie cellular death but could also be involved in activating signaling pathways necessary for the subsequent proliferation of microglia.

Proliferation of post-phagocytic microglia could also be related to Gal3, which triggers proliferation in microglia in response to ischemic injury (Lalancette-Hébert et al., 2012). Gal-3 has been identified to play an anti-apoptotic role. This function has been demonstrated in peritoneal macrophages, where the absence of the protein in Gal-3 deficient mice resulted in increased sensitivity to apoptotic stimuli compared to macrophages from control mice (Hsu et al., 2000). The anti-apoptotic properties of Gal-3 may be related to the fact that this lectin has similarities with Bcl-2, a well-characterized suppressor of apoptosis. Therefore, Gal-3 could also be acting as a protective mechanism against apoptosis. Overall, galectin-3 is a regulator of cell growth and apoptosis and may function through a cell death inhibition pathway involving Bcl-2 (Yang et al., 1996).

Finally, proliferation could result from changes in polyamine synthesis, specifically causing a reduction in the levels of decarboxylated S-adenosylmethionine (dc-SAMe) and an elevation in spermidine and decrease in spermine, leading to an augmented Spd/Spm ratio. The diminished dc-SAMe, a

precursor of the increased spermidine, and the heightened Spd/Spm ratio may imply an enhancement in spermidine production. Polyamines synthesis has been extensively linked to the stimulation of cell division and proliferation, gene expression for the survival of cells, DNA and protein synthesis, regulation of apoptosis, oxidative stress, angiogenesis, and cell–cell communication activity (Lenis et al., 2017). Likewise, spermidine has been described above for its antioxidant role; however, it also participates in cell growth by significantly increasing cell proliferation when cells are exposed to the polyamine (Wei et al., 2022).

Another metabolite that is increased in post-phagocytic microglia is glycerylphosphorylcholine (GPC). GPC is a precursor of phosphatidylcholine (PC), which is a major component of cell membranes in the body and a deficiency in PC synthesis resulted in reduced low-density lipoproteins (VLDLs) and high-density lipoproteins (HDLs) (Cole et al., 2012) both involved in membrane synthesis. Likewise, PC plays a key role in lipid metabolism underlying cell proliferation in the context of cancer that can be extrapolated to other non-malignant cell types (Ridgway, 2013). Thus, GPC appears to be mediating recovery from post-phagocytic damage as well. The metabolite serine, which is involved in protein synthesis showed an increased tendency also after phagocytosis. Serine is classically known for its involvement in protein synthesis, but it is also involved in the synthesis of membrane lipids (Inuzuka et al., 2005; El-Hattab, 2016). Taken together, these two metabolites seem to be involved in cell recovery, spatially in membrane recovery, which could be linked in recovering lysosomes used for phagocytic cargo degradation or recycling cell membrane after pouches are formed.

Overall, stress induced by phagocytosis appears to activate multiple mechanisms that facilitate the recovery of microglia through proliferation.

7.4 ADAPTATIONS DERIVED FROM PHAGOCYTOSIS DIFFER FROM "TRAINED IMMUNITY" DESCRIBED IN MACROPHAGES.

Our results have demonstrated that the post-phagocytic recovery serves to maintain microglial phagocytosis efficiency. This was evidenced by exposing post-phagocytic microglia to a second challenge of apoptotic cells that needed to be cleared, 7 days after the initial phagocytosis. However, due to the limitations of our model, we were unable to confirm whether there was an enhancement of phagocytic function, as observed in the trained immunity described in macrophages. The concept of trained immunity involves prior exposure to pathogens, apoptotic cells, or other threats, leading to metabolic adaptations that impact the cells' epigenetics, enhancing their inflammatory and phagocytic functions on subsequent encounters (Cheng et al., 2014; Weavers et al., 2016; Morioka et al., 2018). Now, we will compare some key aspects of trained immunity that are not recapitulated in microglia, suggesting that the sustained function of microglia involves processes different from those in trained macrophages.

We have observed that phagocytic microglia downregulate mitochondrial respiration and glycolysis. In contrast, trained immunity in macrophages is characterized by a shift that enhances glycolytic metabolism while decreasing mitochondrial respiration (Cheng et al., 2014). Likewise, phagocytosis in macrophages also triggered this shift (Park et al., 2011; Morioka et al., 2018) (Wang et al., 2017). Therefore, unlike macrophages, phagocytosis seems to affect catabolic metabolism in general, differing from the mechanisms activated in trained immunity.

Metabolic alterations induced in trained immunity result in epigenetic reprogramming which underlie the enhanced immune response (Fanucchi et al., 2021). Our results have showed the early post-phagocytic transcriptional changes suggest short-term alterations associated with the process of degrading the phagocytic cargo, such as the increase expression of the lysosomal proteins in the LM cluster. To assess whether there were underlying epigenetic changes, we employed an *in vitro* phagocytosis model and conducted a DNA methylation analysis using RRBS (reduced representation bisulfite sequencing; PhD Thesis Irune Diaz-Aparicio, 2018). The alterations observed included hypo- and hypermethylation, in 5-methylcytosine (5mC) methylation across CHH, CHG, and CpG islands between control and phagocytic microglia at 24 hours (**Figure 48A**). However, these methylation changes were limited, influencing only a small number of genes: 500 genes with a more permissive exclusion criterion (unadjusted $p<0.05$) and 110 genes with a more stringent criterion (p with Bonferroni adjustment<0.05). This gene count differs from the transcriptional changes identified in gene expression arrays within the same model, where alterations were detected in 6,585 genes (Diaz-Aparicio et al., 2020). Remarkably, only 65 genes (0.94%) with differential methylation exhibited altered mRNA expression, and a gene ontology (GO) analysis revealed their predominant association with transcription factors (**Figure 48B**). The limited overlap between the transcriptional changes in the array and the methylated genes, coupled with the observed microglial death, and lack of transcriptional changes at 7d after LCI, suggest that phagocytosis does not induce long-term epigenetic training. This finding differs from what has been observed in macrophages, where an epigenetic reprogramming characterized by the accumulation of specific epigenetic marks, such as H3K4me3 on gene promoters, is evident, ultimately leading to the enhanced response (Fanucchi et al., 2021). Thus, the date supports that microglial post-phagocytic adaptations and trained immunity are distinct processes.

A

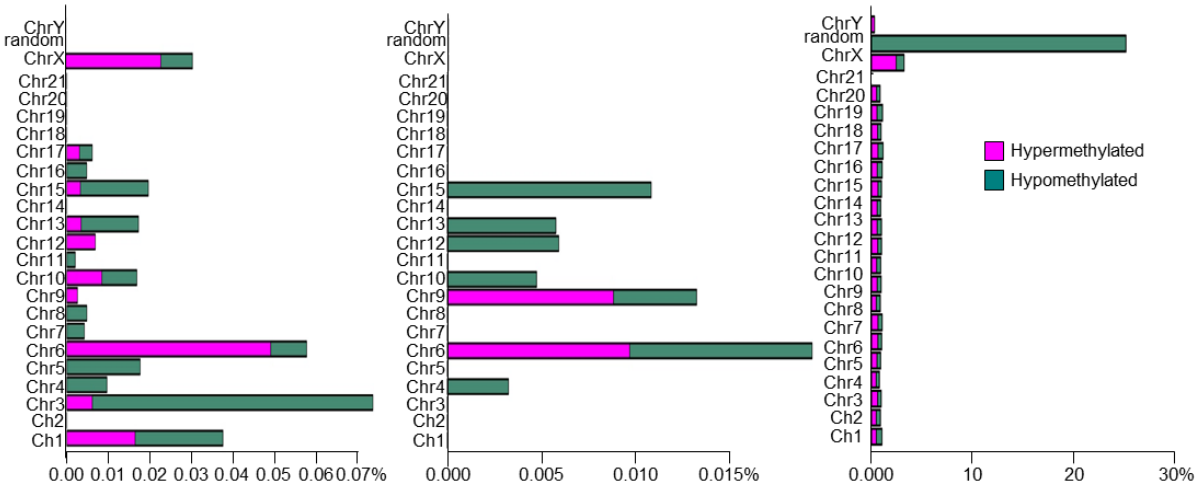

B

BinomP<0.05					
500 genes	Count	%	PValue	Fold Enrichment	Bonferroni
GO:0034765~regulation of ion transmembrane transport	11	2.34	0.0006	3.84	0.75
GO:0006811~ion transport	22	4.69	0.008	1.86	1.00
GO:0006813~potassium ion transport	7	1.49	0.049	2.65	1.00
GO:0006355~regulation of transcription, DNA-templated	36	7.67	0.019	1.47	1.00
GO:0046427~positive regulation of JAK-STAT cascade	5	1.06	0.028	4.30	1.00
GO:0071639~positive regulation of monocyte chemotactic protein-1 production	4	0.85	0.006	10.14	1.00

BinomBonfP<0.05					
110 genes	Count	%	PValue	Fold Enrichment	Bonferroni
GO:0045944~positive regulation of transcription from RNA polymerase II promoter	11	11.34	0.024	2.21	1.00
GO:0006355~regulation of transcription, DNA-templated	11	11.34	0.026	2.17	1.00
GO:0045944~positive regulation of transcription from RNA polymerase II promoter	11	11.34	0.024	2.21	1.00
GO:0006355~regulation of transcription, DNA-templated	11	11.34	0.026	2.17	1.00
GO:0006468~protein phosphorylation	7	7.21	0.048	2.61	1.00

BinomBonfP<0.05 + present in gene array					
65 genes	Count	%	PValue	Fold Enrichment	Bonferroni
GO:0045944~positive regulation of transcription from RNA polymerase II promoter	10	16.4	0.0054	2.95	0.91
GO:0006355~regulation of transcription, DNA-templated	10	16.4	0.006	2.90	0.93
GO:0006468~protein phosphorylation	6	9.84	0.033	3.28	0.99

Figure 48. The results of the DNA methylation analysis using RRBS dismiss the epigenetic reprogramming of post-phagocytic microglia. ***(A)*** *Stacked bar-graphs showing the percentage of methylation across CHH, CHG, and CpG islands.* ***(B)*** *Summary tables with the GO terms of genes that underwent significant methylation. The top table includes genes with lax inclusion criteria (unadjusted p < 0.05). The middle table displays genes included in a more restrictive filtering with Bonferroni adjustment (p*

< 0.05). The last table illustrates the overlaps between methylated gene data and data indicating changes in gene expression arrays analysis. Data obtained by Irune Diaz-Aparicio (PhD Thesis 2018)

In terms of the functional outcome of phagocytosis, we observed that post-phagocytic microglia maintained their phagocytic capacity seven days after their initial phagocytosis. Furthermore, we detected the absence of significant transcriptomic changes indicating an enhancement in immune function. These findings stand in contrast to what is observed in trained immunity, where macrophages enhance their immune function after a first challenge. However, it's important to note that the "superphagocytosis" model has limitations. The initial LCI pulse reduces the pool of proliferating neuroprogenitors, leading to the generation of fewer apoptotic cells in the second LCI pulse. Consequently, microglia are exposed to a lesser phagocytic challenge. While we do not observe formal evidences of a trained response, microglia from the DG are more efficient phagocytose than those in CA, as shown by the phagocytic index of both regions, which is ≈3 times greater in the DG. Therefore, DG microglia, which continuously participate in the phagocytosis of apoptotic cells generated in the neurogenic niche, seem to be trained compared to CA microglia, which do not handle phagocytosis under physiological conditions.

Altogether, and despite the observed increased phagocytic efficiency in DG microglia, the comparison between the mechanisms induced by trained immunity in macrophages and microglial phagocytosis suggests distinct underlying processes. Simultaneously, the functional outcomes of both processes also differ: in trained immunity, cellular function is enhanced, whereas in microglial post-phagocytosis, cellular function undergoes recovery and maintains a stable state.

7.5 THE STUDY OF PHAGOCYTOSIS IN GLIOBLASTOMA EXPOSED TO RT AS AN APPROACH TO UNDERSTAND MICROGLIAL RECOVERY AND TO OPTIMIZE TREATMENTS.

Because of the limitation of our superphagocytosis model to detect training using two sequential LCI challenges, we studied the effect of radiotherapy (RT, 10Gy) in apoptosis and phagocytosis in two distinct Glioblastoma models, (Proneural and Mesenchymal). RT led to apoptosis of both tumor and non-tumor cells, demonstrating that the mentioned RT dose affected healthy cells. Therefore, it would be necessary to optimize it in subsequent studies. In addition to the induced apoptosis, RT also inhibited tumor cell proliferation and ultimately led to phagocytosis by TAMs. In our GBM models, it was challenging to differentiate between microglia and infiltrating monocytes within the tumor site and both of them were characterized as Tumor-Associated Macrophages (TAMs). In the Proneural subtype TAMs in the tumor core did not express the microglial marker P2Y12, whereas in the Mesenchimal subtype, some TAMs expressed the protein. This data suggest, that within the tumor coexist different types of TAMs. Some transcriptomic analyses have revealed the diversity of TAM populations within

tumors (Batchu et al.), identifying up to seven distinct subpopulations, highlighting that the immune landscape in glioblastoma is complex and dynamic. Regardless of the identity of TAMs, these cells were capable of engulfing apoptotic cells. Therefore, our data substantiates the existing evidence that TAMs can engage in phagocytosis within the tumor microenvironment. (Chang et al., 2000; Kulprathipanja et al., 2004). This occurs despite the tumor's immunosuppressive effects on TAMs and its reprogramming of them to contribute to tumor progression (Buonfiglioli et al., 2021b).

The preserved phagocytic function opens interesting treatment options to enhance the elimination of the tumor (Zhai et al., 2021; Chen et al., 2023). However, our observations indicate that TAM phagocytosis is not as efficient as observed under physiological conditions in the neurogenic niche, particularly in the Mesenchymal subtype, where the clearance of apoptotic cells is impaired or delayed. Reprogramming of TAMs within the tumor microenvironment is marked by immunosuppressive responses that facilitate and promote tumor progression, potentially resulting in a diminished or impaired phagocytic capability (Butovsky et al., 2018). Nevertheless, our findings reveal that, despite miroglia perform a more efficient phagocytosis in physiology, phagocytosis is sustained in the tumor context. Thus, we hypothesize that transcriptional and metabolic alterations, which are crucial for maintaining phagocytic function may serve as compensatory mechanisms counteracting TAM reprogramming and preserving phagocytosis. Subsequent investigations could more directly explore potential crosstalk between these reprogramming processes and post-phagocytic changes.

Our initial approach to studying phagocytosis in the tumor context involved a single application of RT. However, in the treatment of brain tumors, radiotherapy is typically administered in sequential doses using a technique known as hypofractionated radiotherapy (HFRT) (Hingorani et al., 2012a), which results in multiple waves of apoptotic cells that microglia must clear. Repeated administration of RT pulses without sufficient time between them could hinder microglial recovery, impairing the phagocytosis of generated apoptotic debris. Therefore, studying the effects of HFRT on microglia is crucial to determine the efficacy of these therapies and optimize them in the future. In our initial exploration of this topic, we assessed phagocytosis after a single irradiation dose.

For this purpose, our laboratory examined phagocytosis of TAMs in tumors exposed to two RT pulses, administered 7 days apart—the microglial recovery time that has proven effective in our previous analyses under physiological conditions. This approach allows us to assess whether this timeframe is sufficient for cell recovery and further phagocytosis of apoptotic cells. The analysis of phagocytosis after a second pulse of apoptotic cells (**Figure 49A**) revealed that RT generated a similar number of apoptotic cells in both pulses and TAMs maintained their Ph index (% of apoptotic cells phagocytosed) after 7 days. The Ph index was high 6h after the RT, in both the first and the second exposure, measuring 73.4 ± 10.3% and 83.7 ± 5.6%, respectively. These parameters remained consistent at 24 hours after RT, with a Ph index of 80.1 ± 5.6% in the

first round, and 85.1 ± 5.7% in the second pulse (**Figure 49B**). This indicates that TAMs were equally efficient phagocytizing apoptotic cells in the first and the second round, confirming the recovery after phagocytosis and sustain of function, as previously assessed in our "superphagocytosis" *in vivo* model.

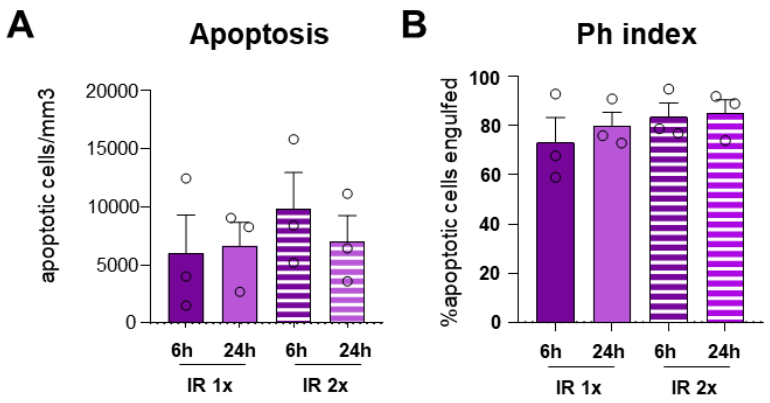

Figure 49. Functional analysis of GBM TAMs phagocytosis exposed to a second apoptotic challenge. ***(A)*** *Number of apoptotic cells per mm3 inside the tumor.* ***(B)*** *Ph index (% of apoptotic cells inside the tumor phagocytosed by TAMs). Data obtained by Xabier Cuesta, TFG 2023.*

Overall, the analysis of phagocytosis in a pathological context such as GBM contradicts the belief that TAMs are impaired in phagocytosis. Instead, the efficiency of TAMs appears to be maintained after phagocytosis, confirming the recovery observed in microglia. The data suggesting that high or closely spaced doses of RT may impact non-tumor cells and hinder the proper recovery of post-phagocytic TAMs also prompts further investigation, opening avenues for optimizing RT treatments. Therefore, ongoing research on phagocytosis in the context of RT is essential to maximize benefits while minimizing potential damage.

8. CONCLUSIONS

8. CONCLUSIONS

8.1 THE "SUPERPHAGOCYTOSIS" IN VIVO MODEL IS A VALID STRATEGY TO ASSESS PHAGOCYTOSIS INDUCED CHANGES IN MICROGLIA

8.1.1 LCI synchronized DG microglia in a phagocytic stage

- We developed an *in vivo* model of phagocytosis based on low cranial irradiation (LCI, 2Gy), which caused apoptosis of neuroprogenitors and boosted microglial phagocytosis at 6h.
- DG microglia were very efficient performing phagocytosis and cleared all the apoptotic corpses by 24h after LCI.
- LCI induced 26.3 times less apoptosis in the non-neurogenic CA than in the DG and phagocytic microglia only represented the 4% in CA region.
- Comparing DG and CA microglia was useful to discriminate the changes induced by irradiation (occurring in both DG and CA) from those induced by phagocytosis (specific of the DG).

8.1.2 The "superphagocytosis" model caused minimal damage in the brain and in microglia themselves

- The use of LCI prevented the breakdown of the blood-brain barrier, which usually happens with higher doses of irradiation, avoiding the massive invasion of monocytes.
- DNA damage assessed by DBS labeling was mainly observed in non-microglial cells located in the in the DG and it resolved over time, reaching non-distinguishable levels at 3 days when compared to control conditions.
- LCI -induced microglial DNA damage, showed by DBS labeling, was 7.2 times lower in microglia than in the rest of nuclei. The damage was also resolved approximately in a 3-day period.
- However, irradiation was not innocuous for microglia, as it caused transcriptional changes involved in cellular survival pathways and inflammatory at short -term (24h), and transcriptional changes involved in the regulation of cell cycle and mitochondrial recovery at long-term (7d).

8.2 MICROGLIAL POST-PHAGOCYTOSIS IS NOT A FIXED STATE; INSTEAD, IT IS A PROCESS WITH VARIOUS STAGES.

8.2.1 Post-phagocytosis was a dynamic process and does not express specific markers for early (24h) post-phagocytic microglia.

- Microglial morphology was simplified during engulfment, while post-phagocytic microglia did not display robust morphological alterations that could validate morphology as a reliable marker of post-phagocytosis
- Early (24h) post-phagocytic microglia underwent transient transcriptomic changes characterized by the overexpression of lysosomal genes and Gal-3.

8.2.2 Late post-phagocytic changes were related to microglial proliferation and death.

- Late (7d) post-phagocytic microglia underwent transient transcriptomic changes of genes involved in proliferation, resulting in an increase of proliferative microglia associated with phagocytosis in DG from 3 to 30 days
- The proliferative program induced by phagocytosis was abortive, as most of the proliferative microglia did not survive, leading to maintain microglial numbers in the DG.
- Microglial proliferation compensated the cell death induced by phagocytosis

8.3 PHAGOCYTOSIS IS STRESFULL FOR MICROGLIA, WHICH SET IN MOTION A RECOVERY PROGRAM.

8.3.1 Phagocytosis lead to oxidative stress and metabolic deficits in microglia that underlie microglial death.

- Phagocytosis affected microglia by increasing the production of ROS, simplifying its mitochondrial network, and reducing its catabolic metabolism, ultimately leading to potential energy failures that may result in cell death.

8.3.2 Microglia underwent changes that facilitate the recovery of phagocytosis efficiency.

- Post-phagocytic microglia increased the synthesis of metabolites involved in the resolution of oxidative stress, such as polyamines and the oxidized form of glutathione.
- Post-phagocytosis proliferation may be triggered by polyamines and Gal-3, both of which are traditionally known to be involved in cell growth and proliferation.
- Recovery mechanisms sustain long-term phagocytosis efficiency of post-phagocytic microglia after the second irradiation 7 days after the first exposure.

8.4 ADAPTATIONS DERIVED FROM PHAGOCYTOSIS DIFFER FROM “TRAINED IMMUNITY” DESCRIBED IN MACROPHAGES FOLLOWING PHAGOCYTOSIS.

8.4.1 Phagocytosis-induced metabolic changes differ from the metabolic shift underlying trained immunity.

- Post-phagocytic microglia globally downregulate catabolic metabolism, in contrast to the metabolic shift observed in “trained immunity”, which enhances glycolysis and suppresses oxidative phosphorylation.

- Post-phagocytic microglia reduce and simplify mitochondrial networks, in contrast to mitochondrial fission observed in post-phagocytic macrophages after phagocytosis.

8.4.2 Phagocytosis induced transcriptional changes do not correlate with the epigenetic changes observed in trained immunity.

- Transcriptional changes in phagocytic microglia did not suggest epigenetic alterations, while in trained immunity, the potentiated function is underpinned by epigenetic changes.

8.4.3 Phagocytosis induced functional consequences differ from the potentiated function observed in trained immunity.

- Post-phagocytic microglia maintained their function after recovery; however, they do not exhibit the enhancement of function observed in macrophages during “trained immunity”.
- DG microglia exhibit a higher phagocytic capacity when compared to their counterparts in the CA, suggesting that microglia located in neurogenic niches were primed to perform phagocytosis.

8.5 IN GBM RT EFFICIENTLY KILLS TUMOR CELLS, WHICH ARE POSTERIORLY PHAGOCYTOSED BY TAMS.

8.5.1 Microglia and infiltrating macrophages share exression markers within the tumor and both of them are categorized as TAMs.

- In the Proneural subtype TAMs in the tumor core lose the characteristic expression of the microglial marker P2Y12.
- In the Mesenchimal subtype some of the TAMs within the tumor partially maintain P2Y12 expression.

8.5.2 RT at a dose of 10Gy induced apoptosis of tumor cells in both Proneural and Mesenchimal GBM subtypes.

- Irradiation caused apoptosis of tumor cells, but also induced apoptosis on healthy cell in both GBM subtypes, suggesting that the dose could be lowered to avoid killing non-tumoral cells.
- Irradiation depleted tumor cell proliferation at 6h, which rapidly returned to basal levels by 24h in both GBM subtypes.

8.5.3 TAMs were able to phagocytose generated apoptotic cells in both Proneural and Mesenchimal GBM subtypes.

- TAMs were able to engulf apoptotic cells in both GBM subtypes, whereas clearance was only observed in the Proneural subtype, suggesting a delayed apoptosis or impaired degradation of cargo by TAMs.
- In both subtypes the phagocytosis performed by TAMs was less efficient when compared to physiological conditions and to the “superphagocytosis” model, showing that the tumor microenvironment partially impair phagocytosis.

9. TESIAREN ITZULPENA EUSKERAZ

9. TESIAREN ITZULPENA EUSKERAZ

Euskal Herriko Unibertsitatea
Medikuntza eta Erizaintza Fakultatea
Neurozientzen saila

Fagozitosiaren ondorio metabolikoak eta funtzionalak mikroglian

Doktore-gradua lortzeko doktorego-tesia.
Mar Márquez Ropero
2024
Tesi-zuzendariak:
Amanda Sierra doktorea
María Domercq García doktorea

AURKIBIDEA

1. LABURDURAK

1. LABURDURAK

AD	Alzheimer's Disease	Alzheimer gaixotasuna,
ALIX	Apoptosis-linked gene 2-interacting protein X	X proteina, apoptosiari lotutako 2 genearekin elkarreragiten duena
ALS	Amyotrophic lateral sclerosis	Alboko esklerosi amiotrofikoa
AP	Anteroposterior	Atzeko aldea
APCs	Antigen-presenting cells	Antigenoak aurkezten dituzten zelulak
ApoE	Apolipoprotein E	E apolipoproteina
APP	Amyloid precursor protein	Amiloidearen proteina aitzindaria
ATP	Adenosine triphosphate	Adenosin trifosfatoa
Aβ	Amyloid β	β amiloidea
Bak	BCL2 Associated K Protein	BCL2ri lotutako K proteina
BAMs	Border associated macrophages	Ertzari lotutako makrofagoak
Bax	BCL2 Associated X Protein	BCL2ri lotutako X proteina
BBB	Blood bran barrier	Hesi hematoentzefalikoa
BDNF	Brain-derived neurotrophic factor	Garunetik eratorritako faktore neurotrofikoa
Birc5	Baculoviral IAP repeat containing 5	IAP errepikapen bakulobirala, 5 duena
BrdU	5-bromo-2-deoxyuridine	5-bromo-2-desoxiuridina
BSA	Bovine serum albumin	Behi-albumina seruma
C	Control	Kontrola
C1q	Complement protein 1q	1q osagarriaren proteina
CA	Cornu Amonis	Cornu Amonis
CaCL2	Calcium Chloride	Kaltzio kloruroa
CAMs	CNS associated macrophages	NSZri lotutako makrofagoak
CD11b	Cluster of differentiation molecule 11B	Differentiation 11B molekularen klusterra
CD68	Cluster of differentiation 68 / Macrosialin	Differentiation 68/Makrosialina klusterra
Cd74	Histocompatibility class II invariant chain peptide Class	Histokonpatibilitateko II. klaseko kate aldaezineko peptidoa
Cenpe	Centromere protein e	Proteina eta zentromeroarena
CK-p25	Calcium/ calmodulin-dependent protein kinase II	Kaltzioa/proteina kinasa, II kalmodulinaren mendekoa
CNS	Central nervous system	Nerbio-sistema zentrala
cpMs	Choroid plexus macrophages	Plexo koroideoaren makrofagoak
CSF	Colony stimulating factor	Koloniak estimulatzeko faktorea
CSF1R	Colony stimulating factor 1 receptor	Kolonien faktore estimulatzailearen hartzailea 1
Cst3	Cystatin 3	Zistatina 3
CTSB	Cathepsins B	B katepsinak
CTSD	Cathepsins D	D katepsinak
CX3CL1	Fractalkine	Fraktalkina
D	Day	Eguna
DAM	Disease-associated microglia	Gaixotasunari lotutako mikroglia

DAMPs	Damage-associated molecular patterns	Kalteei lotutako patroi molekularrak
DAP12	DNAX-activation protein of 12 kD	12 kD-ko DNAX aktibazioko proteina
DAPI	4',6-diamidino-2-phenylindole	4 ', 6-diamidino-2-fenilindol
DAVID	Database for Annotation, Visualization and integrated discovery	Oharrak egiteko, bistaratzeko eta aurkikuntza integratua egiteko datu-basea
DBS	Double-strand breaks	Kate bikoitzeko hausturak
dc-SAMe	Decarboxylated S-adenosylmethionine	S-adenosilmetionina deskarboxilatua
DEPC	Diethyl Pyrocarbonate	Dietilpirokarbonatoa
DG	Dentate gyrus	Hortzdun bira
DMEM	Dulbecco's Modified Eagle Medium	Eagle ingurunea Dulbeccok aldatua
E	Embryogenic day	Egun embiogenikoa
ECM	Extracellular matrix	Zelulaz kanpoko matrizea
EDTA	Ethylenediaminetetraacetic Acid	Azido etilendiaminotetraazetikoa
EGF	Epidermal growth factor	Hazkunde epidermikoaren faktorea
EMPs	Erythromyeloid precursors	Aitzindari eritromieloideak
ER	Endoplasmic reticulum	Erretikulu endoplasmikoa
FAO	Fatty-acid oxidation	Gantz-azidoen oxidazioa
FasL	Fas ligand	Fas ligandoa
FBS	Fetal Bovine Serum	Behien serum fetala
Fcrl2	Fc receptor like 2	2. motako Fc hartzailea
Fcrls	Fc receptor-like S, scavenger receptor	Fc hartzailearen antzeko S, hartzaile sarraskijalea
GAS6	Arrest-specific protein 6	Gelditzeko proteina espezifikoa 6
gCSCs	Glioma cancer stem cells	Gliomako minbiziaren zelula amak
GDNF	Glial cell-derived neurotrophic factor	Zelula glikoetatik eratorritako faktore neurotrofikoa
GFP	Green fluorescent protein	Proteina berde fluoreszentea
γH2AX	Phosphorylated histone H2AX	H2AX histona fosforilatua
GM-CSF	Granulocyte-macrophage colony-stimulating factor	Granulozito-makrofagoetako kolonien faktore estimulatzailea
GO	Gene ontology	Geneen ontologia
GPC	Glycerylphosphorylcholine	Glizerilfosforilkolina
GPR34	G protein-coupled receptor 34	34 hargailua, G proteinara akoplatua
GSSG	Glutathione disulfide	Glutation disulfuroa
Gy	Gray (unit of ionazing radiation)	Gray (erradiazio ionizatzailearen unitatea)
H	Hours	Orduak
H2-Aa	Histocompatibility 2 class II antigen A alpha	A alfa antigenoaren 2. motako histokonpatibilitatea
H2-Ab1	Histocompatibility 2 class II antigen A beta 1	A beta 1 antigenoaren 2. motako histokonpatibilitatea
HAM	Highly-activated microglia	Mikroglia oso aktibatuta
HAMs	Human AD microglia	Alzheimerrarekin lotutako giza mikroglia
HBSS	Hank's balanced salt solution	Hank-en gatz-disoluzio orekatua
HCl	Hydrochloride acid	Azido klorhidrikoa
HEPES	4-(2-hydroxyethyl)-1-piperazineethanesulfonic acid	4- azidoa (2-hidroxietil) -1-piperazinaetanosulfonikoa

Hexb	β-hexosaminidase subunit β	β-hexosaminidasaren β subunitatea
HFRT	Hypofractionated radiotherapy	Erradioterapia hipofrakzionatua
HGF/SF	Hepatocyte growth factor or scatter factor	Hepatozitoen hazkunde-faktorea edo sakabanatze-faktorea
HMGB1	High mobility group box 1 protein	Mugikortasun handiko taldeko 1. kutxako proteina
HSCs	Hematopoietic stem cells	Zelula ama hematopoietikoak
IBA1	Ionized calcium-binding adapter molecule 1	Kaltzio ionizatuari lotzeko 1 molekula egokitzailea
IFIT	Interferon induced protein	Interferonek eragindako proteina
IFIT3	Interferon induced protein 3	Interferonak eragindako 3. proteina
IFN	Interferon	Interferona
IL-10	Interleukin 10	Interleukina 10
IL-1β	Interleukin 1β	Interleukina 1 β
IL-4	Interleukin 4	Interleukina 4
IL-6	Interleukin 6	Interleukina 6
iPLA2	Phospholipase A2 enzyme	A2 fosfolipasa entzima
iPSCs	Induced pluripotent stem cells	Zelula ama pluripotente induzituak
IRM	Interferon responsive microglia	Interferonarekiko sentikorra den mikroglia
Irf7	Interferon regulatory factor 7	Interferoiaren erregulazio-faktorea 7
Isg20	Interferon stimulated exonuclease gene 20	Exonukleasaren genea 20, interferonaz estimulatua
KCl	Potassium Chloride	Potasio kloruroa
kVs	Kilovolts	Kilovoltikoak
LAMPs	Lysosome-Associated Membrane Proteins	Lisosomei lotutako mintz-proteinak
LCI	Low Crenial Irradiation	Garezurreko Irradiazio Baxua
LDAMs	Lipid-droplet-accumulating microglia	Lipido-tantak metatzeko mikroglia
Lgals3	Galectin 3	Galektina 3
LIMPs	Lysosomal Integral Membrane Proteins	Mintz Integral Lisosomaleko proteinak
LM	Lysosomal (transcriptional signature)	Lisosomala (sinadura transkripzionala)
Log	Logaritmic	Logaritmikoa
LPC	Lysophosphatidylcholine	Lisofosfatidilkolina
LPS	Lipopolysaccharide	Lipopolisakaridoa
LysoPS	Lysophosphatydilserine	Lisofosfatidilserina
MACS	Magnetic-Activated Cell Sorting	Magnetismoz aktibatutako sailkapen zelularra
Mcm5	Maintenance complex component 5	Mantentze-lanen multzoaren 5. osagaia
M-CSF	Macrophage colony-stimulating factor	Makrofago-kolonien faktore estimulatzailea
MerTK	Mer tyrosine kinase	Mer tirosina kinasa
MGnD	Microglial neurodegenerative phenotype	Fenotipo neurodegeneratibo mikrogliala
MgSO4	Magnesium Sulfate	Magnesio sulfatoa
MHC	Major histocompatibility complexes	Histokonpatibilitateko konplexu handiak
Mki67	Marker of proliferation Ki-67	Ugalketa-markatzailea Ki-67
MMP	Metalloproteinase	Metaloproteinasa

mMs	Leptomeningeal macrophages	Makrofago leptomeningeoak
MRC1/CD206	Mannose Receptor C-Type 1	C-1 motako esku-hargailua
MS	Multiple sclerosis	Esklerosi anizkoitza
Ms4a7	Membrane spanning 4-domains A7	A7 mintzezko 4 domeinu
NaCl	Sodium Chloride	Sodio kloruroa
NaH2PO4	Sodium Dihydrogen Phosphate	Sodio fosfatoko dihidrogenoa
NaHCO3	Sodium Bicarbonate	Sodio bikarbonatoa
NKs	Natural killer cells	Zelula hiltzaile naturalak
NLR	(nod)-like receptors	Hargailuak (nod) -antzekoak
NO	Nitric oxide	Oxido nitrikoa
NSCs	Neural stem cells	Zelula ama neuralak
Ntv-a	Nestin promoter-driven tv-a	TV-a nestinaren sustatzaileak
Oas	2'-5'-Oligoadenylate synthetase	2 '-5' -Oligoadenilato sintetasa
OCT	Optimal Cutting Temperature	Ebaketa-tenperatura optimoa
Olfml3	Olfactomedin-like protein 3	Olfactomedinaren antzeko 3 proteina
OPCs	Oligodendrocyte progenitors cells	Oligodendrozitoen zelula gurasoak
P2RY12	Purinergic receptor P2Y12	P2Y12 hargailu purinergikoa
PAM	Proliferative-region associated microglia	Eremu ugalkorrari lotutako mikroglia
PBS	Phosphate-Buffered Saline	Fosfatoz tanpoitutako gatz-disoluzioa
PC	Phosphatidylcholine	Fosfatidilcolina
PD	Parkinson disease	Parkinson gaixotasuna
Pf4	Platelet factor 4	Plaketa-faktorea 4
PFA	Paraformaldehyde	Paraformaldehidoa
PFKFB3	6-phosphofructo-2-kinase/fructose-2,6-biphosphatase 3	6-fosfofructo-2-kinasa/fruituak-2,6-bifosfatasa 3
Ph	Phagocytosis	Fagozitosia
Ph-index	Phagocytic index	Indize fagozitikoa
ProS	Protein S	S proteina
PRRs	Pattern recognition receptors	Patroiak ezagutzeko hargailuak
PS	Phosphatidylserine	Fosfatidilserina
pvMs	Perivascular macrophages	Makrofago peribaskularrak
RCAS	Retroviral vectors derived fromavian sarcoma-leukosis virus	Sarkoma-leukosi hegaztiaren birusetik eratorritako bektore erretrobiralak
RGCs	Retinal ganglion cells	Erretinako zelula gongoilak
ROS	Reactive oxygen species	Oxigeno-espezie erreaktiboak
Rpm	Revolutions per minute	Bira kopurua minutuko
RSC	Radial Stem Cell	
RT	Room temperature	Giro-tenperatura
S1P	Sphingosine-1-phosphate	Esfingosina-1-fosfatoa
scRNA-seq	Single-cell RNA sequiencing	RNA zelulabakarraren sekuentziazioa
SDF-1	Stroma-derived factor 1	1. faktorea, estromatik eratorria
Sec	Seconds	Segundoak
SEM	Standard error of the mean	Batezbestekoaren errore estandarra
SGZ	Subgranular zone	Eremu subgranularra

Siglech	Sialic acid binding Ig-like lectin H	Azido sialikoarekin lotzeko lectina H, Ig-ren antzekoa
Socs3	Suppressor of cytokine signalling 3	Zitokinetako seinaleztapenaren ezabatzailea 3
SPF	Specific pathogen-free	Patogenorik gabeko espezifikoa
SPP1	Secreted phosphoprotein 1	Fosfoproteina sekretua 1
Stab1	Stabilin 1	Estabilina 1
Stat2	Interferon alpha induced transcriptional activator	Transkripzio-aktibatzailea, alfa interferoiak induzitua
STI1	Stress-inducible phosphoprotein 1	Estresak eragindako 1. fosfoproteina induzigarria
SVZ	Subventricular zone	Zona subbentrikularra
TAMs	Tumor-associated macrophages	Tumoreei lotutako makrofagoak
TGFβ	Transforming growth factor β	Hazkuntza eraldatzailearen β faktorea
TLR	Toll like receptors	Toll motako hargailuak
TM	Trabecular meshwork	Sare trabekularra
TMEM119	Transmembrane protein 119	Mintz-proteina 119
TNC	Tenascin C	C tenaszina
TNF	Tumor necrosis factor	Nekrosi tumoralaren faktorea
Top2a	DNA topoisomerase II alpha	DNA topoisomerasa II alfa
Tr1 cells	Type 1 Regulatory T cells	1. motako T zelula erregulatzaileak
Trem2	Triggering receptor expressed on myeloid cells-2	Hargailu abiarazlea zelulan adierazita
tSNE	t-Distributed Stochastic Neighbor Embedding	Ondorengoeneko inkrustazio estokastikoa, t forman banatuta
UMAP	Uniform Manifold Approximation and Projection	Kolektore uniformeen hurbilketa eta proiekzioa
vATPases	Vacuolar ATPases	ATPasa bakuolarrak
VNR	Vitronectin receptor	Bitronektina-hargailua
WAM	White matter associated microglia	Substantzia zuriari lotutako mikroglia
WT	Wild-type	Basatia (sagu-basatia)
Xkr8	Xk-related protein 8	8 proteina, Xkekin erlazionatua
µm	Micron	Mikra

2. SARRERA

2. SARRERA

2.1 MIKROGLIAREN SARRERA

Neurozientziak garuna sakonera-maila desberdinetan aztertzen duten eremu ugari biltzen ditu. Neurozientzia Kognitiboak prozesamendua eta informazioaren sorrera ikertzen ditu (Milner, 1998), eta Neurozientzia Molekularrak, berriz, garun-ehuna osatzen duten zelulen prozesu biokimikoak eta molekularrak aztertzen ditu (Revest et al., 1998). Neurozientzia Zelularra garuneko zeluletan zentratzen da, neuronak eta glia zelulak barne. Neuronak nerbio-sistemaren lehen mailako osagai gisa definitu dira, nerbio-bulkada sortzeko eta transmititzeko ardura baitute (Fodstad, 2002). Hala ere, glial zelulen interes gero eta handiago batek aitortu du ehun neuralaren bolumenaren erdia baino gehiago hartzen dutela, 1:1 glia eta neurona arteko proportzioarekin giza garun osoan, eta funtsezko rolak betetzen dituztela garunaren funtzionamendu egokia bermatzeko (Fields et al., 2014; Von Bartheld et al., 2016).

Neuronen eta glia-zelulen lehen deskribapena XIX. mendearen hasieran egin zen (Fan et al., 2018), baina, une hartan, bi zelula horiek zelula-mota bakartzat jotzen ziren. 1856 arte ez zen "neuroglia" ("Nervenkitt") terminoa sortu "nerbio-elementuak" lotuta mantentzen zituen "ehun konektibo" mota bati erreferentzia egiteko (Hirbec et al., 2020), eta, azkenean, zelula horiei glia izena eman zitzaien, grezierazko "itsasgarri" hitzean oinarrituta. Hala ere, finkatze- eta tindatze-prozeduren hobekuntzek (Deiters, 1865; Golgi, 1873), geroago Ramón y Cajalek (Ramón y Cajal et al., 1894; Andres-Barquin, 2002) optimizatuak, neurona eta zelula glial bakoitza gainerako zeluletatik anatomikoki bereizita zegoela erakutsi zuten, garuneko zelulen egiturazko indibidualtasunaren lehen ebidentzia histologiko zuzena emanez (Ramón y Cajal, 1888; Ramón y Cajal, 1913; Fan et al., 2018). Cajalek nerbio-sistema zentralaren "hirugarren elementu" bat ere identifikatu zuen, "lehen elementua" (neuronak) eta "bigarren elementua" (astrozitoak) bereizita (Tremblay et al., 2015; Sierra et al., 2016; Fan et al., 2018). "Hirugarren elementua" oligodendrokitoek eta mikrogliak osatzen zuten, Pío del Río Hortegak, Cajaleko eskolako ikasleetako batek, Cajalen lehen deskribapena egin eta urte batzuetara aurkitu zuenez (De Río-Hortega, 1919; Sierra et al., 2016). Halaber, Rio Hortegaren lehen behaketek mikrogliak estimuluei erantzuteko duen gaitasuna deskribatu zuten, eta, gainera, eskualde-banaketa eta zelula mikroglialen heterogeneotasuna deskribatu zituzten (del Río-Hortega, 1919; Sierra et al., 2016).

Río-Hortegaren hasierako aurkikuntzen ondoren, mikroglial ikerketa-eremua 1960ko hamarkadaren amaierara arte gelditu zen, Georg Kreutzbergen taldeak mikrogliak terminal sinaptikoak ezabatuz aurpegi-nukleoaren lesio-osteko berrantolaketan zuen partaidetza aurkitu zuen arte (Blinzinger et al., 1968). Harrezkero, mikrogliari buruzko gure ezagutza esponentzialki hazi da, hiru arlo espezifikotan egindako aurrerapenei esker: mikroglia primarioaren kultibo zelularra, zelula bizi eta finkatuen irudiak lortzeko metodoak, eta mikrogliaren gen eta proteina espezifikoen identifikazioa. XXI. mendearen etorrerarekin, eremu honek erritmo esponentzialean izan zuen bilakaera, mikrogliaren ulermen

holistikoa eraginez (Sierra et al., 2019; Paolicelli et al., 2022). Gaur egun, mikroglia nerbio-sistema zentraleko parenkimako (CNS) makrofagoak dira, garuneko parenkima etengabe zaintzeaz arduratzen dira eta garuneko sistema immunologikoaren hesi zelular nagusia osatzen dute (Paolicelli et al., 2022).

Doktorego-tesi honek mikrogliaren funtzio nagusietako bat du ardatz: material biologiko kaltegarriaren fagozitosia parenkimaren barruan, zehazki zelula apoptotikoen fagozitosia. Mikroglia bidezko zelula apoptotikoen fagozitosiaren (eferozitosiaren) prozesua asko aztertu da, bai fisiologian, bai gaixotasunean (Napoli et al., 2009; Sierra et al., 2013), eta hainbat fase ditu zelula apoptotikoa ehunetik erabat ezabatu arte (Diaz-Aparicio et al., 2016). Gainera, fagozitosia ez da prozesu terminala, haien ingurunean eragina baitu eta mikroglia transkripzio-aldaketetara eramaten baitu. Horrek emaitza funtzionalak ekar ditzake, doktoretza-tesi honen helburu nagusi gisa aztertuko direnak (Diaz-Aparicio et al., 2020; Márquez-Ropero et al., 2020). Hurrengo ataletan, xehetasun handiagoz azalduko dugu nola sortzen den mikroglia, garuna nola inbaditzen zein kolonizatzen eta azkenik, nola garatzen den. Ondoren, mikrogliak bere funtzio bereizgarriak nola hartzen dituen deskribatzen dugu, batez ere zelula apoptotikoen fagozitosian zentratuz. Azkenik, fagozitosiaren ondorioak testuinguru patologiko jakin batean aztertzearen garrantzia azaltzen dugu, garuneko tumoreetan hain zuzen ere.

2.2 ONTOGENIA MIKROGLIALA

2.2.1 Leinu eta jatorri mikroglikoa

Zelula mikroglialak bereziak dira nerbio-sistema zentraleko beste zelula batzuen artean, jatorri desberdina dutelako. Gainerako burmuineko zelulak ektodermotik, enbrioiaren kanpoko geruzatik (Fujita et al., 1975) datozen bitartean, mikrogliak beste makrofagoekin partekatzen du bere jatorria, eta mesodermo enbrioitik sortzen da (Ross et al., 2020), zehazki zaku bitelinotik, enbrioiari itsatsitako mintz sac -tik, bi bereizketa bide nagusiri jarraituz. Alde batetik, ehunean dauden zenbait makrofago eta monozito populazio batzuk, zelula ama hematopoietikoetatik (HSC) sortzen dira. Zelula horiek zaku bitelinoan jaiotzen dira eta, ondoren, fetu-gibelera migratzen dute. Han, behin betiko HSCak sortzen hasten dira enbrioi-egunaren inguruan (Kumaravelu et al., 2002; Márquez-Ropero et al., 2020). Fetuaren gibeleko hematopoiesiak makrofagoen populazio ezberdinak sortzen ditu, transkripzio faktorea c - Myb adierazten eta eskatzen dutenak garapen egokirako, hala nola albeolar edo bihotzeko makrofagoak, besteak beste (Mucenski et al., 1991; Sumner et al., 2000).

Bestalde, beste makrofago batzuek, hala nola mikroglia eta CNS lotutako makrofagoek (CAM), mugako makrofago elkartuak (BAM) bezala ere ezagutzen direnak, jatorri ezberdina dute HSCetatik sortutako makrofagoen aldean. Mikroglia parenkimaren makrofago egoiliartzat hartzen da, CNS interfazeetan CAMak aurkitzen diren bitartean, non makrofago peribaskularrak (pvMs), makrofago duralak eta leptomeningeo subduralak (mMs) eta plexus macrophages koroideak (cpMs) dauden, espazio peribaskularrean, meningetan eta plexus koroidean, hurrenez hurren (Prinz et al, 2021). Zelula-mota biak

eritromieloide-aitzindarietatik (EMP) sortzen dira, HSCak baino lehenago (E7.5-8.5 inguruan, saguetan), eta ez dute c-Myb adierazten edo eskatzen garatzeko eta heltzeko (Ginhoux et al., 2010; Hoeffel et al., 2012; Schulz et al., 2012). (**1. irudia**).

CAMen eta mikrogliaren destino zelularra Mannose Receptor C-Type 1 (MRC1 edo CD206) proteinen adierazpenaren mende dago, eta CD206+ eta CD206- zelulak E10.5.ean garunaren inbasioaren aurreko zaku bitelinoan bereizten dira. CD206+ zelulak, batez ere, garatzen ari diren plexus koroideoan eta meningetan ikusten dira, CAMak irudikatuz, eta CD206- zelulak, berriz, parenkiman zehar banatzen dira, eta zelulak positiboak ziren P2Y12 proteinarentzat, zelula mikroglialak irudikatuz (Goldmann et al., 2016; Utz et al., 2020; Prinz et al., 2021). Arbaso mikroglialak garuna kolonizatzen dute E10.5 saguetan (Ginhoux et al., 2010; Ginhoux et al., 2015) eta 4. eta 24. haurdunaldiko astea gizakietan (Menassa et al., 2018). Arbaso horiek leptomeningetatik eta alboko bentrikuluetatik sartzen dira CNSra, eta garuna populatzen dute odol-ontzien eraketarekin eta birmoldaketarekin paraleloan (Bonney et al., 2020). Ontzi-eraketaren eta mikroglia heldugabeen sarreraren arteko formazio paraleloak zelula hauei parenkima kolonizatzeko aukera ematen die (Checchin et al., 2006; Pont, Lezica et al., 2011). Mikroglia garunean sartu ondoren, kolonizazio osoa perinatikoki gertatzen da eta abiadura desberdinetan gertatzen da garuneko egitura bakoitzaren garapenaren arabera (Monier et al., 2007; Verney et al., 2010; Menassa et al., 2018). Mikroglia ezartzen denean, garun heldu baten egoera fisiologikoan, oso erritmo baxuan berritzen dira monocytes zirkulatzailearen ekarpenik gabe (Ajami et al., 2007; Bruttger et al., 2015; Goldmann et al., 2016; Zhan et al., 2019; Utz et al., 2020; Prinz et al., 2021). Laburbilduz, mikroglia bizitza luzeko zelulak dira, CNS parenchyma bizi den zaku bitelinotik eratorriak, eta helduaroan irauten dute autoberrikuntza prozasuaren eraginez, monozitoen ekarpenik gabe, gutxienez baldintza fisiologikoetan.

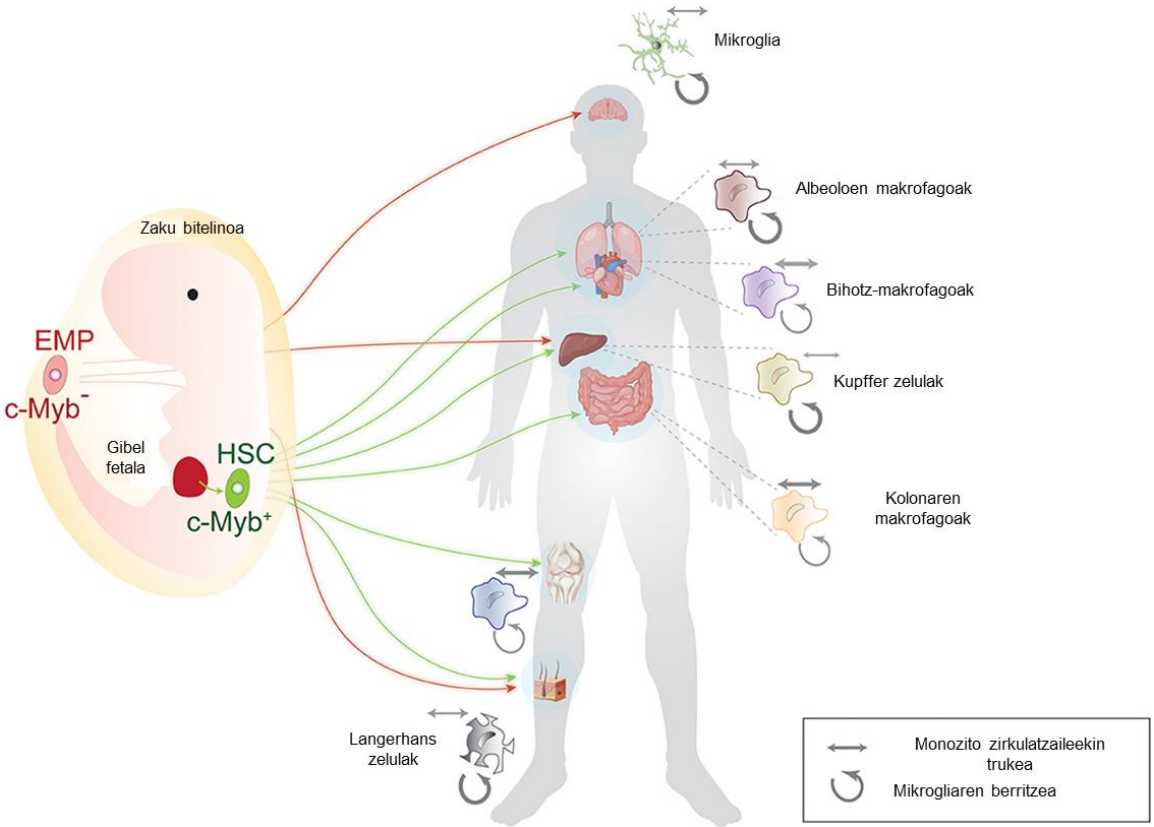

1. irudia. Makrofagoen populazio nagusien jatorri, leinu eta dinamika demografikoaren laburpena. *Mikroglia, z-Myb-Negatibo eritromieloide-aitzindari goiztiarretatik (EMP) sortua zaku bitelonian. Koloretako geziek (berdea, gorria) makrofagoen eta mikrogliaren sorleku nagusia adierazten dute. Makrofagoen populazio bakoitzaren ondoan dauden gezi haztatuek adierazten dute autoberritzearen ekarpen erlatiboa (gezi zirkularrak) vs. zirkulatzen ari diren monoklitoekin (alde biko geziak) trukatzea populazio zehatz horri. Mikroglia, nagusiki, bere burua berritzen ari da; beste makrofago batzuek, berriz, hezur-muina behar dute, monocyte eratorriak beren belaunaldirako. Bektore-grafiko batzuk Vecteezy.com bidez lortu ziren baimenarekin. Irudia argitaratu zen (Marquez-Ropero et al., 2020).*

2.2.2 Nortasun mikrogliala

Populazio mikrogliala garunean sortzeko, hau kolonizatzeko eta bertan ezartzeko prozesuan zehar, nortasun bakarra ematen dion transkribapen-profila lortzen du. Mikroglial nortasunaren gaur egungo definizioa mikroglian oso aberastuta dauden eta normalean "markatzaile mikroglial" gisa definitzen diren geneen adierazpenean oinarritzen da. Komunitate zientifikoaren barne adostasuna da mikroglia honako hauek adieraz ditzaketela transkripzio-faktoreen bidez: Pu.1; markatzaile zitoplasmatikoak, hala nola kaltzio ionizatuari lotzen zaion molekula egokitzailea 1 (IBA1); eta mintz zelularreko markatzaileak, hala nola P2YR12 hargailu purinergikoa, 119 mintzaz haraindiko proteina (TMEM119) eta kolonietako faktore estimulatzailearen hartzailea 1 (CSF1R) (Paolicelli et al., 2022).

Mikrogliak lotura handia du CAMekin, eta bi populazio horiek, batzuetan, azterlanetan nahasten dira, non partekatutako proteinak erabiltzen diren isolatzeko eta/edo aztertzeko (Mildenberger et al., 2022). Adibidez, 11b

klusterraren (CD11b) desberdintze-molekularen proteina, mikrogliaren eta makrofagoen bidez partekatua, mikroglia hautatzeko eta beste zelula batzuetatik bereizteko erabili ohi da sailkapen-prozesuan zehar (normalean fluoreszentzia bidez edo zelulak magnetikoki bereizteko estrategien bidez aktibatutako sailkapen zelularra (FACS edo MACS)), eta hori da hasierako urratsa zelula bakarraren RNAren sekuentziazio-azterketa gehienetan (scRNA-seq). Horrela, sailkatutako eta sekuentziatutako Cd11b zelulek mikroglia eta CAMak barne hartzen dituzte (Gerrits et al., 2020). Hala ere, berriki egindako ikerketek CAMetarako markatzaile espezifikoak definitu dituzte. Horiek hainbat gene komun biltzen dituen transkripzio-sinadura zentral bat partekatzen dute, hala nola MRC1, plaketa-faktorea 4 (Pf4), mintzetik hedatzen diren 4 domeinutako A azpifamiliako 7. kidea (Ms4a7), besteak beste. Gainera, azpimota bakoitza bere sinadura genetikoaren bidez definitzen da (Jordao et al., 2019; Mildenberger et al., 2022). Oro har, datu horiek, zenbait CAM azpipoluzaio daudela erakusten dute, eskualde-kokapenaren eta sinadura-geneen arabera definituta, ezaugarri batzuk mikroglia parenkimatosoarekin partekatzen dituztenak eta sekuentziazio-azterketetan nahas daitezkeenak. Transkripzio-faktore intrintsekoek zein garuneko parenkimaren kanpo-seinaleek CAMen eta mikrogliaren garapen zuzena bermatzen dute. Hurrengo atalean, mikrogliaren heldutasuna lortzeko beharrezkoak diren transkripzio-faktoreak eta ingurumen-sainaleak sakonduko ditugu.

2.2.2.1 Transkripzio-faktoreak

Pu.1 transkripzio-faktoreak berebiziko garrantzia du hematopoiesiaren erregulazioan, eta progenitore-hematopoietikoen patua zehazten du; azken batean, leinu zelularretan (adibidez, linfoide-leinuak, eritroidea eta makrofagoa) bereizten dira, Pu.1 dosiaren mende (Kastner et al., 2008; Mak et al., 2011). Gainera, Pu.1 programak CD11b adierazpena eta 1 eta 2 hazkundeari emandako erantzun goiztiarra arautzen ditu (Egr1/2). Horiek guztiak kritikoak dira makrofagoak bereizteko (Laslo et al., 2006). Azken finean, knock-out (KO) saguetan Pu.1 transkripzio-faktorerik ez egoteak makrofagoen, neutrofiloen, T eta B zelulen eta mikrogliaren falta eragiten du (McKercher et al., 1996; Mezey et al., 2000). Pu.1 beste transkripzio-faktore batekin elkarreragiten du, 8 interferoiaren faktore erregulatzailearekin (IRF8). **IRF8** funtsezkoa da leinu mieloideak garatzeko, monozitoak/makrofagoak eta zelula dendritikoak barne (Xia et al., 2020). Pu.1 ez bezala, IRF8ren adierazpen ezak ez du erabat eragozten mikrogliak CNSa kolonizatzea (Kierdorf et al., 2013). Hala ere, honek IBA1 adierazpenak murina-mikroglian murriztera garamatza, hazkunde-faktoreei, defizit funtzionalei eta morfologia- eta mugikortasun-aldaketei hiper-erantzun bat ematera, eta faktore horrek funtzio mikrogliala behar bezala garatzeko duen garrantzia nabarmentzen du (Horiuchi et al., 2012; Masuda et al., 2014). Beraz, transkripzio-faktore biak funtsezkoak dira mikro-sorkuntzarako, eta horiek gero heltzea eta funtzioak eskuratzea sustatzen dute.

2.2.2.2 Ingurumen-seinaleen

Mikroglia, halaber, bere garapenaren faseak gidatzen dituzten eta bere hektzean zehazten duten ingurumen-seinaleen mende dago. Hartzaile nagusietako bat CSF1R da, eta haren CSF1 eta IL-34 ligandoek funtsezko eginkizuna dute

mikrogliaren garapenean. CSF1ek piztutako seinaleztapena beharrezkoa da mikrogliaren garapenerako eta bereizketarako, enbrioi-garapenean ugalketa sustatuz (Lee et al., 1993; Imai et al., 2002; Ginhoux et al., 2010; Smith et al., 2013). Era berean, 34-ILak garapenean zehar ugaritzea, bereiztea eta bizirautea arautzen du, eta zitokinen/kimiozinen adierazpena sustatzen du, baita zelulen atxikipena eta migrazioa ere, mikroglia CNSan ezarri ondoren (Lin et al., 2008; Elmore et al., 2014; Masteller et al., 2014; Zhao et al., 2018). Bi ligando horiek erabakigarriak dira, bakoitza modu ezberdinean adierazten baita garun-eskualdearen arabera. CSF1ek nortasun mikrogliala hartzea bultzatzen du zerebeloan, IL-34ren eraginik gabe, eta programa molekular bakar baten adierazpena eragiten du. Programa horrek aurreko garuneko mikroglia zerebelosotik bereizten zuen (Kana et al., 2019). Hipoeremuan, bi ligando horiek beharrezkoak dira biziraupen mikroglialerako (Easley-Neal et al., 2019). CSF1R bidezko seinaleztapena anormala denean, IL-34 eskasiaren kasuan bezala, populazio mikrogliala murriztu egiten da % 20 (Erblich et al., 2011; Nayak et al., 2014). Gainera, CSF1R-/- saguek zelula mikroglialen erabateko galera erakusten dute, eta horrek iradokitzen du hartzailea beharrezkoa dela garapen eta biziraupen mikroglialerako (Erblich et al., 2011). Horrela, bada, CSF1Rren bidezko seinaleztapena ez da soilik erabakigarria mikrogliaren garapenerako, baizik eta erabat ez agertzea eragin dezake adierazten ez denean.

Mikrogliaren heltzeak kontrolatzen duen beste molekula ba,t beta hazkunde transformatzaileko faktore zitokina da (TGF-β). Hasiera batean TGF-βren papera mikrogliaren garapenean ezin izan zen aztertu, izan ere, Tgfb1 KO saguek sindrome autoinflamatorio hilgarria garatu zuten jaio eta gutxira (Kulkarni et al., 1993). T zelulen IL2 sustatzailearenpean CNSaren Tgfb1-/- espezifiko bat sortzeari esker, TGF-β1aren eskasiak mikroglian dituen ondorioak aztertu ahal izan ziren. Horrez gain, TGF-β1aren faltak 20 eguneko saguen mikroglia-kopurua murrizten duela, adinarekin berreskuratzen ez zena (IBA1+ zelulak). Gainera, TGF-1 eskasiak P2YR12 markagailu mikroglial kanonikoaren adierazpena eragotzi zuen (Butovsky et al., 2014). Hori dela eta, TGF-βa beharrezko faktore bat da, heltze mikroglialaren hainbat urratsetan eragiten duena eta sinadura mikroglial kanonikoa eskuratzeaz ziurtatzen duena.

Laburbilduz, aitzindari mikroglialak Pu.1 eta Irf8-dependentzia bideen bidez garatzen dira. Kanpoko ingurumen-faktoreen menpe daude, hala nola CSF1, IL-34 eta TGF-, 1 heltzerako eta fenotipoa behar bezala eskuratzeko. Beraz, mikrogliak informazio endogenoa eta exogenoa behar du erabat garatzeko eta bere funtzioak eraginkortasunez betetzeko.

Atal honetan, nortasun mikroglialaren ikuspegi globala eman dugu, CAMetatik bereiziz. Mikrogliaren ezaugarriei eta funtzio bereizgarriei laguntzen dieten barne-faktoreak eta kanpo-seinaleak eztabaidatu ditugu, mikroglia-identifikazioaren ikuspegi orokorra eskainiz. Mikrogliaren ezaugarriak erabakigarriak dira egoera mikroglialak hobeto ulertzeko. Kontzeptu dinamiko horrek hainbat mailatako aldaketak hartzen ditu kontuan (transkribomikoa, proteomikoa, ultraegitura, etab.), mikrogliak aurre egin beharreko testuinguruaren edo erronkaren arabera (Paolicelli et al., 2022).

2.2.3 Egoera mikroglialak

Mikroglia, kanpoko faktoreei modu uniformean erantzuten zien biztanleria homogeneotzat hartu izan da urte askotan (Butovsky et al., 2018). Dena den, Pío del Río Hortegaren lehen behaketek, mikroglia hainbat eragileengatik estimulatua zenean, erantzuteko modu desberdinak eta desberdintasun morfologikoak zituela erakutsi zuten (Sierra et al., 2016). 70.eko hamarkada erdialdera arte, zenbait ikerketek mikrogliak estimulu desberdinei emandako erantzun morfologikoak detektatu zituzten. Horrek, mikroglia "atsedenean" eta "aktibatuta" banatzen zuen sailkapen dikotomikoa ekarri zuen. Joera horri jarraituz, 2000.eko hamarkadan, makrofagoek hainbat estimuluri *in vitro* egoeran emandako erantzunean oinarritutako nomenklatura bat erabiltzen hasi zen, egoera mikroglialak definitzeko "M1" (proinflamatorioak) edo "M2" (antiinflamatorioak) aktibazio motak sortzen zituena. "M1" mikroglia fenotipo aktibatu bati lotzen zitzaion, morfologia ameboidea zuena eta zitokina proinflamatorioak askatzen zituena; "M2" mikrogliak, berriz, beste azpimota bat irudikatzen du. Mikroglia azpimota honek morfologia adarkatua zuen eta hanturaren aurkako faktoreak askatzen zituen (Gaikwad et al., 2013). Hala ere, nomenklatura hori laster geratu zen zaharkituta. mehatxu-mota desberdinengatik estimulatuak zirenean era ugariagotan eta konplexuagotan erantzuten zuten. Era berean, scRNA-seq teknologia iritsi zenean, burmuin bizian mikroglia ez zela kategoria horietako bakar batean ere polarizatzen frogatu zen, askotan M1 eta M2 markatzaileak adieraziz (Ransohoff, 2016; Paolicelli et al., 2022). Ondorioz, mikroglia dikotomikoki kategorizatzeari utzi zitzaion.

Beraz, mikrogliaren kategorizazio dikotomikoak ez du kontuan hartzen mikrogliak erantzuteko gai den estimulu sorta zabala eta zelula horiek betetzen dituzten funtzio ugari. Azken urteotan, sekuentziazio-azterketen garapenek eta gorakadek (bulk RNA-seq, scRNA-seq, eta abar) egoera mikroglialak ebaluatzen lagundu dute, eta horiek xehetasun handiagoz deskribatuko dira jarraian (**2. irudia**) (Paolicelli et al., 2022).

Mikroglia testuinguru aldakorretara egokitzeko edo egoera desberdinei erantzuteko moduei "egoera mikrogliala" deritze. Egokitzapen horiek aldaketa nabarmenak eragiten dituzte jarduera transkripzionalean zein metabolikoan, eta testuinguru-egokitzapenen adierazpen biologiko gisa balio dute. Fagozitosiak egoera desberdinak eragiten ditu, prozesu honen etapa bakoitzak transkribapen-egokitzapen bereizgarriak eragiten dituela erakusten duen bezala (Diaz-Aparicio et al., 2020).

Doktorego-tesi honen helburu nagusia, fagozitosiak egoera bereizien azpian dauden egokitzapenak eragiten dituen aztertzea da. Horien bidez mikroglia zelula apoptotikoak irentsi ondoren igarotzen baitira. Beraz, atal honetan mikrogliak har ditzakeen egoerak delineatuko ditugu; aldaketa transkripzionalak, metabolikoak eta beste mota batekoak orkestratuz morfologian eta proteina adierazpenean. Egoera mikroglial horiek ulertzea funtsezkoa da fagozitosiari erantzunez gerta daitezkeen aldaketa potentzialak ebaluatzeko. Jarraian, egoera mikroglialak modulatzen dituzten faktoreen deskribapenean sakonduko dugu. Hortaz aparte, mikroglia bere testuingurura nola egokitzen den ere,

transkribatzea eta metabolismoa modulatuz eta biak heterogeneotasun mikroglialaren sorreran inplikatuz.

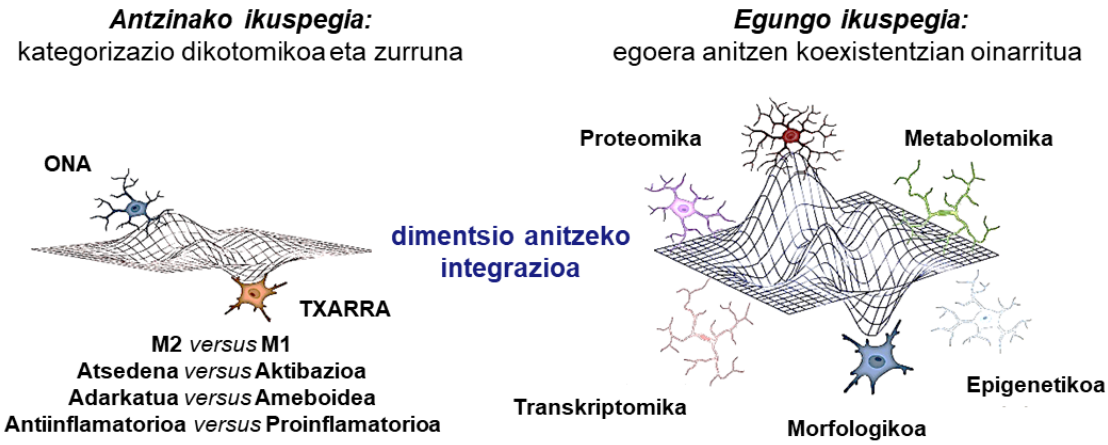

2. irudia. Nomenklatura mikroglialak: iragana eta etorkizuna. *Mikroglia kategoria dikotomikoetan kokatu izan da tradizioz, baina datu epigenetiko, transkriptomiko, metabolomiko eta proteomikoen gaur egungo integrazioak aldi berean dauden egoeren integrazio multidimentsionala errazten du. Irudia argitaratu zen (Paolicelli et al., 2022).*

2.2.3.1 Testuinguruaren araberako heterogeneotasun mikrogliala.

Mikroglia aldatzen duten eta egoera heterogeneoetara eramaten duten faktoreen artean adina, sexua, denbora zirkadianoa, CNSaren seinaleak, seinale periferikoak, mikrobiotaren aldaketan eta baldintza patologikoak (Erny et al., 2015; Thion et al., 2018; Chen et al., 2021) daude. Mikrogliaren bizitzaren zeharreko gidatze-aldaketetan, adinak eragina du. Etapa bakoitzak (enbrioia, jaiotza-ingurukoa, heldua eta zahartzea) berariazko faktore erregulatzaileak eta adierazpen genetikoko profilak adierazten ditu. Garapenaren etapa goiztiarrenetan, hala nola jaio osteko garapen goiztiarrean, mikroglia oso heterogeneoa bihurtzen da transkribatzean, helduen CNSan, berriz, heterogeneotasun mikrogliala murriztu egiten da (Hammond et al., 2019). Hala ere, nahiz eta helduen mikroglian heterogeneotasun transkripzionala murriztu egiten den, oraindik ere desberdintasun batzuk daude, batez ere eskualde-kokapenak bultzatuta. Mikroglia hipokanpalak eta zerebelosoak desberdintasun transkripzionalak erakusten dituzte beste eremu batzuekin alderatzen direnean, immunitatean inplikatutako geneen adierazpen handiagoarekin batera (Grabert et al., 2016). Era berean, mikrogliak antzemaezin diren seinaleei ere.erantzuten die, kortex sentsoriomotorraren geruzetan ikusitako aldaketa fenotipikoek erakusten duten bezala, non neurona piramidalek mikroglialaren dentsitatean eta

egoera molekularrean eragiten duten (Stogsdill et al., 2022). Sexu-desberdintasunek ere eragina dute egoera mikroglialetan, ustez kromosoma sexualengatik eta hormona gonadalengatik. Gizonezkoen eta emakumezkoen mikrogliak desberdinak dira transkriptoman, proteoman eta morfologian, eta berez mantentzen dira sexu desberdineko garun batera transplantatu ondoren ere (Hanamsagar et al., 2017; Guneykaya et al., 2018; Villa et al., 2018). Bitxia bada ere, sexu-desberdintasunek mikroglian duten eragina funtsezkoa izan daiteke hainbat arlotan, sexu-dimorfismoa erakutsi duten patologietan, hala nola prebalentziaren adierazpenean eta tratamenduari emandako erantzunean (Lynch, 2022).

CNSak emandako ingurumen-seinaleez gain, mikrogliak sarrera periferikoei ere erantzuten die. Traktu gastrointestinaleko mikrobiotan eta patogenoak detektatu ondoren makrofago periferikoek sortutako zitokinetan aldaketak hautemateko gaitasuna barne. Alde batetik, mikrobiotak heldutasuna eta funtzio mikrogliala kontrolatzen duela dirudi, mikrobiotatik eratorritako kate laburreko gantz-azidoen bidez, zeintzuek heste-garun ardatzaren bitartekariak baitira (Erny et al., 2015; Thion et al., 2018; Erny et al., 2021). Bestalde, erantzun immunitario periferikoak ere hautematen ditu mikrogliak. Hantura sistemiko akutuak Interleuzina-1 beta (IL-1) hantura-bitartekariaren ekoizpena eragiten du, eta horrek iradokitzen du, "gaixotasun-portaeran" (adibidez, lozorroa, jateko gogoa galtzea, logura, etab.), infekzio batean zehar, mikroglia inplikatua egon daitekeela.

Laburbilduz, aurkeztutako datuek mikrogliaren moldagarritasun nabarmena erakusten dute, izen ere, seinale ugariri erantzuten baitie. Egokitze-erantzun horiek bizitzan zehar parenkimaren hainbat eskualdetan ikusitako heterogeneotasunaren azpian daude. Mikrogliak, transkroptazioaren eta metabolismoaren alterazioen bidez lortzen ditu egokitzapen horiek. Aipaturiko aldaketak ondorengo eztabaidan argituko dira, transkripzio-egoeren miaketarekin hasita.

2.2.3.2 Transkripzio-egoerak

Aurreko atalean funtzio mikrogliala modulatzen duten eta heterogeneotasunaren oinarria osatzen duten hainbat testuinguru eta ingurune deskribatu ditugu. Bere aldakortasun funtzionalaren funtsezko determinatzaile bat adierazpen genikoaren modulazio dinamikoa da, transkripzio-egoera desberdinak sortzen dituena. Mikroglia aktibatuta edo geldirik dagoela kategorizatzen duten M1 eta M2 egoera klasiko eta sinplistetatik haratago, scRNA-seqen azken ikerketek ezagutza berriak ekarri dituzte mikroglia-aniztasuna ulertzeko, era berean, mikroglia-egoerak definitzeko kontzeptu berriak sartu dituzte. Lehen ere egin izan den bezala, mikroglia-egoerek mikrogliak hainbat ingurune edo estimulutara egiten dituen egokitzapenak biltzen dituzte, eta hainbat mailatako aldaketak hartzen dituzte barnean. Zelula bakarreko ikerketek aukera ematen dute mikroglia kategorizatzeko, transkribatzean oinarrituta, zehazki, funtsezko geneen adierazpenean, eta, horrela, hainbat egoera identifikatzen dira. Atal honetan, scRNA-seq azterketetan adierazitako sinadura nagusietan sakonduko dugu.

Mikroglia homeostatikoa

Mikroglia homeostatikoaren definizioa, baldintza fisiologikoetan dauden zelulei buruzkoa da. Hauek, hainbat egoera morfologikoak eta funtzionalak erakusten dituzte, CNSaren mikroingurumen-seinaleen arabera (Paolicelli et al., 2022). Saguaren mikroglia homeostatikoa, espezifikoki P2yr12, Tmem119, H azido sialikoarekin lotzen den Ig motako lektina (Siglech), G 34 proteinari akoplatutako hartzailea (Gpr34), 3 zitokinen seinaleztapenaren ezabatzailea (Socs3), -hexosaminidasa (Hexb) azpiunitatea, olfactomedina 3 motako proteina (Olfml3) eta S scavenger motako hartzailea (Fcrls) (Butovsky et al., 2018). Gene mikroglial horietako batzuk giza mikroglian ere ikusi ziren, P2RY12 eta TMEM119 barne (Butovsky et al., 2014; Satoh et al., 2016; Zrzavy et al., 2017). Mikrogliaren transkripzio-sinadura homeostatiko horren identifikazioak tresna solidoen garapena hobetu zuen, baita mikrogliarako antigorputz espezifikoak eta sagu transgenikoak ere. Zehazki mikrogliara zuzentzeko, mikrogliaren sorrera induzitutako zelula ama pluripotentzialetatik abiatuta (iPSC) (Muffat et al., 2016; Douvaras et al., 2017).

DAM mikroglia

ScRNA-seq analisian aurkitutako beste sinadura bat gaixotasunari lotutako mikroglia (DAM) izan zen. Sinadura hori Alzheimer (AD) gaixotasunaren eredu genetiko batean aurkitu zen lehen aldiz. Eredu genetiko horren ezaugarria amiloidearen metaketa da eta gaixotasunaren bereizgarri nagusietako bat da (Keren-Shaul et al., 2017). Alde batetik, azpipopulazio horrek markatzaile homeostatikoen adierazpen murritza zuen. Hala nola, Tmem119 eta P2ry12, baita mikrogliak adierazitako beste proteina batzuena ere, zehazki, P2ry13 hargailu purinergikoa, kimiokinen hartzailea (C-X3-C) 1 (Cx3cr1), 3. zistatina (Cst3) eta CSF1R. Bestalde, DAM mikrogliak hainbat generen adierazpena handitu egin zela erakutsi zuen, adibidez mieloide 2 zeluletan (Trem2) adierazitako hartzaile eragilea, E apolipoproteina (Apoe) eta Dectina-1 (Clec7). DAM enpresa giza mikroglian ere identifikatu zen, goraka erregulatu baitzituen APOE eta TREM2 (Olah et al., 2020). Garrantzitsua da nabarmentzea bai APOE bai TREM2 giza AD gaixotasuna garatzeko arrisku-geneak dira, eta horrek iradokitzen du DAMek gaixotasunaren progresioan eragina izan dezakeela (Chen et al., 2021). ADtik haratago, DAM mikrogliak ere aurkitu ziren beste gaixotasun eredu batzuetan, hala nola alboko esklerosi amiotrofikorako SOD1-G93A ereduan (ELA) (Deczkowska et al., 2018) eta esklerosi anizkoitzan (EM) (Krasemann et al., 2017). DAMekin batera, antzeko sinadurak aurkitu ziren gaixotasun neurodegeneratiboaren beste eredu batzuetan, zehatz mehatz fenotipo neurodegeneratibo mikroglialean (MGnD), EAko giza mikroglian (HAMs), esklerosi anizkoitzean handitutako mikroglian (EM), eta lipido-tantak metatzen dituzten mikroglian (LDAMs),

HAM mikroglia

Gaixotasun neurodegeneratiboetan atzemandako sinadura mikroglialetatik haratago, patologia neurodegeneratibo elkarturik gabeko zahartze-eredu batek mikroglia oso aktibatuta (HAM) (Jin et al., 2021) definitutako sinadura bat

erakutsi zuen. HAM mikroglia 18 hilabeteko saguetan soilik ikusi zen, eta horietan zenbait markatzaileren adierazpen espezifikoa, hala nola lipasa lipoproteina (Lpl), galektina-3 (Lgals3), F zistatina (Cst7) eta Cd74. HAM mikrogliak erantzun immunodistiratsuak eragin zituen garun zahartuetan, neuronek askatutako makrofagoen migrazioaren faktore inhibitzailea (Mif) detektatu ondoren. HAMeko Cd74 hartzailearen bidez jardunez, Mifek mikrogliaren jarduera immunokimiotaktikoa sustatu zuen. Beraz, badirudi HAM sinadura mikrogliaren ezaugarria dela patologia neurodegeneratiborik gabe zahartutako garunetan.

MHC mikroglia

ScRNA-seq azterketak egin dira beste gaixotasun-eredu batzuetan, horien artean saguaren neurodegenerazio-ereduan, giza proteinaren gainadierazpenean oinarrituta p25, kaltzio/kalmodulinaren mendeko (CK -p25) kinasa II proteinaren kontrolpean (Cruz et al., 2006). Badirudi EA duten pazienteetan metatzen dela eta lotura estua duela heriotza neuronalarekin. CK-p25 saguetan beste azpimultzo mikroglial bat identifikatu zen, MHC-II edo MHC mikroglia (Mathys et al., 2017). Azpimultzo espezifiko horrek antigenoen aurkezpenarekin lotutako geneen adierazpen genikoaren maila handiak erakutsi zituen, histokonpatibilitateko II. klaseko A alfa antigenoa (H2-Aa), histokonpatibilitateko II. klaseko A beta 1 antigenoa (H2-Ab1) eta histokonpatibilitateko II. klaseko kate-peptido aldaezina (Cd74, DAM sinaduran ere adierazia) barne. Modu esanguratsuan, CAM sinadurak arestian aipatutako II. klaseko MHCarekin lotutako geneen adierazpen-maila handiak erakutsi zituen. Hala ere, gene beste gene batzuek adierazpen handiagoa ere erakutsi zituzten, besteak beste, Mrc1, plaketa faktorea 4 (Pf4), mintza 4 domeinuak 4 A7 (Ms4a7), egonkortzea 1 (Stab1), eta Fc hartzailea 2 (Fcrl2) (Prinz et al., 2021) – horietako batzuk CAM- biztanlerian deskribatu dira aldez aurretik –, eta horrek iradokitzen du erlazio bat egon daitekeela bi populazio zelular horien artean. Gainera, MHC-IIrekin lotutako geneak handitu egin ziren neurodegenerazioaren progresioan CK-p25 eredu neurodegeneratiboan (Mathys et al., 2017) eta proteina aitzindari amiloidearen knock-in saguaren ereduan (APP) (APP^{NL-G-F}) EArako (Sala Frigerio et al., 2019). Horrek, patologiaren exazerbazioak... dezakeela iradokitzen du.Hala, badirudi gaixotasun neurodegeneratiboek areagotu egiten dutela CAMen presentzia ehun patologikoan.

IFN mikroglia

Interferonarekin edo IFNrekin lotutako mikrogliaren klusterra CK-p25 ereduan ere deskribatu zen lehen aldiz (Mathys et al., 2017), eta, gainera, beste gaixotasun-eredu batzuetan aurkitu zen (adibidez, Aβ-ren metaketan (APP-PS1), tauopatietan (P301S eta P301L), alboko esklerosi amiotrofikoan, kuprizonak eragindako desmielinizazioan, iskemian, lipopolisakaridoen esposizioan, infekzio biraletan eta gliometan) (Friedman et al., 2018). IFN klusterrak interferoiak estimulatutako gene ezagun asko zituen, hala nola 2 '-5' -Oligoadenilato sintetasa familietako kideak (Oas1, Oas2, Oasl1, Oasl2), eta interferoiak eragindako proteinak (Ifit1, Ifit2, Ifit3), interferoiak estimulatutako 20 exonukleasaren genea (Isg20), eta interferoia erregulatzen duen faktorearen transkripzio-faktoreak (Irf7) eta alfa interferoiak eragindako transkripzio-aktibatzailea (Stat2) (Mostafavi et al.,

2016). Gene horiek infekzio biralaren aurrean eragin zuten gehien, baina LPSrekin tratatutako saguetan eta glioma-ereduetan ere gehiegi adierazi ziren. Gainera, biboteen ezabatze partziala erabiltzen duen sagu-eredu batean, somatosensorialeko azalaren zirkuitu neuralaren birmoldaketa bizkortzen duen faktore estresatzaile ezagun batean, IFNrekiko sentikorra den populazio mikroglial bat aurkitu zen (Dorman et al., 2022). Ikertzaileek ikusi zutenaren arabera, IFN geneak (adibidez, Ifit3) gehiegi adierazten zituen mikrogliak neuronak irensten zituen, eta horrek iradokitzen du IFN mikrogliak fagozitosian parte hartzen duela.

Mikroglia ugalkorra

Aurretik aztertutako talde/sinadura mikroglial homeostatikoez, DAMez, MHCz eta IFNz gain, IHrako 5xFAD ereduan egindako scRNA-seq-ei buruzko azken ikerketek bosgarren talde mikroglial bat identifikatu zuten: mikroglia ugalkorra. Populazio horrek, nabarmeki aberastuta zegoen hazkunde-fasean zeuden zeluletan (G) 2/mitikoan (M), eta ugalketarekin lotutako geneen goranzko erregulazioa erakusten zuen. DNA topoisomerasa II alfa (Top2a), Ki-67 ugaltze-markatzailea (Mki67), proteina eta zentromeroa (Cenpe), minikromosomaren mantentze-konplexuaren 5. osagaia (Mcm5) eta proteina 5 bakulobirala, IAP errepikapenak dituena (Birc5) (Chen et al., 2021) bezalako geneen adierazpena du ezaugarri. Mikroglia ugalkorraren identifikazioak aurreko txostenak berretsi zituen, 5xFAD (Wang et al., 2016) saguetako Aβ, plaken inguruko Ki67 ugalketa-markatzailea eta eredu neurodegeneratiboetako gene mitotikoen gehikuntza adierazten zituen mikroglia-taldea identifikatuz (Friedman et al., 2018). Hala, bazirudien mikroglia ugaritzen ari zela neuroendekapenari erantzunez, eta aldez aurretik ikusitakoa berresten zuela zenbait baldintza neurodegeneratibotan, hala nola EAn eta Creutzfeldt Jakob gaixotasunean (Gómez-Nicola et al., 2013).

PAM mikroglia

Duela gutxi, eskualde ugalkorrekin lotutako talde mikroglial bat hauteman da, eskualde ugalkorrekin lotutako mikroglia izenekoa (PAM) (Li et al., 2019). Transkripzio-sinaduraren ezaugarri nagusiak honako hauek dira: gene homeostatikoen adierazpen moteldua, hala nola Tmem119, P2ry12 eta Siglech, eta fosfoproteina sekretuaren gainadierazpena 1 (Spp1), melanoma ez-metastasikoaren glikoproteina B (Gpnmb), 1 intsulinaren hazkunde-faktorea (Igf1), C-type lectin domain-containing 7A (Clec7a), lipasa lipoproteina (Lpl), CD9 (Cd9), CD63 (Cd63), galektina 3 (Lgals3), 5 gantz-azidoekin lotzen den proteina (Fabp5), X alfa integrinaren azpiunitatea (Itx). PAMak, edo eskualde ugalkorrei lotutako mikrogliak, nagusiki garatzen ari den gorputz isilean eta zerebelo-substantzia zurian agertzen dira jaio ondorengo lehen astean (Li et al., 2019). Denbora-esparru espezifiko hori bat dator eratu berri diren oligodendrozitoen fagozitosian parte hartzearekin. Ondorioz, behaketa horiek PAMak zelula fagozitikoak direla erakusten/frogatzen dute.

Laburbilduz, scRNA-seq azterketek sinadura mikroglial ugari identifikatzen dituzte, animalien garapen-adinaren eta hainbat gaixotasunen testuinguruan.

Populazio horietako batzuk hertsiki lotuta daudela dirudi, ibilbideen analisiak zenbait populazio mikroglialen arteko erlazioak jorratzen baititu (Ellwanger et al., 2021).Mikroglia homeostatikoa *continuum* baten bidez bereizten da, azkenik, lau ibilbide bereizitan adarkatzen dela erakutsiz: DAM, IFN-I, MHC eta mikroglia ugalkorra. Horrela, badirudi mikrogliak modu malguan trantsizionatzen duela transkribapen-sinadura batetik bestera, eta horietako bakoitza, beharbada, egoera bakarrarekin lotuta dagoela, inguruneko eskaeren arabera.

Hala ere, scRNA-seq azterketek ere mugak dituzte. Gene-adierazpenaren sinadurek bide biologikoak adierazten dituzten arren, transkripzio-sinadura horien eta azpipopulazio egonkorren ondorio funtzionalak ez daude argi oraindik. Gainera, laginak prozesatzeko tresnek eta espezieen arteko desberdintasunek zaildu egiten dituzte konparazioak zein datuen integrazioa, ikerketa-taldeen arteko adostasuna saihestuz (Gosselin et al., 2017; Wu et al., 2017; Geirsdottir et al., 2019; Marsh et al., 2022). Adostasun ezak izen desberdinak ekar ditzake kluster bererako, baita klusterren gehiegizko zatiketa ere. Beraz, scRNA-seq-en azterketek egoera mikroglialen aniztasuna ulertzeko informazio baliagarria ematen duten arren, funtsezkoa da egoera mikroglialak definitzen hastea. Ez bakarrik RNAm-ren adierazpen-mailak kontuan hartuta, baita konplexutasuneko beste geruza batzuk aztertuz ere (adibidez, sinadura epigenetikoak, transkripzionalak, translazionalak eta metabolikoak). Azken batean fenoma zelularra (hau da, motilitatea, morfologia eta ultraegitura) eta funtzioa (Paolicelli et al., 2022) zehaztuko dituztenak. Jarraian, bi gai jorratuko ditugu: lehenik, egoera mikroglialekin lotutako aldaketa metabolikoak, eta, bigarrenik, testuinguruko hainbat faktoreren eragina, hala nola espeziea, sexua, espazio-kontsiderazioak eta garapen-unea dibertsitate mikroglialean.

2.2.3.3 Egoera metabolikoak

Beren egoera transkribatzaileetatik haratago, mikrogliak profil metaboliko espezifikoak erakusten ditu, aurkitzen dituzten ingurumen zantzuei lotuta daudenak. Profil metaboliko horiek testuinguru nagusiak ezarritako eskakizun funtzionalei erantzuteko egokituta daude. Immunitate-zelula askok, T zelulek eta makrofaseek barne, malgutasun metaboliko nabarmena dute, eta horrek aukera ematen die hantura-baldintza aldakorretara egokitzeko eta, horrela, erantzun immunologiko koordinatuak laguntzeko (Bernier et al., 2020b). Era berean, immunologikoak ez diren beste zelula batzuk, hala nola tumore-zelulak, fosforilazio oxidatzaile mitokondrialetik energia ekoizpen bizkorrago batera pasatzen dira, glikolisiaren bidez (Warburg efektua) eta ugaltzea eraginez (Vaupel et al., 2021). Minbizi-zelulez gain, ugaztunen zelulak azkar ugaltzen dira, ehunak zorrotz birsortzen dira eta giza globulu gorri helduak Warburg-en motako glukosa-metabolismora aldatzen dira (Ghashghaeinia et al., 2019; Sun et al., 2019). Era berean, metabolismo oxidatzailetik egoera glikolitiko indartura igarotzea mekanismo bat da, bakterio- eta onddo-hormako konposatu baten eraginpean dauden makrofaseetan sortzetiko immunitatea garatzeko. Glukosaren eraginpean dauden saguen makrofagoek Warburgen aldaketa metabolikoa jasaten dute, dectin-1-Akt-mTOR-HIF-1α bidea aktibatuz. Horrez gain, aldaketa epigenetikoak eragiten dituzte, epe luzera hobetutako bigarren mailako infekzioen erantzun funtzionalen eragileak direnak (Cheng et al., 2014). Berezko memoria hori ez dator bat egokitze-memoriarekin; izan ere, memoria

hori honela definitzen da: immunitate-erantzun oso espezifikoen sorkuntza T eta B zelulen ekintzaren bidez. Erantzun immune horiek antigeno espezifikoak ezagutzen eta gogoratzen dituzte, hala nola proteinak edo patogenoen beste molekula batzuk, inbaditzaile zehatz horien aurka epe luzera babesa emateko. Horrela, zelula immunologiko mota ezberdinek metabolismoa erabiltzen dute funtzioa aldatzeko eta egokitzeko.

Mikrogliak mikroingurune metaboliko paregabe bati egin behar dio aurre, garunak, gorputzaren pisuaren % 2 ordezkatzen duen organoak, gorputzaren glukosaren eta oxigenoaren % 20 kontsumitzen baitu (Mergenthaler et al., 2013). Odolaren eta garunaren arteko hesiak (BBB) substratuak garuneko parenkiman sartzea arautzen du, astrozitoak izanik giltzarri nagusiak glukosaren gorakadan eta laktato-anezkan. Azken finean, neuronak energia iturri gisa erabiltzen ditu (Jurcovicova, 2014). Baina mikroglaziarrek ingurune metabolikoa ere somatzen dute, nahiz eta glukosa, aminoazidoak eta gantz-azidoak metabolizatzeko aukera ematen dieten transposizio eta entzimak izan (Bennett et al., 2016). Oinarrizko baldintza homeostatikoetan, mikrogliak glukosa metabolizatzen du. Mikrogliak, hala ere, *in vitro* malgutasun metabolikoa erakusten du eta metabolismo oxidatiboa mantentzeko gaitasuna erakusten du glukosa, glutamina, piruvatoa, laktatoa edo ketona gorputzak erabilgarri dauden substratu bakarrak direnean (Nagy et al., 2018). Glukosarik ez dagoenean, adibidez intsulinak eragindako hipogluzemian, mikroglaziarra glutaminan oinarritzen da, eta azkar aldatzen da glikolisitik glutaminolisira, fosforilazio oxidatzailea eta haien zaintza-gaitasuna mantentzeko (Bernier et al., 2020a). Horrela, mikroglia gai da substratu desberdinak barneratu eta metabolizatzeko, ingurunearen gorabehera metabolikoetara egokitzeko gaitasuna erakutsiz.

Hala ere, mikroglia ez da inguruko ingurumen metabolikora egokitzen den eragile pasibo bakarrik, aldaketa metabolikoak jasaten ditu estimulu inflamatorioen ondorioz. Adibidez, hanturazko inguruneetan, mikrogliak etengailu metaboliko bat jasaten du, eta horrek fosforilazio oxidatzailea gutxitzen du, fisio mitokondrialari eta glikolisi upregulatu bati lotuta (Orihuela et al., 2016; Nair et al., 2019). Aldaketa glikolitiko honek trukaketak dakartza entzimen erregulazioan eta glikolisiaren seinaleztapen-bidean parte hartzen duten gene metabolikoen transkripzioan. Adibidez, GLUT1 glukosa-hartzaileak zein 6 fosfofrukto-2-kinasa/fruktosa-2,6-bifosfatasa 3 entzimak (PFKFB3), mikroglian gehiago transkribatuak daudela erakusten dute (**3. irudia**), mikroglia zelulak estimulu pro-inflamatorioen eraginpean daudenean, bai eta hantura areagotzen den gaixotasunetan ere, hala nola ADan.

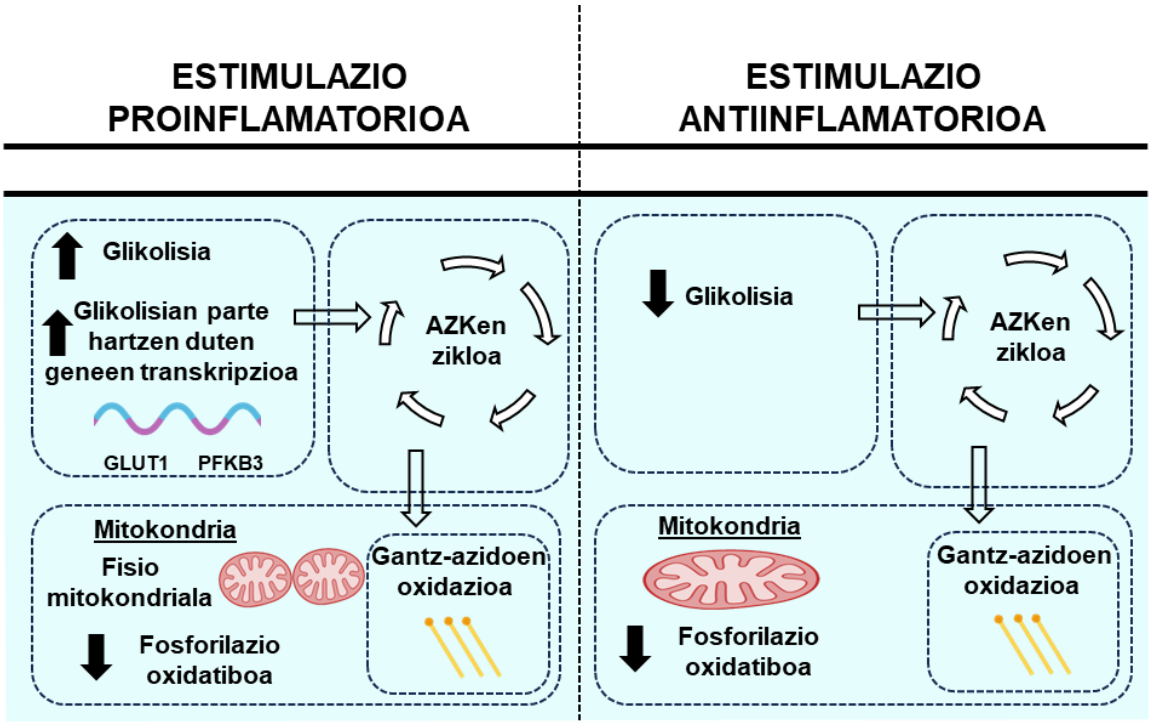

3. irudia. Mikrogliaren egokitzapen metabolikoak estimulazio pro eta antiinflamotorioaren ondoren. *Proinflamatorio-faktoreekin mikroglia estimulatzeak etengailu metaboliko bat eragiten du, eta horrek glikolisia potentziatzen du, fosforilazio oxidatzailea murrizten duen bitartean. Estimulu antiinflamatorioek, berriz, gantz eta azido oxidazioa murrizten dute. BioRender.com-ekin sortua eta moldatua (Márquez-Ropero et al., 2020).*

Laburbilduz, mikrogliak, ingurumen-erronkei erantzuteko moldagarritasun nabarmena du. Horrek, mikroglia-egoera ezberdinetara garamatzan adierazpen genikoaren eta metabolismoaren alterazioen ondorio da. Atal honetan egoera mikroglikoetan eragina duten hainbat faktore azaldu diren arren (adibidez, garapen-denbora, adina, sexua, eskualde parenkimala, eta abar), fagozitosiak egoera mikroglikoari nola eragiten dion gaur egungo ezagutza oraindik mugatua da (1.5.2 atalean berrikusiko da). Gure laborategiaren ikerketek dagoeneko frogatu dute *in vitro* mikroglia fagozitosiaren ondorengo eraldaketa transkriptazionalak jasaten dituela, metabolismo zelularrean inplikatutako gene batzuekin, eta horrek iradokitzen du fagozitosiak mikroglian egokitzapen transkripzional eta metabolikoak eragiten dituela (Diaz-Aparicio et al., 2020). Ondorioz, doktorego tesi honen helburu nagusienetako bat fagozitosiak eragindako mikroglia aldaketa transkriptional eta metabolikoak xehetasun handiagoz argitzea eta deskribatzea da.

Horrela, mikrogliak beren profil transkriptomikoa eta metabolismoa birmoldatu egiten ditu hartutako egoera zehatzetara eta, azken batean, estimulazio zorrotz edo kronikoari erantzuten dioten funtzio espezifikoak egitera. CNSn mikrogliak betetzen dituen funtzioetan sakontzeko, hurrengo atalean funtzio mikroglikoak zehatzago deskribatuko ditugu.

2.3 FUNTZIO MIKROGLIALAK

Garuneko parentimaren makrofago egoiliar gisa, mikrogliak rol integrala betetzen du nerbio-sistema zentralaren (NSZ) funtsezko funtzio batzuetan. Funtzio immunitario klasikoen artean, hantura-erantzuna eta fagozitosia daude, eta

horiek deskribatuko dira lehenik. Hanturan zein fagozitosian parte hartzen duten mekanismoen bidez, hala nola faktore disolbagarriak askatuz eta hondakinak ezabatuz, mikrogliak garunaren funtzio espezifikoak betetzen ditu, gliogenesia, baskulogenesia, neurogenesia, mantentze sinapikoa eta mielinizazioa barne hartzen dituztenak (**4. irudia**). Hurrengo ataletan, funtzio immunitario klasikoen ikuspegi orokorra emango dugu: hantura eta fagozitosia, eta, ondoren, mikrogliak betetzen dituen garunaren funtzio espezifikoen azterketa zehatza. Funtzio horien artean, mikrogliak etengabe arakatzen du bere ingurunea, lehenik deskribatuko den zaintza izeneko prozesu batean.

2.3.1 Zaintza edo parenkimaren eskaneatzea

Inguruneko aldaketei eraginkortasunez erantzuteko, mikrogliak, inguratzen duen ehuna "sentitu" behar du eta haren alterazioak hauteman behar ditu. Horretarako, prozesu mikroglialek etengabe eskaneatzen dute garun-ehuna eta prest daude edozein alterazio gertatzen denean jarduteko (Hanisch et al., 2007). Mikrogliak ingurumen-aldaketa ugari hautematen ditu, hala nola mikrobio inbaditzaileak, kaltetutako edo hildako zelulak, inguruko ehunaren pH-aren alterazioak, zelulaz kanpoko matrizearen osotasunaren edo osotasunaren aldaketak eta hainbat substantziaren askapena, horien artean, zitokinak eta kimiokin inflamatorioak (Hickman et al., 2013). Gainjarri gabeko esplorazio-eskualdeak dituzten prozesu zelularren bidez egiten da zaintza (Nimmerjahn et al., 2005). Gainera, proba emergenteek iradokitzen dute prozesu mikroglialek modu autonomoan jardun dezaketela, mikroglia fagozitikoan ikusten den bezala; izan ere, prozesu batek fagozitosia lantzen du, eta beste batek inguruko lurraldea zaintzen jarraitzen du eraginkortasun berarekin (Kamei et al., 2023). Hala ere, zenbait baldintza patologikok, hala nola iskemiak (Beccari et al., 2023), epilepsiak (Abiega et al., 2016) eta ADak (Franco-Bocanegra et al., 2019), aldatu egiten dute mikro-higikortasuna, eta horrek are gehiago eragiten die zaintzari eta ondorengo funtzioei.

2.3.2 Erantzun immunitarioa

Erantzun immunitarioa honela banatzen da: berezko erantzun immunitarioa (immunitate innatoa) eta erantzun immunitario egokitzailea (adaptazio immunitatea). Lehenengoa organismoak patogenoen aurka duen lehen defentsa-lerroa da, eta erantzun azkarra eta zehaztugabea du ezaugarri. Patogenoak organismora iristen direnean, izatezko immunitate-sistemak lehen defentsa-lerro gisa jokatzen du (Riera Romo et al., 2016; McComb et al., 2019). Sortzetiko immunitate-sistema osatzen duten zelulak zelula hiltzaile naturalak (NK), zelula dendritikoak eta globulu zuriak dira, baita tisulu-makrofagoak ere, mikroglia eta garuneko CAMak barne (Turvey et al., 2010; Prinz et al., 2021). Estimulu kaltegarri bat detektatu ondoren, zelula immunitario horiek mehatxuari aurre egiteko bi mekanismo jartzen dituzte martxan: hantura eta fagozitosia. Sortzetiko immunitate-sisteman, entrenatutako immunitateak memoria-prozesu gisa funtzionatzen du, eta, horren bidez, bigarren aldiz infekzio baten eraginpean jartzeak, sistemaren erantzun biziagoa eragiten du (Netea, 2013).

Aitzitik, immunitate moldagarria patogenoei zuzentzen zaie, zehazki, horiek ezagutu ondoren, eta horrek erantzun immunitario atzeratua eta eraginkorragoa

ematen du. Gainera, aurrez azaldutako patogenoak ezagutzeko gaitasuna du, memoria immunologiko gisa definitzen dena (Janeway Jr et al., 2001; Brandes et al., 2019). Hala ere, bi memoria-forma horiek desberdinak dira: memoria moldagarria espezifikoa da, eta zelula immunitarioak aurrez esposizioan egon diren patogeno zehatzei erantzuten die; sortzetiko immunitatearen memoria, berriz, ez-espezifikoa eta orokorra da.

Berezko immunitatea eta egokitze-immunitatea hainbat mekanismoren bidez konektatuta daude. Honen adibide da, berezko sistemaren zelulen zitozinen askatzea, egokitze-sistemako zelulak aktibatzeko, edo antigenoak aurkezten dituzten zelulen bidez (APC), agente kaltegarrien antigenoak harrapatu eta prozesatzen dituztenak, histokonpatibilitateko konplexu handiagoen bidez immunitatean aurkezteko (MHC-I eta MHC-II) (Kumar et al., 1994; Hoebe et al., 2004; Rossi et al., 2005). Mikrogliak eginkizun bat izan dezake sortzetiko erantzunaren eta erantzun moldagarriaren arteko loturaren bitartekaritzan, potentzialki antigenoak aurkezten dituzten zelulak (APC) bezala parte hartuz (Aloisi, 2001; Gregerson et al., 2004; Sutter et al., 2022). Hori horrela iradoki den arren, proba argiak falta dira immunitate immunitate moldagarrian duten zereginari buruz.
Hala ere, mikrogliaren ezaugarri bereizgarri bat sortzetiko immunitatearen esparruan parte hartzea da. Bereziki hantura-erantzunaren eta fagozitosiaren espezializazioan, berezko immunitateari atxikitako bi funtzio klasiko direlarik. Lehenik eta behin, hanturaren efektu molekularrei buruz hitz egingo dugu eta, hurrengo atalean, fagozitosian sakonduko dugu, doktorego-tesi honen gai nagusia dena.

2.3.2.1 Hantura

Hantura estimulu kaltegarriek eragiten dute, hala nola patogenoek, substantzia toxikoek, irradiazioak edo kaltetutako zelulek. Ezaugarri bezala, mina, beroa, gorritzea, hantura eta funtzio tisularraren galera ditu (Lucas et al., 2006; Isailovic et al., 2015). Hanturaren helburu nagusia mehatxua ezabatzea eta ehuna are gehiago lehengoratzea da (Chen et al., 2018). Garuneko parentimaren barruan, mikroglia da hantura-erantzunaren orkestratzaile nagusia, hantura-bitartekariak askatuz, hala nola zitozinak, kimiozinak eta osagarriaren proteinak (Nayak et al., 2014).

Zitozinen familiak molekula txikiak barne hartzen ditu, horien artean: peptidoak, proteinak eta glikoproteinak, eta zelula ekoizleengan eragiten dute, modu autokrinoan, zein inguruko zeluletan modu parakrinoan (Borish et al., 2003). Zitozinak proinflamatorioetan eta antiinflamatorioetan sailkatzen dira, funtzioaren arabera. Zitozina proinflamatorioek hantura-erantzuna eragiten dute, eta antiinflamatorioek, berriz, konpondu egiten dute. Jarraian, xehetasun handiagoz deskribatuko ditugu.

Zitozina proinflamatorioak molekula seinalatzaileen multzo bat dira, eta hantura sustatzeko askatzen dira. Mikrogliak estimulu kaltegarriak detektatu ondoren patroiak ezagutzeko hargailuen bidez, hala nola Toll motako hargailuak (TLR), NLR motako hargailuak eta TREM hartzaileak, besteak beste (Franchi et al., 2009; Hanamsagar et al., 2012; Owens et al., 2017). Estímulo kaltegarrien

identifikazioak hartzeile hauen bidez, hanturazko erantzuna hasten duten zitokinen ekoizpena jartzen du martxan (Vezzani, 2005). Zitozina proinflamatorioak sortzea beharrezkoa da kanpoko mehatxuei aurre egiteko, baina askapen gogortu batek ondorio kaltegarriak izan ditzake, hala nola, ehun lesioak (Raziyeva et al., 2021). Garunaren kasu partikularrean, zenbait patologiak, hala nola EA, Parkinson gaixotasuna (EP), esklerosi anizkoitza (EM), epilepsia eta iktusa, zitokina proinflamatorioen mailen igoera anormala erakutsi dute, patologiaren okertzearekin lotuta egon ohi direnak (Schwartz et al., 2010; Fung et al., 2012). Zitozina horiek beste hantura-bitartekari batzuk sortzea eta askatzea eragiten dute, oxigeno-espezie erreaktiboak (ROS) eta oxido nitrikoa (NO) adibidez. Horiek neurotoxikoak izan daitezke, ekintza mugatu ezean (Bilbo et al., 2012; Lyman et al., 2014). Zitozinak kontrolik gabe askatzearen ondorio kaltegarririk ohikoenak hauek dira: neuronen eta zelula glialen apoptosia, BBBren iragazkortasuna areagotzea, eta, horrekin batera, migrazioa areagotzea eta zelula immuneak garuneko parentimarantz infiltratzea: horrek kaltea areagotzen du (Ramesh et al., 2013; Salmina et al., 2021).

Zitozina antiinflamatorioek aldiz, hanturaren ebazpenean parte hartzen dute. Interleuzinaren hartzailearen antagonista (IL) -1 (IL-1ra) izan ezik, hanturaren aurkako zitozina guztiek ere ezaugarri proinflamatorio batzuk dituzte gutxienez (Opal et al., 2000). Hanturaren aurkako zitozina ezagunenen, 4 interleuzina daude: interleuzina 4 (IL-4), interleuzina 10 (IL-10) eta B hazkunde eraldatzailearen faktorea (TGF-β) (F. Su et al., 2016). Zitozina horiez gain, zitozinen inhibitzaile espezifikoak eta zitozinen hartzaile disolbagarriak daude, zitozinen funtzio proinflamatorioa arintzen laguntzen dutenak (Opal et al., 2000). Mikrogliaren kasu partikularrean, hanturaren aurkako zitozinen askapenak eta detekzioak erantzun babeslea ematen du baldintza patologikoetan. Antigenoen presentzia gutxitzeak eta zitozina proinflamatorioen, kimiozinen eta oxido nitrikoaren (NO) askapena murrizteak eraginda (Aloisi, 1999; Loane et al., 2010).

Zitozina proinflamatorioez eta antiinflamatorioez haratago, beste zitozina mota batek, kimiozinek, hainbat zelularen mugigarritasuna sustatzen dute lesioaren lekurantz, non hanturazko erantzuna are gehiago hasiko duten (Hughes et al., 2018). Horrela, kimiozinek kimiotaxi izeneko migrazio zelularreko prozesu batera eramaten dute, eta hori ere baldintza fisiologikoetan gauzatzen da, hala nola garapenean zehar identitate neuronalak (neural patterning) eskuratzean (Jin et al., 2008). Mikrogliak CX3CR1 makrofagoen kimiokina adierazten du, eta horiek, CX3CL1 ligandoarekin batera, funtsezkoak dira neurona-mikroglia komunikazio-ardatzerako (Wolf et al., 2013). Proposatu da kimiocinak eta horien hartzaileak goranzko joeran erregulatzea zenbait egoera patologikotan, hala nola EA, EM, garuneko traumatismoak edo istripu zerebrobaskularrak (Mennicken et al., 1999; Ubogu et al., 2006; Savarin-Vuaillat et al., 2007), eta badirudi eragina dutela leku patologikoetarako migrazio mikroglialean (El Khoury et al., 2007).

Erantzun inflamatoriotik askatutako beste osagai gako bat osagarriaren sistema da, apopiloaren defentsan eta hanturan berebiziko garrantzia duena. Osagarriak mehatxuei azkar erantzuten dieten 30 proteina, hartzaile eta modulatzaile baino gehiago ditu (Morgan & Harris, 2015). Osagarriaren aktibazioa patogenoak opsonizatzean eta fagozitoek ezabatzean gertatzen da, eta opsoninek eragiten dute, fagozitosia eragiteko eduki kaltegarriarekin lotzen diren proteina

estrazelularrek (Sarma et al., 2011). Beraz, osagarriaren sistema aktibatzea funtsezkoa da fagozitosiari ekiteko, eta xehetasun handiagoz deskribatuko da hurrengo atalean.

2.3.2.2 Fagozitosia

Fagozitosia zelula-prozesu bat da, eta, horren bidez, kaltegarri izan daitekeen elementu bat fagozito batek ezagutzen, irensten eta digeritzen du. Zelula horrek partikula handiak irensteko gaitasuna du (0,5mtik gorakoak) (Mukherjee et al., 1997). Organismo zelulabakarretan, fagozitosia oinarrizko nutrizio-prozesua da; organismo zelulaniztunetan, berriz, zelula-mota desberdinek egiten dute fagozitosia, ehunen homeostasia mantentzeko. Horien artean, zelula espezializatuek, fagozito profesionalek, modu eraginkorrean egiten dute fagozitosia, eta berehala erantzuten diete mehatxuei. Fagozito gehienek hantura-erantzuna eta funtzio fagozitikoa konbinatzen dituzte patogenoak eta substantzia toxikoak desagerrarazteko eta garbitzeko. NSZren fagozito profesional gisa, mikrogliak karga-barietate zabal baten fagozitosia egiten du, ondoren deskribatuko direnak.

Mikrobioak. NSZ patogenoek inbaditzeko aukera txikia da, BBBk oztopo fisiko zaila baita inbaditzaileentzat (Pardridge, 2005). Hala ere, birusak, bakterioak, onddoak edo parasitoak bezalako organismoak NSZn sartzen direnean, mikrogliak berehala antzematen ditu eta erantzun immunitarioa ematen du (Dando et al., 2014). Patogenoen ezagutzatik haratago, mikrogliak eraginkortasunez ezabatzen ditu organismo horiek, lipopolisakaridoen estimulazioaren ondoren bakterioak irensten dituzten labore mikroglialetan frogatu den bezala (Diesselberg et al., 2018; Cockram et al., 2019). Bakterioen fagozitosiak eta LPSekiko esposizioak hantura-erantzuna eragin zuten mikroglian, eta, beraz, LPS bidezko estimulazioa giza sepsia imitatzeko eredu gisa ezarri zen (Deitch, 1998). Bakterioak bezala, onddoak ere in vitro eta in vivo mikrogliak fagozitatzen ditu (Neglia et al., 2006; Lionakis et al., 2011). Beraz, mikrogliak eraginkortasunez borrokatzen ditu mikrobio inbaditzaileak NSZn.

β-Amiloidea. Aβ 36-43 aminoazidoez osatutako peptidoa bat da, amiloide proteina aitzindariaren (APP) deribatua (Hamley, 2012). IHren ezaugarri patologiko nagusietako bat da garunean Aideren askapena, oligomerizazioa eta lagapena (Hardy et al., 2014) (Ondrejcak et al., 2010). Behin parenkiman metatzen hasten denean, gertaeren ur-jauzi kaltegarri bat sortzen du, sinapsia eta neuroendekapena galduz hasten dena, eta narriadura kognitiboarekin eta oroimenaren galerarekin amaitzen dena. Zenbait ikerketek adierazi dute IHren progresioak zerikusia izan dezakeela A○ eiren argitze eskas batekin (Mawuenyega et al., 2010; «Prozamanian et al.», 2020). Hala eta guztiz ere, mikrogliaren papera oraindik ere eztabaidagarria da A, fagozitosian. Nahiz eta in vitro laborantzetan A○ fagocita mikroglia, mikrogliaren papera in vivo plaka kentzeko oraindik ez dago argi (Majumdar et al., 2011; Hellwig et al., 2015; Feng et al., 2020). Ikerketa batzuek frogatu dute mikrogliak ez duela eraginik gaixotasunean; izan ere, mikrogliaren agortzeak ez dio eragiten A, plakaren tamainari (Grathwohl et al., 2009). Beste ikerketa batzuek, berriz, mikrogliak ondorio onuragarriak dituela iradokitzen dute, plakaren tamaina murriztuz, fagozitosiarekin lotutako kinasa-tirosinako Axl eta Mertk hartzaileen jardueraren

bidez (Huang et al., 2021). Era berean, beste hartzaile mikroglial bat ere, TREM2, gaixotasunean inplikatuta dago, haren gozamenak plaka-pilaketa eragiten baitu (Ulrich et al., 2017) (Yuan et al., 2016). Beraz, mikroglia IHren progresioan inplikatuta dago, nahiz eta gaixotasunaren garapenean eta mantentzean betetzen duen zeregin zehatzaren inguruan eztabaida sortzen den oraindik.

Sinapsiak. Sinapsiek,neuroek arteko konexio dinamikoak irudikatzek dituzte: horrez gain, jarduera neuronalaren, garapenaren eta neurodegenerazioaren ondorioz aldatzen dira (Hong et al., 2016). Gehiegizko sinapsia sortzen denean, gehiegizko hori inausketa sinaptikoaren bidez ezabatzen da. Fenomeno hori garapenean zehar sinapsia gehiegi eratu den egoeretan hauteman da (Katz et al., 1996; Hua et al., 2004), eta zenbait ikerketek mikrogliaren barruan osagai sinapikoak daudela ere adierazi dute. Adibidez, kontaktu sinaptikoen ondoren prozesu mikroglialek proteina presinaptikoak (SNAP25) eta postsinaptikoak (PSD95) dituztela ikusi da.. Hala ere, oraindik ez da argitu nola gertatzen den prozesu hori, eta ez dira zehaztu prozesuan inplikatutako seinaleztapen-etapa eta -bideak (Paolicelli et al., 2011; Lim et al., 2021). Inausketa sinaptikoa fraktina (Paolicelli et al., 2011), osagarriaren sistema eta MERTK bide fagozitikoak (Schafer et al., 2012; Chung et al., 2013) bezalako faktoreek erregulatzen dutela iradoki da. Beraz, sinapsi-fagozitosia zuzentzen duten mekanismoak erabat ulertzeko ikerketa gehiago behar bada ere, aurkikuntza horiek biziki iradokitzen dute mikrogliak modu eraginkorrean irensten duela material sinaptikoa, inausketa sinaptikoaren prozesuan lagunduz.

Mielina. Prozesu hori, batez ere, eraso baten ondoren mielina galtzea eragiten duten gaixotasunetan aztertu da, hala nola EMn edo iktus iskemikoan (Jia et al., 2022; Sen et al., 2022). EMn, hanturazko lesioek kalte oligodendrokitarioa eta desmielinizazioa eragiten dituzte, eta mikrogliak aktiboki parte hartzen du mielina-hondarrak ezabatzen, eta horrek ondorengo erremielinizazioa sustatzen du (Trapp et al., 1998; Napoli et al., 2010; Dobson et al., 2019). EMko animalia-ereduetan egindako ikerketetan, haien artean lesio desmielinazaitzealeko ereduak, mikrogliak erremielinizazioan funtsezko zeregina duela frogatu dute; izan ere, CX3CR1 eta TREM2 hargailu mikroglialetako sagu eskasek mielina-hondarrak motelago argitu zituzten, erremielinazio motelagoarekin batera (Lampron et al., 2015; Cignarella et al., 2020). Axoiak eta mielina ere, kaltetu egiten dira istripu zerebrobaskular iskemiko baten ondoren eta mikrogliak mielina ezabatzen laguntzen du. Hori burutzeko X gibeleko hargailuaren seinalepean, mikrogliak hantura funtzioa jartzen du martxan eta eta oligodendrozitoak bereizteko eta berreskuratzeko ingurune egokia sortzen du (Liu et al., 2020).

Zelula apototikoak. Tesi proiektu honetan, zelula apoptotikoak eta haien fagozitosia aztertuko ditugu. Apoptosia, edo programatutako zelula-heriotza, erregulartasunez gertatzen da, bai testuinguru fisiologiko normaletan (bai garapenean edo orekari eustean), bai gaixotasun-egoeretan (Henson et al., 2001). Zelula apoptotikoak gertaera fisiologikoetatik edo gaixotasunarekin lotutako gertaeretatik sortzen badira ere, ezinbestekoa da mikrogliak zelula horiek eraginkortasunez ezabatzea. Zelula apoptotikoen fagozitosi mikroglialak hilzorian dauden zelulak modu egoki eta eraginkorrean ezabatzea bermatzen du, ehuenen homeostasia sustatuz eta kaltegarriak izan daitezkeen zelula-hondarrak

eta seinale proinflamatzaileak askatzea saihestuz, bestela neuroinflamazioa eta ehun-kaltea eragin baititzakete (Neher et al., 2012; Sierra et al., 2013).

Hurrengo atalean (**1.4 atala**), garunaren funtzio espezifikoen deskribapen xehatua egin ondoren, zelula apoptotikoen fagozitosiaren garrantzian sakonduko dugu, eta zehatzago azalduko ditugu prozesuaren faseak, funtzio hori aztertzeko prozedura esperimentalak eta fagozitosiak zelula mikroglialetan dituen ondorioak.

2.3.3 Mikrogliaren funtzio espezifikoak burmuinean

Zaintzaren eta hanturarekin zein fagozitosiarekin lotutako mekanismoen bidez, hala nola faktore disolbagarriak askatzearen eta hondakinak kentzearen bidez, mikrogliak garunaren funtzio espezifikoak betetzen ditu, besteak beste, neurogenesia, mantentze sinapikoa, gliogenesia, baskulogenesia, BBBren iragazkortasuna eta mielinizazioa.

Garatzen ari den garunean, mikrogliak neurogenesia erregulatzen du ugaztunen garuneko bi nitxo neurogeniko nagusietan: hipoeremuaren biraketa horzdunaren (DG) eremu subgranularrean eta azpibentrikularrean (SVZ) (Saharan et al., 2013). SGZ murinan, mikrogliak neuroblasta apoptotikoak fagozitatzen ditu jaio osteko garai goiztiarrean, hipoeremuko zirkuituetan sartzea erregulatzeko, eta funtzio hori betetzen jarraitzen du helduaroan ere (Sierra et al., 2010). SVZn, mikrogliak ere fagozita neuropadres (NPC) eta NPC populazioaren dentsitatea erregulatzen du (Cunningham et al., 2013; Fourgeaud et al., 2016). Mikrogliak zitokina proinflamatorioak askatzea eragiten duten baldintza patologikoen ondorioz, neurona berriak gutxiago sortzen dira GDn (Ekdahl et al., 2003; Monje et al., 2003). Era berean, fenotipo mikroglialaren zuzeneko modulazioak neuroblastoen bereizketa ere deuseztatzen du (Buttgereit et al., 2016), eta horrek, neurogenesiari eusteko, mikrogliaren funtzionamendu egokia oso garrantzitsua dela iradokitzen du. Oro har, aurkikuntza horiek agerian uzten dituzte mikrogliak neurogenesia erregulatzeko dituen forma ugariak.

Neurogenesiaz haratago, mikroglia enbrioi-garapenaren ondoren jaio berri diren neuronen biziraupenaren eta jardueraren erregulatzaile zentrala ere bada. Mikrogliak hainbat estrategia gauzatzen ditu funtzio neuronala moldatzeko. Mintzeko hargailu batzuen bidez seinaleztatuz, hala nola fractalkina eta Cx3cr1, mikrogliak, erretinako fotohartzaileen heldutasunean eta biziraupenean laguntzen du (Jobling et al., 2018). Era berean, mikrogliak biziraupen neuronalaren bitarteko zitokinak eta hazkunde-faktoreak askatzen ditu, eta gainera, TGF-β seinaleztapena etetearen bidez heltze mikrogliala aldatzen dela frogatu da (Frade et al., 1998; Sedel et al., 2004; Ueno et al., 2013). Mekanismo sekretuez gain, prozesu mikroglialak zuzenean neuronekin harremanetan jar daitezke hargailu purinergikoen bidez, eta horrek kaltzio neuronalaren karga erregulatzen du eta neurona-konektibitatea are gehiago modulatzen du (Cserép et al., 2020). Oro har, aurkikuntza horiek adierazten dutenez, mikroglia ezinbestekoa da populazio neuronalak mantentzeko eta gainera, ezinbestekoa da ere jarduera neuronala modulatzeko.

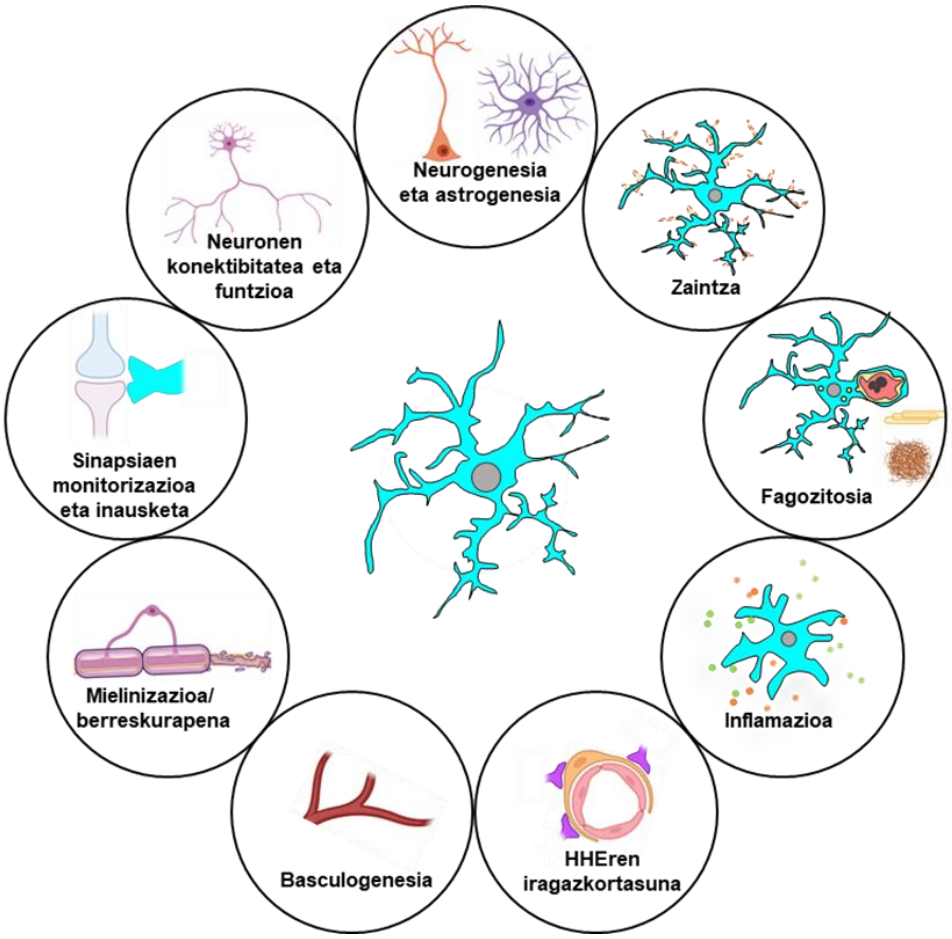

4. irudia. Mikrogliaren funtsezko funtzioak. *Mikrogliak funtsezko hainbat eginkizun betetzen ditu, bai fisiologian, bai garunaren patologian. Etengabeko zaintzan, mikrogliak ingurumen-aldaketak detektatzen ditu eta horiei erantzuten die. Garuneko zelula immunitario gisa, mikrogliak sortzetiko immunitate-funtzioak betetzen ditu, baldintza patologikoei erantzunez. Hantura-faktoreak askatzen dituzte eta zelula-hondarrak fagozitatzen dituzte (adibidez, zelula apoptotikoak, proteina-agregatuak eta mielina-zatiak). Horrez gain, mikrogliak funtsezko hainbat zeregin egiten ditu baldintza fisiologikoetan, egoera patologikoetan alda daitezkeenak. Zeregin horien artean, lehen aipatutako fagozitosia dago, garapenean eta nitxo neurogenikoetan eta monitorizazioan eta inausketa sinaptikoan ere funtsezkoa dena. Mikroglia moldakorra da, garuneko beste zelula mota batzuekin elkarreragin baitezake, eta eragina izan dezake bere jardueretan. Interakzio hori neuronetara eta horien sare-konexioetara, zelula ama neuraletara (NSC) eta neurogenesi-prozesura, oligodendrozitoetara eta axoien mielinizazio/erremelinizaziora, zelula endotelialetara eta garuneko odol-hodien eraketa/eraberritzera hedatzen da, baita astrozitoetara eta hesi hematoentzefalikoaren (BHE) iragazkortasunera ere. BioRender.com sortu eta egokitu (Sierra et al., 2019).*

Mikrogliak neuronen funtzionamendu egokia bermatzeko betetzen duen funtsezko beste zeregin bat sinapsiak birmoldatzea da. Mikrogliak sinapsiari forma ematen dioten hainbat funtziotan parte hartzen du, hala nola formazioan, heltzean eta fintzean. Sinapsia sortzean, garunetik eratorritako faktore neurotrofikoak (BDNF) garapen sinaptikoaren erregulatzaile indartsu gisa jarduten du, eta BDNF mikrogliala ezabatzeak sinapsia murriztea ekarri zuen

(Parkhurst et al., 2013). Era berean, mikrogliak funtsezko zeregina betetzen du heltze sinaptikoan, CX3CR1 hartzailerik ez duen mikroglian ikus daitekeen bezala, eta horrek atzerapena eragiten du kolonizazio mikroglialean eta atzerapena heltze sinaptikoan (Hoshiko et al., 2012). Mikrogliak egindako aldaketa sinapikoen azpian proposatzen diren mekanismoen artean stripping-a dago. Mekanismo hori ez da fagozitikoa, mikrogliak mintz presinapikoaren eta postsinapikoaren eta trogozitosiaren artean duen interposizioan oinarritzen baita. Trogozitosia mintzaren fagoitosi partzial gisa definitzen da, eta biek eragiten diote eszitagarritasunari edo egonkortasun sinaptikoari (Eyo et al., 2023). Aldaketa sinaptikoez gain, mikrogliak sinapsia ezabatzen ere parte hartzen du, aurreko **1.3.2.2 atalean** berrikusi dena (Sinapsi-fagozitosia). Laburbilduz, mikrogliak sinapsien funtzio egokia sustatzen du, sinapsiak heltzeko etapa desberdinetan jardunez eta beharrezkoa denean horiek argituz.

Gainera, mikrogliak baskulatura eta zelula ez-neuronalak sortzea sustatzen du, hala nola oligodendrozitoak eta astrozitoak, bereziki garapenean zehar. Garuneko baskulatura neurogenesiarekin paraleloan eratzen da eta denborarekin heltzen da (Checchin et al., 2006). M-CSF seinaleztapen mikrogliala eteteak zein agortze mikroglialak baskulaturaren konplexutasuna murrizten dute, eta horrek agerian uzten du mikrogliak odol-hodiak behar bezala garatzeko duen garrantzia (Checchin et al., 2006; Kubota et al., 2009). Mikrogliak ere parte hartzen du mielinizazioan, oligodendrozitoen biziraupena eta ugalketa sustatzen duten hazkunde-faktoreak askatuz (Pang et al., 2013). Erremielinizazioan, mikrogliak endekatutako mielina fagozitatzen du (Domingues et al., 2016), oligodendrozitoen aitzindarien erreklutamendua eta bereizketa sustatuz (Domingues et al., 2016; Voet et al., 2019). Hala ere, zitokina proinflamatorioak askatzeak erremielinizazioa muga dezake EM bezalako patologietan, gaixotasunari lotutako hantura kronikoak mikrogliaren funtzionamendu egokia hondatzen duela frogatuz (Guerrero et al., 2020). Astrozitoen sorrera ere mikrogliak eragiten du, eta hainbat faktore sekreturen bidez (1. eta 6. interleuzioa (IL-1 eta IL-6), leuzemiaren inhibitzaileak (Lif) eta oxido nitrikoak (NO) astrogenesia estimulatzen dute (Nakanishi et al., 2007; Béchade et al., 2011). Horrela, mikrogliak sekretatutako faktoreak lehen mailako mekanismo bat dira, zeinaren bidez mikrogliak astrozitoen garapen putatiboa erregulatzen duen. Oro har, mikrogliak zelula ez-neuronalak sortzen eta garatzen laguntzen du, eta hori funtsezkoa da garuneko parenkimaren funtzionamendu egokiari eusteko.

Laburbilduz, mikrogliak garun-ingurunera egokitutako funtzio-multzo bat betetzen du, eta funtzio horiek guztiak ezinbestekoak dira parenkimak organismo baten bizitzan zehar behar bezala funtzionatzeko. Doktorego-tesi honek mikrogliaren funtzio bat izango du ardatz: zelula apoptotikoen fagozitosia.

2.4 ZELULA APOPTOTIKOEN FAGOZITOSIA

Apoptosia zelulen heriotza programatuaren modu oso erregulatua da, bi bide nagusik abiarazia: bide intrintsekoa (mitokondriala) eta bide estrintsekoa (heriotza-hartzailea) (Vitale et al., 2017; Galluzzi et al., 2018). Apoptosi intrintsekoa hainbat seinale intrazelularren bidez sortzen da, hala nola DNAren

kaltea, estres oxidatiboa edo biziraupen-seinaleen galera. Seinale horiek Bcl-2 familiako proteina proapoptotikoak aktibatzen dituzte, hala nola BCL2ri lotutako X proteina (Bax) eta BCL2ri lotutako K proteina (Bak) (Roufayel, 2016). Bax eta Bak-en aktibazioak kanpo-mintz mitokondriala iragazkortzera eramaten du, eta horrek c zitokromoa eta zitosolean beste faktore apoptotiko batzuk askatzea dakar. Honek, era berean, entzima kaspasak aktibatzen ditu (D 'Orsi et al., 2017), proteinak zatitzeko eta degradatzeko funtsezkoak direnak. Kaspasen aktibazioak apoptosi intrintsekoa eta estrintsekoa gurutzatzen diren etapa. Kanpoko bidea hasteko, zelulaz kanpoko inguruneko heriotza-ligondoak lotzen dira, hala nola tumore-nekrosiaren faktorea (TNF) eta Fas ligandoa (FasL), zelula-gainazaleko heriotza-hartzaileei dagokienez. Elkartze horrek heriotza-hartzaileak seinaleztatzeko konplexuak sortzea eragiten du, eta, azken batean, kaspasak aktibatzea eragiten dute (Nair et al., 2014). Apoptosiaren azken etapetan, zelulek zatiketa nuklearra (cariorrexia), kromatinaren kondentsazioa (piknosia), zitoplasmaren murrizketa eta gorputz apoptotikoen eraketa jasaten dituzte (Santavanond et al., 2021). Prozesu horretan zehar, zelulak bere mintz plasmatikoaren osotasunari eusten dio, bere eduki zitoplasmatikoak, inguruko ehunarentzat toxikoa denak, ihes egitea saihesteko. Fagozitosi akastun batek zaildu egingo luke babes hori, eta, horren ondorioz, zelula apoptotiko primarioek bigarren mailako egoera nekrotikorantz egingo lukete, baldin eta beren mintz plasmatikoa arriskuan jartzen bada, eta horrek zelula-barneko eduki kaltegarriaren gainezkatzea eragingo luke (Dias et al., 2021).

Baldintza fisiologikoetan, apoptosiak zelula-kopurua erregulatzen du gehiegizko zelula-ugalketa bati erantzunez (Oppenheim, 1991; Paronetto et al., 2016). Enbrioaiaren garapenean zein jaio osteko garapenean, apoptosiak funtsezko eginkizuna betetzen du zelula ugalkorren gehiegizko orekan, eta organismo helduetan, berriz, apoptosia funtsezkoa da zelulen ordezkapenerako (Pellettieri et al., 2007; Voss et al., 2020). Baldintza patologikoetan, apoptosia patogenoekiko esposizioari erantzunez gertatzen da, eta gaixotasun neurodegeneratiboetan ere ikusten da, hala nola Alzheimer gaixotasunan, alboko esklerosi amiotrofikoan (ELA), Parkinson gaixotasunean eta Huntington gaixotasunean (Czabotar et al., 2023). CNSan, apoptosiaren kausa fisiologikoa edo patologikoa edozein dela ere, mikrogliaren ardura gorpuak ezabatzea da, ehunen homeostasia bermatzeko.

Prozesu fagozitiko mikrogliala asko deskribatzen den testuinguruetako bat apoptosia jasaten duten zelula progenitoreeen irensketa da. Zehazki, erretinan jaio eta gutxira (Anderson et al., 2019), erretinako zelula ganglionarren fagozitosia lantzen du mikrogliak (CGR), bai eta gorputz kaltziosoan oligodendrozitoen zelula gurasoena ere (Nemes-Baran et al., 2020). Garun helduetan, apoptosia oraindik ere gertatzen da nitxo neurogeniko helduetan, hala nola subbentrikularrean (SVZ) eta hipoeremuaren GDan. GDn, zelula jaioberri gehienek apoptosia izaten dute zirkuituan integratu aurretik (Xavier et al., 2015). Mikrogliak zelula apoptotikoen fagozitosi eraginkorra hiru etaparen bidez egiten du: “aurkitu nazazu”, “jan nazazu” eta “digeritu nazazu”.

2.4.1 Fagozitosiaren etapak

Zelula apoptotikoen fagozitosia sekuentzialki gertatzen da hainbat seinalek gobernatutako prozesu batean. Lehenik eta behin, zelula apoptotikoek "aurkitu nazazu" seinaleak askatzen dituzte mikroglia haiengana erakartzeko, eta horrek mikrogliala fagozitatu beharreko kargarantz mugitzea eragingo du (Sierra et al., 2013; Yu et al., 2022). Ondoren, mikrogliak zuzenean eragingo dio zelula apoptotikoari, zelula apoptotikoetan eta mikroglian dauden ligandoen eta "jan nazazu" hargailuen bidez. Urrats horrek zelula apoptotikoak ezagutzea eta akoplatzea ahalbidetzen du, eta karga apoptotikoa fisikoki irenstera eramaten du. Karga horretan, mikrogliak poltsa fagozitikoa eratzen du, zelula apoptotikoa barneratzea ahalbidetzen duena (Gardai et al., 2006; Sierra et al., 2010; Li, 2012; Sierra et al., 2013). Karga apoptotikoa barneratzeak fagosoma sortzea dakar, eta lisosomari ematen zaio, azkenean fagolisosoma osatzeko eta azken urratsean "digeritu nazazu" fasean, karga guztia degradatzeko (Kinchen et al., 2008a; Kinchen et al., 2008b; Hochreiter-Hufford et al., 2013) (**5. irudia**). Jarraian, prozesu osoan inplikatutako molekulen eta hartzaileen multzoa deskribatuko dugu, banan-banan, eta parte hartzen duten urratsaren arabera sailkatuko ditugu.

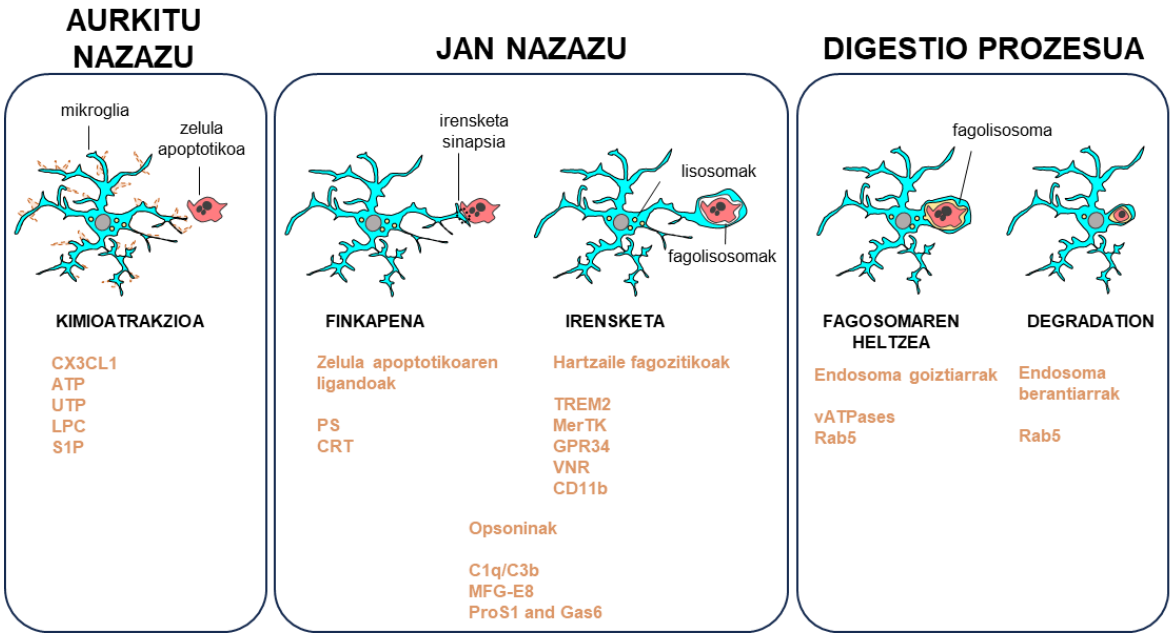

5. irudia. Prozesu fagozitiko mikrogliala eta haren etapak. *Mikrogliak zelula apoptotikoen fagozitosia hiru etapatan banatzen du: "aurkitu nazazu", "jan nazazu" eta "digeritu nazazu" (digestio prozesua). Lehenik eta behin, zelula apoptotikoek, beren heriotza-prozesuan zehar, kimioatrakzio-prozesuan parte hartzen duten molekulak askatzen dituzte, mikrogliaren mugimendua kaltetutako zelularantz estimulatuz. Mikrogliak kaltetutako zelulara iristen denean, zelula apoptotikoaren ligandoak hartzaile mikroglialekin elkartzen dira, prozesu mikrogliala zelula apoptotikoarekin lotzeko. Urrats horretan, opsoninek gorputz apoptotikoak ezagutzea errazten dute. Ezagutu eta finkatu ondoren, mikrogliak zelula apoptotikoa irensten du, zelularen inguruan poltsa fagozitiko bat eratuz. Azkenik, irentsitako karga lisosometara eramaten da, eta azkenean degradatu egiten da. Sierra 2013 aldatua.*

2.4.1.1 “Aurkitu nazazu” etapa

Zelula apoptotikoek askatutako molekulen artean honako hauek daude: "aurkitu" seinaleak deiturikoak, kimiokina fractalkina (CX3CL1), zelulaz kanpoko nukleotidoak (ATP, UTP) eta lisofosfatidilcolina (LPC) eta esfingosina-1-fosfato (S1P) (Truman et al., 2008; Arandjelovic et al., 2015) daude.

Fractalkina (CX3CL1). CX3CL1 mintzari lotutako proteina bat da, eta proteolitikoki banatu behar da zelula apoptotikoetatik askatzeko. Ondoriozko molekula disolbagarria kimikokinen 1. hartzailearekin lotzen da mikrogliaren berariazko CX3C (CX3CR1) dela eta, fagozitoak zelula apoptotikoen lekura migratzea sustatuz (Jung et al., 2000; Truman et al., 2008; Mizutani et al., 2012; Eyo et al., 2016).

Nukleotidoak (ATP, UTP). ATP eta ADP nukleotidoak zelula apoptotikoetatik askatzen dira kanal baten bidez, 3. kaspasaren aktibazioaren ondoren (Elliott et al., 2009; Chekeni et al., 2010). Zelulaz kanpoko espazioan kokatu ondoren, nukleotiko horiek eta haien ADP eta UDP forma hidrozatuak, mikroglian adierazitako hartzaile purinergikoen pletoragatik ezagutzen dira. Hori, azkenean hilzorian dagoen zelularen ondoand dauden fagozitoen erakarpenean gertatzen da (Inoue, 2008; Domercq et al., 2013).

Lisofosfatidilkolina (LPK). Prozesu apoptotikoan, fosfatidilcolina A2 (iPLA2) entzima fosfolipasak zatitzen ditu, eta LPC bihurtzen ditu; azken batean, G G2A hartzaile akoplatuarekin bat egiten du, mikrogliaren migrazio kimioerakargarria sustatuz (Lauber et al., 2003) (Peter et al., 2008; Xu et al., 2016).

Esfingosina-1-fosfatoa (S1P). S1Pa, esfingosinatik sortzen da, esfingosina zinasatik zehazki, 3. kaspasa aktibatu ondoren. S1Pa askatzen denean, mikroglian adierazitako S1P hargailuekin bat egiten du, eta horrek kimioatrakzio-prozesu bat sortzen du, oraindik gutxi ezagutzen dena (Gude et al., 2008; O 'Sullivan et al., 2018).

Mikroglia zelula apoptotikora hurbildu ondoren, fagozitosiaren bigarren etapari ekiten zaio, "jan nazazu" deituriko etapari. Etapa horretan, mikrogliaren eta diana-zelula baten arteko kontaktu fisikoa gertatzen da, zelula apoptotikoa ezagutzeko eta finkatzeko (Sierra et al., 2013).

1.4.1.2 "Jan nazazu" fasea

"Jan nazazu" faseak zelula apoptotikoek askatutako molekulen pletora bat dakar ("jan nazazu" ligandoak), baita mintza mikroglialaren hargailuek ("jan nazazu" hartzaileak) eta opsoninek eta zubi-molekulek askatutako molekulen pletora bat ere. Hauek diana zelula apoptotikoekin lotzen dira fagozitosia errazteko.

- "Jan nazazu" ligando apoptotikoak

Fosfatidilserina (PS). PS mintz plasmatikoaren barne-xaflan dagoen fosfolipido bat da, estimulu apoptotikoen aurrean gainazal zelularrera kanporatzen dena (Fadok et al., 1998). PSren kanporatze-prozesua atzeraezina da, Xkekin (Xkr8)

lotutako 8. proteinaren ekintzagatik, bai eta ATP11C ATPasaren inaktibazioagatik ere, 3 kaspasak eragindako zatiketaren ondorioz (Suzuki et al., 2016) (Segawa et al., 2014).

Kalretikulina (CRT). CRT sortu berri diren proteinen kalitate-kontrolean parte hartzen duen erretikulu endoplasmikoari (RE) lotutako proteina bat da, eta REaren estresak zein apoptosiaren seinaleztapenak zelulen gainazalean esposizioa eragiten dute (Kleizen et al., 2004; Obeid et al., 2007). CRT esposizioa PSrekin lotuta edo bakarrik gertatzen da, eta dentsitate txikiko lipoproteinen hartzaile mikroglialak (LRP) detektatzen ditu, zelula apoptotikoen xurgapena sustatuz (Gardai et al., 2003; Wijeyesakere et al., 2016).

- Fagozitoen hartzaileak

TREM2. TREM2 immunoglobulina motako mintzaz haraindiko hargailua da, eta zelula dendritikoetan (CD), makrofagoetan eta mikroglian adierazten da (Neumann et al., 2007). TREM2 12 kD-ko (DAP12) DNAX aktibazio-proteina izeneko proteina egokitzailearekin lotzen da, eta TREM2 edo DAP12ren alterazioak narriadura eragiten du mikrogliak zelula apoptotikoak hartzean (Paloneva et al., 2002) (Hsieh et al., 2009; Thrash et al., 2009). Horrez gain, TREM2k IHn A-ren errekonozimenduan parte hartzen du, eta IHren patologiari lotuta dagoen E (ApoE) apolipoproteinaren hartzaile gisa jarduten du (Atagi et al., 2015; Parhizkar et al., 2019; Joshi et al., 2021).

Mer tirosina kinasa (MerTK). MerTK gehien aztertutako TAM hartzailea da (Tyro3, Axl eta Mer) (Lemke, 2013). DCetan, makrofagoetan eta mikroglian adierazten da, eta zelula apoptotikoekin elkarreragiten du PSri lotutako proteina disolbagarrien bidez, hala nola 6. gelditze-proteina espezifikoa (GAS6), S proteina (ProS) eta Galectina-3ren (Gal-3) bidez *in vitro* zelula apoptotikoen ezabatzean bitartekari egiten du (Wu et al., 2005; Caberoy et al., 2012; Lemke, 2013; Jiménez-García et al., 2022).

34 hargailua, G proteinari akoplatua (GPR34). GPR34 hartzaileen PY2 familiakoa da (Lin et al., 2017). Batez ere mikroglian eta makrofagoetan adierazten da, baita zelula immuneen beste populazio batzuetan ere, hala nola B zeluletan eta linfoide zeluletan (Makide et al., 2013; Schoeneberg et al., 2018) (Wang et al., 2021). GPR34 ligando nagusia lisofosfatidilserina (LysoPS) da, lehen aipatutako PSren (Makide et al., 2013) forma desazetilatua, "jan nazazu" ligando bat bezala jarduten duena. GPR34k mikroglian duen gabeziak, zelula apoptotikoak eta mielina irensteko gaitasun txikiagoa dakar (Preissler et al., 2015), eta horrek ageriak uzten du hartzaileak fagozitosian duen garrantzia.

Bitronektina-hargailua (VNR). VNRa atxikipen makrofagikoko molekulen integrinen superfamiliakoa da. MFG-E8 opsoninarekin (milk fat globule EGF factor 8) bat egiten du, eta opsoninak zehatzago deskribatzen dituguneanaipatuko dugu (Hanayama et al., 2002; Lauber et al., 2004). Zelula apoptotikoaren eta fagozitoaren lotura-prozesuak, *in vivo* zein *in vitro*, mikrogliaren zitoeskeletoaren antolaketa eragiten du, Hurrats honetan VNR eta MerTK hartzaileen eragin kobinatua ezinbestekoa da, antolaketa hori burutzeko (Wu et al., 2005; Brown et al., 2014; Arcuri et al., 2017).

3. osagarriaren hartzailea (CR3/CD11b). CR3 beta-2 integrinen familiako kide bat da, eta osagarriaren ur-jauziko hainbat molekularekin bat egiten du, hala nola C1q edo C3b (Linnartz et al., 2012; Vorup-Jensen et al., 2018). Paper garrantzitsua betetzen du zelula patogenoen eta apoptotikoen zelula-atxikipena eta fagozitosia ahalbidetuz *in vitro* mikroglian (Trouw et al., 2008). Horrez gain, CR3k erantzun antiinflamatorio bat ematen du mikroglian, tolerantzia immunitarioari eusten lagunduz (Fraser et al., 2010).

- Opsoninak eta zubi-molekulak

Fagozitosia errazteko, beste molekula disolbagarri batzuk, hala nola opsoninak eta zubi-molekulak, irentsi behar diren zeluletara bideratzen dira. C1q eta C3b osagarriaren osagaiak, opsonina klasiko deskribatuenak dira. Bestalde, fagozitosi mikroglialean, zubi-molekula gisa jardunez PSrekin lotzen diren molekulek esnearen gantz-globuluen (MFG-E8) EGF 8 faktorea eta lehen aipatutako MerTK Gas6 eta ProS ligandoak barne hartzen dituzte.

C1q eta C3b osagarriaren osagaia. C1q proteinak hainbat funtzio betetzen ditu sortzetiko immunitate-sisteman, hala nola zelula-lisia, hantura-erantzuna, birusen neutralizazioa eta opsonizazioa (Beurskens et al., 2015). Opsonizazioan zehar, C1q zelula apoptotikoaren mintzarekin elkartzen da eta C3ren zatiketa sustatzen du, C3b opsonina sortuz (Martin et al., 2016). Zelula apoptotikoen gainazalean dagoen opsonina-biltegiak, azkenik, fagozitosi mikroglialera eramaten du (Diaz-Aparicio et al., 2019).

Esne-gantzezko globuluen EGF 8 faktorea (MFG-E8). DCk, makrofagoek eta mikrogliak ekoiztuta, MFG-E8k PSrekin bat egiten du zelula apoptotikoetan, eta horrek fagozitosia eragiten du (Aziz et al., 2011; Spittau et al., 2015). MFG-E8 bidez erdietsitako fagozitosia zuzenean ebaluatu da in vitro zein *in vivo* makrofagoetan (Hanayama et al., 2002; Akakura et al., 2004) eta *in vitro* mikroglian (Fuller et al., 2008).

S proteina (ProS1) eta gas6. ProS1 eta Gas6 proteina homologoak dira, K. bitaminaren mendekoak. Bi molekula disolbagarri horiek TAM hargailuen ligandoak dira, eta PSrekin lotzen dira, zelula apoptotikoak ezagutzeko eta irensteko zubi-molekula gisa jardunez (Manfioletti et al., 1993; Lemke et al., 2008).

Behin “jan nazazu” fasea amaituta, gorputz apoptotikoa hiru dimentsioko poltsa fagozitikoak inguratzen ditu, eta mikrogliaren barruan barneratzen da. Ondoren, mikrogliak, karga eman behar die lisosomei, digestio-prozesua garatzeko. Hurrengo atalean zehatasun handiagoz azalduko da (Yu et al., 2008), eta hurrengo atalean azalduko da xehetasun handiagoz.

Laburbilduz, fagozitosia hiru urrats nagusitan multzokatzen diren molekula ugarik parte hartzen duten gertaeren ur-jauzi bat da: “aurki nazazu”, “jan nazazu” eta “digeritu nazazu”. Etapa horiek behar bezala eta modu integratuan funtzionatu behar dute, horietako edozein aldatzeak kalte egingo baitio prozesu osoari, eta horrek fagozitosia kaltetuko edo zailduko du. Fagozitosi eraginkor baterako

zelula-makineria hori aktibatzeak ondorioak izan ditzake mikrogliarentzat. Seguraski, mikrogliak sistema berrezarri nahiko du, geroko jarduera fagozitikoetarako. Doktorego-tesi honen helburuetako bat, fagozitosiak zelula mikroglialei nola eragiten dien aztertzea da. Hurrengo atalean, mikroglia fagozitikoa identifikatzeko erabili diren hainbat estrategia deskribatuko ditugu, eta in vitro eta in vivo metodoak zehaztuko ditugu, fagozitosia ebaluatzeko.

2.4.2 Fagozitosia aztertzeko metodoak

Fagozitosi mikroglialaren analisia zeharkako metodoetan oinarritu izan da tradizioz, morfologia mikroglialaren ebaluazioa edo markatzaile espezifikoen adierazpena barne, fagozitosia gertatzen dela uste den testuinguruetan (Diaz-Aparicio et al., 2016). Atal honetan, aldaketa morfologikoak eta fagozitosiarekin lotutako proteinak irudikatuko ditugu. Gainera, fagozitosi mikrogliala erreproduzitzen duten metodoen berrikuspen sakona egingo dugu, in vivo eta in vitro ikuspegiak erabiliz (**6. irudia**).

2.4.2.1 Fagozitosi-markatzaileak

Fagozitosia identifikatzeko zeharkako metodoei dagokienez, denbora luzez lotu da morfologia ameboide bat fagozitosi mikroglialarekin (Young et al., 2018), baina gure laborategiak frogatu du mikroglia adarkatua oso eraginkorra dela fagozitosia eginez, bai baldintza fisiologikoetan, bai morfologia hipertrofikoagoa erakutsiz LPSrekin estimulatu ondoren (Sierra et al., 2010; Sierra et al., 2013).

Mikroglia fagozitikoa etiketatzeko proposatutako proteinen artean, mintzari lotutako proteinak eta lisosomei lotutako proteina zitoplasmatikoak iradoki dira. Lehenengo kategorian Axl, MerTK, TREM2 eta CD11b sartzen dira; horiek izan dira, fagozitosiaren markatzaile gisa proposatu direnak, prozesu fagozitikoaren lehen etapetan inplikatutako mintz-hartzaile bezala, batez ere "jan nazazu" etapan. Atal honetan, lehenik eta behin, horiei buruz arituko gara. Proteina zitoplasmatikoei dagokienez, entzima lisosomalak, lisosomekin lotutako mintzeko proteinak (LAMP) eta lipidoen metabolismo degradatzailearekin lotutako beste proteina batzuk sartzen dira. Proteina horiek fagozitosiaren "digeritu nazazu" fasean parte hartzen dute batez ere, eta mintzeko proteinen ondoren deskribatuko dira. Bi kategoria horietatik haratago, IBA1 bezalako beste proteina batzuk fagozitosiarekin lotu dira.

IBA1 proteina mikroglia fagozitikoaren adierazle gisa erabili da (Hendrickx et al., 2017; Nelson et al., 2017). Hala ere, proteina hori, mikroglian oinarri-oinarrian adierazia, handitu egiten da estimulu askoren ondorioz, hala nola entzefalitisa (Mori et al., 2000), iskemia (Ito et al., 1998) edo garuneko tumoreekiko esposizioa (Tran et al., 1998). Hortaz, IBA1ek adierazpen handiagoa erakusten du hainbat estimuluri erantzuteko, fagozitosiaz haratago, eta ezin da fagozitosiaren markatzaile gisa erabili.

Axl eta MerTK fagozitosi-markatzaile gisa ere proposatu dira (Jenkins et al., 2023). Biak TAM hargailuetakoak dira, zelula apoptotikoen irenspenean

bitartekari direnak (Scott et al., 2001; Burstyn-Cohen et al., 2012), baina bi hartzaileen adierazpena handitzea dakarten berezko erantzun immunitarioetan ere parte hartzen dute, hantura-maila altuak erakusten dituzten baldintzetan, hala nola gaixotasun neurodegeneratiboak eta zahartze-maila (Ransohoff et al., 2010; Zagórska et al., 2014; Fourgeaud et al., 2016). Beraz, TAM hartzaileen adierazpena handitzea ezin da fagozitosiaren ondoriotzat bakarrik hartu.

Gauza bera gertatzen da TREM2rekin, zeinen adierazpen eraldatuak zelula apoptotikoen bilketa eskasa eragiten du (Paloneva et al., 2002; Hsieh et al., 2009; Thrash et al., 2009), eta sinapsiaren fagozitosian ere inplikatu da (Filipello et al., 2018). Hala ere, nabarmendu behar da TREM2, askotan, IHko A fagozitosiaren markatzailetzat hartzen dela, IH garatzeko arriskuarekin eta gaixotasunaren progresio handiagoarekin ere erlazionatu dela (Frank et al., 2008; Lue et al., 2015; Wang et al., 2016).

Era berean, CD11b azaleko proteinak, partikula opsonizatuen fagozitosian parte hartzeagatik ezaguna (Fu et al., 2014), fagozitosiaren inhibizioa eragiten du proteina blokeatzen denean (Allendorf et al., 2020). Hala eta guztiz ere, CD11b-k bere adierazpenaren igoera ere jasaten du, irain proinflamatorioen (adibidez, LPS) eta estres oxidatiboaren (adibidez, H2O2) (Roy et al., 2008) ondorioz.

Oro har, gainazaleko hartzaile horiek, fagozitosi-markatzaile gisa erabili direnak, berebiziko garrantzia dute prozesu honetan. Hala ere, beste prozesu batzuetan ere parte hartzen dute, eta adierazpen handiagoa ezin da fagozitosiarekin bakarrik lotu.

Zenbait proteina lisosomal proposatu dira (adibidez, entzimak eta LAMPak) fagozitosiaren markatzaile potentzial gisa (Colombo et al., 2021), jarduera lisosomalak fagozitosiaren azken etapan duen paper erabakigarria dela eta. Proteina lisosomalak substratuen azidotzea eta degradazioan parte hartzen duten entzimetan sailka daitezke, hala nola hidrolasa azidoetan eta katepsinetan eta horien inhibitzaileak zistatinetan. Proteina horiek eginkizun nagusia dute mikrogliaren digestio-jardueran, eta, horren ondorioz, handitu egiten da entzima lisosomalen jarduera fagozitosiaren ondoren (Axline et al., 1970).

Entzima horien artean, katepsinak zelula-prozesuetarako funtsezkoak diren proteasa-entzimen talde bat dira. Prozesu horietako bat bereziki, lisosomen barruko proteinen degradazioa da (Repnik et al., 2012). Badirudi katepsinen funtzionamendu egokia funtsezkoa dela fagozitosi-prozesuan. Fagozitosiaren ondoren, zenbait katepsinak, hala nola B katepsinak, gorantz erregulatzen dira erronka fagozitiko bati erantzunez (Porter et al., 2013). Era berean, K katepsinaren eskasiak digestio eskasa eta fagozitatutako kargaren metaketa eragiten ditu (Everts et al., 2003). Zistatinek katepsinen inhibitzaile gisa jarduten dute, zisteina proteasak baitira. Zistatinen funtzio nagusia katepsinekin bat egitea eta jarduera entzimatikoa inhibitzea da (Turk et al., 2012). B zitatinaren agortzeak fagozitosi mikrogliala hondatzen du hipokanpoan Cstb KO sagu eredu batean (Sierra-Torre et al., 2020); AD saguaren eredu batean aldiz, B zistatinaren agortzeak kontrako ondorioak erakusten ditu jarduera lisosomala handitzean (Yang et al., 2014). Beraz, fagozitosiaren degradazio-fasean katepsinek eta zistatinek duten zeregina esanguratsua dela dirudi.

Halaber, lisosoma-mintzeko proteinak ere badaude, lisosomen egituran, funtzioan eta egonkortasunean ezinbesteko eginkizunak betetzen dituztenak. Horren adibide, lisosomei lotutako mintzeko proteinak (LAMP)eta mintz integral lisosomaleko proteinak dira (LIMP) (Saftig et al., 2010). Lisosomaren mintzaren proteinak ezinbestekoak dira degradazioan, lisosomak fagosomekin behar bezala funtzionatzeko beharrezkoa baitira (Huynh et al., 2007). LAMP makrosialina familiako proteinak (CD68 proteina lisosomala ere esaten zaio) mikroglia fagozitikoa markatzen du EP eredu batean (Silva et al., 1999). Horrez gain, Niemann-Pick genean (NPC1) mutazio batek eragindako neuroendekapenaren ereduan, mikrogliaren scRNA-seq sinadura bat identifikatzen da, ezaugarri bezala, CD68 genearen eta proteina lisosomalak kodetzen dituzten beste gene batzuen (LAMP1, LAMP2) adierazpenaren handitzea duena, eta lehen aipatutako D eta B katepsinekin batera (CTSD eta CTSB) (Colombo et al., 2021). Populazio mikroglial horrek mielinaren bilketa fagozitiko handiagoa ere erakusten du. Azterlan horrek berak identifikatzen du funtzio lisosomalaren gehikuntzarekin lotutako sinadura mikroglialean mielinaren fagozitosiarekin lotutako geneen goranzko erregulazioa dagoela, hala nola LGALS3 eta LPL, biak ere sagu zahartuetan detektatutako beste sinadura batean deskribatuak, oso aktibatuta dagoen mikroglia gisa deskribatua (HAM) (Jin et al., 2021).

Gainera, LGALS3 produktuak, galektina-3 (Gal-3), *in vitro* neuronen antzeko zelulen fagozitosian ere parte hartu zuen (Nomura et al., 2017), eta haren adierazpen areagotuak, LPLrekin batera, PAM (Li et al., 2019) sinaduran ere jaso dira mikroglian. Hala ere, badirudi Gal-3 gorantz araututa dagoela mikrogliaren profil transkriptomikoan, hainbat ingurune neurodegeneratibotan eta kaltetutako leku zerebraletan. Halaber, proinflamazio-erantzunaren abiaraztean inplikatuta dago, Toll-like (TLR) (García-Revilla et al., 2022) hargailuekin duen interakzioaren bidez.

Ondorioz, gaur egun ez da fagozitosirako markatzaile espezifikorik zehaztu. Aitzitik, fagozitosiaren ondoren erregulatutako proteina asko beste estimulu eta testuinguru batzuen ondorio ere badira. Arazo nagusia, fagozitosia egoera mikroglial bat dela interpretatzea da, prozesu bat izan beharrean. Mikrogliak irensketa prozesua burutzen dago poltsa fagozitikoak dituenean, degradazio prozesua egiten du karga digeritzen duenean, eta, geroago, egokitzapen postfagozitikoak garatzen ditu. Beraz, fagozitosirako markatzaile espezifikoez hitz egitea ez da zuzena, mikrogliak hainbat alterazio erakutsiko baititu etapa horietako bakoitzean. Doktorego-tesi honetan, fagozitosiari lotutako alterazio transkripzionalak, metabolikoak eta funtzionalak identifikatuko ditugu *in vitro* eta *in vivo* ereduak erabiliz.

2.4.2.2 Fagozitosi-ereduak

Fagozitosia in vitro sistemak erabiliz aztertu izan da tradizionalki. Fagozitosiaren in vitro modelizazioak prozesuan esku hartzen duten seinaleztapen-bideak aztertzea eta inplikatutako mekanismoak disekzionatzea ahalbidetzen du. Hala

ere, fagozitosiaren *in vivo* hurbilketek guztiz laburbiltzen dute prozesu fagozitikoa organismo bizidunean, eta aukera ematen dute prozesuaren beraren eta fagozitosiaren emaitza funtzionalaren azterketa integratuagoa egiteko. Jarraian, *in vitro* zein *in vivo* fagozitosia modelizatzeko erabiltzen diren teknikak zehaztuko ditugu.

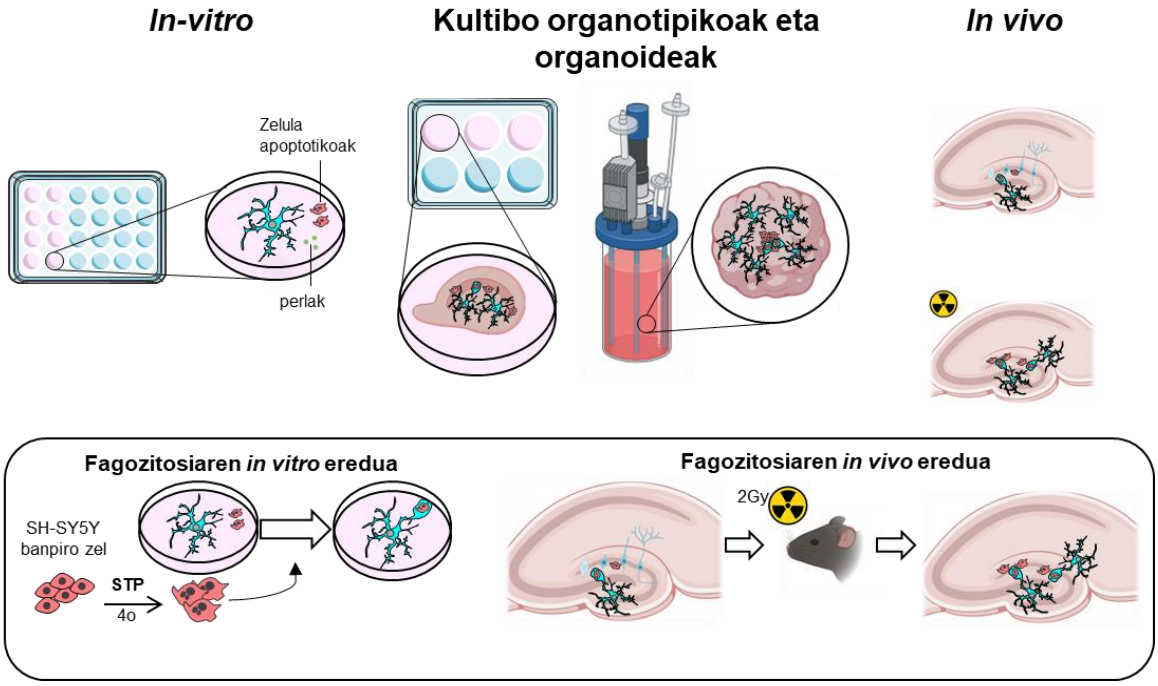

6. irudia. Fagozitosi mikrogliala aztertzeko metodoak. *Gaur egun, hainbat eredu erabiltzen dira fagozitosia aztertzeko. Eredua aukeratzea azterlanaren helburuen araberakoa da. In vitro ereduek aukera ematen dute zelula mikroglial isolatuetako fagozitosia ikertzeko, hazkuntzan sartutako zelula apoptotikoen edo perlen kantitatea zehatz kontrolaturik. In vitro ikuspegia zenbatezina da fagozitosian inplikatutako zelulaz kanpoko eta zelula-barneko mekanismoak aztertzeko. Labore organotipikoetan eta organoideetan garatutako ereduek in vitro eta in vivo sistemen arteko bitarteko ikuspegiak adierazten dituzte, eta ingurune kontrolatu batean elkarreragin konplexuagoak aztertzea ahalbidetzen dute. Azkenik, in vivo sistemek aukera ematen dute mikroglia baldintza fisiologikoetan ikertzeko, apoptosi basalak biraketa horzdunean analisirako oinarrizko lerro bat eskaintzen baitu. Doktorego-tesi hau garatzeko in vitro eredu bat zein in vivo eredu bat erabili dira. In vitro eredua giza zelula apoptotikoekin "elikatutako" saguaren mikroglia primarioa haztean datza. Aldiz, in vivo "superfagozitosia" garezurreko irradiazio baxua (LCI) 2 G-tan erabiltzean datza, oinarrian gertatzen den apoptosia eragiteko eta fagozitosia indartzeko. In vivo ikuspegi honek aukera ematen du baldintza fisiologikoetan erantzun mikrogliala eta ingurune esperimental kontrolatu batean fagozitosia sustatzeko duen gaitasuna hurbiletik aztertzeko. BioRender.com-ekin sortua.*

Fagozitosia aztertzeko *in vitro* metodoak

1986an, Guilianek eta Bakerrek, fagozitosi mikrogliala aztertzeko lehen hurbilketa egin zuten, mikroglia primarioaren kultiboa ezarriz eta substratu fagozitiko potentzialak dituzten zelulak "elikatuz" (Giulian et al., 1986). Ikerketa honek honek oinarriak ezarri zituen arloan, eta fagozitosi mikrogliala kultibo primarioak erabiliz aztertzen hasi ziren (Sierra et al., 2013). Kultibo primarioez gain, zelula mikroglialen lerroak, hala nola BV2 linea mikroglial hilezkorra (Blasi

et al., 1990), fagozitosi-saiakuntzetan erabili izan dira eta oraindik ere erabiltzen dira (Bocchini et al., 1992). Horrez gain, azken urteetan, zelula ama pluripotente induzituen (iPSCs) teknologiaren garapenak, giza mikroglia deribatua sortzea ahalbidetu du, non fagozitosia ere aztertu den (Healy et al., 2018; Dräger et al., 2022). Laburbilduz, hiru ikuspegi horiek prozesu fagozitikoa aztertzeko erabili ohi dira. Horietako bakoitzak hainbat abantaila eta eragozpen ditu, eta saiakuntza motaren arabera aldatuko dira, adibidez, laboreari gehitzen zaion substratu fagozitikoaren arabera. Jarraian, eredu bakoitzaren ezaugarriak zehaztuko dira, baita substratu fagozitiko egokiena aukeratzearen garrantzia ere. Lehenik, hainbat mikroglia erabiltzearen alde onak eta txarrak eztabaidatuko ditugu (lerro zelular hilezkorrak, labore primarioak eta zelula ama pluripotente induzituetatik eratorritako zelula mikroglialak), laboreei gehitu ohi zaizkien substratuekin jarraitzeko (mikroesferak eta zelula apoptotikoak).

Mikrogliaren elikaduran oinarritutako kultibo zelularrak:
In vitro elikadura-sistemek esperimentuen kontrolagarritasuna bermatzen dute, eta zelula mikroglial indibidualizatuetan tratamenduaren eragina zuzenean ebaluatzea ahalbidetzen dute. Hainbat mikroglia-iturri erabiliz egin daitezke. Zelula-lerro mikroglialak erraz mantentzen dira eta oso eskuragarri daude, murrizketarik gabe ugaltzeko eta erraz biltegiratzeko duten gaitasunagatik (Timmerman et al., 2018). Aipatutako horma-lerro zelular erabilienetako bat, BV2 izenekoa, LPSri dagokio eta ahalmen fagozitikoa du (Stansley et al., 2012). Kultibo primarioek, gainera, homogeneotasun genetikoa eta patogeno espezifikorik gabeko populazioa (SPF) eskuratzearen abantaila dute, horiek sortzeko erabilitako karraskarien jatorria dela eta (Timmerman et al., 2018). Era berean, iPSCek ere abantailak dituzte, giza ezaugarri mikroglialak laburbiltzen baitituzte (Healy et al., 2018). Hala ere, *in vitro* sistemek ere mugak dituzte. BV2 zelulek ez dute fenotipo mikrogliala erabat erreplikatzen, eta sagu helduaren garunaren mikrogliaren profiletik nabarmen bereizten dira. Ondorioz, zelula horiek kimiozinei erantzuteko mugigarritasun murriztua erakusten dute, LPSei erantzuteko gaitasun txikiagoa eta TGF-a bidearen beheranzko erregulazioa (Butovsky et al., 2014; Das et al., 2016; He et al., 2018). Mikrogliaren kultibo primarioek ez dute beharrezko ingurumen-seinalerik ondorengo heltzerako, eta horrek profil transkripzional heldugabe batera garamatza (Butovsky et al., 2014). Horrez gain, burmuinean mikrogliak seinale jakin batzuk jasotzen ditu etengabe, fraktalkina adibidez, ingurunearen egoera homeostatikoaren berri ematen dutenak. Estimulu horien faltak mikrogliaren hantura-profila handitzea dakar, garuneko mikrogliaren egoera homeostatikoa laburbildu gabe. Honek, zenbait artefaktu eragin ditzake (Wolf et al., 2013). Kultibo primarioaren beste handicap bat karraskarien mikrogliaren eta gizakiarenaren arteko aldea da, gizakiek eragindako mikroglia primarioaren bidez konpontzen saiatu baitira. Hala ere, giza garun-ehunen (osasuntsu) eskuragarritasun mugatuak, giza mikroglia primarioa erabiltzeko aukera zailtzen du (Watkins et al., 2014; Timmerman et al., 2018). iPSCek mutagenesia izateko eta onkogeneak aktibatzeko arrisku handiagoa dute (Friedman et al., 2018); muga hori gorabehera, giza mikroglia antzerateko eredurik zehatzena izaten jarraitzen dute (Hasselmann et al., 2020). Hori dela eta, *in vitro* ikuspegiak baliotsuak dira kontrolatutako ingurune batean mekanismo zelularrak aztertzeko. Hala ere, landutako mikrogliak eta in vivo homologoak desberdinak dira, eta haien funtzioak ez du garun-ingurunearen konplexutasuna erabat erreplikatzen.

Substratua aukeratzea ere funtsezkoa da *in vitro* fagozitosi-saiakuntzetan. Latexko perlak, eskuarki, perlak serumarekin estaltzea eskatzen duen prozedura batean erabili izan dira, fagozitoarekin elkarreragina sustatzeko. Duela gutxi proposatu da laborantza-serumean dagoen C1q-ak zelula apoptotikoen fagozitosian parte hartzea, eta horrek agerian uzten du, halaber, aktibatu gabeko seruma erabiltzearen garrantzia fagozitosi-saiakuntzak egitean (Fraser et al., 2010; Diaz-Aparicio et al., 2019). Hala ere, mikroesferek ez dituzte kimiokinak askatzen, horrela "aurkitu nazazu" etapa fagozitikoan substraturantz mikroglia-kimioatrakzioa sahiesten dute. Are gehiago, partikula horiek ezin dira degradatu, eta ezin da aztertu fagozitosiaren azken urratsa. Beraz, baldintza fisiologikoetan fagozitosia imitatzeko, gure laborategiak *in vitro* fagozitosi-saiakuntza bat erabili du, mikroglia neurona apoptotikoekin "elikatuz", C1q (seruma aktibatu gabe) presentzian. Metodoak aukera ematen du zelula apoptotikoetatik "aurkitu nazazu" seinaleak askatzeko eta, ondoren, horiek digestionatzeko, mikrogliak fagozitatu ondoren (Diaz-Aparicio et al., 2020).

Kultibo organotipikoak eta organoideak:
Zelula apoptotikoekin tratatutako kultibo zelularrez gain, beste metodo batzuek, fagozitosia 3D inguruneetan aztertzeko aukera ematen dute, hala nola kultibo organotipikoak eta garuneko organoideak. Hipokanpoaren xerra organotipikoetan apoptosia modu naturalean gertatzen da, mota zelular neuronal guztiak daude eta konektibitatea zaintzen da; beraz, fagozitosi fisiologikoa imitatzeko zein epilepsia edo iktusa bezalako hainbat gaixotasun modelatzeko erabil daitezke (Garbayo et al., 2011; Abiega et al., 2016; Gerace et al., 2021). Hala ere, ebakidura organotipikoek zenbait desabantaila dituzte, hala nola ingurunea aldatzea kultibo-ingurunea gehitu ondoren, beste garun-eremu batzuekiko konexioa galtzea eta ebaketa organotipiko batek garun oso baten konplexutasun eta funtzionaltasun osoa ez hartzea (Humpel, 2015; Abiega et al., 2016). Duela gutxi, garuneko organoideek giza garuna modelizatzea ahalbidetu dute, heterogeneotasun zelularra mantenduz eta egitura osoak ehun baten antzera jokatuz (Sabate-Soler et al., 2022). Ezaugarri guzti horiek, organoideak garapen neuronalerako eta nahaste neurologikoa aztertzeko sistema oso osatuak bihurtzen dituzte (Lancaster et al., 2013; Lindborg et al., 2016). Dena den, urte askotan, mikroglia ez zen garuneko organoideetan egon. Mikrogliaren jatorri mesodermikoa dela eta, ezin da bereizi ehun neuroektodermikoaren eta burmuineko organoideen artean, eta, beraz, iPSCetatik eratorritako mikroglia kanpotik mihiztatu behar da kultibo sistemetan (Fagerlund et al., 2021; Popova et al., 2021). Azken aldian, hezkidetzako protokolo hauek erakutsi dutenez, mikrogliak gaitasun fagozitikoa du zelula mikroglikoen barruan kaspasa3 partikula behatu ondoren (Xu et al., 2021; Zhang et al., 2023). Hortaz, organoideek ikerketa-eremu berri bat ireki dute, non giza burmuina plaka batean modelatu daitekeen, animaliekin esperimentuak egin beharrik gabe. Dena den, honen berritasunak eta garapen eskasak *in vivo* ereduak beharrezkoak egiten ditu oraindik.

Fagozitosia aztertzeko *in vivo* metodoak

In vivo fagozitosia aztertzeko, karga apoptotikoa mikrogliaren barruan behatu behar da. Poltsa fagozitikoak, normalean mikroglia-prozesu batean kokatutako

egitura tridimentsionalak, gorputz apoptotikoa inguratzen du eta behaketa honen bidez fagozitosia ebaluatuko da. Gaur egun, irudi-teknikek aukera ematen digute poltsa tridimentsionala eta barruko edukia zuzenean ikusteko. Gure laborategiak immunofluoreszentzia eta irudi konfokala erabiltzen ditu. Horri esker, immunolabellazioa eta mikrobioak, zelula apoptotikoak eta beste eduki fagozitiko batzuk ikus daitezke, hala nola mielina edo hondakin axonalak. (Sierra et al., 2013). Hala ere, ehun finkoko irudien analisiak denbora-puntu jakin batean informazioa emateko muga du. Arazo hau, 2fotoizko mikroskopioaren zuzeneko irudien teknika erabiliz konpon daiteke, zehazki zebrafish arrainak erabiliz. (Sieger et al., 2012; Abiega et al., 2016; Kamei et al., 2023).

Gure laborategiak DGaren nitxo neurogenikoa erabili du *in vivo* eredu gisa, fagozitosia baldintza fisiologikoetan aztertzeko. DG hipokanpalean gertatzen den neurogenesi-prozesuan, ur-jauzi neurogenikoa izenez ezagutzen den prozesu batean, zelula jaioberri batzuk hil egiten dira. Apoptosi basal horri esker, fagozitosi mikroglialaren oinarrizko lerro bat ezar daiteke baldintza fisiologikoetan (Sierra et al., 2010). Gure taldea aitzindaria izan zen fagozitosi mikroglialaren azterketan DGan, eta mikrogliaren analisiaren bidez, zelula apoptotikoen eta zelula apoptotiko fagozitoen zenbakiak zehaztu ziren, eraginkortasun fagozitikoa adierazten duten parametroak kalkulatzeko erabilgarriak izan direnak (Sierra et al., 2010). Baldintza fisiologikoetan, zelula apoptotiko gehienak (% 90 inguru) mikrogliak irentsi zituen, eta gainerako zelula apoptotikoak, haien ezaugarri apoptotiko goiztiarra dela eta, oraindik ez zituen mikrogliak ezagutu (Sierra et al., 2010). Mikrogliak eragindako zelula apoptotiko fagozitatuen ehunekoa, indize fagozitikoaren bidez definitzen da (Ph indizea) eta ahalmen fagozitiko mikrogliala adierazten du. Gainera, fagozitosia azkar gertatzen da, zelula apoptotikoa 90 minutu inguruko argitze-denboran ezabatuz. Era berean, mikroglia fagozitiko bakoitzeko poltsa fagozitikoen kopuruak, (ustez zelula apoptotiko fagozitikoak adierazten dituztenak), zelulen gaitasun fagozitikoa adierazten du. Oinarrizko baldintzetan, mikroglia fagozitiko gehienek gorputz apoptotiko bat duen poltsa fagozitiko bat erakusten dute (Sierra et al., 2010). Beraz, fisiologian mikrogliak eraginkortasunez ezabatzen ditu DG nitxoaren zelula apoptotikoak apoptosiari akoplatutako fagozitosiaren bidez.

Hala ere, ereduak baditu muga batzuk. Apoptosia ustekabean eta noizean behin gertatzen da. Ondorioz, nitxo neurogenikoan dauden zelula mikroglial guztien artean, zelula gutxi batzuk baino ez dira arituko fagozitosian. Hori dela eta, sagu helduen eta gazteen hipoeremuaren nitxo neurogenikoan, mikroglia fagozitikoen eta ez fagozitikoen populazio nahasia dago. Gai honi heltzeko, doktorego-tesi honetan *in vivo* "superfagozitosi" eredu bat garatu dugu, garezurreko irradiazio baxua (LCI) erabiltzean datzana, DGan neuroprogenitoreak apoptosia eragiteko eta fagozitosia indartzeko. Eredu honek apoptosi masibo bat sortzen du, DGaren mikroglia egoera fagozitiko batean sinkronizatzea ahalbidetzen duena, eta aldi berean, kaltetutako zelulak eta egoera fagozitiko bat sortzen ditu, behin garbituak izan eta gero. Horrek nabarmen handitzen du GDko mikroglia fagozitikoen kopurua, eta, horri esker, aldaketa postfagozitikoak azter daitezke.

2.5 FAGOZITOSIAREN ONDORIO FUNTZIONALAK

Azken atalean azaldu den bezala, fagozitosi mikrogliala oso eraginkorra da GDko baldintza fisiologikoetan, zelula apoptotikoak azkar irensten eta ezabatzen baititu. Mikrogliak hondakin apoptotikoak behar bezala ezabatzeak ondorioak ditu inguruko nerbio-ehunean eta zelula mikroglialetan. Jarraian, bi efektuak xehetasun handiagoz deskribatuko ditugu.

2.5.1 SNCren inguruneko fagozitosiaren emaitza funtzionala

Mikrogliak hondakin apoptotikoak azkar eta eraginkortasunez kentzeak eduki intrazelular apoptotikoa isurtzea saihesten du; izan ere, zelula apoptotiko primarioak mintzaren osotasuna galtzen du eta zelula apoptotiko edo nekrotiko sekundarioak bihurtzen dira (Kolb et al., 2017). Jakina da zelula-barneko edukia zelulaz kanpoko espaziora askatzeak hantura-erantzuna eragiten duela; alabaina, DNA, RNA, nukleotidoak edo kromatinaren proteina batzuk, hala nola HMGB1 (mugikortasun handiko taldearen 1. kaxako proteina), kalteari lotutako patroi molekularrak (DAMP) deritzenak, mikrogliak adierazitako patroiak (PRR) ezagutzeko hartzaileek ezagutzen dituzte, eta hantura-erantzun immune konplexu bati ekiten diote (Huber-Lang et al., 2018). Alde batetik, fagozitosi ez-eraginkor bat hantura-erantzun orokor batean eta ehunaren kaltean gertatzen da, gure laborategian asko aztertu den epilepsia-saguaren *in vivo* eredu batean ikusten den bezala. Bertan, fagozitosi hondatua mikroglia bidezko hantura-profilari lotuta dago (Abiega et al., 2016; Morioka et al., 2019). Bestalde, zelula apoptotikoen fagozitosia egiten duen *in vitro* mikrogliak, erantzun motelduak erakutsi zizkien hanturazko estimuluei, hala nola LPSri (Magnus et al., 2002; De Simone et al., 2003). Aitzitik, gure laborategiak, LPSren erangipean dagoen in vitro mikroglia primarioak zitokinen adierazpen-profila, mikroglia fagozitokoaren oso antzekoa dela frogatu du (Diaz-Aparicio et al., 2020). Laburbilduz, itxuraz kontraesankorrak diren eta prozedura-desberdintasunekin lotuta egon daitezkeen aurkikuntzen gorabehera (adibidez, fagozitazio osteko denbora edo LPS dosia), datu horiek, fagozitosi mikroglialak eragin immunomodulatzaileak dituela iradokitzen dute (Szondy et al., 2017; Morioka et al., 2019).

2.5.2 Fagozitosiak eragindako ondorioak mikroaglia zeluletan.

2.2.3.3 atalean, funtzio mikrogliala eta, bereziki, hanturazko erantzunak metabolismoan eta transkripzioan izandako aldaketek nola arautzen dituzten aztertu dugu. Beraz, fagozitosi mikroglialak aldaketa transkripzionalak eta metabolikoak ere eragin ditzake.

Makrofagoetan, fagozitosiak funtzio immunitarioaren modulaziora daraman egokitzapen transkripzional eta metabolikoko errepertorioa eragiten du, sortzetiko immunitatearen entrenamendua deritzon prozesua (2.2.3.3 atala). Izan ere, fagozitosiak fisio mitokondriala eragiten du (Wang et al., 2017; Morioka et al., 2018), eta mintz mitokondrialaren potentziala murrizten du proteina desakoplatzaile mitokondrialaren bidez (UCP2) (Park et al., 2011). Horiek, glukolisia areagotzearekin batera (Morioka et al., 2018), gorpuak etengabe atzematea bermatzen dute. Horrez gain, laktatoaren askapenaren gorakadak ingurune antiinflamatorio bat ezartzea sustatzen du (Morioka et al., 2018). Hala ere, fagozitosiak eragindako egokitzapen metabolikoek, fagozitosian eragina

izateaz gain, ondorio iraunkorrak ere sortu dituzte. Fagozitosiak makrofagoen funtzioa nola birprogramatzen duen erakusten duten hainbat adibide daude. Esaterako, Drosophilaren garapen goiztiarrean, makrofagoak ez dira sentikorrak ehunen kalteen edo infekzioen aurrean. Hala ere, gorpuak hartu ondoren, makrofagoak gai dira kaltetutako eskualdeetara migratzeko eta patogeno bakterianoak fagozitatzeko. Hau, Jun kinasa seinaleztapen-bidea aktibatuz eta Draper kalteen hartzailearen adierpena handituz egiten dute (Weavers et al., 2016). Beraz, makrofagoetako gorpu apoptotikoen fagozitosiak egokitzapen metabolikoak eragiten ditu, eta egokitzapen horiek berehala modulatzen dute funtzio zelularra, eta epe luzera ere ere, fagozitoa indartzea bultzatzen du.

Aldiz, ezer gutxi dakigu mikrogliako fagozitosirako egokitzapen metabolikoei buruz. Kultiboan, mikroglia fagozitikoak modulazio transkripzionalak esperimentatzen ditu, denboraren araberako adierazpen-aldaketak erakusten dituztenak. Gene batzuk aldi baterako erregulatzen dira fagozitosiaren ondorengo 3 orduetan, baina gehienak degradazio osteko fasean erregulatzen dira, fagozitosiaren ondorengo 24 orduetan (Diaz-Aparicio et al., 2020). Gene horietako batzuk metabolismo zelularrean inplikatuta zeuden, eta horrek, fagozitosiak mikroglian, egokitzapen metabolikoak eragiten dituela iradokitzen du (Diaz-Aparicio et al., 2020). Doktorego-tesi honetan, hipotesi hau frogatuko dugu: fagozitosiaren ondoren, mikrogliak bere metabolismoa birmoldatu eta bere funtzioan eragina izan dezakeela.

2.6 FAGOZITOSIA GARUNEKO TUMOREETAN

Mikrogliaren aldaketa postfagozitikoen azterketa funtsezkoa da mikrogliak fagozitosia nola egiten duen ulertzeko, denbora tarte laburretan zelulak etengabe desafiatzen direnean estimulu apoptoikoak direla eta. Fagozitosi errepikakorra beharrezkoa den kasu patologiko bat, garuneko tumoreena da. Hauek normalean erradioterapia bidez tratatzen dira garuneko minbiziko tumore-zelulak kentzeko (Scaringi et al., 2018). Tratamendua dosi sekuentzialetan eman ohi da (Hingorani et al., 2012), eta horrek mikrogliak ezabatu behar dituen zelula apoptotikoen uholdeak eragiten ditu. Atal honetan, garuneko hainbat tumore mota aztertuko ditugu, glioblastoma eta berari loturiko tratamendu- modalitateak bereziki. Azken hau, garuneko tumore gaizto primarioen formarik prebalente eta oldakorrena da. Bestalde, mikrogliak mikrogiro tumoralean duen zereginean sakonduko dugu, eta, azkenik, tumore-zelulen fagozitosi mikroglialean jarriko dugu arreta.

2.6.1 Garuneko tumoreen kategoriak

Garuneko tumore nagusienak hiru kategoriatan sailkatzen dira: minbizi sistemikoen garezur barneko metastasia, meningiomak eta gliomak (McFaline-Figueroa et al., 2018). Garuneko tumore metastasikoak bigarren mailako garuneko tumoretzat hartzen dira, garunean sortzen ez direlako eta haien prebalentzia lehen mailako tumoreena baino 10 aldiz handiagoa delako (Arvold et al., 2016). Garuneko metastasi gehienak gaixotasun sistemiko aurreratu baten ondorio direnez, pronostikoak txarra izaten jarraitzen du (Sperduto et al., 2012). Garuneko tumore primarioen artean, meningiomak zelula meningotelialetatik

sortzen dira, aurrerago garezurreko gainazalean edo azalera duralean garatzen dira eta pronostiko ona dute, gehienak onberak dira (Buerki et al., 2018). Alderantziz, gliomak zelula glialetatik sortzen dira, eta horien artean astrozitomak, oligodendrogliomak, ependimomak, glioblastomak eta histologia ezohikoa duten tumore ugari daude. Gliomen artean, glioblastomak garuneko tumore gaizto primario ohikoenak eta erasokorrenak dira, eta tratamenduaren eraginkortasun mugatua eta biziraupen-tasa txikiak erakusten dituzte (Fu et al., 2014). Orain arte, eskuragarri dauden tratamenduek ez dute lortu biziraupen-tasak handitzea, eta pazienteen bizi-itxaropena hilabete gutxi batzuetara soilik handitu dute (Silantyev et al., 2019). Beraz, tratamenduen optimizazioa funtsezkoa da glioblastoma duten pazienteen bizi-kalitatea eta bizi-itxaropena hobetzeko.

Glioblastomen sailkapen berriak, ezaugarri molekular eta histologikoetan oinarritzen denak, diagnostiko eta terapia egokiagoak lortzea du helburu, baina abordatze terapeutiko klasikoak neurokirurgia, erradioterapia eta kimioterapia konbinatzen ditu (McFaline-Figueroa et al., 2018). Lehenik eta behin, tumorearen erresekzioa egiten da. Erresekzioak minbizi-ehuna ahalik eta gehien erauztea bermatu behar du, garuneko funtzioetan eragin edo eragin gutxi izan gabe (Sanai et al., 2011). Ondoren, "Stupp protokoloa" aplikatzen da, prozedura hori ebakuntza ondoko tratamendurako adostasun-estandarra baita. Protokoloa erradioterapia hipozatikatuko (HFRT) 6 astetan oinarritzen da. Bertan erradiazio dosi osoa dosi txikiagoetan banatzen da eta sekuentzialki ematen da (60Gy egunean 2Gy zatikitan zatituta, bost egunean bi eguneko atsedenaldiak baimenduz) temozolamida gehigarriarekin batera. Hau egunero ematen da erradioterapian zehar eta ondorengo sei zikloetan ere (Stupp et al., 2005). Dena den, hainbat frakzio eta dosi aztertu dituzten HFRTri buruzko azken ikerketek ez dute lortu biziraupen-denbora nabarmen handitzen (Liu et al., 2021). Horrez gain, HFRTren optimizazioak sarritan alde batera utzi du fagozitoek tumore-zelula apoptotikoak deuseztatzeko duten funtsezko zeregina, mikrogliak tumore-zelulen fagozitosiari buruzko ikerketa nahiko mugatua baita oraindik, hurrengo atalean deskribatuko dugun bezala. Beraz, erradiazio osteko fagozitosia gehiago aztertu behar da tratamenduak optimizatzeko.

2.6.2 Mikroglia eta TAM tumore-mikroingurunean

Tumorean, mikroglia, BBB iragazkortu ondoren tumorean infiltratzen diren monozito zirkulatzaileekin batera existitzen da, eta biek tumoreei lotutako makrofagoak (TAM) izeneko populazio mistoa osatzen dute. TAMak tumore-masaren % 30-40 inguru dira, eta bi norabideko harremana dute minbizi-zelulekin eta tumore-mikroingurunearekin (Badie et al., 2000; Watters et al., 2005; Buonfiglioli et al., 2021). Erlazio horren ondorioz, TAMek tumorea okertzen laguntzen duela proposatu da, bai tumore-progresioa sustatuz, bai funtzio immunoezabatzaileak gauzatuz (Buonfiglioli et al., 2021) (**7. irudia**).

TAM-glioma-zelulak diafoniaren bitartekoak dira bai TAM errekrutatzen laguntzen duten glioma-zelulek askatutako molekula kimioatrayenteak, bai tumore-progresioa sustatzen duten TAMek askatutako faktoreak (Buonfiglioli et al., 2021). Tumore-zelulek askatutako faktoreen artean, tumore-lekuetara TAM errekrutatzea errazten duten honako proteina kimioerakargarri hauek daude:

CCL2 eta CCL7 zitozinak, 33 interleuzina (IL-33) eta hazkunde-faktoreak, hala nola granulozito-makrofagoen kolonien faktore estimulatzailea (GM-CSF), hepatozitoen hazkunde-faktorea edo sakabanatze-faktorea (HGF/SF), estromatik eratorritako 1. faktorea (SDF-1) eta glia-zeluletatik eratorritako faktore neurotrofikoa (GDNF) (Wang et al., 2012; Ku et al., 2013; Sielska et al., 2013; Chen et al., 2017a; Chen et al., 201b. Era berean, tumore-zelulek beste agente batzuk askatzen dituzte, hala nola CSF1 eta 1. fosfoproteina sekretua (SPP1). Horiek, TAMak erakartzeaz gain, fenotipo Immusupresiboa baterako aldaketa ere eragiten dute TAMetan (Sielska et al., 2013; Wei et al., 2019). Azkenik, tumoreak jariatutako proteinek ere tumorearen beraren progresioa errazten dute. Hori da Versicanen kasua, Toll motako hartzaileekin (TLR) bat egiten duena tumore-hazkuntza zuzenean bultzatuz. Hauek Tenascina C (TNC) zelula-atxikipeneko molekula, tumorearen ugalketa TAMen bidez modu positiboan erregulatzen dute (Hu et al., 2015; Xia et al., 2015). Oro har, glioblastomako zelulek molekulak ekoizteko eta askatzeko prozesu konplexu bat osatzen dute, eta horiek, aldi berean, TAMen ekintzaren bidez haztea eta hedatzea errazten dute.

Tumore-zeluletatik eratorritako faktoreak birprogramatu ondoren, TAMek tumore-progresioan laguntzen dute askatutako faktoreen bidez. TAMen kasuan, zitozinen, TGF-βaren eta 1. eta 6. iterleukinen (IL-1, eta IL-6) ekoizpena handituta dago, eta horietako bakoitzak tumore-progresioan laguntzen du, hainbat modutan. TGF jariakinak zelulaz kanpoko matrizea (MEC) aldatzen du eta, beraz, glioblastoma-zelulen inbasioa areagotzen du (Wick et al., 2001). IL-1alden gainadierazpenak gainera tumore-zelulak eta ugalketa sustatzen ditu; eta IL-6 tumore-progresioan inplikatuta dago, tumore-zelulek odol-hodiak sortzen laguntzen baitute (Feng et al., 2015; Zhang et al., 2017). Halaber, estresak eragindako fosfoproteina 1 askatzeak (STI1) eta hazkunde epidermikoaren faktoreak (EGF) zein metaloproteinen ekoizpenak (MMP14, MMP2 eta MMP9), TLRren aktibazioaren bidez, tumoreen hazkundea eta inbasioa sustatzen dute (Markovic et al., 2009; Coniglio et al., 2012; Vinnakota et al., 2013; da Fonseca et al., 2014; Hu et al., 2014). Beraz, TAMek zuzenean laguntzen dute tumore-hazkuntzan, eta horrek diana terapeutiko interesgarria adierazten du, tumore-progresioa geldiaraz dezakeena.

Gainera, TAMek erantzun immunitarioa ere moteltzen dute, beste zelula batzuetan eraginez, hala nola T zeluletan, eta beren funtzio immunitarioak murriztuz, hala nola fagozitosia. Tumore-zelulen ezagutzari dagokionez, T zelulek antigenoak ezagutu behar dituzte aukeratutako zeluletatik eta TAMetatik eta zelula kantzerigenoen identifikazioa errazten dute (Sakaguchi et al., 2007; Qian et al., 2018). Tumore-zelulak aztertzeaz ari garenean, T zelulek xede-zelulen antigenoak eta TAM zelulak ezagutu behar dituzte, antigenoak (APC) aurkezten dituzten zelulak baitira, eta minbizi-zelulak identifikatzea errazten dute. Hala ere, gliomatik eratorritako faktoreek antigenoen agerpena murriztu zuten TAMen II klaseko CMH adierazpenaren narriaduraren bidez, eta horrek tumore-progresiora daraman T zelulen jarduera moteldu zuen (Qian et al., 2018). Horrela, TAMek tumore-progresioan ere laguntzen dute, inguruko zelula immunitarioetan eragiten baitute.

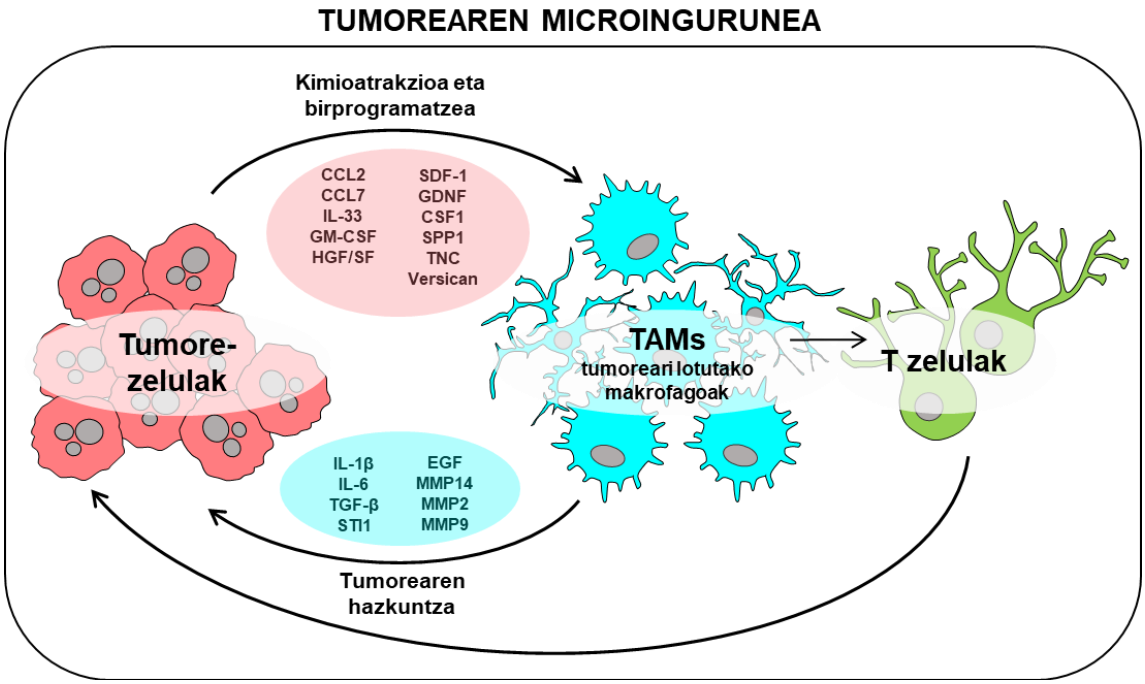

7. irudia. TAMs-tumore-zelulen interakzioa tumore-mikroingurunean. *TAM/Tumore-zelulak interakzioan tumore-mikroingurunean askatutako faktoreek tumore-hazkundea sustatzen dute eta erantzun immunitarioa murrizten dute. Glioma-zelulek TAMak errekrutatzen eta birprogramatzen dituzten molekula kimioerakargarriak askatzen dituzte. Era berean, TAMek tumore-progresioa sustatzen duten substantziak askatzen* dituzte eta immunitate-sistema moldagarriaren erantzuna moteltzen dute (T zelulak). BioRender.com-ekin sortua eta egokitua (Buonfiglioli et al., 2021).

2.6.3 Tumore-zelulen fagozitosia

TAMek tumore-mikroingurunean fagozitosia egiteko duten gaitasuna kontraesankorra da oraindik. Alde batetik, TAMek ez dituzte tumore-zelulak fagozitatzen; izan ere, zelula osasuntsuek bezala, fagozitosia eragozten duten "ez nazazu jan" seinaleak dituzte (Cockram et al., 2021; Kelley et al., 2021). Gainera, tumore-mikroingurunean "ez nazazu jan" seinaleak areagotu egiten dira, hala nola gainazal antifagozitikoko proteinaren adierazpen areagotua ("ez nazazu jan") CD47, SIRPa hartzailearekin bat egiten duena TAM zeluletan fagozitosia inhibitzeko (Willingham et al., 2012; Li et al., 2021). Ildo horretan, anti-CD47 antigorputzen bidezko tratamenduak TAMen tumore-fagozitosia eragin zuen glioblastomako xenoinjertoaren eredu batean, eta tumore-hedapena murriztu zuen (Hutter et al., 2019). Bestalde, gutxienez *in vitro* kasuan, TAMek mikroperlen gaitasun fagozitiko txikia erakutsi zuten glioma minbiziaren zelula amen eraginpean jarri zirenean (gCSC) (Wu et al., 2010). Hala ere, agente zitotoxikoen edo UV argiaren bidez tumorean apoptosia eragiten denean, astrozitoak, glioma-zelulak eta TAM zelulak gai dira tumore-mikroingurunean fagozitosia egiteko (Chang et al., 2000; Kulprathipanja et al., 2004). Gainera, TAMek irentsitako zelula apoptotikoen kopurua astrozitoek eta glioma-zelulek irentsitakoena baino lau aldiz handiagoa zen, eta horrek adierazten zuen TAMak zirela garuneko tumoreetan fagozitorik eraginkorrenak (Chang et al., 2000). Erradioterapiak apoptosian zein fagozitosian duen eragina ez da hain esploratua

izan. Beraz, erradioterapia glioblastoma tratatzeko estrategiarik ohikoena denez, doktore-tesi honen helburu nagusietako bat TAMek tumore-zelula apoptotikoen fagozitosia ebaluatzea da. Erradiazioak apoptosian eta TAM bidezko tumore-zelulen ondorengo fagozitosian duen eragina ulertzeak bide berri bat irekiko du HFRT aztertzeko, glioblastomari aurre egiteko gehien erabiltzen den terapia baita.

3. HIPOTESIA ETA HELBURIAK

3. HIPOTESIA ETA HELBURUAK

Zelula apoptotikoen fagozitosi mikrogliala asko aztertu da, bai fisiologian, bai gaixotasunean, eta hainbat fase ditu zelula apoptotikoa ehunetik erabat ezabatu arte (Napoli et al., 2009; Diaz-Aparicio et al., 2016). Gainera, fagozitosia ez da prozesu terminala, eragina baitu bai ingurumenean, bai mikroglia zeluletan bertan. Fagozitosiaren ondorioek zelula-barneko eduki apoptotikoaren isuria saihestu egiten dute eta erantzun inflamatorioa galarazten dute (Kolb et al., 2017; Huber-Lang et al., 2018). Era berean, fagozitosiak urjauzi neurogenikoa erregulatzen du faktore neuromodulagailuak sortuz (Diaz-Aparicio et al., 2020). Gisa honetan, mikroglia fagozitosiaren ondorioz aldaketa funtzionalak jasaten dituela argituz. Ikerketa honetan hipotetizatzen dugu fagozitosiak aldaketak eragingo dituela mikrogliaren maila ezberdinetan, potentzialki haien transkripzio egoeran eta euren egoera metabolikoan eta, ondorioz, euren funtzio fagozitikoan eraginez.

1. helburua. Superfagozitosi eredu bat garatu eta balioztatu. Eredua garatzeko, garezurreko irradiazioan (8Gy) oinarritutako eredu bat egokituko dugu. Irradiazio eredu honek neuroarbasoen apoptosia eta fagozitosi mikrogliala eragiten da DGn (Beccari et al., 2023). Eredu hori garezurreko irradiazio baxuko (LCI) eredu batera (2Gy) egokitzeak sortutako zelula apoptotikoen kopurua eta albo-ondorioak murrixtuko ditu. Ondoren, immunofluoreszentzia eta irudi konfokalak erabiliko ditugu ereduaren eraginkortasuna ebaluatzeko. Horrela, eredua mikroglia egoera fagozitikoan sinkronizatzeko gai den ala ez aztertuko dugu, baita DNAren kaltea eta monozitoen estrabasazioa.

2. helburua. Fagozitosiak morfologia mikroglialean eta transkripzio-egoeran eragindako aldaketak aztertzea. Fagozitoaren osteko mikrogliaren markatzaileak aurkitzeko, fagozitosiaren ondoren aldaketak izan ditzaketen parametroak aztertuko ditugu, hala nola aldaketa morfologikoak eta adierazpen genikoan gertatutako aldaketak. Morfologia mikrogliala immunofluoreszentzia eta irudi konfokalaren bidez aztertuko da; mikrogliaren egoera transkripzional postfagozitikoa, berriz, zelula bakarraren RNAren sekuentziatzioaren (scRNA-Seq) bidez, baita ondoren egindako bailozkotzeen bidez (immunofluoreszentzia eta RNAscope) ebaluatuko da.

3. helburua. Fagozitosiaren ondoren mikroglia estresatzen dituzten mekanismoak argitzeko, mikroglia postfagozitikoaren zelula barneko hainbat funtzio eta osagai aztertuko ditugu. Hala nola estres oxidatiboa, mitokondriak eta zelulen metabolismoa. Hauek guztiak estresari eta zelulen heriotzari lotuak daudelako. Estres oxidatiboa, mitokondriak eta metabolismo zelularra aztertzeko, fagozitosiaren in vitro eredu bat erabiliko da. Ondoren, analisi-metodo hauek erabiliko dira: fluoreszentzia bidezko adierazpen-analisia, mikroskopia konfokala eta mikorskopia elektroniko bidezko analisia, Seahorse bidezko analisi metabolikoa eta masa-espektrometria, hurrenez hurren.

4. helburua. Fagozitosi osteko estresaren ondorengo funtzio fagozitiko mikrogliala aztertzea. Funtzio mikrogliala aztertzeko, in vivo "superfagozitosi" eredua erabiliko da, eta, ondoren, immunofluoreszentzia eta irudi konfokalak.

5. helburua. Erradioterapiaren eraginpean dauden glioblastoma-tumoreetan fagozitosi mikrogliala aztertzea, erradioterapia hipofrakzionatuaren (HFRT) testuinguruan fagozitosia aztertzeko aurretiazko ikuspegi gisa. Bi animalia-eredu erabiliko ditugu, saguetan glioblastoma-subtipo proneurala eta mesenkimala laburbiltzen dituztenak (Lenting et al., 2017). Animalia hauek erradioterapia-pultsu (RT) baten eraginpean egongo dira et fagozitosia immunohistokimikaren, immunofluoreszentziaren eta irudi-tekniken bidez ebaluatuko da.

4. EMAITZAK

4. EMAITZAK

4.1: In vivo “superfagozitosi” ereduaren baliozkotzea

Mikroglia bidezko zelula apoptotikoen fagozitosia funtsezkoa da garuneko parenkimatik hondakin toxikoak behar bezala ezabatzeko. Prozesu hau azkar eta modu eraginkorrean gertatzen da. Horrez gain, zelulen heriotzatik eratorritako eduki zitotoxikoaren isuriak eragindako ehunen kaltean saihesten ditu Hala ere, fagozitosia ez da prozesu terminala, eta aldaketa transkribatzaile ugari eragiten ditu mikroglian. Aldaketa hauek inguruko zeluletan eragina dute; gure laborategian deskribatu dugun bezala, neurogenesi prozesuan parte hartzen dute (Diaz-Aparicio et al., 2020). Mikroglian fagozitosiak eragindako aldaketen inplikazioak sakonago aztertzeko, fagozitosiaren *in vitro* eredu bat erabili dugu (Diaz-Aparicio et al., 2020), eta *in vivo* superfagozitosi eredu bat garatu dugu, helburu honetan zehatz-mehatz deskribatuko dena. In vivo superfagozitosiaren eredua hauxe zen: apoptosia eragiteko eta fagozitosia bultzatzeko garezurreko irradiazio baxua (LCI) erabiltzea. Irradiazioak nabarmen eragiten die zelula ugaritzaileei (Jiao et al., 2022), hala nola zelula ama neuronal erradialei (RSC) eta haien alaba zelulei, granulezko zelula jaioberriei. Zelula horiek guztiak hipokanpoan daude, zehazki hortzdun biraren (DG) eremu azpigranularrean (SGZ), nitxo neurogenikoa dagoen lekuan.

Iraganean frogatu dugun irradiazioak (8Gy) neuroprogenitoreen apoptosia eta fagozitosi mikrogliala eragiten ditu DGn (Beccari et al., 2023). Doktorego-tesi honetan 2Gy irradiazio-dosi txikia erabili dugu. Dosi hau, saguetan tumoreen aurkako tratamenduetan erabiltzen dena baino 15-25 aldiz txikiagoa da (Gan et al., 2016). Horrela, zelula ez-ugalkorrei kalte gutxiago egiten diegu eta albo-ondorioak minimizatzen ditugu.

In vivo “superfagozitosiaren” eredu honek in vivo mikroglia fagozitikoaren aldaketa transkriptibo eta funtzionalak aztertzeko aukera eman zigun. Horrela, *in vitro* eredutik lortutako datuak osatu genituen. Atal honetan *in vivo* “superfagozitosi” eredua aurkeztuko dugo eta mikroglia etapa fagozitiko batean sinkronizatzen dela erakutsiko dugo. Zehazki sinkronizazio hau DGn gertatzen dela erakutsiz. Hala ere, atal honetan egiaztatu dugu LCIak kalterik eragiten ote zuen mikrogliaren DNAn eta monozitoen infiltrazioan.

4.1.1 Mikroglia superfagozitiko bihurtzen da DGn LCIaren ondoren.

Irradiazioak apoptosian eta mikrogliako fagozitosian dituen ondorioak aztertu ditugu eta irradiazioak kaspasa 3 aktibatua duten zelula apoptotikoen kopurua handigotzen duela antzeman dugu (**8. irudia**). Gero kontrol saguak (erradiatu gabea) eta sagu sakrifikatuak LCIaren osteko denbora-puntu desberdinekin alderatu (6o, 24o, 3e, 7e eta 30e) genituen (**9. A irudia**). Ondoren, immunofluoreszentzia eta irudi konfokalak egin genituen mikroglia eta zelula apoptotikoak behatzeko. Mikrogliak erreportari berdea adierazten du

(ingelesezko siglak: EGFP) Csf1r (kolonietako faktore estimulatzailearen hartzailea 1) sustatzailearen menpean (fms-EGFP saguak). Zelula apoptotikoak 4 '-6-diamidino-2-fenilindol (DAPI) ADN tindaketa erabiliz, bereiztu ziren haien morfología nuclear anormalari (piknosia, kariorresia) erreparatuz (**9. B, C irudia)**. Zelula apoptotikoak eta mikroglia errazago aurkitzeko, kaspasa-3 aktibatua eta Pu.1 nukleoak ere erabili ziren, hurrenez hurren (**9. B, C irudia**). LCIak apoptosia eragin zuen DGko EAGn 6 ordura. Zelula piknotiko/karriorretiko eta kaspasa-3 aktibatuta adierazten zituzten zelulak kopuruz haunditu baitziren LCIaren ondorioz (**8. irudia, 9.B irudia, D**).

Zelula apoptotiko horietako gehienak prozesu mikroglialek irentsi zituzten, bere inguruan 3D poltsa fagozitikoak sortuz (**9. C irudia**). Fago. indizeak (mikrogliak irentsitako zelula apoptotikoen %) horrela erakusten du. Kontrol-saguetan, mikrogliaren fagozitosia oso eraginkorra izan zen (Fago. indizea 93,6 ± % 2,7), baina apur bat murriztu zen 6 ordutara LCIaren ondoren (% 75,7 ± 2,5) (**9. E,F irudia**). Murrizketa hori, ziurrenik, apoptosia asko handitu delako gertatu da.

6 ordu LCIaren ondoren, mikrogliak apoptosiaren gehikuntzari aurre egin zion, guztizko ahalmen fagozitikoa handituz (mikroglia bakoitzak zituen poltsa fagozitikoen batez bestekoa). Kontrol-baldintzetan mikrogliaren % 9,1 ± 3,5 baino ez zen fagozitikoa, eta 6 orduan, berriz, mikrogliaren % 83,3 ± 14,9 fagozitikoa bihurtu zen, eta zelula bakoitzak 1-6 poltsa fagozitiko zituen (**9. C, G, H irudia**). Fagozitosi aktibo eta sinkronizatu horrek zelula apoptotikoen ezabapen eraginkorra ekarri zuen, eta 24 ordutan LCIak eragindako zelula apoptotikoak desagertu egin ziren DGtik (**9. B-D irudia**). Zifra horiek, halaber, zelula bakoitzeko 46,4 ± 8,5 min-ko ezabatze-denboraren gutxi gorabeherako kalkulua ematen dute. Kalkulu hori honela kalkulatzen da: zelula apoptotikoen proportzioa 6 ordu eta 24 ordu artean, denbora-tartearekin (18 ordu) biderkatuta, eta poltsa fagozitikoen kopurua mikrogliarekin 6 orduan (Fago. ahalmena) (**9. I irudia**). Ondorengo denbora-puntuetan (3e-30e), apoptosia eta fagozitosia maila basaletara itzuli ziren (**9. D-H irudia**), eta horrek baieztatzen du zelula apoptotikoen sorrera masiboa eta ondorengo fagozitosia LCIaren eragina direla.

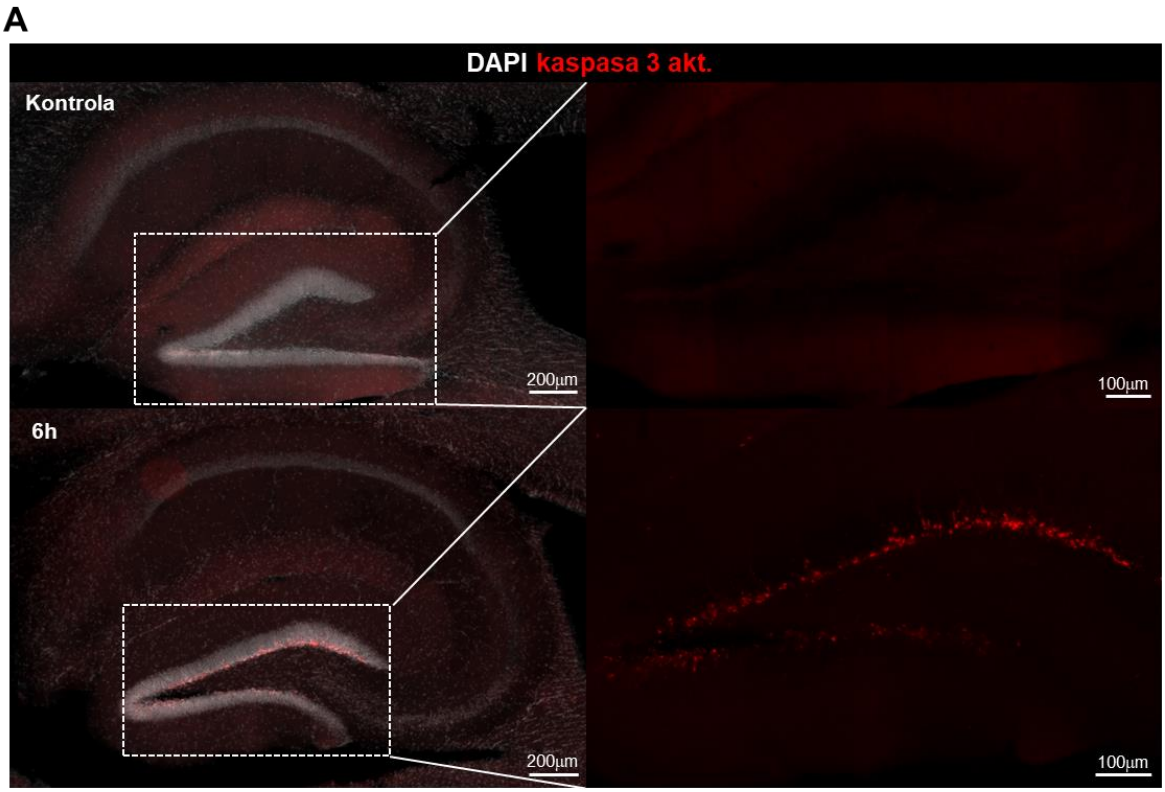

8. irudia. Apoptosiaren indukzioa hipokanpoko nitxo neurogenoan LCIaren ondoren. *(**A**) Hipokanpoaren irudi adierazgarriak kontrol-egoeran eta 6 ordu LCIaren ondoren. Irudiak DAPI (zuria) eta kaspasa aktibatua 3 (gorria) tindaketak erakusten dituzte. Puntukako lerroaren barruan dagoen eremuaren xehetasunean, hipokanpoko hortzdun biraren (DG) eremu azpigranularreko (SGZ) zelula apoptotikoen kontzentrazioa ikusten da. Eskala-barrak = 200µm, 100µm [irudiaren xehetasuna].*

Oro har, datu horiek iradokitzen dute LCIak apoptosia eragin zuela eta mikroglia fase fagozitiko batean sinkronizatu zuela 6 ordutan. Zelula horiek azkar eta eraginkortasunez ezabatu zituzten hipokanpoan sortutako hondakin apoptotikoak, eta postfagozitiko bihurtu ziren 24 ordura. Beraz, "superfagozitosi" eredu horrek aukera eman zigun fagozitosiak mikroglian duen eragina aztertzeko. Jarraian, apoptosia eta fagozitosia DGra mugatuta zeuden ala ez zehaztuko dugu.

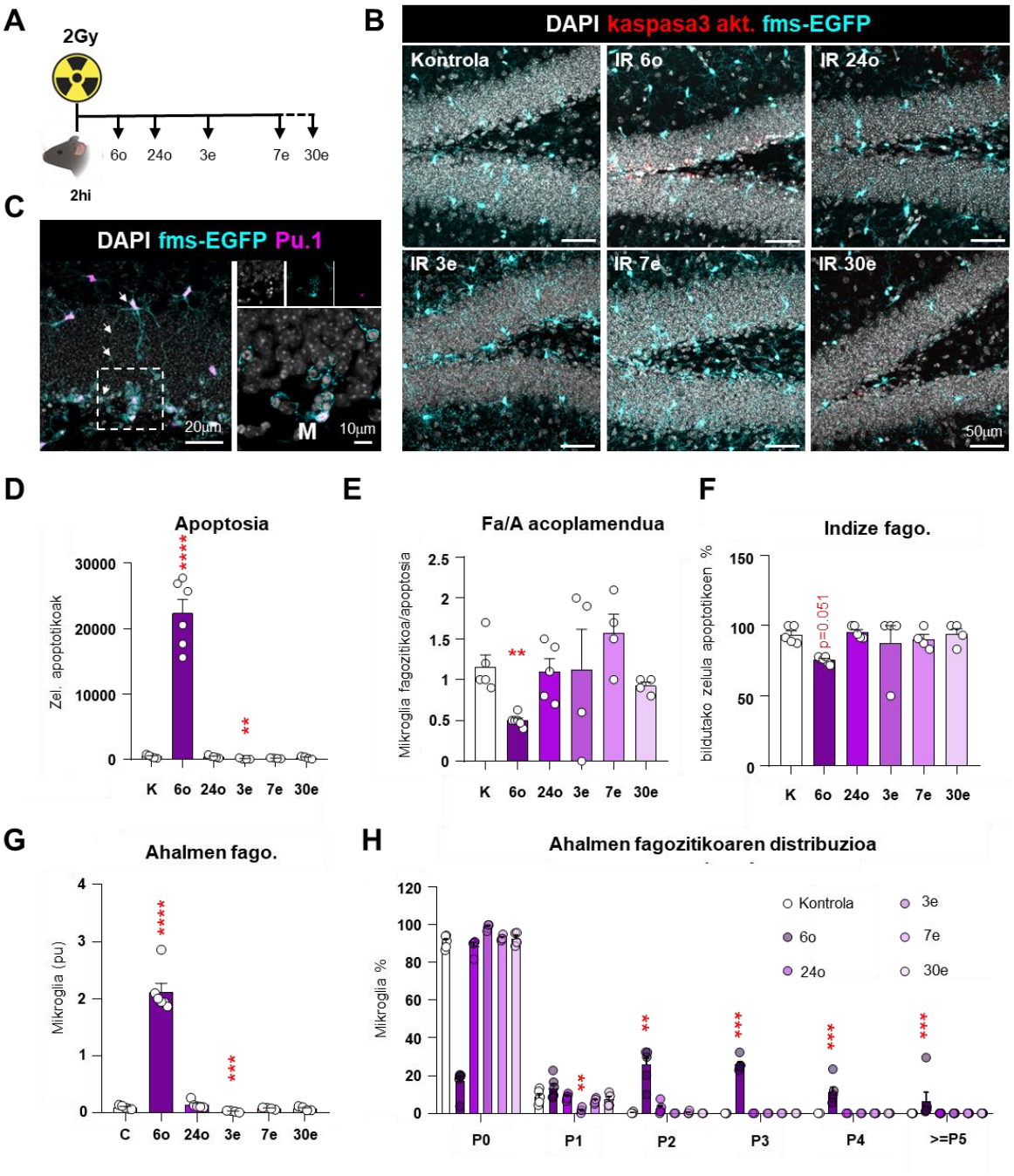

9. irudia. Garezurreko Irradiazio Baxuak (LCI) bultzatutako in vivo superfagozitosi eredua. (**A**) LCI bidezko superfagozitosiaren diseinu esperimentala. (**B**) Baldintza esperimentalen irudi konfokal adierazgarriak (Kontrol, 6o, 24o, 3e, 7e, 30e). Irudiak DAPI (zuria), kaspasa 3 aktibatua (gorria) eta GFP (ziana) tindaketak erakusten dituzte. (**C**) Irudi adierazgarriak, LCIaren ondoren. Irudiak DAPI (zuria), Pu.1 (magenta) eta GFP (zian) tintaketak erakusten dituzte. (**D**) DGko zelula apoptotikoen kopurua Hipokanpo septal bakoitzeko. (**E**) Fago/Apo akoplamendua gehikuntza-aldaketan adierazita (fagozitosi garbia, fagozitosiaren guztizko mailei dagokienez). (**F**) Indize fagozitikoa

(mikrogliak fagozitatutako zelula apoptotikoen %) (**G**) Ahalmen fagozitiko haztuta (mikroglia bakoitzeko nukleo apoptotikoz betetako poltsa fagozitikoen kopurua). Neurri honek poltsa fagozitioak microglía unitatezko adierazten ditu. (**H**) Ahalmen fagozitikoaren distribuzioa (poltsa fagozitikoak dituzten mikroglien %) LCIaren ondorengo hainbat denbora-puntutan (Kontrol, 6o, 24o, 3e, 7e, 30e) (**I**) Mikrogliak zelula apoptotiko bat ezabatzeko behan duen duen batez besteko denbora erakusten duen ezabatze denbora. Barrek n = 4-6 saguren batez bestekoa ± batez bestekoaren errore estandarra adierazten zituzten. Datuak bide bateko ANOVA baten bidez aztertu ziren, eta, ondoren, Holm-Sidak proba post hoc bidez, bidezkoa zenean. Datu batzuk [D, E, G, H] Log eraldatu ziren homozedastizitatea betetzeko. Homozedastizitatea bete ez zenean, Kruskal-Wallis proba egin zen [F, H]. Asteriskoek kontrolaren eta LCIaren arteko aldaketa esanguratsuak adierazten dituzte (6o, 24o, 3e, 7e, 30e). *** p < 0,01,*** p < 0,001 irudikatzen du. Eskala-barrak = *50µm [**B**], 20µm [**C**], 10µm (iruadiaren xehetasunak [**C**]n); z=21µm, z=17.5µm, z=25.2µm, z=13.3µm, z=16.1µm, z=14.7µm [**B**], z=13.3µm [**C**], z=4.2µm (iruadiaren xehetasunak [**C**]n).* BioRender.com *– ekin sortua.*

4.1.2 Mikroglia fagozitikoa DGn zehazki kokatua dago.

Ondoren, apoptosia eta fagozitosia ea zehazki nitxo neurogenoan zeuden ala ez zehaztu genuen, LCIak kalteak eragin baititzake eremu ez-neurogenoetan. Zehazkiago azalduta, hipokanpoko eremu ez-neurogeno batean, CAn (Cornu Ammonis) aztertu genuen apoptosia eta fagozitosia. Analisia LCIatik 6 ordura egin zen, eta immunofluoreszentzia eta irudi konfokala erabili genituen. GFP erabili zen behatzeko; eta zelula apoptotikoak DAPIrekin behatu ziren (**10. A irudia**).

LCIaren ondoren apoptosi indukzio txiki bat hauteman zen CAn (**10. B irudia**). Hala ere, CAn sortutako apoptosia DGn sortutakoa baino 26,3 ± 2,3 txikiagoa zen (**9. D irudia eta 10. B irudia).** CAn, fagozitosia ez zen gertatu kontrol saguetan, eta 6 ordutara, Fago. indizea 2,7 ± 0,6 aldiz txikiagoa zen DGn baino (**9. D irudia eta 10. C irudia**). DGrekin konparatuz, CAn kokatutako mikroglia fagozitikoaren ehunekoa 28,9 ± 10,3 aldiz txikiagoa zen eta bakarrik mifrogliaren % 4 ± 1,5 ari zen fagozitatsen (**9. H eta 10. D irudia**).

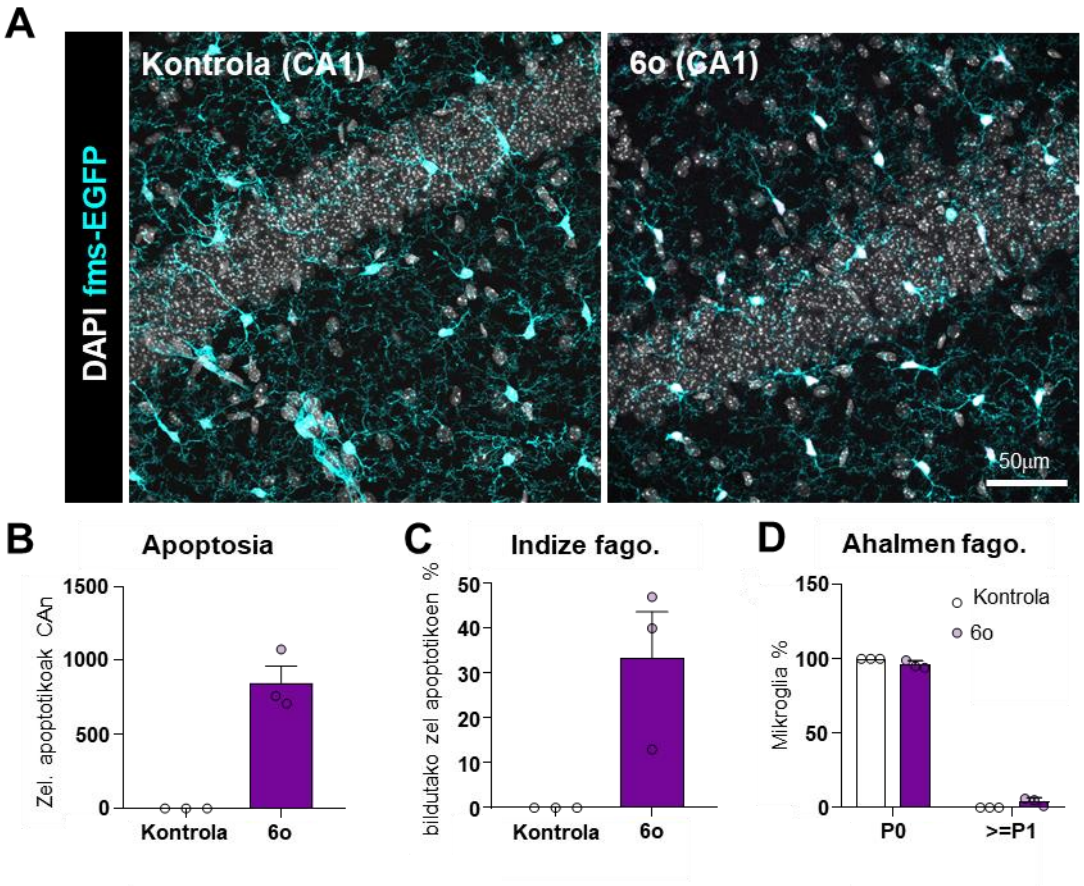

10. irudia. Fagozitosiaren analisia CA eremuan 6 ordu LCIaren ondoren. *(**A**) CAren irudi konfokal adierazgarriak, hainbat baldintza esperimentaletan (Kontrol eta 6o). Irudiak DAPI (zuria) eta GFP (zian) tindaketak erakusten dituzte. (**B**) CAko zelula apoptotikoen kopurua hipokanpo sekpal bakoitzeko. (**C**) Indize fagozitikoa (mikrogliak bildutako zelula apoptotikoen %). (**D**) Ahalmen fagozitikoa (poltsa fagozitikoak dituzten mikroglia) LCIaren ondorengo hainbat denbora-puntutan (Kontrol, 6o, 24o, 3e, 7e, 30e). Homozedastizitatea lortu ez zenean [B, C ,D], Mann Whitney proba egin zen. Barrek n = 3 saguren batez bestekoa ± batez bestekoaren errore estandarra adierazten zituzten Eskala-barrak = 50 m. [A], z = 14 m., z = 21 m.*

Oro har, datu hauek erakusten dute LCIak apoptosi gutxiago eragiten zuela CAn DGn baino. Halaere, CAko mikroglia ez zen hain eraginkorra hondakin apoptotiko fagozitatzen, DGko mikrogliarekin konparatzen badugu. Honek iradokitzen du CAkp zelulak ez direla hain sentikorrak LCIaren efektuari, eta eremu hartako mikroglia ez zegoela hain prestatuta fagozitosarako. Horrela, baieztatu genuen mikroglia fagozitikoa hipokanporen DGn zegoela kokatua. Horregatik, hurrengo ataletan DGko eta CAko mikroglia konparatuko dugu irradiazioak eragindako aldaketak (DGn zein CAn gertatzen direnak) eta fagozitosiak eragindakoak (DGren espezifikoak) bereizteko.

4.1.3 LCIak ez du kate bikoitzeko hausturarik (DSB) eragiten mikroglian.

Jarraian, LCIak mikrogliari kalte egiten ote zion ebaluatuko dugu, kate bikoitzeko hausturak aztertuz (DBS). H2AX fosforilatuaren (gamma-H2AX izenaz ere adierazita) adierazpena aztertuko dugu, irradiazioak ADNn eragindako kalte aztertzeko (Kavanagh et al., 2013). Horretarako, immunofluoreszentzia eta irudi konfokala egiten genituen. Irudien analisia nukleo guztietan (DAPI bidez markatuta) edo nukleo mikroglialen barruan (Pu.1 bidez markatuta) γH2AXren kopurua aztertu zuten. Bi adierazpen-eredu aurkitu genituen: γH2AX + nukleoak, larriki kaltetutako zelulak irudikatzen zituztenak; eta γH2AX punkta zuten nukleoak, hain kaltetuak ez zeuden zelulak irudikatzen zituztenak (Scarpato et al., 2013). γH2AX+ nukleo-kopurua eta H2AX punkta bolumena nukleoen barruan 6 ordura igo ziren, eta behera egin zuten ondorengo denbora-puntuetan (R3A, C irudia). Garrantzitsua da nabarmentzea γH2AX+ nukleoetako bat bera ere ez zela mikrogliarena (Pu.1 bidez identifikatuak), eta H2AX punktaren bolumen txiki bat baino ez genuen aurkitu nukleo mikroglialetan. DGko gainerako nukleoak baino 7,2 ± 1 aldiz txikiagoa zena (**11. B, E irudia**). Datu horiek iradokitzen dute LCIak kalte handia eragin zuela DGko nukleoen ADNn, baina kalte askoz hondarragoa ADN mikroglialean, ziurrenik mikroglia kieszentea delako eta ez delako ugaritzen baldintza fisiologikoetan (Reu et al., 2017). Horrela, baieztatzen dugu gure fagozitosi-eredua estrategia ona zela fagozitosiak eragindako aldaketak aztertzeko, mikrogliaren irradiazioaren eragin minimoekin.

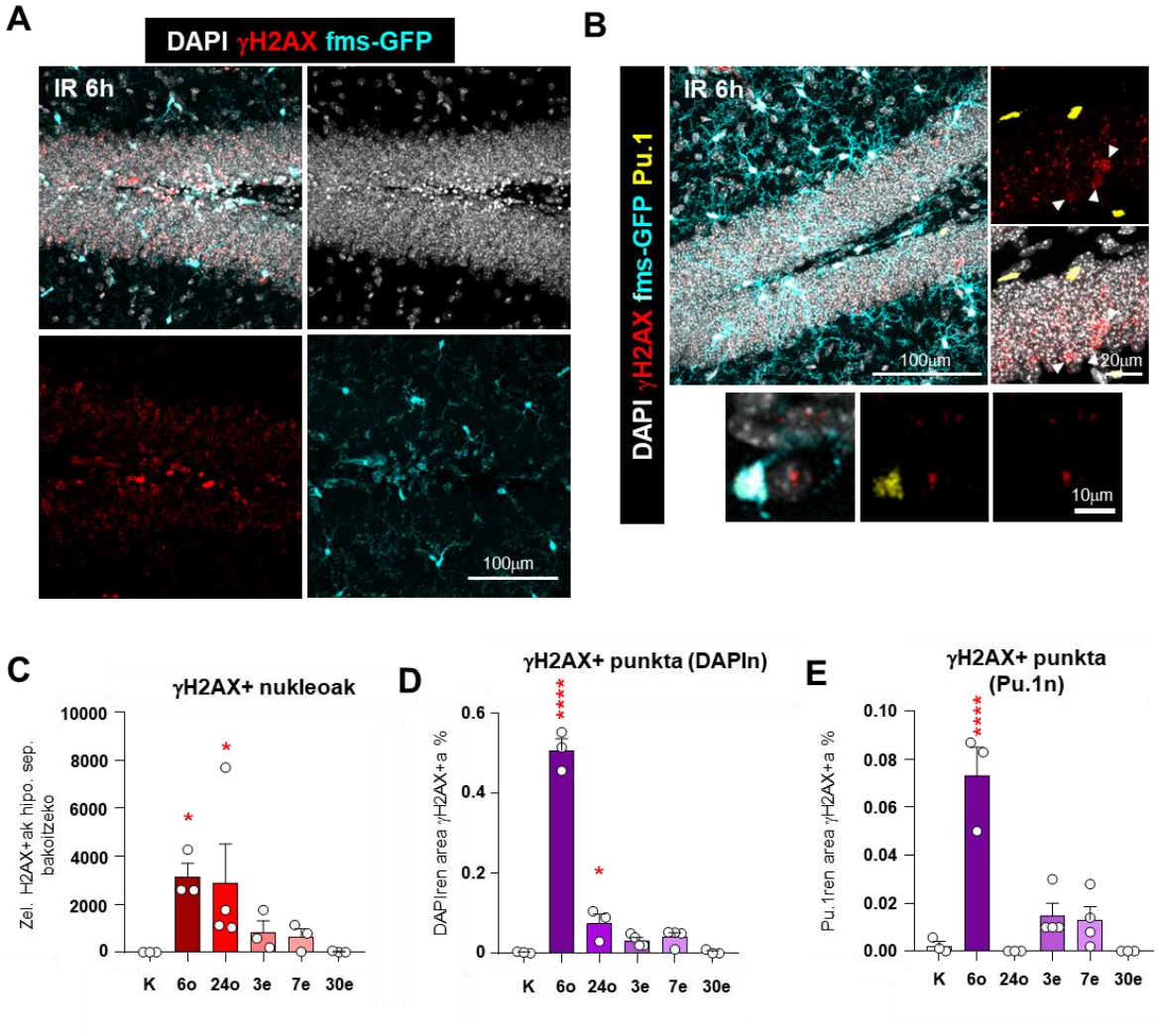

11. irudia. ADNn eragindako kaltearen azterketa, KBHen ebaluazioaren bidez. *(**A**) H2AX punktaren LCIaren 6 ordura irudikatzen duten irudi konfokalak, DAPI tindaketa (zuria), H2AX tindaketa (gorria) eta GFP tindaketa (ziana) erakusten dutenak. (**B**) Zelula H2AX+ (gorri)en nukeoaren eta DAPI (zuria) ez-mikrogliaduna zein DAPI+Pu.1 (zuria eta horia)z edukitutako mikrogliadun nukeoaren irudi adierazgarriak, gezi-punta zuriz adierazita daudenak. Mikroglia GFP tindaketarekin erakusten da (zian). (**C**) DGko H2AX+ zelula-kopurua hipokanpo septal bakoitzeko. (D) Bolumen nuklearraren ehunekoa (DAPIn), γH2AX punktaz okupatutaz. (**E**) Bolumen nuklear mikroglialaren (Pu.1) ehunekoa, γH2AX punktaz okupatua. Barrek n = 3-4 saguren batez bestekoa ± batez bestekoaren errore estandarra erakusten dute. Datuak bide bakarreko ANOVA probaren bidez aztertu ziren, eta, ondoren, Holm-Sidaken post hoc probak, egokia izan zenean. Homozedastizitatea lortu ez zenean, Kruskal-Wallisen proba egin zen [C]. Asteriskoek kontrolaren eta beste denbora-puntuen (6o, 24o, 3e, 7, 30e) arteko aldaketa esanguratsuak adierazten dituzte. * p < 0,05,*** p < 0,001 irudikatzen du. Eskala-barrak = 100µm [A], 100µm [B], 20µm, 10µm ([C]n txertatuak); z=16.8µm [A], z=26.6µm, z=0.7µm [B]*

4.1.4 LCIak ez du monozitoen infiltraziorik eragiten.

LCIak eragindako kalteen hedadura ebaluatzeko, monozitoen infiltrazioa ebaluatu genuen, jakina baita erradiazio ionizatzaileak arriskuan jartzen dutela garunaren muga hematoentzefalikoa (HH) (Trnovec et al., 1990). Gure fms-EGFP animali-ereduan mikroglia eta makrofagoek GFP adierazten dutenez, GFPrako eta P2Y12 (Paolicelli et al., 2022) mikroglia-markatzailerako immunofluoreszentzia egiten genuen bi populazioak bereizteko. Ikusi genuen irradiazioak ez zuela monozitoen (GFP+/P2Y12-) ehunekoa handitzen LCIaren ondorengo edozein denbora-puntutan (**12. A-B irudia**), LCIaren ondoren monozito infiltraziorik ez zegoela iradokiz.

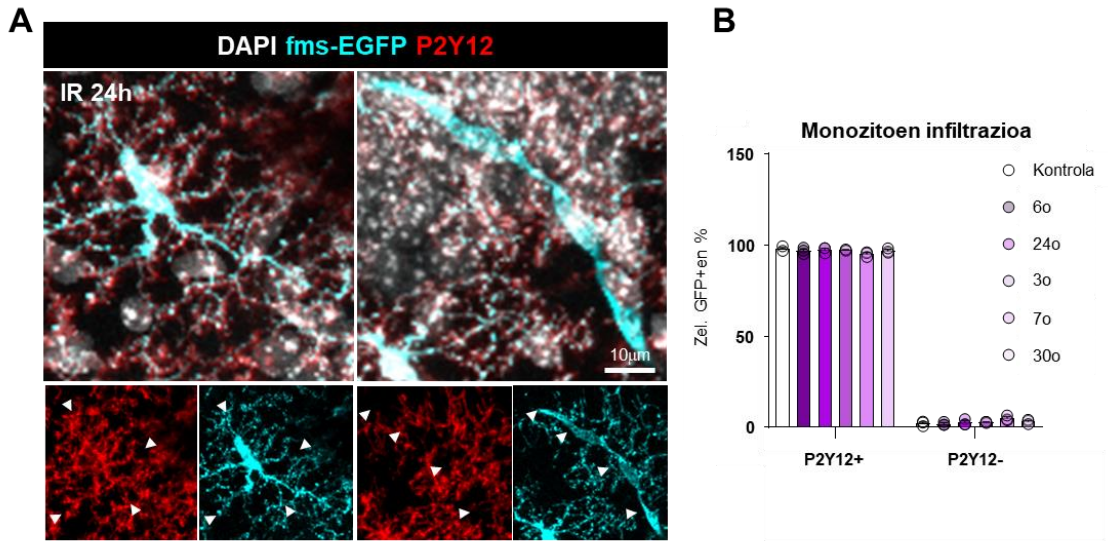

***12. irudia. LCIaren osteko infiltrazio monozitikoaren analisia**. (**A**) Mikrogliaren eta monozitoen konfokal irudiak 24 ordu LCIaren ondoren. Mikrogliak P2Y12 (gorria) eta GFP (ziana) ditu; monozitoek, berriz, GFP (ziana) baino ez dute adierazten. DAPI bidezko tindaketak (zuria) nukleoak erakusten ditu. Zelulak gezi punta zuriekin adierazten dira. (**B**) Mikrogliak (GFP+/P2Y12+) eta monozitoak (GFP+/P2Y12-) diren GFP+ zelulen ehunekoa. Barrek n = 3 saguren batez bestekoa ± batez bestekoaren errore estandarra erakusten dute. Eskala-barra: 10µm; z= 17,5µm.*

Laburbilduz, in vivo "superfagozitosi" ereduaren baliozkotzeak agerian utzi zuen eredu hori baliagarria zela mikrogliaren aldaketa postfagozitikoak aztertzeko, DG mikroglia fase fagozitiko batean sinkronizatzen zuelako, ADN mikroglialean kalte minimoa eraginez eta monozitoen infiltraziorik eragin gabe.

Horrela, LCIak aukera eman zigun hipokanpoaren DGan kokatutako zelula fagozitikoetan aberastutako mikroglia-populazioa lortzeko. Hurrengo ataletan, hainbat estrategia deskribatuko ditugu mikroglia postfagozitikoa identifikatzeko markatzaile posibleak aurkitzeko. Horretarako, mikrogliaren aldaketa morfologikoak eta transkripzionalak aztertuko ditugu fagozitosiaren ondoren, eta horietakoren bat mikroglia fagozitikoaren identifikatzaile gisa baliagarria den aztertuko dugu.

4.2: Mikroglia postfagozitikoa identifikatzea eta ezaugarritzea.

Emaitzen lehen atalean, DG mikroglia estadio fagozitiko batean sinkronizatzen zuen "superfagozitosi" eredua baliozkotu genuen. Honetaz baliatuz, fagozitosiak zelula horietan zituen ondorioak aztertu genituen. Atal honetan, fagozitosiaren ondoren aldaketak izan ditzaketen hainbat parametro aztertuko ditugu, fagozitoen ondorengo zelulen markatzaileak aurkitzeko, hala nola morfologian eta geneen edo proteinen adierazpenean aldaketak behatzeko.

4.2.1 Morfologia mikroglialak ez ditu zelula postfagozitikoak identifikatzen.

Morfologia mikrogliala bere funtzioaren adierazle gisa erabili ohi da (Young et al., 2018). Hala ere, funtzioaren eta morfologiaren arteko lotura asko eztabaidatu da, baina ez da haien arteko lotura ondorioztatu (Paolicelli et al., 2022). Adibidez, "ameboide" morfologia mikroglia fagozitikoarekin lotu da. Alabiana, orain argi dago mikroglia adarkatuak bere adar terminalen bidez gauzatzen duela fagozitosia egoera fisiologikoetan (Sierra et al., 2010), eta gaixotasun batzuetan bakarrik (adibidez, epilepsian eta iktusean) aposizio bidezko fagozitosia egiten dutela, zelula-gorputzetatik hurbil dauden zelula apoptotikoak bakarrik irentsiz (Abiega et al., 2016; Beccari et al., 2023). Gure "superfagozitosi" in vivo ereduan morfologia mikrogliala aztertzeko, mikrogliaren Sholl analisi bat egiten dugu, LCIaren ondoren mikrogliaren prozesuen luzera eta prozesu kopurua kuantifikatzeko (**13. A irudia**).

Ez ditugu desberdintasunik aurkitzen zelula-zentrotik neurtutako prozesuen luzeraren banaketan, ezta prozesuen gehieneko luzeran ere (**13. B-C irudia**) esperimentuan definitutako denboretan zehar (6h, 24h, 3d, 7d, 30d). Era berean, ez ditugi desberdintasunik aurkitzen prozesu-kopuruaren maiztasunen banaketan, ezta prozesuen guztizko kopuruan ere (**13. D-E irudia**). Fagozitosiaren eragina modu espezifikoagoan aztertzeko, zelula "superfagozitikoak" eta ez-fagozitikoak alderatzen ditugu LCIaren ondorengo 6 orduetan. Zelula "superfagozitikoek" prozesu gutxiago eta prozesuekiko distantzia maximoan beheranzko joera zutela ikusi genuen (**13. F-I irudia**). Beraz, mikrogliak fagozitosia burutzen duen bitartean, poltsiko fagozitikoak erakusten zituen eta morfología sinpleago bat erakusten zuen. Horrek, fagozitosia burutzen duen bitartean, mikrogliaren zaintza murriztuta egon ahal dela iradokitzen du. Hala ere, fagozitosiaren osteko mikrogliak ez zuen morfologia aldaketa sendorik erakutsi, morfologia postfagozitosiaren adierazle fidagarri gisa balora zezakeenik. Laburbilduz, gure datuek erakusten dute morfologia ez dela adierazle egokia mikroglia postfagozitikoa identifikatzeko.

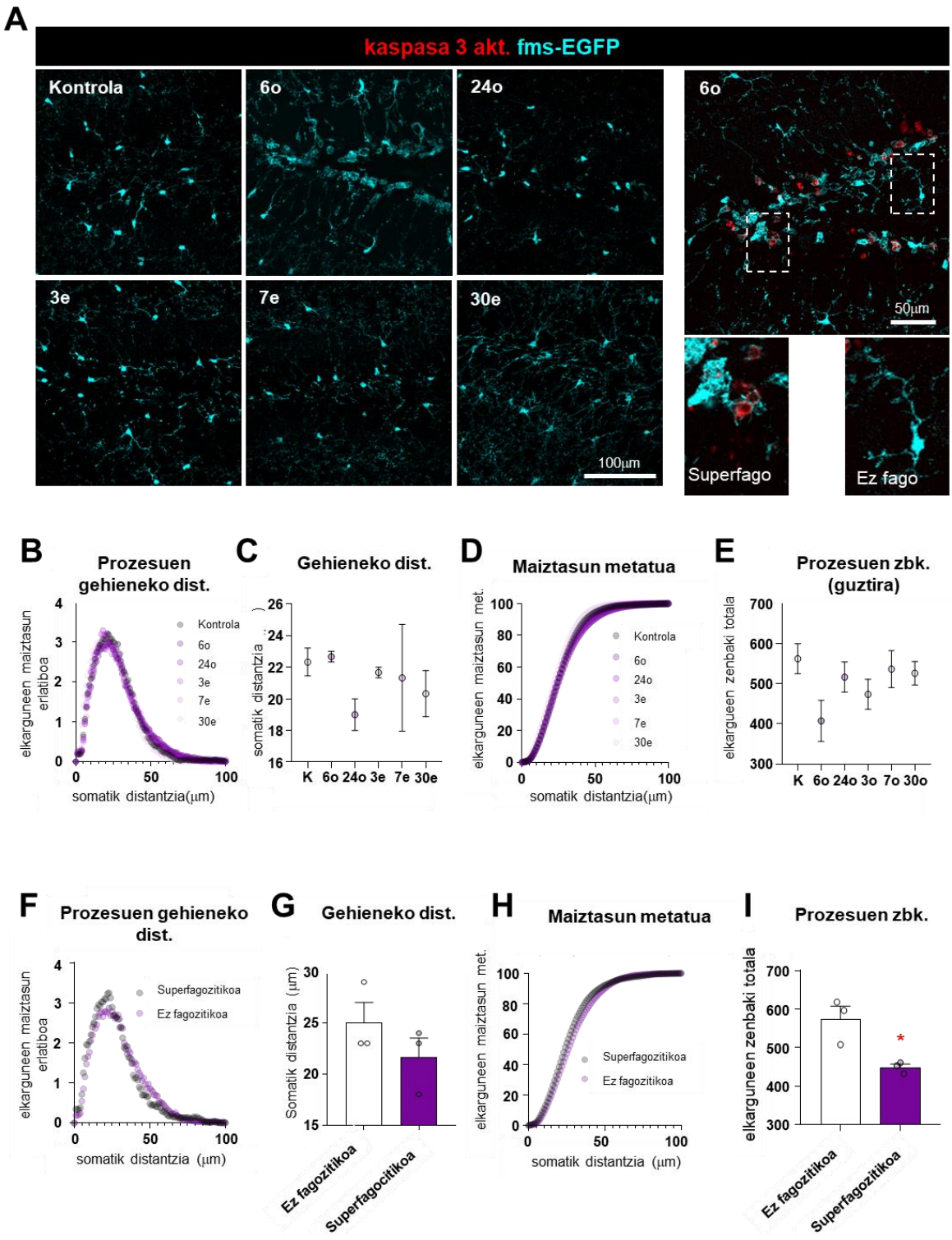

13. irudia. Fagozitosiaren osteko mikrogliaren analisi morfologikoa. *(**A**) Hainbat baldintza esperimentaletan (Kontrol, 6h, 24h, 3d, 7d, 30d) morfologia mikrogliala irudikatzen duten irudi konfokalak, eta "superfagozitikoa" eta fagozitikoa ez den mikrogliaren xehetasun adierazgarri bat (karratu zuri punteztatua), 6 ordutan, 3 aktibatutako kaspasa-tindaketa (gorria) eta GFP tindaketa (ziana) erakutsiz. Mikroglia-morfologiaren sholl analisia, LCIren ondoren, honako hauek alderatuz: Kontrola, 6h, 24h, 3d, 7d eta 30d, honako hauek erakutsiz: (**B**) elkarguneen maiztasun erlatiboa, somatik dagoen distantziarekin korrelazioan; (**C**) prozesurik distalenaren gehieneko distantzia; (**D**) elkarguneen maiztasun metatzailea, somatik dagoen distantziarekin korrelazioan;*

*(**E**) intersekzioen guztizko kopurua, prozesuen guztizko kopurua adierazten duena. Morfologia mikroglialaren Sholl analisia, LCIren 6 orduren ondoren, mikroglia ez-fagozitikoa eta superfagozitikoa alderatuz: (**F**) elkarguneen maiztasun erlatiboa, somatik dagoen distantziarekin korrelazioan, (**G**) prozesurik distalenaren gehieneko distantzia, (H) elkarguneen maiztasun metatzailea, somatik dagoen distantziarekin korrelazioan, (I) prozesu kopuru osoa adierazten duen elkarguneen guztizko kopurua. Puntu koloreztatuek n = 3 saguren batez besteko balioak erakusten dituzte. Errore-barrak dituzten [C, E] kolore-puntuek esperimentu independenteen ± SEM batez bestekoa erakusten dute. Datuak norabide bakarreko ANOVAren bidez aztertu ziren, eta, ondoren, Holm-Sidaken hoc osteko probak egin ziren [C, E] bidezkoa zenean, eta Student-en t probaren bidez [G, I]. Izartxoek ez-fagozitikoaren eta superfagozitikoaren arteko esanahia adierazten dute.* p < 0,05 adierazten du. Eskala-barrak =100µm [A], 50µm [A, 6h detail]. z=21µm, z=15.4µm, z=18,9; z=8.4µm, z=14µm, z=12.6µm[A], z=11,9µm [A, 6h detail].*

4.2.2 Mikroglia hipokanpalaren zelula bakarren RNAseq-a, DGko biztanleria "superfagozitikoa" identifikatzeko tresna gisa.

Morfologia mikroglia postfagozitikoa identifikatzeko baliagarria ez zenez, jarraian, transkripzio-aldaketek LCI ereduaren mikroglia fagozitikoa identifika zezaketen ebaluatuko dugu, Horretarako, zelula bakarren RNA sekuentziazioa erabiliko da (scRNA-Seq), eta aldaketa horiek in situ baliozkotuko ditugu, immunofluoreszentzia eta RNAScope teknikak erabiliz. Transkripzio-aldaketa batzuk irradiazioaren ondorio izatea espero genuen (nukleo mikroglialetan kalte txikia izan arren), eta beste transkripzio-aldaketa batzuk, fagozitosi osteko egokitzapenen ondoriozkoak. Irradiazioak aldaketa handiagoak eragingo lituzke mikroglia osoan, kokapena edozein dela ere, eta fagozitosiak, berriz, aldaketa espezifikoak eragingo lituzke DGn.

Gure laborategiak, aldez aurretik, fagozitosiak *in vitro* mikroglian eragindako transkripzio-aldaketak identifikatu zituen, zelula apoptotikoak irentsi zituzten mikroglia aztertuz eta gorantz edo beherantz 3 ordu eta 24 ordura aldatutako milaka gene agerian utziz (Diaz-Aparicio et al., 2020). Datu horietan oinarrituta, epe laburreko (24 ordu) eta epe luzeko (7d) "superfagozitosi" *in vivo* ereduan izandako aldaketa postfagozitikoak ebaluatzen ditugu, bi taldeak dagozkien kontrol irradiatu gabeekin alderatuz (24 orduko kontrola eta 7d kontrola) (**14. A-B irudia**). Lehenik eta behin, monozito zirkulatzaileak kentzen ditugusaguen perfusioan gatz-disoluzioa, eta, ondoren, CD11b+ zelulak aukeratzen ditugu, mikroglia eta SCNri lotutako makrofagoak barne (Masuda et al., 2022). Ondore zelula horiek kapsulatzen ditugu 10X Genomics mikrofluido-ganbera bat erabiliz. Horri esker, liburutegiak sortu eta ondorengo analisi bioinformatikoa egin ahal izan genuen (**14. A irudia**).

Sekuentziazio-datuak Jose Pascual López Atalaya eta Ángel Márquez Galerarekin (Instituto de Neurociencias - CSIC/UMH) batera iragazi eta aztertu ziren. Gure analisiak kalitate-kontrola izan zuen. Ondorioz, kalitate txikiko zelulak iragazi ziren. Jarraian, datuak bistaratzeko teknikak trazatu genituen, eta puntu-lainoan nabarmentzen ziren klusterrak aukeratu genituen. Ondoren, kluster txikiak ezabatu genituen(< 200 zelula), eta gainerako klusterrak definitu genituen, haien adierazpen genikoan eta aurretiazko literaturan oinarritutuz. Azkenik,

klusterren aldaketa espezifikoak aztertu genituen (klusterren eta geneen tamaina) eta *in situ* baliozkotuko ditugu (**14. B irudia**).

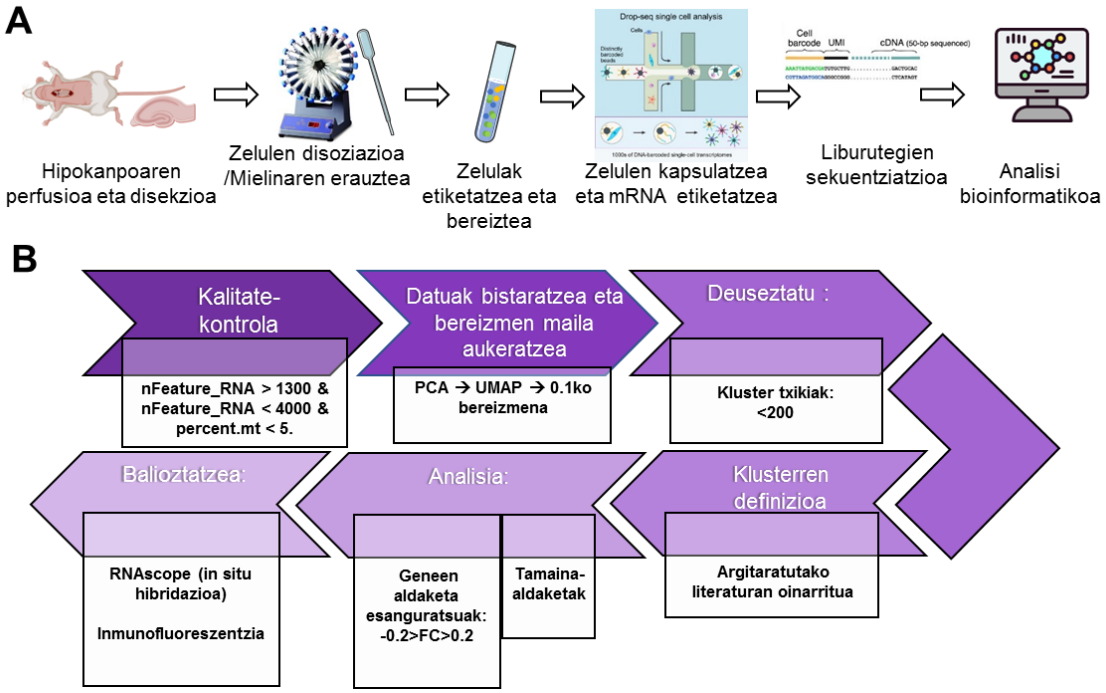

14. irudia. Zelula-bakarren RNAseq analisiaren laburpen grafikoa (laginak prozesatzea eta datuak iragaztea). (***A***) *Laginen prozesamenduaren laburpena.* (***B***) *Datuak iragazteko, aztertzeko eta baliozkotzeko kronograma.*

4.2.3. ScRNA-Seq datuen kalitate-kontrola.

Lehenik, baldintza esperimental desberdinen transkripzio-datuen kalitate-kontrola egin genuen, hiru gertaera mota ezabatuz: 1, multiplete putatiboak, hau da, behar bezala indibidualizatu ez diren zelulak (>4.000 geneko zelulak); 2, kalitate txikiko zelulak (< 1.300 generekin); eta 3, kaltetutako zelulak (>%5 gene mitokondrialekin). Iragazteak 18.484 zelula deuseztatzea ekarri zuen, azken emaitza 46.861 zelula izan zirelarik. (**15. Irudia**).

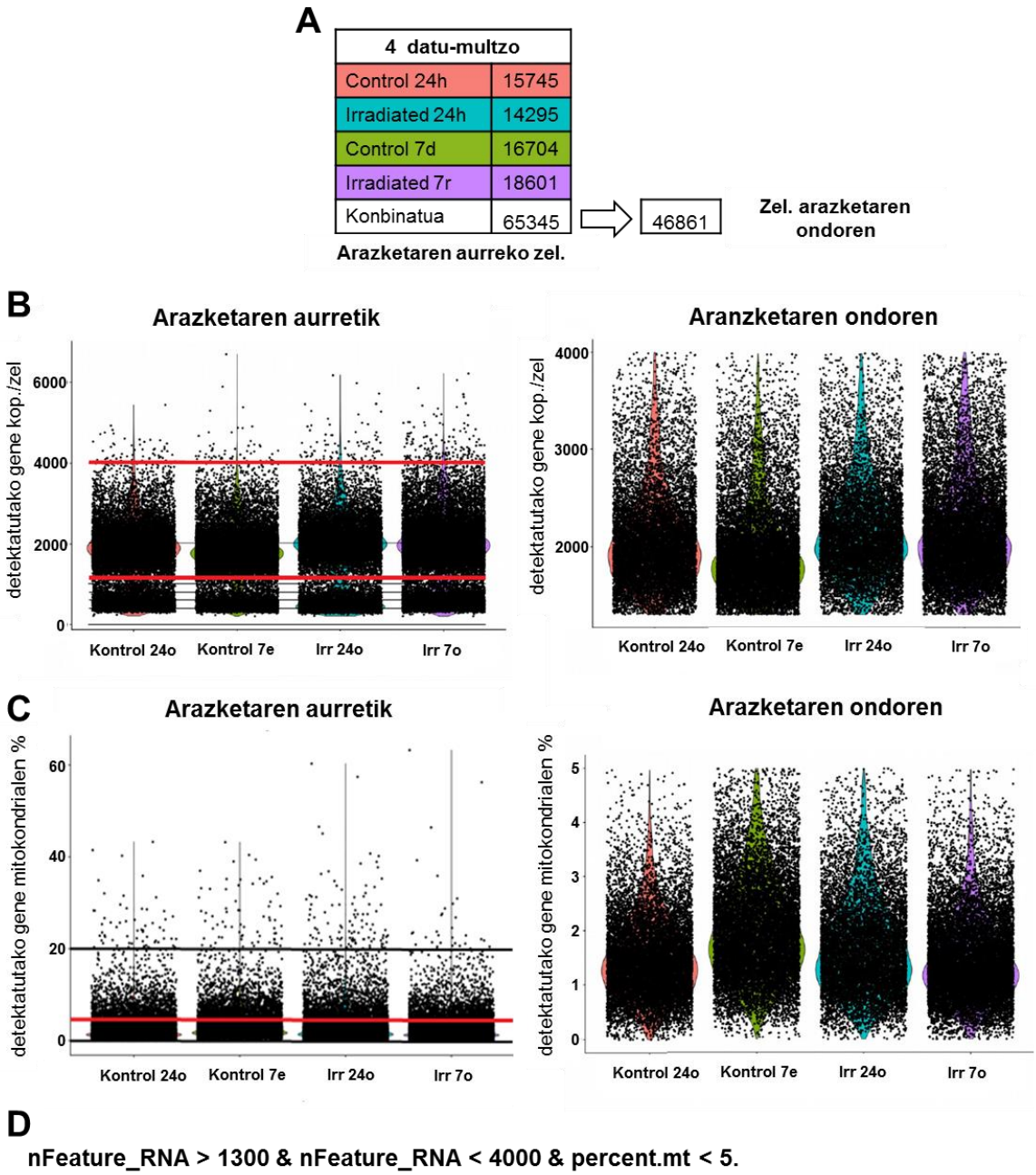

15. irudia. Zelula bakarreko RNAseq datuen kalitate-kontrola. (**A**) Baldintzaren arabera sekuentziatutako zelulen guztizko kopuruaren laburpen-taula eta (**B**) Violin-plot iragazketaren ondoren iragazi aurretik (ezkerrean) eta iragazi ondoren (eskuinean) zelula bidez detektatutako geneen kopurua. Marra gorriek iragazteko ezarritako atalaseak adierazten dituzte. (**C**) Zelulaz detektatutako gene mitokondrialen %eko biolin-plota, iragazi aurretik (ezkerrean) eta iragazi ondoren (eskuinean). Marra gorriek iragazteko ezarritako atalaseak adierazten dituzte.

4.2.4 Tamaina murriztea, bereizmena hautatzea eta kluster txikiak ezabatzea.

Multipletak, kalitate gutxiko zelulak eta zelula kaltetuak ezabatu ondoren, datu-multzoaren zelula-konglomeratuak aztertuko ditugu, dimentsionalitatea murriztuz. Dimentsionalitatearen murrizketa honetan datza: zelula bakoitzaren transkriptorearen informazioa duen dimentsio handiko jatorrizko matrizea seinale erabilgarriekin aberastutako azpiespazio txikiago batean eraldatzea (Nguyen, 2022). Lehenik eta behin, osagai nagusien analisia egiten dugu, datuak koordenatu-sistema berri batean linealki eraldatzeko, eta, ondoren, multiploen hurbilketa eta proiekzio uniformea (UMAP) gauzatzen da (**16. A-B irudia**). UMAP, zelula bakarreko RNAseq datuak bistaratzeko urrezko estandar bat da, zelulak transkribapen-antzekotasunen arabera marrazten ditu, haien arteko erlazioak aurkitzeko (taldekatzea) erabili ohi dena (Sivarajah, 2020). Gainbegiratu gabeko taldekatze-analisi bat ere egiten dugu, hurbileneko bizilagun partekatuaren (SNN) modularitatearen optimizazioan oinarritutako taldekatze-algoritmoa erabiliz. Hori UMAP grafikoan bistaratu zen. Zelulen klusterrak identifikatzen ditugu, ondoren aztertzeko, eta, horretarako, bereizmen-parametroa erabiltzen dugu. Parametro horrek zelulak klusterretan banatzen ditu, haien artean dauden desberdintasun transkripzionalen arabera. Bereizmen altua aplikatuta, sentsibilitate handiagoa lortzen da desberdintasun horiek hautematean; balio baxuagoek, berriz, sentsibilitate txikiagoa adierazten dute. 3 bereizmen-balio desberdin probatu genituen (gutxieneko distantzia = 0,8, 0,5 eta 0,1), eta gutxieneko bereizmena aukeratu genuen (0,1), hobeto adierazten baitzuen UMAPen irudikatutako hodei-forma, nahiz eta kluster mikroglialetan (16C irudia) aldaketa sotilak izan. Bereizmen horrekin, 8 konglomeratu identifikatu genituen (0-7), eta horietatik 5, 6 eta 7 konglomeratuak ezabatu egin ziren zelula-kopuru txikiaren ondorioz (< 200). Hautatutako ebazpenak, 0,1ekoak, ez zuen gainjartzerik ekarri, kluster txikiak babestuz, hala nola 3. eta 4. azpipopulazioak, tamaina berari eutsi baitzioten. Horrek, aukeratutako ebazpenak ondo definitutako populazioak eraginkortasunez mantendu zituela iradokitzen du. Gainerako multzoak (0, 1, 2, 3 eta 4) jarraian aztertu ziren (**16. D-E irudia**).

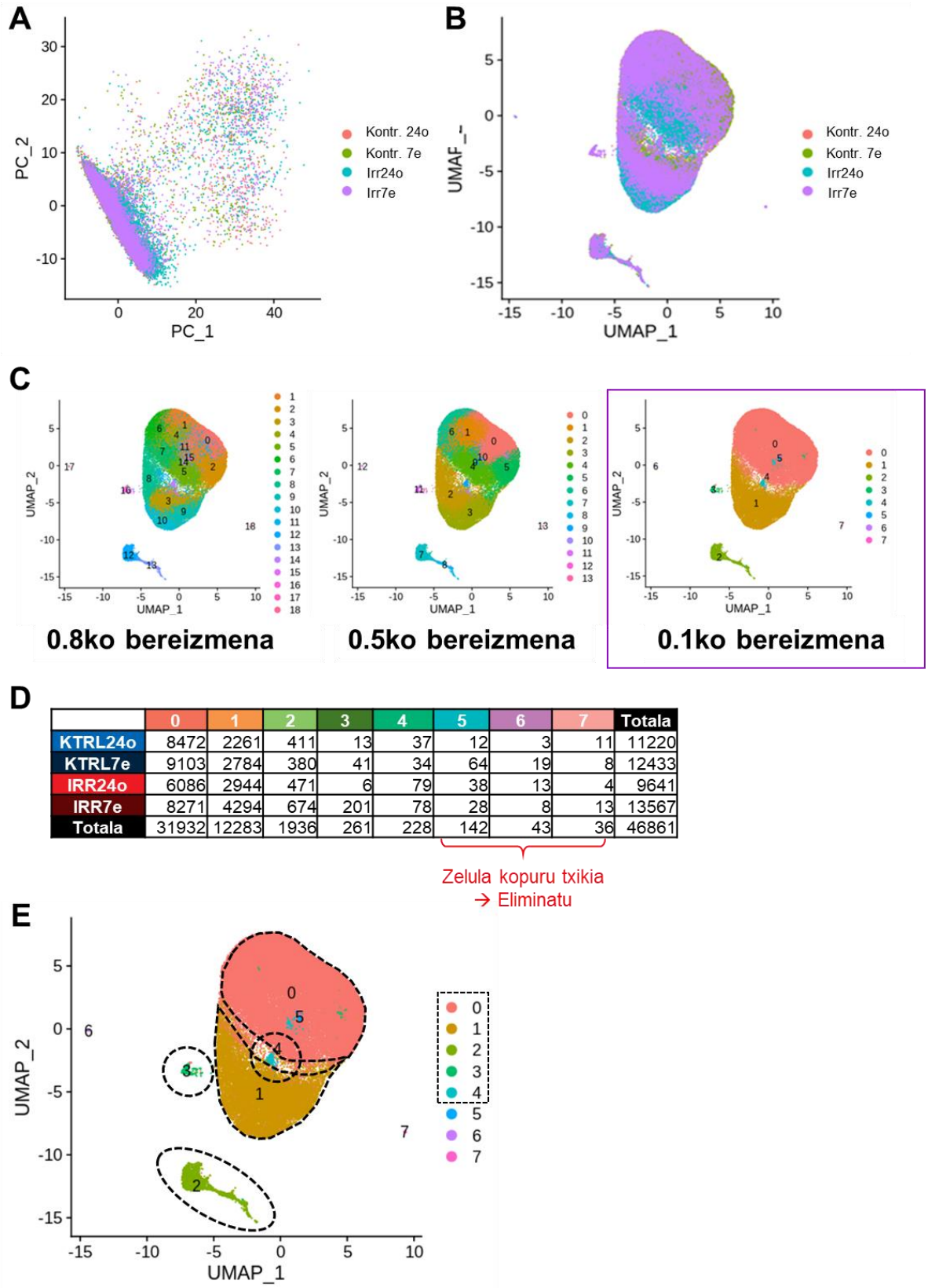

	0	1	2	3	4	5	6	7	Totala
KTRL24o	8472	2261	411	13	37	12	3	11	11220
KTRL7e	9103	2784	380	41	34	64	19	8	12433
IRR24o	6086	2944	471	6	79	38	13	4	9641
IRR7e	8271	4294	674	201	78	28	8	13	13567
Totala	31932	12283	1936	261	228	142	43	36	46861

Zelula kopuru txikia
→ Eliminatu

16. irudia. Tamaina murriztea, bereizmena aukeratzea eta tamaina txikiko konglomeratuak ezabatzea. *(**A**) PCA analisia. (**B**) Hainbat tratamenduren datu fusionatuen UMAP bistaratzea. (**C**) UMAP grafikoak, kluster-irteerak bereizmen-parametro desberdinekin erakutsiz (0,8, 0,5 eta 0,1). (**D**) Kluster eta tratamendu bidez*

*detektatutako zelulen laburpen-taula. Gorriz idatzitako oharrek ezabatutako klusterra erakusten dute, zelula-kopuru txikiaren ondorioz. (**E**) Hautatutako klusterren UMAP, beltzez punteatutako lerroekin inguratuta.*

4.2.5 Klusterrak izendatzea

Azkenean hautatutako klusterrak identifikatzeko, haien gene bereizgarriak aztertuko ditugu (gehien adierazitako 20 geneak) eta aurreko literaturan oinarrituta dagoen arabera definituko ditugu (**17. A-B irudia**). Duela gutxi egindako scRNA-Seq azterketek mikrogliako 5 kluster nagusi definitzen dituzte: homeostatikoa, gaixotasunarekin lotutakoa (DAM), histokonpatibilitateko konplexu handiagoa (MHCII), interferonarekiko sentikorra (IFN) eta ugaritzailea (Chen et al., 2021). Gainera, makrofago espezializatuen beste populazio batzuk ere badaude, hala nola CAMak, gure prestaketan presente egon daitezkeenak (Masuda et al., 2022). Gainera, mikrogliak ex vivo ehunaren prozesamenduari erantzuten dio, eta horrek transkripzio-sinadura artifizial bat sortzen du (Marsh et al., 2022b), analisitik kendu behar dena. Gure analisian lortutako sinadura-geneak ikerketa horien sinadura-geneekin parekatzean, gure klusterrak definitu genituen, CAM klusterra identifikatu genuen eta prozesamenduak zein zelula aktibatu zituen zehaztu genuen.

0 klusterra "homeostatiko" gisa identifikatu genuen, lau gene (P2RY12, SIGLECH, HEXB, TMEM119) bat zetozelako sinadura genetiko homeostatikoarekin. 1. taldea "ex vivo aktibatuta" (exAM) gisa identifikatu genuen, zazpi gene (EGR1, ZFP36, NFKBIZ, CCL4, FOS, JUNB, ATF3) bat zetozelako prozesamendu erreaktiboko sinadurarekin (Marsh et al., 2022b). 2. klusterra "MHC" gisa identifikatu genuen, lau gene (CD74, H2-EB1, H2-AA, H2AB1) bat zetozelako MCHII sinadurarako deskribatutako geneekin. Hala ere, 2. klusterraren sinaduraren beste hiru gene beste sinadura batzuetan identifikatu dira: APOE (DAM sinadura), eta PF4 eta MS4A7 (CAM sinadura). Beraz, sinadura-gene gehienak MHC populazioari zegozkionez, kluster horri izen hori eman zitzaion azkenean. 3. klusterra "ugaritzaile" gisa identifikatu genuen, lau gene (TOP2A, H2AFZ, MKI67, CENPE) bat zetozelako sinadura ugaritzailearekin. 4. taldea "IRM" gisa identifikatu genuen (interferonarekiko mikroglia sentikorra), bost gene (IFITM3, ISG15, IRF, USP18, OASL2) bat zetozelako IRM sinadurarekin. (**17B irudia**).

Beraz, aldez aurreko azterlanetan oinarrituta, gure klusterrak honela definitzen ditugu: homeostatikoa (0), erreaktiboa (1), MHCII (2), ugalkorra (3) eta IRM (4) (**17C irudia**). Jarraian, kluster homeostatikoen, MHCIIren, ugalketa-klusterren eta MRIren aldaketak aztertuko ditugu, tamainan eta adierazpen genikoan, kluster horietako zein zegoen fagozitosiarekin lotuta identifikatzeko. Cluster erreaktiboa, laginaren prozesamenduak eragindako artefaktua, ez zen gehiago aztertu.

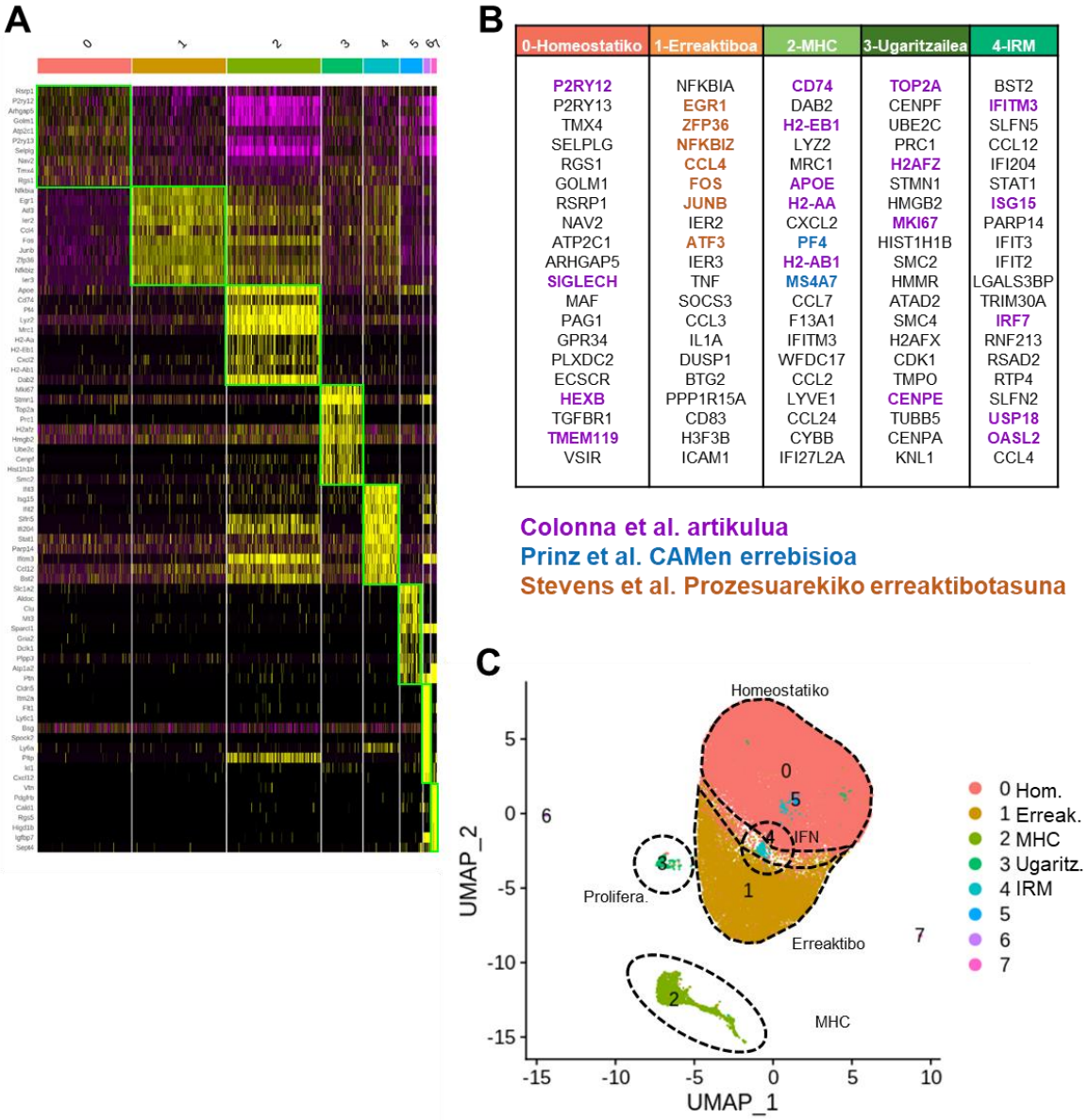

17. irudia. Klusterrak scRNA-seq-en aurretiazko azterketetan oinarrituta identifikatzea. *(**A**) Klusterrak gehien adierazitako 10 geneen heatmap-a. (**B**) Laburpen-taula, kluster bakoitzeko 20 gene nagusiekin. Purpura ilunean, Colonnaren laborategiak definitutako hainbat azpipopulazio mikroglialetarako deskribatutako geneak (Chen et al., 2021). More argian, Prinzen laborategiak CAMentzat deskribatutako geneak (Masuda et al., 2022). Laranjaz, Steven (Marsh et al., 2022b) (**C**) UMAPen laborategiak prozesatzeko mikroglia erreaktiborako deskribatutako geneak, beltzezko puntu-lerroek inguratuak eta dagozkien izenekin etiketatuak.*

4.2.6. LCIak eragindako aldaketak transkribapen-tamainan eta -sinaduran

Mikrogliako klusterrak identifikatu ondoren, tratamenduen arteko kluster bakoitza nola aldatzen zen aztertuko dugu (24 h eta 7 d kontrolak, 24 h eta 7 d irradiatuak), eta horien kokapena (profil transkripzionala) eta tamaina (biztanleriaren tamaina) ebaluatuko ditugu UMAPen. Kluster homeostatikoa beherantz mugitu zen

irradiazioaren ondoren 24 orduko cluster erreaktiborantz, eta 7d-ko oinarrizko egoerara itzuli zen. Horrek iradokitzen du LCIk populazio homeostatikoan mikroglia erreaktiboko geneen transkripzioa eragiten duela. Beste aldaketa nabarmen bat kluster ugaltzailean gertatu zen, nabarmen handitu baitzen bere tamaina 7d irradiazioaren ondoren (**18. irudia**). Jarraian, kluster guztietako gene-adierazpenaren aldaketak ebaluatuko ditugu.

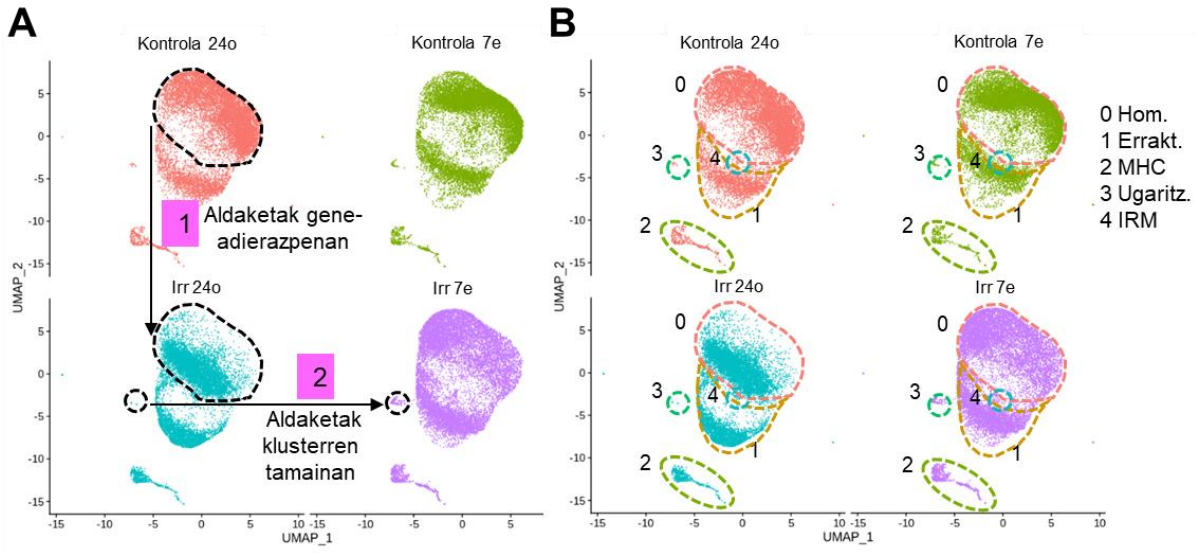

18. irudia. Klusterren tamainaren eta transkriptomaren aldaketen azterketa orokorra. *(**A**) UMAP, klusterraren tamainaren aldaketa eta klusterraren transkriptorearen aldaketa deskribatzen duten oharrekin (purpura) egindako tratamenduena. (**B**) puntu-lerroekin egindako tratamenduen UMAPa, kluster bakoitzaren jatorrizko banaketa adieraziz (24 orduko kontrola) (0 = homeostatikoa, 1 = erreaktiboa, 2 = MHC, 3 = ugaritzailea, 4 = IRM).*

4.2.7 Klusterren artean partekatutako geneen transkripzio-aldaketak

Fagozitosiak eragindakoen eta irradiazioak eragindako transkripzio-aldaketen artean bereizteko, lehenik eta behin LCIaren ondorengo 24 h eta 7d adierazpen geniko globala aztertuko dugu kluster konbinatu guztietan, eta hurrengo atalean kluster bakoitzaren aldaketa espezifikoei erreparatuko diegu. Bi gene mota aurkitu ditugu, LCIaren ondoren adierazpena aldatu zutenak: kluster desberdinetan adierazitako geneak (gene partekatuak), beharbada irradiazioak eragindako aldaketa globalak irudikatzen dituztenak; eta kluster bakoitzarenak ziren geneak, horietako batzuk fagozitosiarekin lotuta egon daitezkeenak. Jarraian, DAVID oharpen funtzionaleko tresnarekin dituen ondorio funtzionalak aztertuko ditugu. DAVIDek, gure gene interesgarriak idazteko eta talde funtzional aberastuak identifikatzeko aukera ematen du. Geneen Ontologian (GO) oinarrituta dago, normalean hiru eremu barne hartzen baititu: funtzio molekularra, prozesu biologikoa eta osagai zelularrak (Huang et al., 2007).

LCIk transkripzio-aldaketa handiak eragin zituen 24 ordura, eta horrek 140 gene partekaturi eta klusterreko 114 gene espezifikori eragin zien (**19A irudia**). DAVID analisiaren arabera, gene partekatuak GO espezifikoekin lotuta zeuden, hala nola B kinasa proteina seinaleztatzeko prozesu biologikoekin (GO: 0043491) eta hanturazko erantzunarekin (GO: 0006954) (19C irudia). B kinasa proteinaren seinaleztapena zelulen biziraupenerako bideetan inplikatuta dago, prozesu apoptotikoak inhibitzen baititu (Chen et al., 2001). Garuneko hantura-erantzuna mikrogliak gauzatzen du, normalean, neurodegenerazioa edo kaltea dagoenean (Muzio et al., 2021a). Horrek mikroglia hipokanpalak LCIare erreakzionatu duela iradokitzen du, autobabes-erantzun bat eraginez eta inguruko ehun kaltetua berrezarri dezaketen immunitate-funtzioak betez.

7 egunera, LCIk partekatutako 32 gene eta klusterreko 61 gene espezifikoren adierazpena eragin zuen (**19. B irudia**), eragindako geneen murrizketa erakutsiz, eta irradiazioaren ondorioak desagertzen ari zirela aditzera emanez.DAVID analisiak agerian utzi zuen gene partekatuak GO espezifikoekin erlazionatuta zeudela, hala nola ziklinaren mendeko proteina zinasaren konplexu holoentzimatikoaren goranzko osagai zelularrarekin (GO: 0000307), ziklo zelularraren erregulazioan inplikatua, eta mitokondriaren beheranzko osagai zelularrekin (GO: 0005739), barne-mintz mitokondrialarekin (GO: 0005743) eta arnasketa zelularrarekin (GO: 0045333) (**19. D-E irudia**). Horrek, mikrogliak epe luzera berreskuratzen jarraitzen duela aditzera eman zuen. Beraz, aurkitutako DNAn kalte txikiena izan arren (**11. irudia**), LCIa ez zen kaltegabea izan mikrogliarentzat, zelula hauek irradiazioaren ondoren bizirauteko eta denboran zehar errekuperatzeko mekanismoak jarri baitzituen martxan.

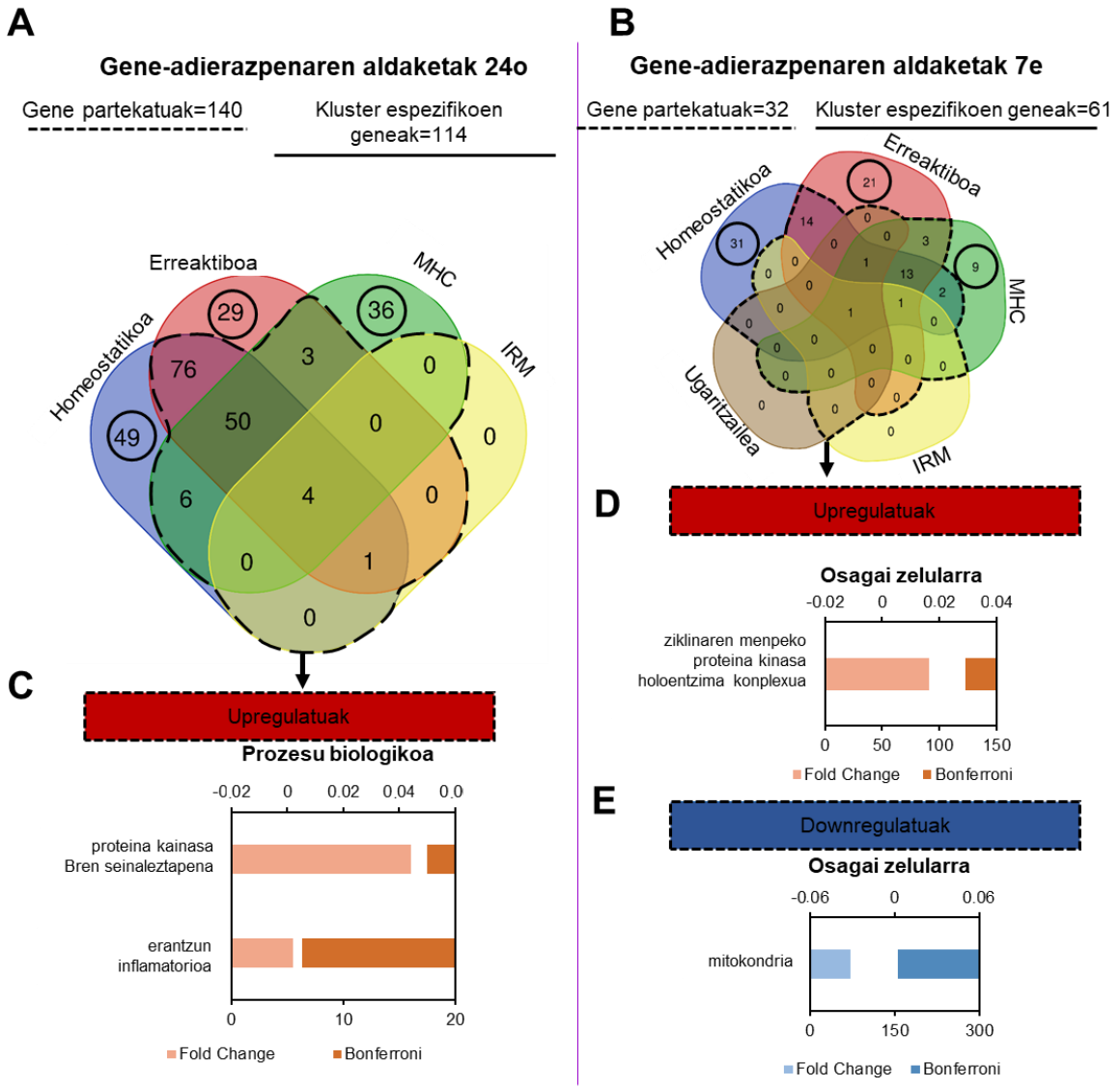

19. irudia. Aldaketa transkripzionalak klusterrek partekatutako geneetan. *(**A, B**) Vennen diagrama, klusterreko gene partekatu eta espezifikoetako adierazpen-aldaketak erakusten dituena 24 ordu (**A**) eta 7 d (**B**) LCIren ondoren. Zirkulu beltzek klusterraren gene espezifikoak adierazten dituzte; puntu-lerroek, berriz, geneen ontologian (GO) oinarrituta sakonago aztertu ziren gene partekatuak adierazten dituzte. (**C**) Goranzko prozesu biologikoen analisia, 24 ordutan DAVID erabiliz. (**D**) Gorantz eta beherantz (E) erregulatutako osagai zelularren analisia DAVID bidez 7etan. Ezkerreko ardatzak funtzio biologiko bakoitzaren tolestura aberastea adierazten du, eta eskuineko ardatzak GO termino bakoitzaren p balio doitua. Estatistikoki esanguratsuak diren aldaketak bakarrik erakusten dira. Estatistikoki esanguratsuak diren aldaketak (GO domeinuak: prozesu biologikoa eta osagai zelularra) dituzten GO terminoen eremuak soilik erakusten dira.*

4.2.8 Transkripzio-aldaketak talde mikroglial homeostatikoan

LCIk gene partekatuetan eragindako transkripzio-aldaketez gain, klusterraren transkripzio-aldaketa espezifikoak daude, eta horietako batzuek mikroglia fagozitikoa adieraz dezakete.

Lehenik eta behin, aldaketa horiek kluster homeostatikoan aztertu genituen, baina ez zen oso probablea populazio fagozitikoa izatea, kontrol-saguetan populaziorik handiena zelako eta LCIaren ondoren tamainaz murriztu zelako (**20. A, C irudia**). Aitzitik, mikroglia fagozitikoa, hipokanpoaren zelula guztien artean gutxiengoa, LCIaren ondoren handitzea espero dugu. Talde horrek zelula sekuentziatuen % 80 osatzen du, eta LCIaren eraginpean egon ondoren, murriztu egiten da haien tamaina. Datu horiek ez datoz bat gure aurreko emaitzekin. Horien arabera, DGan mikroglia fagozitikoa % 9,1 ± 1,5etik % 83,1 ± % 14,9ra igotzen zen kontrol-baldintzetan, LCIrekiko esposizioko 6 orduetan (**9. irudia**).

Kluster homeostatikoan, LCIak aldaketa transkripzionalak eragin zituen klusterreko 49 gene espezifikotan 24 ordutan eta klusterreko 31 gene espezifikotan 7 detan (**20. D irudia**). 80 gene espezifiko horietatik 8 aldatu egin ziren bi uneetan. 24 ordura araututako geneak zenbait GOrekin erlazionatuta zeuden, hala nola goraka erregulatutako C3HC4 motako RING domeinuaren loteslea (GO: 0055131), lotura-funtzio molekularrarekin erlazionatuta; eta beherantz erregulatutako erribosoma zitosolikoaren osagai zelularrarekin (GO: 0022626) (**20E-F irudia**). C3HC4 motako RING finger domeinuak funtsezko zeregina betetzen du ubikitinazioan (Guo et al., 2022), proteina gehienak degradatzen dituen prozesu biokimikoan; eta erribosomaren beheranzko funtzio erregulatu batek proteinen sintesia murriztea ekar dezake. Horrek zelularen barruko proteinak birziklatze-prozesu baten eraginpean jarri direla iradokitzen du, agian irradiazioaren zein fagozitosiaren ondorioz sor daitekeen kaltea arintzeko duten ekintzaren ondorioz.

7d-ko gene aldatuak goranzko GO erragulazioarekin lotuta zeuden, eta honako prozesu biologiko hauetan inplikatuta zeuden: kaltzio ioiarekiko emandako erantzun zelularra (GO: 0071277), RNA polimerasa II-ren sustatzailearen transkripzioa (GO: 0006367) eta AMPc-ren erantzuna (GO: 0051591) (**20. H irudia**). Oro har, gene horiek RNA mezulariaren (RNAm) aitzindarien DNA transkripzioan parte hartzen dute, eta horrek kluster homeostatikoa berriz epe luzerako transkripzio-mailan aktibatzen dela iradokitzen du (7 egun irradiazioaren ondoren). Gainera, zelulek kaltzioa eta adenosina ziklikoaren monofosfatoa (AMPc) bezalako seinaleei erantzuten dietela dirudi, eta horrek mikroglia homeostatikoak bere jarduera sentsorioa epe luzera berreskuratzen duela adierazten du. Bestalde, beherantz erregulatutako GOek 7detan arnasketa aerobikoaren prozesu biologikoa barne hartzen dute (GO: 0009060) (**20. I irudia**), eta horrek jarduera mitokondrial txikiagoa eta zelulek energia gutxiago ekoizten dutela iradokitzen du. Beraz, litekeena da aipatutako berreskurapena erabat osatu ez izana eta zelulek oraindik ere konpondu beharreko defizit metabolikoak izatea. Bi denbora-puntuetan araututako geneei dagokienez, kate bikoitzeko DNAren lotura-funtzio molekularraren goranzko GO arautuarekin lotuta zeuden (GO: 0003690). Funtzio molekular horrek beste funtzio espezifikoago batzuk biltzen ditu, hala nola transkripzioa, paketatzea edo DNAren zatiketa, eta horrek mikrogliak maila nuklearrean aldaketak izaten

dituela iradokitzen du. Horrela, LCIk epe luzera suspertzen saiatzen diren zelula homeostatikoen transkripzioa murrizten du. Hala ere, susperraldi hori partziala da, metabolismo mikroglialak epe luzera beherantz erregulatuta jarrai dezakeelako.

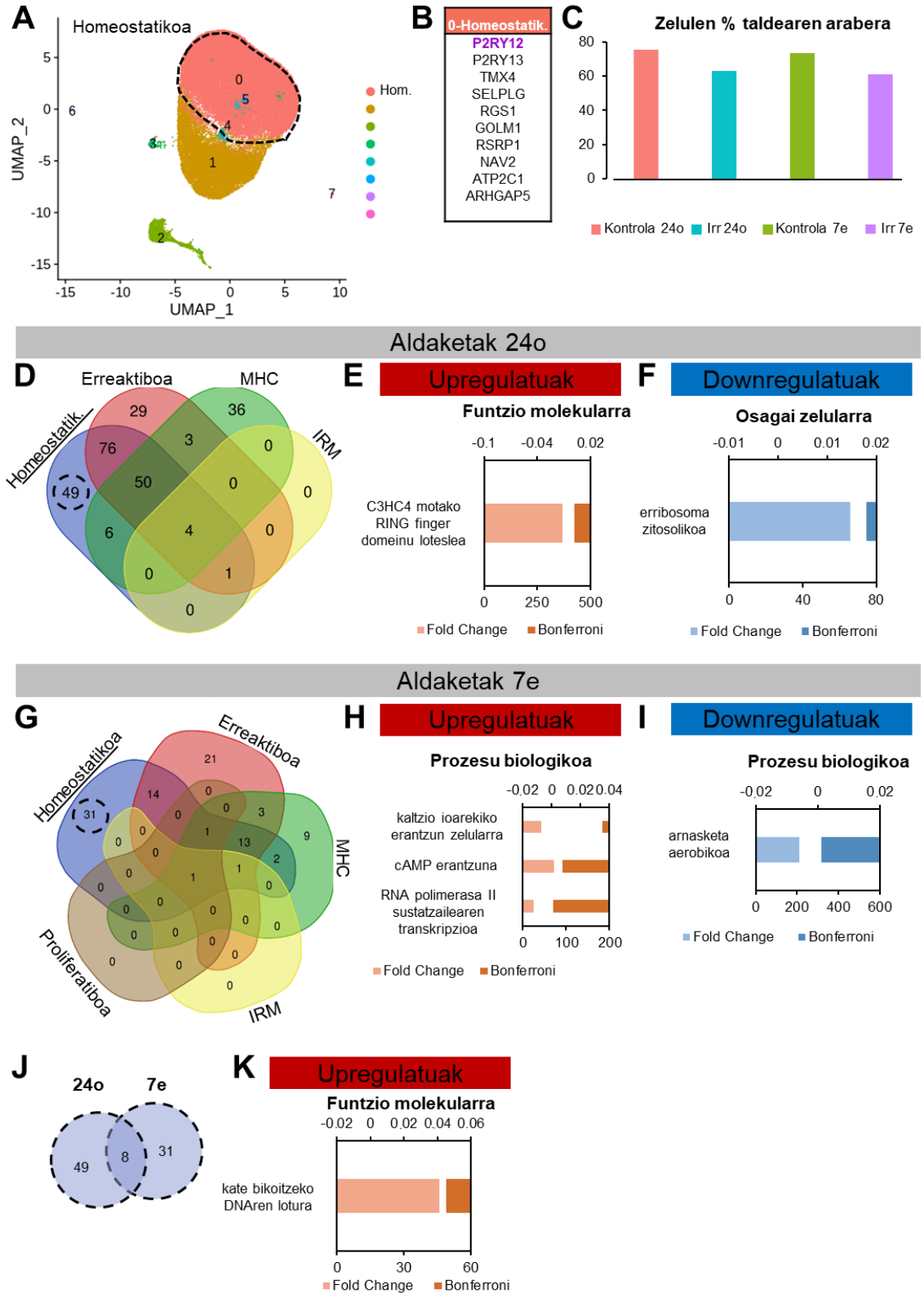

20. irudia. Aldaketa transkripzionalak kluster homeostatikoan. *(**A**) UMAPek kluster homeostatikoa erakusten du, puntu-lerro batez inguratua. (**B**) Kluster homeostatikoaren gene bereizgarrien zerrenda. (**C**) baldintza esperimental bakoitzean kluster homeostatikoko zelulen %. (**D, G, J**) Vennen diagrama, klusterreko gene partekatu eta espezifikoetan 24:00etan (**D**) eta 7d (**G**) LCIaren ondoren egiten diren adierazpen-aldaketak erakusten dituena, bi denbora-puntuen (J) artean partekatzen diren kluster-gene espezifikoak barne. Goranzko (**E**) eta beheranzko (**F**) GO arautuak 24 ordutan aztertzea, DAVID softwarea erabilita. Goranzko (**H**) eta beheranzko (**I**) GO arautuak aztertzea 7 egunera, DAVID softwarea erabilita. Denboran partekatutako geneen goranzko GO arautuen analisia (**J**). Ezkerreko ardatzak tolesturetan aberastea adierazten du, eta eskuineko ardatzak GO termino bakoitzaren p balio doitua adierazten du. Estatistikoki esanguratsuak diren aldaketak bakarrik erakusten dira.*

Beraz, kluster homeostatikoa baztertu egin zuten hautagai gisa biztanleria fagozitikoa ordezkatzeko, eta gainerako klusterrak zehatzago aztertu zituzten.

4.2.9. Transkripzio-aldaketak MHC klusterrean

MHC klusterra populazio fagozitikoa hartzeko hautagai potentzial bat izan zen, LCIri epe laburrean eta luzean erantzuteko tamaina handitu baitzen (**21. C irudia**). Hala ere, kluster horrek CAMak ere adieraz ditzake, klusterraren gene batzuk (MSA47 eta PF4) CAM sinaduran identifikatu baitira (**21. B irudia**). Tratamenduak MHC populazioan eragiten dituen klusterraren transkripzio-aldaketa espezifikoak aztertzen jarraitzeko, klusterrak epe laburrean eta luzean egiten dituen transkripzio-aldaketa espezifikoak aztertuko ditugu.

MHC klusterrean, LCIk aldaketa transkripzionalak eragin zituen klusterreko 36 gene espezifikotan 24 ordutan eta klusterreko 9 gene espezifikotan 7 ordutan, eta gene espezifiko bat partekatu zuen bi denbora-puntuen artean (**21. D irudia**). DAVIDekin egindako gene horien analisiak ez zuen esan GO bakar batean ere modu esanguratsuan inplikatuta zeudenik, ziur asko inplikatutako geneak gutxi zirelako. Beraz, gene bakoitzaren funtzioa aztertu zen eta antzeko prozesuetan inplikatuta zeudenak taldekatu ziren.

24 ordu eta 7 ordu bitarteko geneak funtzioaren arabera sailkatu ziren kategoria hauetan: metabolismoa, fagozitosia/degradazioa, hantura, antigenoak izatea, oxidazio/zelula-estresa, DNAn kalteak berreskuratzea, apoptosia/hazkundea erregulatzea, RNAren metabolismoa, mintz-hartzailea eta funtzio ezezagunak (**21. F irudia**). Bitxia bada ere, bi denbora-puntuen artean partekatutako Lgals1 geneak goranzko eredu erregulatua erakutsi zuen eta zelula-zelula eta zelula-matrize interakzioetan inplikatuta egon zen, hazkunde negatiboko faktore gisa jardun zuen eta biziraupenaren aldeko ondorioak izan zituen (Ruvolo et al., 2020).

Oro har, emaitza horiek MHC populazioak LCIaren ondoren, epe laburrean, aldaketak pairatzen dituela iradokitzen dute. Bitxia bada ere, aldaketa horietako batzuk estres oxidatiboa areagotzearekin eta MHC klusterraren funtzio nagusian, antigenoen aurkezpenean, inplikatutako geneen beheranzko erregulazioarekin lotuta zeuden. Epe luzera, badirudi MHC populazioa bere onera itzultzen ari dela

estres oxidatibotik, baina alterazio batzuk erakusten jarraitzen du fagozitosian, inflamazioan, RNAm-ren metabolismoan, apoptosiaren erregulazioan eta zelulen metabolismoan. Hurrengo atalean, aurkikuntza horiek RNAscope *in situ* hibridazioarekin baliozkotuko ditugu gure ehunean. Hoenen helburua MHC populazioa identifikatzea da.

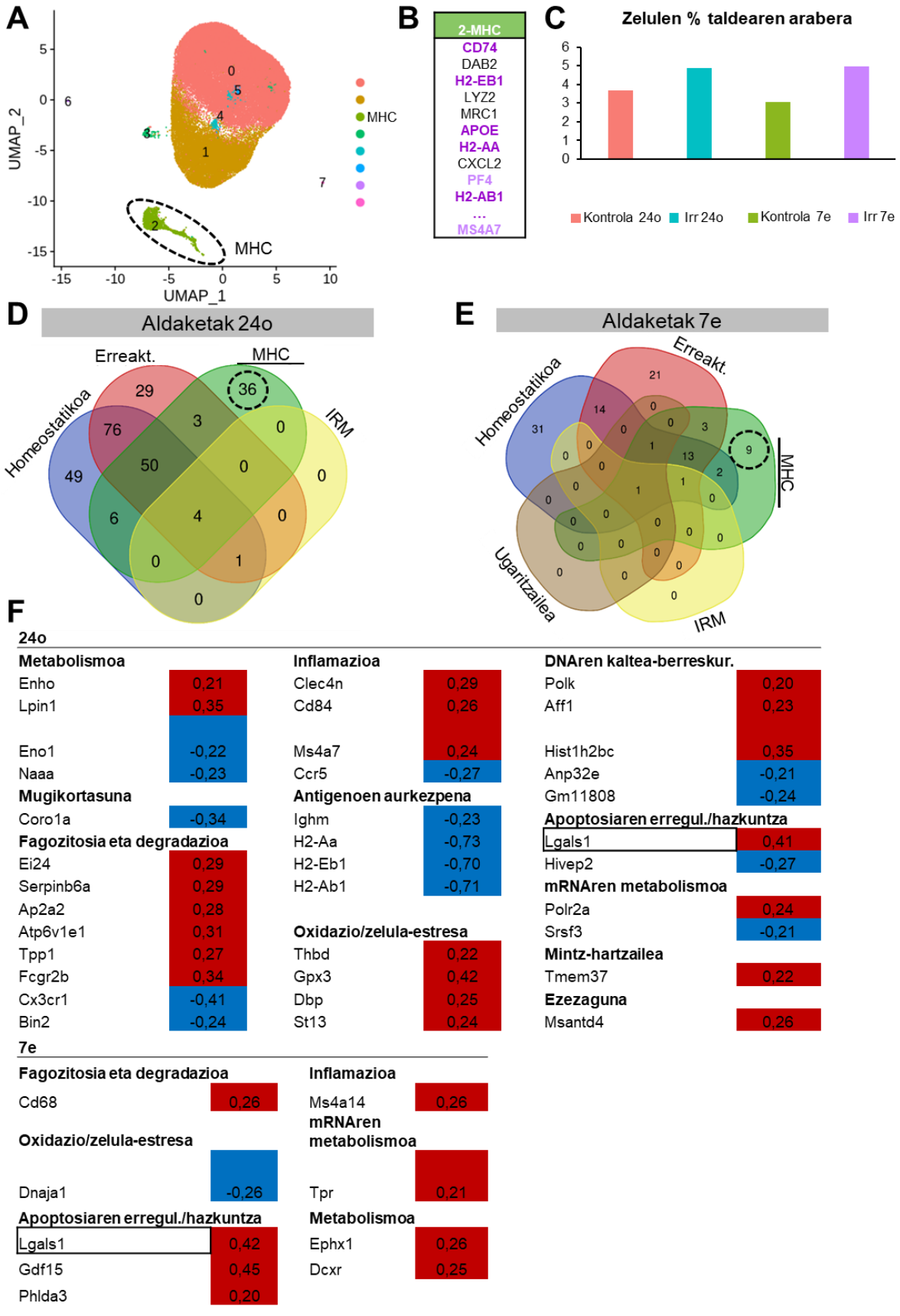

21. irudia. Aldaketa transkripzionalak kluster homeostatikoan. *(**A**) UMAP, MHC populazioa puntu-lerro batez inguratuta erakusten duena. (**B**) MHC klusterreko gene*

*bereizgarrien zerrenda. Purpura iluna, hainbat azpipopulazio mikroglial deskribatu geneak Chen et al. 2021 (Chen et al., 2021). More argian, CAMentzat deskribatutako geneak Masuda et al. 2022 (Masuda et al., 2022). (**C**) MHC klusterreko zelulen %, baldintza esperimental bakoitzean. (**D, E**) Gene partekatuen eta klusterreko gene espezifikoen Vennen diagrama, 24:00etan (D) eta 7: 00etan (**E**), LCIren ondoren. MHC klusterraren aldaketa espezifikoen inguruan puntu-lerro bat dago. (**F**) Klusterraren aldaketa genetiko espezifikoen laburpen-taula, sailkapen funtzionalaren arabera taldekatuta. FCk tolesturak aldatzea esan nahi du. Lauki gorrien zenbakiek gorantz erregulatutako geneak adierazten dituzte; lauki urdinen zenbakiek, berriz, beherantz erregulatutako geneak. Ertz beltza duten laukiek gene errepikatua adierazten dute bi denbora-puntuetan.*

4.2.10. MHC geneak in situ adieraztea LCIren ondoren.

MHC klusterra populazio fagozitikoa izateko hautagai potentziala zen; izan ere, LC) 24 ordura eta 7 ordura handitu zen. Hala ere, kluster horrek CAMak ere adieraz ditzake, klusterraren gene batzuk (MSA47 eta PF4) CAM (Prinz et al., 2021) sinaduran identifikatu baitira (**21. B-C irudia**). Kluster honek mikroglia fagozitikoa ordezkatzen ote zuen aztertzeko, sinadura honen geneetako bat aukeratu genuen, MS4A7, mintz hedapeneko 4A geneen familiako kide bat, leinu monokitikoan heldutako funtzio zelularrarekin lotuta dagoena (Mattiola et al., 2021).

MS4A7 MHC klusterreko zelulen % 81ean adierazi zen, pct.1 irudian erakusten den bezala (baldintzarako klusterrean genea detektatzen den zelulen ehunekoa), eta beste kluster batzuetako zelulen % 1ek bakarrik adierazi zuten, pct.2 irudian erakusten den bezala (baldintzarako beste klusterretan batez besteko genea detektatzen den zelulen ehunekoa) (**22. A irudia**), pct1/pc2 erlazioa 57,57koa zen, eta horrek MS4A7 MHC populazioa identifikatzeko hautagai sendoa zela iradokitzen zuen. Gainera, gene hori 0,24 aldiz handitu zen (FC, fold-change) MHC klusterrean LCIren ondoren 24 ordura (**22. A-B irudia**). MS4A7 in situ adierazpena aztertuko dugu, RNAScope erabiliz. MS4A7ren adierazpena mugatua zenez aztertutako eskualdeetan, APOE zundaren adierazpena erabili zen barne-kontrol gisa (**22. D, E irudia**). Helduen mikroglian, APOE espresioa baxua da (Lee et al., 2023), eta gure irudiek ez dute erakusten P2Y12 eta APOE markatzaileen arteko kokapenik (**22. F irudia**), hibridazio-prozesuak behar bezala funtzionatzen zuela frogatzen dueña.

MS4A7-rako zelula positiboek P2Y12-ren adierazpen baxua zuten, morfologia ameboidea zuten, eta P2Y12+ populazio mikroglialaren ehuneko oso txikia adierazten zuten DG-n. Gainera, nahiz eta MS4A7ren adierazpena DGn CAn aurkitutakoa baino handiagoa izan (**22. D irudia**), M24A7+ zelulen P2Y12 adierazpen baxuak eta morfologia ameboideak MHC klusterrak CAMak irudikatzen dituela iradokitzen du.

A

Gene	avg_logFC	pct.1	pct.2	ratio	Espresio aldaketak klusterraren barnean tratamenduaren 24 ordutara? (FC)	Espresio aldaketak klusterraren barnean tratamenduaren 7 egunetara? (FC)
Ms4a7	2,39	0,81	0,01	57,57	0,24	no

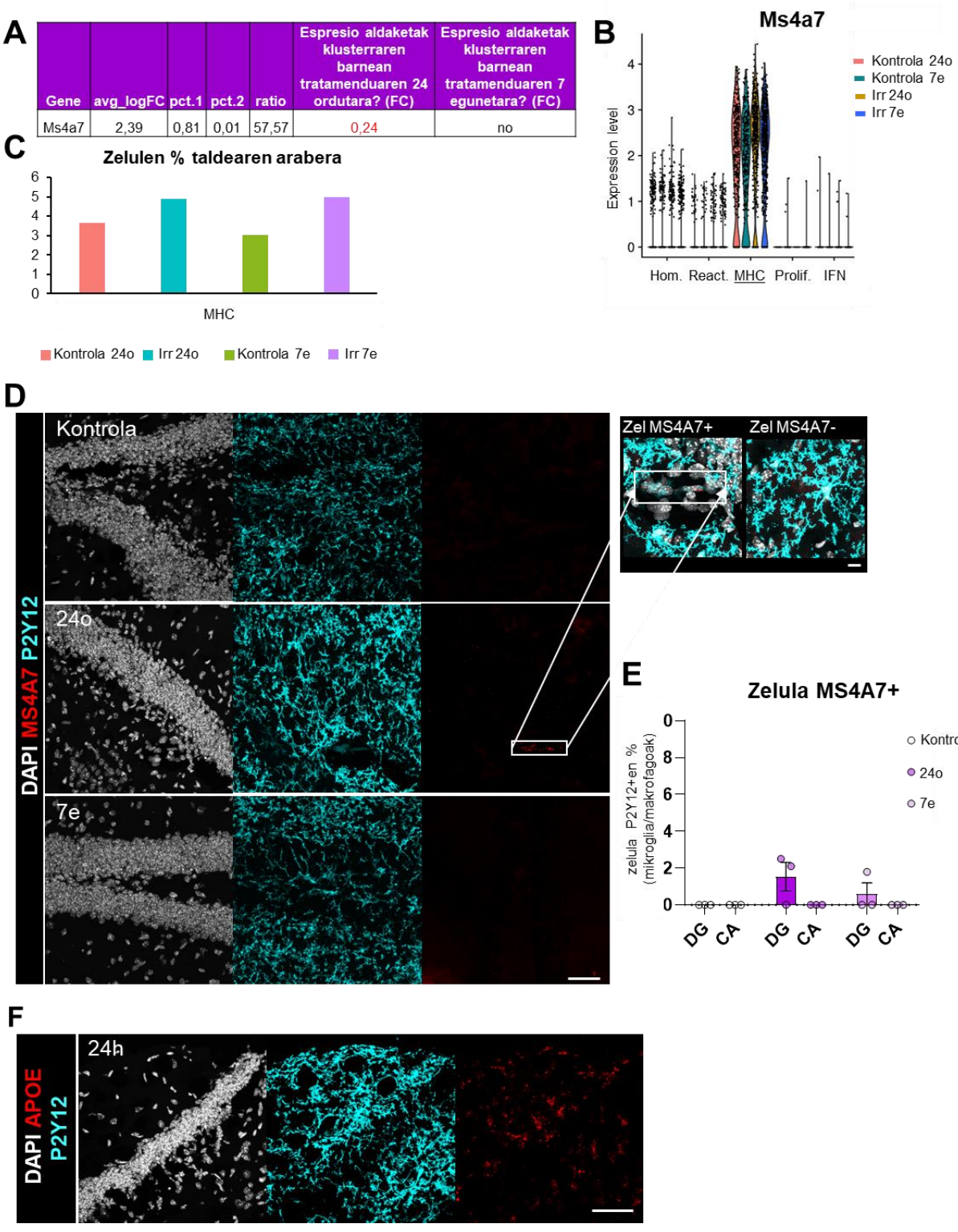

22. irudia. MHC klusterraren markatzailea adieraztea LClaren ondoren. *(**A**) MS4A7 genearen adierazpenaren laburpen-taula MHC klusterrean. Parametro hauek erakusten dira: batez besteko FC, pct1, pct2, pct1/pct2 erlazioa eta adierazpen-aldaketak LClaren ondoren (24h eta 7d). (**B**) Violin-plots, MS4A7 erakusten hainbat klusterretan, hainbat baldintzen artean. (**C**) MHC klusterreko zelulen %, baldintza esperimental bakoitzean. (**D**) DGa irudikatzen duten irudiak, DAPI (zuria), MS4A7 (gorria) eta P2Y12 (cian) tindaketa erakusten dutenak, hainbat baldintza esperimentaletan (kontrola, 24h eta 7d).*

*Laukizuzen zuriaren barruan MS4A7+ zelulak adierazten dira. (**E**) RNAm MS4A7 eduki handia adierazten duten zelulen analisia, DG eta CA eskualdeetako zelulen ehunekoa hainbat baldintza esperimentaletan erakutsiz (kontrola, 24h eta 7d). (**F**) DGren irudi adierazgarriak, APOE (gorria) kontrol positiboaren etiketak erakutsiz, DAPI (zuria) eta P2Y12 (cian) ere erakutsiz. Barrek n = 3 saguren ± SEM batez bestekoa erakusten dute. Datuak norabide bakarreko ANOVAren bidez [D] aztertu ziren, eta, ondoren, Holm-Sidaken post hoc probak, hala zegokionean. Eskala barrak = 50µm, 10µm ([D]-n txertatuak). z = 16,45µm, z = 17,5µm, z = 8,75µm [D]; z = 15,4µm [F].*

4.2.11. Transkripzio-aldaketak IRM klusterrean eta IRM geneen adierazpena in situ LCI ondoren.

MHCaren kasuan bezala, IRM klusterra populazio fagozitikoa izateko hautagai potentziala ere zen; izan ere, kluster txiki bat zelako, tratamenduari (LCI) erantzuteko 24 eta 7 ordutara tamainaz handitzen zuena. Gainera zuen aldaketarik erakusten gene-adierazpenean (hau da, ez zuen aldaketa transkripzional espezifikorik klusterrean) (**23. A, C irudia**). Sinadura mikroglial hori, fagozitosia eragiten duten zeluletan ikusi da garapen kortikalean zehar (Escoubas et al., 2021). Horrela, IRM klusterra *in situ* baliozkotzeko eta identifikatzeko, IFIT3 gene sinaduraren RNAscope teknika burutu genuen.

IFIT3k IRM klusterreko zelulen % 80an adierazi zuen (pct.1), eta beste kluster batzuetako zelulen % 4k bakarrik adierazi zuen (pct.2), 44,61eko pct.1/pct.2 ratioa erakutsiz. Horrek IFIT3 IRM hautagai indartsua zela populazioa identifikatzeko iradokitzen du (**23. D-E irudia**). Zelula mikroglialak IFIT3+ edo IFIT3- bezala sailkatu ziren, ARNm IFIT3 edukiaren arabera. IFIT3 eduki nabaria zuten zelulak IFIT3+ gisa kategorizatu ziren, eta zehatzago aztertu ziren populazio mikroglialaren barruan. Nahiz eta baldintza basaletan IFIT3+ mikrogliaren populazioa ugariagoa izan DGn CAn baino (25,1 ± 1,0 eta 0,7 ± 0,7), IFIT3+ zelulen ehunekoa ez zen aldatu tratamendua eman ondoren (**23. F-G irudia**), eta datu hauek talde horrek ere ez duela mikroglia postfagozitikoa adierazten iradokitzen du. Gainera, emaitza horiek berresteko, IFITM3ren, kluster honen beste gene bereizgarri baten, adierazpena aztertuko dugu, immunofluoreszentzia bidez. Analisiak IFITM3 batez ere odol-hodietan adierazten zela agerian utzi zuen (**23. H irudia**), zelula mikroglialekin kokatu gabe. Beraz, IRM klusterrak ez du mikroglia postfagozitikoaren populazioa adierazten.

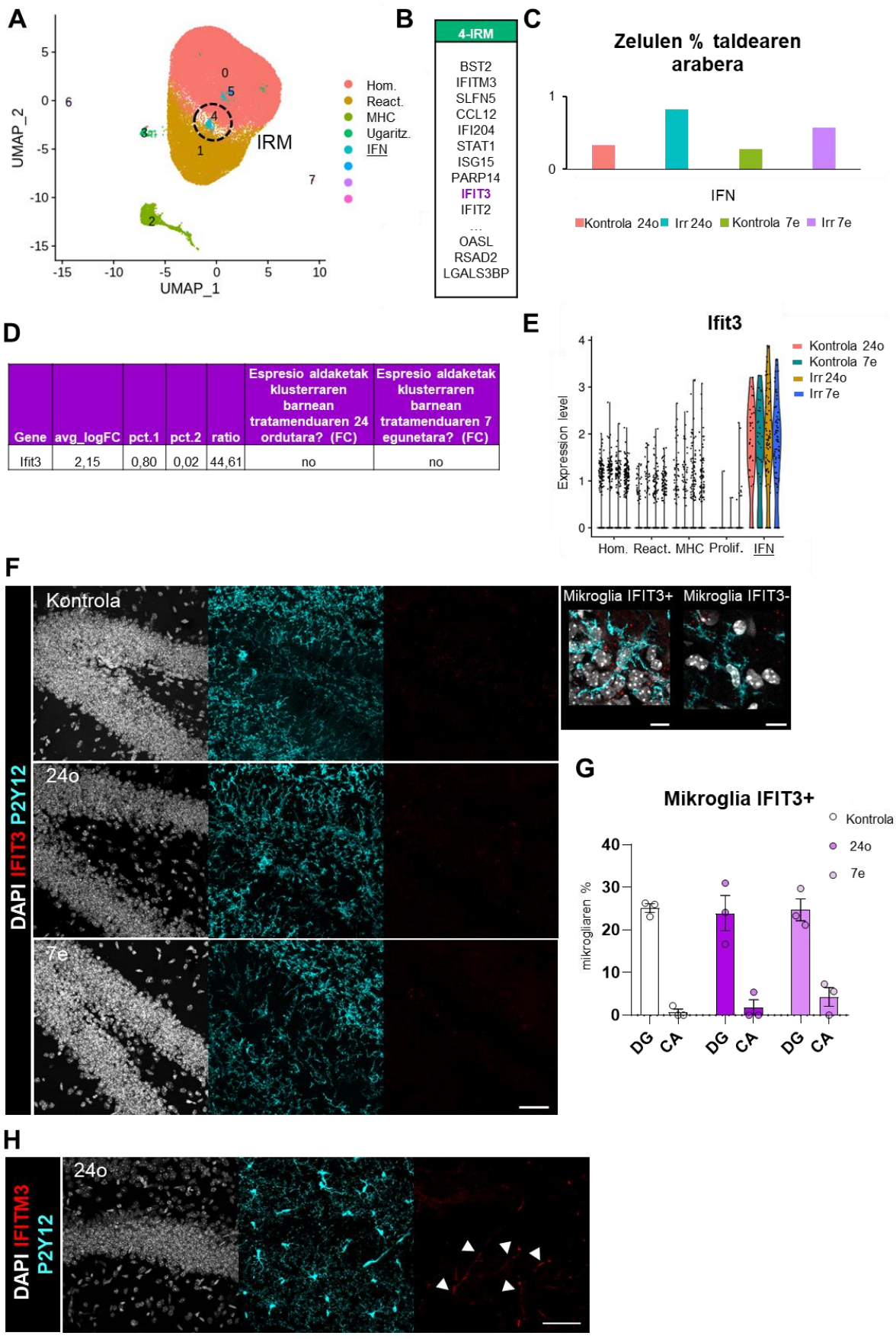

23. irudia. IRMren konglomeratuen markagailuaren adierazpena, LCIren ondoren. *(**A**) UMAPek puntu-lerro batez inguratutako IRM populazioa erakusten du. (**B**) IRM*

*klusterreko gene bereizgarrien zerrenda. (**C**) IRM klusterreko zelulen ehunekoa baldintza esperimental bakoitzean. (**D**) IFIT3 gene-adierazpenaren laburpen-taula IRM klusterrean. Parametro hauek erakusten dira: batez besteko FC, pct1, pct2, pct1/pct2 erlazioa eta LCIaren ondorengo adierazpen-aldaketak (24h eta 7d). (**E**) Violin-plots, hainbat baldintzaren arteko klusterretan IFIT3 erakusten. (**F**) DGaren irudi adierazgarriak, DAPI tindaketa (zuria), IFIT3 (gorria) eta P2Y12 (ziana) erakutsiz, hainbat baldintza esperimentaletan (kontrola, 24h eta 7d). (**G**) DG eta CA eskualdeetako IFIT3+en ehunekoaren analisia, hainbat baldintza esperimentaletan (kontrola, 24h eta 7d). (**H**) DGaren irudi adierazgarriak, DAPI (zuria), IFITM3 (gorria) eta P2Y12 (ziana) tindaketa erakusten dutenak. Barrek n = 3 saguren ± SEM batez bestekoa erakusten dute. Datuak norabide bakarreko ANOVAren bidez [D] aztertu ziren, eta, ondoren, Holm-Sidaken post hoc probak, egokia izan zenean. Eskala barrak = 50µm, 10µm ([F]-n txertatua). z=12.25µm, z=11.2µm, z=10.15µm [F]; z=27.3µm [G] z=40µm [H].*

4.2.12. Mikroglia fagozitikoak CD68 eta galektina 3-ren adierazpen handia du ezaugarri.

Populazio postfagozitikoa scRNA-Seq bidez identifikatutako talde bakar batean ere aurkitu ez zenez, fagozitosiari lotutako proteinen bilaketa bibliografiko bat egin genuen, hala nola CD68 eta galektina 3 (Gal3) (Rotshenker, 2009; Rotterman et al., 2020). CD68 zelulen konpartimentu endosomal eta lisosomaletan kokatzen da nagusiki, eta aktiboki parte hartzen du zelulaz kanpoko materialen degradazioan (Bobryshev et al., 2013). Gainera, CD68 fagozitosi-prozesuekin lotu da, eta haren adierazpena goranzko joeran erregulatzen da testuinguru fagozitikoetan, hala nola iskemia edo garapenean zehar ugaltzen diren eskualdetan (Silva et al., 1999; Li et al., 2019). Gal3, galektinen familiako kidea da, oso ezaguna da bere izaera pleiotropikoagatik eta erantzun immuneen abiaraztean duen inplikazioagatik (Sciacchitano et al., 2018). LGALS3 genea, Gal3rako kodetzen duena, gorantz erregulatzen da mikrogliak mielina eta oligodendrozitoak fagozitatzen dituenean (Nomura et al., 2017; Li et al., 2019). Hau kontuan hartuta, bi proteinen adierazpena immunofluoreszentzia bidez aztertu zen kontrolean eta LCIaren ondoren (24h eta 7d) (**24. A, C irudia**).

Mikroglia CD68+en ehunekoak LCIaren ondoren, bai 24 ordutara, baita 7 ordutara, gora egin zuen DGn, baina ez zen aldaketarik izan CAn (**24. A-B irudia**). Era berean, Gal3+ mikrogliaren ehunekoak LCIren ondoren 24 eta 7 ordutara handitu egin zen DGn. Igoera hori DGn bakarrik gertatu zen eta CAn, berriz, ez zen aldaketarik izan (**24. C-E irudia**). DGko Gal3+ mikroglia, DGko eremu subgranularrean (SGZ) kokatu zen zehazki, fagozitosia nagusiki gertatzen den eskualdean (Sierra et al., 2010) (**24. G irudia**). DGn ez bezala, non Gal3+ mikroglia espezifikoki SGZn kokatzen zen, CAko Gal3+ mikroglia geruza desberdinetan banatzen zen. Horrek DGren mikrogliak SGZn gertatzen ziren aldaketa espezifikoei erantzuten ziela iradokitzen du (**24. H, F irudia**). Era berean, DG Gal3+ mikrogliak Gal3ren maila altuagoak erakutsi zituen, zelula gehienek intentsitate ertain-altua erakutsi baitzuten, eta CA Gal3+ mikrogliaren gehiengoak intentsitate txikia erakutsi zuen, DG mikrogliaren eta CA mikrogliaren arteko aldeak agerian utziz. (**24. E-F irudia**). Horrela, CD68 eta Gal3 adierazpen altua duen mikroglia populazio bat adierazten zuen populazio ba identifikatu genuen. Populazio honek SGZan zegoen kokatua eta fagozitosiaren ondoren

handitzen zuen bere tamaiana eta horrek CD68 eta Gal3 mikroglia postfagozitikoaren markatzaile gisa erabili ahal iradokitzen du.

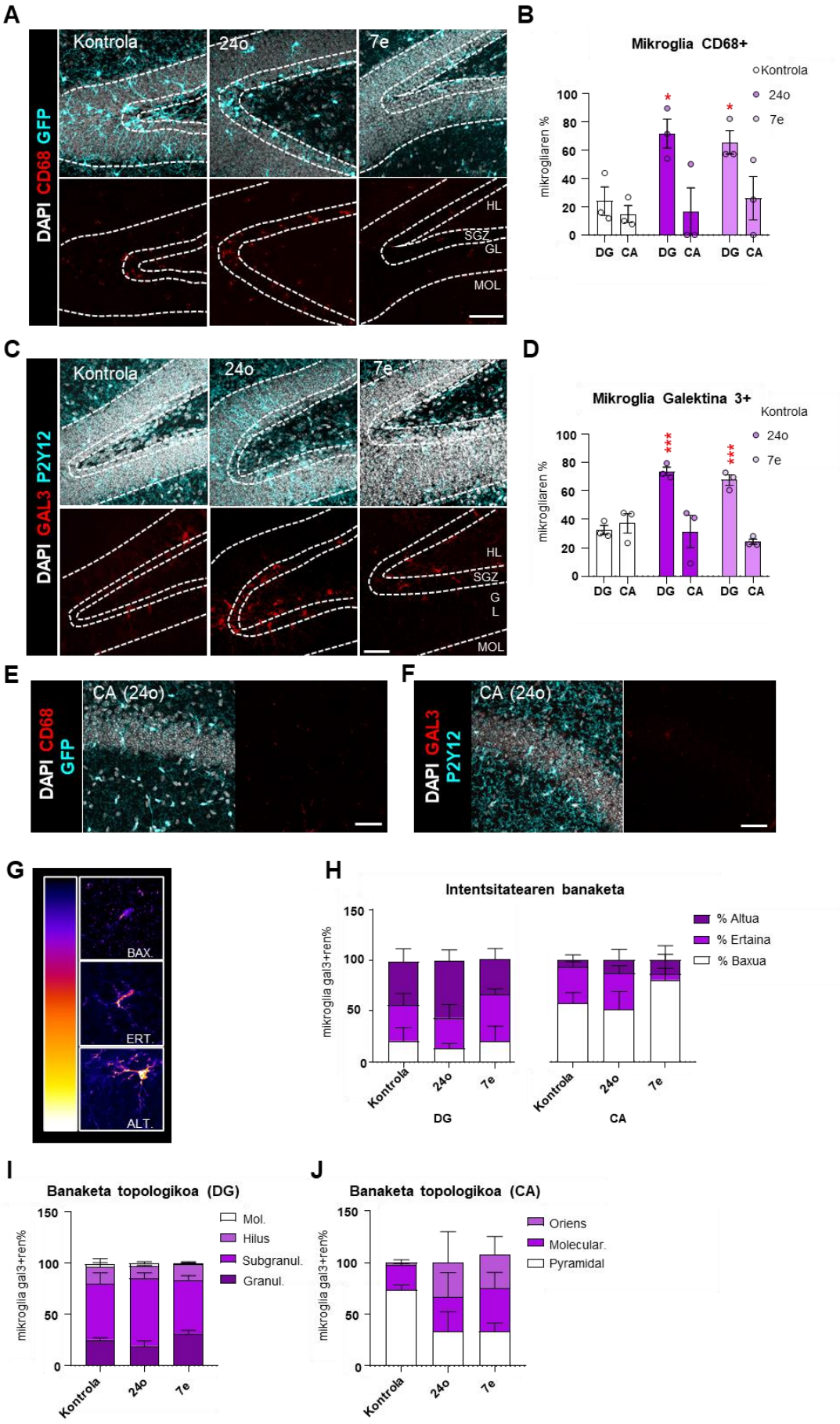
A
Kontrola
24o
7e
DAPI CD68 GFP
HL
SGZ
GL
MOL
B
Mikroglia CD68+
Kontrola
24o
7e
mikrogliaren %
DG CA DG CA DG CA
C
DAPI GAL3 P2Y12
HL
SGZ
G
L
MOL
D
Mikroglia Galektina 3+
E
CA (24o)
DAPI CD68 GFP
F
DAPI GAL3 P2Y12
G
BAX.
ERT.
ALT.
H
Intentsitatearen banaketa
mikroglia gal3+ren%
% Altua
% Ertaina
% Baxua
DG
CA
I
Banaketa topologikoa (DG)
Mol.
Hilus
Subgranul.
Granul.
J
Banaketa topologikoa (CA)
Oriens
Molecular.
Pyramidal

24. irudia. LCIaren osteko fagozitosiarekin lotutako proteinen adierazpena. *(**A**) Mikrogliaren irudi konfokal adierazgarriak, DGan CD68 adieraziz baldintza esperimental desberdinetan (Control, 24h, 7d), DAPI tindaketa erakutsiz (zuria), CD68 (gorria), eta GFP (cian). Geruza zelularrak (haria, HL; eremu subgranularra, SGZ; geruza pikortsua, GL; molekularra, MOL) marra zuri etenez markatuta daude. (**B**) DG eta CA eskualdeetako CD68+ mikrogliaren ehunekoaren analisia, hainbat baldintza esperimentaletan (kontrola, 24h eta 7d). (**C**) DGn galektina3 adierazten duten mikrogliaren irudi konfokalak, baldintza esperimental desberdinetan (Control, 24h, 7d), DAPI tindaketa (zuria), galectina3 (gorria) eta P2Y12 (cian) erakutsiz. Geruza zelularrak (haria, HL; eremu subgranularra, SGZ; geruza pikortsua, GL; molekularra, MOL) marra zuri etenez markatuta daude. (**D**) DG eta CA eskualdeetako Gal3+ mikrogliaren ehunekoaren analisia, hainbat baldintza esperimentaletan (kontrola, 24h eta 7d). (**E**) DAPI tindaketa (zuria), CD68 tindaketa (gorria) eta GFP tindaketa (ziana) erakusten dituen AC 24 orduan CD68k adierazten duen mikrogliaren irudi konfektiboa. (F) DAPI (zuria), GAL3 (gorria) eta GFP (ziana) bidezko tindaketa erakusten duen AC 24 orduan GAL3k adierazten duen mikrogliaren irudi konfocala. (**G**) Zelulak Gal3ren intentsitatearen arabera definitzeko sailkapen-irizpideen irudikapen grafikoa, J irudiaren LUT (bilaketa-taula) bat erabilita. (**H**) Gal3+ mikrogliaren ehunekoa GDan, banaketa topologikoaren arabera taldekatuta (granularra, subgranularra, hilioa, beste batzuk). (I) Gal3+ mikrogliaren ehunekoa GDan, banaketa topologikoaren arabera taldekatuta (granularra, subgranularra, haria, molekularra). (**J**) Gal3+ mikrogliaren ehunekoa ACan, banaketa topologikoaren arabera taldekatuta (orienak, molekularrak, piramideak). Datuak norabide bakarreko ANOVAren bidez aztertu ziren [B, D, F, G, H], eta, ondoren, Holm-Sidaken post hoc probak egin ziren, bidezkoa zenean. Izartxoek kontrolaren eta LCIaren arteko esanahia adierazten dute (24h eta 7d).* p < 0,05 adierazten du. Eskala barrak= 50µm. z=20.3µm, z=8.4µm, z=23.1µm [A]; z=12.6µm, z=28.7µm; z=18.98µm [C]; z=17.5µm [E]; z=17.5µm [F].*

4.2.13. Aurretiko scRNA-seq datuen analisi berrituak, CD68/GAL-3 adierazpen handiko kluster mikroglial bat identifikatu zuen.

Cd68 eta Lgals3ren adierazpena gure hasierako txertaketan aztertu genuen, eta gene horien koadierazpen eredu ezberdinak identifikatu genituen UMAP grafikoaren lurralde zehatzetan (**25. irudia**). Hala eta guztiz ere, gure hasierako gainbegiratu gabeko elkartze-planteamenduak (hurbileneko bizilagunaren (SNN) modularitate-optimizazioan oinarrituriko algoritmo taldekatzailea, 0,1 erresoluzio-parametroarekin) ez zuen zelula horientzako populazio definiturik adierazten, eta multzo hori mikroglia homeostatikoaren kategoriari esleituta agertzen zen. Hori kontuan hartuz, gure hasierako planteamenduak ez zuela oreka onik lortzen azpibatzearen eta gainbatzearen artean pentsatu genuen. Horregatik, mikrogliaren konposizio-heterogeneotasuna sakonago ulertzeko, beste analisi bat egin genuen, kartografiatutako datu berberak erabiliz (beheko taulara jo bi analisien parametro garrantzitsuen laburpena behatzeko (**1. taula**)).

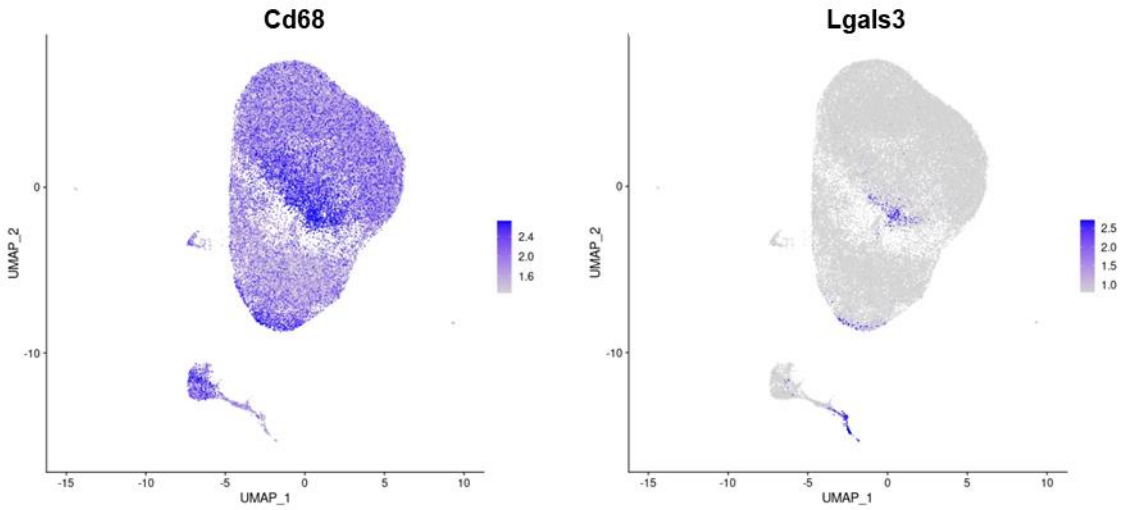

25. irudia. Cd68k eta Lgals3k UMAP grafikoaren lurralde espezifikoetako baterako adierazpen-ereduak erakusten dituzte.

Labur esanda, dobleteen identifikazio konputazionala Scrublet tresnaren bidez egin genuen (Wolock et al., 2019). Jarraian, zelulak iragazten ditugu, hasierako analisiaren parametro berberak erabiliz, irakurritako edukietan eta gene mitokondrialen proportzio erlatiboan oinarritutuz. Ondoren, eredu lineal orokorra egin genuen (GLM), datuen normalizazioa eta bariantza egonkortzeko SCT v2 erabiliz (Choudhary et al., 2022). Gure hasierako analisiarekin alderatuta, alde nabarmena dago. Lehenengo analisian datuak log-normalizazioa estandarra erabiliz normalizatu baitziren (UMI zenbaketak sekuentziazioaren sakontasun osoak ("tamaina faktoreak")) eta jarraian sasi-zenbaketaren gehikuntzak eta log-transformazioak egin baitzirelako, analisi honeta gertatzen ez dena (Satija et al., 2015; Hafemeister et al., 2019). Bigarren analisi honetarako, taldekatze gainbegiratuaren ikuspegia egin genuen, SNN algoritmoan hainbat bereizmen parametro erabiliz (0,1, 0,5, 0,8) eta klusterrak sortutako UMAP embedding batean bistaratu ziren 30 dimentsio esanguratsuenak (PC) erabiliz, osagaien analisi nagusitik abiatuta (PCA) (hasierako hurbilketan erabilitako 12 PCen aldean) (**3. taula, 26. A irudia**). Azkenik, zelula ez-mieloideak, MHC CAMak eta ex vivo mikroglia "aktibatua" ("erreaktiboa") iragazi genituen eta mikroglia azpimultzoa (32.591 zelula) dimentsio baxuko espazioan birtxertatu genuen hasierako Seurat objektuaren 30 dimentsio esanguratsuenak erabiliz (**27. A irudia**).

	1. ANALISIA	2. ANALISIA
Doublet detection	No	Yes (Scrublet)
QC filtering	<1000; >4000; mt<5%	<1000; >4500; mt<5%
Normalization	Log norm	SCT v2
UMAP	12 PCs	30 PCs
Clustering	SNN, res=0.1 (unsupervised)	SNN, res=0.1;0.5;0.8 (supervised)

3. taula. ScRNAseq-en datuak aztertzeko pipelinetan egindako urrats nagusien laburpena.

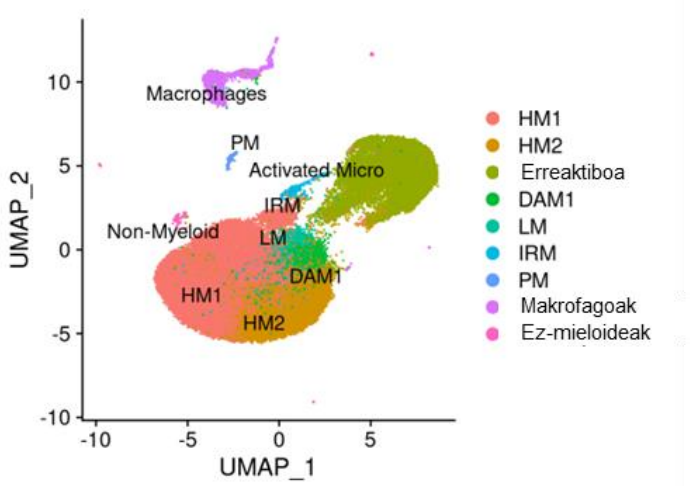

26. irudia. UMAPek ikuskatutako talde baten emaitzak erakusten ditu. *Analisi hau Osagai Nagusien Analisiaren bidez lortutako 30 dimentsio esanguratsuenetatik (Osagai Nagusiak, PC) eratorritako informazioan oinarritzen da.*

Ikuspegi horrek erakutsi zuen mikroglia, neurri handi batean, homogeneoa dela, aurreko azterlanekin bat zetorrena (Keren-Shaul et al., 2017; Hammond et al., 2019; Marsh et al., 2022a) (**27. A irudia**). Mikroglia homeostatikoaren bi populazio nagusiz gain (HM1, 19050 zelula; HM2, 9818 zelula), beste lau mikroglia-populazio txikiago ere identifikatzen ditugu, klusterraren gene markatzaile espezifikoetan oinarrituta (Chen et al., 2021): gaixotasunari lotutako mikroglia 1 (DAM1; 1.944 zelula; APOE, B2M), mikroglia lisosomala (LM; 1.319 zelula; APOE, CTSB, CST7, LPL, AXL, ITGAX), interferoiarekiko sentikorra (IRM; 278 zelula; IFITM3, IRF7) eta proliferatiboa (PM; 180 zelula; adibidez, TOP2A, MKI67). Zehazki, LCIa HM2 taldeko zelulen proportzioaren murrizketa esanguratsuarekin eta LM eta IRM taldeetako zelulen proportzioaren igoera nabarmena izan zuen 24 ordutan (**27. B irudia**). Beraz, badirudi LCIk epe laburreko ondorioak eragiten dituela mikrogliaren transkribatzean eta zelulen funtzionamendu homeostatikoari eragiten diola, **6.2.8 atalean** adierazi den bezala.

LM populazioak mikroglia homeostatikoko *bona fide* markatzaileen murrizketa nabarmena erakutsi zuen, hala nola P2ry12 eta Tmem119 (**28. A irudia**). LCI bidezko tratamendua egin eta zazpi egunera, mikrogliaren populazioen proportzioak kontrol-baldintzaren antzekoak ziren, ugalketa-zelulen gorakada nabarmenagatik izan ezik (**28. B irudia**). LM biztanleriak jarduera lisosomalarekin lotutako gene-maila handiagoak erakutsi zituen, CTSB, CTSZ,

CD68, ATP6V0 eta CD63 barne (**28. D irudia**). Gainera, talde horrek Lgals3ren adierazpen espezifikoa erakutsi zuen (**28. D-E irudia**), baita Cd68ren maila handiagoa ere (**28. B-C irudia**). Horrela, LM populazio postfagozitikoa dela baieztatu zen.

Cd68ren igoera karga fagozitikoaren degradaziorako lisosomen igoeraren ondorio izan daitekeela uste dugu (Chistiakov et al., 2017), eta Gal3ren gorakada, berriz, kaltetutako lisosomen berreskurapenean duen parte-hartzearekin lotuta egon daitekeela (Rotshenker, 2022). LM klusterrak PAMekin antzekotasun batzuk ditu, fagozitosiarekin lotu direnak; izan ere, biek sinadura zentraleko geneak partekatzen dituzte, hala nola CD9, CD63 eta LGALS3 (Li et al., 2019). Hemen aurkeztutako datuek erakusten dutenez, fagozitosiaren ondorengo gertaera goiztiarrek testuinguru fagozitiko desberdinen (LCI eta PAMek burututako fagozitosia) artean partekatutako eta zelularen jarduera degradatzaileekin modu ulergarrian lotutako transkripzio-sinadura iragankorra adierazten dute. Beraz, mikroglia fagozitikoak transkripzio-egoera iragankorra hartzen du, karga fagozitikoa behar bezala degradatzeko beharrezko funtzioei lotuta.

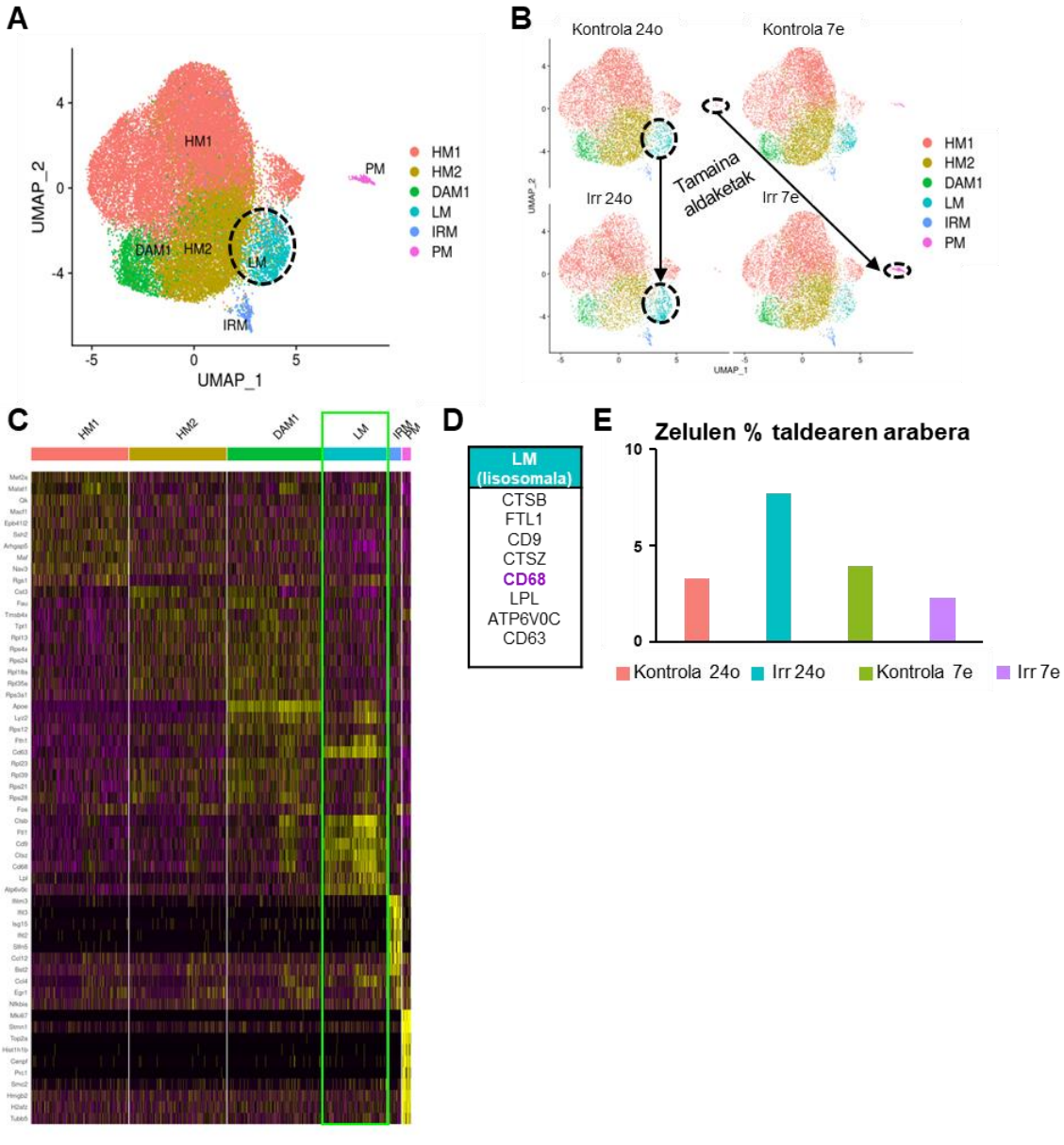

27. irudia. Kluster lisosomalak detektatzea, lehendik zeuden sc-RNA-seq datuak berriz aztertuta. *(**A**) Hautatutako klusterren UMAP, non LM klusterra beltzez punteatutako lerroek inguratzen duten. (**B**) LCIaren ondoren LM 24h gehitzea erakusten duten oharrekin egindako tratamenduen UMAP. (**C**) Klusterrak gehien adierazten dituen geneen bero-mapa. LM klusterra berde argiz inguratuta dago. (**C**) Laburpen-taula, LM klusterrean gehien adierazitako 10 geneekin. More ilunean CD68 agertzen da (oso adierazia zelula postfagozitikoetan). (**D**) LM klusterreko zelulen ehunekoa baldintza esperimental bakoitzean.*

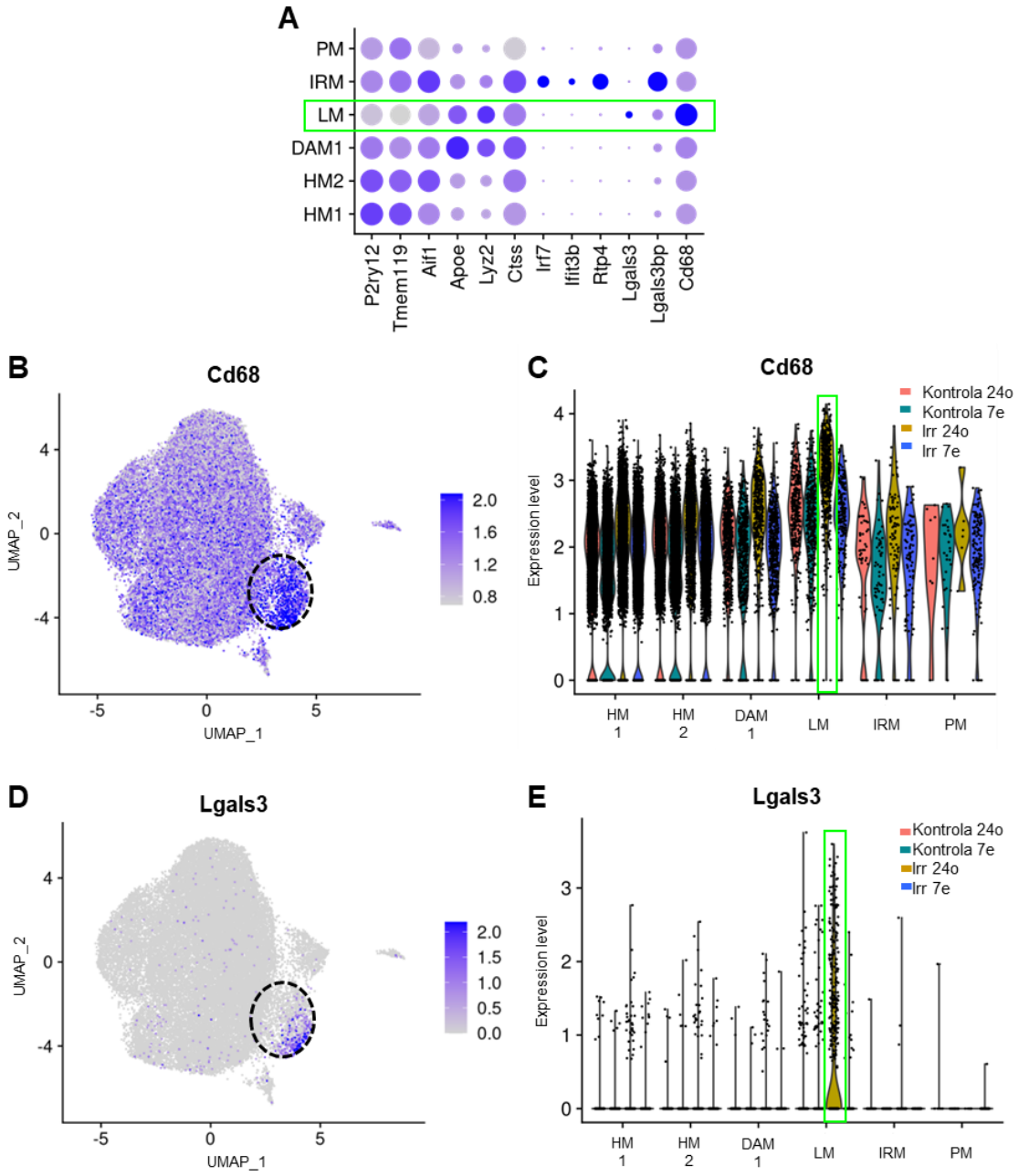

28. irudia. LM klusterra ezaugarritzea. LM klusterra ezaugarritzea. *(**A**) Klusterren arteko adierazpen-aldaketa nagusiak erakusten dituen puntu-diagrama. LM klusterra laukizuzen berde argi batek inguratzen du. (**B**) UMAPek FCk adierazitako CD68 adierazpena erakusten du. LM klusterra beltzean punteatutako lerroek inguratzen dute. (**C**) Biolin-plotak, hainbat baldintzaren arteko klusterretan CD68 erakusten dutenak. Laukizuzen berde argi baten bidez adierazten da LM klusterraren adierazpena LCIren ondorengo 24 orduetan handitzea. (**D**) UMAPek LGALS3-ren adierazpena erakusten du, FCk adierazia. LM klusterra beltzean punteatutako lerroek inguratzen dute. (**E**) Violin-plots, LGALS3 hainbat klusterretan erakutsiz, hainbat baldintzen artean. LM klusterrean LCIaren ondorengo 24 orduetan adierazpenaren gehikuntza laukizuzen berde argi batekin adierazten da.*

4.2.14. Mikrogliak gora egiten du fagozitosiaren ondoren

Epe laburreko fagozitosiak eragindako aldaketak definitu ondoren (24 ordu), epe luzeko aldaketa transkripzionalak aztertu ziren (7e). Bai scRNA-seq-en lehen analisiak, bai bigarrenak eta bai taldekatzeak talde ugaritzaile bat erakutsi zuten, LCIaren ondoren tamainaz handitu zena, 7 egunetara zehazki (**29. C irudia**).

Hipokanpoaren DGan populazio ugaltzailea baliozkotzeko eta identifikatzeko, mikrogliaren eta Ki67ren immunofluoreszentzia eta irudi konfokalak egiten ditugu. MKi67 bidez kodetutako KI67 proteina, ugalketarekin lotutako proteina nuklear bat da. Proteina honen azterketa control-baldintzan (irradiatu gabea) eta LCIren ondorengoko zenbait denboretan analizatuko da (6o, 24o, 3e, 7e eta 30e) (**30. A irudia**) zelula ugaritzaileak identifikatzeko.

DGn, LCIaren ondoren (6 ordu eta 24 ordu), Ki67 zelulen guztizko kopurua murriztu egin dela ikusi dugu. Hala ere, zenbaki horiek denborarekin berreskuratzen dira (**30B irudia**). Murrizketa horrek eta ondorengo errekuperazioak LCIk neurogurasoen ugalketari kalte egin ziola iradoki zuten. DG mikroglia ez zen ugaritzen kontrol-saguetan; hala ere, LCIa baino 7 egun geroago, ugaritzen hasi ziren, eta joera horrek gora egiten jarraitu zuen ondorengo denbora-puntuetan (30d) (**30. A, C irudia**). Gainera, ugalketa mikrogliala DGren espezifikoa izan zen, ia ez baitziren aurkitu zelula mikroglial ugalkorrik CAn. Horrek fagozitosiak ugalketa mikrogliala eragin zuela iradokitzen du (**30. D irudia**). Horrela, fagozitosiak mikrogliaren ugaltze mikrogliala eragiten zuela 7 egunetara balioztatu dugu. Halaber, datu hauek sc-RNASeq bidez ikusitako populazio ugaltzailearen aldaketak fagozitosiaren ondorio zirela ere balioesten dituzte. Beraz, fagozitosiak programa ugaltzaile luze bati ekin zion mikroglian.

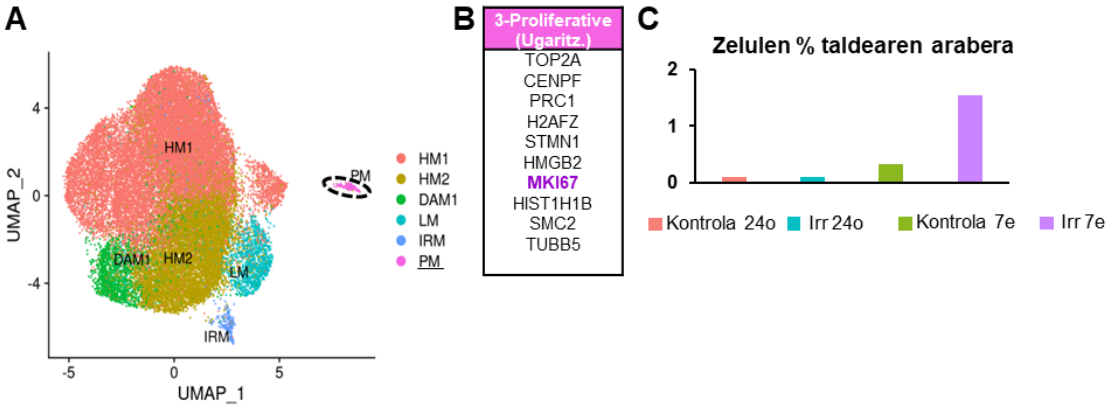

29. irudia. Talde ugaltzailea ezaugarritzea eta aztertzea. *(**A**) UMAPek populazio ugalkorra erakusten du, puntu-lerro batez inguratua. (**B**) Kluster ugaltzailearen gene bereizgarrien zerrenda. (**C**) baldintza esperimental bakoitzean, kluster ugaltzaileko zelulen %.*

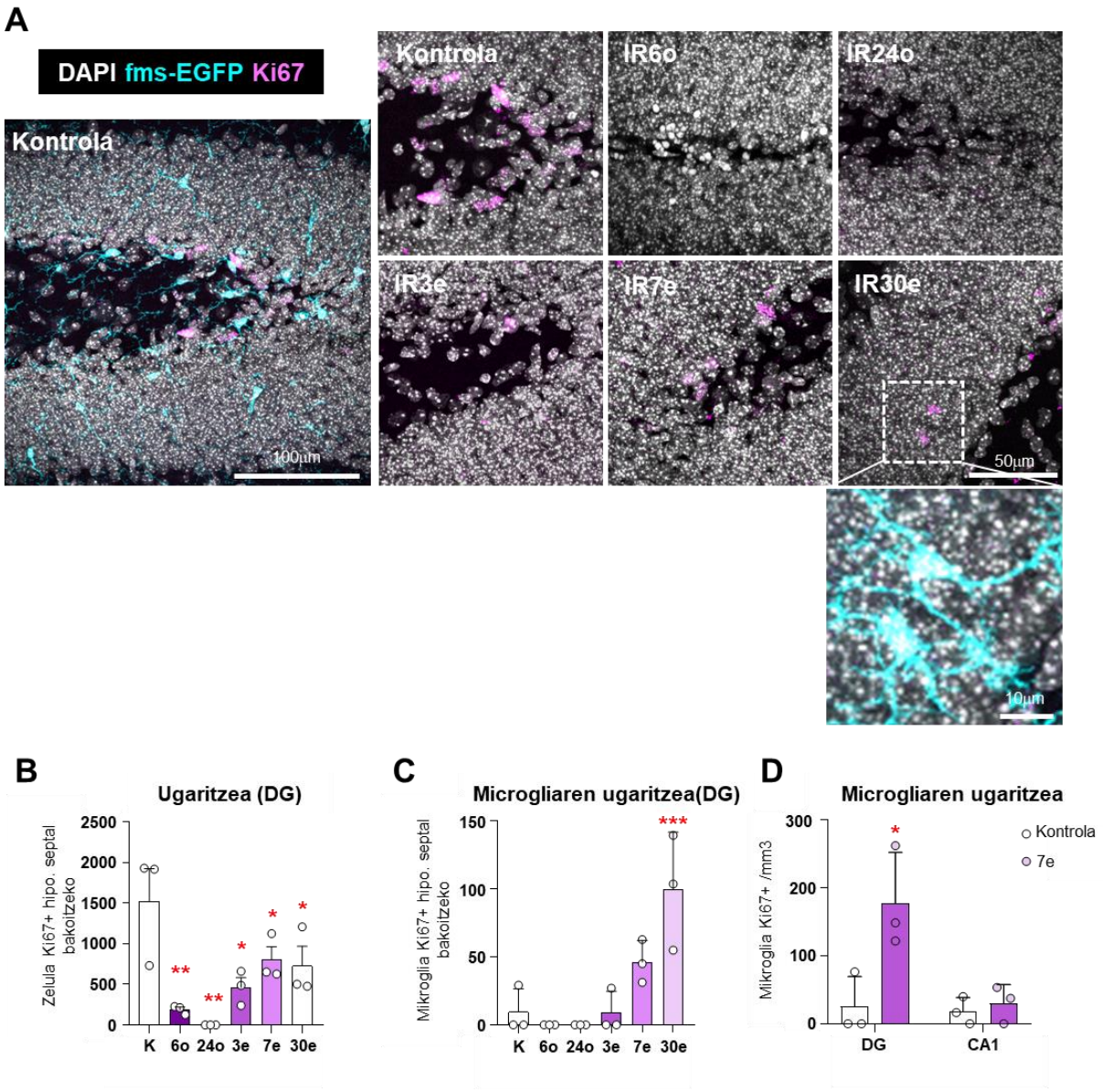

30. irudia. LCIaren osteko ugalketa aztertzea. *(**A**) Baldintza esperimental desberdinen (kontrola, eta 6h, 24h, 3d, 7d, eta LCIren ondorengo 30d) irudikapen-irudiak, DAPI tindaketa (zuria), Ki67 (magenta) eta GFP (cian) erakutsiz. Mikroglia ugaltzailearen xehetasuna lauki punteatu zuriaren barruan adierazten da. (**B**) Ki67+ zelula-kopurua GDn hipoeremu septal bakoitzeko. (**C**) DGko Ki67+ mikroglia-kopurua hipoeremu septal bakoitzeko. (**D**) Ki67+ mikroglia kopurua mm3-ko DG eta CA eskualdeetan. Barrak n = 3 saguren batez bestekoa ± SEM erakusten du. Datuak norabide bakarreko ANOVAren bidez [B, C] aztertu ziren, eta, ondoren, Holm-Sidaken post hoc probak, hala zegokionean, eta Student-en t probaren bidez [D]. Izartxoek kontrolaren eta JLaren arteko esanahia adierazten dute (6h, 24h eta 7d) [B, C] eta kontrolaren eta JLren artekoa [D].* $p < 0,05$,** ordezkatzen du $p < 0,01$,*** irudikatzen du $p < 0,001$. Eskala-barrak = 100µm and 50µm hurrenez-hurren [A], 10µm ([A]-n txertatua); z=8.4µm, z=11.2µm, z=16.1µm, z=14.7µm, z=16.1µm, z=16.1µm [A].*

4.2.15. Fagozitosia eragindako programa ugaltzailea abortiboa da

Jarraian, programa ugaltzaile horrek mikroglia-kopurua aldatzen ote zuen ebaluatuko dugu. Populazio mikrogliala 24 ordura murrizten zela ikusi genuen, baina maila basalak geroago berreskuratzen ziren (**31. A irudia**), eta horrek zeluletako batzuk fagozitosia gertatu eta gutxira hil daitezkeela iradokitzen du. Mikroglia jaioberriaren jarraipen zuzena egiteko, LCIa egin eta 7 egunera bromodesoxiuridina (BrdU) injektatzen dugu, zelularen S fasean DNAri gehitzen zaion timidina nuklerraren analogo sintetikoa, eta zelula ugaltzaileak etiketatzen ditugu (Duque et al., 2015). Mikroglia ugaritzailearen bizi-denbora aztertzeko, burmuinaren azterketa mikroskopikoa injekzioaren osteko 24 eta 48 orduetara (hpi / oio) egin zen. Horretarako mikrogliaren (fms-EGFP) eta BrdUren immunofluoreszentzia eta irudi konfokalak egin genituen (**31. A-B irudia**). Aztertutako bi denbora-puntuetan (24hpi(oio) eta 48hpi(oio)), BrdU+en populazio osoa ez zen aldatu. Hala ere, 48oio baldintzan jaitsiera bat pairatu zuen (**31. C-E irudia**). Oro har, datu horiek erakusten dute fagozitosiak eragindako ugalketa mikrogliala abortiboa izan zela, eta horrek zelula sortu berri gutxi batzuk bakarrik epe luzera mantentzen direla iradokitzen du.

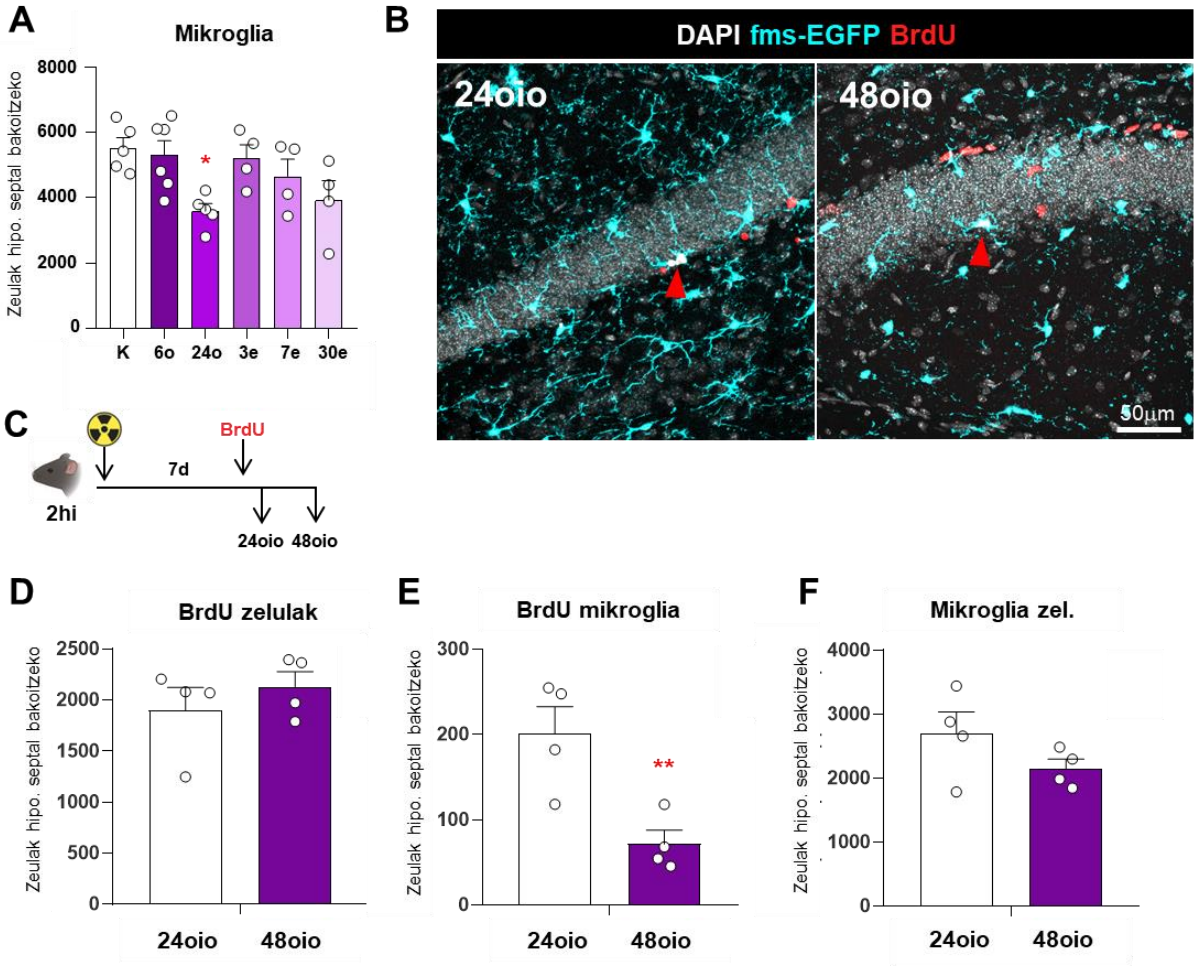

31. irudia. Fagozitosiaren ondorengo ugalketa funtzionalaren analisia. *(**A**) DGko mikroglia kopurua hipoeremu septal bakoitzeko, LCIaren ondorengo hainbat puntu tenporaletan (Control, 6h, 24h, 3d, 7d, 30d). (**B**) Baldintza esperimental desberdinen*

*adierazgarri diren irudi konfokalak (24hpi(oio), 48hpi(oio)), DAPI tindaketa (zuria), BrdU (gorria) eta GFP (ziana) erakutsiz. (**C**) BrdUren saiakuntzaren diseinu esperimentala, LCIren "superpagozitosiaren" ereduaren ondoren. (**D**) Hipokanpo septal bidezko GDko BrdU+ zelula-kopurua. (**E**) DGko BrdU+ mikroglia-kopurua hipoeremu septal bakoitzeko. (**F**) DGko mikroglia kopurua hipoeremu septal bakoitzeko, 24hpi eta 48hpi. Barrek n = 4 saguren ± SEM batez bestekoa erakusten dute. Datuak Student-en t probaren bidez aztertu ziren. Izartxoek 24hpi eta 48hpi arteko esanahia dute.** p < 0,01 adierazten du. Eskala-barra = 50µm; z=13.3µm, z=27.3µm.*

4.2.16. Mikrogliaren ugaritzeak konpentsatu egiten du fagozitosiaren ondoren eragindako zelula-heriotza

LCIaren ondoren (**31. A irudia**), mikrogliaren 24 orduko murrizketa ikusten dugunez, heriotza mikroglial goiztiarra modu zuzenagoan ebaluatzen dugu jarraian, eta fagozitosian inplikatutako mikroglia apoptotikoa 6 ordura ikusten dugu (Pu.1 nukleo piknotikoak/karrioretikoak) (**32. A irudia**). Hala ere, zenbakia txikiegia zen kuantifikatzeko, beharbada hurbileko mikrogiliek berehala fagozitatu zituztelako. Heriotza mikrogliala fagozitosiaren ondorio ote zen modu independentean aztertzeko, *in vitro* fagozitosi-saiakuntza bat egiten dugu, SH-SY5Y zelula apoptotikoekin (Diaz-Aparicio et al., 2020) (**32. B-C irudia**). Fagozitosiaren ondoren, mikrogliak handitu egin zuen apoptosian (GO apoptosia: 0006915) eta ugaritzean (GO proliferation: 0008283) (**32. D irudia**) inplikatutako geneen adierazpena, eta mikroglia apoptotikoaren areagotzea antzeman zen neurona apoptotikoekiko esposizioaren ondoren (% 2,3 ± 1,2). Joera horrek gora egiten jarraitu zuen denborarekin, 24 ordura iritsi arte (% 12,6 ± 0,9) (**32. E irudia**). Beraz, fagozitosiak mikrogliaren apoptosi goiztiarra (6-24 ordu) eragiten duela dirudi, *in vivo* zein *in vitro*, eta ondoren ugaritze abortiboa jartzen du martxan (3-30e).

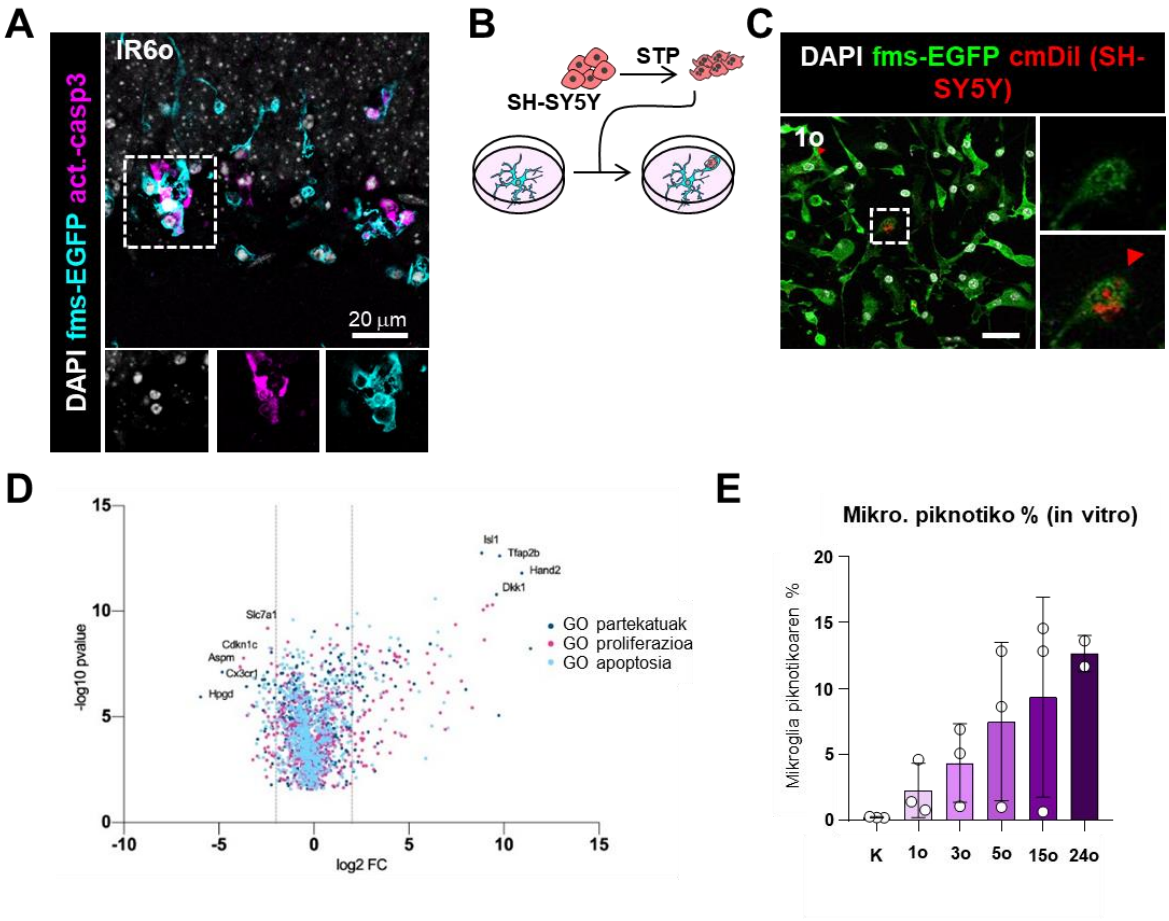

32. irudia. Heriotza mikroglialaren analisia, fagozitosiaren ondoren. *(**A**) Mikroglia apoptotikoaren irudi konfocal adierazgarria, DAPI (zuria), caspasa 3 aktibatua (magenta) eta GFP (cian) tindaketa erakusten duena. Xehetasuna punteatutako karratu baten barruan agertzen da. (**B**) In vitro fagozitosi-saiakuntzaren diseinu esperimentala. (**C**) DAPI (zuria), SH-SY5Y banpiroarekin (gorria) eta GFParekin (ziana) tindaketa erakusten duten in vitro a 1h fagozitosiaren irudi konfuzalak. SH-SY5Y edukiaren xehetasuna mikroglian. (**D**) Sumendiaren diagrama, mikroarraian gehien adierazten diren geneak erakusten dituena. (**E**) Mikroglia piknotikoaren ehunekoa fagozitosiaren ondoren. Barrek 3 esperimentu independenteren ± SEM batez bestekoa erakusten dute. Datuak norabide bakarreko ANOVAren bidez aztertu ziren, eta, ondoren, Holm-Sidaken post hoc probak, egokia izan zenean. Izartxoek kontrolaren eta LCIaren arteko esanahia adierazten dute (6h, 24h eta 7d).* p < 0,05 adierazten du. Eskala-barrak =30µm [B], 20µm [E]; z=6.3µm [B], z=0.7µm [E].*

Laburbilduz, mikroglia postfagozitikoa ezaugarritzen/identifikatzen duten parametro desberdinen miaketak bi populazio postfagozitiko desberdin identifikatzea ekarri zuen: Fagozitosiaren osteko populazio goiztiarra (24o), Gal3 espezifikoki adierazten zuena eta CD68aren adierazpena areagotzen zuena; eta fagozitiko osteko populazio berantiarra (7e), fagozitosiak eragindako heriotzari erantzuteko ugaritzen zena.

Heriotza mikrogliala eragin zuen mekanismoa zein zen zehazten jarraitzeko, hurrengo helburuan estres oxidatiboa, alterazio mitokondrialak eta aldaketa metabolikoak aztertuko ditugu heriotza mikroglialaren kausa posible gisa.

Ondoren, berritutako populazio horrek epe luzerako ahalmen fagozitikoa berreskuratzen duen aztertuko dugu.

4.3: Fagozitosiaren ondoren mikrogliari eragiten dioten mekanismoak argitzea

Emaitzen bigarren atalean, mikroglia postfagozitikorako identifikatzaileak aurkitzea proposatu genuen. Atal horretan, ondorengoko aurkikuntzak egin genituen, alde batetik, fagozitosiaren ondorengoko epe laburran Gal3+ mikrogliaren populazioa ugaritu zen. Beste aldetik, fagozitosiaren epe luzera, fagozitosiak eragindako heriotza konpentsatzen duen mikroglia ugalkorreko populazio bat identifikatu genuen. Atal honetan, heriotza zelularraren azpiko mekanismoak aztertuko ditugo mikroglia postfagozitikoan. Bereziki azpimarratuko ditugu: estres oxidatibo postfagozitikoa, mitokondriak eta metabolismo zelularra, faktore hauek guztiak erlazionatuta daudelako eta zelularen heriotzarekin lotuta daudelako ere.

4.3.1 Fagozitosiak OEEn ekoizpena handitzen du mikroglian

Lehenik eta behin, oxigeno-espezie erreaktiboen (ROS-OEE) ekoizpena aztertu genuen, hainbat zelula-prozesutan sortzen dena, hala nola zelulen ugaritzean, desberdintzean, egokitzapen metabolikoan, immunitatearen erregulazioan (Glasauer et al., 2013) eta fagozitosian (Dupre-Crochet et al., 2013). Fagozitosian, OEEak fagosoman sortzen dira eta karga degradatzen laguntzen dute (Minakami et al., 2006). Hala ere, OEE maila handiegiak proteina, azido nukleiko, lipido, mintz eta organuluetan kalteak eragiten ditu, eta horrek heriotza zelularreko prozesuak aktibatzea ekar dezake, hala nola apoptosia (Redza-Dutordoir et al., 2016). Beraz, fagozitosiaren ondoren estres oxidatzailea sortzen zen eta estres horrek zelulari kalte handiagoa eragin ziezaiokeen aztertzeko, fagozitosiaren *in vitro* eredua erabili zen. Eredu honetaz baliatuz OEE maila neurtuko da CellROX zunda fluorogenikoarekin. Fagozitosia gertatu eta 6 ordura, OEEn mailak 2,1 ± 0,3 aldiz handiagotu zen, naïve mikrogliarekin koparatzen badugu. 24 ordura, berriz, beheranzko joera ikusi zen, eta horrek iradokitzen du OEEn mailak naïve mikrogliaren mailetara itzultzen ari zirela (**33. irudia**). Datu horiek iradokitzen dute OEEn ekoizpena zelulen disfuntziora eta ondorengo heriotzara daraman estres oxidatiboaren sorreran inplikatuta egon daitekeela. Hala ere, emaitza hori berretsi egin behar da, antioxidatzaileek efektu hori irauli dezaketen eta fagozitosiaren ondoren heriotza mikrogliala saihestu dezaketen aztertuz.

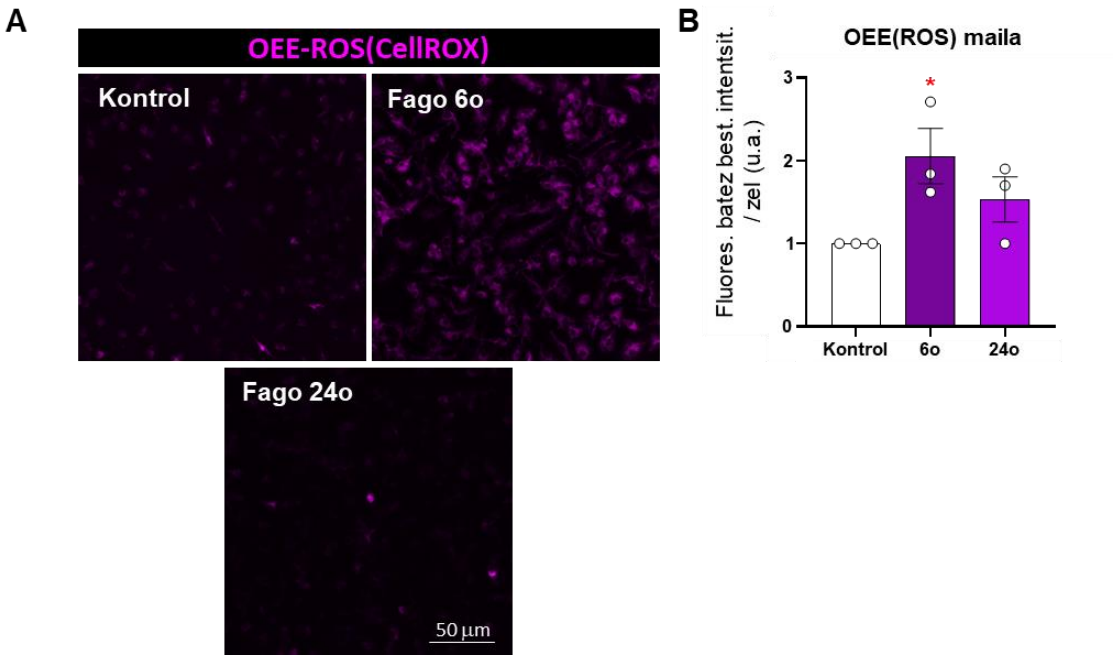

33. irudia. Fagozitosiaren osteko OEEn analisia. ***(A)*** *Mikroglia primarioen OEEn adierazpena baldintza desberdinetan irudikatzen duten irudi adierazgarriak (Kontrola, 6 ordu eta 24 ordu).* ***(B)*** *Unitate arbitrarioetan (u.a.) adierazitako OEEn mailak. Barrek n = 3 esperimentu independenteen batez bestekoa ± batez bestekoaren errore estandarra erakusten dute. Datuak bide bakarreko ANOVA probaren bidez aztertu ziren, eta, ondoren, Holm-Sidaken post hoc probak, egokia izan zenean. Asteriskoek mikroglia kontrolaren eta mikroglia fagozitikoaren (6o eta 24o-tara) arteko aldaketa esanguratsuak adierazten dituzte. * p < 0.05 adierazten du. Eskala-barra = 50 µm*

4.3.2 Fagozitosiak mitokondriak birmoldatzen ditu, mitokondria-kopurua gutxituz eta sareak sinplifikatuz.

Mitokondriek OEEn 90% inguru sortzen dituzte (Tirichen et al., 2021). Gainera, OEEn ekoizpen honek kalte mitokondriari kaltea eragiten dio, eta mitokondriek aldaketak pairatzen dituzte, hala nola birmoldaketa morfologikoa (Muliyil et al., 2014) eta mitofagia (Schofield et al., 2021). Fagozitiko osteko mikrogoliaren mitokondrien alterazioak 24 ordura xehetasun handiagoz aztertzeko, mitokondria-sarea, morfologia eta ultraestruktura aztertuko ditugu, gure *in vitro* fagozitosi-eredua erabiliz, bai BV2 mikroglia zelula-lerroarekin, bai mikroglia primarioarekin. Mitokondria-sarea eta morfologia GFP-Mito-7 plasmidoarekin transfektatutako BV-2 zeluletan aztertu ziren (García-Moreno et al., 2014). Plasmido horrek mitokondriak etiketatzen dituzte C oxidasa zitokromoaren VII. azpi-unitatera loturaren ondorioz (Olenych et al., 2007). Mitokondriak mikroskopia konfokalaren bidez bistaratu ziren. Ondoren, sare mitokondrialak (Fiji erabiliz) eta 3Dko morfologia mitokondriala (Huygens erabiliz) aztertu zen (**34. A irudia**). Bi analisi-mota horiek baliokideak izan ziren, eta zelula bakoitzeko objektu mitokondrialen kopuru konparagarria detektatu zuten (**34. B irudia**), metodoen arteko korrelazio handia erakutsiz (R2 = 0,89). Mitokondria-sarearen analisiak objektu mitokondrialak modu sinplifikatuan irudikatu zituen, sarearen

oinarrizko forma erakusten zuen erdiko lerro edo eskeleto bat sortuz, eta, horri esker, haren konplexutasuna aztertu ahal izan genuen. Horrela, ikus dezakegu fagozitosiak mitokondrien banakako kopurua nahiz sareak osatzen dituzten mitokondrien kopurua murrizten zuela. Luzera, adarrak eta loturak murrizteko joera ere ikusten dugu, eta horrek sarearen konplexutasuna murriztea iradokitzen du (**34. C irudia**). Morfologia mitokondrialaren analisiak ere agerian utzi zuen fagozitosiaren ondoren objetu mitokondrialak gutxitu egin zirela, guztizko kopurua eta haien luzera osoa murriztuz. Hala ere, ez zen aldaketarik izan objetu mitokondrialen batez besteko dimentsioetan (bolumena eta luzera) (**34. D irudia**). Datu horiek, fagozitosiak BV2 zelula-lerroan mitokondrien murrizketa eragin zuela erakurtsi zuten.

Aldaketa horiek baliozkotzeko, fagozitosi-saiakuntza bera egiten dugu mikroglia primarioan, eta mitokondriak aztertu ziren transmisio-mikroskopia elektronikoaren bidez (TEM) (**35. A irudia**). Fagozitosiaren ondoren, eremu zitoplasmatiko gutxiago hartzen zuten objektu mitokondrial gutxiago zeudela ikusi genuen (**35. B-C irudia**). Fagozitosiaren ondoren, objektu mitokondrialak txikiagoak ziren, eta horrek aurretik ikusitako sare mitokondrialaren konplexutasun txikiagoa bermatzen du (**35. D irudia**). Oro har, datu horiek iradokitzen dute fagozitosiak mitokondrien kopurua murriztu zuela eta sareak sinplifikatu zituela. Murrizketa mitokondrial hori OEEn ekoizpenaren ondorio izan daiteke; izan ere, OEEn mailen igoerak dinamika mitokondriala aldatzen du eta mitofagia eragiten du (Chuang et al., 2020). Gainera, mitokondriek zelulen metabolismoan eginkizun nagusia dutenez, horiek murrizteak metabolismo katabolikoaren gutxitzea sortarazi dezake eta ondorioz heriotza mikrogliala eragin dezake.

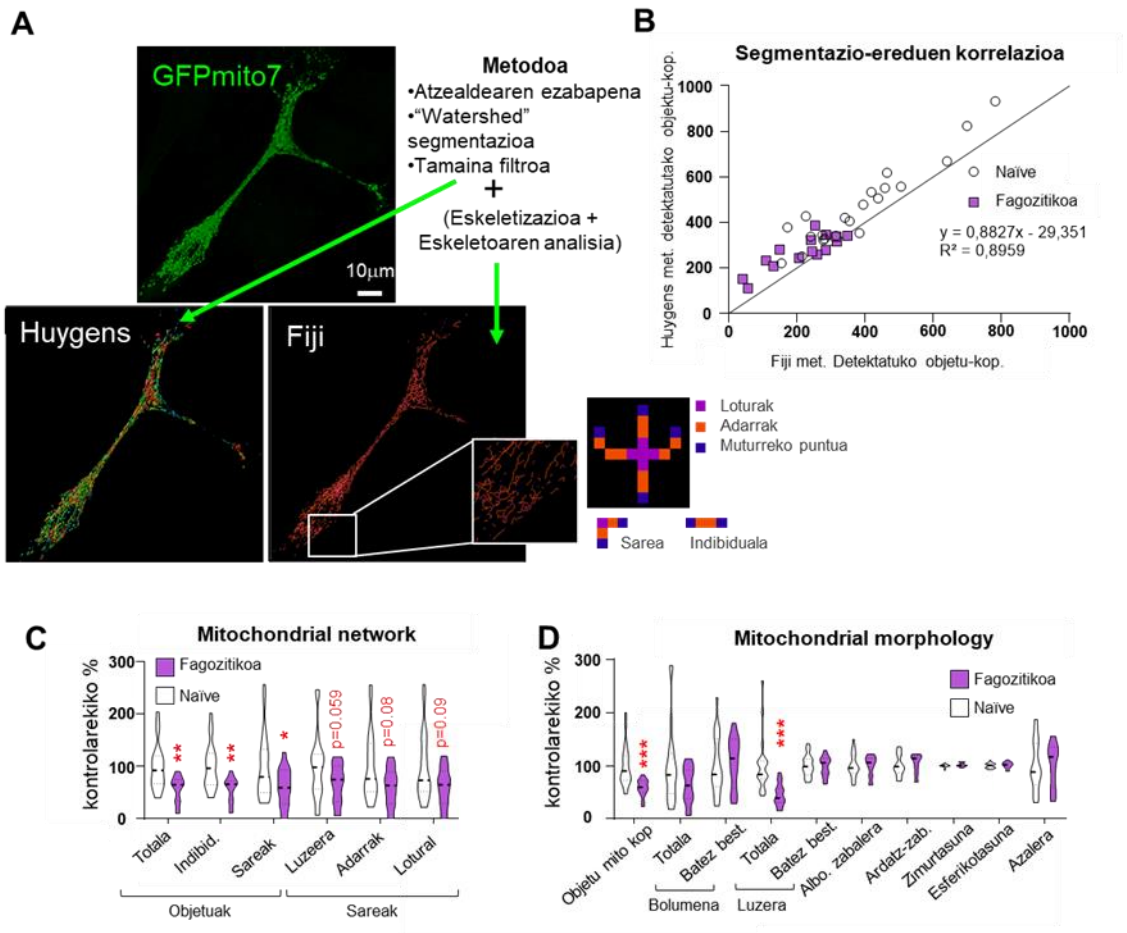

34. irudia. Mitokondrien mikroskopia konfokal bidezko analisia BV2 zeluletan, fagozitosiaren ondoren. (**A**) Analisi-metodoen laburpen grafikoa. Irudiek GFPmito7 (berdea) markatutako mitokondriak eta morfologia mitokondrialaren analisia erakusten dituzte, Huygens eta Fiji irudiak aztertzeko programen bidez, hurrenez hurren. (**B**) Objektu mitokondrialen analisiaren korrelazioa Fiji eta Huygens bidez. (**C**) Sare mitokondrialaren analisia, kontrolarekiko zenbait parametro mitokondrial normalizaturen ehunekoa erakutsiz. (**D**) Morfologia mitokondrialaren analisia, kontrolarekiko parametro mitokondrial normalizatuen ehunekoa erakutsiz. Puntu zuriek eta karratu koloreztatuek detektatutako balioen (zelulako objektu mitokondrialen kopurua) eta analisi-metodo bakoitzaren arteko korrelazioa erakusten dute. Biolin-grafikoek datuen banaketa erakusten dute, muturreko balioak barne; beheko eta goiko bisagrak hirugarren kuartilari dagozkio, hurrenez hurren. Datuek n = 3 esperimentu independente erakusten dituzte. Datuak t Student probaren bidez aztertu ziren. Datu batzuk [C, D] Log eraldatu ziren homozedastizitatea betetzeko. Normaltasuna eta homozedastizitatea bete ez zirenean, Mann-Whitney proba egin zen [C, D]. ** p <0.05 adierazten du, ** <0.01 adierazten du, *** <0.001 adierazten du. Eskala-barra= 10µm; z=7.64µm.*

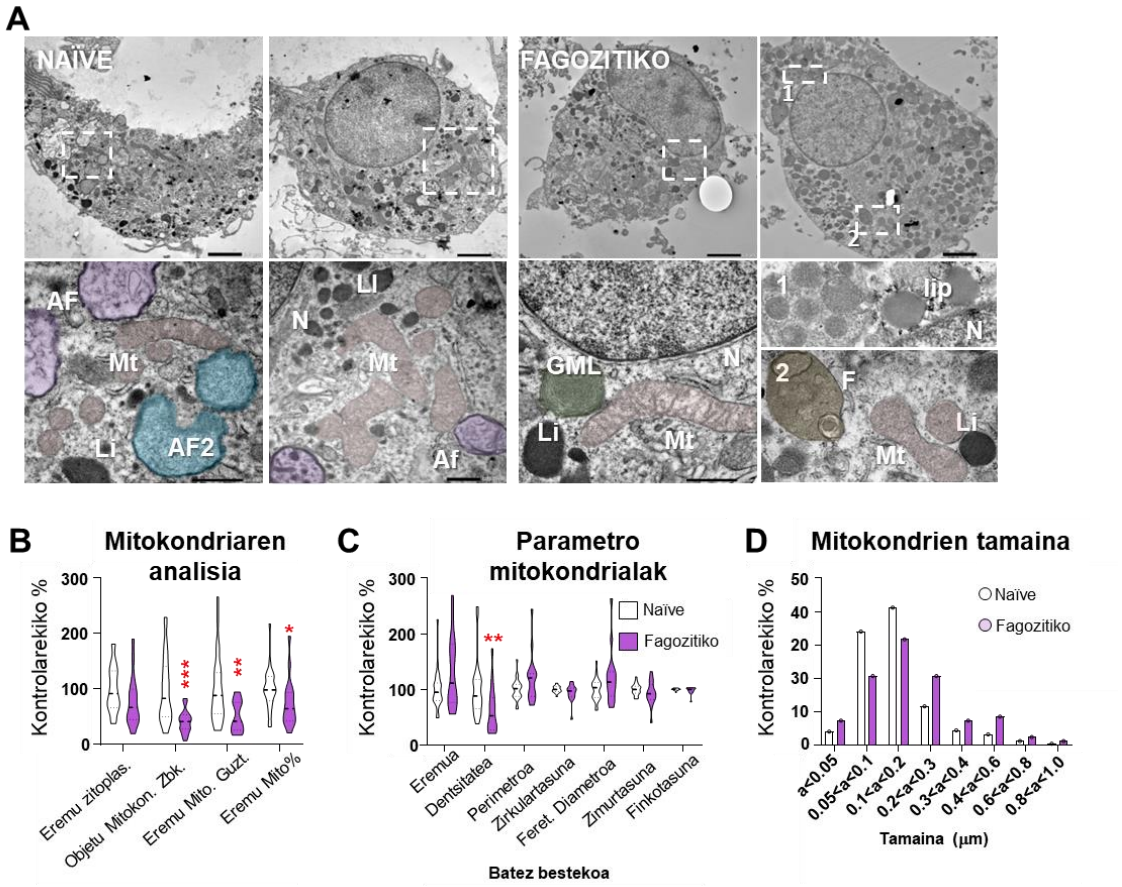

35. irudia. Mitokondrien TEM analisia mikroglia primarioan, fagozitosiaren ondoren. *(**A**) Naïve mikrogliaren eta mikroglia fagozitikoaren TEM irudiak. Irudiek mitokondriak (arrosa, Mt) eta beste organulu batzuk erakusten dituzte, hala nola lisosomak (iluna, Li). Kontrol-zeluletan autofagosoma primario eta sekundario ugari ikusten dira (purpura eta urdina, hurrenez hurren; AF); zelula fagozitikoetan, berriz, zenbait organulu degradatzaile ikusten dira, hala nola gorputz multilamelatuak (berdea, GML). Zelula fagozitikoetan ere aurkitu ziren eduki lipidikoak (lip) eta fagosomak (F). (**B**) Zitoplasma mikroglialeko objektu mitokondrialen kopuruaren eta eremuaren EM analisia, kontrolean normalizatutako neurrien ehunekoa erakutsiz. (C) Parametro mitokondrialen EM analisia, kontrolean normalizatutako neurrien ehunekoa erakutsiz. (**D**) Objektu mitokondrialen sailkapena, tamainaren arabera (mitokondrien %). Biolin-grafikoek datuen banaketa erakusten dute, muturreko balioak barne; beheko eta goiko bisagrak hirugarren kuartilari dagozkio, hurrenez hurren. Aztertu beharreko datuak t Student probaren bidez aztertu ziren. [B, C] datu batzuk Log eraldatu ziren homozedastizitatea eta/edo normaltasuna betetzeko. * p < 0,05,** adierazten du p < 0,01,** adierazten du p < 0,001. Eskalako barra, 2µm-koa zelula osoen irudietarako eta 0,5µm-koa xehetasunetarako [A].*

4.3.3 Fagozitosiak metabolismo katabolikoa murrizten du.

Mitokondriak funtsezkoak dira zelulek behar duten energia sortzeko. Arnasketa zelularra izeneko prozesu baten bidez, bide metaboliko batzuk eta organulu horiek, glukosa eta beste erregai batzuk ATP bihurtzen dituzte, zelulen dibisa energetiko unibertsala (Judge et al., 2020). Fagozitosiak mitokondria-sarea

birmoldatu eta mitokondria-kopurua murrizten duenez, fagozitosiaren ondoren metabolismo katabolikoari eragiten ote zion aztertuko dugu, eta tartean dauden bideak aztertuko ditugu (glikolisia, azido trikarboxilikoaren zikloa (ATZ) eta arnasketa mitokondriala (**36. A irudia**). In vitro fagozitosi-eredua erabiliz, 24 orduko aldaketa metaboliko postfagozitikoak aztertu genitue, metabolomika eginez eta azidotasun estrazelularra (AE) eta oxigeno-kontsumoaren tasa (OCR) neurtuz, Seahorse teknologiaren bidez (Zhang et al., 2019) eta metabolitoak masa-espektrometriaren bidez.

Analisi metabolomikoak ez zuen mikroglia post-fagozitikoetan aldaketarik hauteman, zehazki glikolisian (glukosa) eta TCA zikloan (sukzinatoa, fumaratoa eta malatoa) inplikatutako metabolito nagusien ekoizpenean (**36. B-E irudia**). Seahorse teknika erabiliz bide glukolitikoa zehatzago aztertzeko, glukolisiak ECARi egiten dion ekarpena aztertuko dugu, prozesu horrek sortutako protoien estrusio-tasa (PER) neurtuz (**36. F irudia**). PER analisiak erakutsi zuen glukolisiak mikroglia naïvean azidotzearen % 71,4 ± 13,8ra lagundu zuela, eta arnasketa mitokondrialak, berriz, gainerako % 28,6 ± 13,8ra. Mikroglia fagozitikoan, berriz, glukolisiak azidotzeari egindako ekarpena % 92,43 ± 1,2ra igo zen (**36. G irudia**). Beraz, fagozitosiaren ondoren mitokondriak murrizteak glukolisiak azidotasun estrazelularrari egiten dion ekarpena handitzen zuela zirudien. Hala ere, glukolisi konpentsatorioaren analisiak, Rotenona eta A (Rot/AA) antimizinarekin arnasketa mitokondriala blokeatu ondoren PER glukolitikoa neurtuz aztertu zenak, erakutsi zuen, mikroglia naïvean ez bezala, mikroglia fagozitikoa ez zela gai fosforilazio oxidatiboa inhibitu ondoren glukolisia handitzeko (R24H irudia). Beraz, fagozitosiak kalte egin zion metabolismo glukolitikoari, mikrogliak energia-eskaerei aurre egiteko zuen erreserba-ahalmena murriztu baitzuen, arnasketa mitokondriala farmakologikoki kaltetuta dagoenean.

Jarraian, metabolismo mitokondriala aztertuko dugu OCR (**36. I irudia**) neurtuz ATP sintasaren inhibitzaileen aurrean, eta ikusiko dugu fagozitosiak protoien ihesa areagotzen zuela, funtzionamendu mitokondrial txarraren neurri bat, eta, aldi berean, ATPren ekoizpena murrizten zuela (**36. I-J irudia**). Jarraian, OCRaren neurketak, FCCP agente desakoplantatzailearen aurretik eta ondoren (karbonilo 4 zianuroa (trifluorometoxi) fenilhidrazona), protoien gradientea barne-mintz mitokondrialaren bidez eteten duena, mitokondrien gehieneko edukiera erakutsi zuen. Fagozitosiaren ondoren, arnasketa maximoak eta erreserba-gaitasunak beheranzko joera erakutsi zuten. Gainera, mikroglia fagozitikoaren erreserba-ahalmena nayve mikrogliarenera normalizatu zenean, ikusten dugu zelulek gaitasun txikiagoa dutela OCRa handitzeko energia-eskaera handiagoari erantzuteko (**36. J-K irudia**). Gainera, inhibizio glikolitikoaren eta mitokondrialaren ondoren (**36. H-J irudia**) OCR eta ECARen gorakadak agerian utzi zuen beste bide metaboliko batzuk goraka araututa egon zitezkeela fagozitosiaren ondoren. Oro har, fagozitosiak beherantz erregulatutako metabolismo katolikora garamatza, arnasketa mitokondrial alteratuarekin eta glukolisi konpentsatzaile batekin; beste bide metaboliko konpentsatzaile batzuk, berriz, areagotu egiten direla dirudi. Beherantz erregulatutako metabolismo katoliko hori izan liteke ROSek eragindako kalte mitokondrialaren kausa, eta zelulen heriotza eragin lezake.

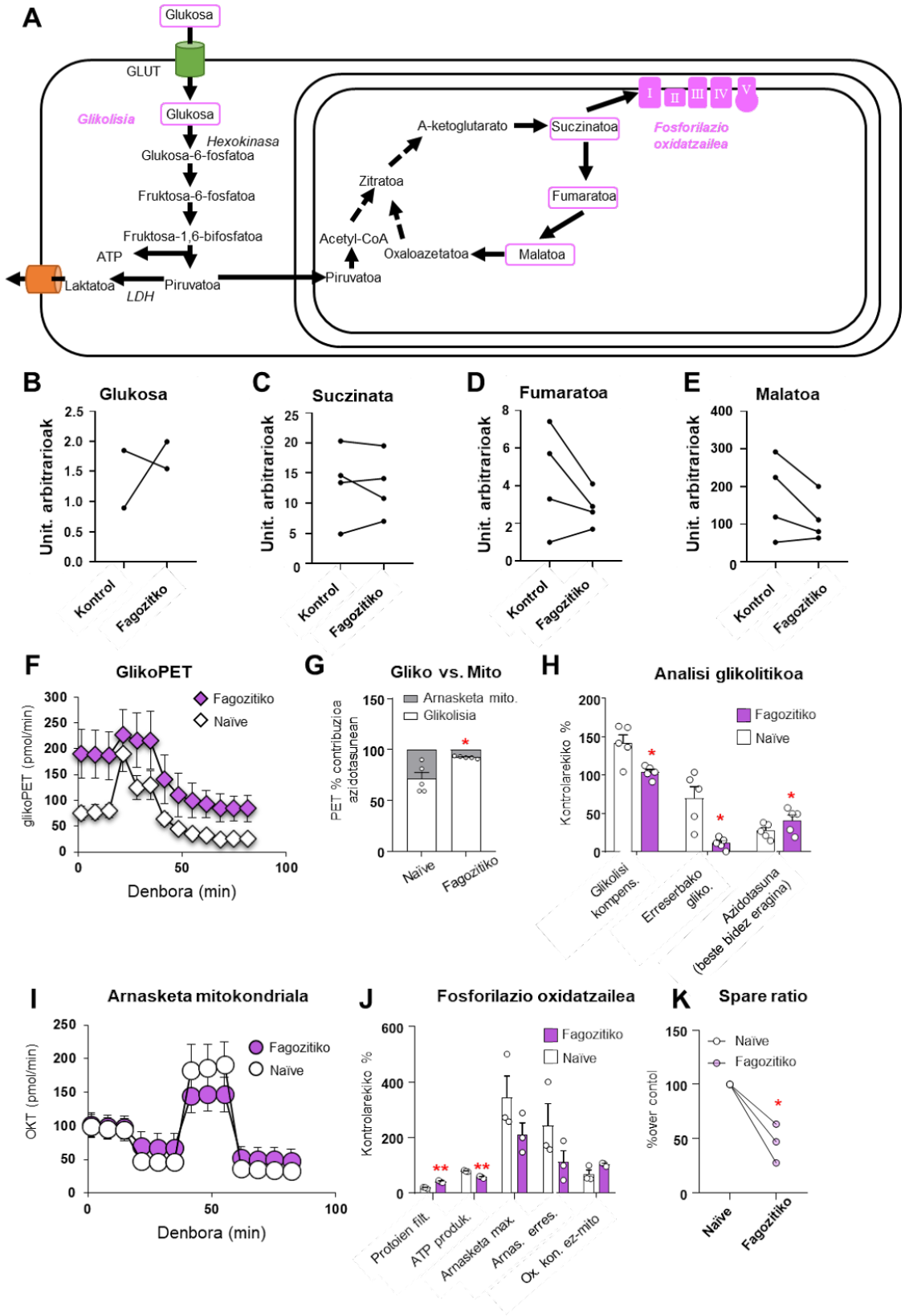

36. irudia. Fagozitosiaren osteko metabolismo katolikoaren analisia. *(**A**) Esploratutako bide metabolikoen laburpen grafikoa. Masa-espektrometria bidez aztertutako metabolitoak magentan markatuta daude. (**B**) Glukosa-mailak, unitate arbitrarioetan neurtuta (u.a.). (**C**) Unitate arbitrarioetan neurtutako suzzinato-mailak (u.a.). (**D**) Fumarato-mailak, unitate arbitrarioetan neurtuta (u.a.). (**E**) Malato-mailak,*

*unitate arbitrarioetan neurtuta (u.a.). (**F**) Protoien estrusio-tasa (PET) pmol/min-tan, mikroglia naïve eta fagozitikoaren glukolisiak eragindakoa (esperimentu adierazgarri baten datuak aukeratu ziren). (**G**) Glukolisiak zein fosforilazio oxidatiboak sortutako PETaren ehunekoa. (**H**) Glukolisiaren analisia, oinarrizko lerroarekiko PETaren aldaketak neurtuz. (**I**) Oxigeno-kontsumoaren tasa (OKT) mikrogliaren pmol/min naïve eta mikroglia fagozitikoan (esperimentu adierazgarri baten datuak erakusten dira). (**J**) Fosforilazio oxidatiboaren analisia, oinarri-lerroaren gaineko OKT aldaketak neurtuz. (**K**) Arnasketa mitokondrial normalizatuaren erreserba-ahalmena kontrolari dagokionez. Puntuek neurketa indibidualak adierazten dituzte eta lineek esperimentu independenteak (B-E) konektatzen dituzte. F-ren eta J-ren ikonoek (erronboak eta zirkuluak) esperimentu adierazgarri baten baldintza ezberdinen batez bestekoa adierazten dute, errore-barrek desbideratze estandarra (DE) erakusten duten bitartean. Barrek n = 3/5 esperimentu independenteen batez bestekoa ± batez bestekoaren errore estandarra erakusten dute. Datuak Student-en t probaren bidez aztertu ziren. Datu batzuk ([G, J]) Logaritmikoki eraldatu ziren homozedastizitatea betetzeko. Homozedastizitatea bete ez zenean, t de Welch-en ([K]) proba egin zen. Izartxoek kontrol-mikrogliaren eta microglia fagozitikoaren arteko esanahia adierazten dute.* p < 0,05 adierazten du. ** p < 0,01 adierazten du.*

4.3.4 Fagozitosiaren ondorengo analisi metabolomikoak estres oxidatiboarekin eta ugalketa zelularrarekin erlazionatutako metabolitoen ekoizpena areagotzen dela erakusten du

Fagozitosiaren ondoren gorantz erregulatuta zeuden beste bide metaboliko batzuk zehatzago behatzeko, masa-espektrometria erabiltzen dugu ondorengoko bide metabolikoak aztertzeko: folatoaren zikloko beste metabolito garrantzitsu batzuk identifikatzeko (serina), metioninaren zikloa (metionina, muinoa, betaina, GPC, SAMe eta dc-SAMe) eta bide interkonektatuak (treonina, glutamato eta glutamina), funtsezko funtzio batzuetan esku hartzen dutenak, hala nola glutatio antioxidatzailearen sintesia (GSH, GSSG) eta poliaminen sintesia (espermidina eta espermina) (**37. irudia**).

Mikroglia postfagozitikoak glutatioiaren forma oxidatua (GSH), glutatioi-disulfuroa (GSSG) (**37. D irudia**) nabarmen handitu zuen mikroglia kontrolarekin konparatuz. Glutatioi-disulfuroa antioxidatzaile gisa jarduten duenean sortzen da (Owen et al., 2010), eta horrek iradokitzen du glutatioiak estres oxidatiboaren ebazpenean parte hartu zuela. Gainera, fagozitosiak ere aldaketak eragin zituen poliaminen sintesian, S-adenosilmetionina deskarboxilatuaren (dc-SAMe) kantitatea murriztuz, eta espermidina-mailak handituz espermina gutxitzen zuen bitartean. Honek Epd/Epm erlazioa handitu zuen (R25B-C irudia). Poliamina horiek estres oxidatiboaren berreskurapenean inplikatuta daude (adibidez, espermidina gehitzeak estres oxidatiboa arintzen du, OEE mailak murriztuz (Kumar et al., 2022)), eta zelulen ugalketa eta desberdintze prozesuan hartzen dute parte (Pegg, 2016). Dc-SAMren gutxitzeak, eta Epd/Epm ratioaren areagotzeak espermidinaren ekoizpena indartuta dagoela iradokitzen dute, eta badirudi sintesiaren ondoren erabiltzen dela, gerora ez baita esperminan bihurtzen. Gainera, fagozitosiak metabolito glizerilfosforilkolinaren (GFC) mailak ere handitu zituen (**37. C irudia**), fosfatidilkolinaren aitzindaria (FC), organismoan zelula-mintzen osagai nagusia dena. Metabolito serinak,

proteinen sintesian parte hartzen duenak, fagozitosiaren ondoren ere goranzko joera erakutsi zuen. Oro har, datu metabolomikoek iradoki zuten fagozitosiaren ondoren mikrogliak sintetizatu egin zituela estres oxidatiboaren bereizmenean parte hartzen duten molekulak; zelulen berreskurapenean, prozesu fagozitikoak degradatuak izan daitezkeen proteinak eta mintz lipidikoak sortuz; eta zelulen ugalketan parte hartzen dutenak.

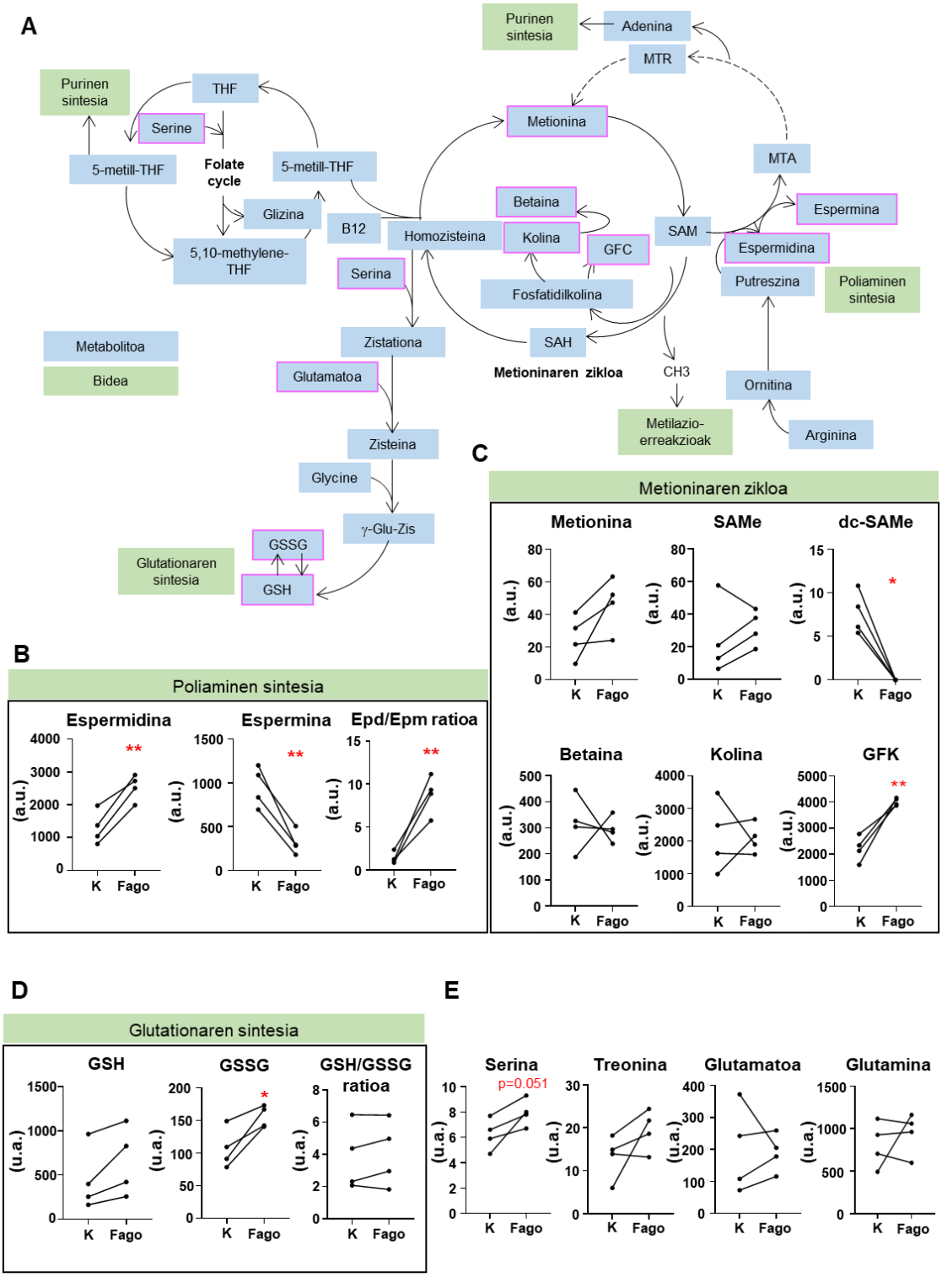

37. irudia. Metioninaren zikloko, poliaminen sintesiaren eta glutatioiaren sintesiaren metabolitoen analisia. *(**A**) Masa-espektrometria bidez eta inplikatuta dauden bide metabolikoaren bidez aztertutako metabolitoen (purpura) laburpen grafikoa. (**B**) Poliaminen sintesi-metabolitoen neurketak (espermidina, espermina, Epd/Epm erlazioa) unitate arbitrarioetan (u.a.). (**C**) Metioninaren zikloko metabolitoen neurketak (metionina, SAMe, dc-SAMe, betaina, kolina, GFK) unitate arbitrarioetan (u.a.). (**D**) Glutatioi-sintesiaren metabolitoen neurketak (GSH, GSSG, GSH/GSSG) unitate arbitrarioetan (u.a.). (**E**) Metioninaren zikloan inplikatutako beste metabolito batzuen neurketak (serina, treonina, glutamatoa, glutamina) unitate arbitrarioetan (u.a.). Puntuek neurketa indibidualak adierazten dituzte eta lineek esperimentu independenteak konektatzen dituzte (n = 3). Datuak t Student-en probaren bidez aztertu ziren. Datu batzuk [B, C] Logaritikmikoki eraldatu ziren homozedastizitatea betetzeko. Normaltasuna eta homozedastizitatea bete ez zirenean, Mann-Whitney proba egin zen [C].* p < 0,05 adierazten du, ** p < 0,01 adierazten du.*

4.3.5 Fagozitosiaren eraginkortasuna epe luzera berreskuratzen da.

Jarraian, fagozitosiak eragindako estresaren ondoren mikrogliak bere funtzioa berreskuratzeko gai ote zen aztertu genuen. Aldaketa metaboliko eta mitokondrial horiek mikroglian funtzio fagozitikoa mantentzen ote zuten aztertzeko, honako esperimentu hau egin genuen. Mikrogliari desafio egin genion sekuentzialki, gure *in vivo* eredua erabiliz eta LCIa bi aldiz administratuz, 7 eguneko denbora-tartean. Horrela, mikroglia, fagozitatu behareko zelula apoptopikoen 2 pultsoen eraginpean jarri genuen, eta bigarren esposizioaren ondoren fagozitatutako mikrogliaren eraginkortasuna aztertu genuen, haren eraginkortasun fagozitikoa (6 ordu) eta ezabapenekoa (24 ordu) aztertzeko (**38. irudia**).

GIRren bigarren pultsuak apoptosia eragin zuen, nahiz eta heriotza hori lehen pultsuan sortutakoa baino 7,8 ± 0,78 aldiz txikiagoa izan zen (**38. B-C irudia**). Gutxiera honek, lehen pultsuaren ondoren gertatutako ama zelula neuralen heriotza eta murrizpenaren ondorio da (**38. B irudia**). Hala ere, mikrogliaren ahalmena zelula apoptotikoak ezabatzeko berdina izan zen lehen eta bigarren pultsuetan, zelula apoptotiko guztiak 24 ordutan desagertu baitziren (**38. B-C irudia**). Era berean, indize fagozitikoa eta mikroglia kopurua ez zen aldatu irradiazio bikoitzaren ondorioz, eta horrek iradokitzen du heriotza postfagozitikoa proportzionala izan daitekeela mikrogliak garbitu behar dituen zelulen kopuruarekiko (**38. D-E irudia**). Bigarren irradiazioaren ondoren erronka fagozitiko txikiagoa sortzen duen ereduaren mugak gorabehera, fagozitoaren osteko mikrogliak bere ahalmen fagozitikoa mantentzen zuela zirudien, eta hondakin apoptotikoak eraginkortasunez ezabatzeko gai izan zen. Beraz, fagozitosiaren ondoren mikrogliak jasaten dituen egokitzapen mitokondrial eta metabolikoek epe luzerako funtzioa mantentzen dutela dirudi.

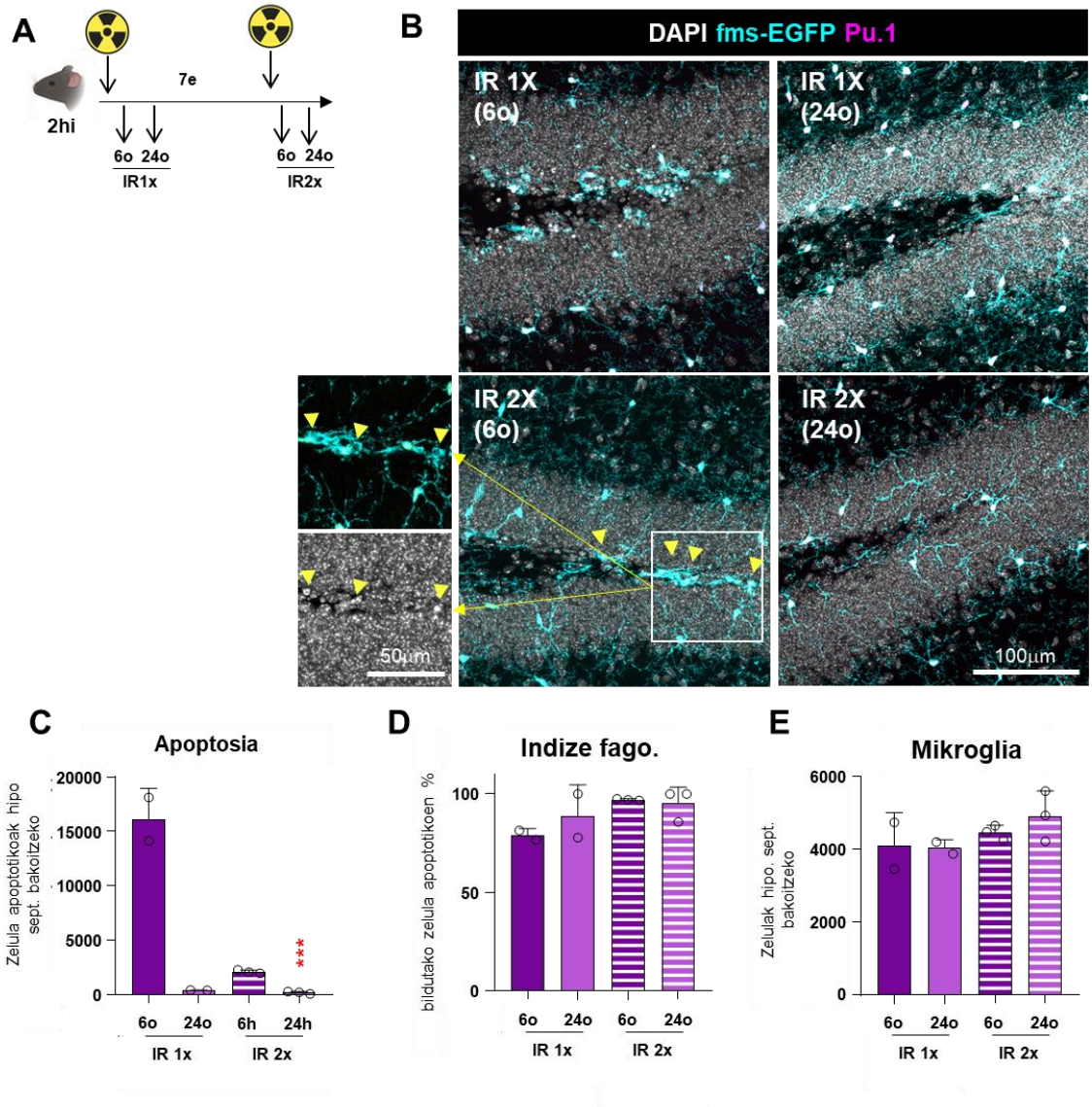

38. irudia. Bigarren erronka apoptotiko baten eraginpean dagoen fagozitosi mikroglialaren analisi funtzionala. *(**A**) Fagozitosi bikoitzaren diseinu esperimentala, LCIaren eraginpean saguak bi aldiz jarriz. (**B**) Baldintza esperimental desberdinen (IR 1x 6o eta 24o, eta IR 2x 6o eta 24o) irudi adierazgarriak, DAPI (zuria), Pu.1 (magenta) eta GFP (cian) tindaketak erakutsiz. Karratu zuri baten barruan adierazitako mikroglia fagozitikoaren xehetasuna. Poltsa fagozitikoak gezi punta horiz adierazten dira. (**C**) Zelula apoptotikoen kopurua DGn hipokanpo septal bakoitzeko. (**D**) Fago. indizea (mikrogliak fagozitatutako zelula apoptotikoen %). (**E**) Mikroglia kopurua DGn hipokanpo septal bakoitzeko. Barrek n = 3 saguren batez bestekoa ± batez bestekoaren errore estandarra erakusten dute (n = 2 kontrol positiboetarako). Datuak t Student-en probaren bidez aztertu ziren, denboraren araberako aldeak alderatu zirenean (6 ordu vs 24 ordu).*** p < 0,001 adierazten du. Eskala-barra = 100 µm [B], 50 µm ([B] -n txertatzeak); z = 16,1 µm, z = 17,5 µm, z = 18,2 µm, z = 13,3 µm [B].*

Laburbilduz, emaitzen 3. atal honetan, fagozitosiaren ondoren mikrogliari eragiten dioten mekanismoen azterketa egiten da, eta honako aldaketa nabermen hauek antzeman dira: mikroglia zelulek OEEn ekoizpena areagotu zuten, haien mitokondriak eta metabolismo katabolikoa murriztu zituzten, eta, aldi

berean, ugaritzearekin lotutako poliaminen sintesia areagotu zuten. Azken batean, funtzio fagozitikoa berreskuratu zen.

Fagozitosiak mikrogliari nola eragiten dion eta ondoren nola berrezkuratzen den ulertzea funtsezkoa da, batez ere fagozitosia jarraia egin behar denean zelula apoptotiak etengabe sortzen direlako. Honen adibide bat, garunean gertatutako minbiziak dira. Garuneko tumoreen eta horien tratamenduaren kasuan, erradioterapia garuneko minbizian tumore-zelulak kentzeko erabili ohi da (Scaringi et al., 2018), eta dosi sekuentzialetan eman ohi da (Hingorani et al., 2012). Horren ondorioz, mikrogliak sortutako zelula apoptotikoak desagerrarazi egin behar ditu erradioterapiak hiltzen duen bakoitzean. Hala ere, ikerketa gutxi dago mikrogliak egiten duen hondarren ezabatzearen inguruan eta ez dakigu zehantz-mehatz nola funtzionatzen duen. Hurrengo atalean, glioblastomaren, garuneko minbizi oso oldarkorraren, fagozitosi mikrogliala aztertuko dugu, erradiazioarekiko esposizioaren ondoren.

10. BIBLIOGRAPHY

10. BIBLIOGRAPHY

A

Abiega, O., Beccari, S., Diaz-Aparicio, I., Nadjar, A., Laye, S., Leyrolle, Q., Gomez-Nicola, D., Domercq, M., Perez-Samartin, A., Sanchez-Zafra, V*., et al.* (2016). Correction: Neuronal Hyperactivity Disturbs ATP Microgradients, Impairs Microglial Motility, and Reduces Phagocytic Receptor Expression Triggering Apoptosis/Microglial Phagocytosis Uncoupling. PLoS Biol *14*, e1002554.

Absinta, M., Maric, D., Gharagozloo, M., Garton, T., Smith, M. D., Jin, J., Fitzgerald, K. C., Song, A., Liu, P., and Lin, J.-P. (2021). A lymphocyte–microglia–astrocyte axis in chronic active multiple sclerosis. Nature *597*, 709-714.

Adwas, A. A., Elsayed, A., Azab, A., and Quwaydir, F. (2019). Oxidative stress and antioxidant mechanisms in human body. J Appl Biotechnol Bioeng *6*, 43-47.

Ajami, B., Bennett, J. L., Krieger, C., Tetzlaff, W., and Rossi, F. M. (2007). Local self-renewal can sustain CNS microglia maintenance and function throughout adult life. Nature neuroscience *10*, 1538-1543.

Akakura, S., Singh, S., Spataro, M., Akakura, R., Kim, J.-I., Albert, M. L., and Birge, R. B. (2004). The opsonin MFG-E8 is a ligand for the αvβ5 integrin and triggers DOCK180-dependent Rac1 activation for the phagocytosis of apoptotic cells. Experimental cell research *292*, 403-416.
Alcantara Llaguno, S. R., Chen, J., and Parada, L. F. (2009). Signaling in malignant astrocytomas: role of neural stem cells and its therapeutic implications. Clinical Cancer Research *15*, 7124-7129.

Allendorf, D. H., Puigdellívol, M., and Brown, G. C. (2020). Activated microglia desialylate their surface, stimulating complement receptor 3-mediated phagocytosis of neurons. Glia *68*, 989-998.

Aloisi, F. (1999). The role of microglia and astrocytes in CNS immune surveillance and immunopathology. The Functional Roles of Glial Cells in Health and Disease: Dialogue between Glia and Neurons, 123-133.

Aloisi, F. (2001). Immune function of microglia. Glia *36*, 165-179.

Anderson, S. R., Zhang, J., Steele, M. R., Romero, C. O., Kautzman, A. G., Schafer, D. P., and Vetter, M. L. (2019). Complement targets newborn retinal ganglion cells for phagocytic elimination by microglia. Journal of Neuroscience *39*, 2025-2040.

Andres-Barquin, P. J. (2002). Santiago Ramón y Cajal and the Spanish school of neurology. The Lancet Neurology *1*, 445-452.

Arandjelovic, S., and Ravichandran, K. S. (2015). Phagocytosis of apoptotic cells in homeostasis. Nature immunology *16*, 907-917.

Arcuri, C., Mecca, C., Bianchi, R., Giambanco, I., and Donato, R. (2017). The pathophysiological role of microglia in dynamic surveillance, phagocytosis and structural remodeling of the developing CNS. Frontiers in molecular neuroscience *10*, 191.

Arganda-Carreras, I., Fernández-González, R., Muñoz-Barrutia, A., and Ortiz-De-Solorzano, C. (2010). 3D reconstruction of histological sections: Application to mammary gland tissue. Microscopy research and technique *73*, 1019-1029.

Arvold, N. D., Lee, E. Q., Mehta, M. P., Margolin, K., Alexander, B. M., Lin, N. U., Anders, C. K., Soffietti, R., Camidge, D. R., and Vogelbaum, M. A. (2016). Updates in the management of brain metastases. Neuro-oncology *18*, 1043-1065.

Atagi, Y., Liu, C.-C., Painter, M. M., Chen, X.-F., Verbeeck, C., Zheng, H., Li, X., Rademakers, R., Kang, S. S., and Xu, H. (2015). Apolipoprotein E is a ligand for triggering receptor expressed on myeloid cells 2 (TREM2). Journal of Biological Chemistry *290*, 26043-26050.

Axline, S. G., and Cohn, Z. A. (1970). In vitro induction of lysosomal enzymes by phagocytosis. The Journal of Experimental Medicine *131*, 1239-1260.

Aziz, M., Jacob, A., Matsuda, A., and Wang, P. (2011). milk fat globule-EGF factor 8 expression, function and plausible signal transduction in resolving inflammation. Apoptosis *16*, 1077-1086.
Badie, B., and Schartner, J. M. (2000). Flow cytometric characterization of tumor-associated macrophages in experimental gliomas. Neurosurgery *46*, 957-962.

B

Ballabio, A. (2016). The awesome lysosome. EMBO molecular medicine *8*, 73-76.

Batchu, S., Hanafy, K. A., Redjal, N., Godil, S. S., and Thomas, A. J. (2023). Single-cell analysis reveals diversity of tumor-associated macrophages and their interactions with T lymphocytes in glioblastoma. Scientific Reports *13*, 20874.

Beccari, S., Diaz-Aparicio, I., and Sierra, A. (2018). Quantifying microglial phagocytosis of apoptotic cells in the brain in health and disease. Current protocols in immunology *122*, e49.

Beccari, S., Sierra-Torre, V., Valero, J., Pereira-Iglesias, M., Garcia-Zaballa, M., Soria, F. N., De Las Heras-Garcia, L., Carretero-Guillen, A., Capetillo-Zarate, E., Domercq, M*., et al.* (2023).

Microglial phagocytosis dysfunction in stroke is driven by energy depletion and induction of autophagy. Autophagy, 1-30.

Béchade, C., Pascual, O., Triller, A., and Bessis, A. (2011). Nitric oxide regulates astrocyte maturation in the hippocampus: involvement of NOS2. Molecular and Cellular Neuroscience *46*, 762-769.

Becher, O. J., Hambardzumyan, D., Walker, T. R., Helmy, K., Nazarian, J., Albrecht, S., Hiner, R. L., Gall, S., Huse, J. T., Jabado, N*., et al.* (2010). Preclinical evaluation of radiation and perifosine in a genetically and histologically accurate model of brainstem glioma. Cancer Res *70*, 2548-2557.

Bennett, M. L., Bennett, F. C., Liddelow, S. A., Ajami, B., Zamanian, J. L., Fernhoff, N. B., Mulinyawe, S. B., Bohlen, C. J., Adil, A., and Tucker, A. (2016). New tools for studying microglia in the mouse and human CNS. Proceedings of the National Academy of Sciences *113*, E1738-E1746.

Bernier, L.-P., York, E. M., Kamyabi, A., Choi, H. B., Weilinger, N. L., and MacVicar, B. A. (2020a). Microglial metabolic flexibility supports immune surveillance of the brain parenchyma. Nature communications *11*, 1559.

Bernier, L.-P., York, E. M., and MacVicar, B. A. (2020b). Immunometabolism in the brain: how metabolism shapes microglial function. Trends in Neurosciences *43*, 854-869.

Beurskens, F. J., van Schaarenburg, R. A., and Trouw, L. A. (2015). C1q, antibodies and anti-C1q autoantibodies. Molecular immunology *68*, 6-13.

Bhutani, N., Piccirillo, R., Hourez, R., Venkatraman, P., and Goldberg, A. L. (2012). Cathepsins L and Z are critical in degrading polyglutamine-containing proteins within lysosomes. Journal of Biological Chemistry *287*, 17471-17482.

Bilbo, S. D., Smith, S. H., and Schwarz, J. M. (2012). A lifespan approach to neuroinflammatory and cognitive disorders: a critical role for glia. Journal of Neuroimmune Pharmacology *7*, 24-41.
Binley, K. E., Ng, W. S., Tribble, J. R., Song, B., and Morgan, J. E. (2014). Sholl analysis: a quantitative comparison of semi-automated methods. Journal of neuroscience methods *225*, 65-70.

Blasi, E., Barluzzi, R., Bocchini, V., Mazzolla, R., and Bistoni, e. F. (1990). Immortalization of murine microglial cells by a v-raf/v-myc carrying retrovirus. Journal of neuroimmunology *27*, 229-237.

Blinzinger, K., and Kreutzberg, G. (1968). Displacement of synaptic terminals from regenerating motoneurons by microglial cells. Zeitschrift für Zellforschung und mikroskopische Anatomie *85*, 145-157.

Bobryshev, Y. V., Shchelkunova, T. A., Morozov, I. A., Rubtsov, P. M., Sobenin, I. A., Orekhov, A. N., and Smirnov, A. N. (2013). Changes of lysosomes in the earliest stages of the development of atherosclerosis. Journal of Cellular and Molecular Medicine *17*, 626-635.

Bocchini, V., Mazzolla, R., Barluzzi, R., Blasi, E., Sick, P., and Kettenmann, H. (1992). An immortalized cell line expresses properties of activated microglial cells. Journal of neuroscience research *31*, 616-621.

Bonney, S., Mishra, S., Pleasure, S. J., and Siegenthaler, J. A. (2020). Meninges and vasculature. In Patterning and Cell Type Specification in the Developing CNS and PNS, (Elsevier), pp. 1037-1063.

Borish, L. C., and Steinke, J. W. (2003). 2. Cytokines and chemokines. Journal of Allergy and Clinical Immunology *111*, S460-S475.

Brandes, R., Lang, F., and Schmidt, R. F. (2019). Physiologie des Menschen: mit Pathophysiologie: Springer-Verlag).

Brown, G. C., and Neher, J. J. (2014). Microglial phagocytosis of live neurons. Nature Reviews Neuroscience *15*, 209-216.

Bruce, K. D., Gorkhali, S., Given, K., Coates, A. M., Boyle, K. E., Macklin, W. B., and Eckel, R. H. (2018). Lipoprotein lipase is a feature of alternatively-activated microglia and may facilitate lipid uptake in the CNS during demyelination. Frontiers in molecular neuroscience *11*, 57.
Bruttger, J., Karram, K., Wörtge, S., Regen, T., Marini, F., Hoppmann, N., Klein, M., Blank, T., Yona, S., and Wolf, Y. (2015). Genetic cell ablation reveals clusters of local self-renewing microglia in the mammalian central nervous system. Immunity *43*, 92-106.

Buerki, R. A., Horbinski, C. M., Kruser, T., Horowitz, P. M., James, C. D., and Lukas, R. V. (2018). An overview of meningiomas. Future Oncology *14*, 2161-2177.

Buonfiglioli, A., and Hambardzumyan, D. (2021a). Macrophages and microglia: the cerberus of glioblastoma. Acta neuropathologica communications *9*, 1-21.

Buratovic, S., Stenerlöw, B., Fredriksson, A., Sundell-Bergman, S., and Eriksson, P. (2016). Developmental effects of fractionated low-dose exposure to gamma radiation on behaviour and susceptibility of the cholinergic system in mice. International Journal of Radiation Biology *92*, 371-379.

Burstyn-Cohen, T., Lew, E. D., Través, P. G., Burrola, P. G., Hash, J. C., and Lemke, G. (2012). Genetic dissection of TAM receptor-ligand interaction in retinal pigment epithelial cell phagocytosis. Neuron *76*, 1123-1132.

Bussi, C., Heunis, T., Pellegrino, E., Bernard, E. M., Bah, N., Dos Santos, M. S., Santucci, P., Aylan, B., Rodgers, A., and Fearns, A. (2022). Lysosomal damage drives mitochondrial proteome remodelling and reprograms macrophage immunometabolism. Nature Communications *13*, 7338.

Butovsky, O., Jedrychowski, M. P., Moore, C. S., Cialic, R., Lanser, A. J., Gabriely, G., Koeglsperger, T., Dake, B., Wu, P. M., and Doykan, C. E. (2014). Identification of a unique TGF-β–dependent molecular and functional signature in microglia. Nature neuroscience *17*, 131-143.

Butovsky, O., and Weiner, H. L. (2018). Microglial signatures and their role in health and disease. Nat Rev Neurosci *19*, 622-635.

Buttgereit, A., Lelios, I., Yu, X., Vrohlings, M., Krakoski, N. R., Gautier, E. L., Nishinakamura, R., Becher, B., and Greter, M. (2016). Sall1 is a transcriptional regulator defining microglia identity and function. Nature immunology *17*, 1397-1406.

C

Caberoy, N. B., Alvarado, G., Bigcas, J. L., and Li, W. (2012). Galectin-3 is a new MerTK-specific eat-me signal. Journal of cellular physiology *227*, 401-407.

Casciati, A., Dobos, K., Antonelli, F., Benedek, A., Kempf, S. J., Bellés, M., Balogh, A., Tanori, M., Heredia, L., and Atkinson, M. J. (2016). Age-related effects of X-ray irradiation on mouse hippocampus. Oncotarget *7*, 28040.

Chang, G. H.-F., Barbaro, N. M., and Pieper, R. O. (2000). Phosphatidylserine-dependent phagocytosis of apoptotic glioma cells by normal human microglia, astrocytes, and glioma cells. Neuro-oncology *2*, 174-183.
Checchin, D., Sennlaub, F., Levavasseur, E., Leduc, M., and Chemtob, S. (2006). Potential role of microglia in retinal blood vessel formation. Investigative ophthalmology & visual science *47*, 3595-3602.

Chekeni, F. B., Elliott, M. R., Sandilos, J. K., Walk, S. F., Kinchen, J. M., Lazarowski, E. R., Armstrong, A. J., Penuela, S., Laird, D. W., and Salvesen, G. S. (2010). Pannexin 1 channels mediate 'find-me'signal release and membrane permeability during apoptosis. Nature *467*, 863-867.

Chen, D., Varanasi, S. K., Hara, T., Traina, K., Sun, M., McDonald, B., Farsakoglu, Y., Clanton, J., Xu, S., and Garcia-Rivera, L. (2023). CTLA-4 blockade induces a microglia-Th1 cell partnership that stimulates microglia phagocytosis and anti-tumor function in glioblastoma. Immunity *56*, 2086-2104. e2088.

Chen, H., Chong, Z. Z., De Toledo, S. M., Azzam, E. I., Elkabes, S., and Souayah, N. (2016). Delayed activation of human microglial cells by high dose ionizing radiation. Brain research *1646*, 193-198.

Chen, L., Deng, H., Cui, H., Fang, J., Zuo, Z., Deng, J., Li, Y., Wang, X., and Zhao, L. (2018). Inflammatory responses and inflammation-associated diseases in organs. Oncotarget *9*, 7204.

Chen, W. S., Xu, P. Z., Gottlob, K., Chen, M. L., Sokol, K., Shiyanova, T., Roninson, I., Weng, W., Suzuki, R., Tobe, K*., et al.* (2001). Growth retardation and increased apoptosis in mice with homozygous disruption of the Akt1 gene. Genes Dev *15*, 2203-2208.

Chen, Y., and Colonna, M. (2021). Microglia in Alzheimer's disease at single-cell level. Are there common patterns in humans and mice? J Exp Med *218*.

Chen, Z., Feng, X., Herting, C. J., Garcia, V. A., Nie, K., Pong, W. W., Rasmussen, R., Dwivedi, B., Seby, S., and Wolf, S. A. (2017a). Cellular and molecular identity of tumor-associated macrophages in glioblastoma. Cancer research *77*, 2266-2278.

Chen, Z., Feng, X., Herting, C. J., Garcia, V. A., Nie, K., Pong, W. W., Rasmussen, R., Dwivedi, B., Seby, S., Wolf, S. A*., et al.* (2017b). Cellular and Molecular Identity of Tumor-Associated Macrophages in Glioblastoma. Cancer Res *77*, 2266-2278.

Cheng, S.-C., Quintin, J., Cramer, R. A., Shepardson, K. M., Saeed, S., Kumar, V., Giamarellos-Bourboulis, E. J., Martens, J. H., Rao, N. A., and Aghajanirefah, A. (2014). mTOR-and HIF-1α–mediated aerobic glycolysis as metabolic basis for trained immunity. science *345*, 1250684.
Chistiakov, D. A., Killingsworth, M. C., Myasoedova, V. A., Orekhov, A. N., and Bobryshev, Y. V. (2017). CD68/macrosialin: not just a histochemical marker. Laboratory investigation *97*, 4-13.

Choudhary, S., and Satija, R. (2022). Comparison and evaluation of statistical error models for scRNA-seq. Genome biology *23*, 27.

Chuang, K. C., Chang, C. R., Chang, S. H., Huang, S. W., Chuang, S. M., Li, Z. Y., Wang, S. T., Kao, J. K., Chen, Y. J., and Shieh, J. J. (2020). Imiquimod-induced ROS production disrupts the balance of mitochondrial dynamics and increases mitophagy in skin cancer cells. J Dermatol Sci *98*, 152-162.

Chung, W.-S., Clarke, L. E., Wang, G. X., Stafford, B. K., Sher, A., Chakraborty, C., Joung, J., Foo, L. C., Thompson, A., and Chen, C. (2013). Astrocytes mediate synapse elimination through MEGF10 and MERTK pathways. Nature *504*, 394-400.

Cignarella, F., Filipello, F., Bollman, B., Cantoni, C., Locca, A., Mikesell, R., Manis, M., Ibrahim, A., Deng, L., and Benitez, B. A. (2020). TREM2 activation on microglia promotes myelin debris clearance and remyelination in a model of multiple sclerosis. Acta neuropathologica *140*, 513-534.

Ciuntu, A. (2017) The role of tetraspanins in neutrophil survival and phagocytosis, University of Sheffield.

Cockram, T. O., Dundee, J. M., Popescu, A. S., and Brown, G. C. (2021). The phagocytic code regulating phagocytosis of mammalian cells. Frontiers in Immunology *12*, 629979.

Cockram, T. O., Puigdellívol, M., and Brown, G. C. (2019). Calreticulin and galectin-3 opsonise bacteria for phagocytosis by microglia. Frontiers in Immunology *10*, 2647.

Cole, L. K., Vance, J. E., and Vance, D. E. (2012). Phosphatidylcholine biosynthesis and lipoprotein metabolism. Biochimica et Biophysica Acta (BBA)-Molecular and Cell Biology of Lipids *1821*, 754-761.

Colombo, A., Dinkel, L., Müller, S. A., Sebastian Monasor, L., Schifferer, M., Cantuti-Castelvetri, L., König, J., Vidatic, L., Bremova-Ertl, T., and Lieberman, A. P. (2021). Loss of NPC1 enhances phagocytic uptake and impairs lipid trafficking in microglia. Nature communications *12*, 1158.

Coniglio, S. J., Eugenin, E., Dobrenis, K., Stanley, E. R., West, B. L., Symons, M. H., and Segall, J. E. (2012). Microglial stimulation of glioblastoma invasion involves epidermal growth factor receptor (EGFR) and colony stimulating factor 1 receptor (CSF-1R) signaling. Molecular medicine *18*, 519-527.

Cruz, J. C., Kim, D., Moy, L. Y., Dobbin, M. M., Sun, X., Bronson, R. T., and Tsai, L.-H. (2006). p25/cyclin-dependent kinase 5 induces production and intraneuronal accumulation of amyloid β in vivo. Journal of Neuroscience *26*, 10536-10541.

Cserép, C., Pósfai, B., Lénárt, N., Fekete, R., László, Z. I., Lele, Z., Orsolits, B., Molnár, G., Heindl, S., and Schwarcz, A. D. (2020). Microglia monitor and protect neuronal function through specialized somatic purinergic junctions. Science *367*, 528-537.

Cunningham, C. L., Martínez-Cerdeño, V., and Noctor, S. C. (2013). Microglia regulate the number of neural precursor cells in the developing cerebral cortex. Journal of Neuroscience *33*, 4216-4233.

Czabotar, P. E., and Garcia-Saez, A. J. (2023). Mechanisms of BCL-2 family proteins in mitochondrial apoptosis. Nature Reviews Molecular Cell Biology, 1-17.

D

D'Orsi, B., Mateyka, J., and Prehn, J. H. (2017). Control of mitochondrial physiology and cell death by the Bcl-2 family proteins Bax and Bok. Neurochemistry International *109*, 162-170.

da Fonseca, A. C. C., Wang, H., Fan, H., Chen, X., Zhang, I., Zhang, L., Lima, F. R. S., and Badie, B. (2014). Increased expression of stress inducible protein 1 in glioma-associated microglia/macrophages. Journal of neuroimmunology *274*, 71-77.
Dando, S. J., Mackay-Sim, A., Norton, R., Currie, B. J., St. John, J. A., Ekberg, J. A., Batzloff, M., Ulett, G. C., and Beacham, I. R. (2014). Pathogens penetrating the central nervous system: infection pathways and the cellular and molecular mechanisms of invasion. Clinical microbiology reviews *27*, 691-726.

Das, A., Kim, S. H., Arifuzzaman, S., Yoon, T., Chai, J. C., Lee, Y. S., Park, K. S., Jung, K. H., and Chai, Y. G. (2016). Transcriptome sequencing reveals that LPS-triggered transcriptional responses in established microglia BV2 cell lines are poorly representative of primary microglia. Journal of neuroinflammation *13*, 1-18.

De Boeck, A., Ahn, B. Y., D'Mello, C., Lun, X., Menon, S. V., Alshehri, M. M., Szulzewsky, F., Shen, Y., Khan, L., and Dang, N. H. (2020). Glioma-derived IL-33 orchestrates an inflammatory brain tumor microenvironment that accelerates glioma progression. Nature communications *11*, 4997.

De Gaetano, A., Gibellini, L., Zanini, G., Nasi, M., Cossarizza, A., and Pinti, M. (2021). Mitophagy and oxidative stress: the role of aging. Antioxidants *10*, 794.

Del Rio-Hortega, P. (1919). El tercer elemento de los centros nerviosos; I. La microglia en estado normal. II. Intervencion de la microglia en los processos patologic os. III. Naturaleza probable de la microglia. Biol Soc Esp Biol *9*, 68-120.

De Simone, R., Ajmone-Cat, M. A., Tirassa, P., and Minghetti, L. (2003). Apoptotic PC12 cells exposing phosphatidylserine promote the production of anti-inflammatory and neuroprotective molecules by microglial cells. Journal of Neuropathology & Experimental Neurology *62*, 208-216.

Deczkowska, A., Keren-Shaul, H., Weiner, A., Colonna, M., Schwartz, M., and Amit, I. (2018). Disease-associated microglia: a universal immune sensor of neurodegeneration. Cell *173*, 1073-1081.

Deitch, E. A. (1998). Animal models of sepsis and shock: a review and lessons learned. Shock *10*, 442-443.

Deiters, O. (1865). Untersuchungen über Gehirn und Rückenmark des Menschen und der Säugethiere: F. Veiweg).

del Río-Hortega, P. (1919). El "tercer elemento" de Los Centros Nerviosos. II. Intervencion de la microglia en los procesos patologicos (Cellulas en bastocito y cuerpos granulo-adiposos). Bol Soc Esp Biol *9*, 91-103.

Desjardins, M. (1995). Biogenesis of phagolysosomes: the 'kiss and run'hypothesis. Trends in cell biology *5*, 183-186.

Desjardins, M., Celis, J. E., van Meer, G., Dieplinger, H., Jahraus, A., Griffiths, G., and Huber, L. A. (1994). Molecular characterization of phagosomes. Journal of Biological Chemistry *269*, 32194-32200.

Dias, C., and Nylandsted, J. (2021). Plasma membrane integrity in health and disease: significance and therapeutic potential. Cell discovery *7*, 4.

Diaz-Aparicio, I., Beccari, S., Abiega, O., and Sierra, A. (2016). Clearing the corpses: regulatory mechanisms, novel tools, and therapeutic potential of harnessing microglial phagocytosis in the diseased brain. Neural regeneration research *11*, 1533.

Diaz-Aparicio, I., Paris, I., Sierra-Torre, V., Plaza-Zabala, A., Rodriguez-Iglesias, N., Marquez-Ropero, M., Beccari, S., Huguet, P., Abiega, O., Alberdi, E*., et al.* (2020). Microglia Actively Remodel Adult Hippocampal Neurogenesis through the Phagocytosis Secretome. J Neurosci *40*, 1453-1482.

Diaz-Aparicio, I., and Sierra, A. (2019). C1q is related to microglial phagocytosis in the hippocampus in physiological conditions. Matters *5*.

Diaz-Vivancos, P., de Simone, A., Kiddle, G., and Foyer, C. H. (2015). Glutathione–linking cell proliferation to oxidative stress. Free Radical Biology and Medicine *89*, 1154-1164.

Diesselberg, C., Ribes, S., Seele, J., Kaufmann, A., Redlich, S., Bunkowski, S., Hanisch, U.-K., Michel, U., Nau, R., and Schütze, S. (2018). Activin A increases phagocytosis of Escherichia coli K1 by primary murine microglial cells activated by toll-like receptor agonists. Journal of Neuroinflammation *15*, 1-11.

Dieterle, F., Ross, A., Schlotterbeck, G., and Senn, H. (2006). Probabilistic quotient normalization as robust method to account for dilution of complex biological mixtures. Application in 1H NMR metabonomics. Analytical chemistry *78*, 4281-4290.

Dissing-Olesen, L., Ladeby, R., Nielsen, H. H., Toft-Hansen, H., Dalmau, I., and Finsen, B. (2007). Axonal lesion-induced microglial proliferation and microglial cluster formation in the mouse. Neuroscience *149*, 112-122.

Dobson, R., and Giovannoni, G. (2019). Multiple sclerosis–a review. European journal of neurology *26*, 27-40.

Domercq, M., Vázquez-Villoldo, N., and Matute, C. (2013). Neurotransmitter signaling in the pathophysiology of microglia. Frontiers in cellular neuroscience *7*, 49.

Domingues, H. S., Portugal, C. C., Socodato, R., and Relvas, J. B. (2016). Oligodendrocyte, astrocyte, and microglia crosstalk in myelin development, damage, and repair. Frontiers in cell and developmental biology *4*, 71.

Dorman, L. C., Nguyen, P. T., Escoubas, C. C., Vainchtein, I. D., Xiao, Y., Lidsky, P. V., Nakajo, H., Silva, N. J., Lagares-Linares, C., and Wang, E. Y. (2022). A type I interferon response defines a conserved microglial state required for effective neuronal phagocytosis. BioRxiv.

Douvaras, P., Sun, B., Wang, M., Kruglikov, I., Lallos, G., Zimmer, M., Terrenoire, C., Zhang, B., Gandy, S., and Schadt, E. (2017). Directed differentiation of human pluripotent stem cells to microglia. Stem cell reports *8*, 1516-1524.

Dräger, N. M., Sattler, S. M., Huang, C. T.-L., Teter, O. M., Leng, K., Hashemi, S. H., Hong, J., Aviles, G., Clelland, C. D., and Zhan, L. (2022). A CRISPRi/a platform in human iPSC-derived microglia uncovers regulators of disease states. Nature neuroscience *25*, 1149-1162.

Duclos, S., Diez, R., Garin, J., Papadopoulou, B., Descoteaux, A., Stenmark, H., and Desjardins, M. (2000). Rab5 regulates the kiss and run fusion between phagosomes and endosomes and the acquisition of phagosome leishmanicidal properties in RAW 264.7 macrophages. Journal of cell science *113*, 3531-3541.

Duffner, P. K. (2004). Long-term effects of radiation therapy on cognitive and endocrine function in children with leukemia and brain tumors. The neurologist *10*, 293-310.
Dupre-Crochet, S., Erard, M., and Nubetae, O. (2013). ROS production in phagocytes: why, when, and where? J Leukoc Biol *94*, 657-670.

Duque, A., and Rakic, P. (2015). Identification of proliferating and migrating cells by BrdU and other thymidine analogs: Benefits and limitations. Immunocytochemistry and related techniques, 123-139.

E

Easley-Neal, C., Foreman, O., Sharma, N., Zarrin, A. A., and Weimer, R. M. (2019). CSF1R ligands IL-34 and CSF1 are differentially required for microglia development and maintenance in white and gray matter brain regions. Frontiers in immunology *10*, 2199.

Ehninger, D., and Kempermann, G. (2008). Neurogenesis in the adult hippocampus. Cell and tissue research *331*, 243-250.

Ekdahl, C. T., Claasen, J.-H., Bonde, S., Kokaia, Z., and Lindvall, O. (2003). Inflammation is detrimental for neurogenesis in adult brain. Proceedings of the National Academy of Sciences *100*, 13632-13637.

El-Hattab, A. W. (2016). Serine biosynthesis and transport defects. Molecular genetics and metabolism *118*, 153-159.

El Khoury, J., Toft, M., Hickman, S. E., Means, T. K., Terada, K., Geula, C., and Luster, A. D. (2007). Ccr2 deficiency impairs microglial accumulation and accelerates progression of Alzheimer-like disease. Nature medicine *13*, 432-438.

Elliott, M. R., Chekeni, F. B., Trampont, P. C., Lazarowski, E. R., Kadl, A., Walk, S. F., Park, D., Woodson, R. I., Ostankovich, M., and Sharma, P. (2009). Nucleotides released by apoptotic cells act as a find-me signal to promote phagocytic clearance. Nature *461*, 282-286.

Ellwanger, D. C., Wang, S., Brioschi, S., Shao, Z., Green, L., Case, R., Yoo, D., Weishuhn, D., Rathanaswami, P., and Bradley, J. (2021). Prior activation state shapes the microglia response to antihuman TREM2 in a mouse model of Alzheimer's disease. Proceedings of the National Academy of Sciences *118*, e2017742118.

Elmore, M. R., Najafi, A. R., Koike, M. A., Dagher, N. N., Spangenberg, E. E., Rice, R. A., Kitazawa, M., Matusow, B., Nguyen, H., and West, B. L. (2014). Colony-stimulating factor 1 receptor signaling is necessary for microglia viability, unmasking a microglia progenitor cell in the adult brain. Neuron *82*, 380-397.

Erblich, B., Zhu, L., Etgen, A. M., Dobrenis, K., and Pollard, J. W. (2011). Absence of colony stimulation factor-1 receptor results in loss of microglia, disrupted brain development and olfactory deficits. PloS one *6*, e26317.

Eriksson, P., Buratovic, S., Fredriksson, A., Stenerlöw, B., and Sundell-Bergman, S. (2016). Neonatal exposure to whole body ionizing radiation induces adult neurobehavioural defects: critical period, dose—response effects and strain and sex comparison. Behavioural brain research *304*, 11-19.

Erny, D., Dokalis, N., Mezö, C., Castoldi, A., Mossad, O., Staszewski, O., Frosch, M., Villa, M., Fuchs, V., and Mayer, A. (2021). Microbiota-derived acetate enables the metabolic fitness of the brain innate immune system during health and disease. Cell metabolism *33*, 2260-2276. e2267.

Erny, D., Hrabě de Angelis, A. L., Jaitin, D., Wieghofer, P., Staszewski, O., David, E., Keren-Shaul, H., Mahlakoiv, T., Jakobshagen, K., and Buch, T. (2015). Host microbiota constantly control maturation and function of microglia in the CNS. Nature neuroscience *18*, 965-977.

Escoubas, C. C., Dorman, L. C., Nguyen, P. T., Lagares-Linares, C., Nakajo, H., Anderson, S. R., Cuevas, B., Vainchtein, I. D., Silva, N. J., and Xiao, Y. (2021). Type I interferon responsive microglia shape cortical development and behavior. bioRxiv, 2021.2004. 2029.441889.

Everts, V., Hou, W., Rialland, X., Tigchelaar, W., Saftig, P., Brömme, D., Gelb, B., and Beertsen, W. (2003). Cathepsin K deficiency in pycnodysostosis results in accumulation of non-digested phagocytosed collagen in fibroblasts. Calcified tissue international *73*, 380-386.
Eyo, U., and Molofsky, A. V. (2023). Defining microglial-synapse interactions. Science *381*, 1155-1156.

Eyo, U. B., Peng, J., Murugan, M., Mo, M., Lalani, A., Xie, P., Xu, P., Margolis, D. J., and Wu, L.-J. (2016). Regulation of physical microglia–neuron interactions by fractalkine signaling after status epilepticus. Eneuro *3*.

F

Fadok, V. A., Bratton, D. L., Frasch, S. C., Warner, M. L., and Henson, P. M. (1998). The role of phosphatidylserine in recognition of apoptotic cells by phagocytes. Cell Death & Differentiation *5*, 551-562.

Fagerlund, I., Dougalis, A., Shakirzyanova, A., Gómez-Budia, M., Pelkonen, A., Konttinen, H., Ohtonen, S., Fazaludeen, M. F., Koskuvi, M., and Kuusisto, J. (2021). Microglia-like cells promote neuronal functions in cerebral organoids. Cells *11*, 124.

Fan, X., and Agid, Y. (2018). At the Origin of the History of Glia. Neuroscience *385*, 255-271.
Fanucchi, S., Domínguez-Andrés, J., Joosten, L. A., Netea, M. G., and Mhlanga, M. M. (2021). The intersection of epigenetics and metabolism in trained immunity. Immunity *54*, 32-43.

Feng, W., Zhang, Y., Wang, Z., Xu, H., Wu, T., Marshall, C., Gao, J., and Xiao, M. (2020). Microglia prevent beta-amyloid plaque formation in the early stage of an Alzheimer's disease mouse model with suppression of glymphatic clearance. Alzheimer's research & therapy *12*, 1-15.

Feng, X., Szulzewsky, F., Yerevanian, A., Chen, Z., Heinzmann, D., Rasmussen, R. D., Alvarez-Garcia, V., Kim, Y., Wang, B., and Tamagno, I. (2015). Loss of CX3CR1 increases accumulation of inflammatory monocytes and promotes gliomagenesis. Oncotarget *6*, 15077.

Fields, R. D., Araque, A., Johansen-Berg, H., Lim, S.-S., Lynch, G., Nave, K.-A., Nedergaard, M., Perez, R., Sejnowski, T., and Wake, H. (2014). Glial biology in learning and cognition. The neuroscientist *20*, 426-431.

Filipello, F., Morini, R., Corradini, I., Zerbi, V., Canzi, A., Michalski, B., Erreni, M., Markicevic, M., Starvaggi-Cucuzza, C., and Otero, K. (2018). The microglial innate immune receptor TREM2 is required for synapse elimination and normal brain connectivity. Immunity *48*, 979-991. e978.

Fodstad, H. (2002). The neuron theory. Stereotactic and functional neurosurgery *77*, 20-24.

Fourgeaud, L., Través, P. G., Tufail, Y., Leal-Bailey, H., Lew, E. D., Burrola, P. G., Callaway, P., Zagórska, A., Rothlin, C. V., and Nimmerjahn, A. (2016). TAM receptors regulate multiple features of microglial physiology. Nature *532*, 240-244.

Frade, J. M., and Barde, Y.-A. (1998). Microglia-derived nerve growth factor causes cell death in the developing retina. Neuron *20*, 35-41.

Franchi, L., Warner, N., Viani, K., and Nuñez, G. (2009). Function of Nod-like receptors in microbial recognition and host defense. Immunological reviews *227*, 106-128.

Franco-Bocanegra, D. K., McAuley, C., Nicoll, J. A., and Boche, D. (2019). Molecular mechanisms of microglial motility: changes in ageing and Alzheimer's disease. Cells *8*, 639.

Frank, S., Burbach, G. J., Bonin, M., Walter, M., Streit, W., Bechmann, I., and Deller, T. (2008). TREM2 is upregulated in amyloid plaque-associated microglia in aged APP23 transgenic mice. Glia *56*, 1438-1447.

Franklin, K. B., and Paxinos, G. (2019). Paxinos and Franklin's the Mouse brain in stereotaxic coordinates, compact: The coronal plates and diagrams: Academic press).

Fraser, D. A., Pisalyaput, K., and Tenner, A. J. (2010). C1q enhances microglial clearance of apoptotic neurons and neuronal blebs, and modulates subsequent inflammatory cytokine production. Journal of neurochemistry *112*, 733-743.

Friedman, B. A., Srinivasan, K., Ayalon, G., Meilandt, W. J., Lin, H., Huntley, M. A., Cao, Y., Lee, S.-H., Haddick, P. C., and Ngu, H. (2018). Diverse brain myeloid expression profiles reveal distinct microglial activation states and aspects of Alzheimer's disease not evident in mouse models. Cell reports *22*, 832-847.

Fu, R., Shen, Q., Xu, P., Luo, J. J., and Tang, Y. (2014). Phagocytosis of microglia in the central nervous system diseases. Molecular neurobiology *49*, 1422-1434.

Fujita, S., and Kitamura, T. (1975). Origin of brain macrophages and the nature of the so-called microglia. Paper presented at: Malignant Lymphomas of the Nervous System: International Symposium (Springer).

Fuller, A. D., and Van Eldik, L. J. (2008). MFG-E8 regulates microglial phagocytosis of apoptotic neurons. Journal of Neuroimmune Pharmacology *3*, 246-256.

Fung, A., Vizcaychipi, M., Lloyd, D., Wan, Y., and Ma, D. (2012). Central nervous system inflammation in disease related conditions: mechanistic prospects. Brain research *1446*, 144-155.

G

Gaikwad, S. M., and Heneka, M. T. (2013). Studying M1 and M2 states in adult microglia. Microglia: Methods and Protocols, 185-197.

Galluzzi, L., Vitale, I., Aaronson, S. A., Abrams, J. M., Adam, D., Agostinis, P., Alnemri, E. S., Altucci, L., Amelio, I., and Andrews, D. W. (2018). Molecular mechanisms of cell death: recommendations of the Nomenclature Committee on Cell Death 2018. Cell Death & Differentiation *25*, 486-541.

Gan, G. N., Altunbas, C., Morton, J. J., Eagles, J., Backus, J., Dzingle, W., Raben, D., and Jimeno, A. (2016). Radiation dose uncertainty and correction for a mouse orthotopic and xenograft irradiation model. Int J Radiat Biol *92*, 50-56.

Garbayo, E., Raval, A. P., Curtis, K. M., Della-Morte, D., Gomez, L. A., D'Ippolito, G., Reiner, T., Perez-Stable, C., Howard, G. A., and Perez-Pinzon, M. A. (2011). Neuroprotective properties of marrow-isolated adult multilineage-inducible cells in rat hippocampus following global cerebral ischemia are enhanced when complexed to biomimetic microcarriers. Journal of neurochemistry *119*, 972-988.

Garcia-Moreno, F., Vasistha, N. A., Begbie, J., and Molnar, Z. (2014). CLoNe is a new method to target single progenitors and study their progeny in mouse and chick. Development *141*, 1589-1598.

García-Revilla, J., Boza-Serrano, A., Espinosa-Oliva, A. M., Soto, M. S., Deierborg, T., Ruiz, R., de Pablos, R. M., Burguillos, M. A., and Venero, J. L. (2022). Galectin-3, a rising star in modulating microglia activation under conditions of neurodegeneration. Cell Death & Disease *13*, 628.
Gardai, S. J., Bratton, D. L., Ogden, C. A., and Henson, P. M. (2006). Recognition ligands on apoptotic cells: a perspective. Journal of leukocyte biology *79*, 896-903.

Gardai, S. J., Xiao, Y.-Q., Dickinson, M., Nick, J. A., Voelker, D. R., Greene, K. E., and Henson, P. M. (2003). By binding SIRPα or calreticulin/CD91, lung collectins act as dual function surveillance molecules to suppress or enhance inflammation. Cell *115*, 13-23.

Geirsdottir, L., David, E., Keren-Shaul, H., Weiner, A., Bohlen, S. C., Neuber, J., Balic, A., Giladi, A., Sheban, F., and Dutertre, C.-A. (2019). Cross-species single-cell analysis reveals divergence of the primate microglia program. Cell *179*, 1609-1622. e1616.

Gerace, E., Cialdai, F., Sereni, E., Lana, D., Nosi, D., Giovannini, M. G., Monici, M., and Mannaioni, G. (2021). NIR Laser photobiomodulation induces neuroprotection in an in vitro model of cerebral hypoxia/ischemia. Molecular Neurobiology *58*, 5383-5395.

Geric, I., Schoors, S., Claes, C., Gressens, P., Verderio, C., Verfaillie, C. M., Van Veldhoven, P. P., Carmeliet, P., and Baes, M. (2019). Metabolic reprogramming during microglia activation. Immunometabolism *1*.

Gerrits, E., Heng, Y., Boddeke, E. W., and Eggen, B. J. (2020). Transcriptional profiling of microglia; current state of the art and future perspectives. Glia *68*, 740-755.

Ghashghaeinia, M., Köberle, M., Mrowietz, U., and Bernhardt, I. (2019). Proliferating tumor cells mimick glucose metabolism of mature human erythrocytes. Cell Cycle *18*, 1316-1334.

Gimeno-Bayón, J., López-López, A., Rodríguez, M., and Mahy, N. (2014). Glucose pathways adaptation supports acquisition of activated microglia phenotype. Journal of neuroscience research *92*, 723-731.

Ginhoux, F., Greter, M., Leboeuf, M., Nandi, S., See, P., Gokhan, S., Mehler, M. F., Conway, S. J., Ng, L. G., and Stanley, E. R. (2010). Fate mapping analysis reveals that adult microglia derive from primitive macrophages. Science *330*, 841-845.

Ginhoux, F., and Prinz, M. (2015). Origin of microglia: current concepts and past controversies. Cold Spring Harbor perspectives in biology *7*, a020537.

Giulian, D., and Baker, T. J. (1986). Characterization of ameboid microglia isolated from developing mammalian brain. Journal of Neuroscience *6*, 2163-2178.

Glasauer, A., and Chandel, N. S. (2013). Ros. Current Biology *23*, R100-R102.

Goldmann, T., Wieghofer, P., Jordão, M. J. C., Prutek, F., Hagemeyer, N., Frenzel, K., Amann, L., Staszewski, O., Kierdorf, K., and Krueger, M. (2016). Origin, fate and dynamics of macrophages at central nervous system interfaces. Nature immunology *17*, 797-805.

Golgi, C. (1873). Sulla struttura della sostanza grigia del cervelo. Gazzetta Medica Italiana. Lombardia *33*, 244.

Gomes, L. C., Benedetto, G. D., and Scorrano, L. (2011). During autophagy mitochondria elongate, are spared from degradation and sustain cell viability. Nature cell biology *13*, 589-598.

Gómez-Nicola, D., Fransen, N. L., Suzzi, S., and Perry, V. H. (2013). Regulation of microglial proliferation during chronic neurodegeneration. Journal of Neuroscience *33*, 2481-2493.

Gosselin, D., Skola, D., Coufal, N. G., Holtman, I. R., Schlachetzki, J. C., Sajti, E., Jaeger, B. N., O'Connor, C., Fitzpatrick, C., and Pasillas, M. P. (2017). An environment-dependent transcriptional network specifies human microglia identity. Science *356*, eaal3222.

Grabert, K., Michoel, T., Karavolos, M. H., Clohisey, S., Baillie, J. K., Stevens, M. P., Freeman, T. C., Summers, K. M., and McColl, B. W. (2016). Microglial brain region-dependent diversity and selective regional sensitivities to aging. Nat Neurosci *19*, 504-516.

Grathwohl, S. A., Kälin, R. E., Bolmont, T., Prokop, S., Winkelmann, G., Kaeser, S. A., Odenthal, J., Radde, R., Eldh, T., and Gandy, S. (2009). Formation and maintenance of Alzheimer's disease β-amyloid plaques in the absence of microglia. Nature neuroscience *12*, 1361-1363.

Gregerson, D. S., Sam, T. N., and McPherson, S. W. (2004). The antigen-presenting activity of fresh, adult parenchymal microglia and perivascular cells from retina. The Journal of Immunology *172*, 6587-6597.

Gude, D. R., Alvarez, S. E., Paugh, S. W., Mitra, P., Yu, J., Griffiths, R., Barbour, S. E., Milstien, S., and Spiegel, S. (2008). Apoptosis induces expression of sphingosine kinase 1 to release sphingosine-1-phosphate as a "come-and-get-me" signal. The FASEB Journal *22*, 2629.

Guerrero, B. L., and Sicotte, N. L. (2020). Microglia in multiple sclerosis: friend or foe? Frontiers in immunology *11*, 374.

Guneykaya, D., Ivanov, A., Hernandez, D. P., Haage, V., Wojtas, B., Meyer, N., Maricos, M., Jordan, P., Buonfiglioli, A., and Gielniewski, B. (2018). Transcriptional and translational differences of microglia from male and female brains. Cell reports *24*, 2773-2783. e2776.

Guo, H. J., and Tadi, P. (2022). Biochemistry, Ubiquitination. In StatPearls, (Treasure Island (FL)).

H

Hafemeister, C., and Satija, R. (2019). Normalization and variance stabilization of single-cell RNA-seq data using regularized negative binomial regression. Genome biology *20*, 296.

Hambardzumyan, D., Amankulor, N. M., Helmy, K. Y., Becher, O. J., and Holland, E. C. (2009). Modeling adult gliomas using RCAS/t-va technology. Translational oncology *2*, 89-IN86.

Hamley, I. W. (2012). The amyloid beta peptide: a chemist's perspective. Role in Alzheimer's and fibrillization. Chemical reviews *112*, 5147-5192.

Hammond, T. R., Dufort, C., Dissing-Olesen, L., Giera, S., Young, A., Wysoker, A., Walker, A. J., Gergits, F., Segel, M., and Nemesh, J. (2019). Single-cell RNA sequencing of microglia throughout the mouse lifespan and in the injured brain reveals complex cell-state changes. Immunity *50*, 253-271. e256.

Hanamsagar, R., Alter, M. D., Block, C. S., Sullivan, H., Bolton, J. L., and Bilbo, S. D. (2017). Generation of a microglial developmental index in mice and in humans reveals a sex difference in maturation and immune reactivity. Glia *65*, 1504-1520.

Hanamsagar, R., Hanke, M. L., and Kielian, T. (2012). Toll-like receptor (TLR) and inflammasome actions in the central nervous system. Trends in immunology *33*, 333-342.

Hanayama, R., Tanaka, M., Miwa, K., Shinohara, A., Iwamatsu, A., and Nagata, S. (2002). Identification of a factor that links apoptotic cells to phagocytes. Nature *417*, 182-187.

Hanisch, U.-K., and Kettenmann, H. (2007). Microglia: active sensor and versatile effector cells in the normal and pathologic brain. Nature neuroscience *10*, 1387-1394.

Hao, Y., Hao, S., Andersen-Nissen, E., Mauck, W. M., Zheng, S., Butler, A., Lee, M. J., Wilk, A. J., Darby, C., and Zager, M. (2021). Integrated analysis of multimodal single-cell data. Cell *184*, 3573-3587. e3529.

Harrison, R. E., Bucci, C., Vieira, O. V., Schroer, T. A., and Grinstein, S. (2003). Phagosomes fuse with late endosomes and/or lysosomes by extension of membrane protrusions along microtubules: role of Rab7 and RILP. Molecular and cellular biology *23*, 6494-6506.

Hasselmann, J., and Blurton-Jones, M. (2020). Human iPSC-derived microglia: A growing toolset to study the brain's innate immune cells. Glia *68*, 721-739.

He, Y., Yao, X., Taylor, N., Bai, Y., Lovenberg, T., and Bhattacharya, A. (2018). RNA sequencing analysis reveals quiescent microglia isolation methods from postnatal mouse brains and limitations of BV2 cells. Journal of neuroinflammation *15*, 1-13.

Healy, L. M., Perron, G., Won, S.-Y., Rao, V. T., Guiot, M.-C., Moore, C., Bar-Or, A., and Antel, J. P. (2018). Differential transcriptional response profiles in human myeloid cell populations. Clinical immunology *189*, 63-74.

Hellwig, S., Masuch, A., Nestel, S., Katzmarski, N., Meyer-Luehmann, M., and Biber, K. (2015). Forebrain microglia from wild-type but not adult 5xFAD mice prevent amyloid-β plaque formation in organotypic hippocampal slice cultures. Scientific reports *5*, 1-9.

Hendrickx, D. A., Koning, N., Schuurman, K. G., Strien, M. E. v., Eden, C. G. v., Hamann, J., and Huitinga, I. (2013). Selective upregulation of scavenger receptors in and around demyelinating areas in multiple sclerosis. Journal of Neuropathology & Experimental Neurology *72*, 106-118.

Hendrickx, D. A., van Eden, C. G., Schuurman, K. G., Hamann, J., and Huitinga, I. (2017). Staining of HLA-DR, Iba1 and CD68 in human microglia reveals partially overlapping expression depending on cellular morphology and pathology. Journal of neuroimmunology *309*, 12-22.

Hendry, H., and CML WEST, J. (1997). Apoptosis and mitotic cell death: their relative contributions to normal-tissue and tumour radiation response. International journal of radiation biology *71*, 709-719.

Henson, P. M., Bratton, D. L., and Fadok, V. A. (2001). Apoptotic cell removal. Current Biology *11*, R795-R805.

Henson, P. M., and Hume, D. A. (2006). Apoptotic cell removal in development and tissue homeostasis. Trends in immunology *27*, 244-250.

Hickman, S. E., Kingery, N. D., Ohsumi, T. K., Borowsky, M. L., Wang, L.-c., Means, T. K., and El Khoury, J. (2013). The microglial sensome revealed by direct RNA sequencing. Nature neuroscience *16*, 1896-1905.

Hingorani, M., Colley, W. P., Dixit, S., and Beavis, A. M. (2012a). Hypofractionated radiotherapy for glioblastoma: strategy for poor-risk patients or hope for the future? The British journal of radiology *85*, e770-e781.

Hingorani, M., Colley, W. P., Dixit, S., and Beavis, A. M. (2012b). Hypofractionated radiotherapy for glioblastoma: strategy for poor-risk patients or hope for the future? Br J Radiol *85*, e770-781.

Hipolito, V. E., Ospina-Escobar, E., and Botelho, R. J. (2018). Lysosome remodelling and adaptation during phagocyte activation. Cellular Microbiology *20*, e12824.

Hirbec, H., Deglon, N., Foo, L. C., Goshen, I., Grutzendler, J., Hangen, E., Kreisel, T., Linck, N., Muffat, J., Regio, S*., et al.* (2020). Emerging technologies to study glial cells. Glia *68*, 1692-1728.

Hochreiter-Hufford, A., and Ravichandran, K. S. (2013). Clearing the dead: apoptotic cell sensing, recognition, engulfment, and digestion. Cold Spring Harbor perspectives in biology *5*, a008748.

Hoebe, K., Janssen, E., and Beutler, B. (2004). The interface between innate and adaptive immunity. Nature immunology *5*, 971-974.

Hoeffel, G., Wang, Y., Greter, M., See, P., Teo, P., Malleret, B., Leboeuf, M., Low, D., Oller, G., and Almeida, F. (2012). Adult Langerhans cells derive predominantly from embryonic fetal liver monocytes with a minor contribution of yolk sac–derived macrophages. Journal of Experimental Medicine *209*, 1167-1181.

Holland, E. C., and Varmus, H. E. (1998). Basic fibroblast growth factor induces cell migration and proliferation after glia-specific gene transfer in mice. Proceedings of the National Academy of Sciences *95*, 1218-1223.

Holland, R., McIntosh, A., Finucane, O., Mela, V., Rubio-Araiz, A., Timmons, G., McCarthy, S., Gun'ko, Y., and Lynch, M. (2018). Inflammatory microglia are glycolytic and iron retentive and typify the microglia in APP/PS1 mice. Brain, Behavior, and Immunity *68*, 183-196.

Hong, S., Dissing-Olesen, L., and Stevens, B. (2016). New insights on the role of microglia in synaptic pruning in health and disease. Current opinion in neurobiology *36*, 128-134.

Horiuchi, M., Wakayama, K., Itoh, A., Kawai, K., Pleasure, D., Ozato, K., and Itoh, T. (2012). Interferon regulatory factor 8/interferon consensus sequence binding protein is a critical transcription factor for the physiological phenotype of microglia. J Neuroinflammation *9*, 227.

Hoshiko, M., Arnoux, I., Avignone, E., Yamamoto, N., and Audinat, E. (2012). Deficiency of the microglial receptor CX3CR1 impairs postnatal functional development of thalamocortical synapses in the barrel cortex. Journal of Neuroscience *32*, 15106-15111.

Hsieh, C. L., Koike, M., Spusta, S. C., Niemi, E. C., Yenari, M., Nakamura, M. C., and Seaman, W. E. (2009). A role for TREM2 ligands in the phagocytosis of apoptotic neuronal cells by microglia. Journal of neurochemistry *109*, 1144-1156.

Hsu, D. K., Yang, R.-Y., Pan, Z., Yu, L., Salomon, D. R., Fung-Leung, W.-P., and Liu, F.-T. (2000). Targeted disruption of the galectin-3 gene results in attenuated peritoneal inflammatory responses. The American journal of pathology *156*, 1073-1083.

Hu, F., a Dzaye, O. D., Hahn, A., Yu, Y., Scavetta, R. J., Dittmar, G., Kaczmarek, A. K., Dunning, K. R., Ricciardelli, C., and Rinnenthal, J. L. (2015). Glioma-derived versican promotes tumor expansion via glioma-associated microglial/macrophages Toll-like receptor 2 signaling. Neuro-oncology *17*, 200-210.

Hu, F., Ku, M. C., Markovic, D., Dzaye, O., Lehnardt, S., Synowitz, M., Wolf, S. A., and Kettenmann, H. (2014). Glioma-associated microglial MMP9 expression is upregulated by TLR2 signaling and sensitive to minocycline. International Journal of Cancer *135*, 2569-2578.

Hua, J. Y., and Smith, S. J. (2004). Neural activity and the dynamics of central nervous system development. Nature neuroscience *7*, 327-332.

Huang, D. W., Sherman, B. T., Tan, Q., Kir, J., Liu, D., Bryant, D., Guo, Y., Stephens, R., Baseler, M. W., and Lane, H. C. (2007). DAVID Bioinformatics Resources: expanded annotation database and novel algorithms to better extract biology from large gene lists. Nucleic acids research *35*, W169-W175.

Huang, Y., Happonen, K. E., Burrola, P. G., O'Connor, C., Hah, N., Huang, L., Nimmerjahn, A., and Lemke, G. (2021). Microglia use TAM receptors to detect and engulf amyloid β plaques. Nature immunology *22*, 586-594.

Huber-Lang, M., Lambris, J. D., and Ward, P. A. (2018). Innate immune responses to trauma. Nature immunology *19*, 327-341.

Hughes, C. E., and Nibbs, R. J. (2018). A guide to chemokines and their receptors. The FEBS journal *285*, 2944-2971.

Humpel, C. (2015). Organotypic brain slice cultures: A review. Neuroscience *305*, 86-98.

Hutter, G., Theruvath, J., Graef, C. M., Zhang, M., Schoen, M. K., Manz, E. M., Bennett, M. L., Olson, A., Azad, T. D., and Sinha, R. (2019). Microglia are effector cells of CD47-SIRPα antiphagocytic axis disruption against glioblastoma. Proceedings of the National Academy of Sciences *116*, 997-1006.

Huynh, K. K., Eskelinen, E. L., Scott, C. C., Malevanets, A., Saftig, P., and Grinstein, S. (2007). LAMP proteins are required for fusion of lysosomes with phagosomes. The EMBO journal *26*, 313-324.

I

Imai, Y., and Kohsaka, S. (2002). Intracellular signaling in M-CSF-induced microglia activation: role of Iba1. Glia *40*, 164-174.

Inoue, K. (2008). Purinergic systems in microglia. Cellular and Molecular Life Sciences *65*, 3074-3080.

Inuzuka, M., Hayakawa, M., and Ingi, T. (2005). Serinc, an activity-regulated protein family, incorporates serine into membrane lipid synthesis. Journal of Biological Chemistry *280*, 35776-35783.

Isailovic, N., Daigo, K., Mantovani, A., and Selmi, C. (2015). Interleukin-17 and innate immunity in infections and chronic inflammation. Journal of autoimmunity *60*, 1-11.

Ito, D., Imai, Y., Ohsawa, K., Nakajima, K., Fukuuchi, Y., and Kohsaka, S. (1998). Microglia-specific localisation of a novel calcium binding protein, Iba1. Molecular brain research *57*, 1-9.

Ito, D., Tanaka, K., Suzuki, S., Dembo, T., and Fukuuchi, Y. (2001). Enhanced expression of Iba1, ionized calcium-binding adapter molecule 1, after transient focal cerebral ischemia in rat brain. Stroke *32*, 1208-1215.

J

Janeway Jr, C. A., Travers, P., Walport, M., and Shlomchik, M. J. (2001). Principles of innate and adaptive immunity. In Immunobiology: The Immune System in Health and Disease. 5th edition, (Garland Science).

Jenkins, A. K., Lewis, D. A., and Volk, D. W. (2023). Altered expression of microglial markers of phagocytosis in schizophrenia. Schizophrenia Research *251*, 22-29.

Jia, J., Yang, L., Chen, Y., Zheng, L., Chen, Y., Xu, Y., and Zhang, M. (2022). The role of microglial phagocytosis in ischemic stroke. Frontiers in Immunology *12*, 5704.

Jiao, Y., Cao, F., and Liu, H. (2022). Radiation-induced Cell Death and Its Mechanisms. Health Phys *123*, 376-386.

Jiménez-García, L., Mayer, C., Burrola, P. G., Huang, Y., Shokhirev, M. N., and Lemke, G. (2022). The TAM receptor tyrosine kinases Axl and Mer drive the maintenance of highly phagocytic macrophages. Frontiers in Immunology *13*, 960401.

Jin, C., Shao, Y., Zhang, X., Xiang, J., Zhang, R., Sun, Z., Mei, S., Zhou, J., Zhang, J., and Shi, L. (2021). A unique type of highly-activated microglia evoking brain inflammation via Mif/Cd74 signaling axis in aged mice. Aging and disease *12*, 2125.

Jin, T., Xu, X., and Hereld, D. (2008). Chemotaxis, chemokine receptors and human disease. Cytokine *44*, 1-8.

Jobling, A. I., Waugh, M., Vessey, K. A., Phipps, J. A., Trogrlic, L., Greferath, U., Mills, S. A., Tan, Z. L., Ward, M. M., and Fletcher, E. L. (2018). The role of the microglial Cx3cr1 pathway in the postnatal maturation of retinal photoreceptors. Journal of Neuroscience *38*, 4708-4723.

Jordao, M. J. C., Sankowski, R., Brendecke, S. M., Sagar, Locatelli, G., Tai, Y. H., Tay, T. L., Schramm, E., Armbruster, S., Hagemeyer, N*., et al.* (2019). Single-cell profiling identifies myeloid cell subsets with distinct fates during neuroinflammation. Science *363*.

Joshi, P., Riffel, F., Kumar, S., Villacampa, N., Theil, S., Parhizkar, S., Haass, C., Colonna, M., Heneka, M. T., and Arzberger, T. (2021). TREM2 modulates differential deposition of modified and non-modified Aβ species in extracellular plaques and intraneuronal deposits. Acta Neuropathologica Communications *9*, 1-22.

Judge, A., and Dodd, M. S. (2020). Metabolism. Essays Biochem *64*, 607-647.

Jung, S., Aliberti, J., Graemmel, P., Sunshine, M. J., Kreutzberg, G. W., Sher, A., and Littman, D. R. (2000). Analysis of fractalkine receptor CX3CR1 function by targeted deletion and green fluorescent protein reporter gene insertion. Molecular and cellular biology *20*, 4106-4114.
Jurcovicova, J. (2014). Glucose transport in brain-effect of inflammation. Endocr Regul *48*, 35-48.

K

Kaji, K., Takeshita, S., Miyake, K., Takai, T., and Kudo, A. (2001). Functional association of CD9 with the Fcγ receptors in macrophages. The Journal of Immunology *166*, 3256-3265.

Kalm, M., Fukuda, A., Fukuda, H., Öhrfelt, A., Lannering, B., Björk-Eriksson, T., Blennow, K., Márky, I., and Blomgren, K. (2009). Transient inflammation in neurogenic regions after irradiation of the developing brain. Radiation research *171*, 66-76.

Kamei, R., and Okabe, S. (2023). In vivo imaging of the phagocytic dynamics underlying efficient clearance of adult-born hippocampal granule cells by ramified microglia. Glia.

Kana, V., Desland, F. A., Casanova-Acebes, M., Ayata, P., Badimon, A., Nabel, E., Yamamuro, K., Sneeboer, M., Tan, I.-L., and Flanigan, M. E. (2019). CSF-1 controls cerebellar microglia and is required for motor function and social interaction. Journal of Experimental Medicine *216*, 2265-2281.

Kastner, P., and Chan, S. (2008). PU. 1: a crucial and versatile player in hematopoiesis and leukemia. The international journal of biochemistry & cell biology *40*, 22-27.

Katz, L. C., and Shatz, C. J. (1996). Synaptic activity and the construction of cortical circuits. Science *274*, 1133-1138.

Kavanagh, J. N., Currell, F. J., Timson, D. J., Savage, K. I., Richard, D. J., McMahon, S. J., Hartley, O., Cirrone, G. A., Romano, F., Prise, K. M*., et al.* (2013). Antiproton induced DNA damage: proton like in flight, carbon-ion like near rest. Sci Rep *3*, 1770.

Keller, S., Berghoff, K., and Kress, H. (2017). Phagosomal transport depends strongly on phagosome size. Scientific reports *7*, 17068.

Kelley, S. M., and Ravichandran, K. S. (2021). Putting the brakes on phagocytosis:"don't-eat-me" signaling in physiology and disease. EMBO reports *22*, e52564.

Keren-Shaul, H., Spinrad, A., Weiner, A., Matcovitch-Natan, O., Dvir-Szternfeld, R., Ulland, T. K., David, E., Baruch, K., Lara-Astaiso, D., and Toth, B. (2017). A unique microglia type associated with restricting development of Alzheimer's disease. Cell *169*, 1276-1290. e1217.

Kierdorf, K., Erny, D., Goldmann, T., Sander, V., Schulz, C., Perdiguero, E. G., Wieghofer, P., Heinrich, A., Riemke, P., and Hölscher, C. (2013). Microglia emerge from erythromyeloid precursors via Pu. 1-and Irf8-dependent pathways. Nature neuroscience *16*, 273-280.

Kinchen, J. M., Doukoumetzidis, K., Almendinger, J., Stergiou, L., Tosello-Trampont, A., Sifri, C. D., Hengartner, M. O., and Ravichandran, K. S. (2008a). A pathway for phagosome maturation during engulfment of apoptotic cells. Nature cell biology *10*, 556-566.

Kinchen, J. M., and Ravichandran, K. S. (2008b). Phagosome maturation: going through the acid test. Nature reviews Molecular cell biology *9*, 781-795.

Kitay, B. M., McCormack, R., Wang, Y., Tsoulfas, P., and Zhai, R. G. (2013). Mislocalization of neuronal mitochondria reveals regulation of Wallerian degeneration and NMNAT/WLDS-mediated axon protection independent of axonal mitochondria. Human molecular genetics *22*, 1601-1614.

Kleizen, B., and Braakman, I. (2004). Protein folding and quality control in the endoplasmic reticulum. Current opinion in cell biology *16*, 343-349.

Klöppel, G., and La Rosa, S. (2018). Ki67 labeling index: assessment and prognostic role in gastroenteropancreatic neuroendocrine neoplasms. Virchows Archiv *472*, 341-349.

Kolb, J. P., Oguin, T. H., Oberst, A., and Martinez, J. (2017). Programmed cell death and inflammation: winter is coming. Trends in immunology *38*, 705-718.

Krasemann, S., Madore, C., Cialic, R., Baufeld, C., Calcagno, N., El Fatimy, R., Beckers, L., O'loughlin, E., Xu, Y., and Fanek, Z. (2017). The TREM2-APOE pathway drives the transcriptional phenotype of dysfunctional microglia in neurodegenerative diseases. Immunity *47*, 566-581. e569.

Ku, M.-C., Wolf, S. A., Respondek, D., Matyash, V., Pohlmann, A., Waiczies, S., Waiczies, H., Niendorf, T., Synowitz, M., and Glass, R. (2013). GDNF mediates glioblastoma-induced microglia attraction but not astrogliosis. Acta neuropathologica *125*, 609-620.

Kubli, D. A., and Gustafsson, Å. B. (2012). Mitochondria and mitophagy: the yin and yang of cell death control. Circulation research *111*, 1208-1221.

Kubota, Y., Takubo, K., Shimizu, T., Ohno, H., Kishi, K., Shibuya, M., Saya, H., and Suda, T. (2009). M-CSF inhibition selectively targets pathological angiogenesis and lymphangiogenesis. Journal of Experimental Medicine *206*, 1089-1102.

Kulkarni, A. B., Huh, C.-G., Becker, D., Geiser, A., Lyght, M., Flanders, K. C., Roberts, A. B., Sporn, M. B., Ward, J. M., and Karlsson, S. (1993). Transforming growth factor beta 1 null mutation in mice causes excessive inflammatory response and early death. Proceedings of the National Academy of Sciences *90*, 770-774.

Kulprathipanja, N. V., and Kruse, C. A. (2004). Microglia phagocytose alloreactive CTL-damaged 9L gliosarcoma cells. Journal of neuroimmunology *153*, 76-82.

Kumar, G. S., and Das, U. (1994). Effect of prostaglandins and their precursors on the proliferation of human lymphocytes and their secretion of tumor necrosis factor and various interleukins. Prostaglandins, leukotrienes and essential fatty acids *50*, 331-334.

Kumar, V., Mishra, R. K., Ghose, D., Kalita, A., Dhiman, P., Prakash, A., Thakur, N., Mitra, G., Chaudhari, V. D., and Arora, A. (2022a). Free spermidine evokes superoxide radicals that manifest toxicity. Elife *11*, e77704.

Kumar, V., Mishra, R. K., Ghose, D., Kalita, A., Dhiman, P., Prakash, A., Thakur, N., Mitra, G., Chaudhari, V. D., Arora, A., and Dutta, D. (2022b). Free spermidine evokes superoxide radicals that manifest toxicity. Elife *11*.

Kumaravelu, P., Hook, L., Morrison, A. M., Ure, J., Zhao, S., Zuyev, S., Ansell, J., and Medvinsky, A. (2002). Quantitative developmental anatomy of definitive haematopoietic stem cells/long-term repopulating units (HSC/RUs): role of the aorta-gonad-mesonephros (AGM) region and the yolk sac in colonisation of the mouse embryonic liver.

L

Lalancette-Hébert, M., Swarup, V., Beaulieu, J. M., Bohacek, I., Abdelhamid, E., Weng, Y. C., Sato, S., and Kriz, J. (2012). Galectin-3 is required for resident microglia activation and proliferation in response to ischemic injury. Journal of Neuroscience *32*, 10383-10395.

Lampron, A., Larochelle, A., Laflamme, N., Préfontaine, P., Plante, M.-M., Sánchez, M. G., Yong, V. W., Stys, P. K., Tremblay, M.-È., and Rivest, S. (2015). Inefficient clearance of myelin debris by microglia impairs remyelinating processes. Journal of Experimental Medicine *212*, 481-495.

Lancaster, M. A., Renner, M., Martin, C.-A., Wenzel, D., Bicknell, L. S., Hurles, M. E., Homfray, T., Penninger, J. M., Jackson, A. P., and Knoblich, J. A. (2013). Cerebral organoids model human brain development and microcephaly. Nature *501*, 373-379.

Laslo, P., Spooner, C. J., Warmflash, A., Lancki, D. W., Lee, H.-J., Sciammas, R., Gantner, B. N., Dinner, A. R., and Singh, H. (2006). Multilineage transcriptional priming and determination of alternate hematopoietic cell fates. Cell *126*, 755-766.

Lauber, K., Blumenthal, S. G., Waibel, M., and Wesselborg, S. (2004). Clearance of apoptotic cells: getting rid of the corpses. Molecular cell *14*, 277-287.

Lauber, K., Bohn, E., Kröber, S. M., Xiao, Y.-j., Blumenthal, S. G., Lindemann, R. K., Marini, P., Wiedig, C., Zobywalski, A., and Baksh, S. (2003). Apoptotic cells induce migration of phagocytes via caspase-3-mediated release of a lipid attraction signal. Cell *113*, 717-730.

Lee, S., Devanney, N. A., Golden, L. R., Smith, C. T., Schwartz, J. L., Walsh, A. E., Clarke, H. A., Goulding, D. S., Allenger, E. J., and Morillo-Segovia, G. (2023). APOE modulates microglial immunometabolism in response to age, amyloid pathology, and inflammatory challenge. Cell reports *42*.

Lee, S. C., Liu, W., Roth, P., Dickson, D. W., Berman, J., and Brosnan, C. (1993). Macrophage colony-stimulating factor in human fetal astrocytes and microglia. Differential regulation by cytokines and lipopolysaccharide, and modulation of class II MHC on microglia. Journal of immunology (Baltimore, Md: 1950) *150*, 594-604.

Lemke, G. (2013). Biology of the TAM receptors. Cold Spring Harbor perspectives in biology *5*, a009076.

Lemke, G., and Rothlin, C. V. (2008). Immunobiology of the TAM receptors. Nature Reviews Immunology *8*, 327-336.

Lenis, Y. Y., Elmetwally, M. A., Maldonado-Estrada, J. G., and Bazer, F. W. (2017). Physiological importance of polyamines. Zygote *25*, 244-255.

Lenting, K., Verhaak, R., Ter Laan, M., Wesseling, P., and Leenders, W. (2017). Glioma: experimental models and reality. Acta Neuropathol *133*, 263-282.

Li, Q., Cheng, Z., Zhou, L., Darmanis, S., Neff, N. F., Okamoto, J., Gulati, G., Bennett, M. L., Sun, L. O., and Clarke, L. E. (2019). Developmental heterogeneity of microglia and brain myeloid cells revealed by deep single-cell RNA sequencing. Neuron *101*, 207-223. e210.

Li, W. (2012). Eat-me signals: Keys to molecular phagocyte biology and “Appetite” control. Journal of cellular physiology *227*, 1291-1297.

Li, Z., Li, Y., Gao, J., Fu, Y., Hua, P., Jing, Y., Cai, M., Wang, H., and Tong, T. (2021). The role of CD47-SIRPα immune checkpoint in tumor immune evasion and innate immunotherapy. Life Sciences *273*, 119150.

Liesa, M., and Shirihai, O. S. (2013). Mitochondrial dynamics in the regulation of nutrient utilization and energy expenditure. Cell metabolism *17*, 491-506.

Lim, T. K., and Ruthazer, E. S. (2021). Microglial trogocytosis and the complement system regulate axonal pruning in vivo. Elife *10*, e62167.

Lin, H., Lee, E., Hestir, K., Leo, C., Huang, M., Bosch, E., Halenbeck, R., Wu, G., Zhou, A., and Behrens, D. (2008). Discovery of a cytokine and its receptor by functional screening of the extracellular proteome. Science *320*, 807-811.

Lin, H. H., and Stacey, M. (2017). G protein-coupled receptors in macrophages. Myeloid Cells in Health and Disease: A Synthesis, 485-505.

Lindborg, B. A., Brekke, J. H., Vegoe, A. L., Ulrich, C. B., Haider, K. T., Subramaniam, S., Venhuizen, S. L., Eide, C. R., Orchard, P. J., and Chen, W. (2016). Rapid induction of cerebral organoids from human induced pluripotent stem cells using a chemically defined hydrogel and defined cell culture medium. Stem Cells Translational Medicine *5*, 970-979.

Linnartz, B., Kopatz, J., Tenner, A. J., and Neumann, H. (2012). Sialic acid on the neuronal glycocalyx prevents complement C1 binding and complement receptor-3-mediated removal by microglia. Journal of Neuroscience *32*, 946-952.

Lionakis, M. S., Lim, J. K., Lee, C.-C. R., and Murphy, P. M. (2011). Organ-specific innate immune responses in a mouse model of invasive candidiasis. Journal of innate immunity *3*, 180-199.
Liu, S., Zhao, Q., Shi, W., Zheng, Z., Liu, Z., Meng, L., Dong, L., and Jiang, X. (2021). Advances in radiotherapy and comprehensive treatment of high-grade glioma: immunotherapy and tumor-treating fields. Journal of Cancer *12*, 1094.

Liu, Y., Wu, C., Hou, Z., Fu, X., Yuan, L., Sun, S., Zhang, H., Yang, D., Yao, X., and Yang, J. (2020). Pseudoginsenoside-F11 accelerates microglial phagocytosis of myelin debris and attenuates cerebral ischemic injury through complement receptor 3. Neuroscience *426*, 33-49.
Loane, D. J., and Byrnes, K. R. (2010). Role of microglia in neurotrauma. Neurotherapeutics *7*, 366-377.

Lowe, X. R., Bhattacharya, S., Marchetti, F., and Wyrobek, A. J. (2009). Early brain response to low-dose radiation exposure involves molecular networks and pathways associated with cognitive functions, advanced aging and Alzheimer's disease. Radiation research *171*, 53-65.

Lucas, S. M., Rothwell, N. J., and Gibson, R. M. (2006). The role of inflammation in CNS injury and disease. British journal of pharmacology *147*, S232-S240.

Lue, L. F., Schmitz, C. T., Serrano, G., Sue, L. I., Beach, T. G., and Walker, D. G. (2015). TREM 2 Protein Expression Changes Correlate with A lzheimer's Disease Neurodegenerative Pathologies in Post-Mortem Temporal Cortices. Brain pathology *25*, 469-480.

Lumniczky, K., Szatmári, T., and Sáfrány, G. (2017). Ionizing radiation-induced immune and inflammatory reactions in the brain. Frontiers in immunology *8*, 517.

Lyman, M., Lloyd, D. G., Ji, X., Vizcaychipi, M. P., and Ma, D. (2014). Neuroinflammation: the role and consequences. Neuroscience research *79*, 1-12.

Lynch, M. A. (2022). Exploring sex-related differences in microglia may be a game-changer in precision medicine. Frontiers in Aging Neuroscience, 281.

M

Magnus, T., Chan, A., Linker, R. A., Toyka, K. V., and Gold, R. (2002). Astrocytes are less efficient in the removal of apoptotic lymphocytes than microglia cells: implications for the role of glial cells in the inflamed central nervous system. Journal of Neuropathology & Experimental Neurology *61*, 760-766.
Majumdar, A., Capetillo-Zarate, E., Cruz, D., Gouras, G. K., and Maxfield, F. R. (2011). Degradation of Alzheimer's amyloid fibrils by microglia requires delivery of ClC-7 to lysosomes. Molecular biology of the cell *22*, 1664-1676.

Mak, K. S., Funnell, A. P., Pearson, R., and Crossley, M. (2011). PU. 1 and haematopoietic cell fate: dosage matters. International journal of cell biology *2011*.

Makide, K., and Aoki, J. (2013). GPR34 as a lysophosphatidylserine receptor. The journal of biochemistry *153*, 327-329.

Manfioletti, G., Brancolini, C., Avanzi, G., and Schneider, C. (1993). The protein encoded by a growth arrest-specific gene (gas6) is a new member of the vitamin K-dependent proteins related to protein S, a negative coregulator in the blood coagulation cascade. Molecular and cellular biology.

Markovic, D., Vinnakota, K., Chirasani, S., Synowitz, M., Raguet, H., Stock, K., Sliwa, M., Lehmann, S., Kälin, R., and Van Rooijen, N. (2009). Gliomas induce and exploit microglial MT1-MMP expression for tumor expansion. Proceedings of the National Academy of Sciences *106*, 12530-12535.

Marquez-Ropero, M., Benito, E., Plaza-Zabala, A., and Sierra, A. (2020). Microglial Corpse Clearance: Lessons From Macrophages. Front Immunol *11*, 506.

Marschallinger, J., Iram, T., Zardeneta, M., Lee, S. E., Lehallier, B., Haney, M. S., Pluvinage, J. V., Mathur, V., Hahn, O., and Morgens, D. W. (2020). Lipid-droplet-accumulating microglia represent a dysfunctional and proinflammatory state in the aging brain. Nature neuroscience *23*, 194-208.

Marsh, S. E., Walker, A. J., Kamath, T., Dissing-Olesen, L., Hammond, T. R., de Soysa, T. Y., Young, A. M., Murphy, S., Abdulraouf, A., and Nadaf, N. (2022a). Dissection of artifactual and confounding glial signatures by single-cell sequencing of mouse and human brain. Nature Neuroscience *25*, 306-316.

Marsh, S. E., Walker, A. J., Kamath, T., Dissing-Olesen, L., Hammond, T. R., de Soysa, T. Y., Young, A. M. H., Murphy, S., Abdulraouf, A., Nadaf, N.*, et al.* (2022b). Dissection of artifactual and confounding glial signatures by single-cell sequencing of mouse and human brain. Nat Neurosci *25*, 306-316.

Martin, M., and Blom, A. M. (2016). Complement in removal of the dead–balancing inflammation. Immunological reviews *274*, 218-232.

Masteller, E. L., and Wong, B. R. (2014). Targeting IL-34 in chronic inflammation. Drug discovery today *19*, 1212-1216.

Masuda, T., Amann, L., Monaco, G., Sankowski, R., Staszewski, O., Krueger, M., Del Gaudio, F., He, L., Paterson, N., Nent, E.*, et al.* (2022). Specification of CNS macrophage subsets occurs postnatally in defined niches. Nature *604*, 740-748.

Masuda, T., Nishimoto, N., Tomiyama, D., Matsuda, T., Tozaki-Saitoh, H., Tamura, T., Kohsaka, S., Tsuda, M., and Inoue, K. (2014). IRF8 is a transcriptional determinant for microglial motility. Purinergic signalling *10*, 515-521.

Mathews, J. D., Forsythe, A. V., Brady, Z., Butler, M. W., Goergen, S. K., Byrnes, G. B., Giles, G. G., Wallace, A. B., Anderson, P. R., and Guiver, T. A. (2013). Cancer risk in 680 000 people exposed to computed tomography scans in childhood or adolescence: data linkage study of 11 million Australians. Bmj *346*.

Mathys, H., Adaikkan, C., Gao, F., Young, J. Z., Manet, E., Hemberg, M., De Jager, P. L., Ransohoff, R. M., Regev, A., and Tsai, L.-H. (2017). Temporal tracking of microglia activation in neurodegeneration at single-cell resolution. Cell reports *21*, 366-380.

Mattiola, I., Mantovani, A., and Locati, M. (2021). The tetraspan MS4A family in homeostasis, immunity, and disease. Trends in Immunology *42*, 764-781.

Mawuenyega, K. G., Sigurdson, W., Ovod, V., Munsell, L., Kasten, T., Morris, J. C., Yarasheski, K. E., and Bateman, R. J. (2010). Decreased clearance of CNS β-amyloid in Alzheimer's disease. Science *330*, 1774-1774.

McComb, S., Thiriot, A., Akache, B., Krishnan, L., and Stark, F. (2019). Introduction to the immune system. Immunoproteomics: Methods and Protocols, 1-24.
McFaline-Figueroa, J. R., and Lee, E. Q. (2018). Brain tumors. The American journal of medicine *131*, 874-882.

McKercher, S. R., Torbett, B. E., Anderson, K. L., Henkel, G. W., Vestal, D. J., Baribault, H., Klemsz, M., Feeney, A. J., Wu, G. E., and Paige, C. J. (1996). Targeted disruption of the PU. 1 gene results in multiple hematopoietic abnormalities. The EMBO journal *15*, 5647-5658.

Meiffren, G., Flacher, M., Azocar, O., Rabourdin-Combe, C., and Faure, M. (2006). Cutting edge: abortive proliferation of CD46-induced Tr1-like cells due to a defective Akt/Survivin signaling pathway. The Journal of Immunology *177*, 4957-4961.

Menassa, D. A., and Gomez-Nicola, D. (2018). Microglial dynamics during human brain development. Frontiers in immunology *9*, 1014.

Mennicken, F., Maki, R., de Souza, E. B., and Quirion, R. (1999). Chemokines and chemokine receptors in the CNS: a possible role in neuroinflammation and patterning. Trends in pharmacological sciences *20*, 73-78.

Mergenthaler, P., Lindauer, U., Dienel, G. A., and Meisel, A. (2013). Sugar for the brain: the role of glucose in physiological and pathological brain function. Trends in neurosciences *36*, 587-597.

Mezey, E., Chandross, K. J., Harta, G., Maki, R. A., and McKercher, S. R. (2000). Turning blood into brain: cells bearing neuronal antigens generated in vivo from bone marrow. Science *290*, 1779-1782.

Mildenberger, W., Stifter, S. A., and Greter, M. (2022). Diversity and function of brain-associated macrophages. Current Opinion in Immunology *76*, 102181.

Milner, D. (1998). Cognitive neuroscience: the biology of the mind and findings and current opinion in cognitive neuroscience. Trends Cogn Sci *2*, 463.

Minakami, R., and Sumimoto, H. (2006). Phagocytosis-coupled activation of the superoxide-producing phagocyte oxidase, a member of the NADPH oxidase (nox) family. International journal of hematology *84*, 193-198.

Mizumatsu, S., Monje, M. L., Morhardt, D. R., Rola, R., Palmer, T. D., and Fike, J. R. (2003). Extreme sensitivity of adult neurogenesis to low doses of X-irradiation. Cancer research *63*, 4021-4027.

Mizutani, M., Pino, P. A., Saederup, N., Charo, I. F., Ransohoff, R. M., and Cardona, A. E. (2012). The fractalkine receptor but not CCR2 is present on microglia from embryonic development throughout adulthood. The Journal of Immunology *188*, 29-36.

Monier, A., Adle-Biassette, H., Delezoide, A.-L., Evrard, P., Gressens, P., and Verney, C. (2007). Entry and distribution of microglial cells in human embryonic and fetal cerebral cortex. Journal of neuropathology and experimental neurology *66*, 372-382.

Monje, M. L., Toda, H., and Palmer, T. D. (2003). Inflammatory blockade restores adult hippocampal neurogenesis. Science *302*, 1760-1765.

Mori, I., Imai, Y., Kohsaka, S., and Kimura, Y. (2000). Upregulated expression of Iba1 molecules in the central nervous system of mice in response to neurovirulent influenza A virus infection. Microbiology and immunology *44*, 729-735.

Morioka, S., Maueröder, C., and Ravichandran, K. S. (2019). Living on the edge: efferocytosis at the interface of homeostasis and pathology. Immunity *50*, 1149-1162.

Morioka, S., Perry, J. S., Raymond, M. H., Medina, C. B., Zhu, Y., Zhao, L., Serbulea, V., Onengut-Gumuscu, S., Leitinger, N., and Kucenas, S. (2018). Efferocytosis induces a novel SLC program to promote glucose uptake and lactate release. Nature *563*, 714-718.

Mostafavi, S., Yoshida, H., Moodley, D., LeBoité, H., Rothamel, K., Raj, T., Ye, C. J., Chevrier, N., Zhang, S.-Y., and Feng, T. (2016). Parsing the interferon transcriptional network and its disease associations. Cell *164*, 564-578.

Mot, A. I., Liddell, J. R., White, A. R., and Crouch, P. J. (2016). Circumventing the Crabtree Effect: A method to induce lactate consumption and increase oxidative phosphorylation in cell culture. The International Journal of Biochemistry & Cell Biology *79*, 128-138.

Mucenski, M. L., McLain, K., Kier, A. B., Swerdlow, S. H., Schreiner, C. M., Miller, T. A., Pietryga, D. W., Scott, W. J., and Potter, S. S. (1991). A functional c-myb gene is required for normal murine fetal hepatic hematopoiesis. Cell *65*, 677-689.

Muffat, J., Li, Y., Yuan, B., Mitalipova, M., Omer, A., Corcoran, S., Bakiasi, G., Tsai, L.-H., Aubourg, P., and Ransohoff, R. M. (2016). Efficient derivation of microglia-like cells from human pluripotent stem cells. Nature medicine *22*, 1358-1367.

Mukherjee, S., Ghosh, R. N., and Maxfield, F. R. (1997). Endocytosis. Physiological reviews.

Muliyil, S., and Narasimha, M. (2014). Mitochondrial ROS regulates cytoskeletal and mitochondrial remodeling to tune cell and tissue dynamics in a model for wound healing. Dev Cell *28*, 239-252.

Muzio, L., Viotti, A., and Martino, G. (2021a). Microglia in Neuroinflammation and Neurodegeneration: From Understanding to Therapy. Front Neurosci *15*, 742065.

Muzio, L., Viotti, A., and Martino, G. (2021b). Microglia in neuroinflammation and neurodegeneration: from understanding to therapy. Frontiers in neuroscience *15*, 742065.

N

Nadjar, A. (2018). Role of metabolic programming in the modulation of microglia phagocytosis by lipids. Prostaglandins, Leukotrienes and Essential Fatty Acids *135*, 63-73.

Nagy, A. M., Fekete, R., Horvath, G., Koncsos, G., Kriston, C., Sebestyen, A., Giricz, Z., Kornyei, Z., Madarasz, E., and Tretter, L. (2018). Versatility of microglial bioenergetic machinery under starving conditions. Biochimica et Biophysica Acta (BBA)-Bioenergetics *1859*, 201-214.

Nair, P., Lu, M., Petersen, S., and Ashkenazi, A. (2014). Apoptosis initiation through the cell-extrinsic pathway. In Methods in enzymology, (Elsevier), pp. 99-128.

Nair, S., Sobotka, K. S., Joshi, P., Gressens, P., Fleiss, B., Thornton, C., Mallard, C., and Hagberg, H. (2019). Lipopolysaccharide-induced alteration of mitochondrial morphology induces a metabolic shift in microglia modulating the inflammatory response in vitro and in vivo. Glia *67*, 1047-1061.

Nakanishi, M., Niidome, T., Matsuda, S., Akaike, A., Kihara, T., and Sugimoto, H. (2007). Microglia-derived interleukin-6 and leukaemia inhibitory factor promote astrocytic differentiation of neural stem/progenitor cells. European Journal of Neuroscience *25*, 649-658.

Napoli, I., and Neumann, H. (2009). Microglial clearance function in health and disease. Neuroscience *158*, 1030-1038.

Napoli, I., and Neumann, H. (2010). Protective effects of microglia in multiple sclerosis. Experimental neurology *225*, 24-28.

Nayak, D., Roth, T. L., and McGavern, D. B. (2014). Microglia development and function. Annual review of immunology *32*, 367-402.

Neglia, R., Colombari, B., Peppoloni, S., Orsi, C., Tavanti, A., Senesi, S., and Blasi, E. (2006). Adaptive response of microglial cells to in vitro infection by Candida albicans isolates with different genomic backgrounds. Microbial pathogenesis *41*, 251-256.

Neher, J. J., Neniskyte, U., and Brown, G. C. (2012). Primary phagocytosis of neurons by inflamed microglia: potential roles in neurodegeneration. Frontiers in pharmacology *3*, 27.
Nelson, L. H., Warden, S., and Lenz, K. M. (2017). Sex differences in microglial phagocytosis in the neonatal hippocampus. Brain, behavior, and immunity *64*, 11-22.

Nemes-Baran, A. D., White, D. R., and DeSilva, T. M. (2020). Fractalkine-dependent microglial pruning of viable oligodendrocyte progenitor cells regulates myelination. Cell reports *32*.

Netea, M. G. (2013). Training innate immunity: the changing concept of immunological memory in innate host defence. European journal of clinical investigation *43*, 881-884.

Neumann, H., and Takahashi, K. (2007). Essential role of the microglial triggering receptor expressed on myeloid cells-2 (TREM2) for central nervous tissue immune homeostasis. Journal of neuroimmunology *184*, 92-99.

Neumann, J., Sauerzweig, S., Rönicke, R., Gunzer, F., Dinkel, K., Ullrich, O., Gunzer, M., and Reymann, K. G. (2008). Microglia cells protect neurons by direct engulfment of invading neutrophil granulocytes: a new mechanism of CNS immune privilege. Journal of Neuroscience *28*, 5965-5975.

Nguyen, X. (2022). Dimensionality Reduction in Single Cell Genomics.

Nimmerjahn, A., Kirchhoff, F., and Helmchen, F. (2005). Resting microglial cells are highly dynamic surveillants of brain parenchyma in vivo. Science *308*, 1314-1318.

Nomura, K., Vilalta, A., Allendorf, D. H., Hornik, T. C., and Brown, G. C. (2017). Activated microglia desialylate and phagocytose cells via neuraminidase, galectin-3, and mer tyrosine kinase. The Journal of Immunology *198*, 4792-4801.

O

O'Sullivan, S. A., O'Sullivan, C., Healy, L. M., Dev, K. K., and Sheridan, G. K. (2018). Sphingosine 1-phosphate receptors regulate TLR 4-induced CXCL 5 release from astrocytes and microglia. Journal of neurochemistry *144*, 736-747.

Obeid, M., Tesniere, A., Ghiringhelli, F., Fimia, G. M., Apetoh, L., Perfettini, J.-L., Castedo, M., Mignot, G., Panaretakis, T., and Casares, N. (2007). Calreticulin exposure dictates the immunogenicity of cancer cell death. Nature medicine *13*, 54-61.

Olah, M., Menon, V., Habib, N., Taga, M. F., Ma, Y., Yung, C. J., Cimpean, M., Khairallah, A., Coronas-Samano, G., and Sankowski, R. (2020). Single cell RNA sequencing of human microglia uncovers a subset associated with Alzheimer's disease. Nature communications *11*, 6129.

Olenych, S. G., Claxton, N. S., Ottenberg, G. K., and Davidson, M. W. (2007). The fluorescent protein color palette. Curr Protoc Cell Biol *Chapter 21*, Unit 21 25.

Ondrejcak, T., Klyubin, I., Hu, N.-W., Barry, A. E., Cullen, W. K., and Rowan, M. J. (2010). Alzheimer's disease amyloid β-protein and synaptic function. Neuromolecular medicine *12*, 13-26.

Opal, S. M., and DePalo, V. A. (2000). Anti-inflammatory cytokines. Chest *117*, 1162-1172.
Oppenheim, R. W. (1991). Cell death during development of the nervous system. Annual review of neuroscience *14*, 453-501.

Orihuela, R., McPherson, C. A., and Harry, G. J. (2016). Microglial M1/M2 polarization and metabolic states. British journal of pharmacology *173*, 649-665.

Owen, J. B., and Butterfield, D. A. (2010a). Measurement of oxidized/reduced glutathione ratio. Methods Mol Biol *648*, 269-277.

Owen, J. B., and Butterfield, D. A. (2010b). Measurement of oxidized/reduced glutathione ratio. Protein misfolding and cellular stress in disease and aging: concepts and protocols, 269-277.

Owens, R., Grabert, K., Davies, C. L., Alfieri, A., Antel, J. P., Healy, L. M., and McColl, B. W. (2017). Divergent neuroinflammatory regulation of microglial TREM expression and involvement of NF-κB. Frontiers in Cellular Neuroscience *11*, 56.

P

Paloneva, J., Manninen, T., Christman, G., Hovanes, K., Mandelin, J., Adolfsson, R., Bianchin, M., Bird, T., Miranda, R., and Salmaggi, A. (2002). Mutations in two genes encoding different subunits of a receptor signaling complex result in an identical disease phenotype. The American Journal of Human Genetics *71*, 656-662.

Pang, Y., Fan, L. W., Tien, L. T., Dai, X., Zheng, B., Cai, Z., Lin, R. C., and Bhatt, A. (2013). Differential roles of astrocyte and microglia in supporting oligodendrocyte development and myelination in vitro. Brain and behavior *3*, 503-514.

Paolicelli, R. C., Bolasco, G., Pagani, F., Maggi, L., Scianni, M., Panzanelli, P., Giustetto, M., Ferreira, T. A., Guiducci, E., and Dumas, L. (2011). Synaptic pruning by microglia is necessary for normal brain development. science *333*, 1456-1458.

Paolicelli, R. C., Sierra, A., Stevens, B., Tremblay, M. E., Aguzzi, A., Ajami, B., Amit, I., Audinat, E., Bechmann, I., Bennett, M.*, et al.* (2022). Microglia states and nomenclature: A field at its crossroads. Neuron *110*, 3458-3483.

Pardridge, W. M. (2005). The blood-brain barrier: bottleneck in brain drug development. NeuroRx *2*, 3-14.

Parhizkar, S., Arzberger, T., Brendel, M., Kleinberger, G., Deussing, M., Focke, C., Nuscher, B., Xiong, M., Ghasemigharagoz, A., and Katzmarski, N. (2019). Loss of TREM2 function increases amyloid seeding but reduces plaque-associated ApoE. Nature neuroscience *22*, 191-204.

Park, D., Han, C. Z., Elliott, M. R., Kinchen, J. M., Trampont, P. C., Das, S., Collins, S., Lysiak, J. J., Hoehn, K. L., and Ravichandran, K. S. (2011). Continued clearance of apoptotic cells critically depends on the phagocyte Ucp2 protein. Nature *477*, 220-224.

Parkhurst, C. N., Yang, G., Ninan, I., Savas, J. N., Yates, J. R., Lafaille, J. J., Hempstead, B. L., Littman, D. R., and Gan, W.-B. (2013). Microglia promote learning-dependent synapse formation through brain-derived neurotrophic factor. Cell *155*, 1596-1609.

Paronetto, M. P., Passacantilli, I., and Sette, C. (2016). Alternative splicing and cell survival: from tissue homeostasis to disease. Cell Death & Differentiation *23*, 1919-1929.

Pearce, M. S., Salotti, J. A., Little, M. P., McHugh, K., Lee, C., Kim, K. P., Howe, N. L., Ronckers, C. M., Rajaraman, P., and Craft, A. W. (2012). Radiation exposure from CT scans in childhood and subsequent risk of leukaemia and brain tumours: a retrospective cohort study. The Lancet *380*, 499-505.

Pegg, A. E. (2016). Functions of Polyamines in Mammals. J Biol Chem *291*, 14904-14912.

Pellettieri, J., and Alvarado, A. S. (2007). Cell turnover and adult tissue homeostasis: from humans to planarians. Annu Rev Genet *41*, 83-105.

Perego, C., Fumagalli, S., and De Simoni, M.-G. (2011). Temporal pattern of expression and colocalization of microglia/macrophage phenotype markers following brain ischemic injury in mice. Journal of neuroinflammation *8*, 1-20.

Peter, C., Waibel, M., Radu, C. G., Yang, L. V., Witte, O. N., Schulze-Osthoff, K., Wesselborg, S., and Lauber, K. (2008). Migration to apoptotic "find-me" signals is mediated via the phagocyte receptor G2A. Journal of biological chemistry *283*, 5296-5305.

Piers, T. M., Cosker, K., Mallach, A., Johnson, G. T., Guerreiro, R., Hardy, J., and Pocock, J. M. (2020). A locked immunometabolic switch underlies TREM2 R47H loss of function in human iPSC-derived microglia. The FASEB Journal *34*, 2436.

Pont-Lezica, L., Béchade, C., Belarif-Cantaut, Y., Pascual, O., and Bessis, A. (2011). Physiological roles of microglia during development. Journal of neurochemistry *119*, 901-908.

Popova, G., Soliman, S. S., Kim, C. N., Keefe, M. G., Hennick, K. M., Jain, S., Li, T., Tejera, D., Shin, D., and Chhun, B. B. (2021). Human microglia states are conserved across experimental models and regulate neural stem cell responses in chimeric organoids. Cell Stem Cell *28*, 2153-2166. e2156.

Porter, K., Lin, Y., and Liton, P. B. (2013). Cathepsin B is up-regulated and mediates extracellular matrix degradation in trabecular meshwork cells following phagocytic challenge. PloS one *8*, e68668.

Preissler, J., Grosche, A., Lede, V., Le Duc, D., Krügel, K., Matyash, V., Szulzewsky, F., Kallendrusch, S., Immig, K., and Kettenmann, H. (2015). Altered microglial phagocytosis in GPR34-deficient mice. Glia *63*, 206-215.

Prinz, M., Masuda, T., Wheeler, M. A., and Quintana, F. J. (2021). Microglia and central nervous system–associated macrophages—from origin to disease modulation. Annual review of immunology *39*, 251-277.

Q

Qi, X., Man, S. M., Malireddi, R. S., Karki, R., Lupfer, C., Gurung, P., Neale, G., Guy, C. S., Lamkanfi, M., and Kanneganti, T.-D. (2016). Cathepsin B modulates lysosomal biogenesis and host defense against Francisella novicida infection. Journal of Experimental Medicine *213*, 2081-2097.

Qian, J., Luo, F., Yang, J., Liu, J., Liu, R., Wang, L., Wang, C., Deng, Y., Lu, Z., and Wang, Y. (2018). TLR2 promotes glioma immune evasion by downregulating MHC class II molecules in microglia. Cancer Immunology Research *6*, 1220-1233.

R

R Core Team, R. (2013). R: A language and environment for statistical computing.
Rahimian, R., Béland, L. C., Sato, S., and Kriz, J. (2021). Microglia-derived galectin-3 in neuroinflammation; a bittersweet ligand? Medicinal Research Reviews *41*, 2582-2589.

Ramesh, G., MacLean, A. G., and Philipp, M. T. (2013). Cytokines and chemokines at the crossroads of neuroinflammation, neurodegeneration, and neuropathic pain. Mediators of inflammation *2013*.

Ramón y Cajal, S. (1888). Estructura de los centros nerviosos de las aves).

Ramón y Cajal, S. (1913). Contribución al conocimiento de la neuroglia del cerebro humano. Trab Lab Invest Biol *11*, 255.

Ramón y Cajal, S., and Azoulay, L. (1894). Les nouvelles idées sur la structure du système nerveux chez l'homme et chez les vertébrés: C. Reinwald).

Ransohoff, R. M. (2016). A polarizing question: do M1 and M2 microglia exist? Nature neuroscience *19*, 987-991.

Ransohoff, R. M., and Cardona, A. E. (2010). The myeloid cells of the central nervous system parenchyma. Nature *468*, 253-262.

Raziyeva, K., Kim, Y., Zharkinbekov, Z., Kassymbek, K., Jimi, S., and Saparov, A. (2021). Immunology of acute and chronic wound healing. Biomolecules *11*, 700.

Redza-Dutordoir, M., and Averill-Bates, D. A. (2016). Activation of apoptosis signalling pathways by reactive oxygen species. Biochimica et Biophysica Acta (BBA)-Molecular Cell Research *1863*, 2977-2992.

Repnik, U., Stoka, V., Turk, V., and Turk, B. (2012). Lysosomes and lysosomal cathepsins in cell death. Biochimica et Biophysica Acta (BBA)-Proteins and Proteomics *1824*, 22-33.

Réu, P., Khosravi, A., Bernard, S., Mold, J. E., Salehpour, M., Alkass, K., Perl, S., Tisdale, J., Possnert, G., and Druid, H. (2017). The lifespan and turnover of microglia in the human brain. Cell reports *20*, 779-784.

Reu, P., Khosravi, A., Bernard, S., Mold, J. E., Salehpour, M., Alkass, K., Perl, S., Tisdale, J., Possnert, G., Druid, H., and Frisen, J. (2017). The Lifespan and Turnover of Microglia in the Human Brain. Cell Rep *20*, 779-784.

Revest, P., and Longstaff, A. (1998). Molecular neuroscience: Garland Science).

Ridgway, N. D. (2013). The role of phosphatidylcholine and choline metabolites to cell proliferation and survival. Critical reviews in biochemistry and molecular biology *48*, 20-38.

Riera Romo, M., Pérez-Martínez, D., and Castillo Ferrer, C. (2016). Innate immunity in vertebrates: an overview. Immunology *148*, 125-139.

Ross, C., and Boroviak, T. E. (2020). Origin and function of the yolk sac in primate embryogenesis. Nature communications *11*, 3760.

Rossi, M., and Young, J. W. (2005). Human dendritic cells: potent antigen-presenting cells at the crossroads of innate and adaptive immunity. The Journal of Immunology *175*, 1373-1381.

Rotshenker, S. (2009). The role of Galectin-3/MAC-2 in the activation of the innate-immune function of phagocytosis in microglia in injury and disease. Journal of Molecular Neuroscience *39*, 99-103.

Rotshenker, S. (2022). Galectin-3 (MAC-2) controls phagocytosis and macropinocytosis through intracellular and extracellular mechanisms. Frontiers in Cellular Neuroscience *16*, 949079.

Rotterman, T. M., and Alvarez, F. J. (2020). Microglia Dynamics and Interactions with Motoneurons Axotomized After Nerve Injuries Revealed By Two-Photon Imaging. Sci Rep *10*, 8648.

Roufayel, R. (2016). Regulation of stressed-induced cell death by the Bcl-2 family of apoptotic proteins. Molecular membrane biology *33*, 89-99.

Roy, A., Jana, A., Yatish, K., Freidt, M. B., Fung, Y. K., Martinson, J. A., and Pahan, K. (2008). Reactive oxygen species up-regulate CD11b in microglia via nitric oxide: Implications for neurodegenerative diseases. Free Radical Biology and Medicine *45*, 686-699.

Ruvolo, P. P., Ma, H., Ruvolo, V. R., Zhang, X., Post, S. M., and Andreeff, M. (2020). LGALS1 acts as a pro-survival molecule in AML. Biochim Biophys Acta Mol Cell Res *1867*, 118785.

S

Sabate-Soler, S., Bernini, M., and Schwamborn, J. C. (2022). Immunocompetent brain organoids—microglia enter the stage. Progress in Biomedical Engineering *4*, 042002.

Safaiyan, S., Besson-Girard, S., Kaya, T., Cantuti-Castelvetri, L., Liu, L., Ji, H., Schifferer, M., Gouna, G., Usifo, F., and Kannaiyan, N. (2021). White matter aging drives microglial diversity. Neuron *109*, 1100-1117. e1110.

Saftig, P., Schröder, B., and Blanz, J. (2010). Lysosomal membrane proteins: life between acid and neutral conditions. In, (Portland Press Ltd.).

Safwat, A. (2000). The immunobiology of low-dose total-body irradiation: more questions than answers. Radiation research *153*, 599-604.

Saharan, S., Jhaveri, D. J., and Bartlett, P. F. (2013). SIRT1 regulates the neurogenic potential of neural precursors in the adult subventricular zone and hippocampus. Journal of Neuroscience Research *91*, 642-659.

Sakaguchi, S., Wing, K., and Miyara, M. (2007). Regulatory T cells–a brief history and perspective. European journal of immunology *37*, S116-S123.

Sala Frigerio, C., Wolfs, L., Fattorelli, N., Thrupp, N., Voytyuk, I., Schmidt, I., Mancuso, R., Chen, W. T., Woodbury, M. E., Srivastava, G.*, et al.* (2019). The Major Risk Factors for Alzheimer's Disease: Age, Sex, and Genes Modulate the Microglia Response to Abeta Plaques. Cell Rep *27*, 1293-1306 e1296.

Salmina, A. B., Komleva, Y. K., Malinovskaya, N. A., Morgun, A. V., Teplyashina, E. A., Lopatina, O. L., Gorina, Y. V., Kharitonova, E. V., Khilazheva, E. D., and Shuvaev, A. N. (2021). Blood–brain

barrier breakdown in stress and neurodegeneration: biochemical mechanisms and new models for translational research. Biochemistry (Moscow) *86*, 746-760.

Sanai, N., Polley, M.-Y., McDermott, M. W., Parsa, A. T., and Berger, M. S. (2011). An extent of resection threshold for newly diagnosed glioblastomas. Journal of neurosurgery *115*, 3-8.

Santavanond, J. P., Rutter, S. F., Atkin-Smith, G. K., and Poon, I. K. (2021). Apoptotic bodies: mechanism of formation, isolation and functional relevance. New Frontiers: Extracellular Vesicles, 61-88.

Santivasi, W. L., and Xia, F. (2014). Ionizing radiation-induced DNA damage, response, and repair. Antioxidants & redox signaling *21*, 251-259.

Sarma, J. V., and Ward, P. A. (2011). The complement system. Cell and tissue research *343*, 227-235.

Sasmono, R. T., Oceandy, D., Pollard, J. W., Tong, W., Pavli, P., Wainwright, B. J., Ostrowski, M. C., Himes, S. R., and Hume, D. A. (2003). A macrophage colony-stimulating factor receptor–green fluorescent protein transgene is expressed throughout the mononuclear phagocyte system of the mouse. Blood, The Journal of the American Society of Hematology *101*, 1155-1163.

Satija, R., Farrell, J. A., Gennert, D., Schier, A. F., and Regev, A. (2015). Spatial reconstruction of single-cell gene expression data. Nature biotechnology *33*, 495-502.

Satoh, J. i., Kino, Y., Asahina, N., Takitani, M., Miyoshi, J., Ishida, T., and Saito, Y. (2016). TMEM119 marks a subset of microglia in the human brain. Neuropathology *36*, 39-49.

Savarin-Vuaillat, C., and Ransohoff, R. M. (2007). Chemokines and chemokine receptors in neurological disease: raise, retain, or reduce? Neurotherapeutics *4*, 590-601.

Scaringi, C., Agolli, L., and Minniti, G. (2018). Technical Advances in Radiation Therapy for Brain Tumors. Anticancer Res *38*, 6041-6045.

Scarpato, R., Castagna, S., Aliotta, R., Azzara, A., Ghetti, F., Filomeni, E., Giovannini, C., Pirillo, C., Testi, S., Lombardi, S., and Tomei, A. (2013). Kinetics of nuclear phosphorylation (gamma-H2AX) in human lymphocytes treated in vitro with UVB, bleomycin and mitomycin C. Mutagenesis *28*, 465-473.

Schafer, D. P., Lehrman, E. K., Kautzman, A. G., Koyama, R., Mardinly, A. R., Yamasaki, R., Ransohoff, R. M., Greenberg, M. E., Barres, B. A., and Stevens, B. (2012). Microglia sculpt postnatal neural circuits in an activity and complement-dependent manner. Neuron *74*, 691-705.

Schoeneberg, T., Meister, J., Knierim, A. B., and Schulz, A. (2018). The G protein-coupled receptor GPR34–the past 20 years of a grownup. Pharmacology & Therapeutics *189*, 71-88.

Schofield, J. H., and Schafer, Z. T. (2021). Mitochondrial Reactive Oxygen Species and Mitophagy: A Complex and Nuanced Relationship. Antioxid Redox Signal *34*, 517-530.

Schulz, C., Perdiguero, E. G., Chorro, L., Szabo-Rogers, H., Cagnard, N., Kierdorf, K., Prinz, M., Wu, B., Jacobsen, S. E. W., and Pollard, J. W. (2012). A lineage of myeloid cells independent of Myb and hematopoietic stem cells. Science *336*, 86-90.

Schwartz, M., and Shechter, R. (2010). Systemic inflammatory cells fight off neurodegenerative disease. Nature Reviews Neurology *6*, 405-410.

Sciacchitano, S., Lavra, L., Morgante, A., Ulivieri, A., Magi, F., De Francesco, G. P., Bellotti, C., Salehi, L. B., and Ricci, A. (2018). Galectin-3: one molecule for an alphabet of diseases, from A to Z. International journal of molecular sciences *19*, 379.

Scott, R. S., McMahon, E. J., Pop, S. M., Reap, E. A., Caricchio, R., Cohen, P. L., Earp, H. S., and Matsushima, G. K. (2001). Phagocytosis and clearance of apoptotic cells is mediated by MER. Nature *411*, 207-211.

Sedel, F., Béchade, C., Vyas, S., and Triller, A. (2004). Macrophage-derived tumor necrosis factor α, an early developmental signal for motoneuron death. Journal of Neuroscience *24*, 2236-2246.

Segawa, K., Kurata, S., Yanagihashi, Y., Brummelkamp, T. R., Matsuda, F., and Nagata, S. (2014). Caspase-mediated cleavage of phospholipid flippase for apoptotic phosphatidylserine exposure. Science *344*, 1164-1168.

Sen, M. K., Mahns, D. A., Coorssen, J. R., and Shortland, P. J. (2022). The roles of microglia and astrocytes in phagocytosis and myelination: Insights from the cuprizone model of multiple sclerosis. Glia *70*, 1215-1250.

Sheridan, C., Delivani, P., Cullen, S. P., and Martin, S. J. (2008). Bax-or Bak-induced mitochondrial fission can be uncoupled from cytochrome C release. Molecular cell *31*, 570-585.

Sieger, D., Moritz, C., Ziegenhals, T., Prykhozhij, S., and Peri, F. (2012). Long-range Ca2+ waves transmit brain-damage signals to microglia. Developmental cell *22*, 1138-1148.

Sielska, M., Przanowski, P., Wylot, B., Gabrusiewicz, K., Maleszewska, M., Kijewska, M., Zawadzka, M., Kucharska, J., Vinnakota, K., and Kettenmann, H. (2013). Distinct roles of CSF family cytokines in macrophage infiltration and activation in glioma progression and injury response. The Journal of pathology *230*, 310-321.

Sierra-Torre, V., Plaza-Zabala, A., Bonifazi, P., Abiega, O., Díaz-Aparicio, I., Tegelberg, S., Lehesjoki, A. E., Valero, J., and Sierra, A. (2020). Microglial phagocytosis dysfunction in the dentate gyrus is related to local neuronal activity in a genetic model of epilepsy. Epilepsia *61*, 2593-2608.

Sierra, A., Abiega, O., Shahraz, A., and Neumann, H. (2013). Janus-faced microglia: beneficial and detrimental consequences of microglial phagocytosis. Frontiers in cellular neuroscience *7*, 6.

Sierra, A., de Castro, F., del Río-Hortega, J., Rafael Iglesias-Rozas, J., Garrosa, M., and Kettenmann, H. (2016). The "Big-Bang" for modern glial biology: Translation and comments on Pío del Río-Hortega 1919 series of papers on microglia. Glia *64*, 1801-1840.

Sierra, A., Encinas, J. M., Deudero, J. J., Chancey, J. H., Enikolopov, G., Overstreet-Wadiche, L. S., Tsirka, S. E., and Maletic-Savatic, M. (2010). Microglia shape adult hippocampal neurogenesis through apoptosis-coupled phagocytosis. Cell Stem Cell *7*, 483-495.

Sierra, A., Gottfried-Blackmore, A. C., McEwen, B. S., and Bulloch, K. (2007). Microglia derived from aging mice exhibit an altered inflammatory profile. Glia *55*, 412-424.

Sierra, A., Paolicelli, R. C., and Kettenmann, H. (2019). Cien Años de Microglía: Milestones in a century of microglial research. Trends in neurosciences *42*, 778-792.

Silantyev, A. S., Falzone, L., Libra, M., Gurina, O. I., Kardashova, K. S., Nikolouzakis, T. K., Nosyrev, A. E., Sutton, C. W., Mitsias, P. D., and Tsatsakis, A. (2019). Current and future trends on diagnosis and prognosis of glioblastoma: from molecular biology to proteomics. Cells *8*, 863.

Silva, R. P. d., and Gordon, S. (1999). Phagocytosis stimulates alternative glycosylation of macrosialin (mouse CD68), a macrophage-specific endosomal protein. Biochemical Journal *338*, 687-694.

Sivarajah, S. (2020). Dimensionality Reduction for Data Visualization: PCA vs TSNE vs UMAP vs LDA.

Sklar, C. A., and Constine, L. S. (1995). Chronic neuroendocrinological sequelae of radiation therapy. International Journal of Radiation Oncology* Biology* Physics *31*, 1113-1121.

Smith, A. M., Gibbons, H. M., Oldfield, R. L., Bergin, P. M., Mee, E. W., Curtis, M. A., Faull, R. L., and Dragunow, M. (2013). M-CSF increases proliferation and phagocytosis while modulating receptor and transcription factor expression in adult human microglia. Journal of neuroinflammation *10*, 1-15.

Sperduto, P. W., Kased, N., Roberge, D., Xu, Z., Shanley, R., Luo, X., Sneed, P. K., Chao, S. T., Weil, R. J., and Suh, J. (2012). Summary report on the graded prognostic assessment: an accurate and facile diagnosis-specific tool to estimate survival for patients with brain metastases. Journal of Clinical Oncology *30*, 419.

Spittau, B., Rilka, J., Steinfath, E., Zöller, T., and Krieglstein, K. (2015). TGFβ1 increases microglia-mediated engulfment of apoptotic cells via upregulation of the milk fat globule-EGF factor 8. Glia *63*, 142-153.

Srinivasan, K., Friedman, B. A., Etxeberria, A., Huntley, M. A., van Der Brug, M. P., Foreman, O., Paw, J. S., Modrusan, Z., Beach, T. G., and Serrano, G. E. (2020). Alzheimer's patient microglia exhibit enhanced aging and unique transcriptional activation. Cell reports *31*, 107843.

Stansley, B., Post, J., and Hensley, K. (2012). A comparative review of cell culture systems for the study of microglial biology in Alzheimer's disease. Journal of neuroinflammation *9*, 1-8.
Stogsdill, J. A., Kim, K., Binan, L., Farhi, S. L., Levin, J. Z., and Arlotta, P. (2022). Pyramidal neuron subtype diversity governs microglia states in the neocortex. Nature *608*, 750-756.

Stone, H. B., Coleman, C. N., Anscher, M. S., and McBride, W. H. (2003). Effects of radiation on normal tissue: consequences and mechanisms. The lancet oncology *4*, 529-536.

Stupp, R., Mason, W. P., Van Den Bent, M. J., Weller, M., Fisher, B., Taphoorn, M. J., Belanger, K., Brandes, A. A., Marosi, C., and Bogdahn, U. (2005). Radiotherapy plus concomitant and adjuvant temozolomide for glioblastoma. New England journal of medicine *352*, 987-996.

Subramanian, J., Savage, J. C., and Tremblay, M.-È. (2020). Synaptic loss in Alzheimer's disease: mechanistic insights provided by two-photon in vivo imaging of transgenic mouse models. Frontiers in cellular neuroscience *14*, 445.

Sumner, R., Crawford, A., Mucenski, M., and Frampton, J. (2000). Initiation of adult myelopoiesis can occur in the absence of c-Myb whereas subsequent development is strictly dependent on the transcription factor. Oncogene *19*, 3335-3342.

Sun, H., Chen, L., Cao, S., Liang, Y., and Xu, Y. (2019). Warburg effects in cancer and normal proliferating cells: two tales of the same name. Genomics, proteomics & bioinformatics *17*, 273-286.

Sundgren, P. C., and Cao, Y. (2009). Brain irradiation: effects on normal brain parenchyma and radiation injury. Neuroimaging Clinics *19*, 657-668.

Sutter, P. A., and Crocker, S. J. (2022). Glia as antigen-presenting cells in the central nervous system. Current opinion in neurobiology *77*, 102646.

Suzuki, J., Imanishi, E., and Nagata, S. (2016). Xkr8 phospholipid scrambling complex in apoptotic phosphatidylserine exposure. Proceedings of the National Academy of Sciences *113*, 9509-9514.

Szondy, Z., Sarang, Z., Kiss, B., Garabuczi, É., and Köröskényi, K. (2017). Anti-inflammatory mechanisms triggered by apoptotic cells during their clearance. Frontiers in immunology *8*, 909.

T

Thakkar, H., Chen, X., Tyan, F., Gim, S., Robinson, H., Lee, C., Pandey, S. K., Nwokorie, C., Onwudiwe, N., and Srivastava, R. K. (2001). Pro-survival function of Akt/protein kinase B in prostate cancer cells: relationship with TRAIL resistance. Journal of Biological Chemistry *276*, 38361-38369.

Thion, M. S., Low, D., Silvin, A., Chen, J., Grisel, P., Schulte-Schrepping, J., Blecher, R., Ulas, T., Squarzoni, P., and Hoeffel, G. (2018). Microbiome influences prenatal and adult microglia in a sex-specific manner. Cell *172*, 500-516. e516.

Thrash, J. C., Torbett, B. E., and Carson, M. J. (2009). Developmental regulation of TREM2 and DAP12 expression in the murine CNS: implications for Nasu-Hakola disease. Neurochemical research *34*, 38-45.

Timmerman, R., Burm, S. M., and Bajramovic, J. J. (2018). An overview of in vitro methods to study microglia. Frontiers in cellular neuroscience, 242.

Tirichen, H., Yaigoub, H., Xu, W., Wu, C., Li, R., and Li, Y. (2021). Mitochondrial Reactive Oxygen Species and Their Contribution in Chronic Kidney Disease Progression Through Oxidative Stress. Front Physiol *12*, 627837.

Townsend, S. E., and Goodnow, C. C. (1998). Abortive proliferation of rare T cells induced by direct or indirect antigen presentation by rare B cells in vivo. The Journal of experimental medicine *187*, 1611-1621.

Tran, Wolz, Egensperger, Kösel, Imai, Bise, Kohsaka, Mehraein, and Graeber (1998). Differential expression of MHC class II molecules by microglia and neoplastic astroglia: relevance for the escape of astrocytoma cells from immune surveillance. Neuropathology and applied neurobiology *24*, 293-301.

Trapp, B. D., Peterson, J., Ransohoff, R. M., Rudick, R., Mörk, S., and Bö, L. (1998). Axonal transection in the lesions of multiple sclerosis. New England Journal of Medicine *338*, 278-285.
Tremblay, M.-È., Lecours, C., Samson, L., Sánchez-Zafra, V., and Sierra, A. (2015). From the Cajal alumni Achúcarro and Río-Hortega to the rediscovery of never-resting microglia. Frontiers in neuroanatomy *9*, 45.

Trnovec, T., Kallay, Z., and Bezek, S. (1990). Effects of ionizing radiation on the blood brain barrier permeability to pharmacologically active substances. Int J Radiat Oncol Biol Phys *19*, 1581-1587.

Trouw, L., Blom, A., and Gasque, P. (2008). Role of complement and complement regulators in the removal of apoptotic cells. Molecular immunology *45*, 1199-1207.

Truman, L. A., Ford, C. A., Pasikowska, M., Pound, J. D., Wilkinson, S. J., Dumitriu, I. E., Melville, L., Melrose, L. A., Ogden, C. A., and Nibbs, R. (2008). CX3CL1/fractalkine is released from apoptotic lymphocytes to stimulate macrophage chemotaxis. Blood, The Journal of the American Society of Hematology *112*, 5026-5036.

Turk, V., Stoka, V., Vasiljeva, O., Renko, M., Sun, T., Turk, B., and Turk, D. (2012). Cysteine cathepsins: from structure, function and regulation to new frontiers. Biochimica et Biophysica Acta (BBA)-Proteins and Proteomics *1824*, 68-88.

Turvey, S. E., and Broide, D. H. (2010). Innate immunity. Journal of Allergy and Clinical Immunology *125*, S24-S32.

U

Ubogu, E. E., Cossoy, M. B., and Ransohoff, R. M. (2006). The expression and function of chemokines involved in CNS inflammation. Trends in pharmacological sciences *27*, 48-55.
Ueno, M., Fujita, Y., Tanaka, T., Nakamura, Y., Kikuta, J., Ishii, M., and Yamashita, T. (2013). Layer V cortical neurons require microglial support for survival during postnatal development. Nature neuroscience *16*, 543-551.

Ulrich, J. D., Ulland, T. K., Colonna, M., and Holtzman, D. M. (2017). Elucidating the role of TREM2 in Alzheimer's disease. Neuron *94*, 237-248.

Utz, S. G., See, P., Mildenberger, W., Thion, M. S., Silvin, A., Lutz, M., Ingelfinger, F., Rayan, N. A., Lelios, I., and Buttgereit, A. (2020). Early fate defines microglia and non-parenchymal brain macrophage development. Cell *181*, 557-573. e518.

V

Valente, A. J., Maddalena, L. A., Robb, E. L., Moradi, F., and Stuart, J. A. (2017). A simple ImageJ macro tool for analyzing mitochondrial network morphology in mammalian cell culture. Acta histochemica *119*, 315-326.

Valko, M., Rhodes, C., Moncol, J., Izakovic, M., and Mazur, M. (2006). Free radicals, metals and antioxidants in oxidative stress-induced cancer. Chemico-biological interactions *160*, 1-40.
Van Rossum, G., and Drake, F. L. (2009). Introduction to python 3: python documentation manual part 1: CreateSpace).

Vaupel, P., and Multhoff, G. (2021). Revisiting the Warburg effect: Historical dogma versus current understanding. The Journal of physiology *599*, 1745-1757.

Verney, C., Monier, A., Fallet-Bianco, C., and Gressens, P. (2010). Early microglial colonization of the human forebrain and possible involvement in periventricular white-matter injury of preterm infants. Journal of anatomy *217*, 436-448.

Veselkov, K. A., Vingara, L. K., Masson, P., Robinette, S. L., Want, E., Li, J. V., Barton, R. H., Boursier-Neyret, C., Walther, B., and Ebbels, T. M. (2011). Optimized preprocessing of ultra-performance liquid chromatography/mass spectrometry urinary metabolic profiles for improved information recovery. Analytical chemistry *83*, 5864-5872.

Vezzani, A. (2005). Inflammation and epilepsy. Epilepsy Currents *5*, 1-6.

Vieira, O. V., Bucci, C., Harrison, R. E., Trimble, W. S., Lanzetti, L., Gruenberg, J., Schreiber, A. D., Stahl, P. D., and Grinstein, S. (2003). Modulation of Rab5 and Rab7 recruitment to phagosomes by phosphatidylinositol 3-kinase. Molecular and cellular biology *23*, 2501-2514.

Villa, A., Gelosa, P., Castiglioni, L., Cimino, M., Rizzi, N., Pepe, G., Lolli, F., Marcello, E., Sironi, L., and Vegeto, E. (2018). Sex-specific features of microglia from adult mice. Cell reports *23*, 3501-3511.

Vinnakota, K., Hu, F., Ku, M.-C., Georgieva, P. B., Szulzewsky, F., Pohlmann, A., Waiczies, S., Waiczies, H., Niendorf, T., and Lehnardt, S. (2013). Toll-like receptor 2 mediates microglia/brain macrophage MT1-MMP expression and glioma expansion. Neuro-oncology *15*, 1457-1468.

Vitale, I., Manic, G., De Maria, R., Kroemer, G., and Galluzzi, L. (2017). DNA damage in stem cells. Molecular cell *66*, 306-319.

Voet, S., Prinz, M., and van Loo, G. (2019). Microglia in central nervous system inflammation and multiple sclerosis pathology. Trends in molecular medicine *25*, 112-123.

Von Bartheld, C. S., Bahney, J., and Herculano-Houzel, S. (2016). The search for true numbers of neurons and glial cells in the human brain: A review of 150 years of cell counting. Journal of Comparative Neurology *524*, 3865-3895.

Vorup-Jensen, T., and Jensen, R. K. (2018). Structural immunology of complement receptors 3 and 4. Frontiers in immunology *9*, 2716.

Voss, A. K., and Strasser, A. (2020). The essentials of developmental apoptosis. F1000Research *9*.

W

Wang, L., Pavlou, S., Du, X., Bhuckory, M., Xu, H., and Chen, M. (2019). Glucose transporter 1 critically controls microglial activation through facilitating glycolysis. Molecular neurodegeneration *14*, 1-15.

Wang, S.-C., Hong, J.-H., Hsueh, C., and Chiang, C.-S. (2012). Tumor-secreted SDF-1 promotes glioma invasiveness and TAM tropism toward hypoxia in a murine astrocytoma model. Laboratory investigation *92*, 151-162.

Wang, X., Cai, J., Lin, B., Ma, M., Tao, Y., Zhou, Y., Bai, L., Jiang, W., and Zhou, R. (2021a). GPR34-mediated sensing of lysophosphatidylserine released by apoptotic neutrophils activates type 3 innate lymphoid cells to mediate tissue repair. Immunity *54*, 1123-1136. e1128.

Wang, Y., Subramanian, M., Yurdagul, A., Barbosa-Lorenzi, V. C., Cai, B., de Juan-Sanz, J., Ryan, T. A., Nomura, M., Maxfield, F. R., and Tabas, I. (2017). Mitochondrial fission promotes the continued clearance of apoptotic cells by macrophages. Cell *171*, 331-345. e322.

Wang, Y., Ulland, T. K., Ulrich, J. D., Song, W., Tzaferis, J. A., Hole, J. T., Yuan, P., Mahan, T. E., Shi, Y., and Gilfillan, S. (2016). TREM2-mediated early microglial response limits diffusion and toxicity of amyloid plaques. Journal of Experimental Medicine *213*, 667-675.

Wang, Z., Zhang, H., Xu, S., Liu, Z., and Cheng, Q. (2021b). The adaptive transition of glioblastoma stem cells and its implications on treatments. Signal transduction and targeted therapy *6*, 124.

Watkins, L. R., and Hutchinson, M. R. (2014). A concern on comparing 'apples' and 'oranges' when differences between microglia used in human and rodent studies go far, far beyond simply species: comment on Smith and Dragunow. Trends in neurosciences *37*, 189-190.

Watters, J. J., Schartner, J. M., and Badie, B. (2005). Microglia function in brain tumors. Journal of neuroscience research *81*, 447-455.

Weavers, H., Evans, I. R., Martin, P., and Wood, W. (2016). Corpse engulfment generates a molecular memory that primes the macrophage inflammatory response. Cell *165*, 1658-1671.

Wei, J., Marisetty, A., Schrand, B., Gabrusiewicz, K., Hashimoto, Y., Ott, M., Grami, Z., Kong, L.-Y., Ling, X., and Caruso, H. (2019). Osteopontin mediates glioblastoma-associated macrophage infiltration and is a potential therapeutic target. The Journal of clinical investigation *129*, 137-149.

Wei, Z.-x., Cai, L., Zhao, X.-m., Jiang, X.-r., and Li, X.-l. (2022). Effects of spermidine on cell proliferation, migration, and inflammatory response in porcine enterocytes. Frontiers in Bioscience-Landmark *27*, 194.

Wick, W., Platten, M., and Weller, M. (2001). Glioma cell invasion: regulation of metalloproteinase activity by TGF-β. Journal of neuro-oncology *53*, 177-185.

Wijeyesakere, S. J., Bedi, S. K., Huynh, D., and Raghavan, M. (2016). The C-terminal acidic region of calreticulin mediates phosphatidylserine binding and apoptotic cell phagocytosis. The Journal of Immunology *196*, 3896-3909.

Willingham, S. B., Volkmer, J.-P., Gentles, A. J., Sahoo, D., Dalerba, P., Mitra, S. S., Wang, J., Contreras-Trujillo, H., Martin, R., and Cohen, J. D. (2012). The CD47-signal regulatory protein alpha (SIRPa) interaction is a therapeutic target for human solid tumors. Proceedings of the National Academy of Sciences *109*, 6662-6667.

Wolf, Y., Yona, S., Kim, K.-W., and Jung, S. (2013). Microglia, seen from the CX3CR1 angle. Frontiers in cellular neuroscience *7*, 26.

Wolock, S. L., Lopez, R., and Klein, A. M. (2019). Scrublet: computational identification of cell doublets in single-cell transcriptomic data. Cell systems *8*, 281-291. e289.

Wong, A. M., Patel, N. V., Patel, N. K., Wei, M., Morgan, T. E., de Beer, M. C., de Villiers, W. J., and Finch, C. E. (2005). Macrosialin increases during normal brain aging are attenuated by caloric restriction. Neuroscience letters *390*, 76-80.

Wu, A., Wei, J., Kong, L.-Y., Wang, Y., Priebe, W., Qiao, W., Sawaya, R., and Heimberger, A. B. (2010). Glioma cancer stem cells induce immunosuppressive macrophages/microglia. Neuro-oncology *12*, 1113-1125.

Wu, Y., Singh, S., Georgescu, M.-M., and Birge, R. B. (2005). A role for Mer tyrosine kinase in αvβ5 integrin-mediated phagocytosis of apoptotic cells. Journal of cell science *118*, 539-553.
Wu, Y. E., Pan, L., Zuo, Y., Li, X., and Hong, W. (2017). Detecting activated cell populations using single-cell RNA-seq. Neuron *96*, 313-329. e316.

X

Xavier, A. L. R., Kress, B. T., Goldman, S. A., de Menezes, J. R. L., and Nedergaard, M. (2015). A distinct population of microglia supports adult neurogenesis in the subventricular zone. Journal of Neuroscience *35*, 11848-11861.

Xia, S., Lal, B., Tung, B., Wang, S., Goodwin, C. R., and Laterra, J. (2015). Tumor microenvironment tenascin-C promotes glioblastoma invasion and negatively regulates tumor proliferation. Neuro-oncology *18*, 507-517.

Xia, X., Wang, W., Yin, K., and Wang, S. (2020). Interferon regulatory factor 8 governs myeloid cell development. Cytokine & growth factor reviews *55*, 48-57.

Xie, Z., Zhao, M., Yan, C., Kong, W., Lan, F., Narengaowa, Zhao, S., Yang, Q., Bai, Z., and Qing, H. (2023). Cathepsin B in programmed cell death machinery: mechanisms of execution and regulatory pathways. Cell Death & Disease *14*, 255.

Xu, J., Wang, T., Wu, Y., Jin, W., and Wen, Z. (2016). Microglia colonization of developing zebrafish midbrain is promoted by apoptotic neuron and lysophosphatidylcholine. Developmental cell *38*, 214-222.

Xu, R., Boreland, A. J., Li, X., Erickson, C., Jin, M., Atkins, C., Pang, Z. P., Daniels, B. P., and Jiang, P. (2021). Developing human pluripotent stem cell-based cerebral organoids with a controllable microglia ratio for modeling brain development and pathology. Stem cell reports *16*, 1923-1937.

Y

Yang, D.-S., Stavrides, P., Saito, M., Kumar, A., Rodriguez-Navarro, J. A., Pawlik, M., Huo, C., Walkley, S. U., Saito, M., and Cuervo, A. M. (2014). Defective macroautophagic turnover of brain lipids in the TgCRND8 Alzheimer mouse model: prevention by correcting lysosomal proteolytic deficits. Brain *137*, 3300-3318.

Yang, R.-Y., Hsu, D. K., and LIu, F.-T. (1996). Expression of galectin-3 modulates T-cell growth and apoptosis. Proceedings of the National Academy of Sciences *93*, 6737-6742.
Yin, E., Nelson, D., Coleman, M., Peterson, L. E., and Wyrobek, A. (2003). Gene expression changes in mouse brain after exposure to low-dose ionizing radiation. International journal of radiation biology *79*, 759-775.

Young, K., and Morrison, H. (2018). Quantifying Microglia Morphology from Photomicrographs of Immunohistochemistry Prepared Tissue Using ImageJ. J Vis Exp.

Yu, F., Wang, Y., Stetler, A. R., Leak, R. K., Hu, X., and Chen, J. (2022). Phagocytic microglia and macrophages in brain injury and repair. CNS Neuroscience & Therapeutics *28*, 1279-1293.

Yu, X., Guo, C., Fisher, P. B., Subjeck, J. R., and Wang, X.-Y. (2015). Scavenger receptors: emerging roles in cancer biology and immunology. Advances in cancer research *128*, 309-364.
Yu, X., Lu, N., and Zhou, Z. (2008). Phagocytic receptor CED-1 initiates a signaling pathway for degrading engulfed apoptotic cells. PLoS biology *6*, e61.

Yuan, P., Condello, C., Keene, C. D., Wang, Y., Bird, T. D., Paul, S. M., Luo, W., Colonna, M., Baddeley, D., and Grutzendler, J. (2016). TREM2 haplodeficiency in mice and humans impairs the microglia barrier function leading to decreased amyloid compaction and severe axonal dystrophy. Neuron *90*, 724-739.

Z

Zagórska, A., Través, P. G., Lew, E. D., Dransfield, I., and Lemke, G. (2014). Diversification of TAM receptor tyrosine kinase function. Nature immunology *15*, 920-928.

Zhai, K., Huang, Z., Huang, Q., Tao, W., Fang, X., Zhang, A., Li, X., Stark, G. R., Hamilton, T. A., and Bao, S. (2021). Pharmacological inhibition of BACE1 suppresses glioblastoma growth by stimulating macrophage phagocytosis of tumor cells. Nature cancer *2*, 1136-1151.

Zhan, L., Krabbe, G., Du, F., Jones, I., Reichert, M. C., Telpoukhovskaia, M., Kodama, L., Wang, C., Cho, S.-h., and Sayed, F. (2019). Proximal recolonization by self-renewing microglia re-establishes microglial homeostasis in the adult mouse brain. PLoS biology *17*, e3000134.
Zhang, J., and Zhang, Q. (2019). Using Seahorse Machine to Measure OCR and ECAR in Cancer Cells. Methods Mol Biol *1928*, 353-363.

Zhang, L., Xu, Y., Sun, J., Chen, W., Zhao, L., Ma, C., Wang, Q., Sun, J., Huang, B., and Zhang, Y. (2017). M2-like tumor-associated macrophages drive vasculogenic mimicry through amplification of IL-6 expression in glioma cells. Oncotarget *8*, 819.

Zhang, N. (2018). Role of methionine on epigenetic modification of DNA methylation and gene expression in animals. Animal Nutrition *4*, 11-16.

Zhang, W., Jiang, J., Xu, Z., Yan, H., Tang, B., Liu, C., Chen, C., and Meng, Q. (2023). Microglia-containing human brain organoids for the study of brain development and pathology. Molecular Psychiatry *28*, 96-107.

Zhao, Z., Pan, G., Tang, C., Li, Z., Zheng, D., Wei, X., and Wu, Z. (2018). IL-34 inhibits acute rejection of rat liver transplantation by inducing Kupffer cell M2 polarization. Transplantation *102*, e265-e274.

Zrzavy, T., Hametner, S., Wimmer, I., Butovsky, O., Weiner, H. L., and Lassmann, H. (2017). Loss of 'homeostatic'microglia and patterns of their activation in active multiple sclerosis. Brain *140*, 1900-1913.

Zusso, M., Methot, L., Lo, R., Greenhalgh, A. D., David, S., and Stifani, S. (2012). Regulation of postnatal forebrain amoeboid microglial cell proliferation and development by the transcription factor Runx1. Journal of Neuroscience *32*, 11285-11298.